2.5 GEOLOGY, SEISMOLOGY, AND GEOTECHNICAL ENGINEERING

{This section of the U.S. EPR FSAR is incorporated by reference with the following supplements.

The summary includes a synopsis of FSAR Section 2.5.1 through Section 2.5.5, including a brief description of the Site, investigations performed, results of investigations, conclusions, and identification of the organization that performed the work.

This section is intended to demonstrate compliance with the requirements of paragraph (c) of 10 CFR 100.23, "Geologic and Seismic Siting Criteria" (CFR, 2007a). Regulatory Guide (RG) 1.208, "A Performance-Based Approach to Define the Site-Specific Earthquake Ground Motion", (NRC, 2007a) is the primary guidance document for the development of the Site Probabilistic Seismic Hazard Analysis (PSHA) and Ground Motion Response Spectrum (GMRS).

The terms site region, site vicinity, site area, and site are used in this section to describe the specific areas of investigation. These terms correspond to the following areas:

1. The site region is that area within 200 miles (320 km) of the site location.
2. The site vicinity is that area within 25 miles (40 km) of the site location.
3. The site area is that area within 5 miles (8 km) of the site location.
4. The site is that area within 0.6 mile (1 km) of the site location.

SUMMARY

The proposed Bell Bend Nuclear Power Plant (BBNPP) site is located south and west of the existing Susquehanna Steam Electric Station (SSES) in Salem Township, Luzerne County, Pennsylvania. The BBNPP site is found approximately 5 mi (8 km) northeast of the Borough of Berwick, Pennsylvania, and 1.5 mi (2.4 km) to the north and west of the north branch of the Susquehanna River. The major metropolitan centers closest to the site include: Wilkes-Barre, located 19 mi (31 km) to the northeast; Allentown, PA, approximately 50 mi (80 km) to the southeast; and Harrisburg, PA, which is approximately 70 mi (100 km) to the southwest.

The BBNPP Owner Controlled Area (OCA) is 882 ac (357 ha). The BBNPP site occupies an area of 424 acres (172 hectares) within the OCA. The BBNPP is not within the Exclusion Area Boundary for SSES Units 1 and 2.

FSAR Section 2.5 provides information on the seismic, geologic, and geotechnical characteristics of the site and the region surrounding the site. The purpose of this information is to permit an adequate evaluation of the proposed site, to support evaluations performed to estimate the site-specific ground motion response spectrum (GMRS), and to permit adequate engineering solutions to actual or potential geologic and seismic hazards at the proposed site. Details of the studies and investigations performed as well as the findings and conclusions are presented in Section 2.5.1 through 2.5.5.

The primary conclusions of Section 2.5 are as follows:

1. **Section 2.5.1 Basic Geologic & Seismic Information** - The site lies in a stable geologic region, and no geologic or man-made hazards have been identified within the site area. The region has also experienced only minor earthquake activity, with no measured historical epicenter located within 50 miles of the Site.

© 2007-2012 UniStar Nuclear Services, LLC. All rights reserved.
COPYRIGHT PROTECTED

2. **Section 2.5.2 Vibratory Ground Motion** - A PSHA was developed in accordance with Regulatory Guide 1.208, using: (1) the USGS 2002 catalog data update of the United States National Seismic Hazard Maps, (2) the EPRI-SOG 1986 seismic source zones, (3) updated ground motion models (EPRI, 2006), (3) deaggregation and site response analysis according to NUREG 6728-2B; and (4) a performance based Ground Motion Response Spectra (RG 1.208). Sensitivity studies which were performed on the 2002-2007 seismic events for 500 mi (805 km) and the Charlevoix EPRI source zone defined prior to the 1988 Sagueny Earthquake. These studies confirmed the results of the PSHA.

3. **Section 2.5.3 Surface Faulting** - The site vicinity exhibits little evidence of faulting, and all of it is non-capable. In addition, a targeted field investigation for the site vicinity discovered no evidence of paleoliquefaction features.

4. **Section 2.5.4 Stability of Subsurface Materials and Foundations** - Subsurface investigations concluded that the site analysis was bounded by the U.S. EPR FSAR for settlement, bearing capacity, hydraulic gradient and that the subsurface bedrock materials are stable with no potential for soil liquefaction. The Nuclear Island will be founded on the Mahantango Formation, which will be augmented with engineered fill to support the surface founded structures.

5. **Section 2.5.5 Stability of Slopes** - The site exhibits limited natural slopes and the only permanent slopes are those for the ESWEMS Retention Pond. All permanent and temporary slopes are shown to have adequate stability safety factors.

Additional details are summarized below.

Basic Geologic and Seismic Information

Regional Geology

The BBNPP site lies within the Appalachian Mountain Section of the Ridge and Valley Province that consists of long, narrow ridges and broad to narrow valleys exhibiting moderate to very high relief. These ridges and valleys are a direct result of lithologic disparities in erosional resistance and the folded and faulted structures developed in the geologic past, when the mountains were built, during the Alleghanian Orogeny.

This Province is primarily a zone containing Cambrian to Pennsylvanian rocks that were folded and faulted during the Alleghanian Orogeny that occurred during late Pennsylvanian through Permian times, nearly 300 million years ago. In addition to the geologic events that affected the entire Ridge and Valley Physiographic Province, three glacial advances affected the site vicinity during the Pleistocene Epoch.

The BBNPP site region is located in a stable continental region (SCR) characterized by low rates of crustal deformation with no active plate boundary conditions. There is no evidence for late Cenozoic seismogenic activity of any tectonic feature or structure within the site region (within 200 mi, 322 km).

Seismic activity associated with some of the larger tectonic features located beyond the site region has persisted to the present time. The nearest active tectonic feature is associated with the Newbury Liquefaction Features, located approximately 300 miles (480 km) to the northeast of the site. The Newbury feature in northeastern Massachusetts has been assigned to Class "A" status because of eyewitness reports of liquefaction during an earthquake in 1727,

© 2007-2012 UniStar Nuclear Services, LLC. All rights reserved.
COPYRIGHT PROTECTED

but the causative fault responsible for the ground motion and liquefaction remains unidentified. Three other features located beyond the 200-mile (322-km) site region have been included in the calculation of the BBNPP seismic hazard at low frequencies, based on updated models with new paleoseismological data. These features are: the New Madrid Seismic Zone, the Charleston Seismic Zone, and the Charlevoix-La Malbaie Seismic Zone in Canada.

Site Geology

Significant surface and subsurface investigations were conducted for the BBNPP site area foundation investigation, including field surveys, drilling, and geophysical exploration. Additional information was obtained from the Susquehanna Steam Electric Station Units 1 and 2 (SSES) FSAR.

The site is adjacent to the Susquehanna River near the southern edge of glaciation in Pennsylvania. The BBNPP site area is located within the Susquehanna Lowland Section of the Ridge and Valley Physiographic Province and is bordered by the Anthracite Valley Section to the north, and the Anthracite Upland Section to the south. The site area is underlain by folded Late Silurian, Devonian, and Lower Mississippian formations, with the Upper Devonian Mahantango Formation forming the bedrock directly beneath the site at the approximate elevation of 660 ft (20 m) msl. The most recent geologic influence on the site is the Wisconinan glaciation that deposited glacial materials (including kame terrace, moraines and outwash) on the bedrock surface in a layer approximately 40 feet thick.

The topography within 5 mi (8 km) of the site consists of low to moderately high, linear ridges and valleys that primarily follow structural trends of the local geologic formations. Local elevations ranging from about 260 ft (79 m) to nearly 2,368 ft (722 m) msl. The BBNPP is planned to be constructed at a final grade elevation of 674 ft (205 m) msl, approximately 200 ft (61 m) above the Susquehanna River, and will be set back approximately 7,500 ft (2,286 m) from the River bank.

The local geologic formations have been subjected to a series of mountain-building episodes, including the Grenville, Taconic and Alleghanian orogenies. The local structure of the Ridge and Valley Province was imparted to the area during the Alleghanian Orogeny at the end of the Permian Period, nearly 250 million years ago. The Site geologic history has been quiet since the end of the Permian. At that time the local portion of the crust became more stable and tensional stresses predominated through the Cretaceous Period. The only disturbance of this quiet state was the advance of several ice sheets in the Pleistocene. However, since the site is located at the extreme southern limit of the glaciated area, the ice sheets were at their thinnest and any crustal depression or subsequent rebound from the ice load has been minimal.

Geologic studies to determine the site structural characteristics have been performed utilizing data obtained from site borings and geophysical surveys. In addition, bedrock exposures were mapped throughout the site area. A thorough search for faulting and detailed mapping of excavations was also performed. The site occupies a position on the northern limb of the northeast end of the Berwick Anticline. A pair of faults has been mapped near the axis of the anticline, but they have been mapped as being related to the Alleghanian Orogeny, and are not active today. No geologic hazards have been identified during either investigation.

© 2007-2012 UniStar Nuclear Services, LLC. All rights reserved.
COPYRIGHT PROTECTED

The site is located in a region that has experienced only infrequent minor earthquake activity, with no earthquake-related epicentral locations detected within a 50-mile (80 km) radius of the site.

Investigations at the Site have not revealed any adverse geologic conditions that can be attributed to man's activity. The addition or withdrawal of subsurface fluids, including ground water, at the Site has not been significant. Material extraction in the Site vicinity has consisted of minor amounts of sand and gravel for roadbuilding. At present, there are no active mining operations within 11 miles (18 km) of the Site. There has been no mining or petroleum production in the Site area that would cause any surface or subsurface subsidence.

Vibratory Ground Motion

Section 2.5.2 provides a detailed description of the vibratory ground motion assessment that was carried out to develop the BBNPP Ground Motion Response Spectra (GMRS). The GMRS is the first step in defining the Site Safe Shutdown Earthquake (SSE) response spectra. The Site SSE for BBNPP is further defined in Section 3.7.1.1.1 after reconciliation with the Certified Seismic Design Spectra (CSDRS) curves. The vibratory ground motion assessment was performed using a Probabilistic Seismic Hazard Analysis (PSHA). The PSHA was conducted in accordance with RG 1.208.

The PSHA process began with the creation of an updated seismic catalog. The United States Geological Service (USGS) "documentation for the 2002 Update of the National Seismic Hazard Maps"(USGS, 2002) was used as a starting point for earthquake catalog selection. The earthquake catalog was extended to include events up to the end of 2007.

The Electric Power Research Institute-Seismicity Owners Group (EPRI-SOG) seismic source zones defined in the 1989 EPRI/SOG study (EPRI, 1989a) have been adopted for updating the BBNPP site PSHA. Adjustments were required to include characteristic earthquake models that must be used to properly account for more recent information on the seismic activity in the New Madrid and Charleston seismic zones. The hazard contribution of the New Madrid Seismic Zone (NMSZ) was incorporated through a characteristic earthquake model of the New Madrid Fault System (NMFS). Results of several post-EPRI studies have demonstrated that the parameters of the Charleston seismic source need to be updated. The present PSHA for the BBNPP has adopted the Updated Charleston Seismic Source (UCSS) model that was also used in the seismic hazard studies that support the recent FSAR for the CCNPP Unit 3 (UniStar Nuclear, 2007). The Early Site Permit (ESP) Application for the Clinton NPP (EGC, 2006) submitted to the NRC on April 16, 2006 by Exelon Generation Company (EGC), and USGS new interpretations were included in the development of the NMFS characteristic earthquake model.

The following sources are considered for the PSHA at the BBNPP Site:

1. EPRI general area source zones extracted from the 1989 EPRI-SOG study.
2. Updated New Madrid Seismic Zone (NMSZ) as a characteristic model earthquake,
3. The Updated Charleston Seismic Source (UCSS) model

Site response analyses were conducted to evaluate the effect of the site geologic conditions on the generic Central and Eastern United States (CEUS) hard rock ground motions. The intent

© 2007-2012 UniStar Nuclear Services, LLC. All rights reserved.
COPYRIGHT PROTECTED

of the analyses is to develop ground motions at the surface that are consistent with the hazard levels defined for the generic rock conditions.

Uniform Hazard Response Spectra (UHRS) at hard rock are derived as well as their corresponding de-aggregation results for 1E-4, 1E-5, and 1E-6 hazard levels. The low frequency controlling event, 1 to 2.5 hertz, and the high frequency controlling event, 5 to 10 hertz, are identified from the de-aggregation results. These controlling events are prescribed in terms of magnitude (M) and distance (R) pairs. From the M-R pair defining each controlling event, the rock motion time histories whose epicenter distance and magnitude are close to the ones of the controlling event are selected.

For each controlling event, a spectral shape is adopted from the shapes for the Central and Eastern United States (CEUS) site according to the corresponding magnitude and distance pair (NUREG 6728). Then the response spectrum is scaled to match the rock UHRS at the spectral frequencies of 1.75 hertz (low frequency controlling event) and 7.5 hertz (high frequency controlling event). Next, the rock motion time histories are scaled to match the corresponding scaled controlling response spectrum. These scaled time histories are utilized as input to the Site Response Analyses.

A best estimate soil profile, with best estimate shear-wave velocity and material stiffness, density, and damping curves, is developed based on the site specific BBNPP Plant subsurface geophysical and geotechnical investigation. The site analysis uses randomized material properties and layer thicknesses based on the best estimate values and their variability. The results are expressed as mean site amplification functions corresponding to each controlling event. These factors are used to calculate the mean soil UHRS. In turn, the mean site amplification functions and the mean soil UHRS are used to derive the GMRS, with the application of the performance approach defined by RG 1.208. Vertical to horizontal ratios are subsequently used to calculate the vertical GMRS.

Two sensitivity analyses were performed as part of the BBNPP PSHA: (1) to assess the contribution to the hazard from the 2002-2007 seismicity with a 500 mile radius around the site, and (2) to assess the site specific significance of a modified Charlevoix seismic zone. In addition to the sensitivity analyses, recent research and interpretations, related to the St. Lawrence valley, the New England zone, and the Ramapo fault zone, have been evaluated in the context of the BBNPP PSHA. The first sensitivity study concluded that the 2002-2007 data results in a non-conservative prediction, (i.e., would result in additional margin) of seismic occurrence rates when compared to the USGS 2002 catalog. This would be a non-conservative reduction in the PSHA. The second sensitivity analysis concludes that the modification of the Charlevoix seismic zone to properly incorporate post-EPRI 1986 earthquakes does not have an effect in the BBNPP PSHA, mainly due to the distance to the site.

Surface Faulting

In order to assess the potential or lack of potential for surface rupture in the site region, a variety of detailed subsurface and surface investigation tools were employed. A detailed review of existing information was performed, including geologic maps, seismologic survey data, the USGS earthquake catalog, aerial and satellite imagery, local knowledge from local researchers, and published references. Review of the geotechnical drilling information from the adjacent SSES Site was undertaken to verify the lateral continuity of strata across the BBNPP site. In 2007 a surface outcrop survey was carried out within the site area. In addition, in October 2008, additional field investigations were performed by geologists and engineers to

© 2007-2012 UniStar Nuclear Services, LLC. All rights reserved.
COPYRIGHT PROTECTED

assess the presence of paleoliquefaction features along waterways within the site vicinity, and also to ground-truth the presence and surface expression of nearby Paleozoic-age faults.

Seismic refraction studies interpreted by Weston in 2008 show no indication of offset of the top of the Mahantango Shale, which is the local bearing stratum in the site area.

There are no documented zones of Quaternary deformation within the BBNPP site vicinity. No evidence of seismic-related disturbance has been found within the Mahantango Shale or the overlying glacial and post-glacial deposits.

It has been determined that there is no potential for tectonic rupture within the site area, and there are no capable tectonic sources within the site vicinity.

Stability of Subsurface Materials and Foundations

The natural topography at the BBNPP site is gently sloping. The maximum variation in relief is about 144.5 ft (44 m) across the site. Average elevation across the Site is about 680 ft (207 m).

The upper 400 ft (122 m) of the BBNPP soils was the subject of subsurface investigation. The site geology is comprised of glacial and postglacial soil deposits underlain by bedrock, which is on average 38.9 ft (11.9 m) below the ground surface. The subsurface is divided into the following stratigraphic units:

- Overburden Soils: Glacial tills that grade from fine silty and clayey soils at the surface to cobbly sand with boulders at the bottom. These soils cannot be used for foundations, because there is a potential for liquefaction.
- Bedrock Formation: the Mahantango Formation that is a dark gray to black shale, and will provide the foundation for the majority of the principal plant structures.

The field investigation for the site was performed in accordance with NRC Regulatory Guide 1.132, "Site Investigations for Foundations of Nuclear Power Plants" (NRC, 2003a). A thorough field investigation program was planned and implemented, and included the following:

- Boring Program
  - Wash Rotary Drilling and Standard Penetration Test
  - Rock Coring (NQ Wireline)
- In-Situ Pressure meter Testing
- Geophysical Exploration
  - Downhole Tests
  - PS Suspension Logging Tests
  - Deviation Surveys
  - Seismic Refraction Surveys

In total, 48 boreholes were completed for the BBNPP site, of which 27 boreholes were located in the vicinity of the proposed Category 1 structures. Three borings were extended to 400 feet

© 2007-2012 UniStar Nuclear Services, LLC. All rights reserved.
COPYRIGHT PROTECTED

(122 m) for detailed core logging and geophysical testing at the location of the reactor building.

A Hydrogeologic Field Investigation collected site-specific data to support a comprehensive hydrogeological evaluation of the plant site and surrounding areas. The data collected were utilized to support the surface hydrology analysis, hydrogeological characterization, and the development of a groundwater flow model.

A comprehensive laboratory testing program was performed on disturbed and undisturbed soil and rock samples, including the following:

1. Index and engineering classification
2. Strength
3. Consolidation
4. Permeability
5. Chemical Tests
6. Resonant Column Torsional Shear
7. Free-Free Resonant Column

The number and type of tests performed were consistent with the field investigation findings and the overall uniform conditions found at the site, and were performed in accordance with the guidance of the NRC Regulatory Guide 1.138 , "Laboratory Investigations of Soils and Rocks for Engineering Analysis and Design of Nuclear Power Plants" (NRC, 2003b).

Category 1 Granular Structural Fill and Backfill for the eventual construction of the plant was identified from local sources and tested to determine the relevant engineering properties to be used in design analyses.

Recommendations of Soil, Fill and Rock properties were developed for all materials based on a combination of field measurements, laboratory testing, engineering analysis and judgment, and reference materials. Recommended properties are summarized in Section 2.5.4.2.5.

Foundation interfaces between the planned structures and site foundation materials were evaluated, and design parameters selected, in accordance with the requirements for COL applicants referencing the U.S. EPR FSAR.

Stability of Slopes

The BBNPP site is comprised of generally flat topography in the vicinity of the primary structures and components. The Site is planned to be graded to establish the final grade for the project, resulting in minor cuts and fills, as well as slopes.

The stability of temporary and permanent slopes was evaluated using limit equilibrium methods, resulting in a Factor of Safety for the slope section analyzed.

The ESWEMS Retention Pond slopes are the only permanent slopes planned for the BBNPP. Slope stability analysis results indicate that the pond side slopes have Factor of Safety values

© 2007-2012 UniStar Nuclear Services, LLC. All rights reserved.
COPYRIGHT PROTECTED

ranging from 2.0 to 9.2, indicating that the proposed slope design and configuration is stable under all considered loading conditions.

Temporary cut and fill slopes will exist in dry conditions during construction. Slope stability analysis results indicate the temporary slopes have Factor of Safety value of 1.3, indicating that the proposed slope design is stable under all considered loading conditions.}

2.5.1 Basic Geologic and Seismic Information

The U.S EPR FSAR includes the following COL Item in Section 2.5.1:

> A COL applicant that references the U.S. EPR design certification will use site-specific information to investigate and provide data concerning geological, seismic, geophysical, and geotechnical information.

This COL Item is addressed as follows:

{This section presents information on the geological and seismological characteristics of the site region (200 mi (322 km) radius), site vicinity (25 mi (40 km) radius), site area (5 mi (8 km) radius) and site (0.6 mi (1 km) radius). Section 2.5.1.1 describes the geologic and tectonic characteristics of the site region. Section 2.5.1.2 describes the geologic and tectonic characteristics of the site vicinity and location. The geological and seismological information was developed in accordance with the following NRC guidance documents:

- Regulatory Guide 1.70, Section 2.5.1, "Basic Geologic and Seismic Information," (NRC, 1978)
- Regulatory Guide 1.206, Section 2.5.1, "Basic Geologic and Seismic Information," (NRC, 2007) and
- Regulatory Guide 1.165, "Identification and Characterization of Seismic Sources and Determination of Safe Shutdown Earthquake Ground Motion," (NRC, 1997).

2.5.1.1 Regional Geology (200 mi (322 km) radius)

This section discusses the physiography, geologic history, stratigraphy, and tectonic setting within a 200 mi (322 km) radius of the site. The regional geologic map and regional physiographic map, as shown in Figure 2.5-181 and Figure 2.5-5 (USGS, 2002b), respectively contain information on the geology, stratigraphy, and tectonic setting of the region surrounding the BBNPP site. Summaries of these aspects of regional geology are presented to provide the framework for evaluation of the geologic and seismologic hazards presented in the succeeding sections.

Section 2.5.1.1.1 through Section 2.5.1.1.4.4.1.3 are added as a supplement to the U.S. EPR FSAR.

2.5.1.1.1 Regional Physiography and Geomorphology

The BBNPP site lies within the Ridge and Valley Physiographic Province, and the area within a 200 mi (322 km) radius of the site encompasses parts of seven other physiographic provinces. As shown in Figure 2.5-5, these are the Appalachian Plateaus Province, the Piedmont Province, the New England Province, the Atlantic Coastal Plain Province, the Blue Ridge Province, the Central Lowlands Province, and the Adirondack Province (USGS, 2002a). Each of these physiographic provinces is briefly described in the following sections. A map showing the

© 2007-2012 UniStar Nuclear Services, LLC. All rights reserved.
COPYRIGHT PROTECTED

different sections and subsections within the physiographic provinces of Pennsylvania, as depicted by the Pennsylvania Geological Survey (PGS), is shown on Figure 2.5-183.

2.5.1.1.1.1 Physiography and Geomorphology of the Ridge and Valley Physiographic Province

The Ridge and Valley Physiographic Province occupies most of central Pennsylvania, extending from the West Virginia and Maryland borders to northeastern Pennsylvania including most of the Site Vicinity. The Ridge and Valley Province is bordered to the west and north by the Appalachian Plateaus Province and to the southeast by the Piedmont Province as shown in Figure 2.5-182 (Barnes, 2002), Figure 2.5-5 (USGS, 2002b), and Figure 2.5-183 (Sevon, 2000b). On a regional scale, the Ridge and Valley Province extends in a northeast striking zone of varying width from Alabama to New Jersey. The Ridge and Valley Province is primarily a zone containing Cambrian to Pennsylvanian rocks folded and faulted during Alleghenian orogenic events that affected eastern North America during Late Mississippian through Permian times (Hatcher, 1987). Folding resulted in complex geologic structure including synclinal, anticlinal, and nappe structures while faulting resulted in thrust faults, and lateral ramp thrusts. In addition, significant strike slip components are recognized in many Ridge and Valley Faults (Faill,1999a).

The complex geologic structure and varying lithologies, including repetition of some parts of the stratigraphic section, directly affect the geomorphology of the region and site vicinity. The Susquehanna Lowland Section of the Ridge and Valley Province consists of long, narrow ridges and broad to narrow valleys exhibiting moderate to very high relief that exist as a direct result of lithologic disparities in resistance to erosion and location of these resistant lithologies directly related to structure. These ridges typically are the remnant flanks of breached anticlines, typically capped by Cambrian sandstone and quartzite, and synclines underlain by resistant cherty limestones and sandstones of the Upper Silurian and Lower Devonian Keyser and Oriskany formations (DCNR, 2008a).

In addition to the importance of lithology in defining resistance to erosion and the formation of ridges versus valleys, the susceptibility of limestone and dolomite within the Ridge and Valley Province has resulted in significant formation of karst features such as caverns, surface subsidence and collapse, springs, and disappearing streams. Limestone and/or dolomite formations occur in various thicknesses in Cambrian through Pennsylvanian rocks in the Ridge and Valley Province. While not as prevalent as in the Appalachian Plateaus Province, karst is significant in the Ridge and Valley Province. In addition, the abundant fractures, folds, and faults of the Ridge and Valley Province serve as zones where dissolution can initiate and concentrate. However significant the presence of karst throughout some of the Ridge and Valley Province, there is only a small area of potential karst development in the extreme western extent of the site area (5 mi (8km) radius) and based on the lithology of the Mahantango shale and of the Timmers Rock Sandstone, bedrock at the site exhibits no potential for karst development within the site location (0.6 mi (1km) radius).

The Ridge and Valley Province has a sub-section known as the Great Valley Section, as depicted on Figure 2.5-182. The Great Valley Section of the Ridge and Valley Province consists of a very broad lowland that lies south of the Blue Mountain Sub-Section as depicted in Figure 2.5-183 in southeastern Pennsylvania. The lowland has gently undulating hills eroded into shales and siltstones on the north side of the valley and a lower elevation, flatter landscape developed on limestones and dolomites on the south side (DCNR, 2008b). Elevations in the Appalachian Mountain Section range from 440-2,775 ft (134-846 m) (DCNR, 2008e) while elevations in the Great Valley Section range from 140-1,100 feet (43-335 m)

© 2007-2012 UniStar Nuclear Services, LLC. All rights reserved.
COPYRIGHT PROTECTED

(DCNR, 2008b). In addition to the geologic events that affected the entire Ridge and Valley Physiographic Province, four glacial events affected the site region (200 mi (322 km) radius).

Three of four main periods of continental glaciation occurring in Pennsylvania directly affected the site vicinity (25 mi (40 km) radius) as shown on Figure 2.5-184 (Sevon, 2000c). These glacial events occurred in the following order from oldest to youngest; Early Pleistocene, Early Middle Pleistocene, Middle Pleistocene, and Late Pleistocene (Braun, 2004). The oldest glaciation extended the farthest south, with each subsequent glacial event never advancing past the previous one, as shown in Figure 2.5-184. These older glacial advances are more difficult to identify due to the eroding attributes of more recent glaciers. The area south of the Late Pleistocene glacial limit is characterized by extensive colluvial deposits and other features of periglacial origin (Braun, 2004) including frost riving and congelifluction (Sevon, 1999a). The limit of the Late Pleistocene glacial event, also known as the Late Wisconsinan (17,000-22,000 yrs), is marked by heads-of-outwash in the valleys with an indistinct moraine on adjacent hillsides (Braun, 2004) and is labeled as Olean Till as shown in Figure 2.5-184. The overall trend of the Late Wisconsinan margin across northeastern Pennsylvania is approximately west-northwest, and hilltop striae on the Appalachian and Pocono plateaus within 30 mi (48 km) of the margin indicate a regional ice flow direction of north-south to south-southwest (Braun, 1988). The Late Illinoian (132,000-198,000 yrs) glacial event advanced only a few miles from the more recent Late Wisconsinan event, as shown in Figure 2.5-184, and is identified by heads-of-outwash in the valleys and discontinuous patches of till or colluvium derived from till (Braun, 1988). Pre-Illinoian glaciations advanced approximately 20-40 mi (32-64 km) beyond the Late Illinoian limit, as shown in Figure 2.5-184. Glacial lake sediments and two belts of "markedly thicker glacial deposits" suggest that Pre-Illinoian stage (>770,000 yrs) northeastern Pennsylvania was subjected to two glacial events (Braun, 2004). The first of which extended to the maximum glacial limit as shown in Figure 2.5-184, and the second extended only several miles northeast of the maximum glacial limit (Braun, 2004). In addition to the deposition of glacial sediments, surface hydrology has been affected by glacial melt and outwash. During glacial retreats, large volumes of glacial melt-waters formed broad, high energy streams including the Susquehanna, and other neighboring rivers such as the Delaware and Potomac Rivers.

The geologic structure, lithologic makeup, and glacial history of the Ridge and Valley Province define the physiography and geomorphology of the majority of the site vicinity (25 mi (40km) radius and the site area (5 mi (8 km) radius). The site area (5 mi (8 km) radius) physiography is discussed in further detail in Section 2.5.1.2.1.

2.5.1.1.1.2 Physiography and Geomorphology of the Appalachian Plateaus Physiographic Province

Located west of the Ridge and Valley Province, the Appalachian Plateaus Physiographic Province includes the western part of the Appalachian Mountains, and stretches from New York to Alabama. The mountains within the Appalachian Plateaus Province are generally long, narrow, and even crested, while the valleys are highly variable in width and elevation (Way, 1999). Much of the current day landscape of this Province in Pennsylvania developed during multiple periods of glaciation within the Pleistocene period (Way, 1999). The Allegheny Front is the topographic and structural boundary between the Appalachian Plateaus and the Ridge and Valley Province (Clark, 1992). It is a bold, high escarpment, underlain primarily by clastic sedimentary rocks capped by sandstone. In eastern West Virginia, elevations along this escarpment reach 4,790 ft (1,460 m) (Hack, 1989) while in Pennsylvania, its highest point is 3,213 ft (979 m) (DCNR, 2007f). West of the Allegheny Front, the Appalachian Plateaus topographic surface slopes gently down to the northwest. A large portion of the Appalachian

© 2007-2012 UniStar Nuclear Services, LLC. All rights reserved.
COPYRIGHT PROTECTED

Plateaus Province lies within 200 mi (322 km) of the BBNPP site as shown in Figure 2.5-5, and the northern portion of the site vicinity (25 mi (40 km) radius) encompasses the Appalachian Plateaus Physiographic Province as depicted on Figure 2.5-182. Note that no other physiographic province lies within the BBNPP site vicinity (25 mi (40 km) radius).

2.5.1.1.1.3 Physiography and Geomorphology of the Piedmont Physiographic Province

The Piedmont Physiographic Province extends southwest from New York, through southeast Pennsylvania, to Alabama and lies southeast of and adjacent to, the Ridge and Valley Physiographic Province as shown in Figure 2.5-5. The Piedmont Province is about 60 mi (97 km) wide in southeastern Pennsylvania and narrows northward to about 10 mi (16 km) wide in southeastern New York (Figure 2.5-5). Elevation in the Piedmont Province ranges from 20-1,355 feet (6-413 m) (DCNR, 2007b; DCNR, 2007c; and DCNR, 2007d).

In Pennsylvania, the Piedmont Province is divided into the Piedmont Lowland Section, the Gettysburg-Newark Lowland Section, and the Piedmont Upland Section. With the exception of the Piedmont Lowland Section, the majority of the Piedmont Province consists mainly of rolling low hills and valleys (DCNR, 2007a). The Piedmont Lowland Section consists of broad, moderately dissected valleys separated by broad low hills and is developed primarily on limestone and dolomite rock highly susceptible to karst topography (DCNR, 2007b). The Gettysburg-Newark Lowland Section runs adjacent to the Great Valley Section of the Ridge and Valley Province as shown in Figure 2.5-183. The Gettysburg-Newark Section consists of rolling low hills and valleys developed on sedimentary fluvial and lacustrine clastic rock deposits that represent a series of exposed faulted rift basins (Root, 1999). Metamorphic rocks of varying affinity comprise the surface rock outside of the rift basins within the Gettysburg-Newark Lowland Section. The Piedmont Upland Section exhibits gently rolling hills and valleys. Drainage in the Piedmont Upland Section is often controlled by a well developed foliation in predominant schists with drainage developing along foliation or normal to foliation (DCNR, 2007d).

Geologically, the Piedmont Province consists of a variety of sharply folded and faulted supracrustal metasedimentary and plutonic intrusive rocks that are generally younger than the 880-1,000 million year old rocks of the Blue Ridge Province to the west (Milici, 2009). In addition, thick sections of Early Mesozoic sedimentary rocks containing intruded and extruded mafic igneous rocks fill rift basins that are widely distributed in the Piedmont and beneath the Atlantic Coastal Plain. The metasediments within the Piedmont Province may be as young as Ordovician. These Precambrian through Lower Paleozoic crystalline rocks extend to the east under the Upper Jurassic through Cenozoic sediments of the Atlantic Coastal Plain Province.

2.5.1.1.1.4 Physiography and Geomorphology of the New England Physiographic Province

The New England Physiographic Province is bounded on the north by the Ridge and Valley Province and on the south by the Piedmont Province as shown in Figure 2.5-5. The New England Province, aligned in a northeast-southwest direction, extends from the eastern border of Pennsylvania to mid-southeastern Pennsylvania occupying only a small amount of area as compared to the surrounding provinces. The province has an average width of about 5 mi (8 km) within Pennsylvania (Figure 2.5-183), and consists of circular to linear, rounded low hills or ridges that project upward in significant contrast to surrounding lowlands (DCNR, 2007e). The hills and ridges are made up of granitic gneiss, granodiorite, and quartzite thus making them very resistant to erosion (DCNR, 2007e). This province has a local relief ranging

© 2007-2012 UniStar Nuclear Services, LLC. All rights reserved.
COPYRIGHT PROTECTED

from 300-600 ft (91-183 m) with elevations ranging from 140-1,364 ft (43-416 m) (DCNR, 2007e).

2.5.1.1.1.5 Physiography and Geomorphology of the Atlantic Coastal Plain Physiographic Province

The Atlantic Coastal Plain Physiographic Province lies east of, and adjacent to, the Piedmont Province and occupies much of the eastern seaboard, as shown in Figure 2.5-5. In Pennsylvania, this area is designated as the Lowland and Intermediate Upland Section of the Atlantic Coastal Plain Province as shown in Figure 2.5-183. This section consists of a flat upper terrace surface that is cut by numerous short streams, which are typically narrow and steep sided (DCNR, 2008c). The province is aligned in a northeast-southwest direction and is, on average, 6 mi (10 km) wide in Pennsylvania but attains a width of up to 50 mi (80 km) in New Jersey (Figure 2.5-5). The unconsolidated to poorly consolidated sand and gravel deposits of the Coastal Plain, dip gently to the southeast (NJGS, 2003). These sediments rest on various metamorphic rocks (DCNR, 2008c). Local relief is very low in the Lowland and Intermediate Upland Section of Pennsylvania, and elevations range from sea level to 200 ft (61 m) (DCNR, 2008c). The highest elevation of the Atlantic Coastal Plain Province in New Jersey is 391 ft (119 m) (NJGS, 2003).

2.5.1.1.1.6 Physiography and Geomorphology of the Blue Ridge Physiographic Province

The Blue Ridge Province extends less than 50 miles (80 km) into Pennsylvania from the south and is approximately 70 miles (113 km) from the BBNPP site (Figure 2.5-5). The Blue Ridge Physiographic Province is bounded on the east by the Piedmont Province and on the west by the Valley and Ridge Province as shown in Figure 2.5-5 (USGS, 2002b). However, the State of Pennsylvania does not include the Blue Ridge in the statewide designation of physiographic provinces. Instead, this region of Pennsylvania is considered the South Mountain Section of the Ridge and Valley Province as shown in Figure 2.5-183 (Sevon, 2000b). The Blue Ridge Province, also known as the Blue Ridge Thrust Belt Province (Milici, 2009), underlies parts of eight States from central Alabama to southern Pennsylvania in a northeast-southwest direction and is underlain primarily by metamorphosed Precambrian and Early Paleozoic igneous and sedimentary rock (VADOT, 2008). The Blue Ridge Province is recognized as the core of the Appalachian Mountains, emplaced during Alleghanian tectonism along a regional detachment structure (Hatcher, 1987).

Along its western margin, the Blue Ridge is thrust over the folded and faulted margin of the Appalachian basin, so that a broad segment of Paleozoic strata extends eastward for tens of miles, buried beneath these subhorizontal crystalline thrust sheets. At the surface, the Blue Ridge consists of a mountainous to hilly region, the main component of which is the Blue Ridge Mountains that extend from Georgia to Pennsylvania. Surface rocks consist mainly of a core of moderate- to high-rank crystalline metamorphic or igneous rocks, which, because of their superior resistance to weathering and erosion, commonly rise above the adjacent areas of low-grade metamorphic and sedimentary rock (Milici, 2009). The province is bounded on the north and west by the Paleozoic strata of the Appalachian Basin Province and on the south by Cretaceous and younger sedimentary rocks of the Gulf Coastal Plain. It is bounded on the east by metamorphic and sedimentary rocks of the Piedmont Province.

Soils of the Blue Ridge are predominantly colluvium with small amounts of alluvium along the rivers and streams (VADOT, 2008). Residuum occurs locally but is limited in thickness and lateral extent due to aggressive erosive forces caused by steep topography. The Blue Ridge is a long, linear province which ranges in width from about 5 mi (8 km) in Maryland to over 50 mi

© 2007-2012 UniStar Nuclear Services, LLC. All rights reserved.
COPYRIGHT PROTECTED

(80 km) in North Carolina. Elevations in the Blue Ridge Province exceed 6,600 (2,012m) feet in North Carolina and Tennessee.

Reconstructions for the central Appalachians disagree about the boundary between North American native terranes and accreted exotic terranes. Horton (1991) in Kline, 1991, interpreted part of the Virginia Blue Ridge province as an exotic terrane, called the Jefferson terrane, accreted to North America in the Ordovician. Kline (Kline, 1991), implies a common provenance for all the sediments and casts doubt on the exoticity of the Jefferson terrane, based on the presence of a common suite of distinctive detrital grains in Jefferson terrane units and in proven native North American metasedimentary rocks and basement.

2.5.1.1.1.7 Physiography and Geomorphology of the Central Lowlands Physiographic Province

The Central Lowlands Physiographic Province, also known as the Ontario Lowlands, has relatively low relief (Komor, 1998) and is located between the Appalachian Plateaus Province to the south and Lake Ontario to the north as seen on Figure 2.5-5. The Central Lowlands were subjected to glaciation and as a result, consist mainly of unconsolidated surficial materials including mostly sands and gravels (DCNR, 2008d). Elevation within the province ranges from 570 ft (174 m) to approximately 1,000 ft (305 m) as erosion processes along the shores of Lake Erie have created a steep lake-land interface along much of the shoreline (DCNR, 2008d).

2.5.1.1.1.8 Physiography and Geomorphology of the Adirondack Physiographic Province

The Adirondack Physiographic Province has moderate to high relief throughout and its circular shape attains a diameter of over 150 mi (241 km). Elevations within the Adirondack Province range from 1,500 ft. (457 m) to 5,344 ft.(1,629 m) The Adirondack Physiographic Province is located in northern New York and is surrounded by the Ridge and Valley Province to the southeast, the Appalachian Plateaus to the south, the Central Lowlands Province to the west, and the St. Lawrence Valley Province to the north and east as seen in Figure 2.5-5. The bedrocks of the Adirondacks are primarily Precambrian to Early Paleozoic, metamorphic rocks and are part of the great Canadian Shield that has been uplifted to its present day geography (McDonnell, 2008). The bedrock generally supplements long, straight valleys, gently curved ridges, and a radial drainage pattern (Komor, 1998) throughout the province.

2.5.1.1.2 Regional Geologic History

The BBNPP site is located within the Appalachian orogenic belt, a geologic region marked by a complex history of orogenic events, rift sequences, subsequent depositional sequences, eustatic and local sea level changes, and glacial events. The region's position along an active continental margin at intervals in the Proterozoic and Paleozoic Era has developed the structural and stratigraphic characteristics that define the seismotectonic setting. Episodes of continental collisions, depicted on Figure 2.5-6, have produced a series of terranes separated, in part, by low angle detachment faults (Pohn, 2000). Sources of seismicity may occur in the stratigraphy along structures within the North American basement, along the terranes, and over thrust plates. Tectonic episodes of continental rifting (Figure 2.5-6) have produced high angle normal and boundary faults that extend to the aforementioned detachment faults and in some cases through the upper crust. These rift related faults do not extend to within the site vicinity (25 mi (40 km) radius) and have minimal to no influence on BBNPP site (0.6 mi (1 km) radius) seismicity. Direct evidence of these deformational events is visible in the Ridge and Valley province, as described in Section 2.5.1.1.4.3, and borehole data as described in Section 2.5.1.1.3 which identifies the Precambrian rock as Grenvillian. The site region is located currently on the passive margin of the North American plate following latest Permian and

© 2007-2012 UniStar Nuclear Services, LLC. All rights reserved.
COPYRIGHT PROTECTED

Early to Middle Mesozoic Era continental extension and rifting. The events that have affected the site region (200 mi (322 km) are discussed in terms of orogenesis, depositional basins and environments, and their effects on site region (200 mi (322 km) to site vicinity (25 mi (40 km) radius) geology.

2.5.1.1.2.1 Grenville Orogeny

The Grenville Orogeny occurred as a result of the Mesoproterozoic collision of North and South America (Eriksson, 2003) during the construction of the supercontinent Rodinia (Millot, 2001) between 1.0 and 1.20 Ga (Murphy, 2000). The Grenville Orogeny occurred along the southern and eastern margin of the North American craton and resulted in the accretion and crustal evolution of the eastern and southern margins of the North American Craton during the Proterozoic. Crustal evolution along the Grenville has been studied to determine its role in evolution of the Appalachian Orogen (Mueller, 2008). This Proterozoic orogenic province is comprised of a "laterally continuous region of high grade, polymetamorphic terranes and is also recognized as a multiphase orogenic event with distinct zones connected by ductile shear zones (Streepey, 2001). The Grenville Province is also described as primarily orthogneisses (Mueller, 2008). Grenville basement rocks outcrop in numerous locations along the Appalachian mountains from Alabama through Nova Scotia and in Texas (Reese, 2004) and form the basement upon which Paleozoic orogenic and depositional events and sequences occurred. The most significant outcrop of the Grenville Province within the site region is the Adirondack Mountains. The location of the Adirondack physiographic province, comprised of the Grenville age Adirondack Mountains, is depicted on Figure 2.5-5. The site region (200 mi (322 km) radius), site vicinity (25 mi (40 km) radius), site area (5 mi (8 km) and site location (0.6 mi (1 km) radius) all have Grenville rocks as the Precambrian basement. The depth to Grenville basement at the BBNPP site is approximately 33,000 ft (10,058 m) as shown on Figure 2.5-191 and Figure 2.5-187.

2.5.1.1.2.2 Late Precambrian to Late Cambrian Rifting and Late Precambrian to Late Ordovician Deposition

Following the Grenville orogeny, Late Neoproterozoic to Early Cambrian rifting initiated the breakup of the supercontinent, Rodinia, and led to the formation of basins in which Late Precambrian sediments accumulated in the rift-related Appalachian foreland basin. Rift related structures such as the Central Pennsylvania trough, a northeast trending rift graben that exists to the south approximately 50 miles (80 km) from the BBNPP site, is analogous to a series of basement troughs that formed during the opening of the Iapetus Ocean (Gao, 2000). Age analysis of a group of intrusive to hypobyssal rocks associated with rift related normal faulting in the North Carolina and Virginia Blue Ridge reveal age ranges from 760 to 700 Ma (Bailey, 1998) and ages of initial Rodinian breakup have been determined at 780 Ma (Harlan, 2003), indicating a time range for initial rifting. Rifting continued into Earliest Cambrian until the completion of the opening of the Iapetus Ocean and change to a passive continental margin approximately at the Late Cambrian (Gao, 2000). The initiation of rifting was also the onset of the deposition of a thick sequence of terrigenous and volcanic detritus, carbonate rocks, and distal more argillaceous sediment in the Appalachian foreland basin that indicates a predominantly transgressive sea with minor local and temporal exceptions (Kauffman, 1999 and Hasson, 1988). Contribution of detritus to the basin from the Grenville Province is established by a predominance of detrital zircons in Cambrian sandstones (Eriksson, 2003). Sediment load enhanced basin subsidence and faulting, which resulted in localized zones of sequence thickening (Hasson, 1998) during the Middle Cambrian through the termination of rifting. The Waynesboro, Pleasant Hill, and Warrior Formations represent the site area (5 mi (8 km) radius) stratigraphy that is part of this sequence (Figure 2.5-27). Deposition of terrigenous and carbonate sequences continued along the passive margin of the North American craton

© 2007-2012 UniStar Nuclear Services, LLC. All rights reserved.
COPYRIGHT PROTECTED

from the Late Cambrian through the Late Ordovician. Fluctuations in sea level shifted the shoreline and depositional environment throughout this time as indicated by stratigraphic variations from sandstones to shales indicating significant variations in distance of the depositional environment to the sediment source. The west-northwest extent of Iapetan rifting is significant to the current seismic regime. Faults related to Iapetan rifting and the Iapetan passive margin have been identified as the source of seismic activity in Tennessee, Virginia, and Quebec (Wheeler, 1996). Specific seismogenic sources are discussed in detail in Section 2.5.1.1.4.

2.5.1.1.2.3 Taconic Orogeny and Clastic Wedge Deposition

The North American craton became a convergent margin with the onset of the Taconic Orogeny at the end of the Middle Ordovician and continuing through the Middle Silurian (Gao, 2000). The Taconic Highlands, an island arc terrane (Trembley, 1997) converged to the east of the North American craton and became the dominant source of detritus to the Appalachian basin. Along the margin of the craton, especially in New England and Canada, suites of ocean floor and island arc were accreted to the continent along with what is regionally called the Taconic Thrust Belt (Hayman, 2002). Deformation from the Taconic orogeny was imparted throughout the continental margin, as metamorphic events of Taconian (457 Ma) time are recorded in the Blue Ridge of western North Carolina (Moecher, 2004). An example of Taconic deformation within the site region (200 mi (322 km) radius) is the development of the Hamburg Nappe, an overthrusted fold derived from folding of basinal sediment due to thrusting of the Taconic front onto the continent (Faill, 1999b). Behind the Hamburg Nappe were a series of other nappes composed mostly of carbonate cover overlying or wrapping around Grenville crystalline core rocks. Converging from different parts of the continental shelf, they were tectonically superimposed partially overlapping along the Appalachian trend (Faill, 1999b). These nappes are the Lebanon Valley, the Irish Mountain, the Applebutter, the Musconetcong, and the Lyon Station-Paulins Kill which together, compose the Musconetcong nappe megasystem (Faill, 1999b).

Comprised of slabs of the Brandywine Microcontinent during the Taconic Orogeny, the West Chester, Avondale and Woodville Massifs were thrust northwestward upon the continental shelf onto previously emplaced Octoraro Sea deposits (Faill, 1999b). A location map for the West Chester and Avondale massifs is shown in Figure 2.5-211 (Low, 2002). The Street Road Fault separates the Avondale Massif to the southeast from the West Chester Massif to the northwest (Bosbyshell, 2009). The Rosemont Fault to the east of the Avondale Massif separates the massif complex from the Wissahickon (Philadelphia Terrane) and the James Run and Wilmington Complex magmatic arcs (Faill, 1999b). Included and exposed in both the West Chester and Avondale Massifs are basement rocks of the Baltimore Gneiss, including a variety of compositions at amphibolite and granulite grade metamorphism. Granulite facies metamorphism is found in the eastern Avondale, but comprises most of the West Chester Massif, composed of heterogeneous felsic, intermediate and mafic compositions of gneiss (Blackmer, 2005). The idealized cross section in Figure 2.5-213 shows the close relation of these two massifs with the Philadelphia terrane to the SE, as well as the Reading meganappe to the NW.

During this time the site region (200 mi (322 km) radius) existed within the Appalachian basin and received significant amounts of detritus derived from the Taconic Highlands to the east and significantly less detritus from the continent. This led to a clastic wedge thickening to the east toward the Taconic sediment source (Thompson, 1999 and Castle, 2005) and thinning toward the continental margin. The timing of the Taconic Orogeny ranges from the Middle Ordovician into the Middle Silurian. The site vicinity (25 m (40 km) radius) was positioned on

© 2007-2012 UniStar Nuclear Services, LLC. All rights reserved.
COPYRIGHT PROTECTED

the western side of the Appalachian basin during the Taconic Orogeny. The effect of the Taconic Orogeny and Clastic Wedge deposition on the site vicinity (25 mi (40 km) radius) and site area (5 mi (8km) radius) is primarily the deposition of the Middle Ordovician to Lower Silurian strata as noted on Figure 2.5-27. The Martinsburg, Bald Eagle and Juniata Formations were derived from the erosion of the tectonic highland. The composition of the aforementioned Formations is provided in Section 2.5.1.1.3.

2.5.1.1.2.4 Middle Silurian through Early Devonian

During the Middle Silurian through Early Devonian Time the site region (200 mi (322 km) radius) existed as part of an extensive basin of deltaic, reef, alluvial and shallow marine environments (Ver Straeten, 2000, and Diedrich, 1999). The Keefer, Bloomsberg, and Mifflintown Formations are the representative strata for this time. The eastern margin of the North American craton was passive while the eroding Taconic Highlands continued to load sediment into the Appalachian Basin.

2.5.1.1.2.5 Acadian Orogeny

The Acadian Orogeny began at the onset of the Middle Devonian within the site region (200 mi (322 km) radius), the result of the Avalon Terrane and Baltica (Eusden, 2000) converging with the North American craton. The Acadian Orogeny affected the northern Appalachians of New England in the Late Silurian (Bradley, 2002). The site vicinity (25 mi (40 km) radius) remained within the Appalachian basin area while the Acadian mountain range, to the east of the site area, was subjected to erosional processes. These eroded sediments were deposited in the site area and are represented by the modern day black and gray shales of the Marcellus formation that underlie the site (Ver Straeten, 2000). The effect of the Acadian Orogeny is more pronounced in terms of metamorphism and magmatism in the northeastern United States (Maine, New Hampshire, Vermont), but is significant to the site area in that the source material for the formation of the Devonian rocks, notably the Marcellus and Mahantango Formations, that outcrop in the site area was primarily derived from the Acadian Highlands. Ver Straeten (Ver Straeten, 2000) identify the progression of a terrigenous clastic wedge from the orogenic belt to the west during multiple phases of orogenic uplift during the Devonian that was the source of Devonian deposition. Basin flexure and bulging produced local sea level and depositional environment changes that resulted in reef structures that are noted in the Onondaga Formation which outcrops within the site area (5 mi (8 km) radius). The Acadian Orogeny and syn-orogenic deposition within the BBNPP site region (200 mi (322 km) radius) came to a close at the Middle Mississippian period. Upper Devonian and Lower Mississippian strata were deposited in the site vicinity (25 mi. (40 km) radius) but have been eroded by subsequent uplift during the Alleghanian Orogeny. The Middle Mississippian through Middle Pennsylvanian, approximately 350-300 Ma, (Hatcher, 1987) was an orogenic hiatus in which the Mauch Chunk and Pottsville Formations were deposited within the site region and site area. The composition of the aforementioned Formations is provided in Section 2.5.1.1.3.

2.5.1.1.2.6 Alleghanian Orogeny

Convergence of Peri Gondwana with Laurentia at margins identified in modern geographic terms as northwest Africa and eastern North America led to the formation of the supercontinent of Pangaea. The continental collision caused the eastern and southern margins of North America to undergo uplift and deformation in what is referred to as the Alleghanian Orogeny. Late Pennsylvanian dextral transpression (a combination of convergent and transform plate boundaries) was the initial interaction of the aforementioned continents (Engelder and Whitaker, 2006). As the convergent margin evolved in the Early Permian, intense brittle and ductile deformation in the form of thrusting, folding, and varying degrees of metamorphism took place (Steltenpohl, 1988 and Shumaker, 2002). This kinematic change

© 2007-2012 UniStar Nuclear Services, LLC. All rights reserved.
COPYRIGHT PROTECTED

from dominate dextral transpression in the Pennsylvanian to northwestward compressional (shortening) deformation in the Permian was likely due to the oblique nature of the collisional orogen or a plate rotation (Becker, 2006). This inference is supported by detrital zircon age populations of Pennsylvanian and Permian rocks that formed from erosion of the Alleghanian highlands and deposited to the west in the Appalacian basin (Becker, 2006).

The current geologic setting along the eastern, southeastern, and south-central (although much is now buried under Gulf Coast Basin sediment) United States is strongly defined by Alleghanian deformation. In many cases, pre-existing faults related to Grenville, Taconic, or Acadian deformation were reactived to develop regional detachment structures or decollements along which the Piedmont, Blue Ridge, and Ridge and Valley were transported as much as 180 mi (300) km to the northwest in the Middle to Late Permian (Engelder, 2006) This crustal shortening and overthrusting developed the structural setting of deep seated regional thrust faults, intense folding, and varying degrees of metamorphism that is prevalent in the Ridge and Valley, Blue Ridge, and Piedmont Physiographic provinces.

The southern Appalachians seem to have a slightly different kinematic history than the northern salient. Based on calcite twinning patterns, it is thought that oblique convergence at the Laurentian margin left-lateral transpression occurred in the southern segment of the Appalachian salient while dextral transpression occurred in the northern segment of the salient in Pennsylvanian times (Ong, 2007). However, evidence of dextral shear sense on faults in Alabama indicates that the dominant dextral shear became active in the southern Appalachians during the Late Paleozoic (Steltenpohl, 1988). This predominant dextral transpression is at least partially responsible for the oroclinal structures in the Ridge and Valley and Blue Ridge Provinces. A large oroclinal component of the Ridge and Valley exists within the site region (200 mi (322 km) radius) that can be seen on Figure 2.5-182 as the change in regional structural fabric from a north east strike to a east-northeast strike. Change of structural orientation of 19 degrees to the east of dominant strike is measured in northeast Pennsylvania (Harrison, 2004).

Examples of Alleghanian deformation within the site vicinity (25 mi (40 km) radius) and site area (5 mi (8 km) radius) include the Berwick and Light Street Faults, depicted on Figure 2.5-198 and discussed in Section 2.5.1.2.4.1 and Section 2.5.1.2.6.4 These faults are recognized as exhibiting reverse, to the northwest vergence and are classified as Alleghanian thrust faults (Inners, 1978). Field studies did not identify offset in terrace gravels overlying the Light Street and Berwick Faults (Inners, 1978). In addition, the Berwick Anticlinorium, an east-northeast striking, gently northeast plunging anticline trends directly through the site area (5 mi (8 km) radius). The Berwick Anticlinorium is a symmetrical structure in the site area (5 mi (8 km) radius) with both the north-northwest and south-southwest limbs dipping with an averaged 35 degree NNW and SSW repsectively (Inners, 1978). The orientation of this structure is classic Ridge and Valley Alleghanian deformation as presented by Hatcher (Hatcher, 1987). In addition to crustal deformation, the Alleghanian Orogeny had an important effect on the depositional regime in the Appalachian Basin and essentially closed the basin at the end of the Permian. Marked changes in Pennsylvanian rocks are a result of syn-orogenic flysch deposits derived from the uplifted continential margin (Thomas, 2004). The Pottsville, Conemaugh, Allegheny, and Monongahela Formations that lie within the site region (200 mi (322 km) radius) and exhibit lithologies that were influenced by Alleghanian derived detritus exemplify this relationship. Within the site area (5 mi (8km) radius) the Pottsville and Llewellyn Formations, as shown on Figure 2.5-198 exhibit the Alleganian sedimentary source. The Ridge and Valley Province within which the site area mostly lies, (5 mi (8km) radius) is bounded to the northwest by the Allegheny structural front that separates the Appalachian Plateaus

© 2007-2012 UniStar Nuclear Services, LLC. All rights reserved.
COPYRIGHT PROTECTED

province from the Ridge and Valley. Surface expression of Alleghanian deformation within the Appalachian Plateaus Province is less intense than in the Ridge and Valley. Alleghanian stress was accommodated differently in different lithologies, resulting in less pronounced deformation (more gentle folding and fewer thrust faults) within the surface strata (Schumaker, 2002). Deformation during the Alleghanian is most notable as uplift of the Appalachian Plateaus Province and brittle deformation. The current structural setting on cross section view of the site region (200 mi (322 km) radius) is depicted on Figure 2.5-7. The structural and physiographic position of the site area at the end of Pennsylvanian time placed it at elevations above depositional levels, and sub-aerial exposure and erosion ensued.

A recent re-interpretation of the depositional setting of the Spechty Kopf and Rockwell Formations in the central Appalachian basin of Pennsylvania and Maryland indicates that there was a global cooling causing a glacial period Late Devonian (Brezinski, 2010). These deposits are representative of continental glaciers that formed from coalescing valley glaciers from the Alleghanian highlands to the east. This succession constitutes a rarely preserved advance and retreat of a terrestrial glacier that was much more intense than previously inferred. Rapid subsidence of the Appalachian Basin allowed clastic wedge deposits to cover and preserve this thin sequence of glacial and glaciofluvial deposits in a continuous 24.8 mi by 248.5 mi (40 km by 400 km) belt (Brezinski, 2010).

2.5.1.1.2.7 Early Mesozoic Extensional Episode (Triassic Rifting)

During the Late Triassic, at the onset of the breakup of Pangea, the eastern North American plate and African plate began to separate to create the Atlantic Ocean. A series of rift basins, such as the Gettysburg-Newark basin developed in southeastern Pennsylvania and along the North American coastline, respectively in what is referred to as the North American Rift System (Schlische, 2002). The rift basins are arranged primarily in northeast-southwest asymmetric trend and are located from Florida to the Grand Banks of Canada (Withjack, 1998). Normal faulting under the northwest-southeast extensional stress regime often occurred along pre-existing Paleozoic structures (Olsen, 1990).

Subsequently, the basins were filled with sediments such as conglomerates, sandstones and shales and exhibit evidence of syn-rift deposition (lessening of offset upward in the basin deposits) (Schlische, 2002). The Culpepper, Gettysburg, Newark, Hartford, Taylorsville, and Norfolk Basins lie within or close to the outside limit of the site region (200 mi (322 km) radius and are shown on Figure 2.5-208.

Figure 2.5-7 shows the Newark Basin in a cross section of the Middle U.S. Atlantic Passive Margin. Schlische and Withjack (Schlische, 2003; Withjack, 2005) include the Taylorsville and Norfolk Basins (Figure 2.5-208) as part of these Mesozoic Basins. They also consider the Hartford Basin as a sub-basin of the Connecticut Valley Basins, which also includes the small Deerfield sub-basin further North. Figure 2.5-212 (Schlische, 2003) depicts a geologic map and cross sections of an idealized, dip-slip dominated Mesozoic rift basin in eastern North America (a) with syn-rift units thickening toward the border fault in transverse section and thickening toward the center of the basin in longitudinal section. Figure 2.5-212 also shows a geologic map of an idealized rift basin containing multiple sub-basins related to large-scale segmentation of a border-fault system (b). A geologic map of a basin with both dip-slip and strike slipdominated margins is shown in (c). The idealized basin geometry shown in Figure 2.5-212 does not include the effects of basin inversion.

As basin subsidence continued through the Triassic, the depositional environment within the basin became increasingly sub-aqueous. Outboard of the basins, carbonate platform

© 2007-2012 UniStar Nuclear Services, LLC. All rights reserved.
COPYRIGHT PROTECTED

deposition along the nascent continental margin occured. Mantle derived basaltic intrusions occurred within the faulted crust which are evident in diabase dikes and sheets of the Piedmont Province of the eastern United States (Philpotts, 1985). During the Early Jurassic period, the process of seafloor spreading caused deep-seated magma to approach the surface. Volcanic deposits ranging from 6-9.3 mile (10-15 km) thickness formed along the entire U.S Atlantic margin in the Middle Jurassic (Sheridan, 1993). The magma created the basalt located in the Gettysburg-Newark basin of the Piedmont province (Schlische, 2003). Northwest-southeast-directed post rift activities in the Mesozoic basin caused inversion to many structures present during this time (Withjack, 1998). Following rifting, subsidence, and volcanism, the Atlantic Margin became a passive .margin. The structural and seismotectonic influence of Mesozoic rifting affects the site region (200 mi (322 km) with respect to potential seismogenic structures. These structures, such as the Ramapo Fault (Section 2.5.1.1.4.4.2.2), the Martic Fault (Section 2.5.1.1.4.4.4.14), the East Border Fault (Section 2.5.1.1.4.4.4.15), and the Yellow Breeches Fault (Section 2.5.1.1.4.4.4.5) have exhibited seismogenic potential (Ratcliffe, 1971) and are discussed in further detail in these sections.

2.5.1.1.2.8 Late Mesozoic and Cenozoic History

During the Cretaceous Period of the Mesozoic Era, the site vicinity (25 mi (40 km) radius) and the majority of the site region (200 mi (322 km)radius) experience sub-aerial exposure and various rates of erosion based on climate (Sevon, 1999b). The notable exception is the Atlantic Coastal Plain Physiographic Region (Figure 2.5-5) that was inundated by the transgressive Cretaceous sea within which significant deposition took place (Southworth, 2006). The extent of the Cretaceous transgressive sea was well inland of the current Atlantic Coastal Plain limit, but erosion during the Cenozoic Era moved the limit of the sedimentary Atlantic Coastal Plain to the east and southeast (Jordan, 1982; Braun, 2003; Ator, 2005). The Atlantic Coastal Plain remained inundated during much of the Cenozoic Era as exemplified by Paleocene through Pleistocene deposits as shown on Figure 2.5-181. Inland of the shoreline from the Cretaceous Period to Early Cenozoic Era, the majority of the site region (200 mi (322 km) radius) was subjected to chemical and physical weathering and erosion at varying degrees of intensity based on climatic conditions (Sevon, 1999b). The depositional setting that has existed throughout the Cenozoic within the site vicinity (25 mi (40 km) radius) and site area (5 mi (8 km) radius) were topographic lows upon which alluvial and lacustrine deposits accumulated. The notable exception was the advance of glacial ice sheets that had significant effects in terms of exhuming and re-depositing surficial material on a regional scale and changing the loading and unloading conditions (which can initiate deformation in the rock mass) on the site vicinity (25 mi (40 km) radius) and site area (5 mi (8 km)) (Sevon, 1999b).

From Pre-Illinoisan to Late Wisconsian, three major glacial advancements occurred from ice accumulation in Canada advancing into Pennsylvania, and into the BBNPP site area. The glaciers were located at the northern portion of Pennsylvania and covered most of the Appalachian Plateaus province. The earlier glaciers migrated south approximately 770,000 years ago while the most recent occurred about 17,000-22,000 years ago (Barnes, 2002; Braun, 2007). Figure 2.5-184 shows the limit of glacial advance in Pennsylvania with the site vicinity (25 mi (40 km) radius) superposed. A map showing surficial glacial deposits within the BBNPP site (0.6 mi(1km) radius) is presented on Figure 2.5-195.

The glacial advancements scoured valleys and deposited till, sand and gravel outwash material throughout BBNPP site area while the nearby Susquehanna River deposited sand and gravel outwash, filling the bottoms of valleys. During the period of elevated physical weathering, freezing and thawing at the surface caused the breakup of large quantities of rock at the crests of ridges in the Ridge and Valley province (Sevon, 1999a). As a result, the crests of

© 2007-2012 UniStar Nuclear Services, LLC. All rights reserved.
COPYRIGHT PROTECTED

these ridges were lowered by several feet. In addition, loose talus rock accumulated on the slopes of many ridges within central Pennsylvania (Sevon, 1999a).

The geologic history of the site region (200 mi (322 km) radius) is complex. The current geologic processes affecting the site are limited to weathering and erosion of existing material, and to the regional stress field that affects the passive Atlantic margin. Figure 2.5-8 shows the current stress fields in the eastern portion of North America. Minimal isostatic uplift that has remained relatively constant throughout the Cenozoic (Matmon, 2003) is currently a component of the geologic setting. With respect to seismic stability and geologic hazards, the site vicinity (25 mi (40 km) radius) the site area (5 mi (8 km) radius), and site location (0.6 mi (1 km radius) are positioned in a stable geologic setting.

2.5.1.1.3 Regional Stratigraphy

This section contains information and analysis on the regional stratigraphy within the major physiographic provinces in the Northeastern United States that are located within the BBNPP region . The regional geology and generalized stratigraphy within a 200 mi (322 km) radius of the BBNPP site is presented schematically in Figure 2.5-186.

Reports and scientific journal articles, published primarily by staff of the U.S. Geological Survey (USGS) and the Pennsylvania Geological Survey, have been used to develop the following descriptions of regional and local geology. After a thorough search and evaluation of literature ranging from the 1930s to 2008, the references cited in this document are considered to be the leading and most authoritative references relative to BBNPP regional geology, stratigraphic nomenclature, and stratigraphic relationships. In some cases, the best sources of information (most complete and most detailed) for local geology were published in the 1970s and 1980s. In all cases, when more recent publications provide new information, new data, or reinterpretations of old concepts, the newer information has been used and has been cited.

2.5.1.1.3.1 Stratigraphy of the Ridge and Valley Physiographic Province

2.5.1.1.3.1.1 Pre-Cretaceous Basement Rock

####### 2.5.1.1.3.1.1.1 Precambrian

The crystalline basement rock underlying Pennsylvania is of Precambrian age (Saylor, 1999) and rarely exposed, except in the Piedmont Province of southeastern Pennsylvania (Figure 2.5-182). Estimated depth of this basement rock at the BBNPP site is presently at approximately 33,000 ft (10,058 m) below ground surface (bgs), as shown in Figure 2.5-191. Due to the lack of exposure and the relatively great depth to Precambrian rocks in the Ridge and Valley Province, information on Precambrian basement rock is extrapolated from several exploratory wells in western Pennsylvania (Saylor, 1999; Gold, 2008). It is inferred from these deep wells that the Precambrian basement is approximately 1 billion years (Ga) old (Gold, 2008) and it is composed of metamorphosed greenschist or amphibolite. It is also inferred that this Precambrian basement is a regular, gently sloping surface, dipping eastward and forming the western margin of the Appalachian miogeosyncline (Saylor, 1999). Earliest deformation of this basement rock appears to have occurred during the Grenville Orogeny (Saylor, 1999), resulting in multiple folding events and faulting. Due to the heavily metamorphosed state of this Precambrian basement, little is known as to its depositional environment of the original sedimentary deposits.

The closest boreholes to the BBNPP site that penetrate the Precambrian basement rock are located in Erie and Crawford counties, Pennsylvania, located about 200 mi (322 km) northwest of the BBNPP site (Figure 2.5-183). The borings that penetrate the underlying Precambrian

© 2007-2012 UniStar Nuclear Services, LLC. All rights reserved.
COPYRIGHT PROTECTED

basement in northwestern Pennsylvania, eastern Ohio, and northern West Virginia have encountered metamorphic or igneous rocks (Saylor, 1999). For example, a well labeled Temple No. 1 in Mercer County, PA, located approximately 208 mi (335 km) west of the BBNPP site, was drilled into a biotite granite/quartz-biotite gneissic basement rock at 9,810 ft (2,990 m) depth (Saylor, 1999). Another well, labeled Fleck in Mercer County PA, located 205 mi (330 km) west of the BBNPP site, was drilled into basement rock at a depth of 9,136 ft (2,785 m) with rock composition including weathered chloritic schist and granite grading into gneiss (Saylor, 1999). The Precambrian basement rock was only sampled in the drill cuttings and suggests a gneiss/schist from the mineralogy present (i.e., biotite, chlorite, and clear quartz).

2.5.1.1.3.1.1.2 Cambrian Period

Overlying the Precambrian metamorphic and igneous basement of the Ridge and Valley Province are the clastic sedimentary deposits of the Early Cambrian with a transition to the carbonate rich sediments of the Early Ordovician. These Early Cambrian deposits created a wedge of terrigenous sediments, best described today as the Chilhowee Group, which were deposited along the continental margin as the marine waters of the Iapetus (Proto-Atlantic) Ocean slowly transgressed across the continent shortly after the Grenville Orogeny (Kauffman, 1999). Above the clastic sediments of the Chilhowee Group is the brown sandstone interbedded with red and green shale beds of the Waynesboro Group (Kauffman, 1999). The Waynesboro Group, according to Kauffman (Kauffman, 1999) is the oldest exposed outcrop in Central Pennsylvania with an Early to Middle Cambrian age.

As the Early Cambrian seas transgressed in a generally northwesterly direction sandy coastal deposits in Pennsylvania are represented by the Eocambrian Chickies, Weverton and Harpers formations and the Late Middle Cambrian Potsdam Sandstone (Kauffman, 1999) (Figure 2.5-185 and 2.5-114). Deposition of these sediments was followed by deposition of a carbonate platform (Bradley, 1989; Kauffman, 1999) that shows signs of uplift and erosion during the Taconic Orogeny during the Ordovician (Bradley, 1989). Overlying the Potsdam sandstone and Waynesboro Group is a limestone formation identified as the Warrior Formation (Ryder, 1992) of Middle to Late Cambrian age. The lithology of the Warrior Formation is further defined by Kauffman (Kauffman, 1999) as a dark, fossiliferous, fine grained limestone interbedded with silty dolomite and has a thickness of up to 1,340 ft (408 m) in the Ridge and Valley Province. Bordering the Cambrian-Ordovician contact and overlying the Warrior Formation is the Gatesburg Formation Figure 2.5-205. The Gatesburg Formation consists of a series of sequential sandstone and dolomite units and can be labeled as Late Cambrian age through the identification of gastropod fossils in the uppermost member (Ryder, 1992).

2.5.1.1.3.1.1.3 Ordovician Period

Significant deposition of sediment occurred in the Appalachian Basin during the Ordovician Period, and these sediments are present throughout the Ridge and Valley Province from West Virginia up through Maryland eastward to northeastern Pennsylvania and New York (Figure 2.5-186). The Ridge and Valley rocks of Ordovician age are primarily sedimentary in nature, with evidence of uplifting during the Taconic Orogeny. According to Thompson (Thompson, 1999), the Ordovician sedimentation can be broken down into three major phases with Early Ordovician being a depositional environment of a stable carbonate-platform. During Middle Ordovician, there was a submergence of the carbonate-platform, due to the Taconic Orogeny, with marine limestone and siliciclastic sedimentation during the submergence (Thompson, 1999). This submergence resulted in the creation of a basin which was infilled with additional marine limestone and siliciclastic sediments (Thompson, 1999). Stratigraphically, Early Ordovician rocks are generally referred to as part of the Beekmantown

© 2007-2012 UniStar Nuclear Services, LLC. All rights reserved.
COPYRIGHT PROTECTED

Group (Harper, 2003), are composed primarily of dolomite-limestone, and reach a thickness of up to 4,200 ft (1280 m) (Thompson, 1999) (Figure 2.5-185 and 2.5-114). The Middle Ordovician shows a transition zone from the dolomite-limestone to rocks of primarily limestone composition deposited in both shallow and deep-water environments (Thompson, 1999). In central-Pennsylvania, the Loysburg Formation best represents this transition from a tidal-zone to a shallow marine zone with a dolomitic and stromatalite rich limestone underlying a coarse grained, fossiliferous limestone (Thompson, 1999). It is also during the Middle Ordovician that the Iapetus Ocean stopped widening and began to close; meaning this formerly passive area of sedimentation became tectonically active, thus giving birth to the Taconic Orogeny (Cotter, 2008). This active margin setting became the depositional environment of the sandstone and greywacke-shales that comprise almost 3,500 ft (1,067 m) of Late Ordovician formations including the Juniata, Bald Eagle, and Reedsville Formations of central Pennsylvania (Figure 2.5-185 and 2.5-114).

2.5.1.1.3.1.1.4 Silurian Period

During the Early Silurian Period, shallow marine conditions returned to central Pennsylvania (Cotter, 2008) as it became a depositional environment for sediments being eroded and transported from the Taconic highlands in the eastern part of the state. The Silurian basement rocks throughout Pennsylvania have a thickness ranging from 3,000 ft (914 m) in central Pennsylvania to 4,000 ft (1,219 m) in northeastern Pennsylvania (Laughrey, 1999). The Silurian represents a transition from a coastal plain in the east to a delta in the west, through the alluvial clastic deposits of the Shawangunk and Tuscarora formations (eastern and central Pennsylvania respectively) to the offshore facies of the Medina Formation of western Pennsylvania (Laughrey, 1999). The Tuscarora Formation, prevalent throughout the Ridge and Valley Province in central Pennsylvania, is composed primarily of quartzose, sublithic, and argillaceous sandstones and shales (Laughrey, 1999) and ranges in thickness from 492 ft (150 m) to 656 ft (200 m). The Rose Hill, Keefer, and Mifflintown formations (in ascending order) best describe the stratigraphic members of the Middle Silurian (Figure 2.5-186). Rose Hill Formation, which overlies the Tuscarora Formation, is defined as predominantly an olive shale with interbedded layers of hematitic sandstone, purplish shale, and fossiliferous limestone (Laughry, 1999). The Keefer Formation is described mainly as a quartzose and hematitic sandstone with some mudstone and the overlying Mifflintown Formation is composed of shallow marine mudrocks and limestones (Laughry, 1999). The Late Silurian is identified by the Bloomsburg Formation, a grayish-red clay-siltstone with some interbedded sandstone, transitioning to the limestone and thin shale beds of the Tonoloway Formation (Laughrey, 1999).

2.5.1.1.3.1.1.5 Devonian Period

In Pennsylvania, the Devonian-age rocks represent a "westward-thinning wedge of sediments" that range in thickness from 2,400 ft (732 m) in the western portion of the state, to over 12,000 ft (3,658 m) in the east (Harper, 1999). These Devonian sediments are generally broken down into two basic groups: the Pre-Acadian Orogeny comprised of stable shelf sedimentary deposits and Post-Acadian Orogeny strata that emphasize the presence of "tectonism, subsidence, and filling of a foreland basin" (Milici, 2006). The Keyser Formation forms the base for the Devonian-age rocks of the Ridge and Valley Province in Pennsylvania. This formation is primarily composed of gray, fossiliferous limestone (Laughrey, 1999). Above the Keyser Formation lie other stages of the Lower Devonian, including (in ascending order) the cherty limestone of the Helderberg Stage, the quartz rich sandstones, shales and siltstones of the Deerpark Stage, and the detrital sediments of the Onesquethawan Stage (Harper, 1999). The Onesquethawan Stage carries into and becomes the basement for the Middle Devonian timeframe which consists of basinal marine shales to nonmarine sandstone. Other stages

© 2007-2012 UniStar Nuclear Services, LLC. All rights reserved.
COPYRIGHT PROTECTED

within the Middle Devonian Ridge and Valley Province include the fossiliferous shale of the Needmore Formation, the argillaceous and silty Selinsgrove Limestone, the volcanic Tioga ash and shales, and the Marcellus and Mahantango shales of the Hamilton Group (Harper, 1999). The Marcellus shale is a carbonaceous black shale that has recently become the target of much natural gas exploration in Pennsylvania. The Mahantango Formation, which comprises the bedrock of the BBNPP site, is described by Harper (Harper, 1999) as "a complex series of interbedded shales, siltstones, and sandstones ranging from 1,200 ft (366 m) to 2,200 ft (671 m) thick." Milici (Milici, 2006) also refers to the Mahantango Formation as silty shale. The fossiliferous shaley limestone of the Tully Limestone Formation forms the uppermost portion of the Mahantango Formation (Harper, 1999).

The marine and non-marine rocks of the Late Devonian Period represent sediment deposition during the progradation of the Catskill deltaic system (Harper, 1999). This system, as it relates to the Ridge and Valley Province in central Pennsylvania, can be "broadly defined" by four main depositional episodes including (in ascending order) the rarely fossiliferous basinal shales of the Harrell Formation, the interbedded shales, siltstones, and sandstones of the Brallier Formation (equivalent to the Trimmers Rock Formation), the shales, thin siltstone, sandstones, and conglomerates of the Scherr and Lock Haven Formations, and the nonmarine sandstones and mudrock that overlap the Devonian-Mississippian boundary (Harper, 1999).

2.5.1.1.3.1.1.6 Mississippian Period

The Mississippian Period of the Ridge and Valley Province is a topic of on-going research but the most commonly accepted 'boundary' between the Mississippian and Late Devonian is the Spechty Kopf Formation (Berg, 1999). The Spechty Kopf Formation, which ranges up to 1,280 ft (390 m) in thickness, is typically associated with the unconformity lying between the previously discussed Catskill Formation and the fluvial sandstones of the Pocono Formation (Berg, 1999). The Spechty Kopf Formation is predominantly sandstone with some interbedded shale and siltstone. Above it lies the Pocono Formation which, in north-eastern Pennsylvania, consists mainly of medium to coarse-grained sandstones and conglomerates (Brezinski, 1999). In central Pennsylvania, the Pocono Formation is better represented by the Huntley Mountain and Rockwell Formations which are characterized by greenish-gray to tan sandy siltstone and silty shale with some sandstone (Brezinski, 1999). However, more recent studies (Brezinski, 2010) have concluded that the Spechty Kopf formation and the Rockwell Formation are glacial and glaciofluvial deposits. These deposits are restricted to a continuous package within a 24.8 mi by 248.5 mi (40 km by 400 km) outcrop that indicates that the Devonian-Mississippian boundary was a time of global cooling with continental glaciers present in Pennsylvania (Brezinski, 2010). The red shales, sandstones, and conglomerates of the Mauch Chunk Formation (Van Diver, 1993) mark the original uplifting of the Alleghanian Orogeny, as well as the uppermost boundary of the Mississippian strata in the Ridge and Valley Province. The Mauch Chunk Formation varies in thickness throughout the state, but is generally between 3,000 ft (914 m) and 4,000 ft (1,219 m) thick (Brezinski, 1999).

2.5.1.1.3.1.1.7 Pennsylvanian Period

Above the Mauch Chunk Formation in northeastern and central Pennsylvania lies the Lower Pennsylvanian Pottsville Formation, which ranges in thickness from 100 ft (30 m) to 1,600 ft (488 m) and is composed mainly of conglomerate and conglomeratic sandstone, with some sandstone and coal (Edmunds, 1999). Overlying the Pottsville Formation and marking the boundary between the Pennsylvanian and Permian Periods is the Llewellyn Formation. The Llewellyn Formation has a thickness of up to 3,500 ft (1,067 m) and consists mainly of conglomerates and sandstones with numerous coal beds and some clayey shale (Edmunds, 1999).

© 2007-2012 UniStar Nuclear Services, LLC. All rights reserved.
COPYRIGHT PROTECTED

As shown in Figure 2.5-182 and 2.5-186, there are no post-Pennsylvanian age rock units present in the Ridge and Valley Province of Central and Northeastern Pennsylvania. Subsidence and deposition in the northern end of the Appalachian Basin ended in the Pennsylvanian Period and the beginning of the Alleghanian Orogeny (Faill, 1998). Although thrust sheets and alluvial fans may have caused an overburden of 4-5 mi (6-8 km) thick in the region during the Alleghanian Orogeny (Faill, 1998), there is no preserved geologic materials in the Ridge and Valley Province from between the Pennsylvanian period and the Pleistocene glacial epochs. During this long time period, the Paleozoic rocks were subjected to weathering and erosion processes.

2.5.1.1.3.1.2 Tertiary and Quaternary Deposits

No Tertiary or pre-Pleistocene Quaternary deposits have ever been identified in the Ridge and Valley Province.

Pleistocene glaciers advanced over the northeastern end of the Ridge and Valley Province and covered the bedrock with variable thicknesses of glacial deposits, including tills, kame terraces, eskers, and outwash (Sevon, 2000c). The thickest glacial deposits include kame terraces and outwash which was deposited along major valleys leading away from retreating glaciers (Sevon, 1999a). These deposits can be more than 200 feet (60 m) thick and contain boulders, gravel, and coarse sand (Sevon, 1999a).

2.5.1.1.3.2 Stratigraphy of the Piedmont Physiographic Province

There are three distinct sections that comprise the Piedmont Physiographic Province. The first is the Gettysburg-Newark Lowland, the second is the Piedmont Lowland, and the third is the Piedmont Upland (Figure 2.5-183 shows the locations of these sections).

2.5.1.1.3.2.1 Gettysburg-Newark Lowland Section

The Gettysburg-Newark Lowland Section forms a 140-mile (225-km) arc across southeastern Pennsylvania with a series of exposed rift basins of Late Triassic to Early Jurassic age that are filled with fluvial and clastic sediments. Sediments filling the basins include conglomerates, shales, siltstones, and sandstones. These basins are underlain by nonmetamorphic Cambrian and Ordovician basement rocks and are bordered "by a continuous, complex system of normal faults" (Root, 1999).

2.5.1.1.3.2.2 Piedmont Lowland Section

Mesozoic sedimentary rocks of the Piedmont Province occur primarily within the highly folded and faulted region of the Piedmont Lowland section (Figure 2.5-183). The sediments were deposited in a series of northeast-trending basins. Sediments filling the basins include conglomerates, shales, siltstones and sandstones, and basic igneous intrusive dikes, diabase, and lava flows (VADOT, 2008). The Lower Mesozoic sediments deposited in these basins usually are referred to as Triassic basin deposits, although the basins are now known to also contain Lower Jurassic rocks. The folding and faulting of this section, as well as lithologies, are very similar to those found in the Great Valley Section of the Ridge and Valley Province, where Cambrian quartzite and Precambrian gneiss are brought into contact with rocks as young as the Early Ordovician (Gray, 1999).

2.5.1.1.3.2.3 Piedmont Upland Section

Crystalline rocks primarily occur within the Piedmont Upland section of the Piedmont Province. The crystalline rocks consist of deformed and metamorphosed meta-sedimentary and meta-igneous rocks, with overlying saprolite (VDEQ, 2008). The rocks belong to a number

© 2007-2012 UniStar Nuclear Services, LLC. All rights reserved.
COPYRIGHT PROTECTED

of northeast-trending belts that are defined on the basis of rock type, structure and metamorphic grade and are interpreted to have formed along and offshore of ancestral North America (Pavlides, 1994).

Surficial sediments in the Piedmont Province consist of residual and transported material. The residual soils have developed in place from weathering of the underlying rocks, while the transported material - alluvium and colluvium - has been moved by water or gravity and deposited as unconsolidated deposits of clay, silt, sand, and gravel. Surficial sediments in the Piedmont Upland section are interpreted to be the product of Cenozoic weathering, Quaternary periglacial erosion and deposition, and recent anthropogenic activity (Sevon, 2000a).

Residual soil in the Piedmont Province consists of completely decomposed rock and saprolite. Residual soils occur almost everywhere, except where erosion has exposed the bedrock on ridges and in valley bottoms. Saprolite comprises the bulk of residual soil in the Piedmont Province and is defined as an earthy material in which the major rock-forming minerals (other than quartz) have been altered to clay but the material retains most of the textural and structural characteristics of the parent rock. The saprolite forms by chemical weathering, its thickness and mineralogy being dependent on topography, parent rock lithology, and the presence of surface and/or groundwater (Cleaves, 1992).

Colluvium in the Piedmont Province occurs discontinuously on hilltops and side slopes, while thicker colluvium occurs in small valleys lacking perennial streams. Alluvium is present in all valleys with perennial streams (Sevon, 2000a).

2.5.1.1.3.3 Stratigraphy of New England Physiographic Province

The basement rocks of the Reading Prong Section of the New England Physiographic Province are believed to have formed during the Greenville Orogeny and are composed of metamorphosed sedimentary rocks. These rocks were then subjected to the intense thrust faulting and continual folding associated with the Taconic Orogeny, thus creating a complex nappe megasystem (Drake, 1999). Continued folding and faulting during the Alleghanian Orogeny has lead to "extremely complicated geologic relations" (Drake, 1999) within the Reading Prong. The Middle Proterozoic carbonate and crystalline rocks that were transported overtop of the basement rocks (Drake, 1999), were also subjected to folding and faulting and range in sequence depending upon the area of the Reading Prong being studied. Seismic-reflection studies have suggested that the basement of the Reading Prong ranges in thickness from 15,000 ft (4,572 m) in the easternmost part of the Pennsylvania, to 45,000 ft (13,716 m) in Lebanon and Lancaster Counties (Drake, 1999).

2.5.1.1.3.4 Stratigraphy of Atlantic Coastal Plain Physiographic Province

The Atlantic Coastal Plain Physiographic Province is one of the flattest of the many physiographic provinces within the site region. The province covers more than 3,200 mi (5,150 km) from Cape Cod to the Yucatan Peninsula, and forms the continental shelf along the Atlantic Ocean (Komor, 1998). The province represents repeated cycles of transgression and regression of the ocean resulting in over 100 million years of sediment accumulation (Komor, 1998). Underlying most of the Atlantic Coastal Plain Physiographic Province are sediments of Cretaceous and Tertiary age with Pleistocene fluvial sediments overlying areas in and around the part of the province within the state of New Jersey. A record of Cretaceous to Quatemary exhumation of the Appalachians is preserved in the Coastal Plain sediments (Pazzaglia, 2006). These Cretaceous sediments, in addition to glacial outwash deposits from the Pleistocene continental glaciers, comprise the underlying geology of Long Island and the eastern shores of

© 2007-2012 UniStar Nuclear Services, LLC. All rights reserved.
COPYRIGHT PROTECTED

Staten Island (Komor, 1998). The total sediment accumulation in the Atlantic Coastal Plain Province is nearly 30,000 ft (9,144 m) thick (Komor, 1998).

2.5.1.1.3.5 Stratigraphy of Appalachian Plateau Physiographic Province

The Appalachian Plateau Physiographic Province is underlain by rocks that are continuous with those of the Ridge and Valley Province but, in the Appalachian Plateau, the layered rocks are nearly flat-lying or gently tilted and warped, rather than being intensely folded and faulted. Rocks of the Allegheny Front along the eastern margin of the province consist of thick sequences of sandstone and conglomerate, interbedded with shale, ranging in age from Devonian to Pennsylvanian. The stratigraphic formations in the Appalachian Plateau are nearly identical to the strata in the Ridge and Valley Province. Changing paleoclimate particularly influenced depositional patterns during the Upper Middle and Late Pennsylvanian, resulting in cyclothems with altered red beds, thick paleosols, and lacustrine carbonates, rather than the typical coal-clastic cyclothems of the Early and Middle Pennsylvanian to the south (Greb, 2008). In southwest Pennsylvania (Figure 2.5-182) and West Virginia, however, the Appalachian Plateau Province includes sedimentary rocks of Permian age (sandstones, shales, and coal seams) (Hack, 1989).

The Appalachian Plateau Province is the only one of the provinces described above that has rock strata and glacial deposits that are similar to the geologic formations found at the BBNPP site. The rocks of these two provinces (Appalachian and the Ridge and Valley) were deposited in the same general Appalachian structural basin (miogeosyncline) and the sedimentary formations are continuous across the two provinces. There are, however, great differences in geologic age, in structural and tectonic features, and sediment provenance between the Ridge and Valley geologic formations and the geologic materials found in the adjacent physiographic provinces to the east and south.

2.5.1.1.4 Regional Tectonic Setting

The seismotectonic framework of a region, which includes the basic understanding of existing tectonic features and their relationship to the contemporary stress regime and seismicity, forms the foundation for assessments of seismic sources. In the probabilistic seismic hazard study performed by EPRI (EPRI, 1986), seismic source models were developed for the Central and Eastern United States (CEUS) based on tectonic setting; the identification and characterization of "feature-specific" source zones; and the occurrence, rates, and distribution of historical seismicity. The EPRI source model development included the independent interpretations performed by six Earth Science Teams. The seismic source models developed by each of the six teams were based on the tectonic setting and the occurrence, rates, and distribution of historical seismicity. The original seismic sources identified by EPRI (EPRI, 1986) are thoroughly described in the EPRI study reports (EPRI, 1986), and are summarized in Section 2.5.1.1.4.4.5.

The EPRI models reflected the general state of knowledge of the geosciences community in the mid-to-late 1980's.

Since the EPRI study, additional geologic, seismologic, and geophysical research has been performed in the site region. This subsection presents a summary of the current state of knowledge in the regional tectonic setting and highlights the more recent information that is relevant to the identification of seismic sources for the BBNPP site. The following subsections describe the region in terms of:

- Contemporary Plate Tectonic Setting of the Atlantic Margin (Section 2.5.1.1.4.1)

© 2007-2012 UniStar Nuclear Services, LLC. All rights reserved.
COPYRIGHT PROTECTED

- Origin and Orientation of Contemporary Tectonic Stress (Section 2.5.1.1.4.2)
- Gravity and Magnetic Data and Features of the Site Region and Site Vicinity (Section 2.5.1.1.4.3)
- Regional Tectonic Structures (Section 2.5.1.1.4.4)
- Seismic Sources as Interpreted by EPRI Groups (Section 2.5.1.1.4.4.5)

The BBNPP site region is a stable continental region (SCR) characterized by low rates of crustal deformation and no active plate boundary conditions (EPRI, 1986). Nearly 70% of SCR earthquakes with magnitude 6 or greater occurred in areas of Mesozoic and Cenozoic extended crust (EPRI, 1986). Additional evidence shows an association between Late Proterozoic rifts and modern seismicity in eastern North America. However, faults suggested by seismographic data have not been mapped at the ground surface, and there has never been an observation of tectonic fault rupture at the ground surface accompanying a Pennsylvania earthquake (Dewey, 1999). There is also no evidence for Late Cenozoic seismic activity of any tectonic feature or structure in the site region (Crone, 2000) (Wheeler, 2005). No new structures or features have been identified in the site region since 1986 as described in the EPRI study (EPRI, 1986), but recent studies have provided a better understanding of the previously identified tectonic features and their associated seismicity. Among these features are the Ramapo fault and the Reading Prong (Sykes, 2008). These later studies were reviewed as input to this study, and are referenced throughout the subsections.

2.5.1.1.4.1 Contemporary Plate Tectonic Setting of the Atlantic Margin

The Late Precambrian to recent geologic history and plate tectonic evolution of the site region is summarized in Section 2.5.1.1.2 and Figure 2.5-6. Several recent studies have concentrated on the relationship between the stratigraphy and structure during the Paleozoic era as it relates to orogenies and plate tectonics (Pazzaglia, 1994) (Pohn, 2000 and 2001) (Hibbard, 2006) (Cotter, 2008). These three main orogenic phases during the Paleozoic: Taconic, Acadian, and Alleghanian Orogenies, begin with accumulation of marine sediments and volcanic deposits, followed by deformation by structural folding and faulting, and end with tectonic uplift of mountains, and erosion of uplifted land. A particular consequence of orogeny is the production of sediment as uplifted mountains erode. Thus, each phase created a delta, filling shallow seas on the continental side of the orogeny. Clastic fans were deposited in terrestrial, coastal, near-shore, and off-shore settings (Aber, 2001).

During the break up of Pangaea in the Triassic, rift basins developed in eastern North America that were typically asymmetrical and trended northeast to southwest. The current Atlantic passive margin has evolved since this rifting initiated in the Late Triassic. The progression from active continental rifting to sea-floor spreading and a passive continental margin included: (1) initial rifting and hot-spot plume development, (2) thinning of warm, buoyant crust with northwest-southeast extension, normal faulting and deposition of synrift sedimentary and volcanic rocks, and (3) cooling and subsidence of thinned crust and deposition of postrift sediments on the coastal plain and continental shelf, slope, and rise (Klitgord, 1988) (Klitgord, 1995). The transition between the second (rifting) and third (drifting) phases during the Early Jurassic marked the initiation of a passive margin setting for the site region, in which active spreading migrated east, away from the margin.

The continental margin moved away from the spreading center of the mid-Atlantic and horizontal northwest-southeast tension changed to horizontal compression as gravitational potential energy from the spreading ridge exerted a lateral "ridge push" force on the oceanic

© 2007-2012 UniStar Nuclear Services, LLC. All rights reserved.
COPYRIGHT PROTECTED

crust. Northwest-southeast directed post rift activities in the Mesozoic basin caused inversion to many structures present during this time (Withjack, 1998). The transition from a rift to a drift margin through the remainder of the Mesozoic and into the Cenozoic along with the westward push of the continental divide, dominated the tectonic and geomorphic development of the eastern United States up to the modern time period (Schlische, 2003).

Contractional post-rift deformation is interpreted to record the change in stress regime from horizontal maximum extension during rifting to horizontal maximum compression during passive margin drifting. The hypothesis that a change in the stress regime followed rifting existed prior to the 1986 EPRI study (e.g., (Sanders, 1963) (Swanson, 1982) (Wentworth, 1983)). However, significant advances in the characterization of the rift to drift transition and post-rift deformation have occurred since then (Withjack, 1998) (Schlische, 2003).

Latest tectonic processes in the Cenozoic Era include vertical tectonics associated with lithospheric flexure (Pazzaglia, 1993). Vertical tectonics are dominated by cooling of the extended continental, transitional, and oceanic crust as the spreading center migrated eastward, and the erosion of the Appalachian Mountains to the Coastal Plain and extension of the Continental Shelf and Slope.

Based on models of the Cenozoic flexural deformation, surface material from the Appalachian Mountains eroded and was deposited on the Coastal Plain and Continental Shelf (Pazzaglia, 1993). The sediment is mainly deposited in the Salisbury Embayment and Baltimore Canyon Trough (Figure 2.5-7). The flexural hinge that is the axis between deposition and downward pressure to the east and uplift due to ersion to the west is known as the Fall Zone (Pazzaglia, 2006). An elastic model predicts the uplift in the Piedmont province to be as much as 33 ft (10 m) per million years (Pazzaglia, 1994). Figure 2.5-7 illustrates present conditions with location map and composite cross section of the middle U.S. Atlantic passive margin (Pazzaglia, 2004). The Susquehanna River terrace profiles, the Coastal Plain stratigraphic sections, geodynamic model cross-sections, and offshore load volumes are defined along cross section A-A', in the lower part of the same Figure 2.5-7.

2.5.1.1.4.2 Origin and Orientation of Contemporary Tectonic Stress

Since 1986, an international effort to collate and evaluate stress indicator data has resulted in the publication of a new World Stress Map in 1989 that is periodically updated (Heidbach, 2008). The World Stress Map (WSM) is the global repository for contemporary tectonic stress data from the Earth's crust. It was originally compiled by a research group headed by Mary Lou Zoback as part of the International Lithosphere Program (ILP). Since 1995 the WSM is a research project of the Heidelberg Academy of Sciences and Humanities. The WSM research team is integrated into the Tectonic Stress Group of the Geophysical Institute at the Karlsruhe University. The WSM is a task group of the International Association of Seismology and Physics of the Earth's Interior (IASPEI) (Heidbach, 2008).

As observed in Figure 2.5-8 (Heidbach, 2008) throughout the BBNPP site region, the average P axes of the earthquakes are oriented NE-SW and are aligned with the direction of the current plate driving stress that in the BBNPP region is characterized by northeast-southwest-directed horizontal compression. Since the 1986 EPRI evaluation of plate tectonic stress for the CEUS several authors have studied the stress magnitudes in the crust, deformation of intraplate lithosphere, joints and veins in regional tectonic perspective, and contemporary stress variations (Herman, 2005) (Zoback, 2002 and 1991) (Engelder, 2001) (Hancock,1989) (Evans, 1989) (Hickman, 1985) . As indicated in these subsequent studies, the tectonic stress created by the Mid Atlantic ridge forced stress orientation to align northeast to southwest on the

© 2007-2012 UniStar Nuclear Services, LLC. All rights reserved.
COPYRIGHT PROTECTED

North American plate. They also indicated that the lithosphere cannot be deformed more rapidly because of the limited amount of tectonic force available to drive that deformation in the current stress field (Zoback, 2002) and that the stress field for the site region is considered stable. Other potential forces acting on the North American plate are considered minor stress levels of magnitude and orientation.

Study of neotectonic joint attributes by Hancock (Hancock, 1989) and Engelder (Engelder, 1980) that included the Appalachian Plateau and other places in England, France, the Arabian Platform and the Ebro basin in Spain, showed that late-formed joints have potential value for tracking the contemporary stress field in regions where in-situ measurements are not available. Their conclusion showed that these late-formed joints have the characteristics of neotectonic joints and approximately parallel to directions of contemporary horizontal maximum stress (SH) known from in-situ stress measurements. The latter shows that although there may be a slight misalignment between joint strike and the direction of the greatest horizontal stress, these joints reflect the contemporary stress field.

Despite the most common orientation of joints in the Appalachian Mountains being in the northeast-southwest to east northeast-west southwest trend, the vast majority are not neotectonic joints related to the current northeastern U.S. northeast-southwest maximum horizontal compressive stress regime as originally thought (Engelder, 2009). Through study of jointing in the Appalachian foreland of Virginia, Pennsylvania and New York, particularly in the pervasively jointed organic black shales, it was shown that there are three common joint sets (Engelder, 2009). While there are neotectonic east northeast-west southwest joints (J_3), the vast majority of joints in this orientation are early joints (J_1) related to propogation in the pre- or early Alleghenian orogeny times. This became clear when it was observed that these J_1 joints were folded along with bedding (Engelder, 2009). There is also an early east-northeast face cleat development in coal beds throughout the central and southern Appalachians that was initiated during burial that is correlative with the dominant J_1 joint formation (Engelder, 2006). Vertical joints cross-cutting a folded succession are interpreted as J_3 joints related to the contemporary stress regime. The similarity of the J_1 and J_3 orientations is merely a geologic coincidence (Engelder, 2009). The second northewest-southeast oriented joint set (J_2) typically cross cuts J_1 orthogonally when they are observed in the same bed (Engelder, 2009). The J_2 joints, or cross-fold joints, clearly formed later becuase they commonly end at J_1 joints as well as strike across fold axes (Lash, 2009), thereby forming a radial pattern along the oroclinal bend of the central Appalachian Mountains (Engelder, 2009). However, J_1 joints are commonly observed abutting and curving into J_2 joints. This is due to reactivation of short J_1 during Miocene exhumation under the east northeast-west southwest contemporary stress regime (Lash, 2009). The reactivated J_1 joints were driven along curving paths into abutting contacts with the J_2, which is a manifestation of slip on J_2 joints under relatively low contact stress following reactivation of J_1 joints (Lash, 2009).

Current understanding of the tectonic stress in the CEUS based on published reports since the publication of the EPRI source models in 1986 show only slightly different localized characterization of the northeast-southwest orientation of the maximum compressive principal stress (Hancock, 1989). The current characterization of potential activity of tectonic structures for the BBNPP Site remains valid.

2.5.1.1.4.3 Gravity and Magnetic Data and Features of the Site Region and Site Vicinity

Gravity and magnetic anomaly datasets of the site region have been published since the 1986 EPRI study. Regional maps of the gravity and magnetic fields are presented for North America by the Geological Society of America (GSA), as part of the Society's Decade of North America

© 2007-2012 UniStar Nuclear Services, LLC. All rights reserved.
COPYRIGHT PROTECTED

Geology (DNAG) project (Tanner, 1987) (Hinze, 1987) as shown in Figure 2.5-23 and Figure 2.5-26 (Kucks,1999) and Figure 2.5-25 and Figure 2.5-28 (Bankey, 2002).

These maps present the potential field data at 1:5,000,000-scale, and show gravity and magnetic anomalies with wavelengths. Regional gravity anomaly maps are based on Bouguer gravity anomalies onshore and free-air gravity anomalies offshore. The primary sources of magnetic data reviewed for this BBNPP study are from aeromagnetic surveys onshore and offshore (Kucks, 1999). Large-scale compilations (1:2,500,000-scale) of the free-air anomalies offshore and Bouguer anomalies onshore were published in 1982 by the Society of Exploration Geophysicists (Lyons, 1982) (Sheridan, 1988). The DNAG magnetic anomaly maps were based on a prior analog map of magnetic anomalies of the U.S. published in the early 1980's (Zietz, 1982) (Behrendt, 1983) (Sheridan, 1988).

In addition, the DNAG Continent-Ocean transect program published a synthesis of gravity and magnetic data with seismic and geologic data (Klitgord, 1995). No gravity and magnetic data published since 1986 reveal new anomalies related to geologic structures. The following sections discuss the gravity and magnetic anomalies.

2.5.1.1.4.3.1 Gravity Data and Features

Gravity data compiled at 1:5,000,000-scale for the DNAG project provide documentation of previous observations that the Regional Bouguer anomaly gravity field in the site region is characterized by a long-wavelength, east-to-west gradient over the continental margin (Kucks,1999) (Figure 2.5-23, Figure 2.5-215 and Figure 2.5-216). Bouguer gravity values increase eastward from about -80 milligals (mgal) in the Ridge and Valley Province of western Virginia to about +10 mgal in the Coastal Plain Province (Figure 2.5-23, Figure 2.5-215 and Figure 2.5-216). Gravity highs, or positive anomalies, are created by accumulations of dense rock units while gravity lows are from mass deficiencies. The folded and faulted structures, basins, igneous intrusions, lithologic variations, and basement uplifts create variations in mass. Gravity anomalies occur from density contrast in size, depth, and structural depth. Long wavelengths show shallow structures or highly concentrated deep structures. Shorter wavelengths are created by shallower structures (Lavin, 1999). As shown on (Figure 2.5-23, Figure 2.5-215 and Figure 2.5-216), gradient gravity extends from Canada to Alabama and parallels the Appalachian Mountains. The Mesozoic rift basins show gravity lows and northeast-trending border faults (Figure 2.5-216).

The gravity map also shows northeast-trending, long wavelengths of gravity highs and lows. The alignments are variations of thickness of the sedimentary rocks and crustal structures (Lavin, 1999). Low gravity dominates the western part of Pennsylvania and eastern Ohio, including areas such as Beaver Falls gravity low. The Chambersburg anomaly is another low, broad, northeast-trending gravity low which extends the length of the Appalachian Mountain system. The Somerset gravity high in southwestern Pennsylvania is thought to coincide with a regional basemat high that is about 3.5 to 4 mi (6 km) below the surface, though a deeper source has been suggested for this anomaly, while in the northwest the Kane gravity high marks a paleotopographic high that was uplifted from Early Devonian through Early Pennsylvanian time which controlled the sedimentation patterns and composition in the Pennsylvanian Epoch (Figure 2.5-25) (Lavin, 1999). In the northeast, the Scranton gravity high (Feature 34 on Figure 2.5-216 and Figure 2.5-25) is surrounded by the Williamsport and Reading lows. The lows are deep Paleozoic sedimentary basin and/or increased crustal thickness. The Scranton gravity high is related to mafic material during Late Precambrian rifting (Lavin, 1999). The Newport gravity high, directly southwest of the Scranton gravity high, is believed to be a separate, but related feature that might represent the site of a triple

© 2007-2012 UniStar Nuclear Services, LLC. All rights reserved.
COPYRIGHT PROTECTED

junction. All anomalies were known at the time of the 1986 EPRI study. In summary, gravity data published since the mid-1980's (Kucks, 1999) confirm and provide additional documentation of previous observations (i.e., pre-EPRI) across this region of eastern North America, and do not reveal any new anomalies related to geologic structures previously unknown to EPRI (EPRI, 1986) that would impact the BBNPP site.

2.5.1.1.4.3.2 Magnetic Data and Features

Magnetic data compiled for the 2002 Magnetic Anomaly Map of North America reveal numerous northeast-southwest-trending magnetic anomalies, generally parallel to the structural features of the Appalachian orogenic belt (Bankey, 2002) (Figure 2.5-25). The magnetic map allows a visualization of the geological structure of the upper crust in the subsurface showing the spatial geometry of bodies of rock and the presence of faults and folds. Prominent north- to northeast-trending magnetic anomalies in the BBNPP site region (Figure 2.5-217 and Figure 2.5-218) include the interior New York-Alabama Lineament, the New Bloomfield high, subsurface nappes near Scranton and Allentown, anomalies over largely subsurface Proterozoic rocks at the Reading Prong, Philadelphia and Lancaster, and an inferred basement fault located south of Pittsburgh, the Pittsburg-Washington Lineatment (King,1999).

The 994 mi (1,600 km) long lineament in aeromagnetic maps of the eastern U.S. is referred to as the "New York-Alabama Lineament" (NY-AL) (King, 1978) (Feature 28 on Figure 2.5-217). The NY-AL primarily is defined by a series of northeast-southwest trending linear magnetic anomalies in the Ridge and Valley province of the Appalachian fold belt. The NY-AL is located about 50 mi (80 km) northwest of the BBNPP site. Based on studies by King (King, 1999), the NY-AL lineament divides the basement into two magnetically distinct areas (Figure 2.5-25 and Figure 2.5-217). To the southeast, the few anomalies present are very broad and have gentle gradients consistent with the profound basement depths of the region. To the northwest, numerous anomalies indicate a basement composed of large units of rock with strongly contrasting magnetic properties. King (King, 1999) has interpreted the NY-AL to be a major strike-slip fault in the Precambrian basement beneath the thin-skinned, fold-and-thrust structures of the Ridge and Valley province and created a base model for the Appalachian fold belt.

The Clingman-Ocoee lineament is an approximately 750 mi (1,207 km) long, northeast-trending aeromagnetic lineament that passes through parts of the Blue Ridge and eastern Ridge and Valley provinces from Alabama to Pennsylvania (King, 1999). The Clingman-Ocoee lineament is sub-parallel to and located about 30 to 60 mi (48 to 97 km) east of the NY-AL, and about 50 mi (80 km) southeast of the BBNPP site (Figure 2.5-27). The Clingman-Ocoee lineament is interpreted to represent a source or sources in the Precambrian basement beneath the accreted and transported Appalachian terrains (Nelson, 1983). The Clingman-Ocoee block is a Precambrian basement block bounded by the NY-AL and Clingman-Ocoee lineaments (Johnston, 1985b).

The Newark and Gettysburg rift basins consist of Mesozoic clastic rocks (Featured on Figure 2.5-218) that have been downfaulted against Proterozoic and Paleozoic rocks (King, 1999). Magnetic anomalies related to elongated shaped bodies of diabase are preset within these basins.

The Buckingham Mountain anomaly is produced by a fault-bound sliver of Paleozoic and Proterozoic rock creating a northeast trending ridge, and dividing the Newark basin. The faults cut the Mesozoic rocks and are bound to the south by small diabase sheets and bound larger

© 2007-2012 UniStar Nuclear Services, LLC. All rights reserved.
COPYRIGHT PROTECTED

sheets to the north of the anomaly. The Buckingham magnetic high indicates a large subsurface ridge of magnetic Proterozoic rocks extending 15 mi (24 km) southwest from the stateline (King, 1999).

The magnetic anomalies over the Reading Prong (Feature 51 on Figure 2.5-217) are produced by a complex of magnetite-rich, gneissic Proterozoic rocks at the surface (King, 1999). These rocks are related to the center of a nappe system that is over thrusted from the southeast. Small anomalies occur east of Lancaster and are related to gneisses exposed in the Minde Ridge anticline and related structures. The magnetic data indicate similar rocks at shallow depths to the west toward Lancaster and to the east of the Honey Brook Upland, under the Triassic Basin (King, 1999).

In summary, magnetic data published since the mid-1980's (Bankey, 2002) confirm and provide additional documentation of previous observations (i.e., pre-EPRI) across this region of eastern North America, and do not reveal any new anomalies related to geologic structures previously unknown to EPRI (EPRI, 1986) that would impact the BBNPP site.

2.5.1.1.4.4 Regional Tectonic Structures

A tectonic map of the important structures in the BBNPP site region is shown in Figure 2.5-188 and Figure 2.5-232, while a cross section is shown in Figure 2.5-7. Since the EPRI study (EPRI, 1986) was completed, new tectonic features have been proposed and described in the site region, and previously described features have been characterized in more detail. New features identified since the EPRI study (EPRI, 1986) in the BBNPP site region include folds and faults (Pohn 2000) (Wheeler 2006). In the sections below, specific tectonic features and the evidence of their activity, or absence of activity are discussed. Specific descriptions are provided for those features within the BBNPP site region that could have an impact or produce a significant change in the EPRI seismic source model.

Table 2.5-63 contains a listing of the Tectonic Events that have affected the site region, the timing of each event, a brief description of the prevailing conditions during that event, the associated tectonic and non-tectonic features, and the section where these features are discussed. Some features are listed on the table multiple times, to acknowledge their prolonged activity or reactivation through geologic time.

Regional tectonic structures within and outside the 200 mi (322 km) BBNPP site region are described in this section, based on the following breakdown:

- Significant Seismic Sources Beyond 200 mi (322 km) radius that could impact the BBNPP site (Section 2.5.1.1.4.4.1)
- Quaternary Tectonic Features (Section 2.5.1.1.4.4.2)
- Relevant Tectonic Features with Associated Seismicity (Section 2.5.1.1.4.4.3)
- Relevant Tectonic Features with No Associated Seismicity (Section 2.5.1.1.4.4.5)

2.5.1.1.4.4.1 Significant Seismic Sources Beyond 200 mi (322 km) Radius

Description of the tectonic features begins with seismic sources significant to BBNPP, that are outside the BBNPP site Region, or greater than 200 mi (322 km) from the site. The following features are included in this subsection:

- The New Madrid Seismic Zone (NMSZ) (Figure 2.5-9),

© 2007-2012 UniStar Nuclear Services, LLC. All rights reserved.
COPYRIGHT PROTECTED

- The Charleston Seismic Zone (CSZ) (Figure 2.5-10),
- The Charlevoix-La Malbaie Seismic Zone in Canada (Figure 2.5-189), and
- The Saint Lawrence Rift Valley

The Madrid Seismic Zone (NMSZ), the Charleston Seismic Zone (CSZ), and the Charlevoix-La Malbaie Seismic Zone in Canada, are known contributors to the BBNPP seismic hazard at low frequencies, based on updated models with new paleoseismological data on characteristic earthquake events from these sources (see Section 2.5.2 for further details). The Saint Lawrence Rift is not considered a contributor to the BBNPP seismic hazard. However, because it is considered a seismic source in EPRI (EPRI 1986), it is discussed here for completeness.

2.5.1.1.4.4.1.1 New Madrid Seismic Zone (NMSZ)

The New Madrid Seismic Zone (NMSZ) is not a single feature but is defined by the region of abundant seismicity in the central Mississippi River Valley, approximately 800 miles (1290 km) west-southwest of the BBNPP Site. Accordingly, it is not possible to define an average strike, but most of the seismicity is associated with the Reelfoot rift (see below), which has a northeasterly trend. At present, structural and tectonic information about specific seismogrenic faults is limited, in part because the seismogenic faults are not expressed or are poorly expressed at the surface. Furthermore, the entire river valley is covered by Late Quaternary sediments, so only the geologically youngest deformation is expressed at the surface.

In the winter of 1811-1812, at least three major earthquakes occurred in the New Madrid seismic zone, and the area remains the most seismically active area in central and eastern North America. The 1811-1812 earthquakes were among the largest historical earthquakes to occur in North America and were perhaps the largest historical intraplate earthquakes in the world. The New Madrid earthquakes consisted of a series of at least 3 and possibly 4 major (M ? 7.5) events during a period of 2 months in the winter of 1811 and 1812. Strong aftershocks persisted in the region for at least one year. The first major earthquake occurred at 2:15 a.m. (all times are local times) on December 16, 1811. It was followed by another major earthquake at 8:15 a.m. the same day that was the smallest of the 4 major events. Most reports of the New Madrid earthquakes note three principal events, and this event is commonly not cited as one of the principal earthquakes. The next major event occurred at 9 a.m. on January 23, 1812. Historical accounts suggest that this event was intermediate in size between the first and last major shocks. The last and largest earthquake occurred at 3:45 a.m. on February 7, 1812 (Nuttli, 1972; Street, 1990).

The earthquakes produced widespread liquefaction throughout the NMSZ and prominent to subtle surface deformation in several areas, but they did not produce any known surface faulting (Crone, 2000). Furthermore, many features shown on maps of the NMSZ (Figure 2.5-11) are not even associated with discrete faults; the most notable exception is the Reelfoot scarp, which is located along the western shore of Reelfoot Lake in extreme northwestern Tennessee (Crone, 2000). The three most commonly noted features associated with the contemporary deformation are: (1) the Lake County uplift and Reelfoot scarp, (2) areas of suspected co-seismic subsidence, and (3) areas of abundant liquefaction during the 1811-1812 earthquakes. The locations of these features are derived from the digital data used to generate the suite of seismotectonic maps of the New Madrid, Missouri area (Crone, 2000).

© 2007-2012 UniStar Nuclear Services, LLC. All rights reserved.
COPYRIGHT PROTECTED

The most widespread expression of recent strong earthquakes in the New Madrid region is the abundant liquefaction features (sand blows and sand-filled fissures), which are concentrated in a 24.9 to 37.3 mile (40 to 60 km) wide belt from near Charleston, Missouri on the northeast to south of Marked Tree, Arkansas (Obermeier, 1988). Modern or historic earthquakes that induced liquefaction in the same region can serve as calibration events for paleoearthquakes. In the NMSZ, for example, comparison of the size and spatial distributions of historic and pre-1811 sand blows suggests source areas and magnitudes for paleoearthquakes similar to the very large to great earthquakes of 1811-1812 (Tuttle, 2001).

Geologic conditions in the New Madrid region are near optimum for the development of liquefaction features during strong earthquakes: a 6.6 - 26.2 feet (2-8 m) thick, fine-grained "topstratum" deposit overlies water-saturated, unconsolidated "substratum" sand and gravel. Extensive liquefaction occurred during the 1811-1812 earthquakes; locally the ground surface was buried by more than 3.3 feet (1 m) of liquefied sand, and hundreds of square kilometers of the land surface have been mapped as being more than 25 percent covered by liquefied sand (Obermeier, 1988).

Other than the pervasive sand blows throughout the NMSZ, the Reelfoot scarp is the most prominent geomorphic feature that has been produced by the modern tectonism in the NMSZ (Csontos, 2008) and modern seismicity in the NMSZ is intimately associated with it (Braile, 1997). The Reelfoot scarp extends south-southeastward from near the town of New Madrid, Missouri, to a point south of Reelfoot Lake. Recent compilation in Crone (Crone, 2000) have shown that the Reelfoot scarp is approximately 20 miles (32 km) long and the subjacent Reelfoot fault may be as much as 43.5 miles (70 km) long. Despite being a well-defined feature, the Reelfoot scarp is small in comparison to the general dimensions of the seismic zone. However, this fault is the only feature that has conspicuous surface expression and therefore can be studied at the surface. Based on the historical seismicity, there may be other significant but unexposed faults in the NMSZ (Crone, 2000).

Recent studies of the scarp have provided valuable information on the recurrence of deformation on the scarp, calculated uplift rates, and the history of faulting. Based on combined information from seismological, seismic-reflection profiling, geomorphic, and geological studies, the Reelfoot Scarp is interpreted as an east-dipping monocline which is the surface expression of a fault propogation fold associated with the underlying blind Reelfoot thrust fault (Van Arsdale, 1995 and 2000).

The Reelfoot scarp is situated within the Reelfoot rift, which is a northeasterly-trending, 43.5 mile (70 km) wide graben that has as much as 1.2 mi (2 km) of structural relief on magnetic basemat (Crone, 2000). The rift is best defined by the magnetic data, which also reveals the presence of major positive magnetic anomalies along the flanks and axis of the rift that are inferred to be mafic plutons (Braile, 1997).

The contemporary seismicity and current deformation in the New Madrid region is controlled by a regional stress field in which the maximum compressive stress is oriented approximately east-northeast to west-southwest (Van Arsdale, 1995 and 2000). Within this stress field ancient faults, most of which originally formed as extensional features during rifting, have been reactivated mainly as strike-slip faults. The modern seismicity is largely associated with rift related features and is concentrated into three major trends that form a zigzag pattern that has an overall northeasterly trend (Fig. 2.5-11). The southwestern-most trend is a narrow, linear, 74.6 miles (120 km) long zone of earthquakes in northeastern Arkansas and extreme

© 2007-2012 UniStar Nuclear Services, LLC. All rights reserved.
COPYRIGHT PROTECTED

southeastern Missouri (Braile, 1997); this zone of earthquakes roughly coincides with the position of an axial fault zone that is commonly present along the center of most rifts.

Detailed studies of the Reelfoot scarp have documented evidence of three deformation events within the past 2,400 years and characterized the style of near surface deformation associated with the scarp (Kelson, 1996). Late Holocene fluvial deposits are warped into a 26.2 feet (8 m) high, east-facing monocline (Kelson, 1996). Borehole data and trenches at three sites characterized the style of near-surface deformation associated with the scarp and constrain the timing of the three deformation events on the scarp (Kelson, 1996).

Deformation on the scarp associated with the 1811-1812 New Madrid earthquake sequence produced extensive liquefaction, folded the fluvial sediments, and caused minor reactivation of small faults that bound an extensional graben in the uplifted (hanging wall) of the Reelfoot scarp. The penultimate deformation event occurred between A.D. 1260 and 1650 (350-740 yr B.P.), produced about 4.3 feet (1.3 m) of throw in the graben bounding faults, and caused folding and development of the scarp (Kelson, 1996). The oldest documented event associated with the scarp occurred between A.D. 780 and 1000 (1000-1120 yr B.P.), and initially produced the small graben in the hanging wall of the Reelfoot fault. Liquefaction features of similar age to, but of smaller size than, the Daytona Beach sand blow occur near Blytheville (93 mi (150 km) northeast of Marianna) and Montrose, Arkansas (109 mi (175 km) southeast of Marianna) (Tuttle, 2006). A very large ($M > 7.2$) earthquake centered near Marianna about 3500 B.C. might account for the liquefaction in all three areas. The large sand blows at the St. Francis site are similar to compound sand blows in the NMSZ, suggesting that a New Madrid-type earthquake sequence was centered near Marianna about 4800 B.C. (Tuttle, 2006).

Paleoseismic studies have suggested a recurrence interval of about 500-1100 years for earthquakes that are large enough to produce significant surface deformation or liquefaction in various parts of the seismic zone, with most recent studies suggesting that there were about 900 years between the last two New-Madrid-size events (A.D. 900 to A.D. 1811) and that widespread liquefaction occurs every few hundred years (Crone, 2000). However, the record studied thus far is too short to be used for a long-term recurrence rate. Liquefaction data indicate that New Madrid events occurred every 500 ± 300 years during the past 1200 years. Furthermore, this recurrence rate for very large earthquakes is not easily reconciled with the small amount of crustal deformation observed in the region, suggesting that the NMSZ became active during the Quaternary and that New Madrid earthquakes may be temporally clustered in this intraplate region (Tuttle, 2002a). The detailed investigations of the Reelfoot scarp described above provide information that permitted Kelson (Kelson, 1996) to estimate a recurrence interval of 150-900 years, with a more likely range of about 400-500 years. These rate estimates only apply to the Reelfoot scarp, and not to overall behavior of major events for the entire seismic zone.

Epicentral patterns, correlative geophysical data, and historical seismic energy release indicate the significance of New Madrid area seismicity, both within the Reelfoot segment of the rift structures and in areas outside of this segment, particularly to the north (Braile, 1997). It is also clear that deep structure of the crust, including thickness variations in the upper crust and the presence of a high-density lower crustal layer, is a controlling factor in New Madrid seismicity.

Although there are many unanswered questions about New Madrid area seismicity and the causes of earthquakes in this intraplate setting, much has been learned in the past several decades, particularly from the detailed epicentral patterns that are beginning to be illuminated by the seismograph network data and from the geological and geophysical

© 2007-2012 UniStar Nuclear Services, LLC. All rights reserved.
COPYRIGHT PROTECTED

studies (Braile, 1997) of the shallow and deep (crustal and upper mantle) structures within the NMSZ.

Calculations performed for the PSHA for BBNPP determined that the New Madrid Seismic Zone is a contributor to the seismic hazard at the BBNPP Site in the low-frequency range.

2.5.1.1.4.4.1.2 Charleston Seismic Zone (CSZ)

The Charleston Seismic Zone (CSZ) in South Carolina is located 590 miles (950 km) SSW from the BBNPP Site. The Charleston region is considered to have the highest seismic hazard of the east coast of the United States (Jaume, 2006). The CSZ is considered a contributor to the hazard at the BBNPP Site at low frequencies.

The August 31, 1886 Charleston earthquake (magnitude 6.9-7.3) was the largest historical event to strike a well-populated region of the eastern United States (Jaume, 2006). Historical evidence for felt earthquakes in the region before the 1886 event and continuing low- level seismicity in the epicentral area, plus evidence for multiple earthquakes producing liquefaction features in the South Carolina coastal plain, result in this region having the second highest seismic hazard in the continental United States east of the Rocky Mountains (Jaume, 2006).

Geomorphic, geologic, and geophysical data suggest the presence of an approximately 373 mi (600 km) NNE trending buried fault system in the Coastal Plain of the Carolinas and Virginia, named the East Coast Fault System (ECFS), illustrated in Figure 2.5-10 (Marple, 2000). This fault system is expressed by anomalous changes in fluvial geomorphology that locally coincide with one or more than the following features: linear aeromagnetic anomalies, buried faults interpreted from seismic reflection data, surface faults offsetting Pliocene-Pleistocene surficial units, locally brecciated phyllites and argillites, gently up-warped sediments, topographic highs, and seismicity near Summerville, South Carolina.

The suggested fault system traverses the epicentral area of the 1886 Charleston earthquake and lies west of paleoliquefaction sites along the outer South Carolina Coastal Plain. Therefore, this fault system could be the source of the Charleston Earthquake and other large prehistoric earthquakes. Although most features described individually do not provide conclusive evidence of faulting, collectively they strongly suggest the presence of the East Coast Fault System (Marple, 2000).

The shallow subsurface Tertiary stratigraphy of the greater Charleston region reflects the tectonic development and setting of the area over the past 34 Ma. Upper Eocene and Oligocene stratigraphic horizons show a net regional dip toward the southwest or south, whereas Miocene and Pliocene horizons show a shift to net regional dips toward the southeast (Weems, 2002). The tendency for many stratigraphic horizons to pinch out northeastward within the Charleston area indicates that it has been a persistent hinge zone between the Southeast Georgia embayment to the southwest, and the Cape Fear arch to the northeast. Localization of relative strain and motion along this hinge zone probably explains why the Charleston area is much more active seismically than other areas within the Atlantic Coastal Plain (Weems, 2002).

Results from a comprehensive loss assessment for the state of South Carolina (Wong, 2005) indicate that a future repeat of the 1886 earthquake would be catastrophic, resulting in possibly 200 deaths, more than 44,000 injuries, and a total economic loss of $20 billion in South Carolina alone. By characterizing the nature and scope of potential impacts, the study

© 2007-2012 UniStar Nuclear Services, LLC. All rights reserved.
COPYRIGHT PROTECTED

performed by Wong (Wong, 2005) for South Carolina represents a starting point for renewed and hopefully more effective efforts in earthquake hazards and loss mitigation for this, distant to the BBNPP site, capable source.

Calculations performed for the PSHA for BBNPP determined that the Charleston Seismic Zone is a contributor to the seismic hazard at the BBNPP Site in the low-frequency range.

2.5.1.1.4.4.1.3 Charlevoix-La Malbaie Seismic Zone

The Charlevoix-La Malbaie Seismic Zone (CLSZ) area is located 530 mi (853 km) NNE of the BBNPP Site, and 62 mi (100 km) NE of Quebec City, on the north shore of the St. Lawrence River, within the St. Lawrence Rift System (Figure 2.5-189) (Tremblay, 2003). It is considered a contributor to the hazard at the BBNPP Site at low frequencies.

The bedrock of the area mostly consists of metamorphic rocks of the Precambrian crystalline basement (Lemieux, 2000). However, along large segments of the shoreline, as well as in two river valleys ("Du Gouffre" and Malbaie rivers), Paleozoic rocks of the St. Lawrence Lowlands are well exposed and uncomformably overlie the Grenvillian basement (Lemieux, 2000).

The Charlevoix area has been affected by several tectonic events of regional significance. In Late Precambrian to Early Cambrian times, the opening of the Iapetus Ocean is recorded in Charlevoix by isolated and discontinuous segments of the St. Lawrence Lowlands platform. Following the formation of these rift-related faults, the Iapetan ocean is inferred to have covered the Grenvillian basement, which led to the deposition of siliciclastic and calcareous sediments that form the lower part of the St. Lawrence Lowlands in the area (Lemieux, 2000).

Historically, only a few eastern Canadian earthquakes of magnitude greater than 5.5 had observed geological effects such as surface faulting, liquefaction, submarine slumping, rock avalanches, rock falls, landslides, railroad embankment slides, and one tsunami (Lamontagne, 2002). The extent of the Charlevoix Seismic Zone has been defined using instrumentally recorded data (Anglin, 1981). The Charlevoix is the most active region, with five M> 6 events, in 1663, 1791, 1860, 1870, and 1925. Work by Doig (Doig, 1990) has confirmed in part the dates of these earthquakes, based on the relative spacing of the layers and the accelerator-mass spectrometer 14C dating of a twig in one of the cores taken from Lake Tadoussac, in Charlevoix (Doig, 1990). Since 1924, seismicity at Charlevoix has been almost entirely limited to a 44 mi (70 km) zone along the St. Lawrence River (Doig, 1990).

According to available geochronological data, a major meteoritic impact occurred in the Late Devonian, and is recorded by abundant shattercone localities in basement and Paleozoic rocks and by circular topographic features that characterize the Charlevoix area. Within the boundaries of the Charlevoix impact crater, two types of fault related breccias exist: coarse grained cataclastic breccias, and polymictic clastic matrix breccias (Tremblay, 2003).

Finally, the occurrence of a Mesozoic tectonic event has been suggested for the area and consisted of fault reactivation attributed to the opening of the Atlantic Ocean. The geometry and nature of the faults related to impact cratering in the Charlevoix will have to be determined in order to reconstruct and understand the regional tectonic evolution (Lemieux, 2000). Most faults of the Charlevoix Fault Zone are brittle faults, usually normal faults characterized by downdip motion, but strike-slip motion is locally observed; very few faults have been observed with reverse movement (Lemieux, 2000).

© 2007-2012 UniStar Nuclear Services, LLC. All rights reserved.
COPYRIGHT PROTECTED

The Charlevoix area is a region of significant geologic interest, particularly since the discovery of the impact structure. Previous mapping and analysis have revealed a major part of the regional tectonic history of the area but relationships between the inferred impact cratering with structures left by the Iapetan rifting or the Mesozoic reactivation have still to be determined (Lemieux, 2000).

High resolution marine seismic reflection data acquired in the St. Lawrence River estuary (Tremblay, 2003), identify submarine topographic relief attributed to the St. Lawrence rift system. Northwest-trending seismic profiles suggest that normal faults fringing the St. Lawrence river are associated with a major topographic depression in the estuary, the Laurentian Channel trough, with up to 2,997 ft (700 m) of basement relief (Lemieux, 2000). The analysis of some 124 mi (200 km) of deep seismic reflection lines in the CLSZ did not reveal any clear evidence of a surface rupture under the St. Lawrence river including in areas where most M > 4.0 earthquakes occurred in the 20th century (Lamontagne, 2002).

Calculations performed for the PSHA for BBNPP determined that the Charlevoix-La Malbaie is a contributor to the seismic hazard at the BBNPP Site in the low-frequency range.

2.5.1.1.4.4.1.4 Saint Lawrence Rift Valley

The Saint Lawrence Valley or St. Lawrence rift system is a seismically active zone parallel to the Saint Lawrence River which extends approximately 620 mi (1000 km) from Quebec to Newfoundland, at a minimum distance of 450 mi (724 km) NNE of the BBNPP Site (Feature 36 in Figure 2.5-188). The St. Lawrence rift system consists of steeply inclined, dip-slip faults characterized by normal-sense movement along longitudinal faults and a variable component of strike-slip faulting along traverse faults (Tremblay, 2003). In La-Malbaie area most faults display normal-sense motion, but reverse faults have also been observed locally. A predominant northwest-trending fault system accounts for more than 30% of fault data (Lemieux, 2000).

The Charlevoix Seismic Zone, one of the most active seismic regions in eastern Canada, is situated in the Saint Lawrence Valley. The Saint Lawrence Rift System, incorporating the Charlevoix Seismic Zone (described in Section 2.5.1.1.4.4.1.3) has the potential for producing moderate to large earthquakes. The March 1, 1925 earthquake with an estimated magnitude between 6.0 to 6.5 M_b is the largest instrumentally recorded earthquake of the Charlevoix Seismic Zone. Several other large earthquakes, however, have been reported in the region since the first settlements (Bent, 1992). Hypocentral data with additional time has shown no migration of seismicity (Anglin, 1984), which is indicative of confinement of high activity to the same area.

Recent research has been performed in the southeastern corner of Lake Ontario and western Lake Ontario in search for evidence of neotectonic faulting (Wallach, 2002). In the Rochester Basin, vertical separations of layers of unconsolidated sediments and the underlying Paleozoic bedrock had been recognized. In Western Lake Ontario seismic surveys are thought to image a number of monoclonal warps in unconsolidated sediments with different thickness in the imaged layers from the upper and lower blocks across the warp (Wallach, 2002). It was therefore interpreted by Wallach (2002) that these observations are indications that the St. Lawrence Rift System continues much further south than previously mapped, transecting Lake Ontario. The author claims that earthquakes up to magnitude 7m_b might reasonably be expected beneath Lake Ontario and implies that seismic hazards in the area of this lake might be comparable with that of seismically active areas of the St. Lawrence seismic zone. There is no direct geologic evidence to support this conclusion. Finding Quaternary faulting in Eastern

© 2007-2012 UniStar Nuclear Services, LLC. All rights reserved.
COPYRIGHT PROTECTED

North America (ENA) will continue to be difficult. More rigorous study and work is needed in the study area to validate these interpretations.

The EPRI study (EPRI, 1986) excludes the Charlevoix Seismic Zone from the Saint Lawrence Rift System and considers it as a separate seismic zone and that approach was taken for this BBNPP study. The Saint Lawrence Rift System is considered to be a capable tectonic source. Calculations performed for the PSHA for BBNPP determined that the Saint Lawrence Rift Valley (excluding the CLSZ) is not a significant contributor to the seismic hazard at the BBNPP Site.

2.5.1.1.4.4.2 Quaternary Tectonic Features

The U.S. Geological Survey maintains a nationwide database on features that have known or suggested Quaternary tectonic faulting. Geologic information on the Quaternary faults, folds, and earthquake-induced liquefaction in the eastern United States was compiled by Crone (Crone, 2000). An update containing new assessments was published by Wheeler (Wheeler, 2005). Tectonic features, described by Crone and Wheeler (Crone, 2000), and Wheeler (Wheeler, 2005) (Wheeler, 2006) within a 200 mi (322 km) radius (site region) of the BBNPP site were identified, are shown on Figure 2.5-188.

The features within the site region and one outside the region that has demonstrated Quaternary activity, are categorized into one of four Classes, as follows (Crone, 2000). A summary of BBNPP features in each Class is provided as well:

Category	Number of Features	Description
Class A	1	Geologic evidence demonstrates the existence of a Quaternary fault of tectonic origin, whether the fault is exposed by mapping or inferred from liquefaction or other deformational features.
Class B	0	Geologic evidence demonstrates the existence of Quaternary deformation, but either (1) the fault might not extend deeply enough to be a potential source of significant earthquakes, or (2) the currently available geologic evidence is too strong to confidently assign the feature to Class C but not strong enough to assign it to Class A.
Class C	16	Geologic evidence is insufficient to demonstrate (1) the existence of tectonic faulting, or (2) Quaternary slip or deformation associated with the feature.
Class D	0	Geologic evidence demonstrates that the feature is not a tectonic fault or feature. This category includes features such as joints, landslides, erosional or fluvial scarps, or other landforms resembling fault scarps but of demonstrable nontectonic origin.

Note that only one (1) feature was categorized as Class A - demonstrating convincing evidence of Quaternary activity. This is the Newbury Liquefaction Feature. This feature is outside the BBNPP site region (200 mi (322 km) radius). In addition, no features in the site region were identified as having sufficient evidence of Quaternary deformation (Class B).

The sixteen (16) Class C features in the site region are listed in this section and are shown in Figure 2.5-188. Information on these features was reviewed for this study, and these features are not considered in the seismic hazard assessment as characteristic tectonic sources for the BBNPP site.

The known or suggested Quaternary tectonic features that may be significant for the assessment of the seismic hazard at the BBNPP site are described briefly in the following subsections. More detailed discussion of the seismicity and evidence regarding the magnitude

© 2007-2012 UniStar Nuclear Services, LLC. All rights reserved.
COPYRIGHT PROTECTED

and recurrence of earthquakes within the seismic zones is provided in this subsection, and Section 2.5.2.

Following is a list of the seventeen (17) Quaternary features described below.

1. Newbury Liquefaction Feature (Class A)
2. Ramapo Fault System (Class C)
3. Furlong-Flemington Fault System (Class C)
4. Kingston Fault (Class C)
5. New York Bight Fault (Class C)
6. Mosholu Fault (Class C)
7. New Castle County Faults (Class C)
8. Upper Marlboro Faults (Class C)
9. Dobbs Ferry Fault Zone (Class C)
10. Lancaster Seismic Zone (Class C)
11. Cacoosing Valley Earthquake Sequence (Class C)
12. Moodus Seismic Zone (Class C)
13. Clarendon-Linden Fault Zone (Class C)
14. Offset Glaciated Surfaces (Class C)
15. Fall Lines of Weems (Class C)
16. Everona Fault-Mountain Run Fault Zone (Class C)
17. Stafford Fault System (Class C)

2.5.1.1.4.4.2.1 Newbury Liquefaction Features (Class A)

The Newbury area lies in northeastern Massachusetts 300 miles (480 km) to the northeast of the site, and has been the subject of recent research. Crone and Wheeler (Crone, 2000), in their compilation of faults and tectonic features of central and eastern United States selected the name "Newbury Liquefaction Features" for the part of the structure located near Newbury (Essex County, MA) and assigned it to Class "A". Their reason for assignment to Class "A" was eyewitness reports of liquefaction during an earthquake in 1727 (MMI VII, Magnitude = 4.8) and sand dikes that were attributed to the 1727 earthquake. Tuttle (Tuttle, 1991) concluded that the liquefaction was caused by strong ground motion but the causative fault responsible for the ground motion and liquefaction remains unidentified.

The Clinton-Newbury Fault Zones are northeast trending faults that extend from Connecticut to New Brunswick Canada. The fault zones are approximately 262 mi (422 km) northeast of the BBNPP site (Feature 21 in Figure 2.5-188). Strike slip movements have been documented along the fault zone. The trend along this fault system has been the location of several moderate to

© 2007-2012 UniStar Nuclear Services, LLC. All rights reserved.
COPYRIGHT PROTECTED

large earthquakes (EPRI, 1986). Based on research, the fault zone has been assigned an activity probability of 0.2, since location uncertainties prevented association of the apparent trend of earthquakes with the trend of the tectonic feature. The stress information in the area of this tectonic feature was inconclusive (EPRI, 1986). Information on this feature was reviewed for this study, and this feature is considered to be a capable source, but not a characteristic tectonic source for the BBNPP site.

2.5.1.1.4.4.2.2 Ramapo Fault System (Class C)

The Ramapo Fault System is located in northern New Jersey and southern New York State, approximately 124 mi (200 km) north-northeast from the BBNPP site (Figure 2.5-188). This fault system consists of northeast-striking, southeast-dipping, normal faults and classified as border faults for the Mesozoic Newark Basin (Jacob, 2004) (Feature 15 in Figure 2.5-188). Although earlier tectonic episodes characterize parts of the Fault System evolution, it is best characterized as a normal, Mesozoic basin boundary fault (EPRI, 1986). Evidence of the repeated slip since Proterozoic time (including Mesozoic extensional reactivation) is contained in different faults of the system (Ratcliffe, 1971).

Earthquakes have, however, occurred in the general vicinity of the Ramapo Fault System. The term "Ramapo Seismic Zone" (RSZ) is used for the seismically active 7.5 mi (12 km) wide eastern area of Reading Prong (Sykes, 2008). Despite this, reactivation of the Ramapo fault during the Quarternary period has not been clearly demonstrated. Many of the earthquakes have, however, not been well located mainly because of poor seismic station distribution prior to 1970's. Because additional seismographs have been installed in the area of the Ramapo Fault since 1970's a large amount of micro earthquake data has been recorded. Based on earthquake hypocenters and single event focal mechanisms, Aggarwal (Aggarwal, 1978) inferred a reverse slip on a surface dipping 60º-65º southeast from the trace of the Ramapo Fault. The history of repeated slip during the Proterozoic and correlation of fault trend with epicenters, led Aggarwal (Aggarwal, 1978) to conclude that the Ramapo Fault System is active. Based on the scattered epicenters, they also concluded that the seismicity was concentrated along a group of northeast-trending faults of which the Ramapo Fault appeared to be the most active. Yang (Yang, 1981) concluded that the Ramapo Fault System is probably the most active fault system in the greater New York City area.

Examination of small earthquakes and re-evaluation of some focal mechanisms in 1980's did not favor the association of the epicenters with the Ramapo Fault. Seborowski (Seborowski, 1982) studied a sequence of micro earthquakes near Annsville, New York, recorded during January, 1980, and derived a composite focal mechanism solution. Their solution indicated east-northeast compression resulting in thrust motion on a north-northwest striking fault plane. This direction is transverse to the northeast trend of the major structures in the epicentral region including the Ramapo Fault (Aggarwal, 1978). The dominant reverse mechanisms (Aggarwal, 1978) imply east-southeast maximum (horizontal) compressive stress. However, the maximum horizontal compressive stress trend throughout most of the eastern United States including the area of the Ramapo Fault System is east-northeast (Crone, 2000).

An improved 3-D velocity model (Thurber, 1985), which shows 10-15 percent velocity difference across the Ramapo Fault, has changed some of the epicenters and depths of the earthquakes studied by Aggarwal (Aggarwal, 1978). Kafka (Kafka, 1985) used earthquake data of the greater New York City area and refined the catalog to eliminate station and detection bias from the network seismicity. This allowed for uniform measurement of magnitudes and earthquake locations. The results showed half of the earthquakes occurred about 6 mi (10 km) from the Ramapo Fault and about half were located about 31 mi (50 km) from this fault --

© 2007-2012 UniStar Nuclear Services, LLC. All rights reserved.
COPYRIGHT PROTECTED

around the northern part of Newark Basin. Kafka (Kafka, 1985) concludes that "while the Ramapo Fault can by no means be ruled out as a possible source zone for earthquakes in the greater New York City area, the cause of earthquakes in this region is, in the final analysis, still unknown." In general, even though the epicenters align along the Ramapo Fault, the association is less significant than the one suggested by Aggarwal (Aggarwal, 1978). Therefore, the Ramapo Fault system seems to dominate the seismicity (Crone, 2000).

Despite this, many earthquakes in the area have been attributed to the reactivation of the Ramapo Fault by the present-day compressional stress field. However, the results of core analyses (in the area of Ramapo Fault in New York and New Jersey) by Ratcliffe and Burton (Ratcliffe, 1984) are not consistent with the reactivation of Ramapo Fault and related faults in the present-day stress field. Results of further core analyses in six localities of Ramapo and other basin-border faults showed that the most recent slip was extensional at each locality and deformation did not extend beyond the Mesozoic, and there is no evidence of post-Jurassic displacement (Sykes, 2008). Therefore, while the association of earthquakes with the Ramapo Fault System is possible, the uncertainty in the locations allows the association with other structures in the area as well. Since post-1974 earthquakes have been located with higher accuracy, this 7.5 mi (12 km) wide active RSZ cannot be attributed to location errors (Sykes, 2008). Therefore, it has been concluded that more than one fault must be involved in generating the earthquakes (Sykes, 2008).

There is an apparent discrepancy between the distribution of earthquakes in the Ramapo Seismic zone and the lack of displacement in the last 150 Ma in the localities where the cores have been taken (Sykes, 2008). As a possible explanation for this discrepancy, it is assumed that earthquakes may originate from other preexisting faults which may or may not strike similar to Ramapo fault. It is not clear which faults are active. The seismicity data used and processed cannot be solely used to delineate a single fault or multiple faults. Geologic evidence of Holocene fault movements is also very hard to find in the study area.

It is not possible to conclude that the Ramapo fault is an active feature. Therefore, even though it cannot be ruled out as a possible source for some of the observed earthquakes, the cause of the earthquakes is still unknown. This is a conclusion that has been reached by most previous studies (Kafka, 1985). It is not clear which magnitude will probably represent the maximum magnitude for the area or for the Ramapo fault assuming that it is active. The largest observed earthquake in the area is the 1884 (offshore) New York earthquake with m_{bLg} = 5.25. Based on the observed seismicity a maximum magnitude of 6 or slightly higher is appropriate.

The EPRI seismic source model does not consider the Ramapo fault system as a separate seismic source. For the BBNPP PSHA, the maximum magnitudes of the EPRI seismic source zones (that encompass the Ramapo seismic zone) range from 5.3 to 7.1 (EPRI, 1986). These values have been presented in different logic trees by six EPRI teams and adequately characterize the upper level seismicity. Even though a larger source zone (currently used in BBNPP PSHA) tends to diffuse the hazard, this would only have an effect if the RSZ was located closer to the site. Based on the available data and information, the current PSHA results adequately reflect the hazard at the BBNPP from the Ramapo fault zone.

Some branches of the Ramapo fault system (not the Ramapo fault itself) may extend into southeastern Pennsylvania. Those branches have similar distances from the site. Even if it is assumed the Ramapo fault as an active source (with M_{max}~6.0), it cannot produce significant ground motions at the site because of the relatively large distance away.

© 2007-2012 UniStar Nuclear Services, LLC. All rights reserved.
COPYRIGHT PROTECTED

Crone (Crone, 2000) also summarized a few reports that indicate some forms of Quaternary deformation near the Ramapo Fault but argue that none of the reports provide convincing evidence for Quaternary faulting or sudden offset which can be used to distinguish prehistoric seismic slip from aseismic creep. The Ramapo Fault or Fault System is probably capable of generating small or rare large earthquakes but it has been assigned to Class C feature since evidence for quaternary faulting has not been identified (Crone, 2000). Information on this feature was reviewed for this study, and this feature is considered to be a capable source, but not a characteristic tectonic source for the BBNPP site.

2.5.1.1.4.4.2.3 Furlong-Flemington Fault System (Class C)

Furlong Fault is located in the west portion of the Newark Basin, near New Hope in eastern Pennsylvania. This major intrabasinal Mesozoic fault connects to the north, with the Flemington fault in New Jersey (Ratcliffe, 1988). It is located about 75 mi (121 km) southeast of the BBNPP (Feature 24 in Figure 2.5-188). The Furlong and Flemington faults have been considered as one fault system (Root, 1999). Ratcliffe (Ratcliffe, 1988), using data from coring and surface observations, determined that the Furlong-Flemington fault zone consists of two closely parallel faults that dip at 47° to 50° to the southeast. Structural analysis also indicated a normal fault with some component of strike slip for the Furlong fault. Many of the Mesozoic border faults, such as the Ramapo and Flemington faults, coincide with Paleozoic thrust faults. It seems that the reactivation of the Paleozoic thrusts by Mesozoic border faults controlled the overall structure of the basin (Ratcliffe, 1985). However, there is no indication or evidence of later activities for the fault system. Seismicity has not been associated with either Flemington or Furlong faults or with larger Chalfont Fault, which is intersected by the Furlong Fault. Based on the lack of evidence of recent or Quaternary activity, Furlong-Flemington Fault System is not a considered to be a capable tectonic source.

2.5.1.1.4.4.2.4 Kingston Fault (Class C)

The Kingston Fault is located in central New Jersey, approximately 87 mi (140 km) east-southeast of the BBNPP (Feature 6 in Figure 2.5-188). The Kingston Fault is 8 mi (13 km) long, north to northeast striking with a nearly vertical dip (Owens, 1995). The fault is located in the Mesozoic formation of the Newark Basin (Crone, 2000). Parker (Parker, 1990) showed the northern part of the fault trace on his map and reported a dip of 85° SE with extensional slip during the formation of the Basin in the Mesozoic (Stanford, 1995). Results of well, boring, and geophysical data showed movement of southeast side of the fault based on the thickened Pliocene gravel across the fault, which is overlain by Late Pleistocene gravel, which is not offset by the fault, indicating the fault probably moved during Pliocene or Early to Middle Pleistocene (Stanford, 1995). Quaternary activity for the fault can not be demonstrated and the fault slip rate is unknown. Additionally, no paleoseismological study has been performed on the thickness of the Pliocene gravel to determine seismic creep, or different episodes of seismic faulting (Crone, 2000). According to Wheeler (Wheeler, 2005), Kingston Fault was assigned to a Class C feature. No seismicity has been associated with the fault. Based on the information above, the Kingston fault is not considered to be a capable tectonic source.

2.5.1.1.4.4.2.5 New York Bight Fault (Class C)

On the basis of seismic surveys, the New York Bight Fault is characterized as an approximately 31 mile (50 km) long, north-northeast-striking fault, located offshore of Long Island, New York (Schwab, 1997) (Hutchinson, 1985) (Feature 5 in Figure 2.5-188). It is 115 mi (185 km) east of the BBNPP Site, and parallel to the New Jersey coast (Hutchinson, 1985). Based on the results, the fault had offset Upper Cretaceous rocks and Lower Tertiary and Quaternary deposits, therefore it may be as young as the Quaternary (Hutchinson, 1985).

© 2007-2012 UniStar Nuclear Services, LLC. All rights reserved.
COPYRIGHT PROTECTED

The fault was mapped (Crone, 2000) along 24 mi (39 km) of its northern extension and dips almost vertically and was traced to within 6 mi (10 km) of the Long Island Coast (Lotto, 1997). Cretaceous to Eocene strata have been offset by the fault, but an unconformity which separates the Eocene and Miocene strata (and Miocene strata overlying it) are not offset sufficiently within the resolution of the available seismic profiles (Hutchinson, 1985), indicating that the fault is Oligocene at youngest. Later seismic reflection work indicated that middle to Late Quaternary sediments overlay Cretaceous and Tertiary strata at the fault (Lotto, 1997). These Quaternary sediments are not offset more than 3 ft (0.9 m) which is the resolution of the measurement (Crone, 2000).

The seismicity near the fault show small magnitudes (less than 3.00) have been located within 13 mi (21 km) from the fault. The location error for the offshore earthquakes exceeds 6 mi (10 km) (Yang, 1981) because of the seismic station distribution; therefore the location of these events is not reliable. Crone (Crone, 2000) and Wheeler (Wheeler, 2006) classify the New York Bight Fault Zone as a Class C feature, based on the lack of Quaternary activity evidence. Information on this feature was reviewed for this study, and this feature is considered to be a capable source, but not a characteristic tectonic source for the BBNPP site.

2.5.1.1.4.4.2.6 Mosholu Fault (Class C)

The Mosholu Fault is located in Bronx County, New York City, New York (Wheeler, 2006). The fault is approximately 135 mi (217 km) east of the BBNPP (Feature 4 in Figure 2.5-188). The Mosholu Fault was originally mapped and renamed by Baskerville (in Crone, 2000) and has been located by geological mapping and subsurface data (Crone, 2000). The fault is a 5.7 mi (9.2 km) long northwest trending right-lateral oblique-slip fault with a steep dip that crosses the Bronx River channel (Crone, 2000). Merguerian (Merguerian, 1996) suggested that the fault showed postglacial age (since last glacial advance ~12,000 years ago) uplift forming a northwest-trending bedrock high approximately 0.3 mi (0.5 km) northeast of the Mosholu fault trace (Crone, 2000). This bedrock high, or "bulge", is a feature shown by depth-to-bedrock profiles, topographic maps, and surface exposures. The formation of the bulge is thought to have blocked the Bronx River which caused the creation of a lake behind the uplift where clay deposits settled overlying the older glacial deposits. Evidence for this is surface deformation is that the Bronx River changes course to the southeast at the bulge, the existence of the Webster Avenue lowland just south of the bulge and the clay overlying the glacial deposits north of the bulge (Merguerian, 1997). The river would then have diverted southward across the upland, cutting the Snuff Mill gorge, through which the Bronx River currently flows, and eventually draining the lake through the gorge (Crone, 2000). This evidence indicates that the change in river course resulted from neotectonic uplift of a block of bedrock along the northeast side of Mosholu fault in the quarternary period. Crone (Crone, 2000) suggests that the bulge formed in a compressional bend during post-glacial sinistral slip on the Mosholu fault, and that once formed, the topographic expression of the bulge might have been accentuated by post-glacial fluvial erosion. However, Merguerian (Merguerian, 1997) could not conclusively prove that the uplift occurred seismically and mentioned that none of the previous New York City's magnitude approximately 5.0 earthquakes of 1737, 1783, and 1884 have been connected with surface blockage of crustal rocks and was not able to associate historic earthquakes with the faults in the New York City area. Furthermore, earthquakes have not been associated with the Mosholu Fault, but the fault has not been studied in detail for paleoseismolgoical evidence of possible Quarternary activity. There is also no evidence with which to determine whether the uplift, if seismic, occurred in one large earthquake or many smaller ones (Crone, 2000). However, based on the circumstantial evidence from the Bronx River, Merguerian (1997) suggests that NW-trending faults in New York City area, such as the Mosholu Fault and the Dobbs Ferry Fault, are seismically capable.

© 2007-2012 UniStar Nuclear Services, LLC. All rights reserved.
COPYRIGHT PROTECTED

Overall, the attribution of the uplift to post-glacial slip on the Mosholu fault is a reasonable inference, but is not demonstrated (Crone, 2000). The Mosholu Fault has been assigned to Class C by Crone (Crone, 2000). Information on this feature was reviewed for this study, and this feature is considered to be a capable source, but not a characteristic tectonic source for the BBNPP site.

2.5.1.1.4.4.2.7 New Castle County Faults (Class C)

The New Castle County faults are characterized as 146 mi (235 km) long buried north and northeast-striking faults that displace an unconformable contact between Precambrian to Paleozoic bedrock and overlying Cretaceous deposits. The faults are located in northern Delaware, near New Castle, about 150 mi (242 km) southeast of the BBNPP site (Feature 9 in Figure 2.5-188). Based on research (Spoljaric, 1973), a graben is present in New Castle County with a northeastern strike near Delaware City. The graben is bounded by faults that are part of the basement fault that underlies the Coastal Plain of Northern Delaware. The bounded faults have shown displacements ranging from 32 to 98 ft (10 to 30 m) across the basement-Cretaceous boundary (Spoljaric, 1972). Along this fault zone, earthquakes have occurred and have showed magnitudes as high as 3.8. According to studies completed by the Delaware Geological Survey (DGS) (McLaughlin, 2002), a subsurface investigation utilizing seismic reflection and seismic refraction, subsurface drilling, geophysical logging and trench excavation was performed to potentially locate displacement from faults near New Castle, Delaware. No shallow faults were detected during the subsurface drilling program and trench excavation. Seismic section identified extensive faulting in the investigation site where the New Castle fault is projected. DGS concluded that minimal, if any, modern fault activities occurred in the area of New Castle County. Wheeler (Wheeler, 2005) characterizes the New Castle County faults as a Class C features. Based on the above information, including the recent strong evidence as presented by McLaughlin (McLaughlin, 2002), the New Castle County Faults is considered to be a capable source, but not a characteristic tectonic source for the BBNPP site.

2.5.1.1.4.4.2.8 Upper Marlboro Faults (Class C)

The Upper Marlboro Faults are located in Prince Georges County, Maryland approximately 150 mi (241 km) southeast of the BBNPP site (Feature 25 in Figure 2.5-188). The faults are a series of features, which cut the Coastal Plain sediments (Crone, 2000). The faults have a low angle dip, which is more consistent with a surficial origin, and extend to hypocentral depths (Crone, 2000). Wheeler (Wheeler, 2006) related the faults to surficial land slides based on low angle dips. The faults are assigned to Class C feature by Crone (Crone, 2000) and Wheeler (Wheeler, 2006) because no evidence of Quaternary activity has been presented for the faults. Seismicity has not been associated with the fault. Accordingly, the Upper Marlboro Faults are not considered to be a capable tectonic source.

2.5.1.1.4.4.2.9 Dobbs Ferry Fault (Class C)

The Dobbs Ferry Fault is located in Westchester County, New York about 6 mi (10 km) north-northeast of New York City (Wheeler, 2006). The fault is approximately 155 mi (249 km) east of the BBNPP (Feature 3 in Figure 2.5-188). The Dobbs Ferry fault zone is a zone of abundant fractures and joints that extends southeastward from the east bank of the Hudson River and crosses the Bronx River. The fault had dextral slip during the Mesozoic as part of the Pangaea separation (Crone, 2000). Different orientations of superimposed slickensides show more than one episode of slip on the fault. Sinistral slip can be inferred from the majority of slip sense indicators, which is consistent with the present day, east-northeast, regional orientation of the maximum horizontal compressive stress. Some indicators are dextral and older, and perhaps date from Mesozoic extension (Crone, 2000). The October 19, 1985, Ardsley

© 2007-2012 UniStar Nuclear Services, LLC. All rights reserved.
COPYRIGHT PROTECTED

earthquake, with a magnitude of 4.1 along with six aftershocks ranging from 4 to 4.5 in magnitude, occurred in southern Westchester County, New York, approximately 19 mi (30 km) north of central Manhattan, approximately 125 mi (201 km) east of the BBNPP Site. The location of the first six aftershocks (within a week of the main shock) defined a vertical northwest trending rupture zone with an approximate diameter of 2300 ft (700 m) and a depth ranging from 2.8 to 3.4 mi (4.5 to 5.5 km). The rupture zone corresponds directly to a 0.6 mi (1 km) segment of the Dobbs Ferry fault (Hough, 1991). First motion data of the main shock and this group of aftershocks yielded well constrained focal mechanism solutions indicating sinistral slip on a northwest striking plane (Hough, 1991) (Crone, 2000). Later aftershocks defined a northeast striking plane. These results led Seeber (Seeber, 1998) to conclude that the earthquakes probably occurred on the fault zone without surface rupture along its trace. Crone (Crone, 2000) assigns the Dobbs Ferry fault zone to a Class C feature because there is no other paleoseismological evidence for prehistoric Quarternary seismic faulting along the Dobbs Ferry fault zone. The Dobbs Ferry Fault is considered to be a capable source, but not a characteristic tectonic source for the BBNPP site.

2.5.1.1.4.4.2.10 Lancaster Seismic Zone (Class C)

The Lancaster Seismic Zone (LSZ) is located in southeast Pennsylvania and approximately coincides with Lancaster County (Armbruster, 1987). The seismic zone is of circular shape with a diameter of about 31 mi to 38 mi (50 km to 60 km) and is 55 mi (88 km) south of the BBNPP site (Crone, 2000) (Feature 8 in Figure 2.5-188) and has been a source of seismicity for more than 2 centuries. The LSZ consists of short discontinuous north striking faults that transect Triassic and Paleozoic rocks. (Armbruster, 1987) and many studies provide evidence for high density northstriking, near surface structures and fracture zone in the LSZ (Crone, 2000). Some of the previous works summarized by Crone (Crone, 2000) indicate a seismically active fault, or fault zone, in the LSZ.

The age of the faulting occurred during the Early Mesozoic extension relating to the Atlantic margin. The LSZ crosses the Newark-Gettysburg Triassic rift basin which consists of extensional faults associated with Mesozoic rifting. The basin itself and the pre-Mesozoic basement below it appear to be aseismic. The epicenters forming the LSZ reflect this pattern as most well-located epicenters lie directly outside the Gettysburg-Newark Basin (Scharnberger, 2006) occurring on both sides of the basin where the basin is at its narrowest, between the Newark and the Gettysburg portions (Armbruster, 1987).

The LSZ does however mark the southwestern edge of the Newark Basin Seismic Zone (NBSZ) (Crone, 2000). Thrust faults and folds (formed during the Paleozoic Appalachian orogeny) and extensional faults (associated with Mesozoic rifting) are among the main structures along the NBSZ and LSZ (Crone, 2000). This seismicity is part of a belt that correlates with the crystalline slab emplaced on the craton by the Paleozoic detachment (Armbruster, 1987). Regional Jurassic dikes, striking north-northeast, traverse the LSZ. Coinciding with brittle faults, many of these dikes are perhaps among the youngest structures in the region which persist as large planar zones of weakness and cut through the crust (Seeber, 1998).

In the western part of the Lancaster Seismic Zone, the epicenters of 11 events from 1889 through 1994 (with magnitudes 3.04 to 4.61) define a north-south trend that intersects the juncture between the Gettysburg and Newark sub-basins (Armbruster, 1987). The highest magnitude earthquakes were at Marticville in 1984 at a magnitude of 3.7 and Cacoosing Valley in 1994 at a magnitude of 4.6. The earthquakes occurred 31 mi (50 km) apart and were related to tectonic fault lines (Armbruster, 1987).

© 2007-2012 UniStar Nuclear Services, LLC. All rights reserved.
COPYRIGHT PROTECTED

The 1984 Marticville earthquake was the second-largest recorded event of the zone. Armbruster (Armbruster, 1987) suggested a seismogenic shallow fault (centered at 2.5 mi (4.0 km) depth) based on the hypocentral distribution and first motion data from several recorded earthquakes of the 1984 sequence. While not in correlation with the trend of Paleozoic structures in the epicenter area, the 1984 rupture geometry conforms to the strike of the Jurassic dikes and their associated faults. Earthquakes in the zone may have been related with the Rockhill dike in particular (which bisects LSZ and is close to the 1984 rupture area), and its related faults (Armbruster, 1987).

The January 16, 1994 Cacoosing Valley earthquake which struck the northeastern edge of the zone, is known to be the largest earthquake of the LSZ (Seeber, 1998). The Cacoosing Valley earthquake was of magnitude 4.6 and Modified Mercalli Intensity (MMI) VI-VII, The associated earthquake sequence, from 1994 to 1997, is discussed in more detail in Section 2.5.1.1.4.4.2.11. As is the case of 1984 Marticville earthquake, the 1994 Cacoosing Valley earthquake, and its aftershocks, provided seismological evidence for an active fault in the LSZ. The suggested faults, for both the 1984 and 1994 earthquakes, were based merely on seismological evidence. Geological evidence, such as surface rupture or liquefaction, has not been found in either case (Crone, 2000).

No other evidence of Quaternary faulting (e.g., paleoliquefaction) in the LSZ has been reported and it has been assigned to Class C (Crone, 2000). Crone (Crone, 2000) note that even short and shallow faults can host earthquakes as demonstrated by the unusually shallow seismicity of the LSZ. There might be other deeper geologic controls on seismicity which are reflected by the shallow faults of the LSZ (Wise, 1998). None of the EPRI study (EPRI, 1986) groups considered the LSZ as a separate seismic source zone. However, the maximum magnitudes (ranges from 5.2 to 7.2) that have been assigned by the groups to the regions in which the LSZ is situated are larger than any reported earthquakes in the LSZ. Therefore, the EPRI study (EPRI, 1986) adequately characterizes the LSZ in terms of the upper bound magnitude.

Accordingly, the Lancaster Seismic Zone is considered to be a capable source, but not a characteristic tectonic source for the BBNPP site.

2.5.1.1.4.4.2.11 Cacoosing Valley Earthquake Sequence (Class C)

The 1993 to 1997 Cacoosing Valley earthquake sequence occurred along the eastern margin of the Lancaster Seismic Zone with the main shock occurring on January 16, 1994, near Reading, Pennsylvania about 52 mi (84 km) south of the BBNPP site (Crone, 2000) (Feature 7 in Figure 2.5-188). The environment of the Cacoosing Valley consists of many preexisting structures; the Paleozoic thrust and fold belts, Mesozoic rifting which created the Atlantic Ocean, and Jurassic igneous dikes. The maximum magnitude earthquake associated with this sequence is an event of magnitude 4.6 (Crone, 2000). Forty one (41) aftershock hypocenters occurred within 1 mi (1.6 km) diameter and a depth ranging from 0 to 2 mi (0 to 3.2 km) and orientation of N43° W and 54° SW. The main shock occurred at a depth of 1 mi (1.6 km) and aftershocks occurred from that depth to the surface (Seeber, 1998). Most of the permanent damage from the earthquake triggered nontectonic deformation such as sinkholes, which are common in the karst environment (Seeber, 1998).

The main shock occurred under an abandoned quarry. In December 1992, the quarry was allowed to flood with water rapidly. Because the presence of preexisting structures enables weak planes of strain, the biggest factor in Cacoosing earthquake is the mechanical unloading of rock due to the mining. The unloading of the quarry, which then was abandoned and

© 2007-2012 UniStar Nuclear Services, LLC. All rights reserved.
COPYRIGHT PROTECTED

flooded with water, created enough strain to cause the rupture (Seeber, 1998). The zone of the rupture, obtained from the aftershock locations, matched a nodal plane with reverse and left-lateral slip (strike 135°, dip 54° SW) of a focal mechanism obtained from aftershock first motions and main shock waveforms. However, the rupture did not correlate with any of the mapped faults in the area (Seeber, 1998), and the earthquake did not rupture the ground surface.

Wheeler (Wheeler, 2006) defines the seismic event as a feature where there is not sufficient evidence to demonstrate that other faulting occurred in the Quaternary and assigns the Cacoosing Valley earthquake sequence as a Class C feature. Additional information relative to the earthquake is in Section 2.5.1.1.4.4.3.1.

This earthquake sequence is not considered to be related to a capable tectonic source.

2.5.1.1.4.4.2.12 Moodus Seismic Zone (Class C)

The Moodus Seismic Zone is located in Middlesex and New London County, Connecticut (Wheeler, 2005). The seismic zone is approximately 190 mi (306 km) northeast of the BBNPP (Feature 1 in Figure 2.5-188). The town of Moodus is located about 20 mi (32 km) southeast of Hartford, Connecticut. The area around the towns of Moodus and Haddam has been the most seismically active region in Connecticut, and the earliest records of earthquake activity in the area dates back to the second half of the 16th century (Ebel, 1982). The largest historical earthquake occurred in 1791 and had an estimated MMI in the range of VI-VIII (Ebel, 1982) (Crone, 2000). Four shallow microearthquakes occurred in the Moodus Seismic Zone in 1980's (Ebel, 1982) (Ebel, 1989). The seismic sources of the earthquakes were reviewed utilizing geological and geophysical methods (Koch, 1978) (Crone, 2000), but no causative fault has been identified (Crone, 2000). No evidence of liquefaction or paleoliquefaction has been found in the reconnaissance efforts in the Moodus area (Gelinas, 1993). Accordingly, Crone (Crone, 2000) assign the seismic zone as a Class C feature. There is no new information about the seismic zone in Wheeler's (Wheeler, 2005) compilation of possible Quaternary features of the CEUS. Information on the Moodus seismic zone was reviewed for this study, and this feature is considered to be a capable source, but not a characteristic tectonic source for the BBNPP site.

2.5.1.1.4.4.2.13 Clarendon-Linden Fault Zone (Class C)

A major north-south trending system of thrust faults forms the Clarendon-Linden fault zone. The fault zone is approximately 150 mi (241 km) from the BBNPP site (Feature 20 in Figure 2.5-188) where it extends over 62 mi (100 km) from western New York State to northern Allegany County, New York (Fletcher, 1977). According to recent works it further extends into central Allegany County, near the Pennsylvania border (Crone, 2000). The presence of a north-south striking fault was inferred from the surface geology of the area (Herrmann, 1978). Since then, the fault zone has been mapped geologically at the surface and characterized by geophysical methods such as seismic reflection within the subsurface (Crone, 2000).

The August 12, 1929 Attica earthquake, with an estimated magnitude of 5.2 (Street, 1977) and epicentral intensity of VIII, was located near the Clarendon-Linden Fault Zone. Herrmann (Herrmann, 1978) studied two other events (both with epicentral intensities VI) that occurred on January 1, 1966 and June 12, 1967 in the Attica region, and found shallow depth 1 mi to 2 mi (1.6 km to 3.2 km) for both events. The historical seismicity also shows a diffuse east-west trend that does not correlate with the north-south trend of the structure around Attica. Fault plane solutions for 1966 and 1967 events showed similar nodal planes for both events striking

© 2007-2012 UniStar Nuclear Services, LLC. All rights reserved.
COPYRIGHT PROTECTED

about 120° and 20°. The fault plane on the NNE nodal plane is parallel to the Clarendon-Linden structure (Herrmann, 1978).

There is no paleoseismological evidence of Quaternary slip on the fault zone so the zone has been assigned to Class C feature by Crone (Crone, 2000). Tuttle, (Tuttle, 2002b) concluded that the Clarendon-Linden Fault Zone has not generated large events (moment magnitude > 6) during the past 12,000 years. Based on the lack of earthquake-induced liquefaction features along the fault zone, including the area of the 1929 Attica earthquake, the fault zone is probably the source of the 1929 shock. Tuttle (Tuttle, 2002b) concluded that the Clarendon-Linden Fault Zone is capable of producing future M 5 events, and it is considered a seismic source zone by the Bechtel and Dames & Moore EPRI (1986) Groups. Information on this feature was reviewed for this study, and this feature is considered to be a capable source, but not a characteristic tectonic source for the BBNPP site.

2.5.1.1.4.4.2.14 Offset Glaciated Surfaces (Class C)

Small steeply dipping faults offset glacially smoothed rock surfaces at different locations in the northeastern U.S. including Maine, Massachusetts, New Hampshire, New York, and Vermont (Crone, 2000). The closest offset glaciated surfaces are located 75 mi (121 km) northeast of the BBNPP site (Feature 23 in Figure 2.5-188). The dominantly dip slip offsets are typically small in the range of millimeter to decimeter, with some exceptions of larger displacements up to one (1) meter. Crone (Crone, 2000) summarizes a few studies of localities in which such surfaces are located, but indicates that no systematic and comprehensive field or literature search has been done for such localities in the Northeast. Although some studies favor a tectonic origin over other processes (Oliver, 1970), frost heaving was the likely origin for the offset glaciated surfaces (Crone, 2000). In Hudson River Valley of eastern New York, Quebec, and New Brunswick, the small faults show offsets that are uniform in size over distance and are parallel to the strike of cleavage in heaved irregular sized blocks. According to Crone (Crone, 2000), tectonic origin of the small faults in the present-day stress field is unlikely because these small faults have been found in all orientations (Crone, 2000). Ratcliffe (Ratcliffe, 1982) studied Paleozoic slates, which had been summarized as also favoring frost heaving over recent tectonic activity as the origin of the examined small faults.

Crone (Crone, 2000) conclude that evidence supports frost-wedging more than any other process as the likely origin of small faults. Even by assuming a tectonic origin, these small faults do not penetrate deep downward and therefore do not have a significant effect on seismic hazard. Crone (Crone, 2000) mention that offset glaciated surfaces are Quaternary in age but classify them as Class C features based on the conclusion that the small faults with limited length and depth extent do not affect seismic hazard significantly. These small faults have been observed over a large area in 5 states and there has been no seismicity associated with them. Based on the available information and evidence, these small faults are not considered to be capable tectonic sources.

2.5.1.1.4.4.2.15 Fall Lines of Weems (Class C)

Weems (Weems, 1998) identified numerous short stream segments or fall zones with steep gradients while examining longitudinal profiles of major rivers that flow southeastward or northwestward across the Piedmont and Blue Ridge provinces of North Carolina and Virginia. The northeastern tip of the Blue Ridge fall line is located about 140 mi (225 km) southwest of the BBNPP site (Feature 26 in Figure 2.5-188). He noticed the alignment of fall zones of different streams and used the term "fall lines" for the curvilinear trend of the alignments. He defined seven fall lines that trend northeastward, paralleling the regional tectonic fabric and gravitational gradient of the Appalachian Orogeny. The fall lines tend to merge

© 2007-2012 UniStar Nuclear Services, LLC. All rights reserved.
COPYRIGHT PROTECTED

northeastward. Weems (Weems, 1998) states that "limited available evidence favors a neotectonic origin" for the fall lines and rules out climate control. Wheeler (Wheeler, 2005) argues that the identification of fall zones is subjective; therefore Weems' (Weems, 1998) arguments and conclusions depend on the choice of the fall zones. Wheeler (Wheeler, 2005) concludes that tectonic faulting is not yet demonstrated for the fall lines and assigns the fall lines to Class "C." The fall lines of Weems have not been associated with seismicity and they are not considered to be capable tectonic sources.

2.5.1.1.4.4.2.16 Everona Fault-Mountain Run Fault Zone (Class C)

The Mountain Run Fault Zone is a regional geologic and tectonic feature of central Virginia, which extends from the eastern margin of the Mesozoic Culpeper Basin near the Rappahannock River southwestward, to near Charlottesville, VA (Pavlides, 1986) (Pavlides, 1994). The 63 to 94 mi (100 to 150 km) long, northeast trending fault zone is located about 180 mi (290 km) southwest of the BBNPP site (Wheeler, 2006) (see Feature 16 in Figure 2.5-188). The Fault zone forms part of the southeast boundary of Early Mesozoic Culpeper Basin. The Everona Fault occurs in close proximity to the Mountain Run Fault Zone (about 0.6 mi (1.0 km)) and has an estimated age of Late Cenozoic (Crone, 2000) (Bobyarchick, 2007). The fault zone is a reverse fault that dips about 20° NW and truncates layers of rocks in the footwall of the Mountain Run fault zone (Bobyarchick, 2007). This small fault displaces the base of Late Tertiary or Pleistocene gravel located about 0.6 mi (1.0 km) west of the Mountain Run Fault Zone (Wheeler, 2006).

Thrust faulting along the Mountain Run Fault Zone started at the end of Ordovician, as represented by mylonite. Subsequent strike-slip movement in the fault zone related to extension and formation of the Culpeper Basin, occurred prior to Middle Mesozoic, since undeformed basaltic dikes of Jurassic age cut the Mountain Run Fault Zone rocks (Pavlides, 1994). To the northeast, two scarps occur along the fault zone: (1) Mountain Run scarp, located on the southeast side of the Mountain Run Fault Zone extends for 8 mi (13 km), and (2) Kellys Ford scarp, located on the northeast part of Mountain Run Fault Zone, is 1.2 mi (2 km) long and is the southeastern bounding fault of the Mesozoic Culpeper Basin (Pavlides, 1994). Pavlides (Pavlides, 1994) argued that rugged topography of both scarps implies Cenozoic or possibly Pleistocene age. Based on the displaced sub-unconformity saprolites overlaying a basal gravel cover layer in the area, the Everona Fault is a structure of tectonic origin involving the basement, and is not confined to the overlying surficial deposits. (Bobyarchick, 2007).

Crone (Crone, 2000) and Wheeler (Wheeler, 2006) conclude that while the faulting at Everona is likely to be of Quaternary age, no Quaternary activity has been demonstrated for the feature. They classify the feature as Class C, but mention that this feature did not have a detailed paleoseismological study to determine whether it has been a site of Quaternary earthquake. Additional investigation has been done for the North Anna Early Site Permit which shows that Mountain Run Fault Zone has not been active during the Quaternary (Bobyarchick, 2007). Information on this feature was reviewed for this study, and this feature is considered to be a capable source, but not a characteristic tectonic source for the BBNPP site.

2.5.1.1.4.4.2.17 Stafford Fault System (Class C)

The Stafford fault system approaches within 180 mi (290 km) south of the site (Feature 18 on Figure 2.5-188). The 42 mi (68 km) long fault system strikes approximately N35°E for a distance of 45 mi (72 km) along the west bank of the Potomac River in northeastern Virginia (Mixon, 1977) The Stafford Fault System consists of five northwest dipping, high-angle reverse faults and follows the inner margin of the Coastal Plain province. Four faults, the Dumfries Fault Zone, Fall Hill Fault, Hazel Run Fault, and unnamed fault, strike northeast. The fifth fault is the

© 2007-2012 UniStar Nuclear Services, LLC. All rights reserved.
COPYRIGHT PROTECTED

Brooke Fault Zone, northeast of the unnamed fault. Toward its northernmost end, the Brooke Fault Zone is named the Tank Creek Fault (Wheeler, 2005). The Stafford Fault System was originally activated in the Early Cretaceous time. The fault was reactivated at the Fall Hill Fault showing displacement in the Pliocene-Pleistocene sandy gravel, and Cretaceous strata (Mixon, 2000).

Recurrent movement has been demonstrated on the Stafford Fault System by displacements that decrease upward in the Coastal Plain (Mixon, 1977). None of the reports and maps used by Wheeler (Wheeler, 2005) documented Quaternary activity on any faults of the Stafford Fault System. The youngest movement, demonstrating Late Tertiary activity, has been documented on the Fall Hill Fault, of the Stafford Fault System, which offsets Pliocene-Pleistocene sandy gravel (Wheeler, 2005). The Stafford Fault System was assigned to Class C based on lack of evidence of Quaternary slip.

Marple (Marple, 2004) suggested a significantly longer Stafford Fault System which extends from Fredericksburg, Virginia to New York City (Marple, 2004). It was proposed as part of a northeastern extension of the East Coast Fault System, previously postulated by Marple (Marple, 2000). Existing data do not support the extended Stafford Fault System beyond its previous extent and, despite the suggested correlation of some historical earthquakes with the northern extension of the fault system by Marple (Marple, 2000), seismicity data show a poor association between earthquake epicenters and extended segment of the Stafford Fault System.

Based on the foregoing discussion, the Stafford Fault System may not be a capable tectonic source. However it was included as a source zone in the EPRI study (EPRI, 1986). The fault system has a probability of activity of 0.08 in both the Dames and Moore, and the LAW Engineering groups tectonic feature assessments. The numbers mainly reflect the low probabilities assigned by groups because of (1) poor association with seismicity and (2) lack of demonstrated Quaternary slip along the fault.

Information on this feature was reviewed for this study, and this feature is considered to be a capable source, but not a characteristic tectonic source for the BBNPP site.

2.5.1.1.4.4.3 Relevant Tectonic Features with Associated Seismicity

Within a 200 mi (322 km) radius of the BBNPP site, eight (8) Relevant Tectonic Features with Associated Seismicity (Shown on Figure 2.5-188) were identified. Descriptions follow for the eight (8) features that were evaluated as possible contributors to the seismic hazard at the BBNPP Site.

These features are labeled below with the reference numbers utilized on Figure 2.5-188 in parentheses:

1. New York-Alabama Lineament (28)
2. Hudson River Valley Trend (27)
3. Pittsburgh-Washington Lineament (30)
4. Tyrone-Mt. Union Lineament (29)
5. Bristol Block Geopotential Trends (31)
6. Reading Prong (51)

© 2007-2012 UniStar Nuclear Services, LLC. All rights reserved.
COPYRIGHT PROTECTED

7. Peekskill-Stamford Seismic Boundary (52)

8. Dillsburg microearthquake swarm (53)

2.5.1.1.4.4.3.1 New York-Alabama Lineament

The New York-Alabama Lineament (NY-AL) is a northeast trending lineament characterized by aeromagnetic mapping and regional gravity data which extends more than 1,000 mi (1,609 km) from Alabama to New York (King, 1978). The closest approach of the NY-AL is approximately 30 mi (48 km) west of the BBNPP site (Feature 28 in Figure 2.5-188, Figure 2.5-215 and Figure 2.5-217). The NY-AL in Pennsylvania has been disrupted or offset between two major features called the Tyrone-Mt. Union (TMU) lineament and the Pittsburgh-Washington (PW) lineament (Lavin, 1982). TMU and PW crustal features define the boundaries of a northwest trending feature called the Lake Erie-Maryland crustal block. A right-lateral offset of 38 mi (61 km) along TMU is indicated by disruption of NY-AL in southwestern Pennsylvania (Lavin, 1982). Earthquakes have occurred at different locations along the feature, however, their association with the feature cannot be established (EPRI, 1986). Johnston, (Johnston, 1985a) concluded that between 80% and 90% of southern Appalachian earthquakes recorded from 1981 to 1983 lie between the NY-AL and a parallel structure to the southeast called Clingman-Ocoee lineament. Johnston, (Johnston, 1985a) further conclude that the NY-AL and the Clingman-Ocoee lineament do not appear to be seismogenic but rather bound the crustal block that generates the earthquakes. Appalachian seismicity occurs beneath the decollément which separates thrusted and folded Paleozoic rocks from Precambrian basement rocks, indicating that Appalachian seismicity is not related to tectonic and geological features at the surface (Johnston, 1985b).

Kaufman (Kaufmann, 1999) inverted travel time residuals from relocated earthquakes in southeastern Tennessee to obtain the velocity structure of the local upper crust. They stated that the results do not agree with the NY-AL as a linear feature extending through southeastern Tennessee parallel to contours in gravity anomalies. The southeastern Tennessee seismicity is not constrained by major crustal features but is rather associated with low velocity regions in midcrustal depths. Joint hypocenter-velocity inverted on the eastern Tennessee seismic zone suggest a strong low-velocity zone parallel to the seismicity with a northeast trend. The southern margin of this trend coincides with the NY-AL. According to Vlahoic (Vlahoic,1998), research utilizing 3-D velocity earthquake data showed that most earthquakes were located in regions of average velocity or small velocity anomalies, rejecting the association of eastern Tennessee seismicity with low velocity regions in the crust (Vlahoic, 1998).

Information on this feature was reviewed for this study, and this feature is considered to be a capable source, but not a characteristic tectonic source for the BBNPP site.

2.5.1.1.4.4.3.2 Hudson River Valley Trend

Also known as the Hudson River Line (HRL), this feature trends north-south for about 156 mi (251 km) along the Hudson River Valley, coming as close as 120 mi (193 km) NE of the BBNPP Site (Feature 27 in Figure 2.5-188, Figure 2.5-215 and Figure 2.5-217). The feature is weakly associated with the western part of the isostatic gravity low at the New Jersey border to the southeastern edge of Adirondack gravity high. Due to large uncertainty in subsurface geometry, the actual structure of the feature is not determined (EPRI, 1986). Based on early instrumentally recorded seismicity (Yang, 1981), the feature was seismically limited. Subsequent observations of seismicity indicate that few earthquakes are located along some parts of the trend. The moderate-sized earthquakes occur only near the edges of the feature.

© 2007-2012 UniStar Nuclear Services, LLC. All rights reserved.
COPYRIGHT PROTECTED

Therefore the overall seismicity does not indicate the localization of activity along the trend. Recent earthquakes west of the Hudson River range in estimated depth from 9 to 12 mi (14 to 19 km), indicating the possibility of a deep structure, but this is not supported by the isostatic gravity data (Yang, 1981). No evidence of the recent tectonic activity has been demonstrated and based on the forgoing discussion, the seismicity is only poorly associated with the feature. One of the six (6) EPRI (1986) Groups, Woodward-Clyde, considers this to be a capable tectonic source. Information on this feature was reviewed for this study, and this feature is considered to be a capable source, but not a characteristic tectonic source for the BBNPP site.

2.5.1.1.4.4.3.3 Pittsburgh-Washington and Tyrone-Mt Union Lineament

These two major lineaments have been identified from analysis of regional gravity and magnetic patterns, LANDSAT images and geological data (Lavin, 1982). Trending NW-SE, they cross the Appalachian orogen to the vicinity of Lake Erie (EPRI, 1986). The Pittsburgh-Washington (PW) and Tyrone-Mt. Union (TMU) lineaments are expressions of deep crustal fracture zones which extend over a distance of 375 mi (604 km) across western Pennsylvania and parts of surrounding states. The PW-TMU lineaments are located approximately 115 mi (185 km) southwest of BBNPP site (Features 29 and 30 in Figure 2.5-188, Figure 2.5-215 and Figure 2.5-217) (Rodgers, 1984). The TMU and PW lineaments are parallel and form the NE and SW boundaries of the Lake Erie-Maryland crustal block respectively (Lavin, 1982). Major crustal displacements have occurred along the TMU lineament during Late Cambrian to Early Ordovician time. There is no concentration of seismicity along the TMU lineament. Evidence for displacement along PW lineament is not as strong as TMU. Concentration of seismicity has been observed near the northern end of PW lineament in northeastern Ohio but earthquake activity is not localized along the feature in general (EPRI, 1986). The PW and TMU features have been evaluated and the probability of activity for both features is very low (EPRI, 1986). Therefore, it is concluded that the PW-TMU lineament system is not considered to be a capable tectonic source.

2.5.1.1.4.4.3.4 Bristol Block Geopotential Trends

The Bristol Block is an area of magnetic and gravity lows and extends from Tennessee to Pennsylvania. It is bordered by the New York-Alabama lineament on the west, and by the Clingman-Ocoee lineament on the east (Feature 31 on Figure 2.5-188, Figure 2.5-215 and Figure 2.5-217). The northern portion of the Block is located about 80 mi (129 km) southwest of the site (EPRI, 1986). It includes a series of low gravity and magnetic anomalies associated with some earthquakes, since these anomalies extend over a large area. Small earthquakes occur within this block but not all the tectonic features within the block are associated with earthquakes. The Giles County, Virginia seismic zone, which is located within the Bristol block, has been considered separately as seismic source zone (EPRI, 1986). Even though there is associated seismicity with this feature it not considered a capable source, and it is not a characteristic tectonic source for the BBNPP site.

2.5.1.1.4.4.3.5 Reading Prong

The Reading Prong massif is a major Precambrian complex, one of several outcropping between the sedimentary rocks of the Appalachian basin and the Paleozoic metamorphic terrains of New England and the southeastern Piedmont (Wolf, 2003), with its closest approach to the site approximately 50 mi (80 km) east of the BBNPP (Feature 51 in Figure 2.5-188). Metamorphism of the Reading Prong rocks occurred during the Grenville Orogeny, approximately 1.2 billion years ago, and the area was also extensively intruded by synorogenic granites during the same Grenville event. Subsequently, between the Late Proterozoic and the Mesozoic, the rocks throughout the region suffered periodic episodes of deformation that was especially intense during the Late Permian Alleghanian Orogeny when the region was

© 2007-2012 UniStar Nuclear Services, LLC. All rights reserved.
COPYRIGHT PROTECTED

pervasively fractured during the development of imbricated thrust sheets (Wolf, 2003). The rocks of the Reading Prong are allochthonous and represent an overlapping stack of thrust sheets that have been thrust over the Paleozoic Rocks of the Great Valley to the north (Senior, 2006). The thrusting juxtaposed the Precambrian rocks in a structurally high position relative to the thick section of Lower Paleozoic rocks immediately to the west.

A schematic representation of the development of the Reading Prong nappe megasystem is depicted in Figure 2.5-214 (Drake, 1999). In Figure 2.5-214 (Item A), extensional faults related to the opening of a small ocean basin or the Iapetus Ocean formed on the margin of the Laurentian craton during the Late Proterozoic or earliest Cambrian. Continuing in Figure 2.5-214 (Item B), the shelf collapse related to the attempted subduction of Laurentia beneath the Microcontinent at the beginning of the Taconic orogeny allowed the formation of the Martinsburg foreland basin during the Middle Ordovician. Finally in Figure 2.5-214 (Item C) the closing of the small ocean basin or the Iapetus Ocean during the early Late Ordovician Taconic orogeny reactivated the extensional faults as thrust faults, forming the nappe megasystem. Subsequent thrust faulting during the Alleghanian orogeny greatly complicated the nappe megasystem. Rifting related to the opening of the Atlantic Ocean during the Late Triassic reactivated the thrust faults on the southeast as listric extensional faults. The amount, if any, of extensional movement of the other thrust faults is currently not known. This model presented by Drake (Drake, 1999) suggests three periods of movement on the same faults: extensional, contractional, and extensional. Figure 2.5-213, in a non-eroded idealized cross section, shows the close relation between the Reading Prong Province and the nappes that contain the West Chester and Avondale Massifs, as well as the Philadelphia Terrane to the SE. Continental shelf that constitutes the ramp, in which the Reading meganappe and the York terrane are thrust, is shown to the NW.

Sykes (Sykes, 2008) as a result of the observations on a catalog of 383 earthquakes in the Greater New York City - Philadelphia Area, refers that most hypocenters are concentrated in older terranes bordering the Mesozoic Newark basin (Reading, Manhattan, and Trenton prongs) and in similar rocks found at a shallow depth beneath the coastal plain from south of New York City across central New Jersey. The discussion about the seismicity of the reading prong is entirely base on his report.

As a result of Sykes (Sykes, 2008) observations, a belt of activity of about 30 km (18.6 mi) is located to the northwest of the Newark basin and includes the 1881, 1951, 1957, and 2003 shocks plus numerous smaller earthquakes; most of those events, especially those located instrumentally, are concentrated in the eastern Reading prong between the Green Pond syncline and the Mesozoic Ramapo Fault. They also think that earthquakes occur in stronger basement rocks below those younger sediments, with most computed hypocenters in that area being 5-10 km (3-5 mi), and often poorly constrained.

Other activity in the Reading Prong extends as far northwest as the westernmost outcrops of Precambrian rock. A band of high activity strikes about N 100 W and extends from the Ramapo Fault across the entire Reading prong (Sykes, 2008). The lower boundary of activity beneath the reading prong appears to dip southeasterly, maybe controlled by one or more Paleozoic imbricate thrust faults that sole into a master sub horizontal detachment fault whose depth is as great as the 12-15 km (7-9 mi) maximum depth of earthquakes beneath the Ramapo Fault (Sykes, 2008).

Information on this feature was reviewed for this study, and this feature is considered to be a capable source, but not a characteristic tectonic source for the BBNPP site.

© 2007-2012 UniStar Nuclear Services, LLC. All rights reserved.
COPYRIGHT PROTECTED

2.5.1.1.4.4.3.6 Peekskill-Stamford Seismic Boundary

Instrumental data recorded since 1971 shows that activity in the Manhattan prong cuts off abruptly along a nearly vertical, northwest-striking boundary that extends from Stamford, Connecticut, to Peekskill, New York (Feature 52 on Figure 2.5-188). The boundary is named the Peekskill-Stamford boundary (Sykes, 2008), and is considered a newly identified feature. It was possible to identify it after accurate locations and depths of earthquakes, especially those east of the Hudson River, became available with the installation of a seismic station near the New York-Connecticut border in 1971. The Peekskill-Stamford boundary coincides near its western end with the boundary between the Manhattan prong and the Hudson Highlands, and it may be considered as a ramification of the Ramapo Fault Zone. There has been no large magnitude seismicity associated with this feature, though micro seismic records indicate recent activity with defined epicenter locations. The Peekskill-Stamford boundary is incorporated into the BBNPP PSHA as part of area seismic sources that cover the Ramapo Fault Zone. The maximum magnitude considered for those areas exceeds that of any recorded events in this region.

Information on this feature was reviewed for this study, and this feature is considered to be a capable source, but not a characteristic tectonic source for the BBNPP site.

2.5.1.1.4.4.3.7 Dillsburg Microearthquake Swarm

From October 2008 (or earlier) through August 2009, an intense microearthquake swarm of over 600 felt events occurred near Dillsburg, York County, Pennsylvania (Kim, 2009). The area is located near the northern margin of the Gettysburg Mesozoic basin, approximately 80 miles (129 km) southwest of the BBNPP. This enigmatic swarm of activity was studied by Kim (2009) in 2008. Seismograph stations in the mid-Atlantic region detected and located the activity which included 23 larger shocks with magnitudes ranging from 0.8 to 2.9. Based on reports from residents, the apparent center of the seismic activity was around Old York Road and Mandy Lane in York County (Kim, 2009). In an attempt to better characterize and understand the seismic activity, a portable seismograph network was installed around the center of activity from October 24 through December 11, 2008. This network detected 49 microearthquakes distributed along an approximately 1 mile (1.5 km) long northwest-southeast linear trend along Old York Road, but only one (M 1.4) was large enough to be detected by regional permanent networks (Kim, 2009). The hypocenters for these shocks were less than 0.6 mi (1 km), with an average depth of about 1600 ft (0.5 km) (Kim, 2009). Despite their small magnitudes the earthquakes caused booming sounds and noticeable shaking but no significant damage was reported. The shallow depth corresponds roughly to the base of a thick sheet of diabase rather than a well-defined fault (Kim, 2009). The Diabase was mined in the past for iron but the focal depths are deeper than would be expected for the old mines to have a direct role in the origin of the earthquakes. Instead, it is theorized that the activity is due to a concentration of stress along the contact between the diabase and underlying sedimentary rocks due to a contrast in strength between the two different rock types under the current east northeast-west southwest horizontal compressional stress regime in the eastern U.S. (Kim, 2009). The seismic activity may be localized along this contact by the presence of a pre-existing zone of weakness (fractures) in the rock. Another contributing factor could be if there was a recent change in the level of the groundwater table in the area. The exact cause and timing of the earthquake swarm at this point is still unknown and more work needs to be done. It is also not known if more damaging earthquakes will occur in the area in the future. Because the activity is of such low magnitude, and similar swarms elsewhere in eastern North America have not culminated in large earthquakes of magnitude greater than 5 (Kim, 2009), the Dillsburg area is considered to be a capable source, but not a characteristic tectonic source for the BBNPP site.

© 2007-2012 UniStar Nuclear Services, LLC. All rights reserved.
COPYRIGHT PROTECTED

2.5.1.1.4.4.4 Relevant Tectonic Features with No Associated Seismicity

A total of 24 tectonic features have been identified with no associated seismicity.

Of these 24, six are located within the site vicinity (25 mi (40 km) radius). Tectonic structures and features closest to the BBNPP site are relatively more important because of their proximity and are discussed first. These six features and other structures listed in this subsection are shown Figure 2.5-199 (site vicinity), Figure 2.5-188, and Figure 2.5-198 (site area). Based on review of published literature and historical seismicity, there is no reported geomorphic expression, historical seismicity, or Quaternary deformation along any of the twenty four features identified below. Thus they are not considered to be a capable tectonic source for calculating the seismic hazard for BBNPP.

- Berwick Anticlinorium (Section 2.5.1.1.4.4.4.1)
  - Light Street Thrust Fault (Section 2.5.1.1.4.4.4.1.1)
  - Berwick Fault (Section 2.5.1.1.4.4.4.1.2)
- Lackawanna Synclinorium (Section 2.5.1.1.4.4.4.2)
- Anthracite Region (Section 2.5.1.1.4.4.4.3)
- Catawissa-McCauley Mountain Synclinorium (Section 2.5.1.1.4.4.4.4)
- Scranton Gravity High (Section 2.5.1.1.4.4.4.5)
- Yellow Breeches Fault Zone (Section 2.5.1.1.4.4.4.6)
- Rome Trough (Section 2.5.1.1.4.4.4.7)
- Pleasant Valley-Huntingdon Valley Fault (Section 2.5.1.1.4.4.4.8)
- Transylvania Fault Zone (Section 2.5.1.1.4.4.4.9)
- Plummers Island and Pleasant Grove Shear Zones (Section 2.5.1.1.4.4.4.10)
- Newark-Gettysburg Basin (Section 2.5.1.1.4.4.4.11)
- Hartford Basin (Section 2.5.1.1.4.4.4.12)
- Connecticut Basin (Section 2.5.1.1.4.4.4.13)
- Brandywine Fault System (Section 2.5.1.1.4.4.4.14)
- Martic Fault (Section 2.5.1.1.4.4.4.15)
- East Border Fault (Section 2.5.1.1.4.4.4.16)
- Broadtop Synclinorium (Section 2.5.1.1.4.4.4.17)
- Sweet Arrow Fault (Section 2.5.1.1.4.4.4.18)
- Chestnut Ridge Anticline (Section 2.5.1.1.4.4.4.19)
- Philadelphia Structural Block (Section 2.5.1.1.4.4.4.20)

© 2007-2012 UniStar Nuclear Services, LLC. All rights reserved.
COPYRIGHT PROTECTED

- Potomac and Westminster Terranes including the Pleasant Grove Shear Zone (Section 2.5.1.1.4.4.4.21)
- Baltimore Gneiss Terrane (Section 2.5.1.1.4.4.4.22)

2.5.1.1.4.4.4.1 Berwick Anticlinorium

The principal bedrock structure within the site area is the Berwick Anticlinorium (also referred to as the Montour Anticline (Pohn, 2000)), which has been described (Inners, 1978) as "a moderately complex, first order fold which trends in a northeast-southwest direction". The bedrock map and section of the Berwick Quadrangle (Inners, 1978) shows the formations at the BBNPP site area to consist of Silurian, Devonian, and Carboniferous rocks that have been gently folded, with limited faulting (Figure 2.5-193 and 2.5-194). The BBNPP site is situated on the northern limb of the fold, with beds that are dipping between 10 and 20 degrees to the north-northwest. Two faults have been mapped in the vicinity: the Light Street fault located on the northern limb of the fold, and the Berwick fault, inferred to be on the southern limb of the fold. The northeast ends of both faults lie within the site area, but do not directly underlie the site. Both faults are considered folded faults, therefore there is limited chance for these to be reactivated in the contemporary stress regime.

Inners (1978) prepared a lithostratigraphic column along an almost 9 mi (14.5 km) long stretch of the Berwick Quadrangle that intersects much of the BBNPP site area. When these stratigraphic columns are compiled into a cross section (Figure 2.5-194), they collectively provide an almost 9 mi (14.5 km) long, nearly continuous exposure of Silurian, Devonian, and Mississippian formations. Inners (1978) stratigraphic analysis indicates that these Paleozoic formations dip to the north on the north side of the Susquehanna River and dip to the south on the south side. Erosional processes of the Berwick Anticlinorium have produced two mountain ridges, Lee Mountain to the north of the site and Nescopeck Mountain to the south, and have produced similar topography on each mountain (Inners, 1978). The Light Street and Berwick faults are also mapped on this cross section, as seen in Figure 2.5-194. The apparent structural relief of the Berwick Anticlinorium is approximately 12,000 ft (3,658 m) with a wavelength of about 8.2 mi (13.2 km) (Inners, 1978). Quaternary deposits overlying the site show no signs of faulting or folding.

2.5.1.1.4.4.4.1.1 Light Street Thrust Fault

Light Street Thrust Fault is the wedge fault located approximately 2 mi (3.2 km) west of the BBNPP site (Inners, 1978) and is the closest feature to the BBNPP site. The fault was active during the Early Devonian period. Based on studies, the fault dips to the south, at a small angle of 10 to 30 degrees to stratigraphic bedding (Inners, 1978). The strike of the fault has a northeast-southwest orientation. The fault is located in the north side of the Berwick anticlinorium and extends for about 20 mi (32 km) west of Berwick. The fault overlaps the Old Port and Keyser formations. Seismic reflection profiles indicate that the fault originated during the Triassic (Inners, 1978). Based on review of published literature and historical seismicity, there is no reported geomorphic expression, historical seismicity, or Quaternary deformation along the Light Street Thrust Fault. Thus, this feature is not considered to be a capable tectonic source.

2.5.1.1.4.4.4.1.2 Berwick Fault

In conjunction with the Light Street Fault as discussed above, the Berwick Fault is mapped as inferred and is based on limited surface data and a water well log drilled at the Berwick Lumber and Supply Company at 329 West Second Street in Berwick, PA (Inners, 1978). The BBNPP site investigators were unable to locate this well and it was possibly abandoned prior

© 2007-2012 UniStar Nuclear Services, LLC. All rights reserved.
COPYRIGHT PROTECTED

to the site investigation. The inferred Berwick Fault lies within the site area and comes to within approximately 3.5 mi (5.6 km) of the BBNPP site. The exact length of the Berwick Fault is not completely mapped and is believed to be a south-dipping reverse fault on the south flank of the BBNPP (Inners, 1978).

Inners (Inners, 1978) also states that the Berwick fault extends east-northeastward into an exposed third order anticline in the Marcellus-Mahantango interval. Inners (Inners, 1978) attributes the presence of the Berwick Fault to the folding and faulting actions that occurred at the site area during the Alleghanian Orogeny, approximately 250 million years ago. There is no pre-EPRI or post-EPRI study (EPRI, 1986) that associates seismicity with this feature, nor is there any geomorphic evidence of Quaternary deformation. The Berwick fault is not considered to be a capable tectonic source.

A review and interpretation of aerial photography and digital elevation models of the BBNPP site area identified few discontinuous north to northeast-striking lineaments. None of these lineaments were interpreted as fault-related, nor coincident with the Light Street Fault, Berwick Fault, or the other previously inferred Paleozoic structures mapped by Inners (Inners, 1978) and Berg (Berg, 1980). A review of regional geologic sections suggest that the features postulated by Inners (Inners, 1978), if present, are not moderate or prominent structures, and do not deform Quaternary strata. In summary, on the basis of regional and site geologic and geomorphic data, there are no known faults within the site area that pose a structural hazard to the site, including the poorly constrained Light Street and Berwick faults that lie within the southwestern section of the 5 mi (8 km) radius of the site.

2.5.1.1.4.4.4.2 Lackawanna Synclinorium

Lackawanna Synclinorium is a first order fold syncline and its western extents are mapped within the 5 mi (8 km) radius north-northeast of the BBNPP site area (Figure 2.5-188 and 2.5-198) (Inners, 1978) as it trends southwest-northeast. The Lackawanna Synclinorium is a 68 mi (110 km) long structural trough in the Appalachian foreland of northeastern Pennsylvania with a maximum width of 9 mi (15 km) (Harrison, 2006).

There are numerous unnamed faults within the Lackawanna Synclinorium. These are folded faults and as result there is limited chance for these to be reactivated in the contemporary stress regime.

In map view (Figure 2.5-199), its hinge displays a concave-to-the-foreland (concave towards the west) curve. Explanation of its map-view curvature with respect to the regional structural grain has led to multiple tectonic models for the synclinorium and the Pennsylvania salient (Harrison, 2006). The entire synclinorium was thought to be an Alleghanian thin-skinned contractional structure that formed similarly to the fold trains of the central Appalachian Valley and Ridge province (Harrison, 2004). Interpretation of seismic reflection data across the structure, however, suggests that the synclinorium formed primarily by the removal of salt. The trend of the central and northern synclinorium reflects the location of the collapse of the Upper Silurian Salina salt and the north-northwest trend does not represent a significant east-west shortening event (Harrison, 2006; Frey, 1973). In the southern synclinorium, the structure translated northwestward over a thrust ramp joining detachments in the Cambrian Waynesboro Formation and the Salina Group (Harrison, 2004).

Thus, only the southern part of the basin was affected by significant layer parallel shortening (LPS) and folding. The dominant approximately 75-degree LPS fabrics (folds, faults, cleavage) in the synclinorium that parallel the regional folds of the Valley and Ridge, formed in the

© 2007-2012 UniStar Nuclear Services, LLC. All rights reserved.
COPYRIGHT PROTECTED

hanging-wall strata above the Pottchunk fault, a basin-wide Alleghanian detachment (Harrison, 2006). Crosscutting relationships of LPS structures from within the synclinorium indicate that the horizontal component of shortening rotated approximately 45 degrees clockwise through time suggesting that movement along the Salina Group detachment followed movement along the Pottchunk fault (Harrison, 2006). After movement along the Pottchunk fault, collapse of the post-Salina overburden formed much the synclinorium. Thus, the Lackawanna synclinorium is a structure affected by pulses of deformation and overburden collapse (Harrison, 2006).

In addition to the flexural-slip mechanisms responsible for many of the folds in the mapped area of Figure 2.5-199, flexural-flow folding was likely another strong component to their formation (Inners, 1978). Inners (Inners, 1978) identifies several features of flexural-slip folds evident in the Berwick Quadrangle including the common occurrence of slickenlines on bedding surfaces and maintenance of approximately the same bedding thickness across the folds. Flexural-flow folding characteristics, within any structure, include prominent cleavage in argillaceous rocks and thickening of beds within the hinges.

There is no pre-EPRI or post-EPRI study (EPRI, 1986) seismicity associated with the features (Inners, 1978); the hypothetical features are not aligned or associated with gravity and magnetic anomalies, nor is there data to indicate that the features proposed by Inners (Inners, 1978) are capable tectonic sources.

2.5.1.1.4.4.4.3 Anthracite Region

The Anthracite region, located on the diminishing, east-plunging, first-order folds in eastern Pennsylvania, is the most faulted area of the Appalachian Ridge and Valley province (Faill, 1999a). It is composed of four main fields, the Northern, Eastern Middle, Western Middle and Southern Anthracite Fields (Hornbergher, 2004). The Northern Field is situated in the Lackawana Synclinorium described above, and the other three fields make up the Anthracite Upland Section south of the BBNPP Site. According to Wood (1986 in Hornberger, 2004): "Each coal field of the Anthracite Region is a complexly folded and faulted synclinorium, with structural trends between N55°E and N85°E…. The Southern field is the most highly deformed, with several highly faulted, closely spaced synclinal basins. Deformation is most complex toward the southeast, where it is characterized by hundreds of thrust, reverse, tear and bedding plane faults and tightly compressed, commonly overturned folds." The Southern field is structurally complex with large structural features such as the Minersville Synclinorium, the New Bloomfield Anticlinorium and the Broad Mountain Anticlinorium, as well as individual anticlines, synclines and fault complexes within these three major structural features (Hornberger, 2004) (Figure 2.5-199). The dominant faults consist of thrust faults, as part of the base décollement. The thrust faults are dominantly located in the cores of the anticlines. These faults tend to be low angle dipping and transect the bedding planes along the northwest limbs of the folds (Faill 1999a). Other faults associated with these structures are steeply dipping and are parallel to the stratigraphic beds located in the southeast limbs of the anticlines. The highly faulted zone of the Western Middle and Southern fields are as close as 15 mi (24 km) south of the site. However, these fault systems were last active during the post-Carboniferous period (Allegheny Orogeny) and are no longer a seismic hazard. Based on a review of published literature and historical seismicity, there is no reported geomorphic expression, historical seismicity, or Quaternary deformation along the Anthracite region. Although this feature is not considered to be a capable seismic source, there have been reported earthquake epicenters associated with mining activities (collapse, blasting).

© 2007-2012 UniStar Nuclear Services, LLC. All rights reserved.
COPYRIGHT PROTECTED

2.5.1.1.4.4.4.4 Catawissa-McCauley Mountain Synclinorium

The only mention to this structure is in Inners (Inners, 1978) when he refers to the two first order Alleghanian Orogeny related folds structures (Lackawanna Synclinorium and Catawissa-McCauley Mountain Synclinorium) shown Figure 2.5-198 and 2.54-199. The mapped axes of both first-order folds are conjectural when the exact location cannot be determined due to the lack of outcrop in the glaciated valleys (Inners, 1978).

Inners (Inners, 1978) identified in the extreme southeast corner of the Berwick Quadrangle, a synclinal axis that can be mapped in the Mauch Chunk Formation along Nescopeck Creek that may represent the main axis of the Catawissa-McCauley Mountain Synclinorium. Alternatively, Inners (Inners, 1978) also considers that this axis may define only one of several en echelon second-order synclines that form the synclinorium in this area. There is no historic or recorded earthquake epicenters associated with this structure. The Catawissa-McCauley Mountain Synclinorium is not considered to be a capable tectonic source.

2.5.1.1.4.4.4.5 Scranton Gravity High

The Scranton Gravity High (SGH) is located underneath the BBNPP site (Feature 34 in Figure 2.5-216, and in Figure 2.5-23). The SGH extends about 250 mi (402 km) from Albany, New York, to Harrisburg, Pennsylvania. The large gravity anomaly covers portions of the Appalachian Plateaus and Ridge and Valley Provinces (Hawman, 1992). There is no apparent relationship to the seismicity in the area of the SGH, which is sparse. Earthquakes occur southeast of SGH in southeastern Pennsylvania and Western New Jersey, but there is no localization of events along the feature (EPRI, 1986). Therefore, the SGH is not considered to be a capable tectonic source.

2.5.1.1.4.4.4.6 Yellow Breeches Fault Zone

The northeast-striking, southeast-dipping Yellow Breeches Fault is located within the northeastern portion of the Ridge and Valley Physiographic Province in southeastern Pennsylvania (Figure 2.5-188). The fault is a very low angle (sub-horizontal) thrust that divides the Martinsburg/Hamburg foreland segment, separating the Cumberland Valley stratigraphic sequence to the north from the Lebanon Valley stratigraphic sequence to the south of the décollement (Root, 1977b). However, a lithologic comparison can be made between greenschist grade Hamburg succession rocks carried on the Yellow Breeches fault and allochthonous units of lower grade north of that fault emplaced within the main outcrop belt of the Martinsburg foreland basin (Ganis, 2005).

This décollement represents an upper-level detachment above a deeper décollement about 5 mi (8 km) deep (Faill, 1999a). Rock slices of the Lebanon Valley sequence make up the Yellow Breeches thrust plate that is part of the inverted limb of a regional nappe (the southernmost extension of the Reading Prong nappe megasystem) emplaced upon the South Mountain anticlinorium (Root, 1977b). However, Yellow Breeches thrusting is much younger than nappe development and only slightly younger than the South Mountain deformation having formed during the Late Alleghanian orogeny (Root, 1977b). The Yellow Breeches fault zone is not considered a capable tectonic source. Based on published literature, no seismicity is attributed to the Yellow Breeches fault zone and published literature does not indicate that it offsets Late Cenozoic deposits or exhibits geomorphic expression indicative of Quaternary deformation. Therefore, this Paleozoic fault is not considered to be a capable tectonic source (Wheeler, 2006).

© 2007-2012 UniStar Nuclear Services, LLC. All rights reserved.
COPYRIGHT PROTECTED

2.5.1.1.4.4.4.7 Rome Trough

The Rome Trough is a Cambrian extensional graben system that extends from northern Tennessee, northeastward through Kentucky, West Virginia, and into western Pennsylvania (Figure 2.5-216). This northeast-trending graben, which underlies the Appalachian Plateau Province, is mainly characterized by normal faults of Early Paleozoic age. Conversely, complex folds and thrust faults of Late Paleozoic age characterize the eastern Appalachian Plateau (Kulander, 2005). Kulander (Kulander, 2005) studied data from seismic lines across the Rome trough in West Virginia, western Maryland, and southwestern Pennsylvania. Basement-involved thrust faults have been reported in some parts of the Rome trough and attributed it to regional compression dating 0.8-1.0 billion years ago. Major normal movements along the Rome trough boundary faults occurred in the Early to Middle Ordovician, and no other movement seems to have occurred since then (Kulander, 2005). However, the details of basement structure in western Pennsylvania and interpretations of the faults accompanying the Rome trough are based on limited data (Ryder, 1992). The association of this feature with seismicity is also limited. Therefore, the Rome trough is not considered to be a capable tectonic source.

2.5.1.1.4.4.4.8 Pleasant Valley-Huntingdon Valley Fault

Pleasant Valley-Huntingdon Valley Fault is the eastward continuation of the Cream Valley fault. See Feature 12 in Figure 2.5-188. The fault separates the Baltimore Gneiss, overlain by the Chickies and Ledger Formation on the north, from Wissahickon Formation schist on the south. The fault was active during the post Ordovician period and located 120 mi (193 km) south of the site (Crawford, 1999). Major subvertical northeast striking faults, including the Brandywine Manor fault, the Cream Valley fault, the Pleasant Valley-Huntingdon Valley Fault, and the Rosemont fault, intersect through the blocks containing Grenville-age gneisses and juxtaposed them against younger rocks. The Pleasant Valley-Huntingdon Valley Fault borders the Piedmont Upland Section, Piedmont Lowland Section, and Gettysburg-Newark Lowland Section. Based on review of published literature and historical seismicity, there is no reported geomorphic expression, historical seismicity, or Quaternary deformation along the Huntingdon Valley Fault. Therefore, this feature is not considered to be a capable tectonic source.

2.5.1.1.4.4.4.9 Transylvania Fault Zone

The Transylvania Fault Zone, near the latitude 40° N, extends from the Early Mesozoic Gettysburg Basin (Feature 17 in Figure 2.5-188), in Pennsylvania, westward into Ohio and striking at roughly 270 degrees (Dodson, 2008). The fault system is located approximately 170 mi (274 km) west of the BBNPP site (Berg, 1980). The fault zone is mapped as large subvertical east-west trending faults extending through the Blue Ridge, Great Valley and Ridge and Valley provinces. Through the Appalachian Plateau, the fault zones are detected through subsurface records and geophysical studies. Root (Root, 1977a) proposed a zone of east-west trending faults which extend from the eastern margin of the Blue Ridge to the Allegheny front near latitude 40° N, for about 75 mi (121 km). The fault zone transects strata nearly across the entire length of Pennsylvania. In the eastern part of the region two faults, 9 mi (14 km) apart, have been previously mapped for about 23 mi (37 km). These are Shippensburg and Carbaugh-Marsh Creek faults which extend east-west in parallel. Root (Root, 1977a) describe the following faults in the zone: Sideling Hill, Breezewood, Everett gap, and Wills Mountain faults. Root (Root, 1977a) do not consider the fault zone as a major transcurrent fault because the apparent strike-slip movement associated with the fault is no more than 2.5 mi (4 km). Root (Root, 1977a) conclude that the Transylvania fault zone is a fundamental fracture, which possibly extends through the continental plate. The fault system originated in the Precambrian, and was reactivated during the Taconic Orogeny in the Middle Ordovician and

© 2007-2012 UniStar Nuclear Services, LLC. All rights reserved.
COPYRIGHT PROTECTED

again in the Carboniferous Period during the Alleghanian Orogeny. The Transylvania fault also reactivated in the Early Jurassic (Root, 1977a). This fault zone has been included by EPRI (EPRI, 1986) study teams as a tectonic feature but has not been associated with seismicity. Based on review of published literature and historical seismicity, there is no reported geomorphic expression, historical seismicity, or Quaternary deformation along the Transylvania fault zone. Therefore, this feature is not considered to be a capable tectonic source.

2.5.1.1.4.4.4.10 Plummers Island and Pleasant Grove Shear Zones

The Plummers Island Shear Zone and Pleasant Grove Shear Zone are thrust faults that include the Plummers Island fault, Pleasant Grove fault, Hyattstown fault and Martic fault (Kunk, 2004). The faults strike in a northeast-southwest trend with a high angle westerly dipping orientation and are located in the south central Appalachians (Feature 13 in Figure 2.5-188). The fault zones are located 175 mi (282 km) south of the BBNPP site (Kunk, 2004). The faults were active during the Acadian Orogeny in the Early Devonian period and reactivated in the Carboniferous period during the Alleghanian Orogeny, and are part of the south central Appalachians. Based on review of published literature and historical seismicity, there is no reported geomorphic expression, historical seismicity, or Quaternary deformation along the Plummers Island shear zone or the Pleasant Grove shear zone. Therefore, these features are not considered to be capable tectonic sources (Wheeler, 2006).

2.5.1.1.4.4.4.11 Newark-Gettysburg Basin

The Newark-Gettysburg (NG) Basin extends from southeast New York through New Jersey to southern Pennsylvania (Faill, 1973), and is located south approximately 60 mi (97 km) of the BBNPP site (Figure 2.5-208). The NG Basin, one of the several Triassic basins in eastern North America, has been developed either by downthrown block and subsequent sediment deposition from the northwest and southeast direction or as fault-troughs or grabens with faulting and sedimentation occurring at the same time. The Newark and Gettysburg basins are two separate basins that formed the NG Basin. These two basins along with Culpeper Basin and Barboursville Basin (both in Virginia) are the remnants of a larger Triassic feature called the Birdsboro Basin (Faill, 2004). Faults and folds have subsequently tilted and deformed the Birdsboro Basin in the Early Jurassic with a dominant northeast striking structural trend within the basin (Faill, 2004). Border faults, normal faulting and wrench faulting are associated with the NG basin. Significant examples are the Ramapo Fault system in northern New Jersey which bounds the northwest portion of the Newark Basin, and the Furlong Fault, Hopewell Fault and Chalfont Fault which were generated by wrench faulting within the NG basin (Root, 1999).

The Woodward-Clyde Group (EPRI, 1986) concluded that the Newark Basin is seismically limited but the basin may be responsible for the localization of events in the region. Seismicity occurs near the edges of the basin with two notable concentrations of earthquakes. One concentration is near the transition from the Newark Basin into the Gettysburg Basin, which corresponds to the Lancaster Seismic Zone (LSZ) south of the narrowest section of the NG Basin (Armbruster, 1987). The other concentration occurs near the Maryland-West Virginia border, outside the southern edge of the basin. Most well-located epicenters in the LSZ are located just outside the NG Basin (Scharnberger, 2006; EPRI, 1986). A detailed description for the LSZ is provided in Section 2.5.1.1.4.4.2.10.

2.5.1.1.4.4.4.12 Hartford Basin

The Hartford Basin of Connecticut and southern Massachusetts (Figure 2.5-208), along with the much smaller Deerfield and Northfield Basins, are Sub-basins of the larger Connecticut Valley Basin (Resor, 2005; Schlische, 2003). The Hartford Basins' gross structure is a half graben with a master west dipping normal fault on the eastern border and a smaller east-dipping fault

© 2007-2012 UniStar Nuclear Services, LLC. All rights reserved.
COPYRIGHT PROTECTED

on the western border (Resor, 2005). The East Border fault therefore has the larger net vertical slip (Rodgers, 1985) and is located approximately 180 mi (290 km) east of the BBNPP site (Figure 2.5-208) and extends about 130 mi (209 km) from near Bellow Falls, New Hampshire to New Haven, Connecticut (Hibbard, 2006) and further to Long Island Sound. The West Border Fault has much less net slip and is therefore not as significant as the East Border Fault. The East Border Fault strikes generally north and dips west with a listric geometry, and changes in strike to north-northeast from central Connecticut towards the south (Wheeler, 2005). Sedimentation continued until the Early Jurassic period during which the basin also experienced intrusive volcanic activity (Bennington, 2006). Core data from Thompson (1999 in Wheeler, 2005) indicated that stratigraphy at Farm River marsh, nearly 1 mi (1.6 km) inland from the Long Island Sound, showed the downthrown block of the southeastern portion of the marsh with respect to the northwestern portion coincided spatially with the buried trace of the fault. This led to the conclusion that the fault has been active since 2000 years ago having been reactivated as a reverse fault in the present day compressional field (Wheeler, 2005).

Wheeler (Wheeler, 2005) argues that no fault surface has been reported within the overlying marsh deposits. In addition, the downthrown block shows the displacement across a wide slope as opposed to a sharp offset on a fault plane. The area also lacks evidence for sudden movements that would imply tectonic faulting. Wheeler (Wheeler, 2005) concludes that evidence of faulting has not been reported in Quaternary sediments of the Farm River marsh and accordingly classifies the East Border fault as Class C. Seismicity has not been associated with the East Border fault. Therefore, it is concluded that the Hartford Basin is not a capable tectonic source.

2.5.1.1.4.4.4.13 Connecticut Basin

The Connecticut Basin also known as the Connecticut Valley Basin is the largest onshore Mesozoic-age graben in New England (Wheeler, 2005). From Long Island Sound in the south, the basin crosses through central Connecticut and Massachusetts. The basin is located approximately 175 mi (282 km) northeast of the site (Figure 2.5-216 and 2.5-218).This larger basin has sometimes been confused with the smaller Hartford Basin (Wheeler, 2005), which along with the Deerfield and Northfield Sub-basins, comprise the whole of what is known as the Connecticut Valley Basin (Resor and deBoer, 2005). This confusion likely comes from the fact that the Hartford Basin makes up the vast majority of the Connecticut Valley Basin and that both basins were formed by normal movement on the East Border Fault (Section 2.5.1.1.4.4.4.16). Rocks deposited in the basin are of the Newark Super Group sedimentary series (Schlische, 2003) and sedimentation continued until the Early Jurassic period during which the basin also experienced intrusive volcanic activity (Bennington, 2006).

The Connecticut Basin has been evaluated by Rondout Associates Inc. (RAI) tectonic team (EPRI, 1986). RAI considered the basin as seismically active, because they defined the Connecticut Basin feature as containing the Moodus Seismic Zone (Section 2.5.1.1.4.4.5.4). Dames and Moore also included a Connecticut Basin in their tectonic features and seismic zones (EPRI, 1986) but made it a much larger feature extending from New Hampshire to Virginia encompassing the whole of the East Border Fault and other, separate Mesozoic rift basins further south such as the Norfolk and Taylorsville basins (Figure 2.5-208) (Section 2.5.1.1.4.4.5.2). They, however, only have the mapped portions of the basin south of Connecticut as inferred (EPRI, 1986) and no other assessments have concluded such a large continuous basin. However, Law Engineering included a seismic source zone `Buried East Coast Mesozoic Basins' that encompasses the same general area as the inferred portion of Dames and Moore's “Connecticut Basin” (Section 2.5.1.1.4.4.5.3). Weston Geophysical also

© 2007-2012 UniStar Nuclear Services, LLC. All rights reserved.
COPYRIGHT PROTECTED

includes a similar shaped zone of Mesozoic Basins as Law Engineering in their tectonic interpretation (Section 2.5.1.1.4.4.5.5). So while these Mesozoic Basins are legitimate tectonic features, the much larger representation of the `Connecticut Basin' by Dames and Moore is misleading in relation to the geologically accepted boundaries of the Connecticut Basin.

Even though seismicity has been associated with the Connecticut Basin, Quaternary activity has not been demonstrated for the structures within the basin or for its boundary faults. Therefore it is concluded that the Connecticut Basin is not a capable tectonic source.

2.5.1.1.4.4.4.14 Brandywine Fault System

The Brandywine Fault System is located approximately 180 mi (290 km) south of the site and north of the Potomac River (Feature 19 in Figure 2.5-188). The 12 to 30 mi (19 to 48 km) long Brandywine fault system consists of a series of en echelon high angle reverse fault segments with associated flexing of the overlying Coastal Plain sedimentary strata (Cumbest, 2000). The fault system trends north-northeast with displacements ranging from a few feet to 250 ft (76 m). The Brandywine Fault System consists of the Cheltenham Fault and Danville Fault (Cumbest, 2000). The Brandywine Fault System was active in the Cretaceous and Middle Eocene and Middle Miocene (Mixon, 1977).

The Brandywine Fault System is located 6 mi to 12 mi (10 km to 19 km) east of the Stafford Fault Zone and strikes roughly parallel to it. Wheeler (Wheeler, 2005) considers Skinkers Neck and Brandywine as a single fault zone, southeast of Stafford Fault System. Compared to Stafford Fault System, the Skinkers Neck-Brandywine Fault Zone is less known and its boundary is shown by dashed line (inferred) in the map of Mixon (2000). The last activity of the fault was during the Miocene. There is no seismicity associated and no evidence of Quaternary activity with the fault has been demonstrated. Therefore, the Brandywine Fault System is not considered as a capable tectonic source (Wheeler 2005).

2.5.1.1.4.4.4.15 Martic Fault

The Frederick Valley lies near the western edge of the Piedmont physiographic province of Maryland, with the Martic fault being the eastern boundary of this valley (Southworth, 2002). This fault is located 95 mi (153 km) SSW of the BBNPP site (Feature 11 in Figure 2.5-188).

This fault juxtaposes low-grade metamorphic phyllites against Early Paleozoic carbonates. Little difference on topographic relief exists between the Early Paleozoic carbonates of the Frederick Valley and the rocks of the Triassic basins because much of the Triassic bedrock is composed of detrital limestone and dolomite whose clasts are Early Paleozoic in age (Southworth, 2002).

The Martic fault is the structurally lowest fault in a stack of imbricate thrust sheets of the Westminster terrane that were probably active in all orogenies of the Paleozoic era (Southworth, 2002). The other two structurally higher thrusts to the east are the Barnesville-Monrovia, and the Hyattstown thrust faults.

The Martic thrust fault cuts up section westward, placing Ijamsville Phyllite on rocks of the Urbana, Araby, and Frederick Formations; the fault is folded with the footwall rocks. Within the thrust sheet there are early (now folded) and late (cut existing faults) thrust faults, reactivated thrust faults, and numerous small intraformational faults of limited displacement (Southworth, 2002). Rocks of the Ijamsville Phyllite of the Martic thrust sheet have a composite foliation that consists of a transposition foliation that is overprinted with phyllonitic foliation, and several generations of cleavage. Vein quartz that impregnates the rock has been sheared, transposed,

© 2007-2012 UniStar Nuclear Services, LLC. All rights reserved.
COPYRIGHT PROTECTED

and folded into steep isoclines. These steep F1 folds were deformed by westward-verging, inclined F2 folds that plunge steep to gentle in all directions.

There is no seismicity associated with this fault, and it is considered to be non-capable under the present stress regime.

2.5.1.1.4.4.4.16 East Border Fault

The East Border Fault is the eastern limit of the Hartford Basin 180 mi (290 km) east of the BBNPP site (Feature 22 in Figure 2.5-188). The East Border Fault is generally north striking, western dipping normal fault with a listric subsurface geometry (Wheeler, 2005). The East Border Fault of the Connecticut Valley Basin, along with the Deep River Basin in South Carolina, are the only exposed Mesozoic rift basins (half-grabens) that do not have easterly dipping western border faults (Benson, 1992). Southward from central Connecticut the fault curves to strike north-northeast and, farther south, northeast. As the fault crosses the shore of Long Island Sound, it curves more to strike east-northeast before returning to a northeast strike under the Sound (Rodgers, 1985).

Where the fault traces across Long Island, Thompson (2000 and 2001 in Wheeler, 2005) reconstructed the past geographic distributions of high marsh (salt marsh; infrequently flooded by salt water) and low marsh (flooded by tides), relative sea-level rise curves, and paleohistories of vertical offsets of dated, originally horizontal peats at the Farm River Marsh on Long Island. The stratigraphy of the southeastern part of the marsh, which coincides spatially with the buried trace of the East Border fault, is dominated by low marsh and mudflat deposits, while the stratigraphy of the northwestern marsh is predominantly high marsh deposits. The authors indicate that this means that the sea level rose in the southern part of the Farm River marsh more rapidly than in the northwestern part of the marsh implying that the southeastern part of the marsh was downthrown on the East Border Fault with respect to the northwestern marsh.

Several questions remain to be answered with respect to the Quaternary activity of this fault (Wheeler, 2005). Among these is mainly that there is no reported surface faulting within the till or the overlying marsh deposits, an erosive event as a possible alternative explanation for parts of the transition, and lack of evidence that individual increments of the downthrowing occurred suddenly, within the seconds to minutes that an earthquake rupture lasts, or at least more suddenly than could be produced by any alternative, non faulting mechanism (Obermeier, 2009) (Wheeler, 2005).

These questions and possible alternative explanations mean that faulting has not been demonstrated in the Quaternary sediments of the Farm River marsh, and classified the East Border fault as a Class C feature.

2.5.1.1.4.4.4.17 Broadtop Synclinorium

The Broad Top synclinorium is a large regional synclinorium which extends from central Pennsylvania to western Virginia. It is the most western of the synclinoria in the Valley and Ridge province (Jacobeen, 1974) and is located 100 mi (161 km) WSW of the BBNPP site on its closest position (Feature 48 in Figure 2.5-188). The Broad Top Synclinorium is northeast-southwest trending first order fold with a southwest plunge (McElroy, 2007). Although the synclinorium is broken into a series of folded and faulted structures, its basic structural style reflects both basement movement and thin-skinned tectonics.

© 2007-2012 UniStar Nuclear Services, LLC. All rights reserved.
COPYRIGHT PROTECTED

More than 125 mi of seismic surveys, 22 wells, and surface maps were analyzed by Jacobeen (Jacobeen, 1974) to determine the precise relation of basement to thin-skinned tectonics. This relation, as interpreted, indicates that Taconic and older, tension-induced features have a pronounced effect on the localization and genesis of the ramping of décollements. This ramping, in turn, produces many of the large, prominent, first-order structural features in both the Valley and Ridge, and the Plateau provinces of the Appalachian basin, such as the Allegheny Front. The décollement ramping also induces formation of smaller, second-order features and other flexures and faults within the Broad Top synclinorium.

Folds in the Broad Top synclinorium strike in an average N30°E direction and have been mapped as long, continuous features, extending over 100 mi (161 km) (Jacobeen, 1974). Along the strike of the structures, outcrops indicate an en echelon structural trend of anticlinal and synclinal axes that are roughly parallel and doubly plunging as their axes rise and fall in a series of domes and saddles (Jacobeen, 1974). The southwest plunge of the Broad Top Synclinorium results in exposure of the Late Devonian Brallier Formation along its axis. Dips are steeper on its southeast flank and there are smaller folds contained within it while overturning of fold limbs occurs north and west of Garret Knob (McElroy, 2007).

The structure of the Broad Top synclinorium as seen today represents the interaction between Taconic block faulting and Late Paleozoic thrusting. Such Late Paleozoic thrusting, which dominates the structure in the Appalachians, is believed to be modified and localized by older structures in other areas.

There is no seismicity associated with this fault, and it is considered to be non-capable under the present stress regime.

2.5.1.1.4.4.4.18 Sweet Arrow Fault

The Sweet Arrow fault, located between Swatara Gap and New Ringgold, in east-central Pennsylvania, is located 50 miles (80 km) to the southeast of the site (Feature 49 on Figure 2.5-188). It is a thrust fault separating the overturned rocks to the north from the upright rocks to the south (Wood, 1961), and has a dip of 40° to 70° to the south and a throw that can reach several thousand feet. It was recognized by Wood (Wood, 1961) from the thinning and offsetting of stratigraphic units and the truncation of structural features in the area. The fault cuts through rocks of Silurian and Devonian ages, and is buried in many places beneath heavy talus slopes. Wood (Wood, 1961) never mentioned the cross-cutting of younger rocks, including rocks of Quaternary age, but the sense of the motion on the fault (thrust from the southeast) is consistent with the stress regime that existed during the Alleghanian Orogeny, when other similar faults were active. There is no seismicity associated with this fault, and it is considered to be non-capable under the present stress regime.

2.5.1.1.4.4.4.19 Chestnut Ridge Anticline

The Chestnut Ridge anticline is a major regional feature of the Appalachian fold belt (Feature 50 on Figure 2.5-188). Its western limb forms a 100 mi-long (185 km) segment of a physiographic break called the Intra-Plateau Front (Gwinn, 1964). The Front separates the Allegheny Mountains (Figure 2.5-183), with their high-relief open folds (1000 ft [305 m] of relief), from the lowlands and low folds of the Pittsburgh Plateau to the west (Shumaker, 2002).

The original widely accepted structural model for formation of folds in the outer central Appalachian foreland during the Alleghenian Orogeny was partially based on the geologic structure of the North Summit field, a natural gas field on the structural culmination of the

© 2007-2012 UniStar Nuclear Services, LLC. All rights reserved.
COPYRIGHT PROTECTED

long and narrow Chestnut Ridge anticline. The model includes a simple surface anticline that is detached in Silurian Salina Group salts and cored by imbricated Devonian rocks thrust inward toward a depressed axial low (Shumaker, 2002).

More recent reinterpretations of cross-sections across the Chestnut Ridge anticline interpreted from well data indicate a different structural formation (Shumaker, 2002). The old model involves space problems within collapsing synclines above competent reservoir rocks such as the Huntersville-Helderberg lithostructural unit. These problems can be resolved by distortion and evacuation of overlying, incompetent Hamilton Group rocks. Therefore, Huntersville-Helderberg rocks within the Chestnut Anticline deformed into a variety of structural shapes, not solely the imbricated model that traditionally has been applied to Plateau folds of the central Appalachian foreland. There is no seismicity associated with this structure, and it is considered to be non-capable under the present stress regime.

2.5.1.1.4.4.4.20 Philadelphia Structural Block

The Philadelphia Structural Block is located in the Piedmont physiographic province of Pennsylvania and New York (Figures 2.5-213 and 2.5-232). This block is currently comprised of three stratigraphic units; the Wissahickon Formation, the Wilmington Complex, and the Springfield Pluton. Originally the Block was comprised of only the Wissahickon Formation which is thought to have originated as part of a peri- Gondwanan back-arc basin during the Late Cambrian or Early Ordovician (Bosbyshell, 2009). Metamorphism of the Wissahickon Formation began during the Taconic Orogeny with the collapse of the Cambrian-Ordovician Laurentian passive margin beneath the Wilmington Complex, the root of the Taconic volcanic arc. This collapse created the Llanerch Thrust Zone. The Wilmington Complex was then thrust over the Wissahickon Formation, concurrent with the intrusion of the Springfield granodiorite pluton into the Wissahickon (Valentino, 1999).

Significant transcurrent displacements along ductile shear zones indicate a tectonic history of oblique convergence and orogen-parallel displacement (Hill, 2006). These strike-slip shear zones bound and cross-cut the Philadelphia Structural Block. To the northwest the block is bound by the Rosemont Shear Zone, and to the north, the Pleasant Grove- Huntingdon Valley Shear Zone. These shear zones separate the Philadelphia Structural Block from the West Chester and Avondale Grenvillian basement massifs. Another shear zone, the Crum Creek, cross cuts the metamorphic zones of the Wissahickon formation and is thought to be the conjugate pair of the Rosemont shear zone (Valentino, 1995). The most pervasive period of metamorphism in the Wissahickon Formation and the right-lateral transpressive deformation in the Rosemont Shear Zone, and corresponding sinistral movement along the Crum Creek Shear Zone, are Devonian in age (Bobsyshell, 2009). This timing correlates with the Acadian Orogeny in the Central Appalachians.

There is no seismicity associated with this structure, and it is considered to be non-capable under the present stress regime.

2.5.1.1.4.4.4.21 Potomac and Westminster Terranes including the Pleasant Grove Shear Zone

The Westminster and Potomac Terranes are exposed in Maryland, Virginia and Washington DC (Figure 2.5-232). It is proposed that the Potomac was thrust onto the Westminster along the Pleasant Grove Fault during the Devonian Acadian Orogeny (Figure 2.5-230). The Westminster was thrust westward along the Martic Thrust onto the Cambrian/Ordovician continental margin during the Ordovician Taconic Orogeny (Kunk, 2004).

© 2007-2012 UniStar Nuclear Services, LLC. All rights reserved.
COPYRIGHT PROTECTED

The rocks of the Westminster Terrane are dominated by phyllites and are proposed to represent offshore, deepwater, post rift deposits (Kunk, 2004). Rocks of the Potomac Terrane are proposed to be turbidites deposited in a deep ocean trench. Within the Piedmont Province, the Westminster and Potomac Terranes show foliation that mainly strikes northeasterly and dips steeply to the southeast (Southworth, 2006).

The Pleasant Grove Fault, also known as the Pleasant Grove Shear Zone is approximately 60-km long and the zone of deformation is as much as 3-km wide (Southworth, 2006). The shear zone contains dextral strike-slip indicators and similar deformational structures on both the east and west sides of the fault. Along the length of the shear zone, cooling ages range from 371 Ma in the Potomac Terrane to 364-308 Ma north of the Potomac River (Devonian to Carboniferous). The age of most recent dextral shearing is indicated by mica growth and has been dated at approximately 311 Ma (Southworth, 2006). Figure 2.5-230 shows part of Potomac River region depicting the Westminster and Potomac Terranes tectonostratigraphic location and relationships with bordering terranes and associated shear zones.

2.5.1.1.4.4.4.22 Baltimore Gneiss Terrane

The Baltimore Gneiss is defined as the basement gneisses observed at the lowest stratigraphic level in the Central Piedmont. Plank (2000) reports that the gneiss has been observed in the cores of thirteen anticlines, domes and nappes from Baltimore, MD to Philadelphia, PA. It is a Proterozoic age gneiss containing quartz, pink/white feldspar, biotite, garnet, hornblende, magnetite, titanite and zircon. The Glenarm and Wissahickon group rocks were deposited in marine rift basins floored by Baltimore Gneiss (Blackmer, 2005). The gneiss is also exposed in the Avondale and West Chester Massifs and includes amphibolite and granulite grade metamorphic compositions. The Setters Formation and Cockeysville Marble also unconformably overlie the Baltimore Gneiss (Blackmer, 2005). The northeast-southwest belt of metamorphic rocks northwest of Baltimore, which commonly includes exposures of Baltimore Gneiss, is known as the Baltimore Gneiss Terrane. The Grenville-age gneiss and sediments were thrust northwestward into a nappe structure and deformed during the Ordovician Taconic Orogeny (Lang, 1996). Figure 2.5-231 shows the Baltimore Gneiss tectonostratigraphic location within the Eastern Maryland Piedmont depicting the relationships with bordering terranes.

2.5.1.1.4.4.5 Seismic Sources as Interpreted by EPRI Groups

In 1986, the Electric Power Research Institute (EPRI) developed a seismic source model for the Central and Eastern United States (CEUS), which included the BBNPP Site region (EPRI, 1986). The CEUS is a stable continental region (SCR) characterized by low rates of crustal deformation and no active plate boundary conditions. The EPRI source model included the independent interpretations of six Earth Science Teams and reflected the general state of knowledge of the geoscience community as of 1986. Each of these teams developed a tectonic framework, defined as the collection of tectonic features thought to have a non-negligible probability of generating magnitude 5 (m_b) or greater earthquakes in the present stress regime due to tectonic processes, using comprehensive geophysical and seismological databases compiled in initial stages of the project. In order to develop their individual framework each of the six groups did: (1) interpret the crustal stress regime, (2) identify the tectonic features that might produce moderate to large earthquakes, (3) list and evaluate criteria for assessing the likelihood of activity of those features, and (4) quantify the probability of activity of each feature. Using this tectonic framework they later extended the tectonic evaluations and seismic source zones assessment to the entire Central and Eastern United States, for which they estimated seismicity parameters based on advanced and traditional analyses of the

© 2007-2012 UniStar Nuclear Services, LLC. All rights reserved.
COPYRIGHT PROTECTED

historical earthquake data set by means of a consistent, systematic format with full documentation (EPRI, 1986).

Seismic source zones have been configured either to coincide with tectonic features, or to envelope tectonic features and adjacent patterns of observed seismicity. The original seismic sources identified by EPRI are thoroughly described in the EPRI study reports (EPRI, 1986) and details of the interpretations from each of the six Tectonic Evaluation Contractors (TECs) are summarized in Section 2.5.1.1.4.4.5.1 through Section 2.5.1.1.4.4.5.6. Each of these sections presents particulars of the interpretations from each of the six Tectonic Evaluation Contractors (TECs): Weston Geophysical Corporation, Dames & Moore, Law Engineering Testing Company, Woodward-Clyde Consultants, Bechtel Group, Inc., and Rondout Associates Incorporated. The evaluations of each team are supported by figures that show their tectonic interpretation as well as the seismic zones that they specifically defined for the CEUS. All figures include plots of earthquakes with m_b equal to or higher than 3.0 in the updated earthquake catalog, in order to illustrate the spatial relationships between seismicity and the tectonic features and their associated seismicity, if this connection exists. Every TEC was initially responsible for a particular region of the Central and Eastern United States. After these regional tectonics evaluations were made, each of the TECs extended the tectonic evaluations and source zone assessments to the entire Central and Eastern United States (EPRI, 1986).

Section 2.5.1.1.4.4 summarizes specific tectonic features and characteristics within these different source areas, their evolution in time and the current state of knowledge on the tectonic setting and tectonic structures in the site region and beyond. Section 2.5.2 gives details of the procedure by which each of the TEC's resulting seismic source zones distribution was evaluated and the calculation of their Gutenberg-Richter parameters, as well as the integration of the resulting seismic hazard for the BBNPP Site.

2.5.1.1.4.4.5.1 Tectonic Interpretations by Bechtel Group, Inc.

Bechtel Group, Inc. tectonic interpretation and proposed seismic source zone configuration and dependencies are presented in corresponding Figure 2.5-11 and Figure 2.5-17.

Their interpretation for tectonic features affecting the site region (Figure 2.5-11) includes: Charlevoix - La Malbaie (3), Clarendon-Linden Fault (11), Eastern Mesozoic basins (13), Ramapo Fault (14), Stafford Fault (17), Lebanon-Pennsylvania geopotential trend (23), Bristol Block geopotential trends (24), and the New York - Alabama geopotential lineament.

Seismic source zones contributing to 99 percent of BBNPP Site Hazard, illustrated in Figure 2.5-17, are defined by five (5) source zones and five (5) background zones. These seismic source zones are first, and primarily, identified for each tectonic feature with an assessed activity of 0.05 or greater. Four (4) of the five sources zones were defined like this and were given a number designator; they include: La Malbaie/Charlevoix (3), Clarendon-Linden (11), Bristol Block (24), and the New York - Alabama Lineament (25). A second type of seismic source was defined for areas where either no adequate tectonic feature could be identified, or where the features that were identified were not assessed with a high enough likelihood to adequately explain the location of seismicity in the area considered. The remaining seismic source was defined this way and was given a letter designator; this one is the Niagara Area(D). Five (5) background zones are left after all seismic sources have been considered: Atlantic Coastal Region (BZ4), Southern Appalachians (BZ5), Southern Eastern Craton (BZ6), and the Northern Eastern Craton (BZ7), and the Northern Appalachians (BZ8) (EPRI, 1986).

© 2007-2012 UniStar Nuclear Services, LLC. All rights reserved.
COPYRIGHT PROTECTED

2.5.1.1.4.4.5.2 Tectonic Interpretations by Dames & Moore

Dames & Moore tectonic interpretation and proposed seismic source zone configuration and dependencies are presented in corresponding Figure 2.5-12 and Figure 2.5-18.

Their tectonic feature assessment for the site region (Figure 2.5-12) includes: St. Lawrence River Valley Rift (1), La Malbaie/Charlevoix Zone (2), and Clarendon-Linden Fault Zone (27); Newark-Gettysburg Basin (14) as part of the Mesozoic/Cenozoic Rifts; Eocambrian Rifts including Scranton Gravity Anomaly (12) and Pennsylvania Aulacogen (13); and Ramapo Fault (39), as part of the Mesozoic/Cenozoic Faults.

Seismic source zones contributing to 99 percent of BBNPP Site Hazard, illustrated in Figure 2.5-18, are defined by eleven (11) source zones. These eleven seismic source zones are: Adirondacks Zone (3), Appalachian Fold Belts (4), two different kinks within the Appalachian fold belt (4C and 4D), Eastern Marginal Basin (8), Clarendon-Linden Zone (9), Central Virginia Seismic Zone (40), Southern Cratonic Margin (41, Default Source Zone), Newark-Gettysburg Basin (42), Connecticut Basin (47), and La Malbaie/Charlevoix Zone (59) (EPRI, 1986).

2.5.1.1.4.4.5.3 Tectonic Interpretations by Law Engineering Testing Company

Law Engineering Testing Company tectonic interpretation and proposed seismic source zone configuration and dependencies are presented in corresponding Figure 2.5-13 and Figure 2.5-19.

Their interpretation for tectonic features affecting the site region (Figure 2.5-13) comprises: Pennsylvania Aulacogen (B3) and Scranton Gravity High (B4) (Eocambrian Rifts); St. Lawrence Valley Rift (C2a) and Charlevoix-La Malbaie Area (C2d) (St. Lawrence Rift System as part of the Mesozoic Rifts); Adirondacks (D1) (Uplift as part of the Mesozoic Rifts); Stafford-Brandywine Fault Zones (A2), Clarendon-Linden Structure (C14), Ramapo Fault (C18), and Latitude 40° N Fault Zone (C13) (Faults and Shear Zones).

Seismic source zones contributing to 99 percent of BBNPP Site Hazard, illustrated in Figure 2.5-19, are defined by six (6) source zones and six (6) background zones. The six seismic source zones are: Mafic Plutons (M15), a combination of zones 22 & 35 (C11), La Malbaie/ Charlevoix (12), Eastern Basement (17), Reactivated Eastern Seaboard Normal Faults (22) and Clarendon-Linden (20). The six background zones are: Eastern Basement Background (217), Western New England Background (101), Eastern Piedmont Background (107), Adirondacks Background (110), Laurentian Block (111) and Ohio-Pennsylvania Block (112) (EPRI, 1986).

2.5.1.1.4.4.5.4 Tectonic Interpretations by Rondout Associates, Inc.

Rondout Associates, Incorporated tectonic interpretation and proposed seismic source zone configuration and dependencies are presented in corresponding Figure 2.5-14 and Figure 2.5-20.

Their interpretation for tectonic features affecting the site region (Figure 2.5-14) includes: Clarendon-Linden (CL), Gravity Lineament (F), Inboard Mesozoic (IMEF), Niagara Magnetic Anomaly (NMA), New York - Alabama Lineament (NY-AL), Pittsburgh Washington Lineament (PW), Scranton Gravity High (SH), St. Lawrence Rift (SLR), Tyrone-Mt. Union lineament (TMU), and a Gravity Anomaly (X).

Seismic source zones contributing to 99 percent of BBNPP Site Hazard, illustrated in Figure 2.5-20, are defined by five (5) source zones, and one (1) background zone. The five seismic source zones are: Shenandoah (30), Quakers (31), Niagara by the Lake (33), Nessmuk

© 2007-2012 UniStar Nuclear Services, LLC. All rights reserved.
COPYRIGHT PROTECTED

(34), and La Malbaie (37). The Background Region Seismic Sources considered is Grenville Crust (50) (EPRI, 1986).

2.5.1.1.4.4.5.5 Tectonic Interpretations by Weston Geophysical Corporation

Weston Geophysical Corporation tectonic interpretation and proposed seismic source zone configuration and dependencies are presented in corresponding Figure 2.5-15 and Figure 2.5-21.

Their interpretation for tectonic features affecting the site region (Figure 2.5-15) includes: Adirondack Mountains, The Charlevoix-La Malbaie, Clarendon-Linden Structure, N.Y.-Alabama /Clingman lineaments block, St. Lawrence Rift, Appalachian Plateau, Valley and Ridge Fold and Thrust Zone, Mesozoic Basins, and the Moodus Seismic Area.

Seismic source zones contributing to 99 percent of BBNPP Site Hazard, illustrated in Figure 2.5-21, are defined by six (6) source zones and four (4) background zones. The six seismic source zones are: Charlevoix-La Malbaie Seismic Zone (1), Adirondack Mountains (6), Clarendon-Linden (8), New York Nexus (21), and the Zones of Mesozoic Basins (28B and 28A). The four Background Region Seismic Sources are: South Ontario-Ohio-Indiana (101), Appalachian Plateau (102), Southern Appalachian (103) and The Southern Coastal Plain (104) (EPRI, 1986).

2.5.1.1.4.4.5.6 Tectonic Interpretations by Woodward-Clyde Consultants

Woodward-Clyde Consultants tectonic interpretation and proposed seismic source zone configuration and dependencies are presented in corresponding Figure 2.5-16 and Figure 2.5-22.

Their interpretation for tectonic features affecting the site region (Figure 2.5-16) includes: Charlevoix-La Malbaie Structure (12), Adirondack Dome/Uplift (18), Mohawk River Valley Trend (20a), New Jersey Isostatic Gravity Saddle (21), Hudson River Valley Trend (25), Western New York/Southern Ontario Crustal Block (33), Attica-NY intersection Feature (34), Tyrone-Mt. Union Lineament (61), and Pittsburgh-Washington Lineament (63).

Seismic source zones contributing to 99 percent of BBNPP Site Hazard, illustrated in Figure 2.5-22, are defined by fifteen (15) seismic source zones. The fifteen source zones are: Adirondack Uplift (18), Mohawk River Trend (20A), NJ Isostatic Gravity Saddle (21 & 21A), Newark Basin (22), Newark Basin Perimeter (23), Ramapo Fault Zone (24), Hudson River Valley Trend (25), Western NY-Southern Ontario Trend (33), Attica NY Intersection (34), Tyron-Mt. Union Lineament (63), Charlevoix Seismic Zone (12), Pittsburgh-Washington Lineament (61), Moodus Seismic Zone (10), New York-New Jersey-East Pennsylvania Default zone (53). There is one defined background zoning: Susquehanna Background (BZ16) (EPRI, 1986).

2.5.1.2 Site Geology

The U.S. EPR FSAR includes the following COL Item in Section 2.5.1.2:

> Site-specific geology information will be addressed by the COL applicant.

This COL Item is addressed as follows:

Sections 2.5.1.2.1 through 2.5.1.2.6 are added as a supplement to the U.S. EPR FSAR.

© 2007-2012 UniStar Nuclear Services, LLC. All rights reserved.
COPYRIGHT PROTECTED

The following subsections provide a summary of geologic conditions in the BBNPP site area (5 mi (8 km) radius) and site location (0.6 mi (1km) radius). These subsections present information concerning the physiography, geomorphology, geologic history, stratigraphy, structural geology, geologic hazard evaluation, and engineering geology evaluation related to the BBNPP site. The information presented is based on a review of previous reports and documents, a review of geologic literature, communications with geologists and other researchers who are familiar with previous studies in the site area, and geotechnical and geologic field investigations conducted at and in the vicinity of the BBNPP site. A geologic map of site area (5 km (8 km) radius) is shown on Figure 2.5-198, and a geologic map of the site location (0.6 mi (1-km) radius) is shown on Figure 2.5-197.

2.5.1.2.1 Site Area Physiography and Geomorphology

The BBNPP site area is located within the Susquehanna Lowland Section of the Ridge and Valley Physiographic Province and is bordered by the Appalachian Plateaus Province to the west and north, and the New England Province to the east (Figure 2.5-5 and Figure 2.5-183). Additionally, within the Ridge and Valley Physiographic Province, the Anthracite Valley Section of the Ridge and Valley Province borders the Susquehanna Lowland Section to the north of the site and the Anthracite Upland Section borders on the south.

The topography within 5 mi (8 km) of the site consists of low to moderately high, linear ridges and valleys that primarily follow structural trends with elevations ranging from about 463 ft (141 m) msl to 1,778 ft (542 m) (Figure 2.5-3). To the north of the site, elevation increases to greater than 1,500 ft (457 m) msl at the peak of Lee Mountain. With the increase in elevation, the steepness in the slope, from the top of the mountain to the banks of the Susquehanna River, also increases to near vertical northeast of the site. Approximately 10,000 ft (3,048 m) south of the site, on the south side of the Susquehanna River is a steep embankment, which reaches an elevation of approximately 900 ft (275 m). Further to the south of the Site, approximately 4.75 miles (7.6 km), is the ridge of Nescopeck Mountain which reaches over 1,700 feet (520 m) at the edge of the Site Area (5 mile (8 km) radius) (Figure 2.5-3).

The site is well-drained principally by Walker Run, which flows from north to south along the west border of the site then to the south and southwest until it reaches the Susquehanna River. There is also an unnamed, unmapped tributary that flows from east to west just to the south of the site, feeds the mapped wetlands area to the southwest of the, and ultimately drains into Walker Run. Drainage within 5 miles of the site is a primarily a moderately developed trellis pattern with ridges and valleys forming sub-parallel drainage systems. These connect at abrupt incisions nearly normal to a ridge, or at the termination of a ridge, and drain down gradient toward the Susquehanna River. Streams that incise into the glacial deposits establish a dendritic pattern that is not subject to the effect of geologic structure. The longest stream near the site is the previously mentioned Walker Run which is approximately 2 mi (3.2 km) long and ultimately drains into the Susquehanna River. Ephemeral stream channels in the vicinity of the BBNPP site flow directly into the Susquehanna River. These limited stream channels maintain dendritic patterns that are observed to be minimally affected by the geologic structure as they incise into the underlying Trimmers Rock and Mahantango formations and glacial sediments.

The site area bedrock geologic map (Figure 2.5-198), compiled by (Berg, 1980) and (King, 1974) indicates that most of the site area (5 mi (8km) radius) surrounding, and including, the BBNPP site are underlain by Late Silurian, Devonian, and Early Mississippian bedrock. More specifically, the site bedrock is Upper Devonian Mahantango Formation. The most recent geologic influence on the site, not including sub aerial exposure and erosion, is the

© 2007-2012 UniStar Nuclear Services, LLC. All rights reserved.
COPYRIGHT PROTECTED

Wisconinan glaciation that is discussed in Section 2.5.1.1.1. The relevance of this event to the physiography of the site is the deposition of glacial materials. Remnants of kame terrace and outwash labeled as stratified drift deposits of sand and gravel outwash depicted in Figure 2.5-184 are mapped as overlying site area bedrock at approximate elevation 660 ft (210m). This relationship is shown on the geologic cross section of the Berwick Quadrangle (Figure 2.5-194).

Confers Lane and the western boundary for SSES form the eastern boundary of the BBNPP site. The SSES is located approximately 200 ft (61 m) above the Susquehanna River with a long, gradual slope leading from the SSES to the banks of the river. Private property borders the BBNPP site to the immediate south and west. The BBNPP will be constructed at a plant grade elevation of 719 ft (219 m) and will be set back 8,000-10,000 ft (2,438-3,048 m) from the Susquehanna River bank (Figure 2.5-3).

An additional significant geomorphological/physiographic aspect within the site area is the formation of moderate karst geomorphology approximately five miles to the south and west within the Tonoloway and Keyser Formations. The location of these strata are shown to the west of the site in Figure 2.5-198. The Tonoloway Formation is a thinly bedded limestone up to 100 ft. (30 m) thick in the site area (5 mi (8 km) radius) and the Keyser Formation is a fossiliferous limestone up to 125 ft. (38 m) thick (Berg, 1980). Both lithologies are susceptible to the development of karst features due to dissolution of calcium carbonate within the rock. However, the formation of karst geomorphology is not applicable to the site location (0.6 mi (1 km) radius), as carbonate rocks are not at or near the surface of the site. Figure 2.5-27 establishes the depth to carbonate rocks at more than 1,500 ft.(457 m) beneath the surface at the site location (0.6 mi (1 km) radius). Core holes from field studies for the BBNPP site extend to depths as great as 420 ft. (128 m) and do not encounter the stratigraphic position of these formations beneath the site location (0.6 mi (1 km) radius). Quaternary processes affecting the site are limited to weathering and erosion of existing material, and subjection to the regional stress field that affects the eastern half of the continent. The site area (5.0 mile (8km) radius) exhibits no physiographic characteristic that would detrimentally affect the BBNPP site.

2.5.1.2.2 Site Area Geologic History

This subsection presents an overview of the geologic history of the site area. The overall geologic history and tectonic framework of the region are outlined in Section 2.5.1.1.2 and Section 2.5.1.1.4 respectively. A detailed discussion of the surface faulting within 25 mi (40 Km) of the BBNPP site area is provided in Section 2.5.3. The following geologic history of the area around the BBNPP site is summarized based on the recent detailed field studies, and literature review which includes compilations by the Pennsylvania Department of Conservation and Natural Resources and publications by (Braun, 2007). Each has been integral in characterizing the site area (5.0 mile (8km) radius).

The pre-Early Ordivician geologic history of the site area is inferred from scattered borehole data, geophysical surveys and a synthesis of published information. Limited geophysical and borehole data indicate that the basement rock beneath the site most likely consists of a crystalline metamorphosed greenschist or amphibolite (Gold, 2008). Although the basement has not been penetrated directly beneath the site with drill holes, regional geologic cross sections developed from geophysical, gravity and aeromagnetic, as well as limited deep borehole stratigraphic data beyond the site area suggest Precambrian (approximately +542 million years ago) rocks are most likely present at a depth of about 33,000 ft (10,058 m) beneath the site. Figure 2.5-191 shows the inferred depth of the Precambrian basement rocks beneath the BBNPP site.

© 2007-2012 UniStar Nuclear Services, LLC. All rights reserved.
COPYRIGHT PROTECTED

Tectonic models discussed in Section 2.5.1.1.2 and Section 2.5.1.1.4 establish that the crystalline basement was accreted to the Proterozoic North American Craton during the Grenville Orogeny. The depositional environment for the Cambrian bedrock underlying the site is primarily a passive continental martin with a marine carbonate platform extending to a more distal setting upon which clays and silts were deposited (Gao, 2000). These sediments, deposited over a period of nearly 50 million years (approximately 542-488 million years ago), comprise the shales and limestones overlying the Grenville basemat at the BBNPP site. The site area during the Ordovician (approximately 488-444 million years ago) represented an area of continued and increased deposition in an elongated basin along the continental margin. As discussed in Section 2.5.1.1.2.3, the Middle Ordovician to Late Ordovician with respect to the eastern margin of the North American craton, is affected by the Taconic Orogeny (Hurowitz, 2005). As the Taconic allochthon, a suite of oceanic and arc terranes, converged with the North American Craton, uplift of the area began and shifted the depositional environment from that of carbonate platform to a much shallower basin receiving coarser siliciclastic source material (Tremblay, 1997). Deposition of material from the Taconic Allochton, as it approached from the east-southeast, yielded significant amounts of siliciclastic sediment to the basin. Shale and sandstone units that now outcrop in places throughout central Pennsylvania, but underlie the site area by thousands of feet (Thompson, 1999), were deposited at this time. As the Taconic front converged with the craton, portions of the ocean floor and island arc of the Taconic front were obducted onto the craton at the eastern portion of what is now defined as the site region (200 mi (322 km) radius), while some ocean floor subducted under the continent. At the close of the Ordovician, the site area (5 mi (8 km) radius) was located on the western portion of a depositional basin bounded on the west by the North American Craton and on the east by the Taconic Highlands (Thompson, 1999).

The continued erosion of the Taconic Mountains during the early part of the Silurian Period (444-416 million years ago) added to the sedimentation throughout the site area. This early period of sedimentation differed from that of the Ordovician, in that the sand and gravels deposited during the Early Silurian were extremely quartz-rich in mineral composition (Barnes, 2002), thus creating a very erosion-resistant sandstone. After the Taconic Mountains were almost completely eroded away during the Late Silurian, carbonate sedimentation continued through the site area creating shale and limestone intervals (Laughrey, 1999).

The Devonian Period (approximately 416-359 million years ago) primarily marks the Acadian Orogeny (as discussed in Section 2.5.1.1.2.5), the result of the North American landmass colliding with the Avalon Terrane and Baltica (Eusden, 2000). The site area remained a basin area while the Acadian mountain range, to the east of the site area, was subjected to erosional processes. The effect of the Acadian Orogeny is more pronounced in terms of metamorphism and magmatism in the northeastern United States (Maine, New Hampshire, Vermont) (Eusdan, 2000) but is significant to the site area in that the source material for the formation of the Devonian black and gray shales that outcrop, and underlie in the site area was primarily derived from the eroded Acadian Highlands (Ver Straeten, 2000). Ver Straeten (2000) identify the progression of a terrigenous clastic wedge from the orogenic belt to the west during multiple phases of orogenic uplift during the Devonian that was the source of Devonian deposition.

The Carboniferous Period (approximately 359-299 million years ago) is best described in two distinct categories including the older Mississippian and younger Pennsylvanian sub-periods of the Carboniferous Era. The Mississippian (approximately 359-318 million years ago) was a time of continued sedimentation from the Acadian mountains but a change of climate is represented in the lack of oxidation of rocks from this time frame (Barnes, 2002). Near the end

© 2007-2012 UniStar Nuclear Services, LLC. All rights reserved.
COPYRIGHT PROTECTED

of the Mississippian the site and surrounding area likely became poorly drained and was an area of thick forests and swamps. During the Early Pennsylvanian these forests deposited great amounts of organics which did not rot or oxidize due to the water rich environment of the swamps (Edmunds, 1999). These organics were then overlain by sediment deposits and compacted into the coal fields that occupy the Anthracite Valley Section to the north and the Anthracite Upland Section to the south of the site (Edmunds, 1999) (Figure 2.5-183). No Mississippian or Pennsylvanian rocks exist within the site location (0.6 mi (1km) radius) due to uplift and erosion throughout geologic time. However, Mississippian and Pennsylvanian rocks are found within the site area (5.0 mi (8km)) to the north and to the south of the site location as depicted on Figure 2.5-198.

The most significant geologic event to affect the structure of the site area is the Alleghanian Orogeny (discussed in detail in Section 2.5.1.1.2.5). Beginning in the Middle Pennsylvanian, continental convergence of North America and Africa began the multiple phases of the Alleghanian Orogeny which was the primary orogenic event to form the portion of the Appalachian Mountains that extend from northeast Alabama through Pennsylvania. The orogeny formed numerous thrust faults, fractures, anticlines and synclines throughout the Ridge and Valley, Piedmont, and Blue Ridge Physiographic Provinces from Alabama through Pennsylvania including the site area. Convergence from the southeast to the northwest created a structural fabric that strikes primarily northeast and dips to the northwest and southeast. Deformation was both ductile and brittle depending on pressure/temperature conditions. Offset along faults within the Ridge and Valley is primarily reverse dip slip but often has a strike slip component (Pohn, 2000).

The site area was subjected to brittle deformation in the form of folding and thrusting that developed the structural makeup of the Ridge and Valley Province within which the site area lies. The Berwick and Light Street Faults, depicted on Figure 2.5-198 and discussed in Section 2.5.1.2.4.1 are examples of this Alleghanian deformation within the site area (5 mi (8 km) radius), and are not recognized as active. In addition, the Berwick Anticlinorium, an east-northeast striking, gently northeast plunging anticline trends directly through the site area (5 mi (8 km) radius). The Berwick Anticlinorium is a symmetrical structure with both the north-northwest and south-southeast limbs dipping with an averaged 35 degree NNW and SSE respectively (Inners, 1978). The structure imparted by the Alleghanian Orogeny is significant to the topography, drainage, and seismicity of the site area, defining the major landforms (elongated ridges and valleys), drainage patterns, and structural discontinuities within the Paleozoic strata.

By the end of the Permian Period, the Appalachian Mountains had been subjected to significant erosion providing source material for an alluvial plane across the site area (Edmunds, 1999). Publications (Pazzaglia, 2006,) describe the cycle of erosion and isostatic uplift as the dominant geologic process within the site area since the Late Permian, with the exception of discreet glacial periods that significantly altered and even reversed the erosion and uplift process.

The Triassic (approximately 251-199 million years ago), Jurassic (approximately 199-145 million years ago), and the Cretaceous (approximately 145-65 million years ago) Periods, all within the Mesozoic Era, were all time zones of slow erosional processes for many areas of Pennsylvania, including the site area (Barnes, 2002). During these periods of erosion, new drainage patterns and streams were formed. By the end of the Cretaceous Period, chemical alteration became the dominant erosional source of rocks that likely comprised the site area, changing them into clays and saprolite (MacLachlan, 1999). Rifting of Pangea in the Late

© 2007-2012 UniStar Nuclear Services, LLC. All rights reserved.
COPYRIGHT PROTECTED

Permian and throughout much of the Triassic affected the site region (200 mi, (322km) radius) by changing the stress field to an extensional regime. Mesozoic rift basins and intrusive diabase dikes along rift structures mark the extensional effects on the North American Atlantic margin. The aforementioned extension related features do not occur within the site vicinity (25 mi (40-km) radius) nor the site area (5 mi (8 km) radius) (Figure 2.5-208).

Though there is little record as to what happened at or around the site area during the Cenozoic Period (approximately 65 million years to present), much can be inferred from the glacial deposits of the Quaternary Period (approximately 1.8 million years ago to present). It is theorized that during the Tertiary Period (approximately 65-1.8 million years ago) erosion at the site area continued with chemical alteration and erosion, primarily during the Early Tertiary, but transitioned to intense physical erosion during the Late Tertiary (Barnes, 2002). This physical erosion was the result of cooler and drier conditions. It is also believed that during this time many of the modern day rivers and streams, such as the Susquehanna, established themselves (Sevon, 1999b).

During the Quaternary, continental glaciers covered Canada and advanced into a small portion of Pennsylvania, including the site area (5 mi (8 km) radius), and site vicinity (25 mi (40-km) radius) as shown in Figure 2.5-184. The site area was subjected to three different periods of glaciation with the earliest occurring approximately 770,000 years ago and the most recent occurring approximately 17,000 to 22,000 yrs ago. These periods of glacial advance and retreat had both erosional and depositional effects on the site area, the degree of which is difficult to quantify. The main effect of glaciation on the site area was the effect of glacial outwash enhancing drainage patterns that were already in progress (Sevon, 1999a). During and after glacial retreat, the site has been an area of deposition for stratified drift which includes sand and gravel, kame terraces, and outwash. Hence, the surface at the site is comprised of glacial deposits from the Wisconsinan glaciation that is discussed in Section 2.5.1.1.2. Surficial deposits are depicted on Figure 2.5-195 for the site location (0.6 mi (1 km) radius) and on Figure 2.5-196 for the Berwick Quadrangle.

Cenozoic faulting occurred in the Piedmont, especially along the contact of the Piedmont and Coastal plain, where a hinge line of erosional unloading and depositional loading roughly from northwest to southeast (Weems, 1998) is known to exist. Cenozoic faulting is also recognized in the Piedmont (Wentworth, 1983) approximately 50 miles from the site. In addition, Crone (2000) present data for all Quarternary faults and possible tectonic features in the Eastern United States and report two sites in the Pennsylvania Ridge and Valley province. However, no seismic events or tectonic structures are reported within the site area (5 mi (8 km)) or the site vicinity (25 mi (40 km) radius). Capable seismic sources, their location, and affect on the site area (5 mi (8 km) radius) are discussed in Section 2.5.1.2.4.

The surface at the site is comprised of glacial deposits from the Wisconinan glaciation that is discussed in Section 2.5.1.1.2. As briefly discussed in Section 2.5.1.2.1, with respect to physiography, the formation of karst is also part of the geologic history of the site area (5 mi (8 km) radius). Approximately five miles to the west within the Tonoloway and Keyser Formations, as shown on Figure 2.5-198, karst feature development is exhibited. The Tonoloway Formation is a thinly bedded limestone up to 100 ft. (30m) thick in the site area (5 mi (8 km) radius) and the Keyser Formation is a fossiliferous limestone up to 125 ft. (38 m) thick. Both lithologies are susceptible to the development of karst features due to dissolution of calcium carbonate within the rock. However, the formation of karst geomorphology is not applicable to the site location (0.6 mi (1 km) radius), as carbonate rocks are not at or near the surface of the site (Inners, 1978). Figure 2.5-27 notes the stratigraphic position of these

© 2007-2012 UniStar Nuclear Services, LLC. All rights reserved.
COPYRIGHT PROTECTED

formations beneath the site location (0.6 mi (1 km) radius). The Tonoloway and Keyser Formations are at depths as great as 1,500 feet under the site location (0.6 mi (1 km) radius) due to the dip of the northern limb and plunge of the axis of the Berwick Anticlinorium.

The geologic history of the site is complex, but the current geologic processes affecting the site are limited to weathering and erosion of existing material, and subjection to the regional stress field that affects the passive Atlantic margin. Figure 2.5-8, (Heidbach, 2008) shows the current stress fields in the eastern portion of North America, and minimal isostatic uplift. With respect to seismic stability and geologic hazards due to the site area (5 mi (8 km) radius) geologic history, the site area (5 mi (8 km) radius) and site location (0.6 mi (1 km) radius) are positioned in a stable geologic setting.

2.5.1.2.3 Site Area Stratigraphy

As discussed in Section 2.5.1.1, the BBNPP site is located near the deepest portion of the Appalachian structural basin (see Figure 2.5-187). Approximately 33,000 ft (10,058 m) of Paleozoic rocks overlie the Pre-Cambrian basement at the BBNPP site. The regional source of sediments, the types of sediments, and the deformation of these sediments that fill the Basin are described in Section 2.5.1.1. This Section provides more detailed information related to the local stratigraphy, including the nomenclature of the formations, the lithologies, and the thickness of formations. In addition, any characteristics of the geologic media underlying the site that could impact the design or the safety of the BBNPP are presented in this section. Based on the drilling, geologic observations, and laboratory testing results, the rock formations below the BBNPP site are very competent and physically suitable to serve as a stable foundation for the BBNPP.

Site-specific information on the stratigraphy of geologic materials underlying and directly adjacent to the BBNPP site is based on the geologic/geotechnical investigations performed for the BBNPP site and the historical investigations performed at the SSES site. The SSES site is located immediately adjacent to the BBNPP site and observations concerning its soil and rock formations are comparable with those from the BBNPP investigation borings. Given that the geologic conditions at the SSES and BBNPP sites are very similar, the available SSES data and information were used to supplement the BBNPP data and enhance the characterization of subsurface conditions at BBNPP.

A total of 44 boreholes and 51 monitoring wells were completed at BBNPP. Forty one of the monitoring wells were completed in late 2007 and early 2008, with the rest of the boreholes and monitoring wells having been completed in the spring of 2010 for sampling and standard penetration test (STP) purposes. In addition, 3 boreholes were performed for geophysical testing purposes. Of the 47 geotechnical and geophysical borings drilled during the BBNPP site investigation, 12 were 30 to 99 ft (9 to 30 m) deep, 18 were 100 to 199 ft (30 to 61 m) deep, 14 were advanced to a total depth between 200 and 299 ft (61 and 91 m) below ground surface (bgs), and 3 were drilled to a depth between 300 and 420 ft (91 and 128 m) bgs (Table 2.5-28). The deepest geotechnical boring advanced at the BBNPP site was boring G-401, which was drilled to a total depth of 420 ft (128 m) near the proposed centerpoint of the reactor building. All of the geotechnical and geophysical borings penetrated the full thickness of the residual soil deposits and at least 9.5ft (3 m) of the Middle Devonian Mahantango Formation. In addition, approximately 250 exploratory borings were drilled in soil and rock in late 1970, Spring 1971, and 1983 at or near the SSES site. Also, test pits were excavated at selected locations at or near the SSES site.

© 2007-2012 UniStar Nuclear Services, LLC. All rights reserved.
COPYRIGHT PROTECTED

It is estimated that the full thickness of the Mahantango Formation at the BBNPP site is approximately 1,500 ft (457 m) thick (Inners, 1978). Thus, there are approximately 1,100 ft (335 m) or more of Mahantango Formation that lies beneath the deepest geotechnical boring at the BBNPP site. Geological information relative to the uppermost 420 ft. (128 m) of geologic strata at the site was derived from cores and drilling information obtained during the on-site BBNPP subsurface investigations. Stratigraphic information regarding the deeper geologic strata was obtained primarily from publications by the Pennsylvania Topographic and Geologic Survey which focus primarily on this area (e.g., Inners, 1978; Crowl, 1980; and Williams, 1987).

Characteristics of the basement rocks in Pennsylvania are extrapolated from the exposed metamorphic rock in the Piedmont Physiographic Province to the southeast and several exploratory wells in western Pennsylvania (Saylor, 1999). Based on available data (Saylor, 1999), it is likely that the basement rock beneath the site is similar to the schists and gneisses found in the Piedmont Physiographic Province, which is located approximately 50 mi (80 km) to the southeast of the BBNPP site as shown in Figure 2.5-182.

Paleozoic rocks of the Ridge and Valley Province are representative of formations deposited in a foreland basin that have undergone numerous cycles of marine regression/transgression. The Province extends from eastern New Jersey to Alabama and has been subjected to multiple orogenies. Stratigraphic formations, and their depositional environments, are also discussed in Section 2.5.1.1.2 and Section 2.5.1.1.3. A statigraphic column created specifically for the BBNPP Site and Site Area (5-mi (8-km) radius) is shown in Figure 2.5-29. The following Subsections describe each of the stratigraphic formations, in order of oldest to youngest.

2.5.1.2.3.1 Cambrian Formations

The oldest inferred Cambrian Formation underlying the site area is the Waynesboro Formation. The Waynesboro Formation consists of sandstone with interbedded red and green shales and has a thickness of approximately 1,000 ft (305 m) or more (Kauffman, 1999). Overlying the Waynesboro Formation is the Pleasant Hill Formation, which is primarily a limestone formation with interbedded sandy and silty layers throughout (Kauffman, 1999). Overlying the Pleasant Hill Formation is the Warrior Formation. It is a dark, fossiliferous, fine grained limestone interbedded with silty dolomite, with a thickness up to 1,340 ft (408 m) (Kauffman, 1999). Overlying the Warrior Formation, and marking the Cambrian-Ordovician boundary, is the Gatesburg Formation. The Gatesburg Formation consists of a series of sequential sandstone and dolomite units that are fossiliferous (Ryder, 1992) and in excess of 1211 ft (369 m) thick (Gold, 2003). Both the Warrior and Gatesburg formations likely represent a shallow-water carbonate bank or shelf that was subjected to periodic episodes of near-drying conditions (Kauffman, 1999).

2.5.1.2.3.2 Ordovician Formations

Overlying the Upper Cambrian Gatesburg Formation are the Lower Ordovician formations that comprise the Beekmantown Group. These Lower Ordovician formations, from oldest to most recent, include the Stonehenge Formation, Nittany Dolomite, Axemann Limestone, and Bellefonte Dolomite. They are composed primarily of dolomites and limestones (Harper, 2003) and reach a combined thickness of up 4,200 ft (1,280 m) (Thompson, 1999).

The Middle Ordovician strata include the Loysburg Formation, the Black River Group, and the Trenton Group. The Loysburg Formation is typically a dolomitic and stromatalite rich limestone underlying a coarse grained, fossiliferous limestone (Thompson, 1999) with an average thickness of 263 to 475 ft (80 to 145 m). Overlying the Loysburg Formation is the Black

© 2007-2012 UniStar Nuclear Services, LLC. All rights reserved.
COPYRIGHT PROTECTED

River Group that consists of the Snyder and Linden Hall formations (Thompson, 1999) and attains a thickness of about 632 ft (193 m). These formations are composed primarily of siliciclastic clay and shale. Overlying the Black River Group are fine-grained, black, graded limestone and shales of the Solona and Coburn formations of the Trenton Group (Thompson, 1999).

Rocks of the Beekmantown Group, Loysburg Formation, Black River Group, Solona Formation, and Coburn Formation were deposited in marine to marginal-marine environments. Where a platform existed and the seas became progressively shallower, depositional environments became more intertidal (Thompson, 1999). The uppermost rocks within the Trenton Group belong to the Antes Formation, a fossiliferous, generally black, shale (Thompson, 1999) that was likely deposited in shallow water, above the wave base. The Antes, Coburn, and Salona formations collectively attain a thickness of approximately 842 ft (257 m).

Upper Ordovician strata include the Reedsville, Bald Eagle, and Juniata formations (in ascending order). The Reedsville Formation is approximately 600 to 1800 ft (183-549 m) thick and is composed primarily of interbedded shale and sandstone beds, with some limestone (Thompson, 1999; Gold, 2003). Like the Antes Formation underlying it, the Reedsville Formation was likely deposited in shallow water. The Bald Eagle Formation and the Juniata Formation are 700 to 1313 ft (213 to 400 m) and 600 to 1,125 ft (183 to 343 m) thick, respectively (Thompson, 1999; Gold, 2003). Both of these formations consist of nonfossiliferous sandstones, conglomerates, and mudstones, but differ in color with the Bald Eagle being gray and the Juniata red (Thompson, 1999). Unlike the Reedsville Formation, the Bald Eagle and Juniata formations are non-fossiliferous and non-marine. These formations were likely deposited near low-sinuosity streams on alluvial fans (Thompson, 1999).

2.5.1.2.3.3 Silurian Formations

The Tuscarora Formation typically marks the boundary between Late Ordovician and Silurian Periods. The Lower Silurian Tuscarora Formation is quartzose, sublithic, and argillaceous sandstone with few shale beds throughout, and was deposited in a fluvial environment (Laughrey, 1999). The Tuscarora Formation ranges between 400 ft (122 m) and 700 ft (213 m) thick and is extremely resistant to erosion and weathering processes (Laughrey, 1999; Gold, 2003).

Overlying the Tuscarora Formation (in ascending order) are the Rose Hill, Keefer, Mifflintown, Bloomsburg, Wills Creek, Tonoloway, and Keyser formations, all of Silurian age (Figure 2.5-27). The Rose Hill Formation consists of olive shale with interbedded layers of hematitic sandstone, purplish shale, and fossiliferous limestone (Laughrey, 1999). Above the Rose Hill Formation lies the Keefer Formation, a quartzose and hematitic sandstone with some mudstone. The Rose Hill and Keefer formations combine for a thickness that ranges between 600 ft (183 m) and 1070 ft (326 m) (Gold, 2003). The Mifflintown Formation reaches a thickness of about 336 ft (102 m) (Gold, 2003) and is composed of sandy and silty shales, siltstone, and limestone of a shallow marine setting (Laughrey, 1999). The likely depositional environment for the Rose Hill, Keefer, and Mifflintown formations is that of a submarine ramp that deepened from the proximal basin margin (Laughrey, 1999) during the Taconic Orogeny, as discussed in Section 2.5.1.1.2.3 and Section 2.5.1.1.3.

Conformably overlying the Mifflintown Formation is the Bloomsburg Formation (Early Silurian), which consists primarily of grayish-red clay-siltstone with some interbedded fine- to coarse-grained sandstone beds. The Bloomsburg Formation ranges in thickness from 85 ft (26

© 2007-2012 UniStar Nuclear Services, LLC. All rights reserved.
COPYRIGHT PROTECTED

m) to 464 ft (141 m). It is slightly fossiliferous and probably represents sediments deposited in deltaic waters with a high enough salinity to allow some fauna to exist (Laughrey, 1999).

Upper Silurian strata include the Wills Creek, Tonoloway, and Keyser formations. The Wills Creek Formation conformably overlies the Bloomsburg Formation, and consists primarily of claystone to silty claystone with some interbedded grayish-red sandstone and fine-grained argillaceous dolostone and dolomitic limestone. The Wills Creek Formation is approximate 750 ft (229 m) thick (Inners, 1978) and represents deposition in lagoonal, intertidal, and supratidal environments. The Tonoloway Formation is primarily a thinly-bedded limestone deposit with a few thin beds of calcareous shale (Laughrey, 1999); it is about 100 ft (30 m) thick (Inners, 1978). Both the Wills Creek and Tonoloway formations represent numerous shallowing-upward cycles that have been interpreted as repeated progradational events on very large tidal flats (Laughrey, 1999).

The Keyser Formation conformably overlies the Tonoloway Formation and consists mainly of medium to dark gray, fine-grained, fossiliferous limestone with minor interbeds of dark-gray calcareous clay shale. Some dark gray cherty nodules are present toward the upper part of the formation. The Keyser Formation straddles the boundary between the Late Silurian and Early Devonian as the formation represents continuous carbonate sedimentation from both periods and has a thickness of about 125 ft (38 m) (Inners, 1978).

2.5.1.2.3.4 Devonian Formations

The Devonian system of rocks is described as a westward-thinning wedge of sediments with a thickness of almost 11,000 ft (3,353 m) throughout much of Pennsylvania (Harper, 1999). The Upper Keyser Formation makes up the basal unit for the Devonian period formations. Overlying the Keyser Formation is the Old Port Formation, which consists of (in ascending order) the Corriganville Limestone, the Mandata Shale, Shriver Chert, and Ridgeley Sandstone (Harper, 1999). The Corriganville Limestone consists of finely crystalline, thick to thinly bedded limestone and ranges from 10 ft (3 m) to 30 ft (9 m) thick (Harper, 1999). The Mandata Shale is dark gray to black, thinly bedded, siliceous shale, and ranges in thickness from 20 ft (6 m) to 100 ft (30 m) (Harper, 1999). Light colored cherty, mudstones and calcareous siltstones characterize the Shriver Chert (Harper, 1999), which ranges in thickness from 80 ft (24 m) to 170 ft (52 m). The Ridgeley Sandstone ranges in thickness from 8 ft (2 m) to 170 ft (52 m) and is generally white to light-gray, medium grained, quartzose sandstone (Harper, 1999). These units of the Old Port Formation represent the gradual deepening of the Appalachian basin and range in overall thickness from 100 ft (30 m) to 150 ft (46 m) in the site area (Inners, 1978).

The Silurian limestone formations (Wills Creek, Tonoloway, and Keyser) and the Devonian Old Port Formation contain minor dissolution features along bedding planes, fractures, and joints, which makes them relatively good aquifers at shallow depth (see Section 2.5.1.2). The total thickness of these formations is approximately 700 feet (213 m) and they are located at least 1,700 ft (518 m) below the BBNPP site. In general, due to their depth, dissolution features along bedding planes or fractures at this depth are very minor and will have no effect on the structural stability or strength of the overlying rock strata.

The Onondaga Formation (Middle Devonian) disconformably overlies the Old Port Formation and reaches a thickness of about 175 ft (53 m) in the site area (Inners, 1978). The Onondaga Formation consists of silty, shaley, and cherty limestones, and likely represents a shelf margin depositional environment (Harper, 1999). The upper part is a medium dark gray argillaceous, fine-grained, pyritic limestone with interbeds of medium dark gray calcareous clay shale

© 2007-2012 UniStar Nuclear Services, LLC. All rights reserved.
COPYRIGHT PROTECTED

(Selinsgrove Limestone Member) and the lower part is a medium to dark gray, calcareous, slightly silty, clay shale (Needmore Shale Member).

The Marcellus and Mahantango formations together form the Hamilton Group of Middle Devonian age (Figure 2.5-27). The Marcellus Formation, located below the Mahantango Formation, consists of approximately 350 ft (107 m) (Inners, 1978) of dark-gray to black shales that are carbonaceous, and contain pyrite and few fossils (Harper, 1999). The Marcellus Formation was likely deposited in a variety of shallow-water anoxic environments (Harper, 1999).

The Mahantango Formation overlies the Marcellus Shale and is the uppermost bedrock unit at the BBNPP site, as shown in Figure 2.5-27 and Figure 2.5-193. Harper (Harper, 1999) describes the Mahantango Formation as a complex series of interbedded shales, siltstones, and sandstones, ranging from 1,200 ft (366 m) to 2,200 ft (671 m) thick. Inners (Inners, 1978) reports the thickness of Mahantango Formation is approximately 1,500 ft (457 m) in the site area. According to Inners (Inners, 1978), the Mahantango Formation consists primarily of "medium dark to dark gray, silty to very silty claystone (95 percent), with some argillaceous, fine-grained limestone (5 percent) in the uppermost part. Claystone generally in poorly-defined beds 3 to 10 feet (1 to 3 m) thick; massive, often with profuse burrows; noncalcareous to very calcareous; medium-dark-gray, pyritic siderite and limestone nodules, 1 to 4 inches (2.5 to 10 cm) in diameter, are locally abundant and often form distinct bands; several calcareous, fossiliferous horizons 3 to 10 feet (1 to 3 m) thick and abounding in marine invertebrates, can be traced locally." The Tully Member (or Tully Limestone Member) is found at the top of the Mahantango Formation and is medium dark gray (light gray where weathered), fossiliferous, argillaceous, fine-grained limestone and calcareous clay shale. It is approximately 50 to 75 feet (15 to 23 m) thick, but has been eroded from the crest of the Berwick Anticline at the site (Inners, 1978). The Mahantango Formation and the Tully Member represent marine sediments deposited on a shallow subtidal shelf. Harper (1999) suggests that the Mahantango Formation was deposited as a prograding marine shoreline during the early stages of the Catskill Delta.

The shales and siltstones encountered during the BBNPP site investigation were typically dark gray, ranged in hardness from soft to moderately hard, increased progressively in the level of calcareous content with depth, and were slightly pyritic and fossiliferous throughout. The weathered shale that formed the uppermost bedrock surface typically ranges from 5 to 45 ft (1.5 to 13) thick, and is termed the Weathered Zone. Below the weathered shale, the rock becomes much harder and the rock quality designation (RQD) increases, ranging up to 100 percent with an average of 33 percent (see Figure 2.5-200 through 2.5-205).The rock in this zone, termed the Transition Zone, is similar to the sound Mahantango Shale below it, but is highly fractured and can range from non-existent to 84 ft (0 to 25 m) thick. In 8 geotechnical borings, the Weathered Zone and the Transition Zone alternate back and forth. At the point where the highly fractured rock diminishes, the shale is termed the Sound Rock. The Sound Rock zone has an average RQD of 86 percent and in some cases, was so unfractured and competent that the shale cores were removed from the core barrels intact with no breaks at all (Figure 2.5-30). As discussed in Section 2.5.4.2, the Mahantango shale is a hard, competent bedrock unit. According to Inners (Inners, 1978), the Mahantango Formation has "high foundation support strength, suitable for heavy structures if excavated to sound bedrock." Physical properties of the shale bedrock are discussed in detail in Section 2.5.4.2.

The Mahantango Shale is the uppermost bedrock unit present throughout most of the BBNPP site, including all of the areas supporting safety-related structures. Another black shale (the

© 2007-2012 UniStar Nuclear Services, LLC. All rights reserved.
COPYRIGHT PROTECTED

Harrell Shale) is present between the Mahantango Shale and Trimmers Rock Formation in the northern portion of the site and is about 120 ft (37 m) thick (Inners, 1978). It conformably overlies the Mahantango Formation and marks the initial unit of the Upper Devonian strata. The Harrell Formation is typically represented by dark gray to grayish black, pyritic, organic-rich, clay shale and silty clay shales (Inners, 1978; Harper, 1999). The Harrell Shale was deposited in a poorly-oxygenated basinal marine environment. Where exposed today at the ground surface, the shale has moderately developed cleavage, is jointed, and forms splintery and platy fragments. The weathered surfaces can be covered by efflorescent secondary sulfate minerals. Because the shale has low resistance to weathering, it typically forms a swale at the foot of escarpments developed by the Trimmers Rock Formation (Inners, 1978). The swale that runs east to west along the northern edge of the SSES and the BBNPP sites (immediately south of Beach Grove Road) is shown as the outcrop area of Harrell Shale by Inners (Inners,1978; Figure 2.5-193)

While the Mahantango and Harrell formations are the only two bedrock formations exposed at the BBNPP site, other younger Paleozoic Era formations that were deposited after the Harrell Formation exist within the site area (5 mi (8 km) radius), as shown in Figure 2.5-193, Figure 2.5-197, and Figure 2.5-198. These formations comprise the ridges and bedrock outcrops to the north and south of the site, such as Lee and Nescopeck Mountains, respectively.

The Upper Devonian Trimmers Rock Formation lies immediately above the Harrell Shale. It is composed primarily of medium to dark gray siltstone and shale (60 percent), medium to medium dark gray, thinly-bedded, very fine to fine grained sandstone (25 percent), and medium to dark gray silty clay shale (Inners, 1978; Harper, 1999). The Trimmers Rock Formation has a calculated thickness of approximately 3,000 ft (914 m) (Inners, 1978) and likely represents a delta-fed submarine slope of the Appalachian Basin. The Trimmers Rock Formation is resistant to erosion and forms steep escarpments on the north and south sides of the Susquehanna River Valley. The east-west trending unnamed ridge that lies directly north of the BBNPP site is composed of Trimmers Rock Formation and the ground surface rises steeply going up the south flank of this ridge (Figure 2.5-4; 2.5-193).

Above the Trimmers Rock Formation, within the site area, lie the members of the Upper Devonian Catskill Formation including (in ascending order) the Irish Valley, Sherman Creek, and Duncannon Members. Each member of the Catskill ranges in thickness from 150 ft (46 m) to 3,700 ft (1,128 m) and generally consists of gray to red mudstones, claystones, siltstones, and conglomerates that were deposited in mixed continental, fluvial-deltaic, and marginal-marine environments (Inners, 1978; Harper, 1999).

The uppermost unit of Devonian age rocks in the site area is the Spechty Kopf Formation, which also spans into, and identifies the beginning of the Carboniferous Period. The Spechty Kopf Formation has a thickness of about 575 ft (175 m) near the crest of Nescopeck Mountain, but is absent north of BBNPP on Lee Mountain (Inners, 1978). It is composed mainly of medium gray to olive sandstone with other components including siltstone, shale, and conglomerates (Berg, 1999). The likely depositional environment of the Spechty Kopf Formation was that of ephemeral lakes formed on the surface of the Catskill alluvial plain (Berg, 1999).

2.5.1.2.3.5 Mississippian Formations

Mississippian rocks of the site area represent a transition from the prograding deltas of the Late Devonian Period (Brezinkski, 1999) to Pennsylvanian rocks, which primarily represent

© 2007-2012 UniStar Nuclear Services, LLC. All rights reserved.
COPYRIGHT PROTECTED

sedimentary environments within an elongate basin aligned in a northeast to southwest direction (Edmunds, 1999).

The Devonian-Mississippian boundary is marked by the presence of the Upper Spechty Kopf Formation. Unconformably overlying the Spechty Kopf Formation is the Pocono Formation, which was likely deposited on a high-gradient alluvial plain or alluvial fan, is represented by beds of medium to coarse grained sandstone, siltstone, and conglomerates (Brezinski, 1999) with a thickness of about 600-650 ft (183-198 m) (Inners, 1978). Overlying the Pocono Formation within the 5 mile site area radius, is the Mauch Chunk Formation, easily recognizable by it's red to reddish-brown mudstone and siltstone with reddish-brown and greenish-gray sandstones and conglomerates (Brezinski, 1999). The Mauch Chunk ranges in thickness throughout the site area but has been estimated to be between 3,000 ft (914 m) to 4,000 ft (1,219 m) thick (Brezinski, 1999). The depositional environment of the Mauch Chunk Formation was likely that of a broad alluvial plain in which deposits came from two distinct sources. The first source was red clastics, likely derived from the Taconic highlands, and the second was quartz sand from the erosion of the previously deposited (Burgoon) sandstones (Brezinski, 1999).

2.5.1.2.3.6 Pennsylvanian Formations

The Mississippian-Pennsylvanian boundary in the site area is generally considered to be the top of the Mauch Chunk Formation and bottom of the Pottsville Formation. The Pennsylvanian Pottsville Formation overlies the Mauch Chunk Formation conformably and ranges in thickness from 100 ft (30 m) to 1,600 ft (488 m) (Edmunds, 1999). The Pottsville Formation consists mainly of a cobble and pebble conglomerate with some sandstones and finer clastics and coal (Edmunds, 1999).

The youngest rock formation within a 5-mile (8-km) radius of the site area, and overlying the Pottsville Formation, is the Llewellyn Formation. The Llewellyn Formation reaches a thickness of approximately 3,500 ft (1,067 m) through other portions of Pennsylvania and generally consists of subgraywacke clastics, ranging from conglomerates to clay shale and containing numerous coal beds (Edmunds, 1999). The Llewellyn Formation is very resistant to erosion and forms the crest of Lee Mountain near the town of the Shickshinny, as seen in Figure 2.5-3.

2.5.1.2.3.7 Quaternary Deposits

The bedrock at the BBNPP site and the site area is mostly covered with a variable thickness of Pleistocene sediments including kame, kame terrace, outwash, ground moraine and end moraine deposits (Figure 2.5-195). However, on the hill where the most of the BBNPP facilities are to be located, the surface is covered with residual soil with only thin localized patches of glacial till deposits (Inners, 1978). However, maps this hill as Woodfordian End Moraine deposits, but this study does not find such deposits in the extensive investigation completed at the Site. Inners (1978) never performed such a detailed study of this particular location and his mapping therefore must be taken as inaccurate for this location. The hill likely was completely covered by some thickness of till after the glaciers retreated, but has been largely eroded away at this time.

Quaternary deposits of the site area are primarily the result of glacial deposition during at least three known glacial events that are believed to have impacted the site area. Of these three events, Quaternary deposits from two of them comprise the soil overburdens present within the site area. The earliest deposit is of Late Illinoian age (unnamed) and can be stratigraphically correlated to that of the Titusville Till in northwestern Pennsylvania, as shown in Figure 2.5-184. These Unnamed and Titusville Tills are described as a thin, gray to brown

© 2007-2012 UniStar Nuclear Services, LLC. All rights reserved.
COPYRIGHT PROTECTED

and grayish-red clay and sand (Sevon, 2000c). This was almost entirely eroded away during the next glacial advance through the site during the Wisconsinan Epoch (Crowl, 1999). The resulting glacial deposits from the Wisconsinan event is known as Olean Till, which is described as moderately thick, gray to grayish-red sandy till (Sevon, 2000c).

Lower elevations between ridges within the site area (e.g., Susquehanna River floodplain) are covered with thick deposits of stratified drift, as shown in Figure 2.5-196. The stratified drift, as defined by Sevon (2000c), is sand and gravel in eskers, kame terraces, and outwash. Stratified drift has been deposited the site area since the Late Illinoian (Sevon, 2000c), during periods of glacial melting and retreat.

2.5.1.2.4 Site Area Structural Geology

The structural geology of the BBNPP site described in this section has been developed using the following sources:

- the BBNPP site reconnaissance and subsurface explorations performed for this study,
- results of earlier investigations performed at the SSES site, and
- published geologic literature.

There have been no geologic structures identified during this investigation that pose a threat to the BBNPP site operations. The following discussions will support that conclusion by presenting the information on the geologic structures present within 25 miles (40 km) of the BBNPP site, and with increasing detail within the 5 mile (8 km) and 0.6 mile (1 km) distances from the site.

The following discussions present the current understanding of the geologic structures within the site vicinity, starting with the deep crystalline basement, followed by the overlying folded and lithified sedimentary bedrock, and concluding with the on-site investigations conducted for this report. As reported in more detail in Section 2.5.1.1.4, there are faults and folds that occur within the 25 mi (40 km) BBNPP site vicinity (Figure 2.5-193 and Figure 2.5-199). These include the Light Street and Berwick faults within the Berwick Anticlinorium, the Lackawanna Synclinorium and the Catawissa-McCauley Mountain Synclinorium. Each will be discussed in turn in the following sections.

2.5.1.2.4.1 Structures in the Crystalline Basement

Available geophysical data in surrounding areas indicate that the basement likely consists of exotic crystalline magmatic arc material (Hansen, 1986; Glover, 1995). Regional geologic cross sections developed from geophysical, gravity, and aeromagnetic surveys, as well as limited deep borehole data from outside of the BBNPP site area, suggest that complexly deformed, metamorphosed crystalline igneous rocks of Precambrian and Paleozoic age are likely present at approximately -33,000 ft (-10,058 m) msl (Figure 2.5-187 and Figure 2.5-191) (Crawford, 1999; King, 1974; and Gold, 2005). The basement map in Figure 2.5-187 (Gold, 2005) confirms the depth to the basement rocks as well as the relative featureless nature of that surface beneath the site.

To supplement the discussion of basement structures, regional and site vicinity maps of the gravity and magnetic fields are presented in Figure 2.5-23 and Figure 2.5-24 (Kucks,1999) and Figure 2.5-25 and Figure 2.5-26 respectively (Bankey, 2002). Regional Tectonic Features and Basins are depicted on potential base maps in Figure 2.5-215, Figure 2.5-216, Figure 2.5-217 and Figure 2.5-218. None of these data reveal new anomalies related to geologic structures.

© 2007-2012 UniStar Nuclear Services, LLC. All rights reserved.
COPYRIGHT PROTECTED

The following sections discuss the local gravity and magnetic anomalies, as presented in more detail inSection 2.5.1.1.4.3.

2.5.1.2.4.1.1 Gravity Data and Features

Anomalies in gravity data occur from density contrasts in size and depth of geologic structures. Gravity highs, or positive anomalies, are created by abundant thickness or shallow burial of dense features, while gravity lows are from mass deficiencies. Long wavelengths show deep structures or highly concentrated deep structures, and shorter wavelengths are created by shallower structures (Lavin, 1999).

As shown on Figure 2.5-24, the only feature relevant to the site vicinity is the Scranton gravity high, that has a northeast trend that is sub-parallel to the folds in the current mountains. The long wavelength of this high and the shallow gradients along its margins indicates its deep burial. The Scranton gravity high is related to dense mafic material that was emplaced during Late Precambrian rifting (Lavin, 1999).

2.5.1.2.4.1.2 Magnetic Data and Features

Magnetic data compiled for the 2002 Magnetic Anomaly Map of North America reveal numerous northeast-southwest trending magnetic anomalies, generally parallel to the structural features of the Appalachian orogenic belt (Bankey, 2002) (Figure 2.5-27). The magnetic map allows a visualization of the geological structure of the upper crust in the subsurface showing the spatial geometry of bodies of rock and the presence of faults and folds.

The BBNPP site is located in an area with few anomalies and with low gradients between anomalies (Figure 2.5-28). These conditions are consistent with the profound basement depths in the vicinity of the site. The BBNPP site is situated in the middle of a northeast-trending area of low magnetic relief related to a block of Precambrian basement called the Clingman-Ocoee block which is bounded to the northwest by the New York-Alabama Lineament and to the southeast by the Clingman-Ooee Lineament (Johnston, 1985b).

The magnetic data published since the mid-1980's (Bankey, 2002) confirm the interpretations and provide additional documentation of previous observations (i.e., EPRI, 1986) across this region of eastern North America, and do not reveal any new anomalies.

2.5.1.2.4.2 Berwick Anticlinorium

The principal bedrock structure within the site area is the Berwick Anticlinorium (also referred to as the Montour Anticline (Pohn, 2000)), which has been described (Inners, 1978) as "a moderately complex, first order fold which trends in a northeast-southwest direction". The bedrock map and section of the Berwick Quadrangle (Inners, 1978) shows the formations at the BBNPP site area to consist of Silurian, Devonian, and Carboniferous rocks that have been gently folded, with limited faulting (Figure 2.5-193 and Figure 2.5-194). The BBNPP site is situated on the northern limb of the fold. Two faults have been mapped in the vicinity: the Light Street fault located on the northern limb of the fold, and the Berwick fault, inferred to be on the southern limb of the fold. The northeast end of both faults lies within the site area, but do not directly underlie the site.

Unconformably overlying this Paleozoic bedrock is a thin covering of a few flat-lying post-Paleozoic formations composed primarily of glacial till and colluvium overburden, laid down by multiple Quaternary glacial events (Inners, 1978) (Figure 2.5-195 and Figure 2.5-196).

© 2007-2012 UniStar Nuclear Services, LLC. All rights reserved.
COPYRIGHT PROTECTED

2.5.1.2.4.2.1 Light Street Fault

The 28 mile (46 km) (Klawon, 1995) long Light Street fault approaches to within 2 mi (3.2 km) of the BBNPP site (Figure 2.5-193 and Figure 2.5-194). The Light Street Fault brings into contact the Marcellus Formation from the Onondaga and Old Port formations. Based on published data (Inners, 1978; Gillmeister, 1993; Klawon, 1995) the nature of this fault is described as being either (1) a thrust fault that dips in a southerly direction and eliminates a section of the statigraphy between the Wills Creek and Marcellus formations; (2) the detachment of a major décollement that dips to the north; (3) a late stage left-lateral strike slip fault (Gillmeister, 1993); or (4) a combination of (1) and (2) (Inners, 1978). The simplest explanation for the fault occurrence in the area, as well as evidence gathered by Klawon (Klawon, 1995), indicate that it is a south-dipping reverse fault as mapped in Figure 2.5-193 and Figure 2.5-194.

The presence of the Light Street Fault is attributed to the folding and faulting actions that occurred at the site area during the Alleghanian Orogeny, approximately 250 million years ago (Inners, 1978). Figure 2.5-194 shows that the fault does not cut the Quaternary surface deposits overlying the area. This is confirmed by the surficial geologic map (Figure 2.5-196) that also shows no evidence of the fault penetrating those deposits.

There is no historical seismicity that is spatially related to this fault (Figure 2.5-188) (EPRI, 1986). A paleoseismological study of geologic features thought to result from Quaternary tectonic faulting in the Eastern United States (Wheeler, 2006), did not identify this fault as being active.

Because of the age of last motion on this fault, and its lack of historical seismicity, the Light Street Fault is not considered to be a capable tectonic source and poses no threat to BBNPP.

2.5.1.2.4.2.2 Berwick Fault

The Berwick Fault is identified by a repeating of the section of the Old Port and Keyser formations on the southern limb of the fold. The fault is inferred from limited surface data and from a water well log drilled at the Berwick Lumber and Supply Company at 329 West Second Street in Berwick, PA (Figure 2.5-193 and Figure 2.5-194) (Inners, 1978). The investigators were unable to locate this well and it appears to have been abandoned prior to the site investigation. The inferred Berwick Fault lies within the site area and its northeastern end comes to within approximately 3.5 mi (5.6 km) of the BBNPP site. The length of the Berwick Fault is not completely mapped and is believed to be a south-dipping reverse fault on the south flank of the Berwick Anticlinorium (Figure 2.5-194) (Inners, 1978). The Berwick fault extends east-northeastward into an exposed third order anticline in the Marcellus-Mahantango interval (Inners, 1978).

This fault is like the Light Street fault, in respect to both its age and its lack of recent seismicity. Because the Berwick Fault is attributed to the folding and faulting actions that occurred approximately 250 million years ago (Inners, 1978), and because there is no seismicity that is spatially related to this feature (Figure 2.5-188) (EPRI, 1986) (Wheeler, 2006), the Berwick fault is not considered a capable tectonic source, and poses no threat to BBNPP.

2.5.1.2.4.3 Lackawanna and Catawissa-McCauley Mountain Synclinoria

Sectional views of the site geology (Figure 2.5-191 and Figure 2.5-194) show these two folds to be synclines located beneath Lee and Huntington Mountains to the north (Lackawanna Synclinorium), and just beyond Nescopeck Mountain to the south (Catawissa-McCauley Mountain Synclinorium). The southern end of the Lackawanna Synclinorium (Inners, 1978) lies

© 2007-2012 UniStar Nuclear Services, LLC. All rights reserved.
COPYRIGHT PROTECTED

within the site area and a portion of it is shown in the northwest corner of Figure 2.5-193. The Lackawanna Synclinorium is a coal-bearing 68 mi (110 km) long structural trough in the Appalachian foreland of northeastern Pennsylvania (Harrison, 2004), that extends to the northeast of the site. The entire synclinorium was thought to be an Alleghanian thin-skinned contractional structure that formed similarly to the fold trains of the central Appalachian Ridge and Valley province (Harrison, 2004). However, interpretation of seismic reflection data from across the structure suggests that the synclinorium formed primarily by the removal of salt (Harrison, 2004).

The Catawissa-McCauley Mountain synclinorium is represented by the synclinal axis in the extreme lower right corner of Figure 2.5-193, just south of Nescopeck Mountain. The axes of this synclinorium follow the regional trends to the southwest-northeast, parallel with the axis of the Berwick Anticlinorium. This syncline has been delineated from numerous outcrop searches (Inners, 1978), geophysical data and a limited number of deep boreholes that penetrate the crust (Pohn, 2000). This fold is the northern-most part of the Anthracite Region located to the south of the site. The Anthracite region, located within a northeast plunging syncline, is the most faulted area of the Appalachian Ridge and Valley Province (Hornberger, 2004) (Figure 2.5-199). The dominant faults consist of thrust faults, as part of the base décollement which separates thrusted and folded Paleozoic rocks from Precambrian basement rocks. The fault system has not been active since the post Carboniferous period and is located 20 mi (32 km) to the south of the site (Berg, 1980).

These folded features were formed at the same time as the Berwick Anticline (approximately 250 Ma), show limited faulting, and have no historical seismicity spatially related to them (EPRI, 1986) (USGS, 2008). Because of the age of the deformations and the lack of current seismicity related to them, these features are not considered to be capable tectonic sources and pose no threat to BBNPP.

2.5.1.2.4.4 Site Investigations

The investigations at the site include a subsurface investigation for the foundation study, a geophysical investigation, and a field reconnaissance to inspect surface features for evidence of deformation, including folding, faulting and liquefaction. A subsurface investigation was completed at the SSES site, adjacent to the BBNPP site to the east, as part of the FSAR process for that site. The conclusions of that investigation at the SSES location are relevant to the current study by reason of proximity and intended purpose.

2.5.1.2.4.4.1 Subsurface Investigations at the BBNPP Site

Geologic sections developed from geotechnical data collected from 44 boreholes as part of the BBNPP study (as discussed in Section 2.5.4) provide detailed information in the upper 420 ft (128 m) of strata for the presence of structures directly beneath the site. The investigation at the BBNPP site indicates that the site is underlain by unfaulted Middle Devonian shale of the Mahantango Formation. Bedding planes of the formation have been measured at and near the site with strike azimuth measurements ranging predominantly from 61 to 100 degrees and dip angles between 10 and 30 degrees to the north-northwest (Figure 2.5-209). The bedding plane observations within the Mahantango Formation are obscured by strong overprinting from a steeply dipping cleavage. Cleavage planes have been measured at and near the site with strike azimuth measurements ranging from 60 to 92 degrees and dip angles between 58 and 75 degrees to the south-southeast (Figure 2.5-209).

The top of the bedrock shale beneath the site is covered by a layer of residual soil that formed by weathering of the Mahantango Shale itself. Because of the location of the site on a

© 2007-2012 UniStar Nuclear Services, LLC. All rights reserved.
COPYRIGHT PROTECTED

topographic high, the vast majority of any younger sediment deposited during the retreat of the glaciers has been predominantly eroded away leaving only isolated location of thin till remaining. In the lower elevations of the site below the break in slope of the hill where the pond will be located, there is only glacial till and outwash deposits present overlying the bedrock as any residual soils at these elevations were removed by the advance of the glaciers (Figure 2.5-205). Figures 2.5-200 through 2.5-204 show that the residual soils form a blanket over the bedrock surface that mimics the shape of the underlying bedrock surface. Since the time of glacial retreat, weathering and stress relief have left a pattern of weathered and fractured rock overlying the sound rock and underlying the residual soils. Cross sections prepared oblique to the previously mapped northeast-trending Light Street and Berwick faults (Figures 2.5-200 and 2.5-201 show a slightly rolling bedrock surface below the BBNPP site, without offsets that would be characteristic of a faulted area.

Although the bedrock formations underlying the BBNPP site are dipping and have experienced folding during the Alleghanian Orogeny (Williams, 1987; Faill, 1999a), surficial sediments at the site display no signs of faulting or folding during the Pleistocene to Holocene time period, and rest unconformably on the eroded surface of the tilted beds of the local shale bedrock of the Mahantango Formation.

2.5.1.2.4.4.2 Geophysical Investigations

Because earth materials exhibit characteristic wave propagation velocities, they can be classified simply in terms of their seismic velocity. Hence, seismic refraction surveys were performed to support site characterization studies for the BBNPP (Section 2.5.4.2.2.2.3). The seismic refraction data were interpreted to assist in characterizing the local subsurface geologic materials regarding the thickness of the soil overburden, depths to weathered or fractured bedrock, and depths to competent bedrock. Seismic refraction surveys were operated along 9 profile lines totaling 7440 linear feet (2268 m) of coverage. The data for the surveys were collected from May 26 to June 5, 2010 using approved quality assurance procedures. The complete report of this survey (GeoVision, 2010) is included in the Appendices.

Figure 2.5-116 is a map depicting the layout of the 9 lines used during the survey (Lines A1 through A5, oriented east-west; and Lines B1 through B4, oriented north-south). Seismic refraction velocity profiles are presented on Figures 2.5-119 through 2.5-124c with the vertical scale measuring elevation in feet. Tomographic inversion routines are the most appropriate data modeling technique for this site because velocity gradients are assumed to be present within weathered bedrock at this site, and refraction tomography techniques are often able to resolve complex velocity structure (e.g. velocity gradients) that can be observed in bedrock weathering profiles. Layer based modeling techniques such as the Generalized Reciprocal Method (GRM) are not able to accurately model the velocity gradients that can be observed in weathered bedrock such as at the BBNPP. However, The GRM method was used to confirm velocity ranges in the tomographic models.

These interpreted velocity profiles indicate that the elevation of the competent rock is highest in the northern portion of the site, and forms an east-west to southeast-northwest trending depression in the central portion of the site with elevation increasing again to the south. Figure 2.5-118 is a representation of the surface of the competent bedrock. The top of this surface is based on an interpreted velocity in the 11,000 to 13,000 feet per second (ft/s) range (3,400 to 4,000 meters per second (mps)). The approximate locations of the top of the decomposed, weathered and competent shale identified in boreholes within 50 ft (15.2 m) of

© 2007-2012 UniStar Nuclear Services, LLC. All rights reserved.
COPYRIGHT PROTECTED

the seismic lines is included on the seismic models to aid with interpretation (Figures 2.5-119 through 2.5-124c).

Two possible weathered shale units are identified within the tomographic profiles; one based on geologic description (WS1) and the other based on the depth at which RQD exceeds 0% (WS2) (GeoVision, 2010). The locations of the 4,000, 6,000 and 12,000 ft/s (1,200, 1,800 and 3,700 mps) contours from intersecting lines are also shown on the seismic models for discussion. There is a distinct possibility at this site that velocity structure may be slightly different at intersecting lines because of the complex velocity structure of the weathered shale (GeoVision, 2010). Additionally, bedding and fracture attitudes relative to the seismic line orientation may have a significant impact on modeled seismic velocity structure. A review of the data in the figures shows no offsets or abrupt changes in the tops of the bedrock that could indicate recent deformation. See section 2.5.4 for a more detailed discussion of the geophysical analysis.

The map of the top of the competent Mahantango Shale from the boring log data (Figure 2.5-125) shows a surface similar to that shown in Figure 2.5-118 that was developed for the top of competent rock from the geophysical data. Both maps show that the interpreted elevation of the top of the competent rock, as mentioned above, is highest in the northern and southern portions of the site, with an east-west to southeast-northwest trending depression in the center of the site.

Because the interpreted upper surfaces of the decomposed shale and weathered shale (Figures 2.5-118a and 2.5-118b) generally parallel surface topography at the site, the depression in the top of the competent rock in the center of the site is related to a thickened weathered shale layer, as can be seen in the reflection profiles (Figures 2.5-119 through 2.5-124c) and cross-sections (Figures 2.5-200 through 2.5-204). The reason for over-thickened weathered and fractured rock zone in the center of the site is presumably because this zone is located under a gully in the hill, which is oriented parallel to major structural orientations within the Site Area. Within this gully, precipitation is channeled off of the hill and leads to greater subsurface penetration of water within this zone, leading to deeper weathering and fracture propagation in the Mahantango Formation. However, because the top surfaces of the decomposed shale and weathered shale are parallel to the ground surface, with no obvious offset, it is clear that no Quaternary faulting has affected the site.

The close correlation between the seismic data and the boring log data, both in locating the top of rock elevation and in the lack of observed faulting in the rock mass, further confirms the interpretation by earlier researchers in the area (Inners, 1978, Williams, 1987) that there is no evidence of faulting in the Quaternary deposits underlying the site.

2.5.1.2.4.4.3 Interpretation of Aerial Photography and LIDAR Imagery

Aerial reconnaissance within a 25 mi (40 km) radius of the site was conducted by various personnel using aerial photographs from numerous publications. Figure 2.5-128 is a sample of the aerial imagery used, and it contains selected way points from the field reconnaissance. LIDAR imagery of the BBNPP site vicinity was also acquired for review and interpretation (Figures 2.5-220 through 2.5-225). The LIDAR image contains elevation data with a 2 ft (0.6 m) contour interval (PAMAP, 2008). The aerial reconnaissance investigated geomorphology and targeted numerous previously mapped geologic features and potential seismic sources (e.g., Berwick fault, Light Street fault, and Berwick Anticlinorium).

© 2007-2012 UniStar Nuclear Services, LLC. All rights reserved.
COPYRIGHT PROTECTED

Figure 2.5-206 and 2.5-210 contain four topographic cross-sections (A, B, C on Figure 2.5-206, and D on Figure 2.5-210) based on the new LiDAR data set from Luzerne County. The intent of these figures is to review the LiDAR data set in both plan and section view to evaluate the detailed surface of the land as captured by the LiDAR process.

Figure 2.5-209 shows the BBNPP site geology on the LiDAR data base map. Figure 2.5-219 depicts the surficial sediment description including glacial derived features and deposit contacts overlaid on the LiDAR data base map. The same LiDAR data base map without the surficial sediment description is shown in Figure 2.5-220.

The site area geology is presented on the LiDAR data base map in Figure 2.5-221 and Figure 2.5-222 shows the same image without the site area geology. Figure 2.5-223 is similar to Figure 2.5-222 but has the higher altitudes eliminated to show the detail for the lower elevations where the BBNPP site is located.

The site vicinity geology along with the LiDAR base map is presented in Figure 2.5-224. Figure 2.5-225 shows the LIDAR base map without the site vicinity geology. Figure 2.5-224 and Figure 2.5-225 include not only the trace for the Lightstreet and Berwick faults, but also all of the described geologic features at this scale.

The interpretation of the plan-view LiDAR maps incorporates an evaluation of the fracture traces and lineaments visible on the images as linear valleys and swales and straight segments of streams. The features are especially visible for the site on Figure 2.5-220. The orientations of the fractures observed in the outcrop of the Mahantango Shale are within the reported envelope of orientations reported by Inners (1978, Figure 3). There is a single dominant set striking just west of north, with a subordinate set at nearly right angles to the first. These appear to be nearly vertical. The right-angle bend in Walker Run to the southwest of the BBNPP center point, illustrates those trends, as the Run has eroded through the glacial cover to expose the underlying structures. Other orientations are present in the outcrop areas of formations to the north and south of the Mahantango, as is also reported by Inners (1978, Figures 4 and 5).

The topographic cross sections presented in Figures 2.5-206 and 2.5-210 display no offsets that are attributable to the actions of the Berwick or Light Street Faults. The current work confirms the work by Inners (1978) who reports the faults to be locally buried beneath the glacial terrace gravels. In the excavations for the Susquehanna Units, Inners found several slickensided surfaces at low-angles to the bedding planes located less than 1 mile (1.6 km) to the east of the site (Figure 2.5-209). He interpreted these surfaces as wedge faults that usually developed along small-scale drag folds during the folding of the units during the Alleghanian Orogeny, approximately 250 Ma (Inners, 1978). The current investigation found similar slickensided surfaces, the closest at a distance of 0.30 miles (.50 km) to the southwest of the site (Figure 2.5-209), The throw on these faults is usually less than three feet (Inners, 1978), and the field team observed no offset of the glacial materials overlying this feature in the field.

As shown in the following section, field reconnaissance coupled with interpretation of remote imagery (review and inspection of features preserved on the images) shows that there are no geomorphic features indicative of potential Quaternary activity along trends of the postulated folds and faults interpreted by Inners and Williams (Inners, 1978; Williams, 1987). No features suggestive of tectonic deformation were observed in the Quaternary glaciofluvial deposits, and no potential liquefaction features were observed along the Susquehanna River.

© 2007-2012 UniStar Nuclear Services, LLC. All rights reserved.
COPYRIGHT PROTECTED

2.5.1.2.4.4.4 Field Reconnaissance

Information developed from the literature and the imagery interpretation was supplemented by field reconnaissance within a 25 mi (40 km) radius of the site. These field-based studies were performed to verify, where possible, the existence of mapped bedrock faults in the BBNPP site area and to assess the presence or absence of geomorphic features suggestive of potential Quaternary fault activity along the mapped faults, or previously undetected faults. Features reviewed during the field reconnaissance and office-based analysis of aerial photography and LIDAR imagery were based on a compilation of existing regional geologic information in the vicinity of the BBNPP site.

Field reconnaissance was conducted by geologists in teams of two or more. Field reconnaissance visits in 2007, 2008, 2009, and 2010 focused on exposed portions of the Mahantango Formation, other formation exposures along the faces of Lee, Huntington and Nescopeck Mountains, and roads traversing the site vicinity. Key observations and discussion items were documented in field notebooks and photographs. Field locations were logged by hand on detailed topographic base maps and with hand-held Global Positioning System (GPS) receivers (Figure 2.5-209). There were no faults or other forms of deformation noted in the field. No surface expression of either the Berwick or Light Street faults was noted, consistent with the conclusions documented in the literature. Figure 2.5-119 and Figure 2.5-120 (Waypoint 12 on Figure 2.5-207) show that there is no offset in the Quaternary deposits along Syber Creek, where the trace of Light Street Fault crosses it. Photos of the shale bedrock on the site show the steeply dipping nature of the strong persistent cleavage. Bedding dipping to the NNW is visible but highly obscured by this cleavage (Figure 2.5-125 and Waypoint WF3 on Figure 2.5-128). Outcrops in a nearby borrow area show an undeformed contact between the glacial overburden and the shale bedrock (Figure 2.5-126, and Figure 2.5-127 and Waypoint WF5 on Figure 2.5-128).

A supplemental reconnaissance was conducted during the fall of 2008, to investigate the occurrence of potential liquefaction features along the Susquehanna River. The field reconnaissance was carried out by a team of geologists and engineers from Paul C. Rizzo Associates, Inc, and John Sims & Associates from both the land and water approaches to the river banks. The investigation was conducted for the course of the river for a reach of 25 miles (40 km) upstream and downstream of the site (Figure 2.5-207). Because of the prevalent bedrock exposures in both the river banks and the river bottoms, few locations were found where liquefaction conditions were possible and no evidence that liquefaction had occurred. Figure 2.5-121 through Figure 2.5-124 show the rocky nature of the riverbed and its banks and some of the typical exposures found during the investigation (for Waypoints WP1, WP10, WP20, and WP22 respectively).

A third reconnaissance was conducted during the Spring of 2009 to further investigate the occurrence of potential liquefaction features along the Susquehanna River. The study was conducted along approximately 10 miles of the Susquehanna River along the south and east bank in areas accessible by auto and on foot (Figure 2.5-207). The investigated areas lie south and east of the BBNPP site within the Berwick 7.5-minute topographic quadrangle.

Two tributaries of the Susquehanna River, the Wapwallopen and Little Wapwallopen creeks, were found to run on bedrock and are relatively small, but similar to other tributaries of the Susquehanna and this region. These two tributaries, like many other streams in the original study, have been disturbed by coal mining activities.

© 2007-2012 UniStar Nuclear Services, LLC. All rights reserved.
COPYRIGHT PROTECTED

Following the additional reconnaissance, the conclusions about the low potential for liquefaction of the area remain unchanged. The rugged terrain of the Allegheny Mountains, narrow floodplains, and intense modification of the topography through anthracite coal mining confirm those conclusions. The Susquehanna River is a gently meandering river with numerous rock-core islands and boulder-cobble gravel bars. At nearly all sites that were visited, bedrock was present or nearby. The ubiquitous presence of bedrock at or near the surface militates against liquefaction and the presence of paleoliquefaction structures. The tributaries of the Susquehanna have narrow floodplains. Coal mining debris from mine waste dumps, carried by the tributary streams of the Susquehanna, form the visible floodplain deposits of the tributaries.

Fine-grained sediments, when present, are thin and lack the usual prerequisite for preservation of paleoliquefaction features, which is fine to medium sand overlain by 1-2 meters of fine upward silt with a clay cap. However, the banks are commonly vegetated, which significantly reduces accessibility to exposures in the river banks. Further modification of the banks by manmade stone walls, built to prevent erosion or the railroad right-of-way and sections of an early canal, exist through the studied section of the Susquehanna River.

In the spring of 2010, another reconnaissance was undertaken to investigate the portion of the Site Area (5 mile radius (8 km)) that was not investigated during the previous reconnaissance efforts due to the change in Site location. Since the Site location was relocated approximately 1,000 feet (305 m) north-northwest, the difference in the physical area between the two Site Areas forms a crescent shaped zone within the north-northwest edge of the new Site Area. At its thickest, the crescent is approximately 1,000 feet (305 m) wide at its widest and along the curvature it was about 15 miles (24 km) long.

As is typical with most of Pennsylvania and the Site Area, outcrop is limited. For this reason, targets for investigation and ground truthing were areas of known or suspected outcrop within and around the crescent zone. The main areas of investigation were therefore locations on Lee Mountain, Huntington Mountain, Shickshinny Mountain, Penobscot Mountain, and the Mocanaqua, Pond Hill and Berwick Heights areas, as well as a few locations outside of the Site Area where the Light Street Fault has been mapped.

In all outcrops investigated, orientation of bedding, joint surfaces and lineations were measured and rock lithology recorded. Due to prior detailed mapping in the area (Inners, 1978) all rock units had previously been identified. The other main objective of the reconnaissance was to look for any evidence of Quarternary faulting. The observations and measurements made as part of this investigation did not reveal anything inconsistent with the findings of the previous BBNPP reconnaissance efforts or with prior geologic mapping in the areas (Inners, 1978). All measurements were consistent with the mapped structures, all rock lithologies were consistent with unit descriptions and no evidence of recent faulting was observed, including in the area of the mapped Light Street Fault.

2.5.1.2.4.4.5 Prior Work Completed at the SSES Units 1 and 2

A detailed subsurface exploration near the BBNPP site was performed earlier as part of the original SSES FSAR (SSES FSAR, 2003) for the SSES Units 1 and 2 foundation and supporting structures. That exploration covered an area that is located adjacent to the east side of the BBNPP site and addressed the same issues as the current BBNPP FSAR investigation. The high level of detail in that earlier study, and the close proximity to the BBNPP site make that study especially relevant to the current effort. The level of effort for that earlier FSAR study included drilling 250 geotechnical boreholes, collecting down-hole geophysical data, and acquiring

© 2007-2012 UniStar Nuclear Services, LLC. All rights reserved.
COPYRIGHT PROTECTED

seismic refraction data from across the site. Previous site investigations performed for the existing units are summarized in the SSES Final Safety Analysis Report (FSAR) (SSES FSAR, 2003). As cited in the SSES FSAR, these previous investigations provide the following results documenting the absence of Quaternary faults at and within the area of the BBNPP site:

- Interpretation of satellite photos and topographic maps. This interpretation revealed no evidence of surface rupture, surface warping, or offset of geomorphic features indicative of active faulting.
- Interviews with personnel from government agencies and private organizations. These interviews concluded that no known faults are present beneath the existing SSES Units 1 and 2 site area.
- Seismicity Analysis -This analysis showed that no microseismic activity has occurred in the site area; the site is located in a region that has experienced only infrequent minor earthquake activity approximately 35 mi (56 km) northeast of the BBNPP site, around the border of Lackawanna and Wyoming Counties; the closest fault-related epicentral location (the Anthracite Zone) is greater than 25 mi (40 km) away. No earthquake within 50 mi (80 km) of the SSES site has been large enough to cause significant damage in the time the region has been populated, approximately 270 years.
- Approximately 250 exploratory boreholes were drilled at the SSES Units 1 and 2 site area. Borehole data have provided evidence for the lateral continuity of strata across the existing SSES site area (SSES FSAR, 2003). The inspection of soil samples has revealed no adverse effects indicative of geologically recent or active faulting.
- Field reconnaissance of many surface outcrops at the site and within the 25 mi (40 km) radius of the site, coupled with geophysical surveys, provided no evidence for faulting at the SSES site.
- At the time of the original studies for the SSES FSAR in 1975 (SSES FSAR, 2003), published maps showing bedrock faults within a 5 mi (8 km) radius of the SSES site identified only the Light Street fault. The closest significant bedrock faults mapped prior to 1975 were faults located about 80 mi (129 km) southwest of the SSES site near Lewistown, PA (SSES FSAR, 2003).

2.5.1.2.5 Site Area Geologic Hazard Evaluation

This subsection identifies and discusses potential geologic hazards that could be present in the site area (within 5-mi (8-km) radius of the site). These potential geologic hazards include rock dissolution features (caves and karst features), active deformation zones, landslides, abandoned underground mine cavities, and volcanism.

There are no caves or recognized karst features in the site area, and none were discovered during the investigations for BBNPP and SSES. Small- to medium-scale dissolution features occur in the site area where carbonate bedrock formations occur. Formations containing carbonate beds in the area include the Wills Creek, Tonoloway, Keyser, Old Port, and Onondaga formations of Silurian and Lower Devonian strata. These formations are at least 1,600 ft (488 m) below ground surface (bgs) at the BBNPP site and have not been penetrated by any borings at the site. These formations crop out or are located closer to the ground surface approximately 3 to 8 miles (5 to 13 km) southwest of BBNPP. Water wells in the Berwick area (southwest of BBNPP) are screened in the limestone formations and obtain ground water from dissolution features located along joints, fractures, and bedding planes (Inners, 1978). For example, the public water supply wells located in Berwick are screened in the Keyser

© 2007-2012 UniStar Nuclear Services, LLC. All rights reserved.
COPYRIGHT PROTECTED

Formation at depths of 87 to 160 ft (27 to 49 m) bgs and yield up to 500 gallons per minute (gpm) (1893 liters per minute (lpm)) (Williams, 1987). However, one well drilled to a depth of 515 feet (157 m) at the same location produced no water (Williams, 1987). This is an example supporting the general belief that fractures, dissolution features, and secondary permeability of the rock decreases with depth because the confining pressure within the rock increases with depth and causes the fractures to close. This is discussed in greater detail in Section 2.4.12.1.2.8. Because the carbonate formations are located at least 1,600 ft (488 m) bgs, the frequency and magnitude of fracturing and dissolution features should be minimal.

Inventories of caves and karst features in Pennsylvania show no caves or karst to be present in Luzerne or Columbia counties; all significant caves and karst features are located in southeast, central, and southwestern Pennsylvania. The nearest significant cave is Crystal Cave near Kutztown, Pennsylvania, which is located approximately 46 mi (74 km) from BBNPP. In summary, based on the absence of limestone dissolution features in the 0.6-mile (1 km) site radius and the depth of 1,600 ft (488 m) to limestone, karst is not a geologic hazard at the BBNPP site.

Major springs, defined as having flow rates of 100 gpm (379 lpm) or more, can be an indicator of carbonate formations and karst features. An inventory of major springs in the Ridge and Valley Province of Pennsylvania by the USGS (Saad, 1990) identified only one major spring in Luzerne or Columbia counties; this spring (Lu 8) discharges from the Mauch Chunk Formation, approximately 10 miles (16 km) southeast of BBNPP (Saad, 1990). The Mauch Chunk Formation consists of clastic sedimentary rocks ranging from claystone up to conglomeratic sandstones. There are no carbonate strata in this formation and this formation does not underlie the BBNPP site. Thus, there are no documented cases of springs in Luzerne or Columbia counties that infer the presence of karst or significant dissolution features in carbonate rocks.

The last major tectonic events that generated large-scale earthquakes, faults, and deformation along the eastern coast of the United States occurred in the Mesozoic Era (Triassic and Jurassic, approximately 250 Ma). Active deformation processes and seismic activity within the site vicinity have been minimal since the Mesozoic Era, except for the Charlevoix Seismic Zone in Canada and the Charleston Seismic Zone in South Carolina. Thus, active deformation activities are not a source of significant geologic hazard at BBNPP (see also Section 2.5.1.1.4).

Because there are steep slopes and high topographic relief present in this portion of the Ridge and Valley Physiographic Province, landslides and other mass movements (e.g., soil slumping) can occur. Approximately 7.5 miles (12 km) north-northeast of the BBNPP site, is the location of one of the largest landslides in Pennsylvania. Approximately 4,000 years ago (Ka), a rock block landslide on the south side of Schickshinny Mountain caused 20,260,000-27,450,000 yd^3 (15,490,000-20,987,000 m^3) of rock to move 1,250 ft (381 m) onto the Susquehanna River floodplain and partially diverted the Susquehanna River (Inners, 1988). Varnes (Varnes, 1978) defines a rock block slide as "a translational slide in which the moving mass consists of a single unit that is not greatly deformed". Another much smaller landslide located 2 miles (3.2 km) northeast of the first (9.5 miles (15.3 km) northeast of BBNPP), was witnessed in 1947 in which rainfall, that deposited 6 inches of rain within 2 hours, likely caused approximately 122,000 yd^3 (93,277 m^3) to move downslope within a minute or two (Inners, 1988). Including the aforementioned landslides, thirteen rock block slides have been mapped between Nanticoke, PA and Shickshinny, PA (a distance of approximately 9 miles (14.5 km)) along the south side of Schickshinny Mountain, with a total volume of about 56,000,000 yd^3 (42,815,000 m^3) (Inners, 1988). All of these landslides, with the exception of the 1947 landslide, are prehistoric, having a maximum age of approximately 11 Ka, and were the likely results of a combination of the

© 2007-2012 UniStar Nuclear Services, LLC. All rights reserved.
COPYRIGHT PROTECTED

dipslope of Shickshinny Mountain being ultimately underlain by a weak mudstone, a relatively low dipping angle of the rock beds on the slope (approximately 20°), and the undercutting of the sandstone-mudstone bedding planes by the Susquehanna River (Inners, 1988). Inners (Inners, 1988) suggests that even though porewater pressure as a result of high moisture conditions in the area was the most likely cause of many of these historic rock block landslides, the larger landslides probably required a longer 'wet' season and/or multiple year high-moisture conditions. All of these rockslides occurred at least 7.5 miles (12 km) upstream along the banks of the Susquehanna River. No landslides (historic or pre-historic) of this proportion have been recognized or mapped in the BBNPP site area.

Underground coal mining has occurred in the Pennsylvania anthracite fields since the early 1800s. Hundreds of miles of underground workings are located in four different anthracite basins. While underground mining is currently very limited, the abandoned workings still result in mine subsidence immediately over the mine workings. The nearest anthracite basin (the Northern Anthracite Basin) is located at least four miles (6 km) distance from BBNPP, and all coal-bearing formations within the site area have been eroded long ago, so coal mining and mine subsidence at this distance will have no potential effect on the construction or operations of the BBNPP.

Tectonic activities and volcanism have not occurred in the eastern United States since the Mesozoic Era. Volcanic activity during the past 2,000 years has only occurred in the Western United States. The area of greatest volcanic activity is associated with the Cascade Range in the states of Washington, Oregon and California. The last eruption was Mount St. Helens in 1980. This is over 2500 mi (4023 km) away from the BBNPP site. Therefore, volcanism and related hazards are not a geologic hazard at the BBNPP site or vicinity.

Based on the discussion above, there are no geologic hazards that represent a risk to the construction or operation of the BBNPP.

2.5.1.2.6 Site Engineering Geology Evaluation

This section addresses the engineering significance of geologic and geotechnical characteristics of features and materials within the site area (5 mi (8 km) radius) and site location (0.6 mi (1 km) radius).

2.5.1.2.6.1 Engineering Soil Properties and Behavior of Foundation Materials

The overburden soil, based on engineering properties defined in Section 2.5.4., is not an adequate foundation substrate for safety related structures or facilities. The overburden soils are composed of mostly residual silty to clayey sand to poorly graded sand with gravel and poorly graded gravel or silty to clayey gravel with sand. This soil was formed from weathering and decomposition of the Mahantango Shale. Below the soil is a zone of soft weathered rock typically followed by a harder, competent shale that is very fractured. Due to the abundance of fracturing in this zone, these incompetent rock layers are also unsuitable for founding of safety related structures. As a result, the overburden soil and incompetent shale layers will be removed in order to found safety related structures or facilities on bedrock. Sound bedrock of the Mahantango Formation is encountered between 16 and 115.5 ft (5 - 35 m) below ground surface (bgs) at the BBNPP site location (0.6 mi (1 km) radius). Selected Category 1 structures will be founded on sound rock and the rock surface will be improved with removal of weathered and fractured rock, cleaning, and localized concrete fill as necessary. Engineering soil properties, including index properties, static and dynamic strength, and compressibility are discussed in Section 2.5.4. Variability and distribution of properties for the foundation

© 2007-2012 UniStar Nuclear Services, LLC. All rights reserved.
COPYRIGHT PROTECTED

bearing soils will be evaluated and mapped as the excavation is completed. Settlement monitoring will be based on analyses performed for the final design.

2.5.1.2.6.2 Unrelieved Residual Stresses in Bedrock

Due to the fact that bedrock within the site area (5 mi (8 km) radius) and the site location (0.6 mi (1 km) has been buried under a cover of glacial sediments since the Wisconinan glacial event (17,000-22,000 my), it is expected that removal of the glacial overburden will cause unloading effects such as exfoliation jointing or opening of existing joints and subsequent slaking of the rock. Current investigation found that this glacial outwash and till glacial deposits are constricted to the location of the Essential Service Water Emergency Makeup System (ESWEMS), below the break in slope of the hill (Figure 2.5-205). Above the break in the slope, glacial deposits are sparse with the majority of the overburden described as residual soil that formed from weathering of the underlying shale bedrock (Figure 2.5-200, through Figure 2.5-204). The thickness of what could be associated with till deposits, is no more than 3 ft (0.9 m). Where fine grained sandstone layers were found deeper than this, it has been interpreted as being part of the Mahantango Formation, as has been previously described. The superficial deposits in the site were disturbed for agricultural purposes and the surface was cleared of these very sparse erratics, which were plowed and then used to build the stone walls found in the site. The result of a glacial erosion above the break in the slope is found to have only partially removed the top of the weathered bedrock, which is thicker in the top of the site location, and thins down hill towards the location of the Essential Service Water Emergency Makeup System (ESWEMS). The effects of isostatic rebound as a result of rapid erosion due to glacial melt and rapid reduction in normal stress due to glacial retreat is well established in the literature (Pelletier, 2004; Stern, 2005). In addition, geologic mapping in the site vicinity (5 mi (8 km) radius) revealed very continuous, low angle exfoliation fractures in the Mahantango Formation in outcrops which range up to ten feet in height. The presence of these fractures is a typical reaction to stress relief, and is an indication that unloading the rock by excavating overburden will result in the propagation of some low angle fractures that may necessitate further excavation or rock anchoring in some areas.

2.5.1.2.6.3 Zones of Alteration, Weathering, and Structural Weakness

Below the top of competent bedrock (as defined by weathering, fracture density and rock mass rating (RMR) scores), no unusual weathering profiles have been encountered during the site investigation. Calcareous zones, thin pyrite lenses and zones exhibiting increased fracture density at depth observed in isolated areas are the only other discrete zones that vary from the preponderance of the competent rock. The site area bedrock geologic map and site location geologic map (Figure 2.5-198 and Figure 2.5-197, respectively), compiled by Berg (1980) and Schruben (1998) indicates that most of the site area (5 mi (8km) radius) surrounding, and including, the BBNPP site are underlain by Late Silurian, Devonian, and Lower Mississippian bedrock. More specifically, the site location (0.6 mi (1 km) radius) bedrock is Upper Devonian Mahantango Formation (part of the Hamelton group) which serves as the foundation for SSES Units 1 and 2. (SSES FSAR, 2003). The most recent geologic influence on the site, not including sub aerial exposure and erosion, is the Wisconinan glaciation that is discussed in Section 2.5.1.1.1. The relevance of this glacial event with respect to alteration, weathering, and structural weakness is complex. Glacial scour removed weathered rock from the surface of the site area (5 mi (8 km) radius) and glacial deposits left behind after glacial retreat have altered the weathering rate at the bedrock interface; this effect is described in the location of the Essential Service Water Emergency Makeup System (ESWEMS), below the break in slope of the hill (Figure 2.5-205). However, due to the site location being on top of a local hill above the more glaciated valleys, very little of the glacial soils are present here. What remains below residual soil is a slightly to intensely weathered bedrock surface followed by a

© 2007-2012 UniStar Nuclear Services, LLC. All rights reserved.
COPYRIGHT PROTECTED

fractured zone. Based on the performance of the Mahantango Formation as the SSE Units 1 and 2 foundation, it is evident that, with proper excavation and foundation preparation, this rock is a suitable foundation bearing material for Category 1 structures. As noted previously, any zones of alteration, weathering, or increased joint or fracture density will be mapped during excavation and evaluated for removal, cleaning, and treatment to remediate any revealed unsafe conditions.

2.5.1.2.6.4 Deformational Zones

The Light Street fault and the Berwick Anticlinorium (Inners, 1978) have been mapped at or within the 5 miles (8 km) radius of the BBNPP site. The Berwick Anticlinorium is an east-northeast striking, gently northeast plunging anticlinal structure with an axial trace that trends directly through the site area (5 mi (8 km) radius) and site location (0.6 mi (1 km) radius). The Berwick Anticlinorium is a symmetrical structure in the site area (5 mi (8 km) radius) with the north-northwest and south - southeast dipping limbs with an averaged 35 degree NNW and SSE respectively. The relevance of the Berwick Anticlinorium is that the dip of the limbs have the potential to provide sliding planes within an excavation. In addition, axial plane cleavage may have the potential to result in toppling failure from an excavation slope. Any excavations into bedrock or bedrock slopes will be mapped and monitored during excavation and backfill.

Field mapping efforts did not successfully identify surface expression of the Light Street Fault. Deformation including fracturing and folding was mapped in outcrop and is discussed in Section 2.5.3.2. In addition, a thorough literature search was conducted to identify previous studies that have identified any form of deformation in the rock or identified in the stratified glacial deposits.

In addition, two other zones of deformation have been noted within the site area (5 mi (8 km radius). These zones of deformation include the Lackawanna Synclinorium (Inners, 1978),which is located approximately 4 miles (6.4 km) northwest of the site, and the inferred Berwick fault (Inners, 1978), which is inferred to lie approximately 3 miles (4.8 km) southwest of the site (see Section 2.5.1). Neither of these features are considered capable tectonic sources, as defined in Appendix A of Regulatory Guide 1.165 (NRC, 1997).

Based on geologic mapping, interpretation of borehole data and interpretation of geophysical investigation, no deformation zones were encountered in the site investigation for BBNPP that have a detrimental effect the engineering properties of the rock mass. In addition, no deformational zones were encountered during the exploration or excavation for SSES Units 1 and 2. Detailed mapping of the excavation for the proposed excavation for the BBNPP Category 1 structure will document the presence, orientation, continuity, and classification of any deformational zone. Each deformational zone or structure will be evaluated as to its potential affect on the foundation.

2.5.1.2.6.5 Prior Earthquake Effects

Two earthquakes have occurred within 25 miles (40 km) of the site (to the south and southeast) as shown on Figure 2.5-103. There are no reported earthquakes in the BBNPP site area (5 mi (8 km) radius). Studies of the SSES Unit 1 and 2 excavation, available outcrops within the BBNPP site area, and extensive exposures along the road cuts of Nescopeck and Lee Mountain, have not indicated any evidence for earthquake activity that affected the Paleozoic bedrock or Quaternary surficial deposits within the site area. Also, there are no historic accounts of earthquakes in the site area (5 mi (8 km) radius)

© 2007-2012 UniStar Nuclear Services, LLC. All rights reserved.
COPYRIGHT PROTECTED

2.5.1.2.6.6 Effects of Human Activities

Previous investigations performed for the SSES Unit 1 and 2, and for this study identified no activities that would adversely affect the site. However, stones for construction material in the form of crushed rock have been quarried in the site vicinity. Sand and gravel also have been quarried, mostly along the Susquehanna River bank primarily for highway construction. Even though no mineral resources of economic significance and no mine workings are noted at BBNPP site, there are deep anthracite coal mining operations located at 11 miles east of the BBNPP site near the town of Shickshinny. Additionally, oil and gas reserves have been explored near Harveys Lake, approximately 25 miles (40 km) north of the BBNPP site. There is limited withdrawal of groundwater or recharge through impoundments of water in the site area, and adverse effects related to pore pressure change from groundwater withdrawal or injection are not expected to occur at BBNPP site.

2.5.1.2.6.6.1 Oil and Gas Production in the Site Region

The Site Region has had extensive oil and gas exploration and production throughout "recent" history with the vast majority having occurred in the Appalachian Basin, though much of it has not been systematically recorded (Ryder, 1995). Discovery of oil in the Drake well, Venango County, northwestern Pennsylvania in 1859 marked the beginning of the modern petroleum industry not just in the Appalachian Basin, but in the entire country (Milici, 2006). This discovery well, reported to have made at least ten barrels of oil per day for a year, and was the first oil produced commercially from a well drilled in the U. S., was produced from an Upper Devonian stray sandstone at a depth of about 70 ft (21 m) (Milici, 2006). It opened a prolific trend of oil and gas fields producing from Upper Devonian, Mississippian, and Pennsylvanian sandstone reservoirs that extends from southern New York, across western Pennsylvania, central West Virginia, and eastern Ohio, to eastern Kentucky (Ryder, 1995). From 1859 through 1993, approximately 2.3 billion barrels of oil (366 million cubic meters) and 31 trillion cubic feet of gas (TCFG) (878 billion cubic meters) have been produced from the trend (Ryder, 1995). Primary annual oil production in the trend peaked at about 36.3 million barrels of oil (MMBO) (5.7 million cubic meters) in 1900, whereas oil production from secondary recovery peaked at about 37.6 MMBO (6 million cubic meters) in 1937 (Ryder, 1995). Exploration in the trend presently is for gas in low-permeability sandstone reservoirs at depths between 4,500 and 6,000 ft (1370 and 1830 m) (Ryder, 1995).

A second major trend of oil and gas production in the Appalachian Basin began in 1885 continued into the early 1900's in Lower Silurian "Clinton" sandstone reservoirs in Ohio and Lower Silurian Medina Group sandstones in western New York (Ryder, 1995). Hydrofracing techniques introduced in the early 1950's extended the Lower Silurian "Clinton" and Medina sandstone trend across most of central and eastern Ohio, northwestern Pennsylvania, western New York, and a small part of northeastern Kentucky. Current exploration in the trend is for gas in low-permeability sandstone reservoirs at depths between 5,500 and 7,000 ft (1676 and 2134 m) (Ryder, 1995). Important gas discoveries from the Lower Devonian Oriskany Sandstone in Ohio, New York, and West Virginia, in the 1920-1930's opened a major gas-producing trend across parts of New York, Pennsylvania, Maryland, Ohio, West Virginia, Kentucky, and Virginia (Ryder, 1995). Overlying the Oriskany Sandstone is the fractured Middle Devonian Huntersville Chert, which is another important reservoir in the Oriskany trend in Pennsylvania, West Virginia, and Maryland. Exploration is still active in this trend for gas trapped in faulted anticlines at depths between 6,000 and 9,000 ft (1830 and 2743 m) (Ryder, 1995).

Other locations underlain by Appalachian Basin strata have been relatively unsuccessful in production of oil and gas such as deep drilling in the late 1970's and early 1980's for gas in the

© 2007-2012 UniStar Nuclear Services, LLC. All rights reserved.
COPYRIGHT PROTECTED

Appalachian Fold and Thrust Belt east of the Allegheny structural front. Only two small oil fields discovered in southwestern most Virginia and five or six small gas fields elsewhere have been productive in the folded and thrusted rocks of this region (Ryder, 1995).

According to Ryder (1995), nineteen conventional plays and 16 unconventional plays are recognized in the Appalachian Basin Province. However, natural gas prices have steadily increased over the past few years and development of "unconventional" gas resources, such as gas shales have become of great interest (Sumi, 2008). Therefore, in the last ten years or so, Upper Devonian Black shales have become the most prolific and therefore explored play in the region. Upper Devonian Sandstones overlying the Black Shales have been tapped for over a century as they trap gas and oil sourced from the Shales (Ryder, 1995). However, the Devonian black shales themselves are actually the oldest gas play in the U.S. and include the Marcellus Shale, Rhinestreet Shale Member of the West Falls Formation, Pipe Creek Shale Member of the Java Formation, lower and upper parts of the Huron Member of the Ohio Shale, and Cleveland Member of the Ohio Shale (Ryder, 1995). The greatest thickness of combined black-shale units in the basin is in central Pennsylvania, where together, the units are about 1,400 ft (426 m) thick.

Oil and wet thermal gas are the expected hydrocarbon types in the play with production of the unit dependent upon the coincidence of several factors, including relatively abundant organic matter at suitable thermal maturity and a reservoir that is significantly enhanced by a naturally occurring fracture system (Ryder, 1995). Devonian source rocks in western New York and northwestern Pennsylvania are in the zone of oil generation, whereas Devonian source rocks in west-central Pennsylvania, southeastern Ohio, and northern and north-central West Virginia are in the zone of gas generation. The southeastern part of the play in southwestern Pennsylvania and adjoining West Virginia may be over mature with respect to the generation of oil and gas (Ryder, 1995).

Because of its large expanse, abundance of fractures, lower-density and high porosity, the Marcellus shale of the Hamilton Group (which underlies the Mahantango shale at the BBNPP Site) has been the main target of exploration of all the Devonian Black Shales within the past ten to fifteen years in Pennsylvania and surrounding states (Milici, 2006; Sumi, 2008). The Marcellus shale spans a distance of approximately 600 miles (965 km), running from the southern tier of New York, through the western portion of Pennsylvania into the eastern half of Ohio and through West Virginia with an areal extent of about 54,000 square miles (140,000 square km) (Sumi, 2008) (Figure 2.5-233). The shale is extremely variable in thickness, ranging from a few feet to more than 250 ft (76 m) in thickness, and generally becomes thicker to the east. The majority of the Marcellus shale is more than a mile deep, and in some areas it extends 9,000 ft (2743 m) below the surface (Sumi, 2008) (Figure 2.5-234).

Due to its great depth, the Marcellus Shale was not previously considered much of a resource, and is still a very expensive target with drilling costs approaching a million dollars for a traditional vertical well (Sumi, 2008). Because of the variability in geology and depth of the resource, the economic and technical feasibility of extracting the shale gas will vary from region to region, but with the current price of gas and conservative estimates of gas in place for the Marcellus shale at 168 TCFG (4.8 trillion cubic meters) and optimistic estimates up to 516 TCFG (14.6 trillion cubic meters) (Sumi, 2008), exploration is booming.

One of the main reasons that the Marcellus Shale has become such a valued target is because of its known abundance of natural fractures in the Appalachian Plateau as opposed to joint growth in gray shales and siltstones and particularly coarser grained rocks (Engelder, 2009).

© 2007-2012 UniStar Nuclear Services, LLC. All rights reserved.
COPYRIGHT PROTECTED

The most pervasive systematic joints observed in Devonian black shale of the Appalachian Plateau include sub-vertical east-northeast joints (J_1) and younger sub-vertical northwest-striking cross-fold joints (J_2) (Lash, 2009). Their formation was driven exclusively by fluid pressure generated as a consequence of hydrocarbon-related maturation supplemented by subsequent tectonic compaction during the Alleghanian tectonic cycle (Engelder, 2006; Lash, 2009).

Despite the presence of these joints, stimulation techniques to better link up the two crossing sets is taking place in abundance in Marcellus Shale production. This is done through Hydraulic fracting, which is the process of creating and expanding fractures around the wells by injecting a mixture of water, sand and chemicals under pressure. Such induced hydraulic fractures should propagate east-northeast to west-southwest because of the direction of the contemporary tectonic stress field (Engelder, 2009). This can be done in vertical wells, but because of the orientation of the natural joints, hydraulic fracture treatments in vertical wells are not capable of taking full advantage of the bulk permeability anisotropy of black shale, nor the normal-stress induced permeability anisotropy (Engelder, 2009). However, if a well is drilled horizontally through the Marcellus Shale in a north-northwest or south-southeast direction, the bulk permeability anisotropy can be best taken advantage of due to crossing the east-northeast oriented, more permeable J_1 joints (Engelder, 2009). The ability to economically stimulate the formation along the horizontal well bore has made many wells commercial successes and wells that were previously drilled vertically to access Marcellus Formation or other formations can be reused to drill horizontally through the Marcellus Shale (Sumi, 2008).

Overall, the areas of greatest Marcellus Shale gas development are north and northwest of the BBNPP Site in the Appalachian Plateau province, as shown on Figures 2.5-235. Records obtained from the Pennsylvania Department of Environmental Protection (PADEP, 2010), Bureau of Oil and Gas Management show that from January to August 2010 there have been four Marcellus Shale gas well permits issued in Columbia County with no wells drilled, and four permits issued in Luzerne County with one well drilled. These numbers are extremely low compared to the more northern and western counties in Pennsylvania that have over one thousand permits issued and five hundred wells drilled (Figure 2.5-235). The closest well to the BBNPP site is located 9.5 miles (15.3 km) to the east-northeast but is an old well and not related to the Marcellus Shale gas drilling. Thus, the potential to find oil or gas deposits of economic value are very low for the area immediately surrounding the BBNPP and therefore any associated hazards should be of very minimal concern.

2.5.1.2.6.7 Site Groundwater Conditions

A detailed discussion of groundwater conditions is provided in Section 2.4.12. Groundwater in the site area is founded in both the glacial overburden and bedrock formations. In the vicinity of the BBNPP site, the glacial overburden aquifer is the most capable aquifer for transmitting groundwater, and it is the source aquifer for many wells and springs in the county. Groundwater in the bedrock formations is present primarily in secondary openings, including factures, joints, and bedding plane separations. As a result, the ability of the bedrock to store groundwater or yield to well is typically less than the overburden for formations. Because buildings will be founded on sound rock, both the glacial overburden and fractured bedrock aquifers will be affected by construction of the BBNPP. However, active dewatering methods within the sites are expected to limit the adverse effects in the aquifers during excavation and construction (see Section 2.4.12.5.1).

© 2007-2012 UniStar Nuclear Services, LLC. All rights reserved.
COPYRIGHT PROTECTED

2.5.1.3 References

Aber, 2001. Appalachian Mountains, J. S. Aber, Website: http://academic.emporia.edu/aberjame/struc_geo/appalach/appalach.htm, Date accessed: January 23, 2008.

Aggarwal, 1978. Earthquakes, Faults, and Nuclear Power Plants in Southern New York and New Jersey, Science, Volume 200, p 425-429, Y. Aggarwal and L. Sykes, 1978.

Anglin, 1981. Microseismicity in the mid-St. Lawrence Valley Charlevoix zone, Bulletin of the Seismological Society of America, Volume 71, p 1553-1560, F. Anglin and G. Buchbinder, 1981.

Anglin, 1984. Seismicity and Faulting in the Charlevoix Zone of the St. Lawrence Valley, Bulletin of the Seismological Society of America, Volume 74, Number 2, p 595-603, F.M. Anglin, April, 1984.

Armbruster, 1987. The 23 April 1984 Martic Earthquake and The Lancaster Seismic Zone In Eastern Pennsylvania, Bulletin of the Seismological Society of America, Volume 77, Number 2, p 877-890, J. Armbruster and L. Seeber, 1987.

Ator, 2005. A Surficial Hydrogeologic Framework for The Mid-Atlantic Coastal Plain Professional Paper 1680, U.S. Geological Survey, U.S. Department Of The Interior Scott W. Ator, S.W., Denver, J.M., Krantz, D.E., Newell, W.L., Martucci, S.K., 2005.

Bailey, 1998. Late Neoproterozoic Extension-Related Magma Emplacement in the Central Appalachians: An Example from the Polly Wright Cove Pluton, The Journal of Geology, Volume 106, p 347-359, Christopher M. Bailey and Richard P. Tollo, 1998.

Bankey, 2002. Magnetic Anomaly Map of North America, U.S. Geological Survey Open File Report 02-414, scale 1:10,000,000, 1 sheet, V. Bankey, A. Cuevas, D. Daniels, C. Finn, I. Hernandez, P. Hill, R. Kucks, W. Miles, M. Pilkington, C. Roberts, W. Roest, V. Rystrom, S. Shearer, S. Snyder, R. Sweeney and J. Velez, 2002.

Barnes, 2002. The Geological Story of Pennsylvania (3rd ed.), Pennsylvania Geological Survey, 4th ser., Educational Series 4, p 1-44, J.H. Barnes and W.D. Sevon, 2002.

Becker, 2006. Linking Late Paleozoic sedimentary provenance in the Appalachian basin to the history of Alleghanian Deformation, American Journal of Science, vol. 306, p. 777-798, T.P. Becker, W.A. Thomas, and G.E. Gehrels, 2006.

Behrendt, 1983. Structural elements of the U.S. Atlantic margin delineated by the second vertical derivative of the aeromagnetic data, U.S. Geological Survey Geophysical Investigation Map GP-956, scale 1-2,500,000, J. Behrendt and M. Grim, 1983.

Bennington, 2006. Geology of New York and New Jeresey, Hofstra University, 21 p, J. B. Bennington and C. Merguerian, 2006.

Bent, 1992. A re-examination of the 1925 Charlevoix, Quebec, earthquake, Bulletin of the Seismological Society of America, Volume 82, p 2097-2113, A. Bent, 1992.

Benson, 1992. Map of the exposed and buried Early Mesozoic rift basins/synrift rocks of the U.S. Middle Atlantic Continental Margin, Miscellaneous Map Series No. 5, Delaware Geological Survey, University of Delaware, Newark, R. Benson, 1992.

© 2007-2012 UniStar Nuclear Services, LLC. All rights reserved.
COPYRIGHT PROTECTED

Berg, 1980. Geologic map of Pennsylvania, Pennsylvania Geological Survey, 4th ser., Map1, scale 1:250,000, 3 sheets, T.M. Berg, 1980.

Berg, 1999. Part II, Stratigraphy and Sedimentary Tectonics, Chapter 8: Devonian-Mississippian Transition, in C.H. Shultz ed., The Geology of Pennsylvania: Pennsylvania Bureau of Topographic and Geologic Survey Special Publication 1, p 128-137, T.M. Berg, 1999.

Blackmer, 2005. Preliminary Bedrock Geologic Map of a Portion of The Wilmington 30- By 60-Minute Quadrangle, Southeastern Pennsylvania, Open-File Report OFBM-05-01.0, Pennsylvania Geological Survey, Fourth Series, Blackmer, G. C., Harrisburg, 2005.

Bobyarchick, 2007. Kinematics of the Everona Fault, Central Virginia, Bobyarchick Andy R., , Geological Society of America Abstracts with Programs, Session No. 33, Cenozoic Tectonics in the Southeastern United States, Vol. 39, No. 2, p. 89, March 2007.

Bollinger, 1977. Reinterpretation of the intensity data for the 1886 Charleston, South Carolina, earthquake, *in* Rankin, D.W., ed., Studies related to the Charleston, South Carolina, earthquake of 1886 --A Preliminary Report: U.S. Geological Survey Professional Paper 1028-B, p. 17-32, G.A. Bollinger, 1977.

Bosbyshell, 2009. Amphibolite Geochemistry in the Wissahickon Formation, Philadelphia, PA: New Results and Implications for Wilmington Complex- Laurentia Collision, Geological Society of America Abstracts with Programs, Vol. 41, No. 3, H. Bosbyshell.

Bradley, 2002. Emsian Synorogenic Paleogeography of the Maine Appalachians, The Journal of Geology, Volume 110, p 483-492, Dwight Bradley and Robert Tucker, 2002.

Bradley, 1989. Taconic Plate Kinematics as Revealed by Foredeep Stratigraphy, Appalachian Orogen, Tectonics, Volume 8, No. 5, p 1037-1049, D.C. Bradley, 1989.

Braile, 1997. New Madrid Seismicity, Gravity Anomalies, and Interpreted Ancient Rift Structures, Seismological Research Letters, Volume 68, Number 4, p 599-610, Lawrence W. Braile, William J. Hinze, G. Randy Keller, July/August 1997.

Braun, 1988. Glacial Geology of the Anthracite and North Branch Susquehanna Lowland Regions, p 1-25, D. Braun, 1988.

Braun, 2003. Margin of Laurentide Ice to the Atlantic Coastal Plain: Miocene -Pleistocene landscape evolution in the Central Appalachians, in Easterbrook, D.J., ed., Quaternary Geology of the United States, INQUA 2003 Field Guide Volume, [Desert Research Institute], Braun, D.D., Pazzaglia, F.J., and Potter, N., Jr., 2003.

Braun, 2004. Late Wisconsin Deglaciation of the Great Bend- Tunkhannock Region of Northeastern Pennsylvania, Guidebook for the 67th Annual Reunion of the Friends of the Pleistocene, p 1-26, D. Braun, 2004.

Braun, 2007. Surfical Geology of the Red Rock 7.5-Minute Quadrangle, Luzerne, Sullivan, and Columbia Counties, Pennsylvania, Pennsylvania Geological Survey, Fourth series, Open-File Report OFSM 07-10.0, 19p, Portable Document Format (PDF), Duane D. Braun, 2007.

© 2007-2012 UniStar Nuclear Services, LLC. All rights reserved.
COPYRIGHT PROTECTED

Brezinski, 1999. Part II, Stratigraphy and Sedimentary Tectonics, Chapter 9: Mississippian, in C.H. Shultz ed., The Geology of Pennsylvania: Pennsylvania Bureau of Topographic and Geologic Survey Special Publication 1, p 138-147, D.K. Brezinski, 1999.

Brezinski, 2010. Late Devonian glacigenic and associated facies from the central Appalachian Basin, eastern United States, GSA Bulletin, v. 122; no. 112, p. 265-281, David K, Brezinski, C. Blaine Cecil, and Viktoras W. Skema, 2010.

Castle, 2005. Petrophysics of Lower Silurian sandstones and integration with the tectonic-stratigraphic framework, Appalachian basin, United States, AAPG Bulletin, Volume 89, Number 1, p 41-60, James W. Castle and Alan P. Byrnes, January 2005.

CFR, 2007. Geologic and Seismic Sitting Criteria, Title 10, Part 100.23, Code of Federal Regulations, CFR, 2007.

Clark, 1992. Central Appalachian Periglacial Geomorphology, A Field Excursion Guidebook under the auspices of the 27th International Geographical Congress, Commission on Frost Action Environments, Agronomy Series Number 120, G. Clark, R. Behling, D. Braun, E. Ciolkosz, J. Kite and B. Marsh, August 1992.

Cleaves, 1992. Regoliths of the Middle-Atlantic Piedmont and Evolution of the Polymorphic Landscape, Southeastern Geology, Volume 39, Number 3 and 4, p 122-199, E. Cleaves, October, 1992.

Cotter, 2008. The Geologic History of Central Pennsylvania, Introduction, p 1-3, Plate Tectonics, p 1-4, Episode Two, p 1-7, End of Episode Two, p 1-2, Episode Three, p 1-2, Episode Four, p 1-4, E. Cotter, 2008.

Crangle, 2002. Statigraphic Framework of Cambrian and Ordovician Rocks in the Central Appalachian Basin from Lake County, Ohio, to Juniata County, Pennsylvania, Revised and Digitized from Ryder 1992, Stratigraphic Framework of Cambrian and Ordovician Rocks in the Central Appalachian Basin from Medina County, Ohio, through Southwestern and South-Central Pennsylvania to Hampshire County, West Virginia, U.S. Geological Survey, Miscellaneous Investigation Series, Map I-2200. R.D. Crangle Jr., 2002.

Crawford, 1999. Part III, Structural Geology and Tectonics, Chapter 16: Piedmont Upland, in C.H. Shultz ed., The Geology of Pennsylvania: Pennsylvania Bureau of Topographic and Geologic Survey Special Publication 1, p 234-241, M.L. Crawford, W.A. Crawford, A.L. Hoersch, and M.E. Wagner, 1999.

Crone, 2000. Data for Quaternary Faults, Liquefaction Features, and Possible Tectonic Features in the Central and Eastern United States, East of the Rocky Mountain Front, U.S. Geological Survey, Open-File Report 00-260, p 1-332, A.J. Crone and R.L. Wheeler, 2000.

Crowl, 1980. Glacial Border Deposits of Late Wisconsinan Age in Northeastern Pennsylvania, Pennsylvania Bureau of Topographic and Geologic Survey, General Geology Report 71, G.H. Crowl and W.D. Sevon, 1980.

Crowl, 1999. Part II, Quaternary, Chapter 15, in C.H. Shultz ed., The Geology of Pennsylvania: Pennsylvania Bureau of Topographic and Geologic Survey Special Publication 1, p 224-232, G.H. Crowl and W.D. Sevon, 1999.

© 2007-2012 UniStar Nuclear Services, LLC. All rights reserved.
COPYRIGHT PROTECTED

Csontos, 2008. New Madrid seismic zone fault geometry, Geosphere, Volume 4, No 5, p. 802-813, doi: 10.1130/GES00141.1; R. Csontos, and R.V. Arsdale, 2008.

Cumbest, 2000. Comparison of Cenozoic Faulting at the Savannah River Site to Fault Characteristics of the Atlantic Coast Fault Province: Implications for Fault Capability, U.S. Dept. of Energy Contract No. DE-AC09-96SR18500, 51 p, R. Cumbest, D. Wyatt, D. Stephenson, and M. Maryak, 2000.

DCNR, 2007a. Geologic Map of Pennsylvania, Pennsylvania Department of Conservation and Natural Resources, Website: http://www.dcnr.state.pa.us/topogeo/maps/map7.pdf, Date accessed: December 14, 2007.

DCNR, 2007b. Piedmont Lowland Section Piedmont Province, Pennsylvania Department of Conservation and Natural Resources, Website: http://www.dcnr.state.pa.us/topogeo/map13/13pls.aspx, Date accessed: December 14, 2007.

DCNR, 2007c. Gettysburg-Newark Lowland Section Piedmont Province, Pennsylvania Department of Conservation and Natural Resources, Website: http://www.dcnr.state.pa.us/topogeo/map13/13gnls.aspx, Date accessed: December 14, 2007.

DCNR, 2007d. Piedmont Upland Section Piedmont Province, Pennsylvania Department of Conservation and Natural Resources, Website: http://www.dcnr.state.pa.us/topogeo/map13/13pus.aspx, Date accessed: December 14, 2007.

DCNR, 2007e. Reading Prong Section, Pennsylvania Department of Conservation and Natural Resources, Website: http://www.dcnr.state.pa.us/topogeo/map13/13rps.aspx, Date accessed: December 14, 2007.

DCNR, 2007f. Allegheny Mountain Section Appalachian Plateau Province, Pennsylvania Department of Conservation and Natural Resources, Website: http://www.dcnr.state.pa.us/topogeo/map13/13alms.aspx, Date accessed: August 9, 2010.

DCNR, 2008a.Trenton Black River Carbonates: Introduction, Pennsylvania Geological Survey, Pennsylvania Department of Conservation and Natural Resources, Website: http://www.dcnr.state.pa.us/topogeo/tbr/tbrintro.aspx, Date accessed: July 5, 2008.

DCNR, 2008b. Great Valley Section Ridge and Valley Province, Pennsylvania Department of Conservation and Natural Resources, Website: http://www.dcnr.state.pa.us/topogeo/map13/13gvs.aspx, Date accessed: January 22, 2008.

DCNR, 2008c. Lowland and Intermediate Upland Section Atlantic Coastal Plain Province, Pennsylvania Department of Conservation and Natural Resources, Website: http://www.dcnr.state.pa.us/topogeo/map13/13lius.aspx, Date accessed: January 22, 2008.

DCNR, 2008d. Eastern Lake Section Central and Lowland Provinces, Pennsylvania Department of Conservation and Natural Resources, Website: http://www.dcnr.state.pa.us/topogeo/map13/ 13els.aspx, Date accessed: April 10, 2008.

DCNR, 2008e. Appalachian Mountain Section Ridge and Valley Province, Pennsylvania Department of Conservation and Natural Resources, Website: http://www.dcnr.state.pa.us/topogeo/map13/13ams.aspx, Date accessed: August 9, 2010.

© 2007-2012 UniStar Nuclear Services, LLC. All rights reserved.
COPYRIGHT PROTECTED

Dewey, 1999. Part IV. Regional Geophysics, Chapter 27 Seismotectonic Framework, in C.H. Shultz ed., The Geology of Pennsylvania, Pennsylvania Bureau of Topographic and Geologic Survey Special Publication 1, p 339-341, J. Dewey and D. Gordon, 1999.

Diedrich, 1999. Depositional Cyclicity in the Lower Devonian Helderberg Group of New York State, The Journal of Geology, Volume 107, p 643-658, Nathaniel W. Diedrich and Bruce H. Wilkinson, 1999.

Dodson, 2008. Structural Geology of the Transylvania Fault Zone in the Appalachian Thrust Belt, Bedford County, Pennsylvania, Northeastern Section - 43rd Annual Meeting, E. Dodson, March, 2008.

Doig, 1990. 2300 year history of seismicity from silting events in Lake Tadoussac, Charlevoix, Quebec, Geology, Volume 18, p 820-823, Ronald Doig, September 1990.

Drake, 1999. Part III, Structural Geology and Tectonics, Chapter 17: South Mountain and Reading Prong, in C.H. Shultz ed., The Geology of Pennsylvania: Pennsylvania Bureau of Topographic and Geologic Survey Special Publication 1, p 242-255, A.A. Drake, Jr., 1999.

Ebel, 1982. The 1981 microearthquake swarm near Moodus, Connecticut, Geophysical Research Letters, Volume 9, Number 4. p 397-400, J. E. Ebel, V. Vudler, and M. Celata, 1982.

Ebel, 1989. A comparison of the 1981, 1982, and 1987-1988 microearthquake swarms at Moodus, Connecticut, Seismological Research Letters, Volume 60, p 177-188, J. E. Ebel, 1989.

Edmunds, 1999. Part II, Stratigraphy and Sedimentary Tectonics, Chapter 10: Pennsylvanian, in C.H. Shultz ed., The Geology of Pennsylvania: Pennsylvania Bureau of Topographic and Geologic Survey Special Publication 1, p 148-169, W.E. Edmunds, V.W. Skema, and N.K. Flint, 1999.

EGC, 2006. Submittal of Revision 4 to Exelon Generation Company's Early Site Permit Application for Clinton, Including Administrative Information, Emergency Plan, Site Redress Plan, Environmental Report and Site Safety Analysis Report, April 14, 2006.

Engelder, 1980. On the Use of Regional Joint Sets as Trajectories of Paleostress Fields During the Development of the Appalachian Plateau, New York, Journal of Geophysical Research, Volume 85, Number B11, p 6319-6341, Terry Engelder and Peter Geiser, November 1980.

Engelder, 2001. Horizontal slip along Alleghanian joints of the Appalachian plateau: evidence showing that mild penetrative strain does little to change the pristine appearance of early joints, Tectonophysics 336, p 31-41, Terry Engelder, Benjamin F. Haith, Amgad Younes, 2001

Engelder, 2006. Early jointing in coal and black shale: Evidence for an Appalachian-wide stress field as a prelude to the Alleghanian orogeny, Geology, Volume 34, Number 7, p 581-584, Terry Engelder and Amy Whitaker, July 2006.

Engelder, 2009. Joint sets that enhance production from Middle and Upper Devonian gas shales of the Appalachian Basin, AAPG Bulletin, v.93, NO.7, p. 857-889, Terry Engelder, Gary C. Lash, and Redescal S. Uzcategui, 2009.

EPRI, 1986. Seismic Hazard Methodology for the Central and Eastern United States, EPRI Report NP-4726, Electric Power Research Institute, July 1986.

© 2007-2012 UniStar Nuclear Services, LLC. All rights reserved.
COPYRIGHT PROTECTED

EPRI, 1989. Probabilistic Seismic Hazard Evaluations at Nuclear Power Plant Sites in the Central and Eastern United States: Resolution of the Charleston Earthquake Issue, NP-6395-D, Electric Power Research Institute, 1989.

EPRI, 2006. Program on Technology Innovation: Truncation of the Lognormal Distribution and Value of Standard Deviation for Ground Motion Models in the Central and Eastern United States, TR-1014381, Electric Power Research Institute, August 2006.

Eriksson, 2003. Predominance of Grenvillian Magmatism Recorded in Detrital Zircons from Modern Appalachian Rivers, The Journal of Geology, Volume 111, p 707-717, Kenneth A. Eriksson, Ian H. Campbell, J. Michael Palin, and Charlotte M. Allen, 2003.

ESRI, 2007. Street Map Pro [CD-ROM], 2007 State Boundaries, Roads, Streams, County Boundaries, ESRI, 2007.

ESRI, 2008. World Shaded Relief Imagery, ESRI, Redlands, CA, USA, ESRI Website: http:// server.arcgisonline.com/ArcGIS/rest/services, last accessed November 2008.

Eusden, 2000. Timing of the Acadian Orogeny in Northern New Hampshire, The Journal of Geology, Volume 108, p 219-232, J. Dykstra Eusden, Jr., Chris A. Guzofski, Alexander C. Robinson, and Robert D. Tucker, 2000.

Evans, 1989. Appalachian Stress Study, Analysis of Devonian Shale Core: Some Implications for the Nature of Contemporary Stress Variations and Alleghanian Deformation in Devonian Rocks, Journal of Geophysical Research, Volume 94, Number B6, p 7155-7170, Keith F. Evans, Gerhard Oertel, Terry Engelder, June 1989.

Faill, 1973. Tectonic development of the Triassic Newark-Gettysburg Basin in Pennsylvania, Geological Society of America Bulletin, Volume 84, p 725-740, R. T. Faill, 1973.

Faill, 1998. A Geologic History of The North-Central Appalachians, Part 3. The Alleghany Orogeny, American Journal of Science, Vol. 298, P. 131-179, Rodger T. Faill, 1998.

Faill, 1999a. Part III. Structural Geology and Tectonics, Chapter 19 Appalachian Mountain Section of the Ridge and Valley Province, in C.H. Schultz ed., The Geology of Pennsylvania: Pennsylvania Bureau of Topographic and Geologic Survey Special Publication 1, p 268-265, R. Faill and R. Nickelsen, 1999.

Faill, 1999b. Chapter 33 - Paleozoic in The Geology of Pennsylvania, Commonwealth of Pennsylvania, Department of Conservation and Natural Resources, Bureau of Topographic and Geological Survey, in C.H. Shultz ed., The Geology of Pennsylvania: Pennsylvania Bureau of Topographic and Geologic Survey Special Publication 1, Faill, R. T., 1999.

Faill, 2004. The Birdsboro Basin, Pennsylvania Geology, Volume 34, Number 4, p 2-11, R. T. Faill, 2004.

Fletcher, 1977. Earthquakes related to hydraulic mining and natural seismic activity in western New York State, Journal of Geophysical Research, Volume 82, p 3767-3780, J. B. Fletcher and L .R. Sykes, 1977.

Frey, 1973. Influence of Salina Salt on Structure in New York-Pennsylvania Part of Appalachian Plateau, AAPG Bulletin, Volume 57, Number 6, p 1027-1037, M. Gordon Frey, June 1973.

© 2007-2012 UniStar Nuclear Services, LLC. All rights reserved.
COPYRIGHT PROTECTED

Ganis, 2005. Development Of The Martinsburg/ Hamburg Foreland Segment, Geological Society of America Abstracts with Programs, Vol. 37, No. 1, P. 17, G. Robert Ganis, 2005.

Gao, 2000. Along-Axis Segmentation and Growth History of the Rome Trough in the Central Appalachian Basin, AAPG Bulletin, Volume 84, Number 1, p 75-99, Dengliang Gao, Robert C. Shumaker, and Thomas H. Wilson, January 2000.

Gelinas, 1993. Evaluation of liquefaction-susceptible materials near moderate magnitude historical earthquakes in New England, [abs], Seismological Research Letters, Volume 64, p 259-260, R. L. Gelinas, H. M. A. Kempinen, and D. C. Amick, 1993.

GeoVision, 2010. Final Report - Seismic Refraction Investigation Bell Bend Nuclear Power Plant, Luzerne County, Pennsylvania Report 10171-03 Rev. 0, Report Prepared for RIZZO by GeoVision Geophysical Services, Corona, CA, August 2010.

Gillmeister, 1993. The Lightstreet Fault: Possible Alleghenian left-slip Deformation in Northeastern Pennsylvania, Abstracts with Programs - Geological Society of America, Vol. 25, Issue 6, p.165, Norman M. Gillmeister, 1993.

Glover, 1995. E-3 Southwestern Pennsylvania to Baltimore Canyon Trough, Geological Society of America Centennial Continent/Ocean Transect #19, L. Glover III and K. Klitgord, 1995.

Gold, 2003. Geological Report on the Skytop Road Cuts, Pennsylvania State University, Department of Geosciences, p 1-27, D.P. Gold and A.G. Doden, 2003.

Gold, 2005. Precambrian Basement Map of the Appalachian Basin and Piedmont Province of Pennsylvania, David P. Gold of the Department of Geosciences, Pennsylvania State University, in collaboration with S. S. Alexander (Pennsylvania State University), R. Cakir (Department of Geo-Environmental Engineering, Pennsylvania State University), A. G. Doden (GMRE Inc., State College, Pa.), and S.I. Root (Department of Geology, College of Wooster, Ohio), 2005.

Gold, 2008. Basement Depth and Related Geospatial Database for Pennsylvania, Pennsylvania Geological Survey, Open-File General Geology (OFGG) Report OFGG 05-01.0, p 1-6, D.P. Gold, 2008.

Gray, 1999. Chapter 18 Great Valley and Piedmont Lowland, Part III. Structural Geology and Tectonics, p 256-267, C. Gray and S.I. Root, 1999.

Greb, 2008. Appalachian sedimentary cycles during the Pennsylvanian: Changing influences of sea level, climate, and tectonics, *in* Fielding, C.R., Frank, T.D., and Isbell, J. L., eds., Resolving the Late Paleozoic Ice Age in Time and Space: Geological Society of America Special Paper 441, p. 235-248, S.P. Greb, J.C. Pashin, R.L. Martino, and C.P. Eble, 2008.

Gwinn, 1964. Thin Skinned Tectonics in the Plateau and Northwestern Valley and Ridge Provinces of the Central Appalachians: Geological Society of America Bulletin, v.75, p. 863-900, V.F. Gwinn, 1964.

Hack, 1989. Geomorphology of the Appalachian Highlands, R. Hatcher Jr., W. Thomas and G. Viele, eds., The Geology of North America, Volume F-2, The Appalachian-Ouachita Orogen in the United States, Geological Society of America, J. Hack, 1989.

© 2007-2012 UniStar Nuclear Services, LLC. All rights reserved.
COPYRIGHT PROTECTED

Hancock, 1989. Neotectonic joints, Geological Society of America Bulletin, Volume 101, p 1197-1208, 11 figures, Paul L. Hancock and Terry Engelder, October 1989

Hansen, 1986. The Lithology and Distribution of Pre-Cretaceous basement rocks beneath the Maryland Coastal Plain, Department of Natural Resources Maryland Geological Survey Report of Investigations No. 44, 27 p, H. Hansen and J. Edwards Jr., 1986.

Harlan, 2003. Gunbarrel mafic magmatic event: A key 780 Ma time marker for Rodinia plate reconstructions, Geology, Volume 31, Number 12, p 1053-1056, Stephen S. Harlan, Larry Heaman, Anthony N. LeCheminant, and Wayne R. Premo, December 2003.

Harper, 1999. Part II. Stratigraphy and Sedimentary Tectonics, Chapter 7: Devonian, in C.H. Shultz ed., The Geology of Pennsylvania: Pennsylvania Bureau of Topographic and Geologic Survey Special Publication 1, p 108-127, J.A. Harper, 1999.

Harper, 2003. Ordovician Carbonates in Central Pennsylvania, Trenton and Black River Carbonates in the Union Furnace Area of Blair and Huntingdon Counties, Pennsylvania, A Field Trip Guidebook for the Eastern Section AAPG Meeting, J. Harper Ed., J. Harper, May 2003.

Harrison, 2004. The Lackawanna synclinorium, Pennsylvania: A salt-collapse structure, partially modified by thin-skinned folding, Geological Society of America Bulletin, Volume 116, Number 11/12, p 1499-1514, Michael J. Harrison, Stephen Marshak, John H. McBride, November/December 2004.

Harrison, 2006. Fold-Thrust Belt Structures Of The Lackawanna Synclinorium, Pennsylvania: Insight Into The Tectonic Evolution Of The Central Appalachians, Northeastern Geology & Environmental Sciences, v. 28, no. 4, p. 358-367, M.J. Harrison, 2006.

Hasson, 1988. Lithofacies and paleogeography of the Conasauga Group, (Middle and Late Cambrian) in the Valley and Ridge province of east Tennessee, Geological Society of America Bulletin, Volume 100, p 234-246, Kenneth O. Hasson and C. Stephen Haase, February 1988.

Hatcher, 1987. Tectonics of the southern and central Appalachian internides, Annual Reviews of Earth and Planetary Science, Volume 15, p 337-362, R. Hatcher Jr., 1987.

Hawman, 1992. Structure of the crust and upper mantlebeneath the great Valley and Allegheny Plateau of eastern Pennsylvania, II, Gravity modeling and migration of wide-angle reflection data, Journal of Geophysical Research, Volume 97, p 393-415, R. B. Howmann and R. A. Phinney, 1992.

Hayman, 2002. Reactivation of prethrusting, synconvergence normal faults as ramps within the Ordovician Champlain-Taconic thrust system, GSA Bulletin, Volume 114, Number 4, p 476-489, Nicholas W. Hayman and W. S. F. Kidd, April 2002.

Heidbach, 2008. The release 2008 of the World Stress Map (available online at www.world-stress-map.org), O. Heidbach, M. Tingay, A. Barth, J. Reinecker, D. Kurfess and B. Muller, 2008.

Herman, 2005. Joints and Veins in the Newark Basin, New Jersey in Regional Tectonic Perspective, View from the 21st Century, 22nd Annual Meeting of the Geological Association of New Jersey, College of New Jersey, Ewing, New Jersey, p 75-116, Gregory C. Herman, 2005.

© 2007-2012 UniStar Nuclear Services, LLC. All rights reserved.
COPYRIGHT PROTECTED

Herrmann, 1978. A seismological study of two Attica, New York earthquakes, Bulletin of the Seismological Society of America, Volume 68, p 641-651, R. B. Herrmann, 1978.

Hibbard, 2006. Lithotectonic map of the Appalachian Orogen, Canada-United States of America, Geological Survey of Canada Map 02096A, 2 sheets, Scale 1: 1,500,000, J. Hibbard, C. Van Staal, D. Rankin and H. Williams, 2006.

Hickman, 1985. In Situ Stress, Natural Fracture Distribution, and Borehole Elongation in the Auburn Geothermal Well, Auburn, New York, Journal of Geophysical Research, Volume 90, Number B7, p 5497-5512, Stephen H. Hickman, John H. Healy, and Mark D. Zoback, June 1985.

Hill, 2006. The Role of Transcurrent Shear Zones in the History of the Wissahickon Formation, Geological Society of America Abstracts with Programs, Vol. 38, No. 7, pg. 301, M. Hill, October 2006.

Hinze, 1987. Magnetic Anomaly Map of North America, Decade of North American Geology (DNAG), Geological Society of America, W. Hinze and P. Hood, 1987.

Hornberger, 2004. Chapter 2.Geology of the Pennsylvania Coal Regions, Website:http:// www.dep.state.pa.us/dep/deputate/minres/bmr/beneficial_use/10%20CHAPT%202/ Chapter %202%20final.pdf, Date accessed: January 22, 2008.

Horton, 1991. Preliminary Tectonostratigraphic Terrain Map of the Central and Southern Appalachians, U.S. Geological Survey Miscellaneous Investigations Series Map I-2163, J. Horton, A. Drake and D. Rankin, 1991.

Hough, 1991. Seismological constraints on source properties of the m_b=4.0 1985 Ardsley, New York Earthquake: A characteristic rupture?, Journal of Geophysical Research, Volume 96, Number B11, p 18,183-18,195, S. E. Hough and L. Seeber, 1991.

Hurowitz, 2005. Geochemistry of Cambro-Orodvician Sedimentary Rocks of the Northeastern United States: Changes in Sediment Sources at the Onset of Taconian Orogenesis, The Journal of Geology, volume 113, p. 571-587, J.A. Hurowitzh and S.M. McLennan, 2005.

Hutchinson, 1985. New York Bight fault, Geological Society of America Bulletin, Volume 96, p 975-989, D. R. Hutchinson and J. A. Crow, 1985.

Inners, 1978. Geology and Mineral Resources of the Berwick Quadrangle, Luzerne and Columbia Counties, Pennsylvania, Pennsylvania Geological Survey, Fourth Series, p 1-34, J.D. Inners, 1978.

Inners, 1988. Bedrock and Glacial Geology of the North Branch Susquehanna Lowland and the Eastern Middle Anthracite Field, 53rd Annual Field Conference of Pennsylvania Geologists, J.D. Inners Ed., p 120-123, J.D. Inners, October 1988.

Jacob, 2004. Earthquakes and the Ramapo fault system in southeastern New York State, Lamont-Doherty Earth Observatory, K. Jacob, W. Kim, A. Lerner-Lam, L. Seeber, Web Site: http:/ /www.ldeo.columbia.edu/news/2004/04_30_04.htm, Date accessed: April 29, 2008.

Jacobeen, 1974. Structure of Broadtop Synclinorium and Its Implications for Appalachian Structural Style, AAPG Bulletin, Volume 58, Number 3, p 362-375, Frank Jacobeen, Jr. and William H. Kanes, March 1974.

© 2007-2012 UniStar Nuclear Services, LLC. All rights reserved.
COPYRIGHT PROTECTED

Jaume, 2006. Shear Wave Velocity Profiles via Seismic Cone Penetration Test and Refraction Microtremor Techniques at ANSS Strong Motion Sites in Charleston, South Carolina, Seismological Research Letters, Volume 77, Number 6, p 771-779, Steven C. Jaume, November/December 2006.

Jenden, 1993. Mixing of Thermogenic Natural Gases in Northern Appalachian Basin, AAPG Bulletin, Volume 77, Number 6, p 980-998, P. D. Jenden, D. J. Drazan, and I. R. Kaplan, June 1993.

Johnston, 1985a. Seismotectonics of the Southern Appalachians, Bulletin of the Seismological Society of America, Volume 75, Number 1, p 291-312, A.C. Johnston, D.J. Reinbold, and S.I. Brewer, February 1985.

Johnston, 1985b. A basement block model for Southern Appalachian Seismicity, Geological Society of America-Abstracts with Programs, Volume 17, Number 2, p 97, A. Johnston and D Reinbold, 1985.

Jordan, 1982. Statigraphy Of The Sedimentary Rocks Of Delaware, Bulletin No.9, Delaware Geological Survey, Newark, Deleware, Robert R. Jordan, 1982.

Kafka, 1985. Earthquake Activity in the Greater New York City Area: Magnitudes, Seismicity and Geologic Structures, Bulletin of the Seismological Society of America, Volume 75, Number 5, p 1285-1300, A. Kafka, E. Schlesinger-Miller and N. Barstow, 1985.

Kauffman, 1999. Part II, Stratigraphy and Sedimentary Tectonics, Chapter 4: Eocambrian, Cambrian, and Transition to Ordovician, in C.H. Shultz ed., The Geology of Pennsylvania: Pennsylvania Bureau of Topographic and Geologic Survey Special Publication 1, p 59-73, M.E. Kauffman, 1999.

Kelson, 1996. Multiple Late Holocene Earthquakes Along the Reelfoot Fault, Central New Madrid Seismic Zone, Journal of Geophysical Research, v. 101, p. 6151-6170. Kelson, K.I., Simpson, G.D., Van Arsdale, R.B., Harris, J.B., Haraden, C.C., and Lettis, W.R., 1996.

Kim, 2009. The 2008-2009 Earthquake Swarm Near Dillsburg, Pennsylvania, Commonwealth Of Pennsylvania Bureau Of Topographic and Geologic Survey, Open-File Report OFMI 09-01.0 2009. W.Y. Kim, M. Gold, C. Scharnberger, J. Jones, and H. Delano, 2009.

King, 1978. The New York-Alabama lineament: Geophysical Evidence for a Major Crustal Break in the Basement Beneath the Appalachian Basin, Geology, Volume 6, p 312-318, E. King and I. Zietz, 1978.

King, 1999. Part IV. Regional Geophysics, Chapter 24 Aeromagnetics, in C.H. Shultz ed., The Geology of Pennsylvania: Pennsylvania Bureau of Topographic and Geologic Survey Special Publication 1, p 323-327, E. King, 1999.

Klawon, 1995. Light Street Fault Reconsidered in Light of the Structural History of the Berwick Anticlinorium, Abstracts with Programs - Geological Society of America, Vol. 27, Issue 1, p. 61, Jeanne E. Klawon, 1995.

Kline, 1991. Provenance of Arkosic Metasediments in the Virginia Blue Ridge: Constraints on Appalachian Suspect Terrane Models, American Journal of Science, Vol. 291, February, 1991.

© 2007-2012 UniStar Nuclear Services, LLC. All rights reserved.
COPYRIGHT PROTECTED

Klitgord, 1988. U. S. Atlantic Continental Margin: Structural and Tectonic Framework, R. Sheridan and J. Grow, eds., The Atlantic Continental Margin, U.S., Geological Society of America, The Geology of North America, Volume 1-2, p 19-55, K. Klitgord, D. Hutchinson and H. Schouten, 1988.

Klitgord, 1995. Mid-Atlantic Continental Margin: The Mesozoic-Cenozoic Continent-Ocean Boundary, in L. Glover III and K. Klitgord, Chief Compilers, E-3 Southwestern Pennsylvania to Baltimore Canyon Trough, Geological Society of America Continent/Ocean Transect #19, Explanatory Pamphlet, K. Klitgord, C. Poag, L. Glover, R. Sheridan, D. Hutchinson, R. Mixon and R. Benson, 1995.

Koch, 1978. Geology and geophysics of the Moodus seismic area, Connecticut, Geological Society of America Abstracts with Programs, Volume 10, Number 2, p 71, B. F. Koch, R. J. Fahey, S. S. Quarrier, and J. F. Kick, 1978.

Komor, 1998. Sources of Geospatial Data for Central and Western New York - 1998, U.S. Geological Survey, Open-File Report 99-191, 42 p, S.C. Komor, 1998

Kucks, 1999. Bouguer Gravity Anomaly Data Grid for the Conterminous US, http:// tin.er.usgs.gov/metadata/usgravboug.faq.html Kucks, 1999.

Kulander, 2005. Regional Seismic Lines Across the Rome Trough and Allegheny Plateau of Northern West Virginia, Western Maryland, and Southwestern Pennsylvania, US Geological Survey, pamphlet to accompany Map I-2791, C.S. Kulander, and R. Ryder, 2005.

Kunk, 2004. Multiple Paleozoic Metamorphic Histories, Fabrics, and Faulting in the Westminster and Potomac Terranes, Central Appalachian Piedmont, Northern Virginia and Southern Maryland, U.S. Geological Survey, 9 p, M. Kunk, R. Wintsch, C. Southworth, B. Mulvey, C. Naeser and N. Naeser, 2004.

Lamontagne, 2002. An Overview of Some Significant Eastern Canadian Earthquakes and Their Impacts on the Geological Environment, Buildings and the Public, Natural Hazards v. 26, p. 55 -67, M. Lamontagne, 2002.

Lang, 1996. Pressure-temperature-reaction history of metapelitic rocks from the Maryland Piedmont on the basis of correlated garnet zoning and plagioclase-inclusion composition, Helen M. Lang, American Mineralogist, Volume 81.

Lash, 2009. Tracking the burial and Tectonic History of Devonian Shale of the Appalachian Basin by Analysis of Joint Intersection Style, Geological Society of America Bulletin, vol. 121, p. 265-277. Gary G. Lash and Terry Engelder, 2009.

Laughrey, 1999. Part II, Stratigraphy and Sedimentary Tectonics, Chapter 6: Silurian and Transition to Devonian, in C.H. Shultz ed., The Geology of Pennsylvania: Pennsylvania Bureau of Topographic and Geologic Survey Special Publication 1, p 91-107, C.D. Laughrey, 1999.

Lavin, 1982. Major lineaments and the Lake Erie-Maryland crustal block, Tectonics, Volume 1, p 431-440, P. M. Lavin, D. L. Chaffin, and W. F. Davis, 1982.

Lavin, 1999. Gravity, The Geology of Pennsylvania, Part IV. Regional Geophysics, Chapter 23, p 317-321, P. Lavin, 1999.

© 2007-2012 UniStar Nuclear Services, LLC. All rights reserved.
COPYRIGHT PROTECTED

Lemieux, 2000. Stratigraphy and structure of the St. Lawrence Lowland in the Charlevoix area, Quebec: relationships to impact cratering, Geological Survey of Canada, Current Research 2000-D2, p 1-7, Y. Lemieux, A. Tremblay, and D. Lavoie, 2000.

Lotto, 1997. Seismic stratigraphy of the New York bight, NY/NJ continental shelf, Geological Society of America Abstracts with Programs, Volume 29, Number 1, p 62, L. Lotto, M. A. Allison, W. C. Schwab, B. Butman, D. Foster, J. Denny, and W. Corso, 1997.

Low, 2002. Geohydrology of Southeastern Pennsylvania, Water-Resources Investigations Report 00-4166, U.S. Geological Survey, U.S. Department of the Interior, In cooperation with the Pennsylvania Department of Conservation and Natural Resources, Bureau of Topographic and Geologic Survey, Dennis J. Low, Daniel J. Hippe, and Dawna Yannacci.

Lyons, 1982. Gravity Anomaly Map of the United States, Society of Exploration Geophysicists, Scale 1: 2,500,000, P. Lyons and N. O'hare, 1982.

MacLachlan, 1999. Part VI, Geologic History, Chapter 34: Mesozoic, in C.H. Shultz ed., The Geology of Pennsylvania: Pennsylvania Bureau of Topographic and Geologic Survey Special Publication 1, p 435-449, D.B. MacLachlan, 1999.

Marple, 2000. Evidence for a Buried Fault System in the Coastal Plain of the Carolinas and Virginia-Implications for Neotectonics in the Southeastern United States, Geological Society of America Bulletin, Volume 112, Number 2, p 200-220, R. Marple and P. Talwani, February 2000.

Marple, 2004. Relationship of the Stafford Fault Zone to the Right-Stepping Bends of the Potomac, Susquehanna and Delaware Rivers and Related Upstream Along the U.S. Mid-Atlantic Fall Line: In Southeastern Geology, Volume 42, Number 3, p 123-144, R. Marple, 2004.

Matmon, 2003. Temporally and Spatially Uniform Rates of Erosion in the Southern Appalachian Great Smoky Mountains, Geology, v. 31, no. 2, p. 155-158, A. Matmon, P.R. Bierman, J. Larsen, S. Southworth, M. Pavich, M. Caffee, 2003.

McDonnell, 2008. Physical Geography of New York, T. McDonnell, Website: http:// www.nygeo.org/ny_geo.html, Date accessed: April 9, 2008.

McElroy, 2007. Bedrock Geologic Map of the Allensville Quadrangle, Huntingdon and Mifflin Counties, Pennsylvania, Pennsylvania Geological Survey, 4th ser., OpenFile Report OFBM 07-02.0, T.A. McElroy and D.M. Hoskins, 2007.

Mclaughlin, 2002. Results of Trenching Investigations Along the New Castle Railroad Survey-1 Seismic Line, New Castle, Delaware, Delaware Geological Survey, Open-File Report 43, 19 p, P. McLaughlin, S. Baxter, K. Ramsey, T. McKenna and S. Strohmeier, 2002.

Merguerian, 1996. Stratigraphy, Structural Geology, and Ductile- and Brittle Faults of New York City, Website: http://www.dukelabs.com/Abstracts%20and%20Papers/CM1996c.htm, 26 p, Date accessed: March 25, 2008.

Merguerian, 1997. Bronx River diversion- Neotectonic implications, International Journal of Rock Mechanics and Mining Sciences, Volume 34, Number 3-4, Paper Number 298, C. Merguerian and J. E. Sanders, 1997.

© 2007-2012 UniStar Nuclear Services, LLC. All rights reserved.
COPYRIGHT PROTECTED

Milici, 2006. Assessment of Appalachian Basin Oil and Gas Resources: Devonian Shale- Middle and Upper Paleozoic Total Petroleum System, US Geological Survey, Open-File Report Series 2006-1237, p 1-70, R.C. Milici and C.S. Swezey, 2006.

Milici, 2009. The Blue Ridge Thrust Belt Province (068), Piedmont Province (069), Atlantic Coastal Plain Province (070), Adirondack Uplift Province (071), and New England Province (072), U.S. Geological Survey Digital Data Series DDS-30, Release 2, one CD-ROM, Milici, R.C. Online Linkage: http://certmapper.cr.usgs.gov/data/noga95/prov68/text/prov68.pdf.

Millot, 2001. Proterozoic Eon: Mesoproterozoic Era- Greenville Orogeny, L. Sniatkowski ed., J. Millot, 2001.

Mixon, 1977. Stafford Fault System: Structure Documenting Cretaceous and Tertiary Deformation Along the Fall Line in Northeastern Virginia, Geology, Vol. 5, p. 437-440, R. Mixon and W. Newell, 1977.

Mixon, 2000. Geologic Map of the Fredricksburg 30' x 60' Quadrangle, Virginia and Maryland, Report 2607, IMAP, R. Mixon, L. Pavlides, D. Powars, A. Froelich, R. Weems, J. Schindler, W. Newell, L. Edwards, and L. Ward, 2000.

Mitra, 1988. Effects of Deformation Mechanisms on Reservoir Potential in Central Appalachian Overthrust Belt, AAPG Bulletin, Volume 72, Number 5, p 536-554, Shankar Mitra, May 1988.

Moecher, 2004. Precise Time and Conditions of Peak Taconian Granulite Facies Metamorphism in the Southern Appalachian Orogen, U.S.A., with Implications for Zircon Behavior during Crustal Melting Events, The Journal of Geology, Volume 112, p 289-304, David P. Moecher, Scott D. Samson, and Calvin F. Miller, 2004.

Mueller, 2008. Crustal Evolution in the Southern Appalachian Orogen: Evidence from Hf Isotopes in Detrital Zircons, The Journal of Geology, Volume 116, p 414-422, Paul A. Mueller, George D. Kamenov, Ann L. Heatherington, and Joshua Richards, 2008.

Murphy, 2000. Proto-Avalonia: A 1.2-1.0 Ga tectonothermal event and constraints for the evolution of Rodinia, Geology, Volume 28, Number 12, p 1071-1074, J.B. Murphy, R.A. Strachan, R.D. Nance, K.D. Parker, M. B. Fowler, December 2000.

National Atlas, 2008. Shaded Relief (200 Meter) 2008.downloaded from www.nationalatlas.gov/ mld/srld48i.html, U.S. National Atlas, 2008.

Nelson, 1983. The Clingman Lineament: Aeromagnetic Evidence for a Major Discontinuity in the North American Basement, Geological Society of America, Southeastern Section, Abstracts with Programs, Volume 13, Number 1, p 31, A. Nelson and I. Zietz, January 1983.

NGS, 2010. USA Topographic Maps, National Geographic Society, i-cubed. ESRI Server: http://services.arcgisonline.com/ArcGIS/rest/services/USA_Topo_Maps/MapServer Date accessed: July 29, 2010.

NJGS, 2003. Generalized Glacial Sediments of New Jersey, New Jersey Geological Survey, Website: http://www.state.nj.us/dep/njgs/geodata/dgs96-1.gif, Date accessed: December 14, 2007.

© 2007-2012 UniStar Nuclear Services, LLC. All rights reserved.
COPYRIGHT PROTECTED

NRC, 1978. Regulatory Guide 1.70, Standard Format and Content of Safety Analysis Reports for Nuclear Power Plants, LWR Edition, Revision 3, Nuclear Regulatory Commission, 1978.

NRC, 1997. Regulatory Guide 1.165, Identification and Characterization of Seismic Sources and Determination of Safe Shutdown Earthquake Ground Motion, Nuclear Regulatory Commission, March 1997.

NRC, 2003a. Site Investigations for Foundations of Nuclear Power Plants, Regulatory Guide 1.132, Revision 2, Nuclear Regulatory Commission, 2003.

NRC, 2003b. Laboratory Investigations of Soils for Engineering Analysis and Design of Nuclear Power Plants, Regulatory Guide 1.138, Revision 2, Nuclear Regulatory Commission, 2003.

NRC, 2007. Basis Geologic and Seismic Information, Regulatory Guide 1.206, Section 2.5.1, Nuclear Regulatory Commission, June, 2007.

Nuttli, 1972. Contemporary Newspaper Accounts of Mississippi Valley Earthquakes of 1811-1812, Compiled by Otto W. Nuttli, February 1972.

Obermeier, 1988. Liquefaction potential in the central Mississippi Valley, Dept. of the Interior, U.S. Geological Survey; Bulletin 1832, 21 p. S.F. Obermeier, 1988.

Obermeier, 2009. Using Paleoliqufaction-Induced and Other Soft-Sediment Features for Paleoseismic Analysis, in McCalpin, J.P., ed., Paleoseismology: Volume 95, Second Edition, (International Geophysics), San Diego, Academic Press, p. 497-564, Obermeier, S.F., 2009.

Oliver, 1970. Postglacial faulting and seismicity in New York and Quebec: Canadian Journal of Earth Sciences, v. 7, p. 579-590, J. Oliver, T. Johnson, and J. Dorman, 1970.

Olsen, 1990. Transtensional Arm of the Early Mesozoic Fundy Rift Basin: Penecontemporaneous Faulting and Sedimentation, Geology, v. 18, p. 695-698, P.E. Olsen. R.W. Schlische, 1990.

Ong, 2007. Early rotation and late folding in the Pennsylvania salient (U.S. Appalachians): Evidence from calcite-twinning analysis of Paleozoic carbonates, GSA Bulletin, Volume 119, Number 7/8, p 796-804, Philip F. Ong, Ben A. van der Pluijm and Rob Van der Voo, July/August 2007.

Owens, 1995. Geologic map of New Jersey: Central Sheet, U.S. geological Survey Open-File Report 95-0253, 60 p, 3 pls., scale 1:100,000, J. P. Owens, P. J. Sugarman, N. F. Sohl, R. A. Parker, H. F. Houghton, R. A. Volkert, A. A. Drake, R. C. Orndroff, 1995.

PADEP, 2010. Pennsylvania Department of Environmental Protection, Bureau of Oil and Gas Management Home Page, http://www.dep.state.pa.us/dep/deputate/minres/oilgas/2010PermitDrilledmaps.htm, Date accessed: August 19, 2010.

PAMAP, 2008. PAMAP Program Topographic Contours (2 ft interval) of Pennsylvania, PA Department of Conservation and Natural Resources, Bureau of Topographic and Geologic Survey.

© 2007-2012 UniStar Nuclear Services, LLC. All rights reserved.
COPYRIGHT PROTECTED

Parker, 1990. Bedrock geologic map of Monmouth junction quadrangle, New Jersey, U.S. Geological Survey Open-File Report 90-219, 1 pl., scale 1:24000, R. A. parker and H. F. Houghton, 1990.

Pavlides, 1986. Mountain Run fault zone of Virginia, in M. L. Jacobsen and T. R. Rodriguez, comp., National Earthquake Hazard reduction Program, Summaries of Technical Reports, Volume XXIII, U.S. Geological Survey Open-File Report 87-63, p 93-93, L. Pavlides, 1986.

Pavlides, 1994. Early Paleozoic Alkalic and Calc-Alkalic Plutonism and Associated Contact Metamorphism, Central Virginia Piedmont, U.S. Geological Survey Professional Paper 1529, L. Pavlides, J. Arth, J. Sutter, T. Stern and H. Cortesini Jr., 1994.

Pazzaglia, 1993. Stratigraphy, Petrography, and Correlation of Late Cenozoic Middle Atlantic Coastal Plain Deposits: Implications for Late-Stage Passive-Margin Geologic Evolution, Geological Society of American Bulletin, Volume 105, p 1617-1634, F.J. Pazzaglia, 1993.

Pazzaglia, 1994. Late Cenozoic Flexural Deformation of the Middle U.S. Atlantic Passive Margin, Journal of Geophysical Research, Volume 99, Number B6, p 12143-12157, F. J. Pazzaglia and T.W. Gardner, 1994.

Pazzaglia, 2006. Rivers, glaciers, landscape evolution, and active tectonics of the central Appalachians, Pennsylvania and Maryland, *in* Pazzaglia, F.J., ed., Excursions in Geology and History: Field Trips in the Middle Atlantic States: Geological Society of America Field Guide 8, p. 169-197, F.J. Pazzaglia, D.D. Braun, M. Pavich, P. Bierman, N. Potter Jr., D. Merritts, R. Walter, and D. Germanoski, 2006.

Pelletier, 2004. Estimate of three-dimensional flexural-isostatic response to unloading: Rock uplift due to Late Cenozoic glacial erosion in the western United States, Geology, Volume 32, Number 2, p 161-164, Jon D. Pelletier, February 2004.

Philpotts, 1985. Differentiation of Mesozoic basalts of the Hartford Basin, Connecticut. Geological Society of America Bulletin. v. 96: p. 1131 -1139, A.R. Philpotts and I. Reichenbach, 1985.

Plank, 2000. Bedrock Geology of the Piedmont of Delaware and Adjacent Pennsylvania, Delaware Geological Survey, Report of Investigations No. 59, State of Delaware, Margaret O. Plank, William S. Schenck, LeeAnn Srogi, 2000.

Pohn, 2000. Lateral Ramps in the Folded Appalachians and in Overthrust Belts Worldwide- a Fundamental Element of Thrust-Belt Architecture, U.S. Geological Survey Bulletin 2163, p 1-63, H.A. Pohn, 2000.

Ratcliffe, 1971. The Ramapo Fault System in New York and Adjacent Northern New Jersey-A Case of Tectonic Heredity, Geological Society of America Bulletin, Volume 82, p 125-142, N. Ratcliffe, 1971.

Ratcliffe, 1982. Tectonic Versus Frost-Wedging Origin of Faulted Glacially Polished Surfaces in the Lower Hudson River Valley, Geological Society of America Abstracts with Programs, V. 14, no. 1-2, February 1982, p. 76, N.M. Ratcliffe.

© 2007-2012 UniStar Nuclear Services, LLC. All rights reserved.
COPYRIGHT PROTECTED

Ratcliffe, 1984. Brittle fault fabrics, mineralogy, and geometry of border faults of the Newark basin, NY-NJ, from drill-core information, Geological Society of America Abstracts with Programs, Volume 16, Number 1, p 57, N. M. Ratcliffe and W. C. Burton, 1984.

Ratcliffe, 1985. Fault Reactivation Models For Origin of the Newark Basin And Studies Related To Eastern U.S. Seismicity, *in* Proceedings of the Second U.S. Geological Survey Workshop on the Early Mesozoic Basins of the Eastern United States, U.S. Geological Circular 946, G.R. Robinson, Jr., and A.J. Froelich eds., U.S. Geological Survey, N.M. Ratcliffe and W.C. Burton, 1985.

Ratcliffe, 1988. Structural analysis of Furlong fault and the relation of mineralization to faulting and diabase intrusion, Newark basin, Pennsylvania, in A. J. Frolich and G. R. Robinson Jr., eds., Studies of Early Mesozoic basins of the eastern United States, U.S. Geological Survey Bulletin 1776, p 176-193, N. M. Ratcliffe and W. C. Burton, 1988.

Reese, 2004. Kinematic Constraints on Rodinia Reconstructions from the Core of the Texas Grenville Orogen, The Journal of Geology, Volume 112, p 185-205, Joseph F. Reese and Sharon Mosher, 2004.

Resor, 2005. Hartford Basin Cross Section - Southington to Portland, CT, Guidebook for Field Trips in Connecticut, Guidebook no. 8. Ed. McHone, N.W. and Peterson, M.J. Hartford, CT: Department of Environmental Protection, p. 177-189, Phillip G. Resor and J.Z. De Boer, 2005.

Rodgers, 1984. Tyrone-Mt.Union Cross-Strike Lineament of Pennsylvania: A Major Paleozoic Basement Fracture and Uplift Boundary, AAPG Bulletin, Volume 68, Number 1, p 92-105, Michael R. Rodgers and Thomas H. Anderson, January 1984.

Rodgers, 1985. Bedrock Geological Map of Connecticut: Connecticut Geological and Natural History Survey, scale 1:125,000, http://www.tmsc.org/geology/bedrock, J. Rodgers, 1985.

Root, 1977a. North 40° latitude fault zone, Pennsylvania; a new interpretation, Geology, Volume 5, p 719-723, S. I. Root and D. M. Hoskins, 1977.

Root, 1977b. Geology and Mineral Resources Of The Harrisburg West Area, Cumberland and York Counties, Pennsylvania, Atlas 148ab, Pennsylvania Geological Survey, Fourth Series, Harrisburg. Samuel I. Root, 1977.

Root, 1999. Part III, Structural Geology and Tectonics, Chapter 21: Gettysburg-Newark Lowland, in C.H. Shultz ed., The Geology of Pennsylvania: Pennsylvania Bureau of Topographic and Geologic Survey Special Publication 1, p 298-305, S.I. Root and D.B. MacLachlan, 1999.

Ryder, 1992. Stratigraphic Framework of Cambrian and Ordovician Rocks in the Central Appalachian Basin from Medina County, Ohio, through Southwestern and South-Central Pennsylvania to Hampshire County, West Virginia, US Geological Survey Bulletin 1839, p 1-40, R.T. Ryder, A.G. Harris, and J.E. Repetski, 1992.

Ryder, 1995. Appalachian basin province, in Gautier, D.L., Dolton, G.L., Takahashi, K.I., and Varnes, K.L., eds., 1995 national assessment of United States oil and gas resources--Results, methodology, and supporting data: U.S. Geological Survey Digital Data Series DDS-30, 144 p., R.T. Ryder, 1995.

© 2007-2012 UniStar Nuclear Services, LLC. All rights reserved.
COPYRIGHT PROTECTED

Saad, 1990. Large Springs in the Valley and Ridge Physiographic Province of Pennsylvania; A Contribution to the Appalachian Valleys - Piedmont Regional Aquifer-System Analysis Study, U.S. Geological Survey Open-File Report 90-164, D.A. Saad and D.J. Hippe, 1990.

Sanders, 1963. Late Triassic Tectonic History of the Northeastern United States, American Journal of Science, Vol. 261, p 501-524, J. Sanders, 1963.

Saylor, 1999. Part II, Stratigraphy and Sedimentary Tectonics, Chapter 3C: Precambrian and Lower Paleozoic Metamorphic and Igneous Rocks- in the Subsurface, in C.H. Shultz ed., The Geology of Pennsylvania: Pennsylvania Bureau of Topographic and Geologic Survey Special Publication 1, p 51-57, T.E. Saylor, 1999.

Scharnberger, 2006. The Lancaster Seismic Zone of the Southeast Pennsylvania in relation to the Gettyburg-Newark Basin, Geological Society of America, Abstracts with Programs, Volume 38, Number 2, p 83, C. Scharnberger, 2006.

Schlische, 2002. Relative Timing of CAMP, Rifting, Continental Breakup, and Basin Inversion: Tectonic Significance, in Hames, W.E., McHone, G.C., Renne, P.R., and Ruppel, C., eds., The Central Atlantic Magmatic Province, American Geophysical Union Monograph 136, Roy W. Schlische, Martha Oliver Withjack, and Paul E. Olsen.

Schlische, 2003. Progress in Understanding the Structural Geology, Basin Evolution, and Tectonic History of the Eastern North American Rift System, P. Letourneau and P. Olsen, eds., The Great Rift Valleys of Pangaea in Eastern North America, Volume 1, p 21-64, R. Schlische, 2003.

Schruben, 1998. Geology of the Conterminous United States at 1:2,500,000 scale - a Digital Representation of the 1974 P.B. King and H.M. Beikman Map: U.S. Department of the Interior, U.S. Geological Survey Digital Data Series DDS-11 CD-ROM, release 2; display software by Russell A. Ambroziak. P.G. Schruben, R.E. Arndt, and W.J. Bawiec, 1998.

Schwab, 1997. Seafloor Characterization Offshore of the New York-New Jersey Metropolitan Area Using Sidescan-Sonar, U.S. Geological Survey, Open-File Report 00-295,16 p, Schwab, 1997.

Seborowski, 1982. Tectonic implications of recent earthquakes near Ansville, New York, Bulletin of the Seismological Society of America, Volume 72, p 1601-1609, D. D. Seborowski, G. Williams, J. A. Kelleher, and C. T. Statton, 1982.

Seeber, 1998. The 1994 Cacoosing Valley Earthquakes Near Reading, Pennsylvania: A Shallow Rupture Triggered By Quarry Unloading, Journal of Geophysical Research, Volume 103, Number B10, p 24,505-24,521, L. Seeber, J. Armbruster, W. Kim, N. Barstow and C. Scharnberger, 1998.

Senior, 2006. Arsenic, Boron, and Fluoride Concentrations in Ground Water in and Near Diabese Intrusions, Newark Basin, Southeastern Pennsylvania, Lisa A. Senior, Ronald A. Sloto, United States Geological Survey, Scientific Investigations Report 2006-5261, 105 p.

Sevon, 1999a. Pennsylvania and the Ice Age (2nd ed.): Pennsylvania Geological Survey, 4th series, Educational Series 6, 30 p. W.D. Sevon and G.M. Fleeger, 1999.

© 2007-2012 UniStar Nuclear Services, LLC. All rights reserved.
COPYRIGHT PROTECTED

Sevon, 1999b. Part VI, Geologic History, Chapter 35: Cenozoic, in C.H. Shultz ed., The Geology of Pennsylvania: Pennsylvania Bureau of Topographic and Geologic Survey Special Publication 1, p 451-455, W.D. Sevon and G.M. Fleeger, 1999.

Sevon, 2000a. Regolith in the Piedmont Upland Section, Piedmont Province, York, Lancaster and Chester Counties, Southeastern Pennsylvania, Southeastern Geology, Volume 39, Number 3 and 4, p 223-241, W. Sevon, October 2000.

Sevon, 2000b. Physiographic Provinces of Pennsylvania, Pennsylvania Department of Conservation and Natural Resources, Website: http://www.dcnr.state.pa.us/topogeo/maps/map13.pdf, Date accessed: December 14, 2007.

Sevon, 2000c. Glacial Deposits of Pennsylvania, Pennsylvania Department of Conservation and Natural Resources, Website: http://wwww.dcnr.state.pa.us/topogeo/maps/map59.pdf, Date accessed: December 14, 2007.

Sheridan, 1988. The Atlantic Continental Margin, U.S.Geological Society of America, The Geology of North America, Volume 1-2, p 610, R. Sheridan and J. Grow, 1988.

Sheridan, 1993. Deep seismic reflection data of EDGE U.S. mid-Atlantic continental-margin experiment: Implications for Appalachian sutures and Mesozoic rifting and magmatic underplating, Geology, Volume 21, p 563-567, Robert E. Sheridan, Douglas L. Musser, Lynn Glover, III, Manik Talwani, John I. Ewing, W. Steven Holbrook, G. Michael Purdy, Robert Hawman, and Scott Smithson, June 1993.

Shumaker, 2002. Reinterpreted Oriskany structure at the North Summit field, Chestnut Ridge anticline, Pennsylvania, AAPG Bulletin, Volume 86, Number 4, p 653-670, Robert C. Shumaker, April 2002.

Southworth, 2002. Digital Geologic Map and Database of the Frederick 30' x 60' Quadrangle, Maryland, Virginia, and West Virginia, Version 1.0, Compiled by Scott Southworth, Aeromagnetic map and digital topographic map by D. Daniels, Digital compilation by J.E. Reddy and D. Denenny, Pamphlet to accompany Open-File Report 02-437, U.S. Geological Survey, Reston, Virginia, S. Southworth, D. Brezinski, A.A. Drake, W.C. Burton, R.C. Orndorff, and A.J. Froelich, 2002

Southworth, 2006. Central Appalachian Piedmont and Blue Ridge tectonic transect, Potomac River corridor, in Pazzaglia, F.J., ed., Excursions in Geology and History: Field Trips in the Middle Atlantic States: Geological Society of America Field Guide 8, Southworth, S., Drake, A.A., Jr., Brezinski, D.K., Wintsch, R.P., Kunk, M.J., Aleinikoff, J.N., Naeser, C.W., and Naeser, N.D.

Spoljaric, 1972. Geology of the Fall Zone in Delaware, Delaware Geological Survey, p 30, N. Spoljaric, March 1972.

Spoljaric, 1973. Normal Faults in Basement Rocks of the Northern Coastal Plain, Delaware, Geological Society of America Bulletin, Volume 84, p 2781-2783, N. Spoljaric, 1973.

SSES FSAR, 2003. Susquenhanna Steam Electric Station Units 1 and 2 Final Safety Analysis Report, Section 2.5, Geology, Seismology, and Geotechnical Engineering, Rev. 58, Pennsylvania Power and Light, 2003.

© 2007-2012 UniStar Nuclear Services, LLC. All rights reserved.
COPYRIGHT PROTECTED

Stanford, 1995. Possible Pliocene-Pleistocene Movement on a Reactivated Mesozoic Fault In Central New Jersey, Geological Society of America Abstracts with Programs, Volume 27, Number 1, p 83, S. Stanford, D. Jagel, and D. Hall, 1995.

Steltenpohl, 1988. Kinematics of the Towaliga, Bartletts Ferry, and Goat Rock fault zones, Alabama: The Late Paleozoic dextral shear system in the southernmost Appalachians, Geology, Volume 16, p 852-855, Mark. G. Steltenpohl, September 1988.

Stern, 2005. Isostatic rebound due to glacial erosion within the Transantarctic Mountains, Geology, Volume 33, Number 3, p 221-224, T.A. Stern, A.K. Baxter, P.J. Barrett, March 2005.

Streepey, 2001. Early History of the Carthage-Colton Shear Zone, Grenville Province, Northwestern Adirondacks, New York (U.S.A), The Journal of Geology, Volume 109, p 479-492, M. M. Streepey, E. L. Johnson, K. Mezger, and B. A. van der Pluijm, 2001.

Street, 1977. A study of northeastern North American spectral moments, magnitudes, and intensities, Bulletin of the Seismological Society of America, Volume 67, p 599-614, R. L. Street and F. T. Turcotte, 1977.

Street, 1990. The Great Central Mississippi Valley Earthquakes of 1811-1812. Kentucky Geological Survey, University of Kentucky Lexington, Special Publication 14 Series XI, 1990. Street and Nuttli, 1990.

Sumi, 2008. Shale Gas: Focus on the Marcellus Shale, Oil and Gas Accountability Project/ Earthworks, Washington, D.C., L. Sumi, 2008.

Swanson, 1982. Preliminary model for early transform history in central Atlantic rifting, Geology, 10:317-320, M. Swanson, 1982.

Sykes, 2008. Observations and Tectonic Setting of Historic and Instrumentally Located Earthquakes in the Greater New York City - Philadelphia Area, Lynn R. Sykes, John G. Armbruster, Won-Young Kim, and Leonardo Seeber, Bulletin of the Seismological Society of America, Volume 98, Number 4, p. 1696-1719, 2008.

Tanner, 1987. Gravity Anomaly Map of North America, Decade of North American Geology (DNAG), Geological Society of America, J. Tanner, 1987.

Thomas, 2004. Detrital Zircon Evidence of a Recycled Orogenic Foreland Provenance for Alleghanian Clastic-Wedge Sandstones, The Journal of Geology, Volume 112, p 23-37, William A. Thomas, Thomas P. Becker, Scott D. Samson, and Michael A. Hamilton, 2004.

Thompson, 1999. Part II, Stratigraphy and Sedimentary Tectonics, Chapter 5: Ordovician, in C.H. Shultz ed., The Geology of Pennsylvania: Pennsylvania Bureau of Topographic and Geologic Survey Special Publication 1, p 74-89, A.M. Thompson, 1999.

Thompson, 2000. Neotectonics in Coastal Connecticut-Evidence from the Farm River marsh, Branford [abs.]: Eos, Transactions of the American Geophysical Union, v. 80, No 17 (Supplement), p. S86, W.G. Thompson, J.C. Varekamp, E. Thomas, and J.Z. de Boer, 2000.

Thompson, 2001. Fault motions along the east border fault, Hartford basin, CT, over the last 2800 years [abs.]: Eos, Transactions of the American Geophysical Union, v. 81, No 19

© 2007-2012 UniStar Nuclear Services, LLC. All rights reserved.
COPYRIGHT PROTECTED

(Supplement), p. S311, W.G. Thompson, J.C. Varekamp, and E. Thomas, 2001.A.M. Thompson, 1999.

Thurber, 1985. Crustal structure along the Ramapo fault zone, New York State, Earthquake Notes, Volume 56, p 145-152, C. Thurber and T. Caruso, 1985.

Tremblay, 1997. Taconian Obduction and Silurian Exhumation of the Betts Cove Ophiolite, Canadian Appalachians, The Journal of Geology, volume 105, p. 701-716, A. Tremblay, J.H. Bedard, and Kathleen Lauziere, 1997.

Tremblay, 2003. Supracrustal faults of the St. Laurence rift system, Quebec: kinematics and geometry as revealed by field mapping and marine seismic reflection data, Tectonophysics 369, p 231-252, Alain Tremblay, Bernard Long and Manon Masse, 2003.

Tuttle, 1991. Historic and prehistoric earthquake-induced liquefaction in Newbury, Massachusetts, Geology, Volume 19, p 594-597, M. Tuttle and L. Seeber, 1991.

Tuttle, 2001. The use of liquefaction features in paleoseismology: Lessons learned in the New Madrid seismic zone, central United States, Jounal of Seismology, Volume 5, Number 3, p 361-380, Martitia P. Tuttle, 2001.

Tuttle, 2002a. The Earthquake Potential of the New Madrid Seismic Zone, Bulletin of the Seismological Society of America, Volume 92, Number 6, p 2080-2089, Martitia P. Tuttle, Eugene S. Schweig, John D. Sims, Robert H. Lafferty, Lorraine W. Wolf, and Marion L. Haynes, August 2002.

Tuttle, 2002b. Paleoliquefaction study of the Clarendon-Linden fault system, western New York State, Tectonophysics, Volume 353, p 263-286, M. Tuttle, K. Dyer-Williams and N. L. Barstow, 2002.

Tuttle, 2006. Very Large Earthquakes Centered Southwest of the New Madrid Seismic Zone 5,000-7,000 Years Ago, Seismological Research Letters, Volume 77, Number 6, p 755-770, Martitia P. Tuttle, Haydar Al-Shukri and Hanan Mahdi, November/December 2006.

USGS, 1989. 1:24,000 Topographic Maps: Berwick, Pennsylvania, USGS, 1989.

USGS, 2002a. Documentation for the 2002 Update of the National Seismic Hazard Maps, U.S. Geological Survey Open-File Report 02-420, A.D. Frankel, M.D. Petersen, C.S. Mueller, K.M. Haller, R.L. Wheeler, E.V. Leyendecker, R.L. Wesson, S.C. Harmsen, C.H. Cramer, D.M. Perkins, and K.S. Rukstales, 2002.

USGS, 2002b. Physiographic Divisions of the US, Polygon coverage of Physiographic Divisions in the conterminous United States automated from Fenneman and Johnson 1946, 1:7,000,000scale map "Physical Divisions of the United States". http://water.usgs.gov/GIS/ metadata/ usgswrd/XML/physio.xml, USGS, 2002.

USGS, 2008. Documentation for the 2008 update of the United States National Seismic Hazard Maps: U.S. Geological Survey Open-File Report 2008-1128, M.D. Peterson, A.D. Frankel, S.C. Harmsen, C.S. Mueller, K.M. Haller, R.L. Wheeler, R.L. Wesson, Y. Zeng, O.S. Boyd, D.M. Perkins, N. Luco, E.H. Field, C.J. Wills, and K.S. Rukstales, 2008.

© 2007-2012 UniStar Nuclear Services, LLC. All rights reserved.
COPYRIGHT PROTECTED

VADOT, 2008. Aggregate Plant Certification Study Guide, The Virginia Dept. of Transportation, 32nd Ed., Appendix F, P. F-1~F-26, VADOT, 2008

Valentino, 1995. Paleozoic transcurrent conjugate shear zones in the central Appalachian piedmont of southeastern Pennsylvania, Journal of Geodynamics, Volume 19, Issues 3-4, May-July 1995, D. Valentino, and M. Hill.

Valentino, 1999. Interaction between Paleozoic strike-slip and thrust shear zones in the Philadelphia Structural Block, Central Appalachian Piedmont, Geological Society of America, Special Paper 330, D.W. Valentino, R.W. Valentino, and B.J. Lamport.

Van Arsdale, 1995. Northern extension of the Tennessee Reelfoot scarp into Kentucky and Missouri, Seismologial Research Letters, v. 66, no. 5, p. 57-62, Van Arsdale, R.B., Kelson, K.I., and Lurnsden, C.H., 1995.

Van Arsdale, 2000. Displacement history and slip rate on the Reelfoot fault of the New Madrid seismic zone, Engineering Geology, v. 55, p. 219-226, Van Arsdale, R.B., 2000.

Van Diver, 1993. Plate Tectonics, Roadside Geology of Pennsylvania, Roadside Geology Series, 352 p, Van Diver, 1993.

Varnes, 1978. Slope Movement Types and Processes, in Schuster, R.L., and Krizek, R.J., eds., Landslides-Analysis and control: National Research Council, Washington, D.C., Transportation Research Board, Special Report 176, p 11-33, R.L. Schuster and R.J. Krizek, 1978.

VDEQ, 2008. Virginia's Mineral and Energy Resources, Virginia Resource-Use Education Council, Virginia's Natural Resources Education Guide, 17 p., VDEQ, 2008.

Ver Straeten, 2000. Bulge Migration and Pinnacle Reef Development, Devonian Appalachian Foreland Basin, The Journal of Geology, Volume 108, p 339-352, Charles A. Ver Straeten and Carlton E. Brett, 2000.

Vlahoic, 1998. Joint hypocenter-velocity inversion for the eastern Tennessee seismic zone, Journal of Geophysical Research, Volume 103, p 4,879-4,896, G. Vlahoic, C. A. Powell, M. C. Chapman, and S. Sibol, 1998.

Wallach, 2002. The presence, characteristics and earthquake implications of the St. Lawrence fault zone within and near Lake Ontario (Canada-USA), J.L. Wallach, Tectonophysics 353 (2002) 45- 74

Way, 1999. Part IV. Physiography, Chapter 29: Appalachian Mountain Section of the Ridge and Valley Province, in C.H. Shultz ed., The Geology of Pennsylvania: Pennsylvania Bureau of Topographic and Geologic Survey Special Publication 1, p 353-361, J.H. Way, 1999.

Weems, 1998. New recognized en echelon fall lines in the Piedmont and Blue Ridge provinces of North Carolina and Virginia, with a discussion of their possible ages and origins, U.S. Geological Survey Open-File Report 98-374, 52 p, R. E. Weems, 1998.

Weems, 2002. Structural and tectonic setting of the Charleston, South Carolina, region: Evidence from the Tertiary stratigraphic record, GSA Bulletin, Volume 114, Number 1, p 24-42, Robert E. Weems and William C. Lewis, January 2002.

© 2007-2012 UniStar Nuclear Services, LLC. All rights reserved.
COPYRIGHT PROTECTED

Wentworth, 1983. Regenerate Faults of Small Cenozoic Offset - Probable Earthquake Sources in the Southeastern United States, U.S. Geological Survey, Professional Paper 1313-S, C. Wentworth and M. Mergner-Keefer, 1983.

Wheeler, 1996. Earthquakes and the Southeastern Boundary of the Intact Iapetan margin in Eastern North America, Seismological Research letters, Volume 67, Number 5, p 77-83, R. Wheeler, 1996.

Wheeler, 2005. Known or suggested Quaternary tectonic faulting, central and eastern United States-New and updated assessments for 2005, U.S. Geological Survey Open-File Report 20051336, p 37, R. L. Wheeler, 2005.

Wheeler, 2006. Quaternary tectonic faulting in the Eastern United States, Engineering Geology, Volume 82 (2006), p 165-186, R.L. Wheeler, 2006.

Williams, 1987. Groundwater Resources of the Berwick-Bloomsburg-Danville Area, East-Central Pennsylvania, Pennsylvania Bureau of Topographic and Geologic Survey, Water Resources Report 61, J.H. Williams and D.A. Eckhardt, 1987.

Wise, 1998. Lancaster County seismic zone (Penna)- Reactivation of a tectonic structural feature. Geological Society of America Abstracts with Programs, Volume 30, Number 7, p A-320, D. U. Wise and T. R. Faill, 1998.

Withjack, 1998. Diachronous Rifting, Drifting, and Inversion on the Passive Margin of Central Eastern North America: An Analog for Other Passive Margins, AAPG Bulletin, Volume 82, Number 5A, p 817-835, M.O. Withjack, R.W. Schlische, and P.E. Olsen, 1998.

Withjack, 2005. A Review of Tectonic Events on the Passive Margin of Eastern North America, 25th Annual Bob F. Perkins Research Center: Petroleum Systems of Divergent Continental Margin Basins, Martha Oliver Withjack and Roy W. Schlische, Martha Oliver Withjack, and Paul E. Olsen.

Wolf, 2003. Ferroaxinite from Lime Crest Quarry Sparta, New Jersey, Adam Wolf, John Rakovan, Christopher Cahill, Rocks and Minerals, Volume 78, pp. 252-256.

Wong, 2005. Potential Losses in a Repeat of the 1886 Charleston, South Carolina, Earthquake, Earthquake Spectra, Volume 21, Number 4, p 1157-1184, Ivan Wong, Jawhar Bouabid, William Graf, Charles Huyck, Allan Porush, Walter Silva, Timothy Siegel, Gilles Bureau, Ronald Eguchi, and John Knight, November 2005.

Wood, 1961. Sweet Arrow Fault, East-Central Pennsylvania, AAPG Bulletin, Volume 45, Number 2, p 256-263, Gordon H. Wood, Jr. and Thomas M. Kehn, February 1961.

Yang, 1981. Seismotectonics of Northern United States and Adjacent Canada, Journal of Geophysical Research, Volume 86, p 4,981-4,998, J. P. Yang and Y. P. Aggarwal, 1981.

Zietz, 1982. Composite magnetic anomaly map of the United States, Part A: Conterminous United States, U.S. Geological Survey Map GP-54923, Scale 1:2,500,000, I. Zietz, 1982.

Zoback, 2002. Steady-State Failure Equilibrium and Deformation of Intraplate Lithosphere, International Geology Review, Volume 44, p 383-401, Mark D. Zoback, John Townend, and Balz Grollimund, 2002.

© 2007-2012 UniStar Nuclear Services, LLC. All rights reserved.
COPYRIGHT PROTECTED

Zoback, 1991. Stress magnitudes in the crust: constraints from stress orientation and relative magnitude data, Philosophical Transaction of the Royal Society of London, p 181-194, Mary Lou Zoback and Marian Magee, 1991.}

2.5.2 Vibratory Ground Motion

The U.S. EPR FSAR includes the following COL Item for Section 2.5.2:

> A COL applicant that references the U.S. EPR design certification will review and investigate site-specific details of the seismic, geophysical, geological, and geotechnical information to determine the safe shutdown earthquake (SSE) ground motion for the site and compare site-specific ground motion to the Certified Seismic Design Response Spectra (CSDRS) for the U.S. EPR.

This COL Item is addressed as follows:

{This section provides a detailed description of the vibratory ground motion assessment that was carried out for the BBNPP site, resulting in the development of the BBNPP site Safe Shutdown Earthquake (SSE) ground motion response spectra. The assessment follows recommendations provided in NRC Regulatory Guide 1.208, "A Performance-Based Approach to define Site-Specific Earthquake Ground Motion," March 2007, (NRC, 2007a). The assessment includes:

- Characterization of seismic sources based on geological, geophysical, and seismological investigations
- Probabilistic seismic hazard analysis (PSHA) based on the characterized seismic sources and a characterization of ground motion
- Deaggregation of the mean seismic hazard to identify controlling earthquakes
- Analysis of seismic wave transmission at the BBNPP site based on results of the PSHA and geotechnical investigations
- Development of performance-based ground motion response spectra for the Safe Shutdown Earthquake (SSE)

Nuclear Regulatory Commission (NRC) Regulatory Guide 1.208, "A Performance-Based Approach to Define Site-Specific Earthquake Ground Motion," March, 2007, (NRC, 2007a) states in Section B, Discussion:

> "The CEUS is considered to be that part of the United States east of the Rocky Mountain front or east of Longitude 105 West (Refs. 13,14). A Probabilistic Seismic Hazard Analysis (PSHA) in the Central Eastern United States (CEUS) must account for credible alternative seismic sources through the use of a decision tree with appropriate weighting factors that are based on the most up-to-date information and relative confidence in alternative characterizations for each seismic source. Seismic sources identified and characterized by Lawrence Livermore National Laboratory (LLNL) (Refs. 13-15) and the Electric Power Research Institute (EPRI) (Ref. 16, 17) were used for CEUS studies in the past. In addition to the LLNL and EPRI resources, the United States Geological Survey maintains a large database of seismic sources for both the CEUS and the WUS. The characterization of specific seismic sources found in these databases may still represent the latest information

© 2007-2012 UniStar Nuclear Services, LLC. All rights reserved.
COPYRIGHT PROTECTED

available at the time that a PSHA is to be undertaken. However, if more up-to-date information is available, it should be incorporated."

Thus, as a starting point for this assessment of vibratory ground motion concepts from and interpretations presented in EPRI NP-4726, "Seismic Hazard Methodology for the Central and Eastern United States," (EPRI 1986); EPRI-4726-A, "Seismic Hazard Methodology for the Central and Eastern United States," (EPRI 1988); EPRI NP-6395-D-1989, "Probabilistic Seismic Hazard Evaluations at Nuclear Plant Sites in the Central and Eastern United States: Resolution of the Charleston Issue," (EPRI, 1989a) and the 2002 and 2008 National Seismic Hazard maps (USGS, 2002) (USGS, 2008a) were considered and evaluated. In addition, new information, including the Early Site Permit (ESP) Application for the Clinton Nuclear Power Plant site (EGC, 2006) submitted to the NRC on April 14, 2006 by Exelon Generation Company (EGC), was evaluated to assess its impact on existing interpretations.

The base case PSHA was also supplemented by several studies to examine the sensitivity of the BBNPP seismic hazard to source model parameters, such as maximum magnitude, probability of activity, and geometry. These studies included the following:

1. Five Hundred (500) Mile Sensitivity Study

   This study considered an increased area of influence to update the earthquake catalog, from 200 miles (322 km) to 500 miles (805 km). The purpose of this sensitivity study was to investigate the influence of new earthquake activity beyond the BBNPP Site Region. Section 2.5.2.1.2 provides a description of the earthquake catalog update, and Section 2.5.2.4.7 provides the sensitivity study results through comparisons of seismicity rates and hazard curves.

2. Charlevoix Sensitivity Study

   In light of the occurrence of the 1988 Saguenay Earthquake (m_b 5.9) in the vicinity of, but not within, the Charlevoix seismic zone, two sensitivity analyses were considered:

   a. Modification in the geometry of the Charlevoix seismic source zone;

   b. Increase of the maximum magnitude of source zones that included the post-EPRI 1988 Saguenay Earthquake

   Section 2.5.2.2.3.6 presents the nature of modifications in source models and Section 2.5.2.4.7 provides the results and conclusions of the Charlevoix sensitivity studies.

3. Sensitivity Study on Ramapo Fault System

   A recent publication (Sykes, 2008) postulates the existence of new ramifications of seismicity in the vicinity of the Ramapo Zone Fault System. A sensitivity analysis is presented to assess the effects of this feature in a quantitative mode. Section 2.5.2.2.3.3 presents the nature of modifications in source models and Section 2.5.2.4.7 provides the results and conclusions of the Ramapo sensitivity studies.

The following subsections summarize the procedure followed and results from the vibratory ground motion studies that were carried out for the BBNPP site.

© 2007-2012 UniStar Nuclear Services, LLC. All rights reserved.
COPYRIGHT PROTECTED

1. EPRI-SOG tectonic and seismic source zone interpretations (EPRI NP-4726 EPRI, 1986) were examined in light of more recent geological, seismological, and geophysical data under the guidance of NRC Regulatory Guide 1.208, (NRC, 2007a). Section 2.5.2.1 through Section 2.5.2.3 document this review and update of seismicity, geologic and tectonic characteristics of the BBNPP site, and correlation of earthquakes with seismic sources..

2. Section 2.5.2.4 develops PSHA parameters at the BBNPP site assuming the very hard rock conditions implied by currently accepted ground motion attenuation models.

3. Section 2.5.2.5 summarizes information about the seismic wave transmission characteristics of the BBNPP site with reference to more detailed discussion of all engineering aspects of the subsurface in Section 2.5.4.

4. Section 2.5.2.6 describes the development of the horizontal and vertical SSE ground motion for the BBNPP site.

The SSE ground motion is based on the risk-consistent/performance-based approach of Regulatory Guide 1.208 (McGuire, 2007a), with reference to NUREG/CR-6728 (McGuire, 2001), NUREG/CR-6769 (McGuire, 2002), and ASCE/SEI 43-05 (ASCE, 2005b). Horizontal ground motion amplification factors are developed using site-specific data and estimates of near-surface soil and rock properties. These amplification factors are then used to scale the hard rock spectra to develop Uniform Hazard Response Spectra accounting for site-specific conditions using Approach 2B of NUREG/CR-6728 (McGuire, 2001) and NUREG/CR-6769 (McGuire, 2002). A horizontal SSE performance-based surface response spectrum (PBSRS) is developed from these soil Uniform Hazard Response Spectra using the performance-based approach of ASCE/SEI 43-05 (ASCE, 2005b), as implemented in Regulatory Guide 1.208 (NRC, 2007a). The SSE motion is defined at the free-field ground surface. A vertical SSE spectrum is developed by scaling the horizontal SSE by a frequency-dependent vertical-to-horizontal (V/H) factor.

The SSE spectra described herein are performance goal-based (risk-informed) and site specific. As discussed below, the SSE spectra for the BBNPP site have been developed following the graded performance-based, risk-consistent method described in ASCE/SEI Standard 43-05 (ASCE, 2005b). The method specifies the level of conservatism and rigor in the seismic design process such that the performance of structures, systems, and components (SSC) of the plant achieve a uniform seismic safety performance consistent with the NRC's safety goal policy statement.

The SSE spectra, defined at the free-field ground surface, reflect the seismic hazard and geologic characteristics of the BBNPP site and represent the BBNPP site-specific ground motion response spectra (GMRS) of Regulatory Guide 1.208 (NRC, 2007a). These spectra are expected to be modified as appropriate to develop ground motion for design considerations.

The SSE developed in this section meets the requirements of paragraph (d) of 10 CFR 100.23 (CFR, 2007).

2.5.2.1 Seismicity

Probabilistic seismic hazard methodologies often consider that the activity in area seismic sources can be adequately represented by the Gutenberg-Richter (G-R) exponential recurrence equation. A quantitative derivation of the G-R parameters is typically based on historical seismicity, i.e., on catalogs of seismic events. The seismic hazard analysis conducted

© 2007-2012 UniStar Nuclear Services, LLC. All rights reserved.
COPYRIGHT PROTECTED

by EPRI as delineated in NP-6395-D 1989 (EPRI, 1989a) relied, in part, on an analysis of historical seismicity in the Central and Eastern United States (CEUS) to estimate seismicity parameters (rates of activity, a-values, and magnitude distributions, b-values, of the Gutenberg-Richter equation) for individual seismic sources. The historical earthquake catalog used in the EPRI analysis was complete through 1984.

As recognized in NRC Regulatory Guide 1.208 (NRC, 2007a), the United States Geological Survey (USGS) maintains a large database of seismic sources for both the Central and Eastern United States, as part of their efforts to develop National Seismic-Hazard Maps (USGS, 1996) (USGS, 2002)(USGS, 2008a). In Open-File Report 96-532, entitled "National Seismic-Hazard Maps: Documentation June 1996 (USGS, 1996) the USGS states that their CEUS catalog was primarily based on a catalog by Seeber (Seeber, 1991), who conducted a refinement of the EPRI 1986 catalog (EPRI, 1986). The USGS Catalog has been updated for the 2002 and 2008 updates of the National Seismic Hazard Maps (USGS, 2002) (USGS, 2008a). The 2002 version of the catalog includes events up to the end of 2001 and the 2008 version extends through the end of 2006.

Section 2.5.2.1.1 and Section 2.5.2.1.2 are added as a supplement to the U.S. EPR FSAR.

2.5.2.1.1 Regional Seismicity Catalog

Many seismic networks record earthquakes in the CEUS. A large effort is continuously made by the USGS to examine and combine available data on historical earthquakes and to develop a homogeneous earthquake catalog that contains all recorded earthquakes for the region. "Homogeneous" means that estimates of m_b for all earthquakes are consistent, duplicate earthquakes have been eliminated, non-earthquakes (e.g., mine blasts and sonic booms) have been eliminated, and significant events in the historical record have not been missed. Thus, the USGS catalog forms a strong basis on which to estimate seismicity parameters.

The PSHA analysis for the original BBNPP Site location used the USGS 2002 catalog, with events to the end of 2001. There was no homogeneous catalog available for the post-2001 seismicity at the time of the analysis. Sensitivity studies therefore, were performed to evaluate the impact of post-2001 seismicity on the PSHA results. An extended seismicity catalog was compiled by adding the earthquake data for the period 2002-2007 to the existing USGS 2002 catalog. The sensitivity studies also aimed at evaluating the impact of extending the PSHA integration distance to 500 miles. The results of the sensitivity studies are discussed in Section 2.5.2.4.7.

An updated seismicity catalog, which extends through April 2010, was compiled for use in the PSHA analysis of the relocated BBNPP Site (Table 2.5-1). The details of this compilation are presented in Section 2.5.2.1.2.

2.5.2.1.2 Updated Seismicity Data

The USGS catalogs are compiled by examining and combining events listed in several CEUS source catalogs (Mueller, 1997) (USGS, 2002) (USGS, 2008a). In this effort, the USGS intent is to develop a catalog dominated by entries from the most authoritative sources and they use a priority to choose the best location and magnitude from among multiple source catalogs for each earthquake. In addition, the secondary dependent events identified and filtered out as explained in a recent USGS publication (USGS, 2008a). Traditionally, most CEUS earthquake magnitudes are reported as a short-period surface-wave magnitude (m_{bLg}). If an m_{bLg} was not

© 2007-2012 UniStar Nuclear Services, LLC. All rights reserved.
COPYRIGHT PROTECTED

available, a magnitude from a preferred source catalog was assumed by the USGS to be equivalent to m_{bLg}, or simply m_b.

The catalog used in the PSHA for the original BBNPP Site location was the USGS 2002 catalog. Recent license applications, such as the Clinton ESP (EGC, 2006), conclude that the update in seismicity from the 1984 EPRI-SOG catalog does not significantly affect the seismicity parameters, i.e. the slope of the G-R (Gutenberg-Richter) equation (b-value) and seismic rate (a-value) in their respective regions of study. Recurrence rates for source zones included in the BBNPP original PSHA that are located outside the BBNPP Site Region are determined from either a supplemental catalog (e.g., Charlevoix) or from paleoseismic data (e.g., New Madrid, Charleston).

For the seismicity sensitivity studies the USGS 2002 catalog was updated to 2007 using data from available sources. Only 2 earthquakes with m_b greater than 3 occurred in the BBNPP Site Region from 2002 through 2007.

For the BBNPP Site Region, comparison of the impact on b-values, a-values, and PSHA results of using the USGS 2002 catalog versus the updated USGS catalog (through 2007) was examined by a sensitivity analysis. The 2002-2007 update to the catalog did not have a significant effect on the calculation of seismic source zone b-values, seismic occurrence rate, and/or the entire PSHA study at the BBNPP site. The use of the updated earthquake catalog resulted in a marginal reduction of the seismic occurrence rates, when compared to the USGS 2002 catalog. The resulting ground motion exceedance levels were marginally lower. Thus, conservatively, the USGS 2002 catalog was used to assess seismicity parameters in the PSHA for the original BBNPP site.

A sensitivity analysis was also performed to understand the effects of the 2002-2007 seismicity in an area broader than the 200 mi (322 km) BBNPP site region. For this analysis, an earthquake catalog search for 2002-2007 was performed with the following criteria:

- Use of a 500 mi (805 km) circular area centered at the BBNPP site 16W (41.08(N), -76.16(W)) for the USGS earthquake database; selection of the USGS/NEIC (PDE) '1973 - Present' database for magnitudes from 3.0 to 10.0 between the year 2002 and 2007 (USGS web database: http://neic.usgs.gov/neis/epic/epic_circ.html) (USGS, 2008b);

- Use of a rectangular boundary zone with limits from 33.88(N) to 48.27(N) (latitude) and -66.60(W) to -85.70(W) (longitude) for the Advanced National Seismic System (ANSS) earthquake database for magnitude 3.0 to 10.0 between years 2002 to 2007 (ANSS composite web database: http://www.ncedc.org/anss/catalog-search.html) (ANSS, 2008);

For the sensitivity study, the catalog through 2001 (USGS, 2002) was extended through the end of 2006. For this sensitivity catalog, the update methodology adopted the approach described in the USGS open file report 2008-1128 "The 2008 Update of the United States National Seismic Hazard Maps." Magnitude is adopted from the reported values. If more than one magnitude is listed in the original source-catalog record for an earthquake, a preferred magnitude is selected.

For magnitudes less than 5.0, the equivalency between different magnitude scales for different regions are verified using empirical relations. Only about 10 percent of the earthquakes do not have a listed m_{bLg} or m_b (USGS 2008a); in these cases, the preferred

© 2007-2012 UniStar Nuclear Services, LLC. All rights reserved.
COPYRIGHT PROTECTED

magnitude is assumed to be m_{bLg}. For the same event, if the magnitude between databases differs, the larger magnitude is selected.

The final sensitivity catalog was restricted to earthquakes located within 500 mi (805 km) of the BBNPP site.

A search following the approach and using the criteria listed above returned sixty-six (66) earthquakes recorded between 2002 and 2007. These earthquakes are listed in Table 2.5-63 . Assuming all the new earthquakes are independent events, they were added to the catalog used in the BBNPP PSHA sensitivity analysis. Table 2.5-63 provides epicenter coordinates, depth of focus, date, origin time, body wave magnitude (m_b) and reference catalog.

As for the 200 mi (322 km) radius case, this analysis showed that the 2002-2007 update did not have a significant effect on the PSHA study at the BBNPP site. The result was a marginal reduction of ground motion levels, between one and two percent, when compared to use of the USGS 2002 catalog. This result confirmed the conclusion that use of the USGS 2002 catalog to determine G-R seismicity parameters in the original BBNPP PSHA gives slightly conservative hazard results relative to using an updated catalog for the BBNPP Site Region (200 mi (322 km) radius) or an Extended Site Region (500 mi (805 km) radius). Section 2.5.2.4.7 provides information related to the results of the sensitivity analyses.

For the PSHA for the relocated BBNPP Site, a new updated catalog has been compiled. The catalog consists of data for pre-2007 and 2007-2010 time periods. The first part of the data is the USGS 2008 catalog (USGS, 2008a) which includes earthquakes for the period from 1534 to the end of 2006. That catalog, which was compiled for the 2008 update of National Seismic Hazard Maps for the central and eastern United States (USGS, 2008a), is declustered and homogeneous in m_{bLg} magnitude scale and has been critically reviewed by the USGS team. The second part of the compiled seismicity catalog (2007 to April 2010) consists of data from the following sources within 500 miles of BBNPP site:

- Preliminary Determination of Epicenters (PDE) catalog from the USGS/NEIC (USGS, 2010).
- Advanced National Seismic System (ANSS, 2010) catalog. ANSS, which is hosted by the Northern California Data Center, compiles data from several networks, including among others, the Southeastern United States Seismic Network (SEUSSAN) from the Virginia Tech Seismological Observatory, Lamont-Doherty Cooperative Seismographic Network (LCSN) from Lamont-Doherty Earth Observatory, and Weston Observatory from Boston College.
- Ohio Seismic Network catalog from the Ohio Department of Natural Resources (OSN, 2010).
- Earthquake Canada online Bulletin from Natural Resources Canada (EC, 2010).

Data from these sources were combined into a single listing of earthquakes. Duplicated events were eliminated, and possible man-made events were removed. Dependent events were also identified and removed from the catalog. To produce a homogeneous catalog, reported magnitudes were converted, if necessary, into the expected estimate of m_b ($E[_{mb}]$) using the conversion relations proposed in EPRI NP-4726-A (EPRI, 1988). The updated earthquake catalog, which includes events from 1534 through April 2010 is listed in Table 2.5-1.

© 2007-2012 UniStar Nuclear Services, LLC. All rights reserved.
COPYRIGHT PROTECTED

Earthquakes outside the 200 mi (322 km) BBNPP site region that have a significant contribution to the hazard at the BBNPP site have been properly accounted for. Those with significant contribution include the Charlevoix Canada Seismic Zone, the New Madrid Fault Zone, and the Charleston South Carolina Earthquake. These contribute to the low frequency ground motion levels.

Major sources of potential seismic activity such as the New Madrid Seismic Zone (NMSZ) and the Charleston Seismic Zone (CSZ) are located beyond 200 mi (322 km) from the BBNPP site. However, based on new paleo-seismology data, updated characteristic earthquake models have been formulated for the NMSZ and the CSZ. A sensitivity analysis for the BBNPP site using these updated models showed that characteristic earthquake events from both sources are significant contributors to ground motion at the BBNPP site for low response spectral frequencies. The sensitivity analysis also showed that the Charlevoix seismic zone (in Canada) is a contributor to the hazard at low frequencies. Therefore these three sources have been included in the PSHA study for the BBNPP site.

For the NMSZ, a review of the literature regarding seismic source models determined that the Clinton ESP (EGC, 2006) contained an appropriate and up-to-date characterization of the source, including uncertainties. The Clinton ESP (EGC, 2006) also documented paleoliquefaction evaluations in which evidence of soil liquefaction that occurred in prehistoric times is inferred from features such as sand boils or blows, dikes, and sills. By estimating the date and geographical distribution of these features, it is possible to infer the magnitude of the earthquake that originated the features. Earlier investigations of paleoliquefaction features in the southern Illinois basin and in parts of Indiana, Illinois, and Missouri have identified paleoliquefaction occurrences that could have been caused by Holocene and latest Pleistocene earthquakes with estimated moment magnitudes (M) of 6 to 7.8. Details about the paleoliquefaction reconnaissance carried out for the Clinton ESP Site seismic hazard evaluation are given in Section 2.1.4 and Attachment 1 of Appendix B of the Clinton ESP document (EGC, 2006). These details include a discussion of each of the identified features, pictures of the features, results of radiocarbon dating, and criteria for differentiating seismic versus non-seismic liquefaction features. The Clinton ESP was issued by the NRC in March 2007 (NRC, 2007c).

These paleoliquefaction studies have been utilized for developing improved representations of characteristic earthquakes in the New Madrid Fault System. For example, the data support a model in which New Madrid characteristic earthquakes occur as clusters of events, similar to the cluster that occurred in 1811-1812. It was also concluded, from these paleoliquefaction evaluations, that the range of maximum magnitude earthquakes assigned to a random background earthquake in the PSHA for the Clinton ESP site must include events comparable to that estimated for the Springfield, IL earthquake which occurred approximately 22 mi (35 km) northeast of Springfield, IL and 30 mi (48 km) southwest of the Clinton ESP site, that is, M 6.2 to 6.8.

These updates are adapted to the BBNPP site from the Clinton ESP Application. The updated New Madrid Model is discussed in Section 2.5.2.2.3.1.

Another significant source of severe seismic events is the Charleston, South Carolina seismic source that is about 620 mi (998 km) from the BBNPP site. Despite this long distance, it was considered that this source could still have some significant contribution to the hazard at the BBNPP site, particularly ground motion at low response spectral frequencies. Thus, the Charleston seismic source has been included in the present PSHA.

© 2007-2012 UniStar Nuclear Services, LLC. All rights reserved.
COPYRIGHT PROTECTED

Since publication of the EPRI seismic hazard analyses (EPRI, 1989a), paleoliquefaction investigations and other studies have impacted the characterization of the geometry, M_{max}, and recurrence in the Charleston seismic source. Paleoliquefaction studies in the area of the 1886 Charleston earthquake date back to a study performed by Cox and Talwani (Cox, 1983) that identified evidence of earthquake induced liquefaction features preserved in the South Carolina Coastal Plain sediments. Following this discovery, the USGS conducted intensive studies to identify the spatial extent of paleoliquefaction features. USGS studies led to the discovery of sand blows that predated 1886, hence providing a basis for estimating the recurrence interval of large earthquakes in the Charleston area (Obermeier, 1987). More recent studies and interpretations have led to the refinement of the Charleston source zone parameters (Johnston, 1996; Bakun, 2004; Marple, 2000; Talwani, 2001; USGS, 2002; USGS, 2008a). For example, radiocarbon dating techniques in new studies account for the fluctuation of atmospheric C-14 over time while previous studies assumed that the amount of C-14 has remained constant (Talwani, 2001).

Based on the new interpretations, alternative geometries have been used for this zone. Marple (Marple, 2000) proposed an East Coast Fault System (ECFS) in the Coastal Plain of the Eastern US and argued that the southern segment of this fault system is probably the source of the 1886 Charleston earthquake. In their 2008 version of National Seismic Hazard Maps,the USGS (USGS, 2008a) extended the Charleston area source offshore to include the Helena Banks fault zone as a possible source. The USGS (USGS, 2008a) also define another alternative area source which encloses the Woodstock lineament. This area source envelops half of the southern segment of ECFS. These two area sources have equal weights. Bechtel has examined these new data and developed an Updated Charleston Seismic Source (UCSS) model. The UCSS model has been used in development of the FSAR for the Vogtle ESP (SNOC, 2008). The UCSS model as described in the Vogtle ESP (SNOC, 2008) has been adopted here after review and comparison with other models of the Charleston seismic source.

The mean of M_{max} distribution used in the UCSS model (Mw 7.1) is very close to that of USGS (Mw 7.2). The source geometry for the UCSS comprises four source zones with different weights. Beside the area of strong shaking during 1886 Charleston earthquake, this source zone combination accounts for the liquefaction features that are distributed far from the epicentral area. It also includes the southern segment of ECFS (Marple, 2000) as a possible source of the 1886 Charleston earthquake with a low weight of 0.1.

The recurrence interval of the Charleston characteristic earthquake in the UCSS model is based on the work of Talwani (Talwani, 2001). While Talwani (Talwani, 2001) argues that only the 2000 year record of paleoliquefaction data is complete, the UCSS model uses a combination of 2000 year and 5000 year records, thereby considering the possibility that the paleoliquefaction features may have been preserved in the 5000 year data. The 5000 year record, however, has a lower weight (0.2) than the 2000 year data (0.8). Based on comparisons between the UCSS model and other Charleston characteristic earthquake models including the USGS (USGS, 2008a) model, it is concluded that the UCSS model better addresses the epistemic uncertainty in source zone parameters (including recurrence times) and therefore is used here to characterize the Charleston seismic source. This model is discussed in Section 2.5.2.2.3.2. The description of the UCSS model is based on the Vogtle ESP FSAR (SNOC, 2008).

The Charlevoix seismic zone is the most seismically active region of Eastern North America. It is located about 60 mi (97 km) downstream (northeast) from Quebec City. This seismic zone has been the location of numerous small to medium earthquakes as well as five M > 6.0

© 2007-2012 UniStar Nuclear Services, LLC. All rights reserved.
COPYRIGHT PROTECTED

earthquakes in the last 350 years (Mazzotti, 2005). Among the larger events, only the 1925 earthquake, Ms = 6.2, (Bent, 1992) has been recorded by seismographs. The Canadian Geological Survey (CGS) conducted two field surveys in 1970 and 1974 to define the extent of the seismic zone. The results of these two surveys delineated an active seismic zone of about 20 by 55 mi (32 by 86 km) along the Saint Lawrence River (Earthquakes Canada, 2008). Maximum magnitudes of M > 7.0 have been assigned to this seismic zone (Mazzotti, 2005). All six EPRI teams have considered the Charlevoix seismic zone in their source zone models and assigned mean maximum magnitudes close to or larger than 7.0. This seismic zone is located beyond the 200 mile radius region of the site, but a sensitivity analysis showed that it is a contributor to the seismic hazard at lower frequencies. Therefore, this seismic source was included in the final PSHA for the BBNPP site.

2.5.2.2 Geologic and Tectonic Characteristics of Site and Region

As described in Section 2.5.1, a comprehensive review of available geological, seismological, and geophysical data has been performed for the BBNPP site region and adjoining areas. As discussed in Section 2.5.1.2.5.2, excavation mapping is required during construction and any noted deformational zones will be evaluated and NRC notified when excavations are open for inspection. The seismotectonic characteristics of the region constitute the basis for defining the seismic source zones that affect the BBNPP site.

This section summarizes the geologic structure and activity that could potentially result in seismic-related vibratory ground motion at the BBNPP site. The summary addresses Regulatory Positions 1 and 2 within Regulatory Guide 1.208 (NRC, 2007a), which requires that investigation of seismic sources to be performed within a 200 mi (322 km) radius of the BBNPP site. The following sections summarize the EPRI-SOG seismic source interpretations (EPRI, 1986) that lie at least partially within this radius, relevant post-EPRI seismic source characterization studies and updated interpretations based on new data. The evaluation identified no new information which involved a change to the catalog that could impact the outcome of the PSHA.

Three major updates on seismic sources and characteristic earthquake models include:

The East Coast Fault System (ECFS) represents a new postulated seismic source along the Atlantic Seaboard (Section 2.5.1.1.4.4.1.2). The southern segment of the ECFS has been proposed by Marple (Marple, 2000) as being the source of the 1886 Charleston earthquake;

The average recurrence interval for large magnitude earthquakes in the Charleston characteristic model has been updated to 550 years based on paleoliquefaction data. The Charleston seismic source geometry also has been updated to include the southern segment of the ECFS as a possible source of the 1886 earthquake;

Assessments of magnitude, location, and return periods of large characteristic earthquakes of the New Madrid Seismic Zone (NMSZ) have been updated.

Detailed discussions of the updated source models are presented in the Section 2.5.2.2.3.1 and 2.5.2.2.3.2.

Section 2.5.2.2.1 and Section 2.5.2.2.2 are added as a supplement to the U.S. EPR FSAR.

© 2007-2012 UniStar Nuclear Services, LLC. All rights reserved.
COPYRIGHT PROTECTED

2.5.2.2.1 Summary of EPRI Seismic Sources

Evaluations of new information found in previous ESP applications (EGC, 2006) (NRC, 2005) conclude that the EPRI-SOG seismic sources remain appropriate for assessing seismic hazards in the CEUS. Similarly, an evaluation of the EPRI-SOG seismic sources (EPRI 1986) and new information relevant to the relocated BBNPP Site, indicates that the EPRI-SOG seismic sources, with minor modifications and updates, are appropriate for updating the BBNPP site PSHA. Updates and modifications are required for the maximum magnitude distribution for the area sources and for the models used to properly account for the seismic activity in the New Madrid and Charleston seismic zones.

In the 1986 EPRI study (EPRI, 1986), six independent Earth Science Teams (ESTs) evaluated geological, geophysical, and seismological data to develop seismic sources in the CEUS. These sources were used to model the occurrence of future earthquakes and evaluate earthquake hazards at nuclear power plant sites across the CEUS. The six ESTs involved in the EPRI project were: Bechtel Group, Dames & Moore, Law Engineering, Rondout Associates, Weston Geophysical Corporation, and Woodward-Clyde Consultants. Each team produced a report, included in EPRI NP-4726, (EPRI, 1986), that provides detailed descriptions of how they identified and defined seismic sources.

The EPRI-SOG ESTs assigned probabilities of activity to each of the defined source zones. Criteria such as correlation with seismicity, deep crustal expression, and probability of activation in the current stress field, were considered in calculating the probabilities of activity for each source zone. Each EST also provided additional information such as dependencies between the source zones that could be used to develop possible source combinations in their model.

In the original PSHA for the BBNPP site, probabilities of activity and dependencies between the source zones were not considered. This implied that all source zones had a probability of activity equal to one and were independent of each other. This simplification was justified because using probabilities of activity of 1.0 and taking source zones as independently active provides a conservative estimate of seismic hazard. The conservatism was mitigated in some areas by choosing a representative seismic source from among alternatives defined by the EPRI ESTs to explain zones of seismicity.

The current PSHA takes into account the probabilities of activity and dependencies as defined by each EST. This is to remove unnecessary conservatism in the hazard calculations and provide an estimate of seismic hazard that more accurately represents the EPRI-SOG EST interpretations.

The EPRI-SOG ESTs also determined recurrence parameters and maximum magnitudes for each source using the m_b magnitude scale, including their corresponding weights. These siesmic source models were implemented into a probabilistic seismic hazard analysis (PSHA) reported in EPRI NP-6395-D (EPRI, 1989a). EPRI NP-6452-D (EPRI, 1989b) summarized the parameters used in the final PSHA calculations, and this reference is the primary source for defining the geometry of area seismic sources for the BBNPP PSHA presented herein. For the computation of hazard, some of the 1989 EPRI seismic source parameters were updated, as discussed below.

The following sections list the seismic source interpretations in the 1989 EPRI PSHA study (EPRI, 1989a), relevant post-EPRI seismic source characterization studies, and updated interpretations provided by the more recent data. The summary of seismic sources and

© 2007-2012 UniStar Nuclear Services, LLC. All rights reserved.
COPYRIGHT PROTECTED

parameters was developed from the 1989 EPRI project EPRI NP-6452-D (EPRI, 1989b). The listed area seismic sources are those that at least partially lie within the "site region," i.e. within the circle with a 200-mi (322-km) radius centered at the BBNPP site. The list includes the code used by each team to designate each source, the name of the source, the assigned G-R recurrence parameter b-value and the assigned maximum magnitude, and weights assigned to each alternative interpretations of b-value and maximum magnitude to represent epistemic uncertainty.

Figure 2.5-17 through Figure 2.5-22 and Figure 2.5-29 through Figure 2.5-34 present the geometry of the seismic sources contributing to 99% of the hazard at the BBNPP site. The figures also display earthquakes with m_b equal to or higher than 3.0 in the updated earthquake catalog to illustrate the spatial relationships between seismicity and seismic sources. Earthquake epicenters in the updated earthquake catalog include events from the period between 1534 and April 2010, as listed in Table 2.5-1. Following the 1989 EPRI study (EPRI, 1989a) and the 1996, 2002 and 2008 USGS studies (USGS, 1996; USGS, 2002; USGS, 2008a), the recurrence parameters for area seismic sources were computed for each one-degree latitude and longitude cell that intersects any portion of a seismic source.

The PSHA conducted in the EPRI-SOG study, EPRI NP-6395-D (EPRI, 1989a), employed three strong ground motion attenuation relationships developed by Boore and Atkinson (Boore, 1987) and McGuire and others (McGuire, 1988) combined with the response spectral shapes by Newmark and Hall (Newmark, 1982), which are based on Western North America earthquake records. More recently-developed ground motion attenuation models (EPRI, 2004) are supported by a better understanding of earthquake generation and indicate that significant differences in the crustal properties between western and eastern North America lead to significant differences in the frequency content of ground motions between the two regions. In addition, EPRI TR-1014381 (EPRI, 2006a) provides an improved assessment of ground motion variability about median estimates, and thus has been used for this evaluation.

2.5.2.2.1.1 Sources Used for EPRI PSHA - Bechtel Group

The seismic sources identified by Bechtel EPRI-SOG EST (EPRI, 1989a) that are within 200 mi (322 km) of the BBNPP site, as well as their probabilities of activity and recurrence parameters are listed in Table 2.5-3.

Figure 2.5-17 illustrates the locations and geometries of the Bechtel Group seismic sources contributing to 99% of the seismic hazard along with plots of earthquakes with m_b equal to or higher than 3.0 between 1534 and April 2010. Figure 2.5-29 shows the same seismicity and the Bechtel Group seismic source zones for a 50 mi (80 km) radius of the BBNPP site.

2.5.2.2.1.2 Sources Used for EPRI PHSA - Dames & Moore

The seismic sources identified by the Dames & Moore EPRI-SOG EST (EPRI, 1989a) that are within 200 mi (322 km) of the BBNPP sit, as well as their probabilities of activity and recurrence parameterse are listed in Table 2.5-4.

Figure 2.5-18 illustrates the locations and geometries of the Dames and Moore seismic sources contributing to 99% of the seismic hazard along with plots of earthquakes with m_b equal to or higher than 3.0 between 1534 and April 2010. Figure 2.5-30 shows the sameseismicity and the Dames & Moore seismic source zones for a 50 mi (80 km) radius of the BBNPP site.

© 2007-2012 UniStar Nuclear Services, LLC. All rights reserved.
COPYRIGHT PROTECTED

2.5.2.2.1.3 Sources Used for EPRI PSHA - Law Engineering

The seismic sources identified by the Law Engineering EPRI-SOG EST (EPRI, 1989a) that are within 200 mi (322 km) of the BBNPP site, as well as their probabilities of activity and recurrence parameters are listed in Table 2.5-5.

Figure 2.5-19 illustrates the locations and geometries of Law Engineering seismic sources contributing to 99% of the seismic hazard along with plots of earthquakes with m_b equal to or higher than 3.0 between 1534 and April 2010. Figure 2.5-31 shows the same seismicity and the Law Engineering seismic source zones for a 50 mi (80 km) radius of the BBNPP site.

2.5.2.2.1.4 Sources Used for EPRI PSHA - Rondout Associates

The seismic sources identified by the Rondout Associates EPRI-SOG EST (EPRI, 1989a) that are within 200 mi (322 km) of the BBNPP site, as well as their probabilities of activity and recurrence parameters are listed in Table 2.5-6.

Figure 2.5-20 illustrates the locations and geometries of Rondout seismic sources contributing to 99% of the hazard along with plots of earthquakes with m_b equal to or higher than 3.0 between 1534 and April 2010. Figure 2.5-32 shows the same seismicity and the Rondout Associates seismic source zones for a 50 mi (80 km) radius of the BBNPP site.

2.5.2.2.1.5 Sources Used for EPRI PSHA - Weston Geophysical Consultants

The seismic sources identified by the Weston Geophysical EPRI-SOG EST (EPRI, 1989a) that are within 200 mi (322 km) of the BBNPP site , as well as their probabilities of activity and recurrence parameters are listed in Table 2.5-7.

Figure 2.5-21 illustrates the locations and geometries of Weston seismic sources contributing to 99% of the hazard along with plots of earthquakes with m_b equal to or higher than 3.0 between 1534 and April 2010. Figure 2.5-33 shows the same seismicity and the Weston Geophysical seismic source zones for a 50 mi (80 km) radius of the BBNPP site.

2.5.2.2.1.6 Sources Used for EPRI PSHA - Woodward-Clyde Consultants

The seismic sources identified by the Woodward-Clyde Consultants EPRI-SOG EST (EPRI, 1989a) that are within 200 mi (322 km) of the BBNPP site, as well as their probabilities of activity and recurrence parameters are listed in Table 2.5-8.

Figure 2.5-22 illustrates the locations and geometries of Woodward-Clyde seismic sources contributing to 99% of the hazard along with plots of earthquakes with m_b equal to or higher than 3.0 between 1534 and April 2010. Figure 2.5-34 shows the same seismicity and the Woodward-Clyde seismic source zones for a 50 mi (80 km) radius of the BBNPP site.

2.5.2.2.2 Post-EPRI Seismic Source Characterization Studies

Since the EPRI-SOG studies in the 1980's, new information has become available that is relevant to seismic hazard analysis at the BBNPP site. Specifically, updated data and information impact:

Characterization of the rate of earthquake occurrences;

Estimates of the maximum magnitude for seismic sources;

Ground motion models for the CEUS.

© 2007-2012 UniStar Nuclear Services, LLC. All rights reserved.
COPYRIGHT PROTECTED

Studies that have used new data and information are described with emphasis on the items relevant for the evaluation of the seismic hazard at the BBNPP site. These descriptions are provided in Section 2.5.2.2.2.1 and Section 2.5.2.2.2.2.

2.5.2.2.2.1 USGS Studies for the United States National Seismic Hazard Maps

Between 1996 and 2008, the USGS produced seismic hazard maps for the United States based on available seismological, geophysical, and geological information (USGS, 1996)(USGS, 2002) (USGS, 2008a). Each map reflects changes to the earthquake catalog, source models, and attenuation equations used to construct the previous version of the national seismic hazard maps. Among the most significant modifications to the CEUS portion of the source models are changes in the recurrence, maximum magnitude (M_{max}), and geometry of the Charleston and New Madrid sources. Unlike the EPRI models that incorporate many local sources, the USGS source model in the BBNPP site region (200-mi (322 km) radius) includes only three sources that are important to the BBNPP site hazard: the Extended Margin background, Stable Craton background, and New Madrid. Except for the New Madrid zone, where earthquake recurrence is modeled using a characteristic earthquake model, the hazard for the large background or "maximum magnitude" zones is largely based on historical seismicity and the spatial variation of that seismicity.

Since 1996, the USGS characterized the occurrence of large events in the New Madrid seismic zone using a characteristic earthquake model with a characteristic moment magnitude M of 8.0, similar to the estimated magnitudes of the largest events in 1811-12 (USGS, 1996). Uncertainty in the geometry of the New Madrid source was represented using three S-shaped parallel faults encompassing the area of highest historic seismicity. The USGS study used an average recurrence time of 1000 years for the New Madrid characteristic earthquakes.

For background zones, values of the Gutenberg-Richter (G-R) parameter "a" were determined in the 1996 USGS study (USGS, 1996) by counting the number of m_b=3 and larger events within the zone since 1927 and adjusting the rate to equal that since 1976. The area-normalized a-value was then disaggregated into a set of grid cells to calculate the hazard considering the smoothed historical seismicity. The G-R parameter "b" was assigned a value of 0.95, based on calculations for the entire CEUS (USGS, 1996).

In the 2002 USGS study (USGS, 2002), changes that most affected the hazard estimates for the BBNPP site were the use of an updated mean recurrence time, characteristic magnitude, and spatial concentration to characterize the New Madrid sources of large earthquakes. A shorter mean recurrence time of 500 years was adopted and logic trees were developed for the characteristic magnitude related to the same configuration of three fictitious fault sources as in the 1996 maps, giving to the central fictitious source twice the weight of each of the faults to the sides. These changes markedly increased the probabilistic ground motions for the 10% probability of exceedance around the New Madrid area, compared to the 1996 results.

Documentation by the USGS for its 2008 (USGS, 2008a) update of the national seismic hazard maps points out the following changes related to the Central and Eastern U.S.:

Revise catalog and account for magnitude uncertainty

Develop a logic tree for New Madrid (lower recurrence on northern arm and reduced magnitude)

Implement a cluster model for New Madrid earthquakes

© 2007-2012 UniStar Nuclear Services, LLC. All rights reserved.
COPYRIGHT PROTECTED

Modify hypothetical fault geometry for New Madrid

Develop a logic tree for M_{max} area sources

The USGS basic methodology for hazard estimates in the CEUS for the 2008 hazard maps is similar to that implemented in the 1996 and 2002 maps. The methodology includes background-seismicity and fault source models (USGS, 1996)(USGS, 2002)(USGS, 2008a). Background sources account for random earthquakes that occur off known faults and moderate-size earthquakes that occur on modeled faults. The USGS, 2008 background source model (USGS, 2008a) is composed of three smoothed gridded seismicity models, a large regional zone model, and local special seismicity-based zones. The gridded seismicity models are based on recorded historical earthquakes and account for the observation that larger earthquakes occur in regions that have experienced previous smaller earthquakes. Large regional zones account for a low potential of random seismicity in areas without historical seismicity and establish a floor to the seismic hazard calculations. The special local zones allow for local variability in the G-R seismicity parameters. Fault models account for earthquakes on mapped active faults that have paleoseismic or historical evidence of repeated large earthquakes. One of the four CEUS fault models included in 2008 by the USGS is the New Madrid Fault System (NMFS).

In 2008, the USGS (USGS, 2008a) used five fictitious parallel fault traces to represent the NMFS, with each fault having three arms. The use of five parallel faults represents the epistemic uncertainty in the location of future large magnitude earthquakes at New Madrid, in a way similar to the three parallel faults used in the 2002 USGS model. The center of the five traces most closely follows the seismicity pattern and is assigned a weight of 0.7; the traces just outside of the central trace are weighted 0.1 each, and the outer traces are weighted 0.05 each.

The USGS gridded seismicity, large regional zone, and the local seismicity models require a declustered earthquake catalog for calculation of earthquake rates. Gridded seismicity rates are calculated from the USGS seismic catalog for the Central and Eastern United States. The truncated Gutenberg-Richter (Gutenberg, 1944) magnitude-frequency distribution is used to model rates for different sizes of earthquakes in each grid cell or source zone. The USGS estimates completeness levels from the earthquake catalog, and calculates Gutenberg-Richter (G-R) parameters of the magnitude-rate relationship (intercept a and slope b) using a maximum-likelihood method (Weichert, 1980) that accounts for variable completeness. The rates in the gridded cells are spatially smoothed using a two-dimensional Gaussian smoothing operator.

USGS studies have also continuously incorporated developments in ground motion modeling (attenuation equations). In 1996 (USGS, 1996), the USGS adopted attenuation relationships derived for "hard rock conditions" recognizing that most attenuation relations for the CEUS published at that time were based on those site conditions. The USGS noted that it was less problematic to convert these to a firm-rock condition instead of converting them to soil conditions, since there would be less concern over possible non-linearity for the firm-rock site compared to the soil site.

The USGS 2008 study (USGS, 2008a) includes several new simulation-based attenuation relations that were not available in 2002. While in 1996 and 2002 the USGS used ground motion models based on a single corner model (USGS, 1996; USGS, 2002), a double corner and

© 2007-2012 UniStar Nuclear Services, LLC. All rights reserved.
COPYRIGHT PROTECTED

hybrid models were incorporated in the 2008 study (USGS, 2008a). The following is a list of the eight attenuation relationships used by the USGS in 2008, along with their assigned weights:

Single corner - finite fault

Toro and others (Toro, 1997), weight 0.2

Silva and others (Silva, 2002), constant stress drop with saturation, weight 0.1

Single corner - point source with Moho bounce

USGS (USGS, 1996), weight 0.1

Dynamic corner frequency

Atkinson and Boore (Atkinson, 2006), 140 bar stress drop, weight 0.1

Atkinson and Boore (Atkinson, 2006), 200 bar stress drop, weight 0.1

Full waveform simulation

Somerville and others (Somerville, 2001), for large earthquakes, weight 0.2

Hybrid empirical

Campbell (Campbell, 2003a), weight 0.1

Tavakoli and Pezeshk (Tavakoli, 2005), weight 0.1

The 2002 and 2008 USGS efforts (USGS, 2002; USGS, 2008a) have produced ground motion maps for a return period of 2475 years for building code applications.

2.5.2.2.2.2 The Lancaster Seismic Zone

The Lancaster seismic zone (LSZ) is located in southeastern Pennsylvania about 55 mi (89 km) south of the BBNPP site (Section 2.5.1.1.4.4.2.10). Low level seismic activity has persisted in the zone since at least 1889. The largest known earthquake of the LSZ is the January 16, 1994 Cacoosing Valley earthquake of $m_{bLg} = 4.6$ near Reading Pennsylvania (Seeber, 1998). This event was located about 52 mi (84 km) south of the BBNPP site. The Cacoosing Valley event has been attributed to unloading during a quarry process (Seeber, 1998) but it has not been removed from the standard earthquake catalogs used in PSHA studies. The LSZ was not identified as a specific seismic source zone by any of the EPRI-SOG ESTs (EPRI 1986). Rather the seismicity was incorporated in broader seismic source zones covering the region. The range of M_{max} values assigned the broader source zones adequately characterizes the LSZ in terms of the upper bound magnitude (Section 2.5.1.1.4.4.2.10). Therefore, the LSZ is adequately modeled by the EPRI-SOG EST source models and no update is required to address recent seismicity in the zone.

2.5.2.2.2.3 Earthquake Swarm Near Dillsburg, Pennsylvania

Beginning in October 2008 and continuing through 2009, a microearthquake swarm occurred near Dillsburg, York County, Pennsylvania (Kim, 2009) with over 900 events reported as of the end of November, 2009 (Jones, 2010). This earthquake swarm was located about 80 mi (130

© 2007-2012 UniStar Nuclear Services, LLC. All rights reserved.
COPYRIGHT PROTECTED

km) southwest of the BBNPP site. Some of these events were large enough to be recorded at regional seismic stations. The largest event had a magnitude of 2.9 (Kim, 2009). This event occurred on April 24, 2009. Two temporary seismic networks, one in the fall 2008 and the other in the summer 2009, were deployed to record and collect earthquake data from the swarm. The first network was installed on October 24 by personnel from the Lamont-Doherty Earth Observatory of Columbia University and continued operation until December 11, 2008. The network recorded 49 small earthquakes. The epicenters of these earthquakes are distributed along an approximately 1 mile (1.5 km) line trending NW-SE. The average depth of the 49 events was estimated to be about 0.3 mi (0.5 km). Despite their small magnitudes, these rather shallow earthquakes caused booming sounds and noticeable shaking but no damage from the events has been reported (Kim, 2009).

According to Kim and others (Kim, 2009), the spatial distribution of the earthquakes does not define a clear fault plane. Rather it seems that the events originated from a small volume of rock. Depths of the events roughly correspond to the base of a diabase sheet that underlies the area. The cause of these earthquakes is not known, but factors such as the area's mining history, hydrologic conditions, and stress concentrations at the contact between diabase and metasediments are under consideration (Jones, 2010).

No results are yet available from the second portable seismic network that was installed by the Pennsylvania Geological Survey on May 29, 2009 (Kim, 2009). The swarm was still active in mid-2010.

The Dillsburg area seismicity is consistent with seismic sources characterized by the EPRI-SOG ESTs. Thus, definition of a new seismic source zone to account for this activity is not required. The swarm consists of a series of localized small magnitude earthquakes that occur at shallow depths and therefore are unlikely to be associated with structures that might exist deeper in the crust.

2.5.2.2.3 Updated Interpretations Based on New Data

2.5.2.2.3.1 Updated New Madrid Model

As previously noted, seismologic, geologic, and geophysical studies have associated faults within the New Madrid region with the large-magnitude historical earthquakes that occurred during 1811 and 1812. In particular, paleoliquefaction studies indicate that large-magnitude events have occurred on these faults more frequently than the seismicity rates specified in the EPRI-SOG source characterizations. Thus, the updated seismic source evaluations focus on the characteristic large-magnitude events along the New Madrid Fault System.

Fault Geometry

As illustrated on Figure 2.5-66, significant seismic activity occurs in the area of the New Madrid Fault System (NMFS). The severe 1811 through 1812 earthquakes are thought to have ruptured the Reelfoot Fault and fault segments to the south and the north. The precise locations of these three large events are not known. The only evidence of surface rupture appears along the Reelfoot Fault and earthquake locations are generally constrained only by intensity and paleoseismic data. However, the available information indicates that the seismic activity at the NMFS can be attributed to the following three sources:

New Madrid South (NS) Fault;

New Madrid North (NN) Fault; and

© 2007-2012 UniStar Nuclear Services, LLC. All rights reserved.
COPYRIGHT PROTECTED

Reelfoot Fault (RF).

The USGS studies for updating the 1996 U.S. national seismic map (USGS, 1996) considered this seismic activity as a "characteristic" earthquake model. The USGS 1996 study (USGS, 1996) included a moment magnitude M of 8.0 and a recurrence time of 1000 years for such an event. Later, in the USGS work for the 2002 update of the national seismic hazard map (USGS, 2002), significant changes were introduced in mean recurrence time, characteristic magnitude, and spatial concentration of the New Madrid sources of large earthquakes. It was recognized that the locations of the three large 1811-1812 events are generally constrained only by intensity (felt) and paleoseismic data and a logic-tree approach was introduced to represent optional interpretations of fault locations and magnitudes of the New Madrid characteristic events. This logic tree characterized the range of expert opinions on the magnitude of the largest events of the 1811-12 sequence. The 2002 USGS study (USGS, 2002) represented the NMFS as three hypothetical sources to represent epistemic uncertainty in location: one fault with a trace matching the observed microearthquake activity and two adjacent sources situated near the borders of the Reelfoot Rift. Also, a shorter mean return time of 500 years for characteristic earthquakes was used by the USGS in the development of the 2002 maps (USGS, 2002). The end result was that the probabilistic ground motions for the 10% probability of exceedance level increased markedly around the New Madrid area, compared to the 1996 maps.

For the 2008 update of the hazard maps (USGS, 2008a), the USGS takes into account the uncertainty in the locations of characteristic earthquakes by using five fictitious parallel fault-traces, similar to the three used in the 2002 model (USGS, 2002). The central trace is weighted 0.7, the traces just outside of the central traces are weighted 0.1 each, and the outer traces are weighted 0.05 each. The USGS summarized expert opinions on the magnitudes of the 1811-1812 events, which shows that the estimated magnitudes range from M 7.0 up to M 8.1. For the 2008 USGS hazard maps, the characteristic magnitude varies for the three arms (north, central, south) of the NMFS. Of the three largest New Madrid earthquakes, the one in January 1812 is the most likely to have ruptured the northern arm of the seismic zone (Figure 2.5-66). The three leading sets of magnitude estimates for the New Madrid sequence suggest that the January earthquake was 0.2±0.1 magnitude units smaller than the December shock (Johnston, 1996) (Hough, 2000) (Bakun, 2004).

Based on the updated information, for developing the 2008 maps, the USGS has assigned magnitudes for the northern section of the NMFS that are 0.2 units lower than those assigned for the central and southern sections (USGS, 2008a). For the northern arm model the USGS applies the following weighting: M 7.1 (wt 0.15), M 7.3 (wt 0.2), M 7.5 (wt 0.5), and M 7.8 (wt 0.15). The central and southern segments remain characterized as in 2002, i.e., M 7.3 (wt 0.15), M 7.5 (wt 0.2), M 7.7 (wt 0.5), and M 8.0 (wt 0.15).

Regarding large earthquake recurrence for the NMFS, the USGS 2008 study (USGS, 2008a) has used paleoliquefaction data indicating a 500 year recurrence. Three large earthquake sequences are recognized from cross-cutting relationships and radiometric dating of sandblows (liquefaction effects). The USGS refers to Tuttle and others (Tuttle, 2002) who have recognized that events about 900 A.D., 1450 A.D., and 1811-1812 A.D. have occurred. These dates agree with a 500-year mean recurrence. However, citing lack of certainty on whether or not the northern portion of the fault system ruptured in the 1450 A.D. sequence, the USGS consider the possibility of 750-year and 500-year recurrences, equally weighted, for the northern arm of New Madrid. The 500 year recurrence for the southern and central sections remained unchanged based on Tuttle and others (Tuttle, 2002) published evidence that all three of the sequences affected those arms.

© 2007-2012 UniStar Nuclear Services, LLC. All rights reserved.
COPYRIGHT PROTECTED

Another relevant modification made by the USGS in their 2008 New Madrid source modeling (USGS, 2008a) was the inclusion of a clustered large earthquake model in addition to an unclustered model, as used in the 1996 and 2002 studies. A clustered model postulates that the occurrence of a sequence or cluster of large earthquakes closely spaced in time is a persistent characteristic of the NMFS. This hypothesis is supported by geologic data of Tuttle and others (Tuttle, 2002) showing evidence that pre-historic earthquakes on the NMFS typically occur in sequences of three large earthquakes similar to those observed in 1811-1812. The relevance of this consideration is that a particular site will have a larger probability of exceeding a ground motion level if it is affected by three dependent large events rather than one independent event.

The USGS 2008 study assigns equal weight to a clustered model for the NMFS characteristic earthquake and to an unclustered recurrence model. In addition, a more extensive logic tree was used to represent the rates and location of seismic activity at the NMFS.

The recent ESP submitted by Exelon for the Clinton site (EGC, 2006) also recognizes that seismologic, geologic, and geophysical studies have associated faults within the New Madrid region with the large-magnitude historical earthquakes that occurred during 1811 and 1812. The Clinton site was included in the 1989 EPRI-SOG study; however, the Clinton ESP notes that paleoliquefaction studies indicate that large-magnitude events have occurred on the NMFS more frequently than the seismicity rates specified in the EPRI-SOG source characterizations. Thus, Exelon decided to update the seismic source evaluations for the Clinton site focusing on the characteristic large-magnitude events along New Madrid. The Exelon efforts included a thorough review of the technical literature as well as paleoliquefaction studies to identify the fault source geometry and to estimate recurrence parameters in the NMSZ. It was recognized that paleoliquefaction studies indicate that clustered large-magnitude earthquakes have occurred in this zone which can be properly modeled as characteristic events.

A detailed review of the Exelon and the 2008 USGS characteristic earthquake models for the NMSZ was conducted. Estimates of the locations, potential magnitudes, and recurrence of the characteristic events are similar in both models; however, the Exelon model is appreciably more detailed. The main difference is that the USGS also considers an un-clustered model giving only 50% weight to their clustered model while the Exelon model incorporates only the clustered model with a 100% weight. Thus the Exelon approach is conservative relative to the USGS characterization. It is considered that this conservatism is acceptable for assessing the seismic hazard for critical facilities such as nuclear power plants, and the Exelon NMFS source model is adopted for the BBNPP PSHA. The Exelon model for the NMSZ was also adopted by EPRI in the 2008 update of the seismic hazard for nuclear power plant sites in the CEUS (EPRI, 2008).

Based on the Clinton ESP (EGC, 2006), the logic tree used to represent the uncertainty in the model for the NMFS characteristic events is shown on Figure 2.5-35. The first two levels of the logic tree take into account the uncertainty in the location and extent of the fault segments that can rupture in an earthquake sequence, by considering alternative geometries for the NS, RF and NN Faults. The considered fault locations are displayed on Figure 2.5-66. Distances to the BBNPP site for the various options are listed in Table 2.5-9.

For the New Madrid South fault arm, two alternatives are considered:

1. Blytheville arch/Bootheel lineament (BA/BL); weight 0.6, length 82 mi (132 km), and

© 2007-2012 UniStar Nuclear Services, LLC. All rights reserved.
COPYRIGHT PROTECTED

2. Blytheville arch/Blytheville fault (BA/BFZ); weight 0.4, length 71 mi (115 km).

Two alternative total lengths are considered for the New Madrid North fault arm:

1. With a weight of 0.7, rupture of the NN 37-mi (60-km) segment, and

2. The 60 mi (97 km) length including the NN and NNE is given a 0.3 weight.

Two possible alternatives are considered for the Reelfoot arm:

1. A full length segment including the northwest part, with weight 0.7, and

2. A central segment, excluding the northwest part, with 0.3 weight.

New Madrid Characteristic Earthquake Magnitude

Table 2.5-10 contains expected moment magnitudes for characteristic earthquake ruptures for each fault within the New Madrid Fault System along with their corresponding weights. As considered in the Clinton ESP, the size of the next characteristic earthquake is assumed to vary randomly about the expected value following a uniform distribution over a range of ±0.25 moment magnitude units, to represent the aleatory variability in the size of individual characteristic earthquakes.

For the Clinton ESP, constraints on recurrence of characteristic NMFS events were derived from paleoliquefaction and paleoseismic investigations of the Reelfoot fault scarp and associated fold. It was concluded that the NMFS has generated temporally clustered large earthquakes in AD 900±100, AD 1450±150 years and in 1811 to 1812; the time between clustered events may be from 200 to 800 years, with an estimated average of 500 years. Thus, a quantitative assessment of the uncertainty in the dates for prehistoric New Madrid earthquakes was developed, using a Monte Carlo simulation of constraints on the possible dates for the prehistoric earthquakes. The time intervals between these simulated dates were then fit with poissonian and renewal recurrence models. Table 2.5-10 lists the discrete distribution for equivalent annual frequency for characteristic New Madrid earthquakes. In this table, for Model A, all ruptures are similar in size to the 1811 and 1812 earthquakes. In Model B, 1/3 of the sequences consider a smaller (lower magnitude) rupture of the New Madrid North fault and 1/3 of the sequences assume a smaller rupture of the New Madrid South fault. The difference in magnitude from the 1811and 1812 ruptures was set to be no more than 1/2 magnitude unit, and no magnitude ruptures are considered to be less than M 7. Model A and Model B were assigned weights of 2/3 and 1/3, respectively.

New Madrid Characteristic Earthquake Recurrence

The alternative recurrence estimates, based on the poissonian and renewal models, used to represent the occurrence of characteristic New Madrid earthquakes in the Clinton ESP have been used herein, as well as their corresponding weights, as summarized in Table 2.5-10. Because the site is affected by three dependent events, the frequency of exceedance, v(z), of a spectral value z from a characteristic earthquake sequence is where:

$$v(z)_{characteristic} = \lambda_{rate\ of\ cluster}(1-(1-P_1)(1-P_2)(1-P_3))$$

$v(z)_{characteristic}$ is the probability of exceeding ground motion z,

$\lambda_{rate\ of\ cluster}$ is the equivalent mean annual rate of occurrence of the event cluster, and

© 2007-2012 UniStar Nuclear Services, LLC. All rights reserved.
COPYRIGHT PROTECTED

in which P_1, P_2, and P_3 are the probabilities for the three earthquakes of exceeding the ground motion level z, when an earthquake of specified magnitude and distance occurs.

New Madrid Simplifying Assumptions

The New Madrid Fault System lies beyond the 200-mi BBNPP Site Region approximately 1000 miles from the BBNPP Site. A scoping hazard analysis indicates that only the largest earthquakes generated by the source affect the hazard at the BBNPP Site. Thus, only the characteristic earthquake component of the characteristic earthquake recurrence model is implemented in the BBNPP PSHA. That is, the smaller earthquakes with an exponential magnitude-frequency distribution that form part of the characteristic earthquake recurrence model are not included in the PSHA. At the BBNPP Site, exclusion of those earthquakes has a negligible impact on the calculated hazard because of the great distance of the source from the site.

A second simplifying assumption for the NMFS is that the characteristic earthquake rupture always includes the point on each fault segment that is closest to the BBNPP Site and always ruptures to the surface. Thus, the distance used to assess ground motion exceedance is constant for each fault segment. Given the great distance of the NMFS from the BBNPP Site, this assumption is reasonable and has a negligible impact on calculated hazard.

2.5.2.2.3.2 Updated Charleston Seismic Source (UCSS) Model

Results of several post-EPRI-SOG studies have demonstrated that the EPRI-SOG representation of the Charleston seismic source needs to be updated. Aspects of the source characterization that have been examined include geometry (e.g., Marple, 2000; USGS 2002; USGS 2008a), maximum magnitude (e.g., Johnston, 1996; Bakun, 2004; USGS, 2008a), and recurrence model (e.g., Obermeier, 1987; Talwani, 2001). Recent models of the Charleston seismic source are significantly different than the 1986 EPRI-SOG EST characterizations and use a characteristic earthquake model to represent the occurrence of future seismicity. Based on a review of the available literature, it was determined that the Updated Charleston Seismic Source (UCSS) model, described in the Vogtle ESP (SNOC, 2008) and the FSAR for the Calvert Cliffs Nuclear Power Plant (CCNPP) Unit 3 (UniStar Nuclear, 2007) appropriately represents the current state of knowledge and uncertainty. Thus, the UCSS model is adopted for use in the BBNPP PSHA. The description of the UCSS model is based on Section 2.5.2 of the CCNPP Unit 3 FSAR.

UCSS Geometry

The UCSS model includes four mutually exclusive source zone geometries (A, B, B', and C; Figure 2.5-74). These geometries have been defined based on the current understanding of geologic and tectonic features and shaking intensity in the region affected by the 1886 Charleston earthquake; on the distribution of seismicity; and on the geographic distribution, age, and density of liquefaction features associated with both the 1886 and prehistoric earthquakes. These features indicate that most of the evidence related to the Charleston source is concentrated in the Charleston area and is not widely distributed throughout South Carolina.

Geometry A

Geometry A is a northeast-oriented area centered at the 1886 Charleston meizoseismal area (Figure 2.5-74). This geometry encompasses the 1886 earthquake MMI X isoseismal (Bollinger, 1977), most identified Charleston area tectonic features and inferred fault structures and the majority of reported 1886 liquefaction features. Geometry A excludes outlying liquefaction

© 2007-2012 UniStar Nuclear Services, LLC. All rights reserved.
COPYRIGHT PROTECTED

features, because liquefaction occurs as a result of strong ground shaking that may extend well beyond the aerial extent of the tectonic source causing an earthquake.

Existing evidence indicates that the seismic source for the 1886 Charleston earthquake was located in a relatively restricted zone defined by Geometry A. This zone envelops the local tectonic features, the area of ongoing concentrated seismicity, the area with a high density of liquefaction features, and the meizoseismal area of the 1886 earthquake. These observations suggest that future earthquakes with magnitudes comparable to the 1886 Charleston earthquake will likely occur within the area of Geometry A. Thus, a weight of 0.7 has been assigned to Geometry A (Figure 2.5-75).

Geometries B, B', C

Geometries B, B', and C are defined to capture the possibility that future earthquakes may not be restricted to Geometry A. The distribution of liquefaction features along the entire coast of South Carolina suggests that the Charleston source could extend beyond Geometry A. Therefore, Geometries B and B' represent larger source zones, while Geometry C represents the southern segment of the hypothesized East Coast Fault System source zone. Geometry B' is a subset of B and defines the onshore coastal area as a source thus restricting the earthquakes in such onshore regions.

Geometry B - Coastal and Offshore Zone

Geometry B is a coast-parallel source including Geometry A in its entirety and elongated to the northeast and southwest to capture more distant liquefaction features in coastal South Carolina. The source also extends to the southeast region to include the offshore Helena Banks fault zone. This geometry is assigned a weight of 0.1.

Geometry B' - Coastal Zone

Geometry B' is a coast-parallel source that also incorporates all of Geometry A, as well as the majority of reported paleoliquefaction features. However, it does not include the Helena Banks Fault Zone. A weight of 0.1 has been assigned to this geometry.

Geometry C - East Coast Fault System (ECFS South Segment)

Geometry C envelops the southern segment of the proposed East Coast Fault System (Marple, 2000) as a possible source for the 1886 Charleston earthquake. A weight of 0.1 has been assigned to geometry C.

UCSS Characteristic Earthquake Magnitude (M_{max})

Based on currently available data and modern interpretations of the moment magnitude (M) of the 1886 Charleston earthquake (Table 2.5-18), the UCSS model for the magnitude of the Charleston characteristic earthquake modifies the USGS magnitude distribution (USGS, 2002) to include a total of five discrete magnitude values each separated by 0.2 M units (Figure 2.5-75). The UCSS M_{max} distribution includes a discrete value of M 6.9 to represent the Bakun best estimate of the 1886 Charleston earthquake magnitude, as well as a lower value of M 6.7 to capture a low probability that the 1886 earthquake was smaller than the Bakun mean estimate of M 6.9 (Bakun, 2004).

The UCSS magnitudes and weights are as follows:

M Weight

© 2007-2012 UniStar Nuclear Services, LLC. All rights reserved.
COPYRIGHT PROTECTED

6.7	0.10
6.9	0.25
7.1	0.30
7.3	0.25
7.5	0.10

Thisdistribution results in a weighted mean M_{max} of M 7.1 for the UCSS. This is slightly lower than the mean magnitude of M 7.2 in the USGS model (USGS, 2002).

UCSS Characteristic Earthquake Recurrence

The UCSS model incorporates geologic data to characterize the recurrence interval of characteristic earthquakes. Identifying and dating paleoliquefaction features provides a basis for estimating the recurrence of large earthquakes. Recent estimates of M_{max} recurrence intervals are significantly shorter than estimates in the EPRI-SOG EST models. Details regarding the processing, aging, and completeness of Charleston paleoliquefaction features can be found in Talwani (Talwani, 2001) and the CCNPP Unit 3 FSAR (UniStar Nuclear, 2007).

Recurrence data for two time intervals (2000 yr and 5000 yr) are used in the UCSS model. Return periods derived from recorded paleoliquefaction features assume that these features were produced by large M_{max} events and that both the 2000-year and 5000-yr records are complete.

The UCSS model calculates two average recurrence intervals based on the two time intervals, which are used as two branches on the recurrence model portion of the UCSS logic tree (Figure 2.5-75). The first average recurrence interval is based on four events that occurred in the past 2000 years. The second average recurrence interval is based on events that occurred within the last 5000 years. The 2000 and 5000 records have been assigned weights of 0.8 and 0.2, respectively.

2.5.2.2.3.3 The Ramapo Fault

Sykes and others (Sykes, 2008) published an updated synthesis of seismicity and tectonics in the greater New York City-Philadelphia area. During the EPRI-SOG study, the ESTs evaluated a number of tectonic features in this region to assess their seismogenic potential relative to the observed seismicity. One tectonic feature in this region considered by the EPRI-SOG ESTs was the Ramapo fault that borders the Mesozoic-age Newark basin. The Ramapo fault is located 82 - 93 mi (132 - 150 km) from the BBNPP Site. Given the updated synthesis by Sykes and others, possible impacts on the assessment of the Ramapo fault by the EPRI-SOG ESTs is reviewed.

Sykes and others (Sykes, 2008) find that seismicity in the vicinity of the Ramapo fault is not directly associated with displacement along the fault, but rather is distributed in a 7.5-mi (12 km) wide zone in the eastern part of the Reading prong to the west of the fault. Evidence from drillholes that penetrated the fault shows no evidence of post-Jurassic displacement (Sykes 2008). Sykes and others define a "Ramapo Seismic Zone" to describe the seismicity in the vicinity of the fault.

Another aspect of the greater New York City-Philadelphia area seismicity, newly noted by Sykes and others, is a sharp northwest-southeasterly striking boundary to seismicity that extends from Stamford, CT to Peekskill, NY (Sykes, 2008). Northeast of the boundary earthquakes are absent.

© 2007-2012 UniStar Nuclear Services, LLC. All rights reserved.
COPYRIGHT PROTECTED

Sykes and others (Sykes, 2008) find that while certain portions of the greater New York City - Philadelphia area are seismically active, it is not possible with the current data to identify the causative faults. A similar assessment was made by Kafka and others (Kafka, 1985).

Based on the updated seismicity catalog for the greater New York City - Philadelphia area, Sykes and others (Sykes, 2008) used a Gutenberg-Richter recurrence model to extrapolate the rate of seismicity to larger magnitudes than those recorded historically. Using such a model they determine that the return period of a magnitude 6 and 7 earthquake in the study area would be 670 and 3400 years, respectively. While there is no evidence that earthquakes of that size have occurred in the area, the historical record is not of sufficient duration or completeness to rule such events out with certainty. The largest historically documented earthquake in the area occurred in 1884. Sykes and others estimate the earthquake had an m_{bLg} of 5.25 based on its felt area and was located within 30 km of Lower New York Bay (Sykes, 2008).

Based on the available data, it is concluded that the Ramapo fault is not a capable tectonic source. However, the clear history of seismicity in the greater New York City-Philadelphia area, with at least one earthquake with a magnitude likely greater than m_{bLg} 5, indicates that the general area should be considered as a seismogenic source with the specific structures generating earthquakes still undetermined. While the EPRI-SOG EST seismic source characterizations are consistent with the updated Sykes and others findings, two sensitivity analyses are carried out to investigate the impact of source zones based on the Sykes and others work:

(a) Ramapo Seismic Zone

An area seismic source zone is defined based on the Ramapo Seismic Zone discussed by Sykes and others. Figure 2.5-86 shows the zone along with seismicity from the USGS 2002 catalog, supplemented by locations from the PDE through the end of 2007. Seismicity within this zone is insufficient to reliably determine a b-value; therefore a regional value of 0.95 is used. Catalog completeness periods are adopted from the USGS (USGS 2002). These values are similar to those determined by Sykes and others. A maximum magnitude of m_b 6.0 is used for the sensitivity analysis. This value is within the range of weighted mean M_{max} values for typical EPRI-SOG EST source zones defined for the greater New York City-Philadelphia area (Table 2.5-68).

(b) NY-Phil Study Area

An area source zone is defined to coincide with the Sykes and others study area (40° N - 42° N and 73.50° W - 75.5° W). Based on the same USGS 2002 catalog supplemented by PDE locations that is used for the Ramapo Seismic Zone source, a b-value of 0.85 is determined for this zone, which is higher than the 0.7 value determined by Sykes and others (Sykes, 2008). An M_{max} value is 6.0 is used for the sensitivity analysis.

Results of the sensitivity analyses are reported in Section 2.5.2.4.7.

2.5.2.2.3.4 The St. Lawrence Zone

Recent research has been performed in the southeastern corner of Lake Ontario and the western Lake Ontario in a search for evidence of neotectonic faulting (Wallach, 2002). In the Rochester Basin, vertical separations of layers of unconsolidated sediments and the underlying Paleozoic bedrock had been recognized. It may be possible to interpret the observed

© 2007-2012 UniStar Nuclear Services, LLC. All rights reserved.
COPYRIGHT PROTECTED

displacements of the units as due to recent tectonic faulting (Wallach 2002). However, such interpretation remains uncertain. Finding Quaternary faulting in Eastern North America (ENA) will continue to be difficult. More work is needed in the study area to favor or to refute these interpretations.

In addition, historical seismicity, including instrumentally recorded data, show significant seismic activity in 3 areas of the St. Lawrence Seismic Zone (LSZ): (1) the Lower St. Lawrence Seismic Zone, (2) the Charlevoix Seismic Zone, and (3) the area of the 1944 Cornwall-Massena earthquake. The study region in the Lake Ontario south of Cornwell has not experienced high seismicity. According to the Earthquakes Canada website the region of southern Great Lakes has a low to moderate level of seismicity compared to more active zones to the east in general and to Charlevoix in specific. A map of seismicity on the website shows even fewer events for Lake Ontario (Earthquakes Canada, 2008). It may be argued that the seismicity history is short but other zones in the Saint Lawrence Seismic Zone show high levels of activity in the same short period of time. According to the same website, on average, 2 to 3 magnitude 2.5 and larger earthquakes have been recorded in the southern Great Lakes region in the past 30 years. It is postulated that (Wallach, 2002):

> "Because earthquakes of M ~ 5.5-7.0 have been spatially related to the Saint Lawrence fault zone northeast of study area, similar sized earthquakes might reasonably be expected beneath Lake Ontario."

To further investigate the Wallach postulate, different studies conducted to refine the location of earthquakes in Eastern North America (ENA) to correlate the epicenters with existing geologic structures and lineaments were reviewed. Some of these studies have focused on the earthquakes of the Eastern Great Lakes (Dineva, 2004; Ebel, 2002; Seeber, 1993; Mohajer, 1993). The study area is characterized by Paleozoic sedimentary rocks lying on Precambrian basement (Seeber, 1993). Among geologic structures and proposed lineaments that transect the area, only a few seem to correlate with the observed clusters of seismicity. For example, seismicity in the Attica seismic zone has been associated with the Clarendon-Linden fault but even in this case the association is not definitive. The Eastern Great Lakes Basin (EGLB) is an area of low to moderate seismicity and the largest recorded earthquake in this area had a magnitude of less than about 5.5. Some of the mentioned studies have discussed the possibility of future large earthquakes in this area of low seismicity but none provided quantitative results (Ebel, 2002; Seeber, 1993).

Seeber and Armbruster (Seeber, 1993) argue that occurrence of a large earthquake can significantly change the pattern of seismicity and, therefore, favor the models which consider temporal changes in seismicity. This means that present areas of low seismicity may experience large earthquakes in the future. Seeber and Armbruster (Seeber, 1993) note that lack of evidence for substantial accumulated neotectonic displacements on structures such as the Clarendon Linden fault does not necessarily rule out the possibility of large earthquakes from such structures.

Time dependent models of seismicity are not well constrained except for special cases. Therefore, most seismic hazard studies are based on the assumption of stationary seismicity. As Seeber and Armbruster state "seismicity is still the main observable which can offer insight into intracratonic neotectonics and a basis for hazard assessment" (Seeber and Armbruster, 1993). In this case, the areas with low level of seismic activity are the areas with low levels of seismic hazard and this is confirmed by the seismic hazard maps. Unless strong geologic evidence indicates otherwise, observed patterns of seismicity will be the main basis for

© 2007-2012 UniStar Nuclear Services, LLC. All rights reserved.
COPYRIGHT PROTECTED

estimating recurrence parameters in seismic hazards. The geologic evidence should provide quantitative results as input for seismic hazard evaluations. Current available geologic data cannot constrain upper bound magnitude in the study area and most parts of ENA. Seismicity data, although limited, are used for this purpose in many assessments of seismic hazard. Some have adopted the approach in which data from similar tectonic environments supplement the limited existing data.

Ebel and Tuttle (Ebel, 2002) present a summary of seismicity and its relation to stress and geologic structures in EGLB and characterize it as an area with a lower rate of earthquake activity in comparison to the New Madrid, Charlevoix, and Saint Lawrence Valley seismic zones.

Ebel and Tuttle (Ebel, 2002) show seismicity rates per 100 years as contour plots for ENA. The plots clearly shows low levels of activity in Lakes Ontario and Erie compared to other active seismic zones of ENA. Ebel and Tuttle (Ebel, 2002) mention that four paleoseismology studies in the EGLB have found no evidence of large ($M > 6$) earthquakes during recent geologic times. The low seismicity rates may represent a long-term behavior of the region and potential large earthquakes ($M > 6$) in the region may have long recurrence intervals of >12,000 years (Ebel, 2002).

The 2005 version of Canadian National Seismic Hazard Maps (2% in 50 yrs) shows that Lake Erie and Lake Ontario are areas of low to moderate hazard. The maps are for firm ground or soil class C of the National Building Code of Canada (NBCC). The 2008 version of USGS National Seismic Hazard Maps (2% in 50 years) for site class BC conform to the Canadian maps with somewhat lower hazard values for the study area.

The studies provided by Wallach (2002) do not provide any quantitative results or descriptions of tectonic features that could be used for quantitative analyses. The author claims that earthquakes up to magnitude 7 might reasonably be expected beneath Lake Ontario and implies that seismic hazards in the area of this lake might be comparable with that of seismically active areas of the St. Lawrence seismic zone. There is no direct geologic evidence to support this conclusion. Seismicity in the area shows much lower activity levels compared with Charlevoix and other active areas of the St. Lawrence seismic zone. Assuming upper bound magnitudes of 7 or larger for the area would be an overestimation of this parameter while the maximum recorded event had a magnitude of $M < 5.5$. There is not sufficient evidence that could support the westward extension of the seismic zone. The lower St. Lawrence Zone and the Charlevoix zone are properly accounted for by the BBNPP PSHA.

2.5.2.2.3.5 The New England Seismic Source Zone and the Cape Ann Earthquake

The area of seismic activity of the New England region in northeastern United States is called the New England seismic zone. The seismic zone has experienced a low to moderate rate of historical seismicity. The 1755, M 5.9, Cape Ann earthquake (Ebel, 2006) is an example of the moderate historical events in this seismic zone. There is no evidence that earthquakes with magnitudes M 7.0 or larger have happened in this seismic zone. The estimated magnitude of the 1638 New Hampshire earthquake (Estimated M=6.5-7.0) (Ebel, 1996) is also uncertain. The Weston Observatory of Boston College has operated a seismic network to monitor the earthquake activity in the New England seismic zone and adjacent areas. The seismic network can provide more accurate earthquake locations that can be used to explore the possibility of correlation between the epicenters and known tectonic and geologic features. Moderate magnitude events (M=6.0) from this seismic zone (which is located beyond the 200 mile radius) will not result in significant ground motion levels at the BBNPP site.

© 2007-2012 UniStar Nuclear Services, LLC. All rights reserved.
COPYRIGHT PROTECTED

The Cape Ann, Massachusetts earthquake of 1755 was felt over an extensive area along the East Coast around the New England Region. The most likely location of its epicenter is 25 mi (40 km) east-northeast of Cape Ann, Massachusetts (Ebel, 2006). The estimated moment magnitude is M 5.9.

Three different methods have been used to estimate ground motion from the 1755 earthquake (Ebel, 2006): (1) attenuation equations for CEUS assuming a magnitude and distance for the earthquakes; (2) MMI to ground motion conversions; and (3) estimates from chimney and unreinforced masonry damage. Ground motion estimates from the three methods have been given for PGA and 0.3 sec spectral acceleration assuming 5% damping for soil and rock sites at several locations.

For Boston, about 55 mi (87 km) from the epicenter, estimated PGA values for soil sites range from 0.08g to 0.12g and 0.3-sec spectral acceleration values (5%-damped) range from 0.09g to 0.21g. For New Haven, CT, about 175 mi (281 km) from the epicenter, PGA is estimated to be about 0.01g and estimated 0.3-sec spectral acceleration ranges from about 0.02 to 0.07g.

Another earthquake of interest is the 1727 Newbury event. The estimated magnitude for the 1727 event is M 5.6 (Ebel, 2000), which is a moderate event.

Significant zones of seismicity in New England are located at large distances (beyond 250 miles (402 km)) from the BBNPP site. Records of historical seismicity do not include earthquakes with $M \geq 7.0$. There is also no geologic evidence of active or potentially active structures capable of producing such earthquakes.

In summary, investigations of seismicity in the New England region since the EPRI-SOG EST study have not significantly changed the information base used to characterize source zones. Refinements in the location, size, and ground motion produced by significant earthquakes do not change the overall understanding of the seismic potential for the region. Given the large distance of the New England seismicity from the BBNPP Site and the nature of recent investigations, there is no basis to modify the EPRI-SOG EST assessments. For the BBNPP PSHA, only the Bechtel background zone BZ8 and Law zone 22 cover all or some of the New England seismicity and also extend within 200 mi (322 km) of the BBNPP Site and are therefore included.

2.5.2.2.3.6 Charlevoix

As previously discussed, the Charlevoix seismic zone is the most seismically active region of Eastern North America. It is located about 60 mi (97 km) downstream (northeast) from Quebec City (northeast). All six EPRI teams have considered the Charlevoix seismic zone in their source zone models and assigned maximum magnitudes close to or larger than 7.0. This seismic zone is located beyond the 200 mile radius of the BBNPP site, but a sensitivity analysis showed that it is a contributor to the seismic hazard at the BBNPP site for ground motion at lower frequencies.

Section 2.5.2.4.2 provides a discussion of the Gutenberg-Richter b parameter update from the original EPRI-SOG work. The BBNPP evaluation considered that an update is required to the b value of this zone. Values of b for the Charlevoix seismic zone were computed using the USGS 2001 (USGS, 2002) catalog and source zone geometries of Dames and Moore and Woodward-Clyde and a value of 0.7 was obtained in both cases. This is consistent with the b-value obtained by other EPRI EST teams. Therefore, the b value for the Charlevoix seismic zone for those two teams was changed to 0.7. Due to the long distance of the Charlevoix

© 2007-2012 UniStar Nuclear Services, LLC. All rights reserved.
COPYRIGHT PROTECTED

seismic zone from the BBNPP site, the new b value equal to 0.7 does not have a significant impact on the PSHA results.

A post-EPRI-SOG event of interest near the Charlevoix Zone is the November 25, 1988 Saguenay, Quebec earthquake, which occurred 22 mi (35 km) south of Chicoutimi, Quebec and 47 mi (75 km) northwest of the Charlevoix seismic zone (Earthquakes Canada, 2008). The earthquake had an estimated magnitude of 5.9 in both body wave and moment magnitude units (m_b 5.9, M 5.9). A depth of 18 mi (29 km) was estimated for the earthquake. This earthquake was located outside the Charlevoix seismic zone and, according to Earthquakes Canada, it occurred in a relatively aseismic region. The earthquake was felt over a wide area with a maximum epicentral intensity of VII-VIII. The maximum recorded accelerations on rock were 0.156 g on the horizontal component (at 40 mi (64 km) distance) and 0.102 g on the vertical component (at 27 mi (43 km) distance).

The epicenter of the Saguenay earthquake (48.12 N, 71.18 W) was located about 540 mi (870 km) from the BBNPP site. According the intensity map of Earthquakes Canada website, this event was felt with intensity III (MMI scale) in Pennsylvania.

The Saguenay earthquake epicenter is outside the Charlevoix seismic zone as defined by the six EPRI-SOG ESTs. The maximum magnitude distributions for the EPRI-SOG EST defined zones that contain the 1988 earthquake may have been underestimated. Because there was no significant seismicity in the epicentral area prior to the Saguenay earthquakes, most ESTs defined small source zones for Charlevoix based on the well defined area of significant seismicity. Weston has defined an alternative zone to consider the probability that some events outside Charlevoix may indeed belong to this zone. Rondout Associates defined a larger zone for Charlevoix; the 1988 earthquake is outside but very close to the western edge of this zone.

Two sensitivity cases are defined to study the potential impact of the Saguenay earthquake on the EPRI-SOG EST seismic source characterizations for Charlevoix and for the location of the 1988 earthquake:

1. Modify the Charlevoix seismic source zone to include the Saguenay epicentral location. For all 6 ESTs, the geometry of the Charlevoix source zone was modified as shown in the Figure 2.5-87 through Figure 2.5-92. The parameter b and maximum magnitude distribution remained as used in the base case analysis. Because the M_{max} of the existing EPRI-SOG source zones for Charlevoix is about M 7.0 or more, no increase in this value is required given that the magnitude of the 1988 earthquake is only M 5.9. Also, adding the 1988 earthquake to the catalog for Charlevoix events and deriving the b-value results in negligible change. Furthermore, additional earthquakes with epicenters within 625 (1000km) miles radius in the period of 2002-2007 were added to the USGS 2002 catalog and were considered in the evaluation of the impact of the modification of the EPRI source zone model. The radius was selected to incorporate events as far as the Saguenay location. These events are shown in Figure 2.5-87 through Figure 2.5-92.

2. Increase the maximum magnitude distribution (Table 2.5-66) of the current source zones that contain the epicenter of the 1988 earthquake. New earthquakes in the period 2002-2007 inside the 625 mile (1000 km, approximately) radius were updated into the USGS 2002 catalog. The b value and maximum magnitude distribution for the other zones remain without changes. The following adjustments were incorporated as an update sensitivity to the EPRI source zone model:

© 2007-2012 UniStar Nuclear Services, LLC. All rights reserved.
COPYRIGHT PROTECTED

- For the Bechtel EST, the Saguenay Earthquake is outside Source Zone 3 (Charlevoix/La Malbaie) and Source Zone 2 (St. Lawrence), but is located inside the Background Zone 7 (BZ7, Figure 2.5-93). The seismic parameter b and maximum magnitude for BZ7 remains unchanged.

- For the Dames and Moore EST, the Charlevoix Source Zone (Zone 59, Figure 2.5-94) does not include the Saguenay Earthquake, but this event is inside Source Zone 72 (Eastern Canada Province). Consequently, Zone 72 was defined using the maximum distribution indicated in Table 2.5-66 and a parameter b=1.04.

- For the Law Engineering Team EST, a new seismic zone (Zone 109, Figure 2.5-95) was defined in the EPRI source model by using the magnitude distribution indicated in Table 2.5-66. A parameter b=0.970 was considered.

- For the Rondout and Weston Geophysical Source Zones ESTs, the Saguenay Earthquake is not inside the Charlevoix Zone. Source Zones 50-1 and 18 were incorporated and assigned a b value of 1.01 and 0.90, respectively (Figure 2.5-96 and Figure 2.5-97).

- For the Woodward-Clyde EST, the 1988 event is outside Zone 12 (Charlevoix). Because there is not a source zone which includes this event, a new source zone was defined to include this earthquake (Figure 2.5-98). The new source zone was defined with a b value of 0.90 and a maximum magnitude distribution as indicated in Table 2.5-66.

2.5.2.3 Correlation of Earthquake Activity with Seismic Sources

Following Regulatory Guide 1.208 (NRC, 2007a) and 10 CFR 100.23 (CFR, 2007), a PSHA was conducted to support determination of the SSE and to account for uncertainties in the seismological and geological evaluations for the BBNPP site. The probabilistic approach was based on the PSHA conducted by the EPRI for CEUS in the mid to late 1980s (EPRI, 1989a) with changes to incorporate updated data.

The locations of earthquakes were compiled from the an updated USGS catalog (USGS, 2008a), and other sources (Section 2.5.2.1.2), covering events between 1534 and April 2010. The updated catalog has been adopted for assessing the BBNPP site seismic hazard. This update is a refinement of the EPRI-SOG catalog that listed earthquakes between 1627 and 1984 (EPRI, 1988). Figure 2.5-17 through Figure 2.5-22 show the distribution of earthquake epicenters from the updated 2006 USGS (USGS, 2008a) earthquake catalog in comparison to the seismic sources identified by each of the EPRI ESTs. These figures also include updates for seismic activity in the zones for 2007 - April 2010 out to a radius of 500 mi (805 km) from the BBNPP site. The comparison of earthquake distributions from the updated earthquake catalog supports the following conclusions:

- The updated catalog does not show any earthquakes within the BBNPP site region that can be associated with a known geologic or tectonic structure.

- The updated catalog does not show a unique cluster of seismicity that would suggest a new seismic source outside of the EPRI seismic source model (EPRI, 1986).

- The updated catalog does not show a pattern of seismicity that would require significant revision to the EPRI seismic source geometry.

© 2007-2012 UniStar Nuclear Services, LLC. All rights reserved.
COPYRIGHT PROTECTED

2.5.2.4 Probabilistic Seismic Hazard Analysis and Controlling Earthquake

Section 2.5.2.4.1 through Section 2.5.2.4.7 are added as a supplement to the U.S. EPR FSAR.

2.5.2.4.1 Probabilistic Seismic Hazard Analysis

The seismic hazard for the BBNPP was calculated using the original EPRI EST teams area sources, plus the New Madrid and Charleston characteristic earthquakes, and with the EPRI (EPRI, 2004) (EPRI, 2006) ground motion model and aleatory uncertainty model. This calculation was first made for hard rock conditions, and those results were then modified to account for local site conditions.

The analysis of seismic hazard consists of calculating annual frequencies of exceeding different amplitudes of ground motion, for all combinations of seismic sources, seismicity parameters, maximum magnitudes, ground motion equations, and ground motion aleatory uncertainties. This calculation is made for appropriate combinations of the New Madrid zone, the Charleston zone, the seismic sources defined by each of the six EPRI EST teams, and results in a family of seismic hazard curves. The alternative interpretations of seismic sources, seismicity parameters, maximum magnitudes, and ground motion equations making up each branch of the logic tree are weighted, resulting in a combined weight associated with each hazard curve. From the family of hazard curves and their weights, the mean hazard (and the distribution of hazard) are calculated.

The quantification of the Probabilistic Seismic Hazard at hard rock utilized Rizzo's in-house software, Rizzo-Hazard. This code uses the characterization of seismic sources and ground motion models to estimate the annual exceedance probabilities for various levels of spectral accelerations at different spectral frequencies.

The technical methodology generally follows the formulation by Cornell (Cornell, 1968) (Cornell, 1971) and integrates the product of the conditional probability that a ground motion measure will be exceeded given the earthquake magnitude and distance, and the probability distribution of magnitude and distance over all sources that can significantly contribute to the site seismic ground motion. This is expressed as:

$$v(z) = \sum \alpha_n(m_o) \int f(m) [\int f(r|m) P(Z > z|m, r) dr] dm$$

in which:

Z is ground motion level (e.g., peak ground acceleration or pseudo-spectral acceleration at prescribed natural frequencies),

P(Z>z|m,r) is the conditional probability that Z will exceed a value z, given an earthquake of magnitude, m, and distance, r,

f(m) and f(r) are the probability density functions for magnitude and distance, and

$\alpha_n(m_o)$ is the number of earthquakes per year above a prescribed minimum magnitude m_o, in the n-th seismic source.

© 2007-2012 UniStar Nuclear Services, LLC. All rights reserved.
COPYRIGHT PROTECTED

The integration over magnitude is performed from m_o to an upper bound magnitude m^u, and the integration over distance is performed usually over a prescribed radius from the site, typically larger than 186 mi (300 km). The probability density function for distance typically assumes that earthquakes occur randomly over the source areas or faults. The functions f(m) and $\alpha(m_o)$ define the recurrence relationships for the respective source zones.

The PSHA incorporates uncertainties and random variability interpreted to characterize inputs to the hazard calculation. Epistemic uncertainty in seismic sources and ground motion models is described through the use of a logic tree formalism. Alternative interpretations are defined to represent the range of uncertainty consistent with the available data. Then weights are assigned to the alternatives reflecting the degree that they are supported by data. For the EPRI (EPRI, 1989a) interpretations by the six ESTs that are incorporated in the seismic source model for the BBNPP Site, the weights that the teams assessed are used. Similarly, weights assigned to alternative ground motion models in EPRI (EPRI, 2004) are used. For the New Madrid Seismic Zone the characterization described in the Clinton ESP (EGC, 2006) is employed. For the Charleston Seismic Zone, the characterization developed in the Vogtle ESP (SNOC, 2008) was determined to be appropriate for inclusion. Aleatory variability in input parameters is represented by probability distributions within the PSHA integral. Thus, uncertainties and variabilities are appropriately taken into account as required by 10 CFR 100.23. Implementation of the hazard calculation is based on the approach of Frankel (Frankel, 1995) for the CEUS.

2.5.2.4.2 Effects of New Regional Earthquake Catalog

A sensitivity study was done to determine seismicity since the EPRI-SOG study affects the determination of seismicity recurrence parameters for the EPRI EST source zone models. Seismicity rates in the EPRI study (EPRI, 1986) were based on an earthquake catalog that extended through 1984. The USGS 2001 catalog (USGS, 2002) has 17 more years of data. Using the USGS 2001 catalog and completeness periods the b values for some of the EPRI source zones were computed and compared to the b-values obtained by EPRI teams. The differences between the two sets of b-values are small and can be attributed to using different catalogs and different completeness periods. For example, the EPRI b-value for Rondout source zone 31 is 0.96 while the estimated b-value using USGS 2001 catalog is 1.02. For many of the source zones the differences are less than 0.05. Based on these comparisons, it is concluded that, with the exception of source zones characterizing seismicity in the Charlevoix, Quebec vicinity, the b-values determined by the EPRI ESTs are adequate for use in the BBNPP PSHA. For Charlevoix, EPRI ESTs, except Dames and Moore and Woodward-Clyde Consultants, derived a b-value between 0.70 and 0.79. The USGS used a b-value of 0.76 (USGS, 1996) (USGS, 2002) (USGS, 2008a) for this source zone based on the work of Adams and others in the Geological Survey of Canada. Thus, the b-values for the Charlevoix seismic zone in the Dames and Moore (zone 59) and Woodward-Clyde (zone 12) models were reestimated using the updated earthquake catalog 1534 - April 2010 (EPRI, 2010). Values of 0.63 and 0.65 were obtained for the two teams, respectively. These two values, which are more conservative but also more representative of the seismicity of the zone, are used in the current seismic hazard analysis. The choice to use these two updated b-values does not have a significant impact on the overall hazard due to the large distance between the Charlevoix seismic zone and the BBNPP Site. No other changes in EPRI seismicity parameters are required.

2.5.2.4.3 New Maximum Magnitude Information

The upper magnitude, M_{max}, utilized in the magnitude recurrence equation can significantly affect the low probability seismic hazard, in particular from the near field events. In the 1989 EPRI-SOG (EPRI, 1989a) study, each EST developed alternative values of M_{max} for each seismic

© 2007-2012 UniStar Nuclear Services, LLC. All rights reserved.
COPYRIGHT PROTECTED

source in terms of body-wave magnitude (m_b). More recent studies (USGS, 2008a; Bakun, 2004), however, have revised M_{max} for the Charleston, New Madrid, and local sources. In addition, it has been recognized that the large historical events that have occurred at the New Madrid and the Charleston fault systems cannot be adequately modeled by the G-R equation. Instead, the concept of characteristic earthquakes (Schwartz, 1984; Youngs, 1985) has been introduced to more appropriately represent the seismic activity at New Madrid and Charleston. Thus, characteristic events have been adopted in the calculation of the hazard at the BBNPP site. Moment magnitudes M between 7 and 8.1 are incorporated for the New Madrid source and between 6.5 and 6.7 for the Charleston source. Table 2.5-3 through Table 2.5-8 list revised maximum magnitudes and their corresponding weights for the seismic sources selected for the BBNPP site PSHA.

The EPRI-SOG ESTs defined the maximum magnitude for each of their seismic sources using either body wave magnitude, m_b, or seismic moment magnitude, M. Furthermore, the G-R parameters a and b are derived in terms of m_b, while the equations for ground motion models are functions of M. Therefore, conversions from body wave magnitude into moment magnitude are required. The three magnitude-conversion relationships shown in Table 2.5-2 were used in the BBNPP PSHA and were assigned equal weight.

2.5.2.4.4 New Seismic Source Characterizations

For New Madrid and Charleston, new characteristic earthquakesource models have been adopted to reflect updated estimates of the possible geometries and maximum magnitude at both fault zones. For area source zones, the truncated exponential or Gutenberg-Richter (G-R) equation (Gutenberg, 1944) has been used to describe recurrence. This equation was truncated at the maximum magnitude, M_{max}. As noted before, each EPRI EST (EPRI, 1989a) developed G-R parameters a and b for each of their seismic sources, identifying alternative smoothing options, priors, and their corresponding weights. For the BBNPP PSHA, calculation of recurrence parameters uses the spatial smoothing approach developed by USGS (USGS, 2002) (USGS, 2008a). This approach considers only the variation of the intercept parameter a for prescribed constant values of the slope parameter b. The constant values of b have been taken as the averages of the b-values adopted for each seismic source by each EPRI EST (EPRI, 1989a), along with the corresponding weights for each smoothing option. Table 2.5-3 through Table 2.5-8 present the values of the average seismic parameter b for each EPRI EST source model used as input to the BBNPP PSHA.

Four smoothing options are considered for characterizing the recurrence parameter a in the USGS 2008 approach. Each of the first three smoothing options is based on an incompleteness period, a minimum incompleteness magnitude, and a smoothing correlation distance. The fourth option is considered only for the background seismic source since it has negligible effect on main sources such as New Madrid or Charleston that have a much smaller area than the background source. The information for each model is listed in Table 2.5-16.

2.5.2.4.5 New Ground Motion Models

Ground motion prediction equations (attenuation relations) relate the characteristics of the earthquake source and propagation path to the ground motion at a site. Predicted ground motions are typically quantified in terms of a median value (a function of magnitude, distance, site condition, and other factors) and a probability density function of peak horizontal ground acceleration or spectral accelerations.

The estimation of strong ground motion for specified magnitude, distance, and site conditions in the CEUS is difficult due to the paucity of strong motion data. Most of the available data

© 2007-2012 UniStar Nuclear Services, LLC. All rights reserved.
COPYRIGHT PROTECTED

correspond to M < 5.8 and distances exceeding about 31 mi (50 km). Considerable effort has been directed to developing appropriate attenuation relations for the CEUS conditions. In general, the attenuation relationships utilize standard forms to regress on recorded data in the region, augmented by data from other similar tectonic regimes and stochastic time histories tied to source types and styles of faulting.

Since publication of the 1989 EPRI study (EPRI, 1989a), much work has been done to evaluate strong earthquake ground motion in the CEUS. In 2004, EPRI completed a study on strong ground motion prediction in the CEUS following the SSHAC (NRC, 1997b) guidelines for a Level III Analysis. A panel of six ground motion experts was convened during several workshops to provide advice to a Technical Integrator (TI) team on the adequacy of available CEUS ground motion relationships. On this basis, the TI developed a representation of the current scientific understanding on the subject, consisting of "clusters" of ground motion relationships with associated weights to represent the uncertainty in predicting the median ground motion, in terms of moment magnitude. Each cluster corresponds to relationships based on a similar approach for ground motion modeling. The uncertainty in the median model for each ground motion cluster is defined by two additional models: one representing the 5th percentile of the median uncertainty distribution and the other corresponding to the 95th percentile.

Epistemic uncertainty is modeled using multiple ground motion equations and multiple estimates of aleatory uncertainty (sigma), all with associated weights. Different sets of equations are recommended for sources that represent rifted versus non-rifted parts of the earth's crust. Equations are available for spectral frequencies of 100 Hz (equivalent to PGA), 25 Hz, 10 Hz, 5 Hz, 2.5 Hz, 1 Hz, and 0.5 Hz, and these equations apply to hard rock conditions, i.e., rock with a shear wave velocity of 9200 ft/sec (2804 m/sec).

EPRI has published updated estimates of aleatory uncertainty (EPRI, 2006a). This update reflected the observation that sources of the aleatory uncertainties in the original EPRI attenuation study (EPRI, 2004) were probably too large, resulting in over-estimates of seismic hazard. The 2006 EPRI study (EPRI, 2006a) recommends a revised set of aleatory uncertainties (sigmas) with weights that can be used to replace the original aleatory uncertainties published in the 2004 EPRI study (EPRI, 2004).

These EPRI 2004 equations have been adopted for median ground motion estimates, and the Abrahamson log-sigma model (EPRI, 2006a) is used to incorporate aleatory variability. Within this context, Figure 2.5-68 shows the logic tree for general area sources such as background or local source zones, and Figure 2.5-67 shows the logic tree for non-general sources such as New Madrid and Charleston. Adopting the EPRI 2004 ground motion model implies that the seismic hazard is calculated at the location characterized by rock with a V_{S30} of 9200 ft/sec (2804 m/sec).

The EPRI 2004 Report defines four clusters of median ground motion models to represent alternative modeling approaches. Three clusters are used in the ground motion model for general area sources and all four clusters are used for the ground motion model for non-general sources (New Madrid and Charleston). The rift option was selected for the fourth cluster, instead of the non-rift option that is used for area sources. The three branches of the second level of the logic tree on Figure 2.5-75 represent the epistemic uncertainty in the median attenuation relationship for each cluster. The branches incorporate a three-point discrete distribution with weights of 0.63, 0.185 and 0.185 for the median, the 5th, and the 95th percentiles, respectively. The third branching level addresses the uncertainty in the

© 2007-2012 UniStar Nuclear Services, LLC. All rights reserved.
COPYRIGHT PROTECTED

model for the aleatory variability in ground motions about the median attenuation relationship. Models 1A and 1B, as well as their weights, are those proposed by Abrahamson (EPRI, 2006a) (EPRI, 2006b) to account for inter-event and intra-event variability. The EPRI 2004 ground motion attenuation relationships use either the closest distance to the rupture plane or closest distance to the surface projection of the rupture plane (Joyner-Boore distance). For implementation using point sources, the EPRI 2004 document presents adjustments, which are used except for the New Madrid and Charleston non-general sources. For these sources, the earthquake rupture is assumed to always include the closest point to the BBNPP site, which is then used as the distance measure in the ground motion prediction equations.

In assessing aleatory variability in ground motion, EPRI TR-1014381 (EPRI, 2006a) was used in lieu of the Regulatory Guide 1.208 cited document, i.e. EPRI Report 1013105 (EPRI, 2006b). EPRI Report 1013105 (EPRI, 2006b) was an Update Report while EPRI TR-1014381 (EPRI, 2006a) is the final report. For the purposes of revised estimates of aleatory uncertainty in the CEUS, there is no technical difference between the documents. The "Recommended CEUS Sigma" values and "Conclusions" of both reports are identical.

Earthquakes occurring within the area seismic sources were treated as point sources. Thus, the adjustments to the ground motion equations developed in EPRI (EPRI, 2004) to account for this point-source representation were incorporated in the hazard calculations.

2.5.2.4.6 Deaggregation of Probabilistic Seismic Hazard Analysis Results and Identification of Controlling Earthquakes

Figure 2.5-59 through Figure 2.5-65 and Table 2.5-19 through Table 2.5-25 present the hazard curves resulting from the BBNPP PSHA. The hazard curves show ground motion exceedance for seven response spectral frequencies (100 Hz (equivalent to PGA), 25 Hz, 10 Hz, 5.0 Hz, 2.5 Hz, 1.0 Hz, and 0.5 Hz). The mean and fractile (5%, 16%, 50% (median), 84% and 95%) hazard curves are indicated.

Figure 2.5-36 shows mean uniform hazard spectra for 10^{-4}, 10^{-5}, and 10^{-6} annual frequencies of exceedance from these calculations at seven response spectral frequencies. Numerical values of these spectra are documented inTable 2.5-14.

The mean rock hazard has been de-aggregated for 10^{-4}, 10^{-5} and 10^{-6} mean annual frequencies of exceedance. The magnitude and distance bins for the de-aggregation table were taken from Regulatory Guide 1.208 (NRC, 2007a). The results have been plotted in Figure 2.5-37 through Figure 2.5-40, Figure 2.5-76 and Figure 2.5-77, for the 10^{-4} ,10^{-5} , and 10^{-6} annual frequencies of exceedance, respectively. At each annual frequency of exceedance, deaggregation results are shown for a low response spectral frequency range (average of 1 and 2.5 Hz), and a high frequency range (average of 5 and 10 Hz). These figures depict the percent contribution of each magnitude-distance bin to the total hazard.

The deaggregation of the PSHA results was used to identify controlling reference and deaggregation earthquakes for the BBNPP site. Each controlling earthquake is defined by a magnitude and distance. Controlling earthquakes are determined for both the low response spectral frequency range and the high range for 10-4 and 10-5 mean annual frequencies of exceedance. The controlling reference earthquakes (REF) are defined by the mean magnitude and distance from the deaggregation. Because there is a significant contribution to hazard at low response spectral frequencies from distant earthquakes, the mean magnitude and distance for the low frequency controlling reference earthquake is determined from deaggregation results for distances greater than 100 km.

© 2007-2012 UniStar Nuclear Services, LLC. All rights reserved.
COPYRIGHT PROTECTED

In accordance with NUREG/CR-6728 (McGuire, 2001) Approach 2B, the controlling deaggregation earthquakes are used to incorporate the effect of magnitude on site response. Earthquakes with a range of magnitude contribute to seismic hazard at the site for a given mean annual frequency of exceedance. Because the response spectral shape varies as a function of magnitude, the site response potentially varies depending on the magnitude of the earthquakes contributing to a given ground motion level. To incorporate this potential effect in the site response analysis, for each response spectral frequency range three controlling deaggregation earthquakes are identified to represent a low (DEL), middle (DEM), and high (DEH) magnitude.

Response spectral shapes for the REF, DEL, DEM, and DEH are determined following recommendations in NUREG/CR-6728 for CEUS earthquakes. Final response spectra are determined by scaling the spectral shapes to the UHRS at the appropriate response spectral frequency (i.e., 1.75 Hz or 7.5 Hz). Figure 2.5-77 and Figure 2.5-78 show the controlling earthquake response spectra for low and high response spectral frequency ranges for ground motion with a 10^{-4} and 10^{-5} mean annual frequency of exceedance, respectively.

The deaggregation results show that at high response spectral frequency the hazard is dominated by magnitude 5 to 5.5 earthquakes at increasingly close distances as the frequency of exceedance decreases. At low response spectral frequencies, both nearby and distant sources have significant contributions to hazard with distant sources being more important at higher frequencies of exceedance and local sources at lower frequencies of exceedance.

Each of the controlling deaggregation earthquakes, for both the low and high response spectral frequency ranges, was taken as input for the seismic site amplification analyses as described in Section 2.5.2.5.1.5.

2.5.2.4.7 Results of Sensitivity Studies

The following subsections provide results and conclusions of the sensitivity studies performed for the original BBNPP site. The results of these sensitivity studies have been compared to the results of the "base case" PSHA that was performed for the original BBNPP location using the 2001 USGS catalog (USGS, 2002). The results of the current PSHA (relocated BBNPP site) supersedes the original base case and the sensitivity results and therefore should be considered for the BBNPP site.

2.5.2.4.7.1 Five Hundred (500) Mile Catalog Update

Figure 2.5-78 through Figure 2.5-83 show the 2002-2007 events in the 500-mile (805 km) radius centered at the BBNPP site. Events prior to 2002 are omitted for clarity purposes. The figures show the seismic source zones that are either partially or totally within the 500 mile (805 km) radius and contribute to 99% of the hazard at the BBNPP site.

The 500 mi (805 km) sensitivity study results show marginal reduction of ground motion levels, between 0.3 and 2.7%, when compared to the base case PSHA calculation. It is, therefore, concluded that the base case provides adequate estimation of the hazard at the BBNPP site. Table 2.5-63 compares the Uniform Hazard Response Spectra (UHRS) at hard rock conditions between cases considering the updated catalog and the base case analysis. The result is a marginal reduction of ground motion levels, between one and two percent. The more conservative USGS 2002 Guttenberg-Richter b parameters were selected and used in this study. Consequently, this analysis shows that the 2002-2007 extended catalog does not have a significant effect on the PSHA at the BBNPP site due to the decrement of the seismicity rates. As an example, Figure 2.5-84 provides a comparison of the seismicity rates, for the

© 2007-2012 UniStar Nuclear Services, LLC. All rights reserved.
COPYRIGHT PROTECTED

Bechtel EST team and the Source Zone 3 (Charlevoix) and Background Zone. Figure 2.5-85 provides a comparison of the mean hazard curves for Peak Ground Acceleration (PGA).

2.5.2.4.7.2 Charlevoix Sensitivity Study

Table 2.5-64 compares the Uniform Hazard Response Spectra (UHRS) at hard rock conditions between cases considering the original EPRI-SOG base case analysis and the updated Charlevoix geometry for Case 1 of the Charlevoix sensitivity study.

Table 2.5-67 shows a comparison between the Uniform Hazard Response Spectra obtained with the Charlevoix sensitivity analysis Case 2 and those calculated with the EPRI-SOG base case geometry.

Both cases show that no significant changes in the PSHA results occurred. Both cases provide practically equal results which is attributed to the large distance (540 mi (870 km)) between the Charlevoix zone and the BBNPP site. The differences with the base case are mainly due to the 2002-2007 seismicity update for a larger influence region of 625 miles (1006 km). Figure 2.5-99 compares the seismic hazard curves. Figure 2.5-100 provides the seismicity rates for the Charlevoix zone from three of ESTs. The change in the seismicity rates is marginal and, thus, the sensitivity study performed does not affect the PSHA results for the BBNPP site.

2.5.2.4.7.3 Ramapo Fault Sensitivity Studies

Results of the sensitivity analyses are shown in Figure 2.5-101. Contribution of the RSZ to the hazard at 0.1 g ground motion level is not significant. The total hazard curves and values at the BBNPP site already include the seismicity from the RSZ and NY-Ph. However, the seismicity has been taken into account by using the source models of EPRI and not using the specified RSZ and NY-Ph zones. At 0.1 g the contribution from RSZ is about 0.8 % and from NY-Ph less than 7%. The contribution from both zones is accounted for in the BBNPP PSHA. Seismicity rates are provided for the isolated zone by Figure 2.5-102. The final EPRI seismic source zones that contribute to 99% of the seismic hazard at the BBNPP site all include the area of the RSZ and NY-Ph. As was shown earlier, the maximum magnitude of EPRI zones are not underestimated. The definition of new zones or modification of existing ones will not lead to significant changes in the seismic hazard at the BBNPP site. This sensitivity analysis was performed to address the Sykes, 2008 publication in the Bulletin of the Seismological Society of America (BSSA).

2.5.2.5 Seismic Wave Transmission Characteristics of the Site

The uniform hazard spectra presented in Section 2.5.2.4.6 and displayed on Figure 2.5-35 are defined for a hard rock site condition with shear-wave velocity of 9200 ft/sec (2804 m/sec). At the BBNNP site, rock with this shear-wave velocity is located at depths of about 414 ft (126.2 m) below the foundation level. To determine the SSE at the ground surface, it is necessary to adjust the uniform hazard spectra for amplification or de-amplification as the vibratory ground motion propagates through the soil media. As mentioned above, the adjustment was made by conducting Site Response Analyses and following Approach 2B described in NUREG/CR-6728 (McGuire, 2001). These analyses consist of defining the shear wave velocity and material damping characteristics of the soil and rock profile between the ground surface and the depth of hard rock. Then uni-dimensional site analyses are conducted using an equivalent linear procedure (Schnabel, 1972). The results are used to derive site amplification functions for modifying the response spectra at rock to the corresponding response spectra at the ground surface, taking into account the seismic wave transmission characteristics of the soil layers. This section describes the steps involved in the calculation and application of the site

© 2007-2012 UniStar Nuclear Services, LLC. All rights reserved.
COPYRIGHT PROTECTED

amplification functions. The seismic wave transmission characteristics and effects of the BBNPP site soil column on hard rock ground motions are described in this section.

Section 2.5.2.5.1 is added as a supplement to the U.S. EPR FSAR.

2.5.2.5.1 Development of Site Amplification Functions

2.5.2.5.1.1 Methodology

The calculation of site amplification functions is performed in the following 4 steps:

1. Based on the results of geotechnical and geological investigations at the BBNPP Site, develop a best estimate soil and rock column, extending from the surface to the hard rock horizon at depth, consisting of layers defined by their mean low-strain shear wave velocities and by material damping properties, including strain-dependencies. At the BBNPP site, hard rock (V_s = 9200 ft/sec (2804 m/sec)) is found at 414 ft (126.2 m);

2. Develop a probabilistic model that describes the random variability in the above properties, locations of layer boundaries, and correlation between the velocities in adjacent layers, and generate a set of 60 artificial "randomized" profiles;

3. For each of the controlling earthquakes (DEL, DEM, and DEH) associated with ground motions having mean of 10^{-4} and 10^{-5} annual frequencies of exceedance, for both LF and HF spectral frequencies, use the corresponding controlling time histories for input into dynamic response analysis as the outcrop motion at the hard rock elevation;

4. Use an equivalent-linear time-history site-response formulation to calculate the dynamic response of the site for each of the 60 random profiles, and then calculate the mean site response. This step is repeated for each of the three de-aggregated controlling earthquakes.

These steps are described in the following subsections. The calculation of site effects was performed with an in-house version of the computer program SHAKE (Schnabell, 1972). This program computes the response in a system of viscous-elastic, horizontally layered, soil units, overlying a uniform half-space, subjected to transient, vertical travelling shear waves.

The analytical method implemented in SHAKE is based on the solution of the wave equation and the Fast Fourier Transform algorithm. The nonlinearity of the shear modulus and damping is accounted for by the use of equivalent linear soil properties within an iterative procedure to obtain values for modulus and damping compatible with the effective strains in each layer. Therefore, for any set of layer properties, SHAKE performs a linear analysis.

2.5.2.5.1.2 Investigations to Determine the Base Case Soil/Rock Column for the BBNPP Site

Development of a best estimate soil/rock column is described in detail in Section 2.5.4. This section provides an overview of the soil/rock column and the geotechnical and geological investigations carried out to characterize it.

The BBNPP site was investigated using test borings and geophysical methods. The geotechnical investigation is described in detail in Section 2.5.4.

The layers underlying the BBNPP site consist of the following stratigraphic units:

- Overburden Soils:

© 2007-2012 UniStar Nuclear Services, LLC. All rights reserved.
COPYRIGHT PROTECTED

- Glacial Overburdens

- Rock Formations:

  - Mahantango Shale

The Mahantango Shale consists of three horizons: weathered rock, a transition zone, and sound rock. Within the BBNPP site, the overburden soils, weathered rock, and transition zone rock will be excavated and replaced with concrete or engineered fill. The engineered fill and concrete are taken into account in defining the soil/rock column for the BBNPP site response analyses. Section 2.5.4 provides detailed contour information related to the position of the bedrock below the power block's footprint.

The compressional and shear-wave velocities of the in situ materials are taken from geophysical field tests using two different techniques:

1. Three sets of downhole tests,

2. Three sets of suspension logging tests

Of the six geophysical measurements, those from boring G-401 provide the deeper site-specific geophysical information collected during the geotechnical investigation. In this boring, P-S Suspension and downhole tests were performed down to a depth of approximately 400 ft (122 m). This boring is at the center of the projected containment footprint.

The downhole profiles consist of average compressional and shear-wave velocities for layers with thickness varying from about 13 ft (4 m) to 140 ft (42.7 m). The suspension logging profiles provide measurements of compressional and shear-wave velocities at approximately 1.5 ft (0.5 m) spacing. Shear-wave velocities of 9200 ft/sec (2804 m/sec), representing the reference rock condition for which seismic hazard was calculated, were not reached in the geophysical surveys. Thus, the deeper portion of the best estimate profile was developed considering the stratigraphy of the rocks underlying the BBNPP site and the best estimate profile from the previous BBNPP site.

The geologic column at the BBNPP site is an extension of the Mahantango Formation, which is a dark gray to black shale with few to no fractures. Some distinctive features are the presence of calcareous zones, the presence of thin pyrite lenses that increase in abundance with depth, and the presence of calcite veins perpendicular to the bedding plane that are micro-faulted. The upper surface of the Mahantango Formation shows the effects of solution and weathering in a few areas, but is predominatly very competent and indurated.

In addition to the in-situ geophysical testing, laboratory measurements of velocity were carried out on samples obtained from BBNPP site borings. Free-free direct arrival tests were performed on undisturbed rock samples by the University of Texas. The free-free direct arrival test results are provided in Table 2.5-42. The tests provided material velocity and damping values associated with shear waves and compressional waves.

A best-estimate velocity profile was determined taking into account the geophysical borehole measurements, the laboratory measurements, and the geology of the BBNPP site. Figure 2.5-50 shows the best-estimate shear-wave velocity profile along with in-situ velocity data from boring G-401 and laboratory velocity measurements on samples from boring B-401. Also

© 2007-2012 UniStar Nuclear Services, LLC. All rights reserved.
COPYRIGHT PROTECTED

shown is the best-estimate coefficient of variation (COV) profile. Figure 2.5-51 shows the best-estimate profiles without the data.

Resonant Column and Torsional Shear Laboratory Tests were performed on soil and backfill samples. The complete set of results from these tests is reported in Section 2.5.4.2.3. Generic cohesionless soil curves (EPRI, 1993) were adopted to describe the strain dependencies of shear modulus and damping for the backfill based on available results from the BBNPP site investigation. As recommended by Regulatory Guide 1.208 (NRC, 2007a) the damping curves for soils were truncated at 15 percent for the BBNPP site response analysis.

The average of the laboratory test results for damping for the Mahantango Shale is 0.86 percent. Lower values, 0.8 and 0.7 percent, are conservatively used for the analysis. The Mahantango Shale has a very high Rock Quality Designation (RQD) and as a rock mass is capable of transmitting shear waves very efficiently with small amounts of damping. Therefore, the lower reported laboratory values are selected for the analysis. The RQD of the Mahantango Shale is reported in the field boring logs.

For the BBNPP site response analyses, the Mahantango Shale and the concrete underlying the power block basemat are assumed to behave linearly during earthquake shaking.

2.5.2.5.1.3 Representation of Variability and Correlations in Soil/Rock Column Properties

To account for variations in shear-wave velocity across the BBNPP site, 60 randomized profiles were generated. In generating the randomized profiles, the coefficient of variation of V_S is used as an approximation to the standard deviation of $\ln(V_S)$ (Ang and Tang, 1975). These artificial profiles represent the soil column from the top of the ground surface to bedrock with a shear-wave velocity of 9,200 ft/s (2804 m/sec). The model uses as inputs the following quantities:

- The best estimate of the shear-wave velocity profile and other soil properties described above;
- The coefficient of variation of the shear wave velocity as a function of depth, developed using available BBNPP site data (refer to Section 2.5.4);
- The probabilistic characterization of layer thickness as a function of depth, computed assuming a normal distribution;
- The depth to bedrock with a shear-wave velocity of 9200 ft/s (2804 m/s), which is randomized assuming a normal distribution to account for variation in the bedrock-depth data described in Section 2.5.4.

Figure 2.5-43 shows the best estimate V_s and COV profiles for the nuclear island that were used to generate the 60 randomized profiles.

The randomly generated layer thicknesses were computed assuming a normal distribution using a coefficient of variation of 0.15 for each layer. For consistency with the site-specific data, the generated ln-velocities and the generated thicknesses were truncated at ±2 standard deviations according to the recommendations of Toro (Toro, 1996).

Figure 2.5-44 illustrates the 60 randomized V_s profiles . These profiles include uncertainty in depth to bedrock with a shear-wave velocity of 9200 ft/s (2804 m/s). Figure 2.5-45 compares

© 2007-2012 UniStar Nuclear Services, LLC. All rights reserved.
COPYRIGHT PROTECTED

the mean of these 60 V_s profiles to the best estimate V_s profile, indicating very good agreement. This figure also shows the ±1 standard deviation values of the 60 profiles, reflecting the coefficients of variation indicated on Figure 2.5-43.

Mean values of shear stiffness (G/GMAX) and damping for each geologic unit are described in Section 2.5.4. Variation in the properties for each soil/rock column unit are characterized through the use of randomized material property curves. For engineered fill, which is considered a nonlinear material, 60 randomized G/G_{max} and damping curves are developed. For concrete and sound rock, which are considered linear materials, 60 randomized damping curves are developed. For the linear material, G/G_{max} is taken as 1. Figure 2.5-46 and Figure 2.5-47 illustrate the randomized shear stiffness and damping curves for engineered fill at less than 30 ft.

These randomized velocity profiles and material property curves are used to calculate site response taking into account variation in site properties, as described in the following sections.

2.5.2.5.1.4 Development of Smooth Uniform Hazard, Controlling, and Reference Response Spectra

In addition to the characterization of site material properties described in Sections 2.5.2.5.1.2 and 2.5.2.5.1.3, the site response analysis also requires time histories representing earthquakes that control the seismic hazard at various response spectral frequencies. To develop the time histories, first the response spectra associated with controlling earthquakes are developed. Then the time histories are developed to be consistent with the controlling earthquake response spectra. The controlling earthquake response spectra are also used to smooth the UHRS originally defined at the limited number of spectral frequencies for which the PSHA was carried out. Development of controlling earthquake response spectra and their use to smooth the UHRS are described in this section.

The identification of controlling earthquakes on the basis of the PSHA deaggregation is described in Section 2.5.2.4.6. Controlling reference earthquakes are determined for ground motion with mean annual frequencies of exceedance of 10^{-4} and 10^{-5}. At each hazard level, a controlling reference earthquake (REF) is determined for a low response spectral frequency range (average of 1 and 2.5 Hz, or 1.75 Hz) and a high range (average of 5 and 10 Hz, or 7.5 Hz) (Table 2.5-11). In addition, controlling deaggregation earthquakes are determined (Table 2.5-11). The controlling deaggregation earthquakes represent (for each combination of mean annual frequency of exceedance and spectral frequency range) a low, middle, and high magnitude earthquake contributing to the hazard (DEL, DEM, and DEH, respectively). These earthquakes are used to generate input for the site response analysis such that the site response analysis takes into account the effects of the range of earthquake magnitude (i.e., differing spectral shapes) contributing to the hazard at the BBNPP Site. For both the controlling reference earthquakes and the controlling deaggregation earthquakes, response spectral shapes are determined following the recommendations in NUREG/CR-6728 (McGuire, 2001). The response spectral shapes are scaled to the UHRS at the appropriate spectral frequency to give the final controlling response spectra. Figure 2.5-80 and 2.5-81 show the reference earthquake response spectra for the low and high spectral frequency range for 10^{-4} and 10^{-5} mean annual frequencies of exceedance, respectively. Similarly, Figure 2.5-77 and Figure 2.5-78 show the deaggregation earthquake response spectra.

To smooth and extrapolate the UHRS defined from the PSHA results, the spectral shapes of the controlling reference earthquakes are used. In addition to the controlling reference

© 2007-2012 UniStar Nuclear Services, LLC. All rights reserved.
COPYRIGHT PROTECTED

earthquakes for the spectral frequency ranges of 1 to 2.5 Hz and 5 to 10 Hz, to smooth the UHRS, controlling reference earthquake response spectra are also determined for response spectral frequencies of 0.5 Hz and 25 Hz, respectively. For spectral frequencies less than 0.5 Hz, the spectral shape of the controlling reference earthquake for 0.5 Hz is used. For spectral frequencies from 0.5 Hz to 5 Hz, 5 Hz to 10 Hz, and 10 Hz to 100 Hz, the spectral shapes of the 1 to 2.5 Hz, 5 to 10 Hz, and 25 Hz controlling reference earthquakes are used, respectively, to guide the smoothing. The smoothed UHRS are shown in Figure 2.5-49 for ground motion with mean annual frequencies of exceedance of 10^{-4}, 10^{-5}, and 10^{-6}. For mean annual frequencies of exceedance of 10^{-4} and 10^{-5}, the smoothed UHRS are presented on Figure 2.5-77 and Figure 2.5-78 along with the scaled controlling earthquake response spectra.

The smooth controlling response spectra are presented on Figure 2.5-77 and Figure 2.5-78.

2.5.2.5.1.5 Controlling Time Histories

Time histories representing the controlling deaggregation earthquakes are developed by adjusting a seed time history such that its response spectrum matches the associated controlling deaggregation earthquake response spectrum. As an example, a comparison of the time history response spectra to the target response spectrum is shown in Figures 2.5-79 for DEL and DEM controlling earthquakes for the low response spectral frequency range and a 10^{-4} mean annual frequency of exceedance.

The spectral matching is carried out to meet the criteria recommended in Appendix F of Regulatory guide 1.208 (NRC, 2007a). The seed time histories are selected taking into account the magnitude and distance associated with each controlling deaggregation earthquake. For each controlling deaggregation earthquake, two sets of two horizontal time histories are developed, leading to a total of 24 sets (i.e., two sets of time histories x three controlling deaggregation earthquakes x two spectral frequency ranges x two annual frequencies of exceedance). As documented in NUREG/CR-6728 (McGuire, 2001), the seed time histories are strong motion acceleraograms recorded during past earthquakes that have been modified to represent CEUS conditions. The seed time histories used to develop the time histories for the controlling deaggregation earthquakes are listed in Table 2.5-18.

2.5.2.5.1.6 Site Response Analysis

The site response analysis performed for the BBNPP site used a time history-based procedure in conjunction with the following assumptions:

- Vertically-propagating shear waves are the dominant contributor to site response.
- An equivalent-linear formulation of soil nonlinearity is adequate for the characterization of site response.

Sixty response analyses were performed using the Rizzo in-house version of the program SHAKE (Schnabel, 1972) to calculate the site amplification function for each controlling deaggregation earthquake.The 60 randomized velocity profiles were paired with the 60 sets of randomized modulus reduction and damping curves (one profile with one set of modulus reduction and damping curves) to define 60 soil columns. Each of the four spectrally matched time histories corresponding toeach controlling deaggregation earthquake was used to compute the response of the sixty soil columns.

For each analysis, the response spectrum computed at the ground surface was divided, frequency by frequency, by the response spectrum for the hard rock input motion to obtain a site amplification function. The arithmetic mean of these 60 individual response spectral ratios

© 2007-2012 UniStar Nuclear Services, LLC. All rights reserved.
COPYRIGHT PROTECTED

was taken as the mean site amplification function for each controlling deaggregation earthquake. A similar analysis was also carried out for the foundation level to obtain a corresponding mean site amplification function for that BBNPP site.

For each combination of spectral frequency range (LF, HF) and mean annual frequency of exceedance (10^{-4}, 10^{-5}), a weighted average is determined of the mean amplification factors for the DEL, DEM, and DEH controlling earthquakes. The results for the three controlling deaggregation earthquakes are weighted according to their relative contribution to seismic hazard at the BBNPP site.

The following figures and table show results of the site response analysis:

- Figure 2.5-48: individual and mean hard-rock-to-ground-surface amplification functions (factors) for the 60 randomized soil/rock columns for the high spectral frequency range (HF) DEM earthquake representing ground motion with a 10^{-4} mean annual frequency of exceedance
- Figure 2.5-49: maximum strains versus depth for the 60 randomized soil/rock columns for the HF DEM earthquake representing ground motion with a 10^{-4} mean annual frequency of exceedance (left side- 0 to 50 ft, right side- 50 to 450 ft)
- Figure 2.5-50: individual and mean hard-rock-to-ground-surface amplification factors for the 60 randomized soil/rock columns for the low spectral frequency range (LF) DEM earthquake representing ground motion with a 10^{-4} mean annual frequency of exceedance
- Figure 2.5-51:maximum strains versus depth for the for the 60 randomized soil/rock columns for the LF DEM earthquake representing ground motion with a 10^{-4} mean annual frequency of exceedance (left side- 0 to 50 ft, right side- 50 to 450 ft)
- Figure 2.5-52: individual and mean hard-rock-to-ground-surface amplification factors for the 60 randomized soil/rock columns for the HF DEM earthquake representing ground motion with a 10^{-5} mean annual frequency of exceedance
- Figure 2.5-53: maximum strains versus depth for the 60 randomized soil/rock columns for the HF DEM earthquake representing ground motion with a 10^{-5} mean annual frequency of exceedance (left side- 0 to 50 ft, right side- 50 to 450 ft)
- Figure 2.5-54: individual and mean hard-rock-to-ground-surface amplification factors for the 60 randomized soil/rock columns for the LF DEM earthquake representing ground motion with a 10^{-5} mean annual frequency of exceedance
- Figure 2.5-55: maximum strains versus depth for the 60 randomized soil/rock columns for the LF DEM earthquake representing ground motion with a 10^{-5} mean annual frequency of exceedance (left side- 0 to 50 ft, right side- 50 to 450 ft)
- Table 2.5-13: hard-rock-to-ground-surface amplification factors for controlling deaggregation earthquakes, and their weighted average, for HF and LF ranges and ground motion with mean annual frequencies of exceedance of 10^{-4} and 10^{-5}}

2.5.2.6 Ground Motion Response Spectra

The U.S. EPR FSAR includes the following COL Item in Section 2.5.2.6:

© 2007-2012 UniStar Nuclear Services, LLC. All rights reserved.
COPYRIGHT PROTECTED

A COL applicant that references the U.S. EPR design certification will compare the final strain-dependent soil profile with the U.S. EPR design soil parameters and verify that the site-specific seismic response is enveloped by the CSDRS and the soil profiles discussed in Sections 2.5.2, 2.5.4.7 and 3.7.1 and summarized in Table 3.7.1-6, Table 3.7.1-8 and Table 3.7.1-9.

This COL Item is addressed as follows:

{This section and Section 3.7.1 describe the reconciliation of the strain-dependent soil profile and site-specific seismic response for the BBNPP and demonstrates that these parameters are enveloped by the Certified Seismic Design Response Spectra (CSDRS), anchored at 0.3 g PGA, and the soil profiles used in the design of the U.S. EPR.

Table 2.1-1 of the U.S. EPR FSAR identifies shear wave velocity as a required parameter to be enveloped, defined as "Minimum shear wave velocity of 1000 feet per second (Low strain best estimate average value below bottom of basemat)."

Reconciliation of the BBNPP site-specific seismic parameters with the U.S. EPR certified seismic design response spectra (CSDRS) and the soil profiles used for the U.S. EPR is addressed in Section 3.7.1. The evaluation guidelines in U.S. EPR FSAR Section 2.5.2.6 are used to perform the reconciliation.

The steps and conclusions of the seismic parameter reconciliation are summarized below. Summaries of select U.S. EPR structures, systems, and components evaluations which confirm they are adequate for the BBNPP site are also provided as required by seismic reconciliation Step 9.

The seismic reconciliation steps and conclusions:

1. Step 1 of the U.S. EPR FSAR Section 2.5.2.6 seismic reconciliation guidelines is confirmation that the peak ground acceleration for the ground motion response spectrum (GMRS) is less than the PGA for the CSDRS (0.3g or if high frequency content is present, 0.21g and 0.18g for the horizontal and vertical, respectively). The BBNPP site-specific GMRS are described in Section 3.7.1. The peak ground acceleration for the BBNPP site-specific GMRS is confirmed to be less than 0.3g.

2. Step 2 of the U.S. EPR FSAR Section 2.5.2.6 seismic reconciliation guidelines is confirmation that the low strain, best estimate value of the shear wave velocity below the bottom of the foundation basemat of the NI Common Basemat Structures and other Seismic Category I structures is 1000 fps, or greater. The low strain, best estimate value of the BBNPP site-specific shear wave velocity at the bottom of the foundation basemat of the NI Common Basemat Structures and other Seismic Category I structures is confirmed to be greater than 1000 fps.

3. Step 3 of the U.S. EPR FSAR Section 2.5.2.6 seismic reconciliation guidelines is confirmation that the foundation input response spectra (FIRS) for the NI Common Basemat Structure is enveloped by one of the individual design ground motion response spectra, which make up the CSDRS as described in Section 3.7.1.1.1. The FIRS shall be defined using the NEI approach (SHAKE outcrop) of ISG-17. In addition, Step 3 provides confirmation that the input motion, which considers the difference in elevation between each structure and the NI Common Basemat Structures, the embedment of the ESWB, and SSSI effect of the NI Common Basemat Structures is less

© 2007-2012 UniStar Nuclear Services, LLC. All rights reserved.
COPYRIGHT PROTECTED

than the modified CSDRS used for the design of the EPGB and the ESWB (see Section 3.7.1.1.1). Comparison of the BBNPP site-specific GMRS/FIRS with the U.S. EPR CSDRS is described in Section 3.7.1. The site-specific horizontal and vertical GMRS/FIRS exceed the envelope of the U.S. EPR CSDRS ground motions, primarily in the high frequency region. The BBNPP design ground motion response spectra are as described in Section 3.7.1, instead of the CSDRS, because the GMRS/FIRS exceed the CSDRS. This represents a departure from the U.S. EPR FSAR, as described in Section 3.7.1.

4. Step 4 of the U.S. EPR FSAR Section 2.5.2.6 seismic reconciliation guidelines is confirmation that the U.S. EPR design is based on analysis that assumes the underlying layer of soil and rock are horizontal with uniform properties. The U.S. EPR analysis assumes backfill is uniform and the lateral extent of the backfill has no influence on the analysis. The applicant will assess lateral uniformity of the site per Section 2.5.4.10.3.

5. Step 5 of the U.S. EPR FSAR Section 2.5.2.6 seismic reconciliation guidelines is confirmation that a comparison was made of the strain-dependent soil profile including backfill with the U.S. EPR design soil parameters and that the idealized strain-compatible site soil profile is consistent with one of the soil profiles used for the U.S. EPR. The BBNPP idealized site soil profile is described in Section 3.7.1. The BBNPP idealized site soil profile is not considered bounded by the U.S. EPR soil profiles. This represents a departure from the U.S. EPR FSAR, as described in Section 3.7.1. The site soil profile for the backfill and soil columns must be consistent with one of the soil profiles in U.S. EPR FSAR Table 3.7.1-6 that has the same CSDRS curve that was used for comparison in step 3 above. Site soil profiles for the EPGB starting at grade elevation must be consistent with one of the soil profiles in U.S. EPR FSAR Table 3.7.1-8 associated with the modified CSDRS curve used in step 3 above. Site soil profiles for the ESWB starting at grade elevation must be consistent with one of the soil profiles in U.S. EPR FSAR Table 3.7.1-9 associated with the modified CSDRS curve used in step 3 above. The site soil properties for the given soil layer must be consistent with soil properties in U.S. EPR FSAR Table 3.7.2-9.

6. Step 6 of the U.S. EPR FSAR Section 2.5.2.6 seismic reconciliation guidelines is confirmation that the conditions of Steps 1 through 5 are met. The conditions of Steps 3 and 5 are not met for the BBNPP site because the BBNPP site-specific GMRS/FIRS exceed the envelope of the U.S. EPR CSDRS and the BBNPP site-specific idealized site soil profile is not bounded by the soil profiles used for the U.S. EPR. Because the conditions of Steps 3 and 5 are not met for the BBNPP site, seismic reconciliation guideline Step 7 is performed.

7. Step 7 of the U.S. EPR FSAR Section 2.5.2.6 seismic reconciliation guidelines is performance of intermediate-level studies, such as evaluation of the site-specific motion at the top the of the basemat, to demonstrate that the site is bounded by the design of the U.S. EPR. BBNPP site-specific response spectra are developed for the NI Common Basemat Structures basemat and the footprints of the EPGB and ESWB and are compared to the corresponding U.S. EPR design certification spectra. The BBNPP site-specific spectra exceed the envelope of the U.S. EPR certified design spectra; therefore, seismic reconciliation guideline Step 8 is performed.

8. Step 8 of the U.S. EPR FSAR Section 2.5.2.6 seismic reconciliation guidelines is performance of site-specific soil-structure interaction (SSI) analyses with the soil column properties, development of in-structure response spectra (ISRS), and confirmation that the BBNPP site-specific ISRS do not exceed the ISRS for the U.S. EPR

© 2007-2012 UniStar Nuclear Services, LLC. All rights reserved.
COPYRIGHT PROTECTED

design certification. BBNPP site-specific SSI analyses are performed and site-specific ISRS are developed for comparison to the U.S. EPR design certification ISRS. The U.S. EPR design certification SSI analysis methodology is used to perform the site-specific SSI analyses, except as noted in Section 3.7.1 and Section 3.7.2. Performance of the SSI analyses and comparison of the BBNPP site-specific ISRS with the U.S. EPR design certification ISRS is described in Section 3.7.1. The BBNPP site-specific ISRS exceed the envelope of the U.S. EPR certified design ISRS. This represents a departure from the U.S. EPR FSAR, as described in Section 3.7.1. Therefore, seismic reconciliation guideline Step 9 is performed.

9. Step 9 of the U.S. EPR FSAR Section 2.5.2.6 seismic reconciliation guidelines is performance of additional evaluations to confirm that safety-related structures, systems, and components of the U.S. EPR at the building locations where BBNPP site-specific ISRS exceed the ISRS for the U.S. EPR design certification are not affected. These evaluations, summarized below, confirm that the safety-related structures, systems and components of the U.S. EPR are not affected.

The BBNPP average shear wave velocity profile shown in Figure 2.5-53 includes values for engineered fill and concrete forming the basemat. Soils such as Glacial Overburdens will not be used for support of foundations of the BBNPP Nuclear Island. Therefore, shear wave velocity measurements in the BBNPP site soils above elevation 683 ft (208 m) regardless of value, are excluded from this evaluation as they lie above the bottom of the basemat. Results from the above figure indicate that:

1. The BBNPP average shear wave velocity profile below the nuclear island foundation level is bounded by the profiles used for the U.S. EPR.

2. The BBNPP average shear wave velocity profile offers a shear wave velocity belowthe bottom of the basemat (approximate elevation 683 ft (208 m) (or depth=36 ft in Figure 2.5-53)) of 8,510 ft/sec (2,594 m/sec).

3. The minimum shear wave velocity from the BBNPP average shear wave velocity profile is 7,200 ft/sec (2,195 m/sec) .

On the above basis, it is concluded that the BBNPP site shear wave velocity profile is bounded by the soil profiles used for the U.S. EPR and meets the minimum 1,000 ft/sec (305 m/sec) criterion identified in the U.S. EPR FSAR.

As described in Section 2.5.2.5.1.6, the results of the site response analysis are a suite of mean site amplification factors. This section describes the use of the site amplification factors to determine the site-specific response spectra at the ground surface. First, the mean amplification factors for the three controlling deaggregation earthquakes for each combination of spectral frequency range (HF, LF) and mean annual frequency of exceedance (10^{-4}, 10^{-5}) are averaged. In computing the average, the amplification factor for each controlling deaggregation earthquake (i.e., DEL, DEM, DEH) are weighted according to the contribution to the seismic hazard that they represent. This results in weighted average amplification factors high and low spectral frequency ranges for both 10^{-4} and 10^{-5} mean frequencies of exceedance. Table 2.5-13 summarizes the amplification factors.

Next the weighted average amplification factors are used to modify the smooth UHRS for hard rock to give the UHRS at the ground surface. The spectral amplitude for each frequency of the hard-rock UHRS is multiplied by the value of the amplification factor at that frequency. For high frequencies, the weighted average amplification function for the high spectral frequency

© 2007-2012 UniStar Nuclear Services, LLC. All rights reserved.
COPYRIGHT PROTECTED

range is used; for low frequencies, the amplification function for the low range is used. For intermediate frequencies, use of the low or high frequency range amplification function is based on whether the reference earthquake response spectrum for the low or high frequency range lies closest to the UHRS. The resulting surface UHRS for 10^{-4} and 10^{-5} mean annual frequencies of exceedance are shown on Figure 2.5-64.

The ASCE (ASCE, 2005b) performance-based approach was used to derive an SSE ground motion response spectrum (GMRS) from the 10^{-4} and 10^{-5} surface UHRS. The SSE spectrum is derived at each structural frequency as follows:

SSE GMRS = 10^{-4} UHRS x DF

in which

$DF = \max \{1.0, 0.6(A_R)^{0.8}\}$

and

$A_R = (10^{-5}\ \text{UHRS})/(10^{-4}\ \text{UHRS})$

unless A_R is greater than 4.2. In that case,

SSE GMRS = 0.45 (10^{-5} UHRS)

The resulting horizontal performance-based surface response spectrum (PBSRS) for the SSE is plotted in Figure 2.5-57 and listed in Table 2.5-12.

A vertical SSE spectrum was constructed from the horizontal SSE spectrum following the approach described in NUREG/CR-6728 (McGuire, 2001) by deriving vertical-to-horizontal (V/H) ratios and applying them to the horizontal SSE PBSRS.

The vertical SSE surface spectrum is determined from the horizontal SSE PBSRS using a frequency-dependent vertical-to-horizontal response spectral ratio (V/H ratio). The V/H ratio is based on ratios given in NUREG/CR-6728 (McGuire, 2001) for CEUS. These ratios depend on PGA and are for a rock site. To obtain a V/H ratio appropriate for soil conditions, such as are found at the BBNPP Site, a frequency-dependent scaling factor between a rock V/H ratio and a soil V/H ratio is applied. The scaling factor is determined from empirical ground motion relations for active tectonic regions. The analysis is carried out using magnitude, distance, and PGA values for the controlling deaggregation earthquakes associated with ground motion having a 10^{-4} mean annual frequency of exceedance.

The controlling deaggregation earthquakes for ground motion with a 10^{-4} mean annual frequency of exceedance are summarized in Table 2.5-11. PGA values for the DEL, DEM, and DEH events associated with the low spectral frequency range (1 to 2.5 Hz) are 0.15g, 0.07g, and 0.11g, respectively. For the high spectral frequency range (5 to 10 Hz), corresponding values are 0.13g, 0.11g, and 0.08g, respectively. Thus, all controlling deaggregation earthquakes fall in the "less than or equal to 0.2g" category for the NUREG/CR-6728 recommended CEUS rock V/H ratio. Although a weighted average of the ratio associated with the PGA for each controlling deaggregation earthquake is taken for the low and high frequency ranges, because the DEL, DEM, and DEH events fall in the same PGA category, the weighted averages are the same as each individual ratio value.

© 2007-2012 UniStar Nuclear Services, LLC. All rights reserved.
COPYRIGHT PROTECTED

To determine the relation between the V/H ratio for soil and rock, the ground motion prediction equations (GMPEs) of Abrahamson and Silva (Abrahamson, 1997) and Campbell and Bozorgnia (Campbell, 2003b) are used. Magnitude values for the controlling reference earthquakes (REFs) associated with ground motion having a 10^{-4} mean annual frequency of exceedance provide the input to these equations. For the high frequency range the magnitude is 5.8 and for the low frequency range the magnitude is 7.3. PGA values associated with the controlling reference earthquakes are 0.08g (LF) and 0.11g (HF). Distance values for use in the GMPEs are determined such that the distance gives a PGA (rock condition) near the PGA for the respective REF. For the LF REF, distances of 61 km and 54 km are determined, respectively, for the Abrahamson and Silva (Abrahamson, 1997) and the Campbell and Bozorgnia (Campbell, 2003b) GMPEs. Corresponding values for the HF range are 15 km and 14 km, respectively. Using these values of magnitude and distance, V/H ratios for rock (V_{S30} > 760 m/s) and soil (V_{S30} < 360 m/s) conditions were determined for each REF and GMPE. Based on these results, the ratio between V/H_{soil} and V/H_{rock} was determined for each REF and GMPE. The final (V/Hsoil)/(V/Hrock) ratio used to scale the NUREG/CR-6728 CEUS V/H ratio for rock to an equivalent ratio for soil conditions was obtained by enveloping the ratios for the four combinations of REF and GMPE. Figure 2.5-66 shows the CEUS V/H ratio for rock and the CEUS V/H ratio for rock after adjustment for soil conditions as described above.

Also shown on Figure 2.5-66 is the V/H ratio from Regulatory Guide 1.60 (NRC, 1973). Because the Regulatory Guide 1.60 (NRC, 1973) V/H ratio envelopes the CEUS V/H ratio for soil, it is conservatively used to determine the vertical SSE response spectrum from the horizontal SSE PBSRS. The vertical SSE response spectrum is shown on Figure 2.5-65 and listed in Table 2.5-12.

Refer to Section 3.7.1 and Section 3.7.2 for a description of the soil-structure interaction analyses performed for the U.S. EPR design certification.

2.5.2.7 Conclusions

This section is added as a supplement to the U.S. EPR FSAR.

An updated evaluation of the vibratory ground motion has been conducted for the BBNPP site. A Probabilistic Seismic Hazard Analysis (PSHA) was selected as the appropriate basis for evaluating the vibratory ground motion accounting for all credible alternative seismic sources. The alternative seismic sources identified by the Electric Power Research Institute (EPRI) for the Central and Eastern United States (CEUS), Seismic Hazard Methodology for the Central and Eastern United States (EPRI, 1986) issued in 1986 are still considered to constitute an adequate definition of seismic area sources. However, updated information available from databases maintained by the United States Geological Survey has been used to determine recurrence parameters. Since the New Madrid Fault System (NMFS) and the Charleston Seismic Source (CSS) have some contribution to the seismic hazard at the BBNPP site, updated logic-tree representations of the clustered characteristic earthquakes at the NMFS and the un-clustered CSS have been incorporated into the PSHA. The NMFS characterization is provided by Exelon in the Clinton ESP application (EGC, 2006) and the CSS characterization is the one presented in the CCNPP Unit 3 FSAR (UniStar Nuclear, 2007). Both characterizations have been verified with USGS modeling of the New Madrid and Charleston Faults. The PSHA for the BBNPP site makes use of a decision tree approach with appropriate weighting factors that are based on the most up-to-date information and relative confidence in alternative characterizations for each area and characteristic seismic source.

© 2007-2012 UniStar Nuclear Services, LLC. All rights reserved.
COPYRIGHT PROTECTED

On the basis of the PSHA results, mean Uniform Hazard Response Spectra were determined for a hard-rock outcrop. Following Approach 2B of NUREG/CR-6728 (McGuire, 2001) the hard-rock outcrop UHRS were modified to corresponding UHRS for the free-field ground surface. First, controlling earthquake response spectra, based on deaggregation of the PSHA results, and information on the dynamic properties of the soil and rock material at the BBNPP Site, were used to conduct a site response analysis. Site amplification functions determined from the site response analysis were then used to modify the hard-rock outcrop UHRS to produce UHRS for the free-field ground surface.

The Safe Shutdown Earthquake (SSE) response spectra were determined from the UHRS for the free-field ground surface following the guidance of Regulatory Guide 1.208, "A Performance -Based Approach to Define the Site-Specific Earthquake Ground Motion," (NRC, 2007a). The horizontal Ground Motion Response Spectrum (GMRS) for the BBNPP Site was developed from the UHRS for the free-field ground surface. The vertical GMRS was developed from the horizontal GMRS using appropriate V/H spectral ratios.These performance-based spectra adequately represent the regional and local seismic hazards and appropriately include the effects of the local rock and soils at the BBNPP site.

The performance-based approach uses not only the seismic hazard characterization of the site from the PSHA but also basic seismic fragility SSC modeling to define a ground motion that directly targets a structural performance frequency value. It is concluded that the application for the BBNPP site is acceptable from a geologic and seismologic standpoint and meets the requirements of 10 CFR 100.23(d) (CFR, 2007). Deviations from the NRC guidance Regulatory Guide 1.208 (NRC, 2007a), or review criteria in Standard Review Plan 2.5.2 (NRC, 2007b) have been identified and acceptable alternatives, including technical justification, have been provided.

2.5.2.8 References

This section is added as a supplement to the U.S. EPR FSAR.

Abrahamson, 1997. Empirical Response Spectra Attenuation Relations for Shallow Crustal Earthquakes, N. A. Abrahamson and W. J. Silva, Seismological Research Letters, Volume 68, Number 1, pp. 94-127, 1997.

Ang and Tang, 1975. Probabilistic Concepts in Engineering Planning and Design, Volume 1, A.H. Ang and W.H. Tang, John Wiley and Sons, New York, 1975.

Atkinson, 2006. Earthquake Ground-Motion Prediction Equations for Eastern North America," G. M. Atkinson and D. M. Boore, Seismological Society of America, Bulletin, Volume 96, Number 6, pp. 2181-2205, 2006.

ASCE, 2005a. Minimum Design Loads for Buildings and Other Structures, ASCE/SEI 7-05, American Society for Civil Engineers/Structural Engineering Institute, 2005.

ASCE, 2005b. Seismic Design Criteria for Structures, Systems, and Components in Nuclear Facilities, ASCE/SEI 43-05, American Society for Civil Engineers/Structural Engineering Institute, 2005.

ANSS, 2008, ANSS web database, http://www.ncedc.org/anss/catalog-search.html, last accessed November 2008.

© 2007-2012 UniStar Nuclear Services, LLC. All rights reserved.
COPYRIGHT PROTECTED

ANSS, 2010. Online Bulletin, Advanced National Seismic System, Website: <http://www.ncedc.org/anss/catalog-search.html>, accessed April 2010.

Bakun, 2004. Magnitudes and Locations of the 1811-1812 New Madrid, Missouri, and the 1886 Charleston, South Carolina, Earthquakes, W. H. Bakun and M. G. Hopper, Seismological Society of America, Bulletin, Volume 94, Number 1, pp. 64-75, 2004.

Bent, 1992, A re-examination of the 1925 Charlevoix, Bent, A. L., Bulletin of the Seismological Society of America, Vol. 82, No. 5, 2097-2113.

Bollinger, 1977. Reinterpretation of the Intensity Data for the 1886 Charleston, South Carolina, Earthquake in Studies Related to the Charleston, South Carolina, Earthquake of 1886 -A Preliminary Report, in D. W. Rankin, Editor, G. A. Bollinger, U. S. Geological Survey Professional Paper 1028, pp. 17-32, 1977.

Boore, 1987. Stochastic Prediction of Ground Motion Response Parameters at Hard-Rock Sites in Eastern North America, D.M. Boore and G.M. Atkinson, Bulletin Seismological Society of America, Volume 77, Number 2, pp. 440-467, 1987.

Campbell, 2003a. Prediction of Strong Gound Motion Using the Hybrid Empirical Method and Its Use in the Development of Ground-Motion (Attenuation) Relations in Eastern North America, K. W. Campbell, Bulletin of the Seismological Society of America, Volume 93, Number 3, pp. 1012-1033, 2003.

Campbell, 2003b. Updated Near-Source Ground-Motion (Attenuation) Relations for the Horizontal and Vertical Components of Peak Ground Acceleration and Acceleration Response Spectra. K. W. Campbell, and Y. Bozorgnia. Bulletin of the Seismological Society of America. Volume 93, No. 1. pp. 314-331. 2003.

CFR, 2007. Title 10, Code of Federal Regulations, Part 100.23(d), Geologic and Seismic Siting Factors, 2007.

Cornell, 1968. Engineering Seismic Risk Analysis, C.A. Cornel, Bulletin of Seismological Society of America, Volume 58, pp, 1583-1606, 1968.

Cornell, 1971. Probabilistic Analysis of Damage to Structure Under Seismic Loads, C.A. Cornel, Dynamic Waves in Civil Engineering, Chapter 27, edited by D.A. Howells, I.P Haigh, and C. Taylor, 1971.

Costantino, 1996. Recommendations for Uncertainty Estimates in Shear Modulus Reduction and Hysteretic Damping Relationships, C. J. Costantino, 1996, Published as an appendix in "Description and validation of the stochastic ground motion model," W.J. Silva, N. Abrahamson, G. Toro and C. Costantino, 1997, Report Submitted to Brookhaven National Laboratory, Associated Universities, Inc. Upton, New York 11973, Contract No. 770573.

Cox, 1983. Paleoseismic Studies in the 1886 Charleston Earthquake Meizoseismal Area, Geological Society of America Abstracts with Programs, J. Cox and P. Talwani, 1983.

Dineva, 2004, Seismicity of the Southern Great Lakes: Revised Earthquake Hypocenters and possible tectonic controls, Bulletin of the Seismological Society of America, Dineva S., D. Eaton, and R. Mereu, 94, 1902-1918.

© 2007-2012 UniStar Nuclear Services, LLC. All rights reserved.
COPYRIGHT PROTECTED

Earthquakes Canada, 2008, http://earthquakescanada.nrcan.gc.ca/zones/eastern_e.php#SGLSZ, last accessed Nov. 2008.

Ebel, 1996. The Seventeenth Century Seismicity of Northeastern North America, John E. Ebel, Seismological Research Letters, Volume 67, Number 3, p. 51-68, 1996.

Ebel, 2000. A Reanalysis of the 1727 Earthquake at Newburry, Massachusetts, J. E. Ebel, Seismological Research Letters, Volume 71, Number 3, p. 364-374, 2000.

Ebel, 2002, Earthquakes in the Eastern Great lakes basin from a regional perspective, Tectonophysics, Ebel J. E., and M. Tuttle (2002). 353, 17-30.

Ebel, 2006. The Cape Ann, Massachusetts Earthquake of 1755: A 250th Anniversary Perspective, John E. Ebel, Seismological Research Letters, Volume 77, Number 1, p. 74-86, 2006.

EC, 2010. Earthquake Canada, GSC, Earthquake Search (On-line Bulletin), Nat. Res. Can., Website: <http://seismo.nrcan.gc.ca/stnsdata/nedb/bull_e.php>, accessed May 2010

EGC, 2006. Submittal of Revision 4 to Exelon Generation Company's Early Site Permit Application for Clinton, Including Administrative Information, Emergency Plan, Site Redress Plan, Environmental Report and Site Safety Analysis Report, April 14, 2006.

EPRI, 1986. Seismic Hazard Methodology for the Central and Eastern United States, NP-4726, Volumes 1-10, Electric Power Research Institute, July 1986.

EPRI, 1988. Seismic Hazard Methodology for the Central and Eastern United States, NP-4726-A, Revision 1, Volume 1, Part 2, Electric Power Research Institute, 1988.

EPRI, 1988a. A Criterion for Determining Exceedance of the Operating Basis Earthquake, NP-5930, Electric Power Research Institute, 1988.

EPRI, 1989a. Probabilistic Seismic Hazard Evaluations at Nuclear Power Plant Sites in the Central and Eastern United States: Resolution of the Charleston Earthquake Issue, NP-6395-D, Electric Power Research Institute, 1989.

EPRI, 1989b. EQHAZARD Primer, NP-6452-D, Electric Power Research Institute, June 1989.

EPRI, 1993. Guidelines for Determining Design Basic Ground Motions, TR-102293, Volume 1, Electric Power Research Institute, 1993.

EPRI, 2004. CEUS Ground Motion Project Final Report, TR-1009684 2004, Electric Power Research Institute, December 2004.

EPRI, 2006. Program on Technology Innovation: Use of Cumulative Absolute Velocity (CAV) in Determining Effects of Small Magnitude Earthquakes on Seismic Hazard Analyses, Report 1014099, Electric Power Research Institute, Palo Alto, CA, and U.S. Department of Energy, Germantown, MD, 2006.

EPRI, 2006a. Program on Technology Innovation: Truncation of the Lognormal Distribution and Value of the Standard Deviation for Ground Motion Models in the Central and Eastern United States, TR-1014381, Electric Power Research Institute, August 2006.

© 2007-2012 UniStar Nuclear Services, LLC. All rights reserved.
COPYRIGHT PROTECTED

EPRI, 2006b. Program on Technology Innovation: Truncation of the Lognormal Distribution and Value of the Standard Deviation for Ground Motion Models in the Central and Eastern United States, Technical Update 1013105, Electric Power Research Institute, February 2006.

EPRI, 2008. Assessment of Seismic Hazard at 34 U.S. Nuclear Plant Sites, 1016736, Electric Power Research Institute, August 2008.

Frankel, 1995. Mapping Seismic Hazard in the Central and Eastern United States, A.D. Frankel, Seismological Research Letters, Volume 66, Number 4, pp. 8-21, 1995.

Gutenberg, 1944. Frequency of earthquakes in California. B. Gutenberg, and C. F. Richter, Bulletin of the Seismological Society of America, Volume 34, p. 185-188, 1944.

Hough, 2000. On the Modified Mercalli intensities and magnitudes of the 1811-1812 New Madrid earthquakes. S. E. Hough, Armbruster, J.G., Seeber, L., and Hough, J.F Journal of Geophysical Research, Volume 105, Number B10, pp. 23,839-23,864, 2000.

Inners, 1978. Geology and Mineral Resources of the Berwick Quadrangle, Luzerne and Columbia Counties, Pennsylvania, Pennsylvania Geological Survey, Fourth Series, pp. 1-34, J.D. Inners, 1978.

Johnston, 1996. Seismic Moment Assessment of Earthquake in Stable Continental Regions - III. New Madrid 1811-1812, Charleston 1886 and Lisbon 1755, A. C. Johnston, Geophysical Journal International, Volume 126, pp. 314-344, 1996.

Jones, 2010. The Dillsburg, Pennsylvania 2008-2009 Earthquake Swarm, J. L. Jones, C. K. Scharnberger, H. L. Delano, W. Kreiger, and J. Kreiger, Geological Society of America Abstracts with Programs, Vol. 42, No. 1, p. 112, 2010.

Kafka, 1985, Earthquake activity in the Greater New York City area: magnitudes, seismicity, and geologic structures, Kafka, A. L., E. A. Schlesinger-Miller, and N. L. Barstow (1985), Bulletin of the Seismological Society of America, 75 (5), 1285-1300.

Kim, 2009. The 2008-2009 Earthquake Swarm Near Dillsburg, Pennsylvania, W.-Y. Kim, M. Gold, C. Scharnberger, J. Jones, and H. Delano, Pennsylvania Geological Survey, 4th ser., Open-File Report OFMI 09-01.0, 20 p., 2009.

Marple, 2000. Evidence of a buried fault system in the Coastal Plain of the Carolinas and Virginia- Implications for neotectonics in the southeastern United States, R. Marple and P. Talwani, Geological Society of America Bulletin, Volume 112, Number 2., pp. 200-220, 2000.

Mazzotti, 2005, GPS crustal strain, postglacial rebound, and seismc hazard in eastern North America: The Saint Lawrence Valley example, Mazzotti, S., T. S. James, J. Henton, and J. Adamas, Journal of Geophysical Research, Vol. 110, B11301, doi:10.1029/2004JB003590.

McGuire, 1988. Engineering Model of Earthquake Ground Motion for Eastern North America, Electric Power Research Institute Technical Report NP-6074, R. K. McGuire, G.R. Toro and W.J. Silva, 1988.

McGuire, 2001. Technical Basis for Revision of Regulatory Guidance on Design Ground Motions: Hazard- and Risk-consistent Ground Motion Spectra Guidelines, McGuire, R.K., W.J. Silva, and C.J. Constantino, NUREG/CR-6728, U.S. Nuclear Regulatory Commission, 2001.

© 2007-2012 UniStar Nuclear Services, LLC. All rights reserved.
COPYRIGHT PROTECTED

McGuire, 2002. Technical Basis for Revision of Regulatory Guidance on Design Ground Motions: Development of Hazard- and Risk-consistent Seismic Spectra for Two Sites, McGuire, R.K., W.J. Silva, and C.J. Constantino, NUREG/CR-6769, U.S. Nuclear Regulatory Commission, 2002.

Mueller, 1997. Preparation of Earthquake Catalogs for the National Seismic-Hazard Maps: Contiguous 48 States, C. M. Mueller, C., M. Hopper, and A. Frankel, U.S. Geological Survey Open-File Report 97-464, 1997.

Mohajer, 1993, Seismicity and seismotectonics of the western Lake Ontario region, Géographie physique et Quaternaire, Mohajer, A. A., 1993, Vol. 47, 353-362.

Newmark, 1982. Earthquake Spectra and Design, N. M. Newmark and W.J. Hall, Earthquake Engineering Research Institute, Berkeley, California, 1982.

NRC, 1973. Design Response Spectra for Seismic Design of Nuclear Power Plants, Regulatory Guide 1.60, U.S. Nuclear Regulatory Commission, 1973.

NRC, 1997a. Identification and Characterization of Seismic Sources and Determination of Safe Shutdown Earthquake Ground Motion, Regulatory Guide 1.165, U. S. Nuclear Regulatory Commission, March 1997.

NRC, 1997b. Recommendations for Probabilistic Seismic Hazard Analysis: Guidance on Uncertainty and Use of Experts, Prepared by Senior Seismic Hazard Analysis Committee (SSHAC), NUREG/CR-6372, U. S. Nuclear Regulatory Commission, 1997.

NRC, 2005. Safety Evaluation Report for an Early Site Permit (ESP) at the North Anna ESP Site, NUREG-1835, U. S. Nuclear Regulatory Commission, September 2005.

NRC, 2007a. A Performance-Based Approach to Define the Site-Specific Earthquake Ground Motion, Regulatory Guide 1.208, U. S. Nuclear Regulatory Commission, March 2007.

NRC, 2007b. Vibratory Ground Motion, Standard Review Plan, NUREG-0800, Section 2.5.2, Revision 4, U.S. Nuclear Regulatory Commission, March 2007.

NRC, 2007c. Issuance of Early Site Permit for Exelon Generation Company, LLC (ESP-001), Letter from D.B. Matthews (NRC) to M.C. Kray (Exelon Nuclear), March 15, 2007.

Obermeier, 1987. Earthquake Induced Liquefaction Features in the Coastal South Carolina Region, U.S. Geological Survey Open File Report 87-504, S.F. Obermeier, R.E. Weems, R.B. Jacobson, 1987.

OSN, 2010. Online Bulletin, Ohio Seismic Network, Website: <http://www.dnr.state.oh.us/geosurvey/html/eqcat01d/tabid/8296/Default.asp>, accessed May 2010.

Scharnberger, 2006, Earthquake hazard in Pennsylvania, Pennsylvania Geological Survey, S.C. Scharnberger, Pennsylvania Geological Survey, Educational Series 10.

Schnabel, 1972. SHAKE - A Computer Program for Earthquake Response Analysis of Horizontally Layered Sites, P.B. Schnabel, J. Lysmer and H.B. Seed, Report No. EERC 72-12, University of California, Berkeley, 1972.

© 2007-2012 UniStar Nuclear Services, LLC. All rights reserved.
COPYRIGHT PROTECTED

Schwartz, 1984. Fault Behavior and Characteristic Earthquakes: Examples from the Wasatch and San Andreas Fault Zones, Journal of Geophysical Research, D.P. Schwartz and K.J. Coppersmith, Volume 89, Number B7, pp 5681-5698, 1984.

Seeber, 1991. The NCEER-91 earthquake catalog: improved intensity-based magnitudes and recurrence relations for U.S. earthquakes east of New Madrid, L. Seeber and J. G. Armbruster National Center for Earthquake Engineering Research, NCEER-91-0021, 1991.

Seeber, 1993, Natural and induced seismicity in the Lake Erie-Lake Ontario region: reactivation of ancient faults with little neotectonic displacement, Géographie physique et Quaternaire, Seeber, L., and J. G. Armbruster, Vol 47, 363-378.

Seeber, 1998. The 1994 Cacoosing Valley earthquakes near Reading, Pennsylvania: A shallow rupture triggered by quarry unloading, L. Seeber, J. G. Armbruster, W.Y. Kim, N. Barstow, and C. Scharnberger, Journal of Geophysical Research, Volume 103, Number B10, pp. 24,505-24,521, 1998.

Silva, 2002. Development of regional hard rock attenuation relations for central and eastern North America, W. Silva, N. Gregor and R. Darragh, Pacific Engineering Analysis, El Cerrito, CA, 2002.

SNOC, 2008. Early Site Permits - Southern Nuclear Operating Company Application for the Vogtle ESP Site, Revision 4, Southern Nuclear Operating Company, 2008.

Somerville, 2001. Ground-Motion Attenuation Relations for the Central and Eastern United States, P. G. Somerville, N. Collins, N. A. Abrahamson, R. Graves and C. K. Saikia, Report to the USGS, NEHRP External Research Program, Award No. 99-HQ-GR-0098, 2001.

Sykes, 2008. Observations and Tectonic Setting of Historic and Instrumentally Located Earthquakes in the Greater New York City - Philadelphia Area, Lynn R. Sykes, John G. Armbruster, Won-Young Kim, and Leonardo Seeber, Bulletin of the Seismological Society of America, Volume 98, Number 4, p. 1696-1719, 2008.

Talwani, 2001. Recurrence rates of Large Earthquakes in the South Carolina Coastal Plain Based on Paleoliquefaction Data, P. Talwani and W. T. Schaeffer, Journal of Geophysical Research, Volume 106, Number B4, pp. 6621-6642, 2001.

Tavakoli, 2005. Empirical-stochastic ground-motion prediction for eastern North America, B. Tavakoli, B. and S. Pezeshk, Bulletin of the Seismological Society of America, Volume 95, pp. 2283-2296, 2005.

Toro, 1996. Probabilistic Models of Site Velocity Profiles for Generic and Site-Specific Ground Motion Amplification Studies, G. R. Toro, Published as an appendix in W. J. Silva, N. Abrahamson, G. Toro and C. Costantino, 1997, Description and validation of the stochastic ground motion model, Report Submitted to Brookhaven National Laboratory, Associated Universities, Inc. Upton, New York 11973, Contract No. 770573, 1996.

Toro, 1997. Model of Strong Ground Motions from Earthquakes in Central and Eastern North America: Best Estimates and Uncertainties, G. R. Toro, N. A. Abrahamson, and J. F. Schneider, Seismological Research Letters, Volume 68, Number 1, pp. 41-57, 1997.

© 2007-2012 UniStar Nuclear Services, LLC. All rights reserved.
COPYRIGHT PROTECTED

Tuttle, 2002. The Earthquake Potential of the New Madrid Seismic Zone, M. P. Tuttle, E.S. Schweig, J.D. Sims, R.H. Lafferty, L.W. Wolf, and M.C. Haynes, Bulletin of the Seismological Society of America, Vol. 92, No. 6, pp. 2080-2089, 2002.

UniStar Nuclear, 2007. Calvert Cliffs Nuclear Power Plant Unit 3, Combined License Application, Revision 0, Part 2 Final Safety Analysis Report, Section 2.5.2, Vibratory Ground Motion, UniStar Nuclear, 2007.

USGS, 1996. National seismic-hazard maps: documentation, U. S Geological Survey, Open-File Report 96-532, A. Frankel, T. Barnhard, D. Perkins, E. V. Leyendecker, N. Dickman, S. Hanson, and M. Hopper, 1996.

USGS, 2002. Documentation for the 2002 Update of the National Seismic Hazard Maps, U.S. Geological Survey Open-File Report 02-420, A. D. Frankel, M. D. Petersen, C. S. Mueller, K. M Haller, R. L. Wheeler, E. V. Leyendecker, R. L. Wesson, S. C. Harmsen, C. H. Cramer, D. M. Perkins, and K. S. Rukstales, 2002.

USGS, 2008a. Documentation for the 2008 update of the United States National Seismic Hazard Maps: U.S. Geological Survey Open-File Report 2008-1128, M. D. Peterson, A. D. Frankel, S. C. Harmsen, C. S. Muller, K. M. Haller, R. L. Wheeler, R. L. Wesson, Y. Zeng, O.S. Boyd, D. M. Perkins, N. Luco, E. H. Field, C. J. Wills, and K. S. Rukstales, 2008.

USGS, 2008b, USGS web database: http://neic.usgs.gov/neis/epic/epic_circ.html, last accessed November 2008.

USGS, 2010. Online Bulletin, National Earthquake Information Center, U.S. Geological Survey, Website: <http://earthquake.usgs.gov/earthquakes/eqarchives/epic>, accessed April 2010.

Wallach, 2002, The presence, characteristics and earthquake implications of the St. Lawrence fault zone within and near Lake Ontario (Canada-USA), J.L. Wallach, Tectonophysics 353 (2002) pp. 45- 74

Weichert, 1980. Estimation of the earthquake recurrence parameters for unequal observation periods for different magnitudes, D. H. Weichert, Bulletin of the Seismological Society of America, Volume 70, pp. 1337-1356, 1980.

Weston, 2008, www.bc.edu/research/westonobservatory, last accessed November 2008.

Youngs, 1985. Implications of Fault Slip Rates and Earthquake Recurrence Models to Probabilistic Seismic Hazard Estimates, Bulletin of the Seismological Society of America, R.R. Youngs and K.J. Coppersmith, Volume 75, Number 4, pp 939-964, 1985.}

2.5.3 Surface Faulting

The U.S. EPR FSAR includes the following COL Item in Section 2.5.3:

> A COL applicant that references the U.S. EPR design certification will investigate site-specific surface and subsurface geologic, seismic, geophysical, and geotechnical aspects within 25 miles around the site and evaluate any impact to the design. The COL applicant will demonstrate that no capable faults exist at the site in accordance with the requirements of 10 CFR 100.23 and 10 CFR 50, Appendix S. If non-capable surface faulting is present under foundations for

© 2007-2012 UniStar Nuclear Services, LLC. All rights reserved.
COPYRIGHT PROTECTED

safety-related structures, the COL applicant will demonstrate that the faults have no significant impact on the structural integrity of safety-related structures, systems or components.

This COL Item is addressed as follows:

{There is no potential for tectonic fault rupture and there are no capable tectonic sources within a 25 mi (40 km) radius of the BBNPP site. A capable tectonic source is a tectonic structure that can generate both vibratory ground motion and tectonic surface deformation, such as faulting or folding at or near the earth's surface in the present seismotectonic regime (NRC, 1997). The following Sections provide the data, observations, and references to support this conclusion. Information contained in these Sections was developed in accordance with RG 1.165 (NRC, 1997), and is intended to satisfy 10 CFR 100.23, "Geologic and Seismic Siting Criteria" (CFR, 2007a) and 10 CFR 50, Appendix S, "Earthquake Engineering Criteria for Nuclear Power Plants" (CFR, 2007b).

Section 2.5.3.1 through Section 2.5.3.9 are added as a supplement to the U.S. EPR FSAR.

2.5.3.1 Geological, Seismological, and Geophysical Investigations

The following investigations were performed to assess the potential for surface fault rupture out to a 25 mile (40 km) radius of the BBNPP site:

- Site subsurface investigations including geotechnical borings and seismic refraction surveys. (Section 2.5.3.1.1)
- Interpretation of aerial photography and satellite imagery. (Section 2.5.3.1.2)
- Field reconnaissance. (Section 2.5.3.1.3)
- Compilation and review of existing geologic and seismologic data and literature, including a review of seismic data. (Section 2.5.3.1.4)

2.5.3.1.1 Subsurface Investigations at the BBNPP Site

Geologic sections developed from geotechnical data collected from 44 boreholes as part of the BBNPP study (as discussed in Section 2.5.4) provide detailed information in the upper 420 ft (128 m) (Based on deepest boring B-401) of strata for the presence of structures directly beneath the site. The interpretations developed from the previous investigation at the SSES site confirm the interpretation of the new borehole data at the BBNPP site:

Unfaulted Middle Devonian shale shallowly dipping to the north-northwest with a strong south-southeast dipping cleavage, and covered by a layer of undeformed residual soil that formed from weathering of the underlying shale bedrock (Figure 2.5-191, Figure 2.5-192, Figure 2.5-193, Figure 2.5-194, and Figure 2.5-195). However, the location of the Essential Service Water Emergency Makeup System (ESWEMS) is below the break in slope of the hill and is located on glacial outwash and till (Figure 2.5-196).

Although the bedrock formations underlying the BBNPP site have experienced folding during the Alleghanian Orogeny (Williams, 1987; Faill, 1999), residual soils and surficial sediments within the site (Figure 2.5-187) display no signs of faulting or folding during the Quaternary

© 2007-2012 UniStar Nuclear Services, LLC. All rights reserved.
COPYRIGHT PROTECTED

time period, and rest unconformably on the eroded surface of the tilted beds of the local shale bedrock.

Geotechnical boreholes provide additional evidence of the lateral continuity between the residual overburden and the Devonian Mahantango Formation. Figure 2.5-191,Figure 2.5-192, and Figure 2.5-195 display a general thickening of the weathered rock and transition zone sequence that form an east-west to southeast-northwest depression in the solid rock surface in the central portion of the site (Figures 2.5-106 and 2.5-196). This consistency in strata across the site support detailed published reports of the site area local geology, and confirm that recent surficial faulting and folding are absent in the interpreted sections within the BBNPP site.

Seismic refraction surveys were performed to support site characterization studies for the BBNPP (Section 2.5.4.2.2.2.3). Because earth materials exhibit characteristic wave propagation velocities, they can be classified simply in terms of their seismic velocity. Seismic refraction data were interpreted for this study to assist in characterizing the local subsurface geologic materials regarding the thickness of the soil overburden, depths to weathered or fractured bedrock, and competent bedrock. Seismic refraction surveys were performed along 9 profile lines totaling 7440 linear feet (2267 m) of coverage. The data for the surveys were collected from May 26 to June 5, 2010 using approved quality assurance procedures. The complete report of this survey (GeoVision, 2010) is included in COLA Part 11G.

Figure 2.5-105 is a map depicting the layout of the 9 lines used during the survey (Lines A1 through A5, oriented west; and Lines B1 through B4, oriented north-south). Seismic refraction velocity profiles are presented on Figures 2.5-109 through 2.5-117 with the vertical scale measuring elevation in feet. Tomographic inversion routines are the most appropriate data modeling technique for this site because velocity gradients are assumed to be present within weathered bedrock at this site, and refraction tomography techniques are often able to resolve complex velocity structure (e.g. velocity gradients) that can be observed in bedrock weathering profiles. Layer based modeling techniques such as the Generalized Reciprocal Method (GRM) are not able to accurately model the velocity gradients that can be observed in weathered bedrock such as at the BBNPP. However, the GRM method was used to confirm velocity ranges in the tomographic models.

These interpreted velocity profiles indicate that the elevation of the competent rock is highest in the northern portion of the site, and forms an east-west to southeast-northwest trending depression in the central portion of the site with elevation increasing again to the south. Figure 2.5-106 is a representation of the surface of the competent bedrock. The top of this surface is based on an interpreted velocity in the 11,000 to 13,000 feet per second (ft/s) range (3400 to 4000 meters per second (mps)). The approximate locations of the top of the decomposed, weathered and competent shale identified in boreholes within 50 ft (15.2 m) of the seismic lines is included on the seismic models to aid with interpretation (Figures2.5-109 through 2.5-117).

Two possible weathered shale units are identified within the tomographic profiles; one based on geologic description (WS1) and the other based on the depth at which RQD exceeds 0% (WS2) (GeoVision, 2010). The locations of the 4,000, 6,000 and 12,000 ft/s (1200, 1800 and 3700 mps) contours from intersecting lines are also shown on the seismic models for discussion. There is a distinct possibility at this site that velocity structure may be slightly different at intersecting lines because of the complex velocity structure of the weathered shale (GeoVision, 2010). Additionally, bedding and fracture attitudes relative to the seismic line

© 2007-2012 UniStar Nuclear Services, LLC. All rights reserved.
COPYRIGHT PROTECTED

orientation may have a significant impact on modeled seismic velocity structure. A review of the data in the figures shows no offsets or abrupt changes in the tops of the bedrock that could indicate recent deformation. See section 2.5.4 for a more detailed discussion of the geophysical analysis.

The map of the top of the competent Mahantango Shale from the boring log data (Figure 2.5-118) shows a surface similar to that shown in Figure 2.5-106 that was developed for the top of competent rock from the geophysical data. Both maps show that the interpreted elevation of the top of the competent rock, as mentioned above, is highest in the northern and southern portions of the site, with an east-west to southeast-northwest trending depression in the center of the site.

Because the interpreted upper surfaces of the decomposed shale and weathered shale (Figures 2.5-107 and 2.5-108) generally parallel surface topography at the site, the depression in the top of the competent rock in the center of the site is related to a thickened weathered shale layer, as can be seen in the reflection profiles (Figures Figure 2.5-109 through 2.5-117) and cross-sections (Figures 2.5-191 through 2.5-195). The reason for over-thickened weathered and fractured rock zone in the center of the site is presumably because this zone is located under a gully in the hill, which is oriented parallel to major structural orientations within the Site Area. Within this gully, precipitation is channeled off of the hill and leads to greater subsurface penetration of water within this zone, leading to deeper weathering and fracture propagation in the Mahantango Formation. However, because the top surfaces of the decomposed shale and weathered shale are parallel to the ground surface, with no obvious offset, it is clear that no Quaternary faulting has affected the site.

The close correlation between the seismic data and the boring log data, both in locating the top of rock elevation and in the lack of observed faulting in the rock mass, further confirms the interpretation by earlier researchers in the area (Inners, 1978, Williams, 1987) that there is no evidence of faulting in the Quaternary deposits underlying the site.

2.5.3.1.2 Interpretation of Aerial Photography and LIDAR Imagery

Aerial reconnaissance within a 25 mi (40 km) radius of the site was conducted by various personnel using aerial photographs from numerous publications. Figure 2.5-128 is a sample of the aerial imagery used, and it contains selected way points from the field reconnaissance. LIDAR imagery of the BBNPP site vicinity was also acquired for review and interpretation (Figure 2.5-211 through Figure 2.5-216. The LIDAR image contains elevation data with a 2 ft (0.6 m) contour interval. The aerial reconnaissance investigated geomorphology and targeted numerous previously mapped geologic features and potential seismic sources (e.g., Berwick fault, Light Street fault, and Berwick Anticlinorium).

Figure 2.5-197 and 2.5-201 contain four topographic cross-sections (A, B, C on Figure 2.5-197, and D on Figure 2.5-201) based on the new LiDAR data set from Luzerne County. The intent of these figures is to review the LiDAR data set in both plan and section view to evaluate the detailed surface of the land as captured by the LiDAR process.

Figure 2.5-200 shows the BBNPP site geology on the LiDAR data base map. Figure 2.5-210 depicts the surficial sediment description including glacial derived features and deposit contacts overlaid on the LiDAR data base map. The same LiDAR data base map without the surficial sediment description is shown in .

© 2007-2012 UniStar Nuclear Services, LLC. All rights reserved.
COPYRIGHT PROTECTED

The site area geology is presented on the LiDAR data base map in Figure 2.5-212 and Figure 2.5-213 shows the same image without the site area geology coloration and patterns for better clarity. Figure 2.5-214 is similar to Figure 2.5-213 but has the higher altitudes eliminated to better show the detail for the lower elevations where the BBNPP site is located.

The site vicinity geology along with the LiDAR base map is presented in Figure 2.5-215. Figure 2.5-216 shows the LIDAR base map without the site vicinity geology coloration and patterns for better clarity. Figure 2.5-215 and Figure 2.5-216 include not only the trace for the Lightstreet and Berwick faults, but also all of the described geologic features at this scale.

The interpretation of the plan-view LiDAR maps incorporates an evaluation of the fracture traces and lineaments visible on the images as linear valleys and swales and straight segments of streams. The features are especially visible for the site on . The orientations of the fractures observed in the outcrop of the Mahantango Shale are within the reported envelope of orientations reported by Inners (1978, Figure 3). There is a single dominant set striking just west of north, with a subordinate set at nearly right angles to the first. These appear to be nearly vertical. The right-angle bend in Walker Run to the southwest of the BBNPP center point, illustrates those trends, as the Run has eroded through the glacial cover to expose the underlying bedrock structures. Other fracture orientations are present in the outcrop areas of formations to the north and south of the mapped Mahantango Shale, as is also reported by Inners (1978, Figures 4 and 5).

The topographic cross sections presented in Figures 2.5-197 and 2.5-201 display no offsets that are attributable to the actions of the Berwick or Light Street Faults. The current work confirms the work by Inners (1978) who reports the faults to be locally buried beneath the glacial terrace gravels. In the excavations for the Susquehanna Units, Inners found several slickensided surfaces at low-angles to the bedding planes located less than 1 mile (1.6 km) to the east of the site (Figure 2.5-200). He interpreted these surfaces as wedge faults that usually developed along small-scale drag folds during the folding of the units during the Alleghanian Orogeny, approximately 250 Ma (Inners, 1978). The current investigation found a similar slickensided surfaces, the closest at a distance of 0.45 miles (.7 km) to the southwest of the site (Figure 2.5-200). The throw on these faults is usually less than three feet (Inners, 1978), and the field team observed no offset of the glacial materials overlying this feature in the field.

As shown in the following section, field reconnaissance coupled with interpretation of remote imagery (review and inspection of features preserved on the images) shows that there are no geomorphic features indicative of potential Quaternary activity along trends of the postulated folds and faults interpreted by Inners and Williams (Inners, 1978; Williams, 1987). No features suggestive of tectonic deformation were observed in the Quaternary glaciofluvial deposits, and no potential liquefaction features were observed along the Susquehanna River.

2.5.3.1.3 Field Reconnaissance

Information developed from the literature and the imagery interpretation was supplemented by field reconnaissance within a 25 mi (40 km) radius of the site. These field-based studies were performed to verify, where possible, the existence of mapped bedrock faults in the BBNPP site area and to assess the presence or absence of geomorphic features suggestive of potential Quaternary fault activity along the mapped faults, or previously undetected faults. Features reviewed during the field reconnaissance and office-based analysis of aerial photography and LIDAR imagery were based on a compilation of existing regional geologic information in the vicinity of the BBNPP site, as referred to in Section 2.5.3.1.2.

© 2007-2012 UniStar Nuclear Services, LLC. All rights reserved.
COPYRIGHT PROTECTED

Field reconnaissance was conducted by geologists in teams of two or more. Field reconnaissance visits in 2007 , 2008, 2009, and 2010 focused on exposed portions of the Mahantango Formation, other formation exposures along the faces of Lee, Huntington and Nescopeck Mountains, and roads traversing the site vicinity. Key observations and discussion items were documented in field notebooks and photographs. Field locations were logged by hand on detailed topographic base maps and with hand-held Global Positioning System (GPS) receivers (Figure 2.5-200). There were no faults or other forms of deformation noted in the field. No surface expression of either the Berwick or Light Street faults was noted, consistent with the conclusions documented in the literature. Figure 2.5-119 and Figure 2.5-120 (Waypoint 12 on Figure 2.5-198) show that there is no offset in the Quaternary deposits along Syber Creek, where the trace of Light Street Fault crosses it. Photos of the shale bedrock on the site show the steeply dipping nature of the strong persistent cleavage. Bedding dipping to the north-northwest is visible, but highly obscured by this cleavage (Figure 2.5-125 and Waypoint WF3 on Figure 2.5-128). Outcrops in a nearby borrow area show an undeformed contact between the glacial overburden and the shale bedrock (Figure 2.5-126, and Figure 2.5-127 and Waypoint WF5 on Figure 2.5-128).

A supplemental reconnaissance was conducted during the fall of 2008, to investigate the occurrence of potential liquefaction features along the Susquehanna River. The field reconnaissance was carried out by a team of geologists and engineers from Paul C. Rizzo Associates, Inc, and John Sims & Associates from both the land and water approaches to the river banks. The investigation was conducted for the course of the river for a reach of 25 miles (40 km) upstream and downstream of the site (Figure 2.5-198). Because of the prevalent bedrock exposures in both the river banks and the river bottoms, few locations were encountered where liquefaction conditions were possible and no locations were encountered where liquefaction had occurred. Figure 2.5-121 through 2.5-124 show the rocky nature of the riverbed and its banks and some of the typical exposures found during the investigation (for Waypoints WP1, WP10, WP20, and WP22 respectively).

A third reconnaissance was conducted during the Spring of 2009 to further investigate the occurrence of potential liquefaction features along the Susquehanna River. The study was conducted along approximately 10 miles of the Susquehanna River along the south and east bank in areas accessible by auto and on foot. The investigated areas lie south and east of the BBNPP site within the Berwick 7.5-minute topographic quadrangle.

Two tributaries of the Susquehanna River, the Wapwallopen and Little Wapwallopen creeks, were found to run on bedrock and are relatively small, but similar to other tributaries of the Susquehanna and this region. These two tributaries, like many other streams in the original study, have been disturbed by coal mining activities.

Following the additional reconnaissance, the conclusions about the low potential for liquefaction in the area remain unchanged. The rugged terrain of the Allegheny Mountains, narrow floodplains, and intense modification of the topography through anthracite coal mining confirm those conclusions. The Susquehanna River is a gently meandering river with numerous rock-core islands and boulder-cobble gravel bars. At nearly all sites that were visited, bedrock was present or nearby. The ubiquitous presence of bedrock at or near the surface militates against liquefaction and the presence of paleoliquefaction structures. The tributaries of the Susquehanna have narrow floodplains. Coal mining debris from mine waste dumps, carried by the tributary streams of the Susquehanna, form the visible floodplain deposits of the tributaries.

© 2007-2012 UniStar Nuclear Services, LLC. All rights reserved.
COPYRIGHT PROTECTED

Fine-grained sediments, when present, are thin and lack the usual prerequisites for liquefiable deposits, which are a fine to medium sand overlain by 1-2 meters of fine upward silt with a clay cap. However, the banks are commonly vegetated, which significantly reduces accessibility to exposures in the river banks. Further modification of the banks by manmade stone walls, built to prevent erosion of the railroad right-of-way and sections of an early canal, exist through the studied section of the Susquehanna River.

In the spring of 2010, another reconnaissance was undertaken to investigate the new portion of the Site Area (5 mile radius (8 km)) that was made available by relocation of the Site approximately 1000 feet (305 m) to the north-northwest. The area studied forms a crescent shaped zone on the north-northwest edge of the new Site Area that is 1000 feet (305 m) wide at its widest, by approximately 15 miles (24 km) long. As is typical with most of Pennsylvania and the Site Area, outcrop is limited. For this reason, targets for investigation and ground truthing were areas of known or suspected outcrop within and around the crescent zone. The main areas of investigation were therefore locations on Lee Mountain, Huntington Mountain, Shickshinny Mountain, Penobscot Mountain, and the Mocanaqua, Pond Hill and Berwick Heights areas, as well as a few locations outside of the Site Area where the Light Street Fault has been mapped.

In all outcrops investigated, the orientations of bedding, joint surfaces and lineations were measured and rock lithologies recorded. Due to prior detailed mapping in the area (Inners, 1978) all rock units had previously been identified. The other main objective of the reconnaissance was to look for any evidence of Quaternary faulting.

The observations and measurements made as part of this investigation did not reveal anything inconsistent with the findings of the previous BBNPP reconnaissance efforts or with prior geologic mapping in the area (Inners, 1978). All measurements were consistent with the mapped structures, all rock lithologies were consistent with unit descriptions and no evidence of recent faulting was observed, including in the area of the mapped Light Street Fault.

2.5.3.1.4 Compilation and Review of Existing Data and Literature

The existing body of geologic and geotechnical data regarding faulting in the vicinity of the proposed BBNPP site is contained in the following principal sources, as discussed in the three sections below:

1. Work performed for the existing Susquehanna Steam Electric Station (SSES) Units 1 and 2 and complementary structures (SSES FSAR, 2003).

2. Published geologic mapping performed primarily by the USGS and Pennsylvania Department of Conservation and Natural Resources (DCNR, 2007).

3. Seismicity data compiled and analyzed in published journal articles.

2.5.3.1.4.1 Work at the SSES Units 1 and 2

The most detailed previous subsurface exploration near the BBNPP site was performed as part of the original SSES FSAR (SSES FSAR, 2003) for the SSES Units 1 and 2 foundation and supporting structures. That exploration covered an area that is located adjacent to the east side of the BBNPP site and was completed to address the same issues as the current BBNPP FSAR investigation. The high level of detail in that earlier study, and the close proximity to the BBNPP site make that study especially relevant to the current effort. The level of effort for that earlier FSAR study included drilling 250 geotechnical boreholes, collecting down-hole geophysical data, and acquiring seismic refraction data from across the site. Previous site

© 2007-2012 UniStar Nuclear Services, LLC. All rights reserved.
COPYRIGHT PROTECTED

investigations performed for the existing units are summarized in the SSES Final Safety Analysis Report (FSAR) (SSES FSAR, 2003). As cited in the SSES FSAR, these previous investigations provide the following results documenting the absence of Quaternary faults:

- Interpretation of satellite photos and topographic maps. This interpretation revealed no evidence of surface rupture, surface warping, or offset of geomorphic features indicative of active faulting.

- Interviews with personnel from government agencies and private organizations. These interviews concluded that no known faults are present beneath the existing SSES Units 1 and 2 site area.

- Seismicity Analysis -This analysis showed that no microseismic activity has occurred in the site area; the site is located in a region that has experienced only infrequent minor earthquake activity approximately 35 mi (56 km) northeast of the BBNPP site, between Lackawanna and Wyoming Counties; the closest fault-related epicentral location (the Anthracite Zone) is greater than 25 mi (40 km) away. No earthquake within 50 mi (80 km) of the SSES site has been large enough to cause significant damage in the time the region has been populated, approximately 270 years.

- Approximately 250 exploratory boreholes were drilled at the SSES Units 1 and 2 site area. Borehole data have provided evidence for the lateral continuity of strata across the existing SSES site area (SSES FSAR, 2003). The inspection of soil samples has revealed no adverse effects indicative of geologically recent or active faulting.

- Field reconnaissance of many surface outcrops at the site and within the 25 mi (40 km) radius of the site, coupled with geophysical surveys, provided no evidence for faulting at the SSES site.

- At the time of the original studies for the SSES FSAR (SSES FSAR, 2003), published maps showing bedrock faults within a 5 mi (8 km) radius of the SSES site identified only the Light Street fault. The closest significant bedrock faults mapped prior to 1975 were faults located about 80 mi (129 km) southwest of the SSES site near Lewistown, PA (SSES FSAR, 2003).

2.5.3.1.4.2 Published Geologic Mapping

Since the late 1960s, extensive mapping of the BBNPP site region within the Ridge and Valley Province has been performed by the Pennsylvania Geological Survey (PGS) and other governmental agencies to improve knowledge of the Ridge and Valley stratigraphy and other geologic structures within the region (Inners, 1978; Wheeler, 2006). Local mapping includes geologic mapping across the BBNPP site area (Inners, 1978) (Figure 2.5-184), a developed geologic section through the central Appalachian Basin (Ryder, 1992) (Figure 2.5-177) and associated stratiographic column (Figure 2.5-104), and a Precambrian Basement Map (Gold, 2005) based on borehole and seismic reflection data (Figure 2.5-179). This compilation of previous mapping and exploration studies provides the principal basis for the few bedrock faults recognized within the site area.

A local geologic section, oriented approximately north-south within the site area (5 mi (8 km) radius), depicts slightly faulted anticlinal Silurian-Mississippian bedrock that is unconformably overlain by unconsolidated Pliocene-Holocene deposits, as shown in Figure 2.5-185 (Inners, 1978). A review of the SSES FSAR reported the presence of the Light Street Fault but failed to uncover evidence, through either published reports or field investigations, to support the existence of the inferred Berwick fault (SSES FSAR, 2003). Folds, as reported by Inners (Inners,

© 2007-2012 UniStar Nuclear Services, LLC. All rights reserved.
COPYRIGHT PROTECTED

1978), are prevalent structures throughout the bedrock of the BBNPP site, mainly in second- and third-order. The major structure of the area is the Berwick Anticlinorium, a moderately complex, first order fold that passes through the center of Figure 2.5-184 and 2.5-185 (Inners, 1978).

However, the most detailed section of the site area was created by Inners (Inners,1978) as part of a study conducted on behalf of the Commonwealth of Pennsylvania Department of Environmental Resources-Bureau of Topographic and Geologic Survey. This geologic cross-section, Figure 2.5-185 (see Figure 2.5-184 for location of cross-section), was developed extending from just north of Lee Mountain, northwest of the BBNPP site, to near Black Creek, just south of Nescopeck Mountain, south of the BBNPP site. This section depicts moderately dipping, un-deformed geologic contacts between the Middle Devonian Mahantango Formation, the overlying Middle Devonian Harrell Formation, and underlying Marcellus Formation.

As shown on Figure 2.5-184 and Figure 2.5-190, the Light Street Fault (DCNR, 2007) and the Berwick Anticlinorium (Inners, 1978) have been mapped within the 5 mi (8 km) radius of the BBNPP site. In addition, two other structures have been proposed within the 5 mi (8 km) radius of the site, the Lackawanna Synclinorium (Inners, 1978), approximately 4 mi (6.4 km) northwest of the BBNPP site, and the inferred Berwick fault (Inners, 1978) (DCNR, 2007), approximately 3 mi (4.8 km) southwest of the BBNPP site. All of these structural features are consistent with published evidence of the intense folding and faulting that occurred to the bedrock formations during the Alleghanian Orogeny, as discussed in Section 2.5.1 (Faill, 1999; Harper, 1999; Way, 1999). The Light Street fault, inferred Berwick fault (Inners, 1978) (DCNR, 2007) and inferred folds (Inners, 1978) are described previously in Section 2.5.1. None of these features are considered capable tectonic sources, as defined in Appendix A of Regulatory Guide 1.165 (NRC, 1997).

Considering the evidence provided above, as well as the previous site investigations (SSES FSAR, 2003) discussed in Section 2.5.3.1.1, and the field reconnaissance interpretation undertaken for the BBNPP study, no evidence of Quaternary deformation has been reported in the literature or observed on the site for the Light Street or Berwick faults, or the Berwick Anticlinorium.

In summary, numerous investigations of the BBNPP site vicinity have found that the Alleghenian aged folding is not associated with any active deep seated basement faulting beneath the BBNPP site area, and no signs of tectonic deformation exist within the exposed Quaternary deposits near the BBNPP site. Collectively, the published geologic information for the BBNPP site area, combined with regional geologic sections (Inners, 1978; Williams, 1987) and site and aerial reconnaissance, indicate the absence of Pleistocene and younger faulting and folding. A review of local geologic sections (Figure 2.5-185 and Figure 2.5-191) suggest that the features, if present, are not prominent structures and are not developed within the Quaternary age units. In conclusion, there are no known tectonically active faults within the site area, and the Light Street fault and Berwick fault (if present) have been last active in the Late Permian (Inners, 1978).

2.5.3.1.4.3 Recent Seismicity Compilations

The USGS completed a compilation of all Quaternary faults, liquefaction features, and possible tectonic features in the eastern U.S. (Crone, 2000) (Wheeler, 2005) (Wheeler, 2006). These compilations do not show any Quaternary faults or features within a 25 mi (40 km) radius of the site, as shown in Figure 2.5-190. The nearest reported capable Quaternary feature (Crone,

© 2007-2012 UniStar Nuclear Services, LLC. All rights reserved.
COPYRIGHT PROTECTED

2000) is the Cacoosing Valley earthquake (Number 7 on Figure 2.5-180), part of the Lancaster seismic zone (Number 8), approximately 52 mi (84 km) south of the BBNPP site. The closest documented paleo-liquefaction site is known as the Clinton-Newbury liquefaction features (Number 21), and is located over 260 mi (418 km) from the BBNPP site, in northeastern Massachusetts (Crone, 2000).

As was reported in Section 2.5.2, the locations of earthquakes were accounted for by an updated USGS catalog (USGS, 2008), and a new catalog extended to 2010 for assessing the BBNPP site seismic hazard. Figure 2.5-103 shows two earthquakes lying within the 25 mi (40 km) radius of the BBNPP site. Further analysis of these mapped earthquakes revealed that their sources were quarry blasts or mine collapses (Faill, 2004). Neither of these events were fault related or were associated with bedrock/ basement rock deformation. No publications reported vibratory ground motions being felt as a result of either of these seismic events. Based on this information, there are no significant hazard potential faults within a 25 mi (40 km) radius of the BBNPP site.

2.5.3.2 Geological Evidence, or Absence of Evidence, for Surface Deformation

Based on the discussions in the preceding sections, no evidence for surface deformation has been found for this site vicinity. The evidence against that deformation is as follows:

- No subsurface offsets within the site boundary, on the adjacent property for the SSES, or in the site vicinity where literature sources infer faults to exist.
- No capable faults mapped within 25 miles (40 km) of the site (at the local or regional scale).
- No tectonically related seismic activity recorded within 25 miles (40 km) of the site.
- No evidence of prehistoric ground motion (liquefaction features) within the site area.

2.5.3.3 Correlation of Earthquakes with Capable Tectonic Sources

As presented in Figure 2.5-103, two earthquake epicenters occur within the 25 mi (40 km) radius of the BBNPP site, further analysis revealed that the sources for these earthquakes were quarry blasts or mine collapses (Faill, 2004). No reported historical earthquake epicenters have been associated with either of the bedrock faults (Light Street or Berwick faults) located within the 25 mi (40 km) radius of the BBNPP site vicinity. The distribution of earthquakes from the catalog supports the following conclusions:

- There are no earthquakes within the site vicinity that are associated with a known geologic or tectonic structure.
- The updated catalog of earthquake events does not indicate a unique cluster of seismicity in the area that would suggest a local seismic source outside of the EPRI seismic source model (EPRI, 1986).
- The catalog does not show a pattern of seismicity that would require significant revision to the EPRI seismic source geometry.

2.5.3.4 Ages of Most Recent Deformations

As presented in Section 2.5.1.2.4, the local tectonic features located within 5 mi (8 km) of the BBNPP site (the Light Street fault, the inferred Berwick fault, the Berwick Anticlinorium, and the Lackawanna Synclinorium) do not exhibit evidence of Quaternary activity. They are

© 2007-2012 UniStar Nuclear Services, LLC. All rights reserved.
COPYRIGHT PROTECTED

interpreted to have formed during the Paleozoic Era as part of the regional Alleghanian Orogeny and have been inactive since that time (Inners, 1978). This interpretation is based on detailed field mapping that showed that these faults are covered by undisturbed terrace gravels and that the faults and folds are observed to affect only Mississippian and older units (Inners, 1978). Other than highly folded and cleaved Mahantango Shale in the vicinity of the mapped Light Street fault and thickened or missing Devonian units in a limited number of well logs (Inners, 1978), there is no other evidence of these faults. Because of the undeformed surficial cover over the faulted areas, no conclusive evidence that would indicate the nature or orientation of the faults can be observed (Inners, 1978), further supporting that there has been no Quaternary movement on these faults. Lack of Quaternary deformation is further confirmed for the site by the seismic refraction survey performed during all field investigation efforts. All refraction profiles (Figures 2.5-109 through 2.5-117) indicate consistent layering of soils and rock units below the site with no offset of contacts. The profiles indicate that erosion and weathering have been the dominant geologic activities affecting the Mahantango Shale since the Alleghanian Orogeny ended in the Late Permian Period. Through all of the field efforts undertaken during this investigation, absolutely no evidence of Quaternary deformation of any kind was observed in any surficial sediments or at the Quaternary-bedrock interface, confirming the earlier detailed field studies. Based on a review of available published geologic literature, field reconnaissance, and interpretation of aerial photography, tectonic deformation associated with the local structures is constrained to the Late Permian Period, and do not affect Quaternary aged deposits (Inners, 1978) (Williams, 1987) (DCNR, 2007).

2.5.3.5 Relationship of Tectonic Structures in the Site Area to Regional Tectonic Structures

All four of the features evaluated within the 5 mi (8 km) radius of the BBNPP site (Light Street fault, Berwick fault, Berwick Anticlinorium, and Lackawanna Synclinorium) have been linked with regional tectonic events, mainly the Alleghanian Orogeny, and have been inactive since Late Permian time. Tectonic models hypothesize that the crystalline basement underlying the BBNPP site was accreted to a pre-Taconic North American margin during the Precambrian (Eriksson, 2003). Episodes of continental collisions have produced a series of accreted terrains that are separated, in part, by low-angle detachment faults (Pohn, 2000), as discussed in detail in Section 2.5.1.1.2. In association with these continental collisions, the Paleozoic bedrocks of eastern North America, including the Ridge and Valley Province, contain a number of generally northeast striking thrust faults (Schlische, 2003) such as the Light Street fault and the inferred Berwick fault. The Berwick Anticlinorium and Lackawanna Synclinorium are both results of regional extension and compression due to the orogenic events discussed in detail in Section 2.5.1.1.2.

2.5.3.6 Characterization of Capable Tectonic Sources

None of the mapped bedrock structures located within the site vicinity is considered to be a capable tectonic source as defined by Regulatory Guide 1.208 (NRC, 2007). This conclusion is based on the following observations:

- The Light Street and the inferred Berwick faults are inactive, and were most recently active in the Late Permian, approximately 250 Ma.
- There was no deformation of Quaternary age deposits identified in either the literature review or during the site investigations for this study.
- There is no association of historical earthquakes with any local fault or any cluster of seismicity within the site area that would indicate the presence of a capable source.

© 2007-2012 UniStar Nuclear Services, LLC. All rights reserved.
COPYRIGHT PROTECTED

2.5.3.7 Designation of Zones of Quaternary Deformation Requiring Detailed Fault Investigation

There are no zones of Quaternary deformation requiring detailed investigation within the BBNPP site area. A review and interpretation of digital elevation models coupled with aerial reconnaissance identified few discontinuous north to northeast-striking lineaments. None of these lineaments are interpreted as fault-related, or are coincident with the Light Street fault or the inferred Berwick fault.

2.5.3.8 Potential for Tectonic or Non-Tectonic Deformation at the Site

The potential for tectonic deformation at the BBNPP site is negligible. This conclusion is based on the following:

1. No evidence for faulting in the subsurface investigation of the BBNPP site.
2. No evidence of faulting in either the detailed subsurface investigation at the adjacent SSES site, or in outcrops within the site area.
3. No evidence of paleoliquefaction found at the site or surrounding site area.
4. No historical seismic activity or mapped capable faults within the site vicinity.

Collectively, these data support the interpretation for the absence of any Quaternary surface faults or capable tectonic sources within the BBNPP site area. In addition, there is no evidence of non-tectonic deformation at the site, such as glacially induced faulting, collapse structures, growth faults, salt migration, or volcanic intrusion.

2.5.3.9 References

Berg, 1980. Geologic Map of Pennsylvania, Pennsylvania Geological Survey, 4th ser., Map1, scale 1:250,000, 3 sheets, T.M. Berg, et al,1980.

CFR, 2007a. Title 10, Code of Federal Regulations, Part 100, Reactor Site Criteria, 2007.

CFR, 2007b. Title 10, Code of Federal Regulations, Part 50, Appendix S, Earthquake Engineering Criteria for Nuclear Power Plants, 2007.

Crangle, 2002. Stratigraphic Framework of Cambrian and Ordovician Rocks in the Central Appalachian Basin from Lake County, Ohio, to Juniata County, Pennsylvania, Revised and Digitized from Ryder, Stratigraphic Framework of Cambrian and Ordovician Rocks in the Central Appalachian Basin from Medina County, Ohio, through Southwestern and South-Central Pennsylvania to Hampshire County, West Virginia, R.D. Crangle Jr., 2002.

Crone, 2000. Data for Quaternary Faults, Liquefaction Features, and Possible Tectonic Features in the Central and Eastern United States, East of the Rocky Mountain Front, U.S. Geological Survey, Open-File Report 00-260, p 1-332, A.J. Crone and R.L. Wheeler, 2000.

DCNR, 2007. Geologic Map of Pennsylvania, Pennsylvania Department of Conservation and Natural Resources, Website: http://www.dcnr.state.pa.us/topogeo/maps/map7.pdf, Date accessed: December 14, 2007.

© 2007-2012 UniStar Nuclear Services, LLC. All rights reserved.
COPYRIGHT PROTECTED

Eriksson, 2003. Predominance of Grenvillian Magmatism Recorded in Detrital Zircons from Modern Appalachian Rivers, The Journal of Geology, Volume 111, p 707-717, Kenneth A. Eriksson, Ian H. Campbell, J. Michael Palin, and Charlotte M. Allen, 2003.

EPRI, 1986. Seismic Hazard Methodology for the Central and Eastern United States, EPRI Report NP-4726, Electric Power Research Institute, July 1986

ESRI, 2007. Street Map Pro [CD-ROM], 2007 State Boundaries, Roads, Streams, County Boundaries, ESRI, 2007.

Faill, 1999. Appalachian Mountain Section of the Ridge and Valley Province, The Geology of Pennsylvania, Part III. Structural Geology and Tectonics, Chap. 19, p. 268-285, R. Faill and R. Nickelsen, 1999.

Faill, 2004. The Birdsboro Basin, Pennsylvania Geology, Volume 34, Number 4, p 2-11, R. T. Faill, 2004.

GeoVision, 2010. Final Report - Seismic Refraction Investigation Bell Bend Nuclear Power Plant, Luzerne County, Pennsylvania Report 10171-03 Rev. 0, Report Prepared for RIZZO by GeoVision Geophysical Services, Corona, CA, August 2010.

Gold, 2005. Basement depth and related geospatial database for Pennsylvania, Pennsylvania Geological Survey, 4th ser., Open-File General Geology Report 05-01.0, Pennsylvania Department of Conservation and Natural Resources, downloaded from www.dcnr.state.pa.us/topogeo/openfile/basementmap.aspx, D. Gold, 2005.

Harper, 1999. Part II, Stratigraphy and Sedimentary Tectonics, Chapter 7: Devonian, in C.H. Shultz ed., The Geology of Pennsylvania: Pennsylvania Bureau of Topographic and Geologic Survey Special Publication 1, p 108-127, J.A. Harper, 1999.

Harrison, 2004. The Lackawanna synclinorium, Pennsylvania: A salt-collapse structure, partially modified by thin-skinned folding, Geological Society of America Bulletin, Volume 116, Number 11/12, p 1499-1514, Michael J. Harrison, Stephen Marshak, John H. McBride, November/December 2004.

Hibbard, 2006. Lithotectonic Map of the Appalachain Orogen, Canada-United States of America, Geological Survey of Canada Map 02096A, 2 sheets, scale 1:1,500,000, J. Hibbard, C. Van Staal, D. Rankin and H. Williams, 2006.

Jacobeen, 1974. Structure of Broadtop Synclinorium and Its Implications for Appalachian Structural Style, AAPG Bulletin, Volume 58, Number 3, p 362-375, Frank Jacobeen, Jr. and William H. Kanes, March 1974.

Inners, 1978. Geology and Mineral Resources of the Berwick Quadrangle, Luzerne and Columbia Counties, Pennsylvania, Pennsylvania Geological Survey, Fourth Series, p 1-34, J.D. Inners, 1978.

NRC, 1997. Identification and Characterization of Seismic Sources and Determination of Safe Shutdown Earthquake Ground Motion, Regulatory Guide 1.165, U.S. Nuclear Regulatory Commission, March 1997.

© 2007-2012 UniStar Nuclear Services, LLC. All rights reserved.
COPYRIGHT PROTECTED

NRC, 2007. A Performance-Based Approach to Define the Site-Specific Earthquake Ground Motion, Regulatory Guide 1.208, U. S. Nuclear Regulatory Commission, March 2007.

PAMAP, 2008. PAMAP Program Topographic Contours (2 ft interval) of Pennsylvania, PA Department of Conservation and Natural Resources, Bureau of Topographic and Geologic Survey.

Peters Consulting, 2010. As-Built Survey Report Monitoring Wells and Borings for Bell Bend NPP, Salem Township - Luzerne County, PA. Report Prepared for RIZZO by Peters Consultants, Inc., Berwick, Pa, July, 2010.

Pohn, 2000. Lateral Ramps in the Folded Appalachians and in Overthrust Belts Worldwide- a Fundamental Element of Thrust-Belt Architecture, U.S. Geological Survey Bulletin 2163, p 1-63, H.A. Pohn, 2000.

Rodgers, 1984. Tyrone-Mt.Union Cross-Strike Lineament of Pennsylvania: A Major Paleozoic Basement Fracture and Uplift Boundary, AAPG Bulletin, Volume 68, Number 1, p 92-105, Michael R. Rodgers and Thomas H. Anderson, January 1984.

Ryder, 1992 Stratigraphic Framework of Cambrian and Ordovician Rocks in the Central Appalachian Basin from Medina County, Ohio, through Southwestern and South-Central Pennsylvania to Hampshire County, West Virginia, US Geological Survey Bulletin 1839, p 1-40, R.T. Ryder, A.G. Harris, and J. E. Repetski, 1992

Schruben, 1998. Geology of the Conterminous United States at 1:2,500,000 scale - A Digital Representation of the 1974 P.B. King and H.M. Beikman Map: U.S. Department of the Interior, U.S. Geological Survey Digital Data Series DDS-11 CD-ROM, release 2; display software by Russell A. Ambroziak. P.G. Schruben, R.E. Arndt and W.J. Bawiec, 1998.

Schlische, 2003. Progress in Understanding the Structural Geology, Basin Evolution, and Tectonic History of the Eastern North American Rift System, P. leTourneau and P. Olsen, eds., The Great Rift Valleys of Pangea in Eastern North America, Vol. 1, p 21-64, R. Schlische, 2003.

Senior, 2006. Arsenic, Boron, and Fluoride Concentrations in Ground Water in and Near Diabase Intrusions, Newark Basin, Southeastern Pennsylvania, Lisa A. Senior, Ronald A. Sloto, United States Geological Survey, Scientific Investigations Report 2006-5261, 105 p.

Shumaker, 2002. Reinterpreted Oriskany Structure at the Northern Summit field, Chestnut Ridge anticline, Pennsylvania, AAPG Bulletin, Volume 86, Number 4, p 653-670, Robert C. Shumaker, April 2002.

SSES FSAR, 2003. Susquehanna Steam Electric Station Final Safety Analysis Report, Section 2.5, Geology, Seismology, and Geotechnical Engineering, Rev. 58, PPL Susquehanna, LLC, 2003.

Sykes, 2008. Observations and Tectonic Setting of Historic and Instrumentally Located Earthquakes in the Greater New York City - Philadelphia Area, Lynn R. Sykes, John G. Armbruster, Won-Young Kim, and Leonardo Seeber, Bulletin of the Seismological Society of America, Volume 98, Number 4, p. 1696-1719, 2008.

USGS, 2008. Documentation for the 2008 update of the United States National Seismic Hazard Maps: U.S. Geological Survey Open-File Report 2008-1128, M. D. Peterson, A. D. Frankel, S. C.

© 2007-2012 UniStar Nuclear Services, LLC. All rights reserved.
COPYRIGHT PROTECTED

Harmsen, C. S. Muller, K. M. Haller, R. L. Wheeler, R. L. Wesson, Y. Zeng, O.S. Boyd, D. M. Perkins, N. Luco, E. H. Field, C. J. Wills, and K. S. Rukstales, 2008.

Way, 1999. Part IV, Physiography, Chapter 29: Appalachian Mountain Section of the Ridge and Valley Province, in C.H. Shultz ed., The Geology of Pennsylvania: Pennsylvania Bureau of Topographic and Geologic Survey Special Publication 1, p 353-361, J.H. Way, 1999.

Weems, 1998. Newly recognized en echelon fall lines in the Piedmont and Blue Ridge provinces of North Carolina and Virginia, with a discussion of their possible ages and origins, U.S. Geological Survey Open-File Report 98-374, 52 p, R.E. Weems, 1998.

Wheeler, 2005. Known or Suggested Quaternary Tectonic Faulting, Central and Eastern United States-New and Updated Assessments for 2005, U.S. Geological Survey, Open-File Report 2005-1336, R.L. Wheeler, 2005.

Wheeler, 2006. Quaternary tectonic faulting in the Eastern United States, Engineering Geology, Volume 82 (2006), p 165-186, R.L. Wheeler, 2006.

Williams, 1987. Groundwater Resources of the Berwick-Bloomsburg-Danville Area, East-Central Pennsylvania, Pennsylvania Dept of Environmental Resources, Topographic and Geologic Survey, Water Resource Report 61, 76 p., J. Williams and D. Eckhardt, 1987.

Wood, 1961. Sweet Arrow Fault, East-Central Pennsylvania, AAPG Bulletin, Volume 45, Number 2, p 256-263, Gordon H. Wood, Jr. and Thomas M. Kehn, February 1961.}

2.5.4 Stability of Subsurface Materials and Foundations

The U.S. EPR FSAR includes the following COL Item for Section 2.5.4:

> A COL applicant that references the U.S. EPR design certification will present site-specific information about the properties and stability of soils and rocks that may affect the nuclear power plant facilities, under both static and dynamic conditions including the vibratory ground motions associated with the CSDRS and the site-specific SSE.

This COL Item is addressed as follows:

{This section addresses site-specific subsurface materials and foundation conditions. It was prepared based on the guidance in relevant sections of NRC Regulatory Guide 1.206, Combined License Applications for Nuclear Power Plants (LWR Edition) (NRC, 2007a).

Unless otherwise indicated, the information presented in this section is based on results of a subsurface investigation program implemented at the Bell Bend Nuclear Power Plant (BBNPP) site, and evaluation of the collected data. The Susquehanna Steam Electric Station (SSES) Units 1 and 2 Final Safety Analysis Report (FSAR) (PPL, 2004) contains a summary of the geotechnical information collected previously for the construction of SSES Units 1 and 2. The planned Bell Bend NPP is to be located approximately 0.5 mi (0.8 km) west of SSES Units 1 and 2. The geologic and geotechnical work performed for the BBNPP is a "stand-alone" investigation. The outcome and conclusions do not rely on the existing SSES Units 1 and 2 FSAR. This document provides the complete investigation data set, including both geotechnical boring logs, and results from the laboratory testing program. The data is organized within the text, body, tables, and figures to provide an engineering recommendation based on geotechnical

© 2007-2012 UniStar Nuclear Services, LLC. All rights reserved.
COPYRIGHT PROTECTED

parameters. The topographic reference to elevation values in this subsection are based, for the initial ground control and establishment, on the state Plane Coordinates North American Datum of 1983 (NAD83) PA NORTH datum (NGS, 1983). For the establishment of the vertical datum, North American Vertical Datum, 1988 (NAVD 88), is utilized unless stated otherwise (NGS, 1988).

2.5.4.1 Geologic Features

Section 2.5.1.1 addresses the regional geologic settings, including regional physiography and geomorphology, regional geologic history, regional stratigraphy, regional tectonic and non-tectonic conditions, and geologic hazards, as well as maps, cross-sections, and references. Section 2.5.1.2 addresses the geologic conditions specific to the site, including site structural geology, site physiography and geomorphology, site geologic history, site stratigraphy and lithology, site structural geology, seismic conditions, and site geologic hazard evaluation, accompanied by figures, maps, and references. Pre-loading influences on soil deposits, including estimates of consolidation, pre-consolidation pressures, and methods used for their estimation are addressed in Section 2.5.4.2. Related maps and stratigraphic profiles are also addressed in Section 2.5.4.2.

The site lies within the Ridge and Valley Physiographic Province (Inners, 1978). The soils at the site are characterized by glacio-fluvial deposits, and were subjected to both glacial and periglacial events during the Quaternary period. Underneath this glacio-fluvial overburden (glacial overburden) lies the middle Devonian bedrock denominated the Mahantango Formation, part of the Hamilton Group. This formation is characterized by dark gray, slightly fossiliferous, hard shale and was found to be at least 400 ft (122 m) thick based upon the BBNPP site geotechnical investigation. A past report places the total thickness of the Mahantango Formation at approximately 1,500 ft (457 m) (Inners, 1978). Harper (Harper, 1999) describes the Mahantango Formation as "a complex series of interbedded shales, siltstones, and sandstones ranging from 1,200 ft (366 m) to 2,200 ft (671 m)" although Inners (Inners, 1978) reports a site specific thickness of approximately 1,500 ft (457 m). The shales and siltstones encountered during the BBNPP site investigation were typically dark gray, ranged in hardness from soft to moderately hard, increased progressively in the level of calcareous content with depth, and were slightly pyritic and fossiliferous throughout. Harper (Harper, 1999) suggests that the Mahantango Formation was deposited as a prograding marine shoreline during the early stages of the Catskill delta.

The glacial overburden soils and the Mahantango formation were the subject of a detailed subsurface exploration for the COL investigation, as described below.}

2.5.4.2 Properties of Subsurface Materials

The U.S. EPR FSAR includes the following COL Item in Section 2.5.4.2:

> A COL applicant that references the U.S. EPR design certification will reconcile the site-specific soil and backfill properties with those used for design of U.S. EPR Seismic Category I structures and foundations described in Section 3.8.

This COL Item is addressed as follows:

{This section presents the properties of underlying materials encountered at the BBNPP Site. It is divided into five subsections, as follows.

- Section 2.5.4.2.1 provides an introduction to the soil profile and subsurface conditions,

© 2007-2012 UniStar Nuclear Services, LLC. All rights reserved.
COPYRIGHT PROTECTED

- Section 2.5.4.2.2 provides a description of the field investigation program, including borings, sampling, and in-situ tests,
- Section 2.5.4.2.3 provides a description of the laboratory testing program,
- Section 2.5.4.2.4 provides a narrative on the origin and characteristics of the engineered fill soils, and
- Section 2.5.4.2.5 provides the BBNPP recommended soil properties.

2.5.4.2.1 BBNPP Soil Profile

The natural topography at the BBNPP site, at the time of the subsurface exploration, was a gently sloping open field cut across by a highly eroded east-west trending bedrock anticlinorium. The maximum variation in relief was about 144.5 ft (44 m) across the site. Ground surface elevations at the time of exploration ranged from approximately 800 ft to 656 ft (244 to 200 m) mean sea level (msl), with an average elevation of about 680 ft (207 m). The ground surface elevations in the Powerblock area ranged from about 656 ft to 675 ft (200 to 206 m), with the centerline of the BBNPP through the Reactor Building at an elevation of 666.6 ft (203.2 m). The Powerblock includes the Reactor Building, Fuel Pool Building, Reactor Auxiliary Building, Safeguard Buildings, Radioactive Waste Processing Building, Emergency Power Generating Buildings, Essential Service Water System (ESWS) Cooling Towers, and Turbine Building.

The BBNPP subsurface investigation focused on the upper 400 ft (122 m) of the subsurface structure. The site geology is comprised of glacial soil deposits underlain by bedrock, which is, on average, 38.9 ft (11.9 m) below the ground surface. The subsurface structure is divided into the following stratigraphic units:

- Overburden Soil: - Glacial Till
- Bedrock: - Mahantango Formation

Identification of soil and rock layers was based on their physical and engineering characteristics. The characterization of the soils and rocks was based on a suite of tests performed on these soils and rocks, consisting of standard penetration tests (SPT) in soil borings including auto-hammer energy measurements, geophysical testing, pressuremeter tests (PMTs) and laboratory testing.

Figure 2.5-172 provides a general soil column profile. Overall, the subsurface conditions encountered throughout the site are uniform, in both depth and area extension.

The thickness of the glacial till varies from 12.5 (3.8 m) to 62.0 ft (18.9 m). With the exception of some loose sand pockets, the till consists of over-consolidated brown silty sand or sand containing gravel and large rounded cobbles and boulders. The presence of boulders increases with depth.

The overburden soil is not an adequate foundation strata for safety related structures or facilities that will impose high contact pressures. Even though these soils have shear wave velocities in the excess of 1000 ft/sec (305 m/sec), several zones of loose sands were encountered during the investigation. These zones originated from wind deposited processes during the glaciation periods. Low blow counts were recorded in areas at the south side of the power block. Such areas are susceptible to liquefaction.

© 2007-2012 UniStar Nuclear Services, LLC. All rights reserved.
COPYRIGHT PROTECTED

The Mahantango Shale is very dark gray to black, thin bedded to massive bedded, with few to no fractures. There are also calcareous zones, thin pyrite lenses that increase in abundance with depth, and calcite veins perpendicular to the bedding plane that are micro-faulted. The upper surface of the Mahantango Formation shows the effects of solution and weathering in a few areas, but it is predominantly very competent and indurated. For SSES Units 1 and 2, this layer supports large and safety-related structures (PPL, 2004).

The thicknesses and termination elevations of rock are summarized in Table 2.5-26 The table provides the minimums, maximums, and averages from forty eight geotechnical boring logs. The positions of the soil and rock strata are best visualized by cross section drawings and contour elevation plots. These are developed at locations where the main power block and other safety related facilities will be placed. The following plots are presented for visualization purposes:

- Figure 2.5-129, Boring Location Plan
- Figure 2.5-130, Location of Cross Sections
- Figure 2.5-131, Geotechnical Subsurface Section A-A'
- Figure 2.5-132, Geotechnical Subsurface Section B-B'
- Figure 2.5-133, Geotechnical Subsurface Section C-C'
- Figure 2.5-134, Geotechnical Subsurface Section D-D'
- Figure 2.5-135, Surface Elevation Contours
- Figure 2.5-136, Overburden Thickness
- Figure 2.5-137, Thickness of Weathered Rock
- Figure 2.5-138, Elevation of Competent Rock
- Figure 2.5-139, Overburden Thickness and Elevation of Rock (Area near Essential Service Water Emergency Makeup System - ESWEMS)

2.5.4.2.2 Field Investigation Program

A thorough field investigation program was designed and implemented at the BBNPP site. The program included:

- Boring Program,
- Wash Rotary Drilling/ CasiRock Coring (NQ Wireline),
- In-Situ Pressuremeter Testing,
- Geophysical Exploration,
- Downhole Tests,
- PS Suspension Logging Tests,
- Deviation Surveys,

© 2007-2012 UniStar Nuclear Services, LLC. All rights reserved.
COPYRIGHT PROTECTED

- Refraction Surveys.

The field investigation was performed under the guidance provided in NRC Regulatory Guide 1.132, "Site Investigations for Foundations of Nuclear Power Plant" (NRC, 2003a). The work was performed in accordance with work procedures developed specifically for the BBNPP subsurface exploration, including a subsurface exploration plan developed under the Rizzo Quality Assurance Program. Subsection 2.5.4.2.2.1 provides a brief summary of the field investigation conducted for SSES Units 1 and 2, and subsection 2.5.4.2.2.2 details the field investigation program for the BBNPP site.

2.5.4.2.2.1 Previous Subsurface Investigations

Based on information available from the SSES FSAR (PPL, 2004), it was determined that approximately 250 exploratory borings were made in the soil and rock at the site. The subsurface investigations for SSES Units 1 and 2 began in late 1970 (100 and 200 series borings) to establish general geologic relationships over the site area and to determine the general soil and rock conditions at the site. A more intensive program (300 series borings) was conducted in the Spring of 1971 to define foundation conditions in the principal plant structures area. Two 45-degree angle holes were drilled in the reactor area. Additional exploration drilling was necessary to locate the site for the Susquehanna River intake and discharge structures (700-800 series borings), to define soil and rock conditions at the spray pond and ESSW pumphouse (1100 series and some 400 series borings), and to investigate foundation conditions for the cooling towers (borings B1 to B10) and the railroad spur and bridge over State Highway 11 (borings 417 to 455 and 929 to 940). An investigation program (borings 1 through 7) was conducted in 1983 to determine soil and rock conditions in the area of the diesel generator 'E' building. Because of the safety-related (Category 1) function of the spray pond and ESSW pumphouse, the exploration program for there facilities was comprehensive and included split spoon and undisturbed samples, laboratory testing, hydrologic surveys, permeability tests, and seismic cross-hole and up-hole surveys. Split spoon sample laboratory testing, hydrologic surveys, and permeability tests were also performed in the area of the diesel generator 'E' fuel tank. After completion of geologic borings, static water levels were measured in some of the borings drilled on the site.

Geological descriptions in the SSES FSAR (PPL, 2004) indicate that two primary layers existed at the site, the glacial overburden soils and the bedrock. The site is blanketed by till and glacial outwash which grades upward from a gravelly boulder zone to a surface layer of silty fine sands and sandy silt. The surface layer is believed to be reworked loess. The maximum thickness of overburden is around 40 ft (12 m) in the southern half of the site, with bedrock occasionally cropping out at the surface. North of the east-west bedrock ridge situated just north of the reactors, the glacial deposits fill a valley eroded into bedrock to a depth exceeding 100 ft (30.5 m). The upper bedrock at the site area includes the Middle Devonian Mahantango Formation. The upper part of the Mahantango is a dark gray siltstone, with bedding generally delineated by thin, consistent, light gray, fine-grained sandstone stringers. Beneath the upper member, the Mahantango is comprised of 120 to 150 ft (37 to 46 m) of dark gray, hard calcareous siltstone, typically having bedding obscure to absent and displaying cleavage. This member, which supports the SSES power block structures, is harder, more massive, and more resistant to erosion than the upper member. Minor faulting in the form of small bedding-plane slips and intraformational shear zones occur, but they are of no significance to the site. They apparently developed during the Paleozoic (more than 200 million years ago) during the Appalachian Orogeny. The zones are typically healed with calcite and quartz.

© 2007-2012 UniStar Nuclear Services, LLC. All rights reserved.
COPYRIGHT PROTECTED

Comparable observations were made on these soil and rock layers from the BBNPP investigation borings. Given the reasonably parallel geologic conditions between SSES Units 1 and 2, and BBNPP, exploration and testing at BBNPP resulted in enhanced characterization of the subsurface conditions. Findings from previous investigations are not discussed further, unless a differing condition is reported from the previous investigation.

2.5.4.2.2.2 BBNPP Subsurface Exploration

The BBNPP subsurface exploration was performed in accordance with the guidance outlined in Regulatory Guide 1.132 (NRC, 2003a). Deviations are identified at point of use and alternatives and/or basis for deviations are provided.

Regulatory Guide 1.132 (NRC, 2003a) provides guidance on spacing and depth of borings, sampling procedures, in-situ testing, geophysical investigations, etc. This guidance was used in preparing a technical specification, addressing the basis for the BBNPP subsurface exploration. Per Regulation Guide 1.132 (NRC, 2003a), "the minimum required depth of borings in competent bedrock should extend to the greatest depth where discontinuities or zones of weakness or alteration can affect foundations or at least 20 ft (6 m) into sound rock. For safety-related structures, one boring per 10,000 ft^2 (929 m^2) and at least one-fourth of those borings should penetrate into sound rock." In accordance with this guideline, a subsurface exploration program was developed.

In total 45 boreholes were completed for sampling and standard penetration test (STP) puposes. These boreholes are designated as the B-Series boreholes. In addition, 3 boreholes were performed for geophysical testing purposes. These boreholes are designated as the G-Series boreholes.

B-Series boreholes were completed for the BBNPP site, of which 27 boreholes were located in the vicinity of the proposed Category I structures and the remainder were located in other plant locations. It was determined that 1 boring (B-301) should be extended to depth of 400 ft (122 m) for detailed core logging and geophysical testing at the location of the proposed Nuclear Island structure. In addition, 2 borings from the Nuclear Island buildings were extended to about 350 ft (107 m) at a 30^o angle to determine the existence of vertical discontinuities. Such discontinuities were not encountered. Three G-Series destructive drilling boreholes were extended for geophysical testing purposes in the proposed location of the Reactor Building and in two of the ESWS Cooling Towers.

A team consisting of a geologist, a geotechnical engineer, and a member of the project management performed a site reconnaissance prior to start of the field investigation. The focus of this task was to observe the site and assess conditions, locations of borings and wells, and identify potential test relocation areas.

According to Regulatory Guide 1.132 (NRC, 2003a), boreholes with depths greater than 100 ft (30.5 m) should be surveyed for deviation. At the BBNPP site, rock was penetrated at an average depth of 41.1 ft (12.5 m) and deviation surveys were limited to boreholes with geophysical testing. The deviation was taken because bedrock was encountered at an average depth of 41.1 ft (12.5 m).

Regulatory Guide 1.132 (NRC, 2003a) provides guidance for color photographs of all cores to be taken immediately upon removal from the borehole to document the condition of the soils and rocks at the time of drilling. Undisturbed samples were sealed in steel tubes, and could not be photographed. Sample photography was taken of SPT and rock core samples.

© 2007-2012 UniStar Nuclear Services, LLC. All rights reserved.
COPYRIGHT PROTECTED

The BBNPP subsurface geotechnical field exploration was conducted from August 2007 through November 2007. This work consisted of an extensive investigation to define the subsurface conditions at the BBNPP site. Locations of the geotechnical field investigation field tests are shown in Figure 2.5-129 (Boring Location Plan), and information relating to the field tests is summarized in Table 2.5-27. Surveying was conducted in order to establish the horizontal and vertical locations of exploration points as shown in Table 2.5-28. Each boring location was investigated for the presence of underground utilities prior to drilling boreholes.

Subsurface explorations were performed using geotechnical drill rigs mounted on trucks or tracked vehicles. Field borings logs and other field records were maintained by a rig geologist (geologist or geotechnical engineer). A rig geologist was assigned to each rig and was responsible for maintaining the field records associated with activities conducted at a specific exploration point.

Forty-five (45) B-Series borings were advanced with SPT sampling, and 12 undisturbed samples (using Shelby push tubes) collected from the overburden soils. Soils were sampled using the SPT sampler in accordance with ASTM D1586 (ASTM, 1999). Disturbed soil samples were obtained using 1.5-in (3.8-cm) inside diameter split-spoon samplers in conjunction with the SPT, as described by ASTM D1586 (ASTM, 1999). The split spoon sampler was driven a minimum of 18 in (46 cm) or to refusal. The sampling interval was continuous or 2.5 ft (0.7 m) for borings in the vicinity of Category I structures, and 5 ft (1.5 m) in the vicinity of the proposed non-safety-related structures. At least one boring below each proposed safety-related structure was performed with continuous sampling. The recovered soil samples were visually described and classified by the rig geologist in accordance with ASTM D2488 (ASTM, 2006c). Two representative samples of the soil recovered from each SPT were placed in glass jars with moisture-preserving lids. The sample jars were labeled, placed in boxes, and transported to the on-site storage facility.

Undisturbed samples were obtained in accordance with ASTM D1587 (ASTM, 2000b) using the push Shelby tubes. Immediately upon sample retrieval, the disturbed portions at both ends of the tube were removed, both ends were trimmed square to establish an effective seal, and pocket penetrometer (PP) tests were performed on the trimmed lower end of the samples. Both ends of the sample were then sealed with hot wax, filled with sand to the top, covered with plastic caps, and sealed once again using electrician tape and wax to preserve their natural moisture content and prevent soil movement. The tubes were labeled and transported in a vertical orientation to the on-site storage area. Undisturbed samples were stored in an upright position with the top side of the sample up. The locations from which the undisturbed samples were obtained are shown in Figure 2.5-140.

Due to the extremely rocky nature of the overburden, the majority of the borings were advanced using a three inch casing advancer system. The advancer system attached to the three inch casing. The system consisted of a diamond shoe (similar to a diamond drill bit), and a roller bit attached to a carrier that locks and unlocks into the system (similar to a wire line core barrel). The center bit is adjusted to ride just forward of the shoe. The center bit was removed to allow a sampler to be lowered down the casing for SPT sampling. When the boulders were too large for roller bit to penetrate through, a core barrel was placed through the system in-lieu of the roller bit mechanism, allowing the driller to core through the boulder. After coring, the driller switched back to mud rotary to allow sampling of the overburden to the top of bed rock. Once the presence of rock was confirmed, that is, 50 blows/6" or 10 hammer refusals, rock coring was initiated, as summarized below.

© 2007-2012 UniStar Nuclear Services, LLC. All rights reserved.
COPYRIGHT PROTECTED

All boreholes advanced during the field investigation program, penetrated the rock layer. The top of the rock layer was identified by the refusal of the split-spoon sampler and/or by the presence of shale rock fragments in the sampler. Rock coring was performed using wire line core barrels and NQWL dual tube (1.875 in (47.6 mm) core diameter), diamond-tipped rock core tools. Dual tube core barrels, 5 ft or 10 ft (1.5 m or 3 m) in length were used to collect continuous rock samples in accordance with ASTM D2113 (ASTM, 2006e). The recovered rock samples were visually described and classified by the geologist or engineer in accordance with ASTM D5878 (ASTM, 2005d). "Routine care" and "special care" rock core samples were collected during this exploration. Routine care samples were placed directly into wooden rock core boxes with a locking lid and photographed. Wood spacers were place in the core box when needed to stabilize the core laterally. Special care samples were wrapped tightly in a plastic film and aluminum foil, coated with wax, wrapped in a bubble wrap and stored in a polyvinyl chloride (PVC) tube to preserve the in-situ characteristics. The locations from which special care rock samples were obtained are shown in Figure 2.5-141.

The rig geologist visually described the core and noted the presence of joints and fractures, distinguishing mechanical breaks from natural breaks where possible. The rig geologist also calculated percent recovery and Rock Quality Designation (RQD) prior to moving the core from the drill site. Field boring logs and photographs were used to document the drilling operations and recovered materials. In borings to be geophysically logged, PVC casing was grouted in place in lieu of the temporary casing.

An on-site storage facility for soil and rock samples was established prior to initiating the boring exploration program. The site facility had to provide adequate temperature control conditions in accordance with Regulatory Guide 1.132 (NRC, 2003a). The soil and rock samples obtained were logged into an inventory system. Samples removed from the facility were noted in the logbook. A chain-of-custody form was completed for all samples removed from the facility. Material storage and handling was in accordance with ASTM D4220 (ASTM, 2000a) and ASTM D5079 (ASTM, 2006f) for soil and rock samples, respectively.

2.5.4.2.2.2.1 Hammer Calibration and SPT Measurements

The depth of soil and rock penetrated by each borehole is shown in Table 2.5-28. Soil and rock samples retrieved are identified on the boring logs included with the COLA.

Energy measurements were made on the hammer-rod system on 2 of the 4 drilling rigs used in the subsurface investigation. One of the rigs was retired from the investigation due to mechanical failure. This rig was not calibrated, but SPT measurements associated with this rig were only performed at two locations underneath the turbine building. Data from the damaged, non-calibrated rig was not used. Overall, SPT data was only used to establish the potential of the overburden soils. These soils are potentially liquefiable and will be removed from the site. In-situ soils at the BBNPP site will not be used for foundation or lateral support purposes.

A Pile Driving Analyzer (PDA) was used to acquire and process hammer energy data. A summary of measured energies is provided in Table 2.5-29. The total number of measurements made at each boring was ten (10) for borehole B-336, and 9 at borehole B-327A. Energy transfer to the gage locations was estimated using the Case Method, in accordance with ASTM D4633 (ASTM, 2005a). The average energy transfer efficiency measurements ranged from 60 to 87 percent, with an average of 80 percent. As shown in Figure 2.5-131, Figure 2.5-132, Figure 2.5-133, and Figure 2.5-134, the soil on site is relatively

© 2007-2012 UniStar Nuclear Services, LLC. All rights reserved.
COPYRIGHT PROTECTED

consistent, and the blow counts recorded with the CME 75 Track and CME 55 drill rigs are consistent with those taken by other rigs used on-site.

Soil samples were collected from the borings by means of Standard Penetration Test (SPT) and tube samples. Samples were collected more frequently in the borings located in the vicinity of the proposed Category I (safety-related) structures for BBNPP. SPT N-values were measured during the sampling and recorded on the boring logs included with the COLA. SPT N-values ranged from 0 blows/ft to 131 blows/ft (0 blows/m to 437 blows/m), with an average measured N-value of 36 blows/ft (120 blows/m). Most of the recordings were done in the overburden soils. It was possible to take a limited amount of readings in the weathered part of the Mahantango Shale. These were typically above 50 counts. SPT information on the overburden soil layer is presented in Table 2.5-30. The variability of measured SPT N-values is presented in Figure 2.5-142. The figure indicates that there is not a consistent relationship between the SPT values and depth. Some readings are extremely low and they correspond to the presence of loose sand pockets. As the percentage of glacial boulders increased, the SPT process was interrupted at 50 counts when hammer rejection was observed. There were some instances for which the behavior of the hammer allowed for the continuation of the test beyond 50 blow counts. The selected subsurface profiles, Figure 2.5-131, Figure 2.5-132, Figure 2.5-133, and Figure 2.5-134 show the samples collected with their corresponding SPT N-values and classification symbols. The figures indicate if the sample was disturbed or undisturbed, and the number recorded field SPT blows/feet. Additional discussion pertaining to the presence of loose sand pockets is provided in Section 2.5.4.8

SPT hammer energies were measured for 2 of the 4 drilling rigs used for the subsurface exploration. Energy measurements were made in 2 borings (B-336 and B-327A). Because the SPT N-value used in correlations with engineering properties is the value corresponding to 60 percent hammer efficiency, the measured SPT N-values were adjusted based on the energy measurements, in accordance with American Society for Testing and Materials (ASTM) D6066 (ASTM, 2004b). The average energy transfer ratio (ETR) obtained from hammer energy measurements for each drilling rig was applied to the measured SPT N-values. A summary of the measured ETR values for each drill rig is shown in Table 2.5-29. The measured SPT N-values from each boring were adjusted using the ETR value shown in Table 2.5-29 for the drill rig utilized. The adjusted average field-measured N-values are shown in Table 2.5-31.

Figure 2.5-142 indicates the scatter of the SPT blow counts versus the depth. There is no clear pattern and the plot is a reflection of the natural composition of the glacial till. Higher blow counts are attributed to the presence of boulders and consolidated mixtures of sands and gravels. As previously discussed, there are zones with extremely low number of blow counts that originate from wind deposition during the coldest spells of the glaciation process.

2.5.4.2.2.2.2 Pressuremeter Tests

Pressuremeter tests were conducted in four boreholes on the BBNPP site, B-301, B-322, B-325 and B-327 in accordance with ASTM D4917 (ASTM, 2000c) at two depth intervals to measure the volumetric change of a pressurized cell surrounded by in-situ rock, specifically by the weathered Mahantango Formation. The Pressuremeter test is an in situ stress-strain test performed on the wall of a borehole using a cylindrical probe that is expanded in the radial stress direction. The Pressuremeter was field-calibrated using a steel pipe as the surrounding media of the pressure cell. The pressure and displacement gages were properly calibrated and the field geologists matched the serial numbers with the calibration records documentation. Table 2.5-32 presents the results of the borehole pressuremeter tests. These results are later discussed in Section 2.5.4.2.4 within the context of soil and rock properties.

© 2007-2012 UniStar Nuclear Services, LLC. All rights reserved.
COPYRIGHT PROTECTED

2.5.4.2.2.2.3 Geophysical Tests

Geophysical tests were conducted in the three G-Series boreholes, and one B-Series borehole. Geophysical logging consisted of surface seismic refraction surveys, P-S suspension logging surveys, and downhole velocity measurements.

This section provides a summary of the geophysical surveys undertaken for the BBNPP site. Information obtained from these surveys was utilized in the analysis of and discussions pertaining to the site geology and characterization of geologic features as presented in Subsection 2.5.1.2, and surface faulting potential presented in Subsection 2.5.3.

The location, and depth or extent of each test is shown by Figure 2.5-129. Figure 2.5-143, Figure 2.5-144, Figure 2.5-145, and Figure 2.5-146 present the plots for compressional and shear wave velocities. The plots provide the results from the two different surveys performed: downhole test, and P-S Suspension Logging.

A surface seismic refraction survey was performed for the 6 profile lines indicated by Figure 2.5-129. The results of the survey are provided by Figure 2.5-147 through Figure 2.5-153. The findings of the refraction survey are consistent with the boring program in the sense that the rock horizon was defined at the position indicated by the boreholes. The measured compressional shear wave velocities are consistent with those obtained from downhole and PS-suspension logging.

Downhole Seismic Velocity Surveys

Downhole seismic velocity surveys were conducted in borings G-301, G-302, G-303, and B-301. In three of the four borings, installation of PVC casing was critical for acquiring good downhole data. Measurements in an uncased borehole provide more accurate information because the equipment is in direct contact with the rock formation; the casing is installed mainly to protect the instrument from damage. If there is structural integrity of the borehole, it is possible to perform the survey without casing. This was the base at the B-301 location and it was, therefore, able to be an uncased borehole. For those boreholes requiring casings, the space between the outside of the casing had to be backfilled with low-strength grout to ensure that the casing follows the motions of the adjacent soil exactly. The boreholes were purged of water to a depth of 50 ft (15 m) to reduce the effect of tube waves, traveling down the borehole. B-301 was an uncased borehole. Measurements in an uncased borehole provides more accurate information because the equipment is in direct contact with the rock formation; the casing is installed mainly to protect the instrument from damage. If there is structural integrity of the borehole, it is possible to perform the survey without casing. This was the case at the B-301 location.

Downhole seismic velocity surveys are conducted by measuring the time for seismic waves (generated by an impulsive source at the surface) to travel to a sensor located at a sequence of depths in the borehole. A typical sensor consists of three orthogonal geophones. The two horizontal geophones are used to detect shear-wave (S-wave) arrivals and a vertical geophone is used to detect compression-wave (P-wave) arrivals. Various methods are used to align one of the horizontal geophones with the source polarization. At each measurement level, the sensor assembly is locked to the borehole wall using a clamping mechanism so that the geophones will couple with the seismic signals propagating in the earth.

Seismic waveforms for each depth interval are analyzed and the travel time picked from those waveforms. Interval velocities are calculated and reported as seismic velocity versus depth. This procedure is typically repeated every 2.5 ft (0.76 m) through overburden soil, and every 5

© 2007-2012 UniStar Nuclear Services, LLC. All rights reserved.
COPYRIGHT PROTECTED

ft (1.5 m) through bedrock. The shear wave source was a wooden plank approximately 6 inx 6 inx 8 ft (15 cm x 15 cm x 2.4 m) with steel end caps and cleats attached to the bottom to better couple with the ground. The compressional wave (P-wave) source was sledge hammer blows on a steel or aluminum plate adjacent to the borehole.

P-S Suspension Logging

P-S suspension logging was performed in four (4) boreholes. P-S suspension velocity logging was performed in borings B-301, G-301, G-302, and G-303 shown in Figure 2.5-129. The objective of the suspension and downhole logging tests was to obtain shear wave (Vs) and compressional wave (Vp) velocity measurements as a function of depth within each borehole.

In the absence of an accepted ASTM standard, the following procedure was used to perform P-S suspension velocity logging. P-S suspension velocity logging uses a 23 ft (7 m) probe containing a source near the bottom, and two geophone receivers spaced 3.3 ft (1 m) apart, suspended by a cable. The probe is lowered into the borehole to a specified depth where the source generates a pressure wave in the borehole fluid. The pressure wave is converted to seismic waves (P-wave and S-wave) at the borehole wall. At each receiver location, P- and S-waves are converted to pressure waves in the fluid and received by the geophones mounted in the probe, which in turn send the data to a recorder on the surface. At each measurement depth, two opposite horizontal records and one vertical record are obtained. This procedure is typically repeated every 1.6 ft (0.5 m) or 3.3 ft (1 m) as the probe is moved from the bottom of the borehole toward the ground surface. The elapsed time between arrivals of the waves at the geophone receivers is used to determine the average velocity of a 1.6 ft (0.5 m) high column of soil around the borehole.

Surface Seismic Refraction Surveys

Surface seismic refraction surveys are used to generate a cross sectional acoustic image of the subsurface strata. This method identifies mapping depth to bedrock, identifying voids, determining strength and quality of bedrock, and locating faults or steeply dipping contacts. The geophysical refraction seismic survey was performed in 6 selected lines as shown by Figure 2.5-129. The survey is conducted by laying out a series of geophones (typically every 10 ft (3 m)) in intersecting grid lines spaced approximately every 250 ft (76 m), which is then connected to a 24- channel data acquisition system. An individual refraction spread covered 250 linear feet (76 linear meters) and seven "shot points" were operated for each spread. Seismic energy at the shot points was delivered by a sledge hammer striking a metal plate. Depths to which seismic refraction data are acquired are functions of magnitude of the seismic energy source and overall refraction spread lengths. Seismic velocities measured by this technique are used to calculate the mechanical properties of subsurface materials (moduli values), as well as for material identification and for assisting in stratigraphic correlations. Interpretations are made from travel times representing the time required for a compressional seismic wave to travel from an energy source location to each of an array of vibration sensitive geophones. Geophones are located at pre-determined intervals along the ground surface with spacing between individual geophones selected to be appropriate for the intended depth of the investigation (Weston, 2008).

The elastic wave measured in the seismic refraction method, the "P-wave" or compressional wave, is the first arrival of energy from the seismic source at each receiver, or geophone. This elastic wave travels from the energy source in a path causing adjacent solid particles to oscillate in the direction of wave propagation. At shorter distances between source and geophone the first arriving waves will be direct waves that travel near the ground surface through the lower velocity material. At greater distance, the first arrival at the geophone will

© 2007-2012 UniStar Nuclear Services, LLC. All rights reserved.
COPYRIGHT PROTECTED

be a refracted wave that has taken an indirect path through the two layers. The refracted wave will arrive before the direct wave at a greater distance along the spread because the time gained in travel through the higher-speed material compensates for the longer path. For all configurations of seismic sources and receivers, P-wave energy will arrive at a given geophone location in the shortest possible time as required by Fermat's Principal (Dobrin, 1976). This principal was utilized to develop several analytical methods for calculating seismic velocity structure versus depth using only first arrival times of seismic P-wave energy measured along arrays of geophones deployed at ground surface (Weston, 2008).

The results of the survey are provided by Figure 2.5-148 through Figure 2.5-154. The interpretation of the results was performed with borehole data in the form of contour profiles. Figure 2.5-136 through Figure 2.5-138 provide these contours and do not show any evidence of faulting or discontinuity. The thickness of the overburden to top of bedrock constructed from over 45 borings that penetrated the glacial material shows that there has been no thinning or thickening of the glacial material to suggest that this material has been faulted. Further, the surface of the bedrock (i.e., contact between the glacial material and bedrock) is irregular, but is due to glacial scour indicating that post-Devonian faulting has not occurred.

The somewhat irregular surface of the bedrock noted in the Refraction Survey is not interpreted as significant offsets within the Mahantango event that could be attributed to faulting. The irregular surface is mimicked in the overlying glacial till layer suggesting a glacially eroded surface, followed by a folding event associated with the Appalachian Orogeny. Most likely, the apparent irregular surface is the result of glacial scour, an erosional feature, within the upper part of the Mahantango Shale. Other apparent offsets may be a result of low fold (low statistical redundancy) that occurs at the line ends of seismic reflection data and thus reducing the confidence of the interpreted apparent offsets.

The results and interpretation of the geophysical tests are further discussed in the following Sections:

- Section 2.5.3, in the context of surface faulting
- Section 2.5.4.2.5, in the context of recommended soil properties for engineering design purposes,
- Section 2.5.4.4, in the context of the approach to select the best estimate soil column profile for dynamic analysis at the BBNPP site.

2.5.4.2.2.2.4 Hydrogeologic Investigation

The hydrogeologic field investigation included a site specific data collection to support a comprehensive hydrogeological evaluation of the BBNPP site and surrounding areas as required for Section 2.4.

The objective of the hydrogeological field investigation was to collect the necessary data and information to characterize the existing surface water and groundwater flow conditions at the site, including subsurface borings for geological stratigraphy, monitoring of groundwater potential and quality, slug and pumping tests for analysis of aquifer parameters, and gauging of surface water flow in creeks.

The data collected in the field and from other sources (i.e., SSES FSAR, USACE, USGS) were utilized to support the surface hydrology analysis, hydrogeological characterization, and the development of a groundwater flow model. The model has the capability to evaluate the

© 2007-2012 UniStar Nuclear Services, LLC. All rights reserved.
COPYRIGHT PROTECTED

impact of successive rain events on groundwater elevations across the facility as well as the hypothetical discharge of water from facility operations and storage structures to the ground and the resulting impact to groundwater flow and transport of radionuclides from the facility, including the release of radionuclides and other potential contaminants into these flow systems.

Section 2.4 presents the detailed information related to the hydrogeological field investigation.

2.5.4.2.3 Laboratory Testing Program

The laboratory investigation of soils and rocks was performed in accordance with the guidance of the NRC Regulatory Guide 1.138 , "Laboratory Investigations of Soils and Rocks for Engineering Analysis and Design of Nuclear Power Plants" (NRC, 2003b). Soil and rock samples were shipped under chain-of-custody from the on-site storage to the testing laboratories. ASTM Standards ASTM D4220 (ASTM, 2000a) and ASTM D5079 (ASTM, 2006f) provide guidance on standard practices for preserving and transporting soil and rock core samples, respectively. These guidelines were referenced in preparing technical specifications for the BBNPP subsurface investigation, addressing sample storage and transportation, as well as other subsurface investigation and geotechnical requirements.

Laboratory testing consisted of testing soils and rocks samples obtained from the subsurface investigation program. Laboratory testing of soil samples consisted of index and engineering properties on selected SPT disturbed samples, strength, consolidation, permeability, and chemical tests on undisturbed samples, rock cores recovered from borings, and samples gathered from potential borrow areas of fill and backfill. Laboratory tests included the following: engineering classification, moisture (water) content, unit weight, specific gravity, Atterberg limits, grain size (sieve and hydrometer), percent passing #200 sieve, permeability, consolidated-undrained triaxial compression (CŪ), unconfined compression (UC), consolidation, resonant column torsional shear (RCTS), free-free resonant column (FF), resistivity, chloride ion content, and sulphate ion content.

The number and types of tests selected were consistent with the field investigation findings, and the uniform conditions encountered at the site. Overall, the SPT blow counts were very consistent both in depth and spatial distribution. The soil strata at the site were distinguishable and there was a good correlation between the in-situ soil classification and the SPT results. At the BBNPP, the comprehensive index testing program along with refined testing at strategically selected locations has provided the required information to adequately characterize the soil properties.

A summary of laboratory tests and specifications used for the laboratory testing program is shown in Table 2.5-27. The soil and rock laboratory tests listed in Regulatory Guide 1.138 (NRC, 2003b) are common tests performed in most well-equipped soil and rock testing laboratories. Additional tests that are not covered in regulatory guides were also performed for the BBNPP field exploration (i.e. RCTS, FF, and chemical tests).

Resonant Column Torsional Shear (RCTS) tests were performed at Fugro Laboratories.These tests were performed under the Fugro Laboratories Quality Assurance Program. Free-Free Resonant Column (FF) tests were performed at the University of Texas under the RIZZO Quality Assurance Program.

© 2007-2012 UniStar Nuclear Services, LLC. All rights reserved.
COPYRIGHT PROTECTED

The following sections provide a summary of each test, showing the most important and relevant results.

2.5.4.2.3.1 Laboratory Index Tests

Soil samples were classified in the laboratory using the Unified Soil Classification System (USCS) in accordance with ASTM D2487 (ASTM, 2006a). Rock samples were classified in the laboratory using the Unified Rock Classification System (URCS) in accordance with ASTM D5878 (ASTM, 2005d).

2.5.4.2.3.1.1 Grain Size Analyses

Grain size analyses were performed on selected SPT samples of overburden soils. The grain size tests were done in accordance with ASTM D422-63 (ASTM, 2002a). The results of these tests were used for classification and correlation purposes.

2.5.4.2.3.1.2 Moisture Content

Moisture content was determined from samples in accordance with ASTM D2216 (ASTM, 2005c). Moisture content was also obtained during hydraulic conductivity tests on undisturbed samples and during unconfined compressive strength tests of rock core samples. Consistently throughout the site, and down through the depth of the borings, the laboratory results showed natural moisture content in the overburden soils ranging between 5 and 20 percent and an average of 10.7 percent. Moisture content laboratory results are provided by Table 2.5-34 The moisture content of rock samples is extremely low, sometimes not even recorded. This condition is due to the extremely high density of the shales at the site.

2.5.4.2.3.1.3 Unit Weight Determinations

Unit weight determinations were made based on a weight-volume relationship on undisturbed glacial overburden samples and Mahantango Formation rock core samples. Table 2.5-35 lists the samples with the corresponding dry and wet unit weights. On soils, unit weight measurements were performed during resonant column, and hydraulic conductivity tests. Unit weight measurements on rock samples were performed during "Free-Free" tests and during unconfined compressive strength tests.

2.5.4.2.3.1.4 Specific Gravity

Specific gravity tests were performed on Glacial overburden soil samples and Mahantango Formation in accordance with ASTM D854 (ASTM, 2006b). Typical values of specific gravity of most soils lie within the narrow range of 2.7 ± 0.1. For hard rocks samples, ASTM D6473 (ASTM, 2005b) was used to determine the specific gravity. Specific Gravity results are listed in Table 2.5-36.

2.5.4.2.3.1.5 Chemical Classification Tests

Chemical tests were conducted on SPT samples selected from the glacial overburden soils and the Mahantango Formation in accordance with ASME D4972 (ASTM, 2001), AASHTO T290 (AASHTO, 2007), and AASHTO T291 (AASHTO, 2004). These tests provide quantitative information related to the aggressiveness of the soil conditions, and the potential for deterioration of a foundation material. The following chemical tests were conducted on samples from the BBNPP site: resistivity; chloride ion content; and sulphate ion content . The results of the tests are provided in Table 2.5-38.

© 2007-2012 UniStar Nuclear Services, LLC. All rights reserved.
COPYRIGHT PROTECTED

2.5.4.2.3.2 Laboratory Performance Test

2.5.4.2.3.2.1 Unconfined Compression

Unconfined Compression tests were conducted on representative rock core samples to determine their compressive strength, in accordance ASTM D7012-04 (ASTM, 2004a). Table 2.5-38 presents a summary of the Unconfined Compression test results. The core samples of the Mahantango formation are typically a medium to dark gray shale rock with a recovery ratio of 90 percent and a RQD of 70 percent or higher. Therefore, most of the samples did not present problems during the specimen preparation. Section 2.5.4.2.4 provides the recommended geotechnical performance parameters which in part are based on the results of the unconfined compressive strength. The unconfined compressive strength of the specimens from the Mahantango formation is medium high to high with an average slightly above 9000 psi (62 MPa).

2.5.4.2.3.2.2 Rock Sample URCS Engineering Classification

The Mahantango Formation was the main target of the investigation and the specimens showed: minimum to no weathering (Grade A); unconfined compressive strength between 8000 and 13000 psi (55 to 90 MPa) (Grade B); no discontinuities (Grade A); and a unit weight around 170 pcf (27 kN/m^3) (Grade A). The URCS classification of the Mahantango formation is ABAA.

2.5.4.2.3.2.3 Hydraulic Conductivity

Laboratory tests were performed to determine the hydraulic conductivity of undisturbed samples, according to ASTM D5084 (ASTM, 2003). Results of the tests are presented in Table 2.5-39. The tests were performed on undisturbed samples recovered from the overburden glacial soils. Section 2.4 presents detailed information related to the hydrogeological field investigation and additional information regarding permeability and hydraulic conductivity.

2.5.4.2.3.2.4 Resonant Column Torsional Shear

Resonant Column Torsional Shear (RCTS) tests were conducted according to the procedure developed by the University of Texas at Austin (UTA) entitled, PBRCTS-1, Rev. 4, Technical Procedures for RCTS Tests, (UT, 2004a). The tests targeted the Glacial Overburden soils and two remolded samples recovered from borrow area sites. The on-site samples were obtained using thin-walled samplers. One attempt of RCTS test was made on a solid rock core (B-304, R2). The specimen cracked right after subcoring to an approximate diameter of 0.6 in (1.5 cm). The RCTS testing program included a total of five tests, of which one was the cracked rock core. The samples used for testing are listed by Table 2.5-40. It was anticipated that the RCTS tests on Glacial Overburden would reflect the behavior of the finer particle matrix rather than that of the gravelly fragments. For the case of the fill samples, laboratory staff had to scalp the specimens so that the largest particles had a diameter less than 1/6th of the specimen diameter. The focus of the RCTS testing program was to evaluate the material that will likely form the foundation fills for the plant facilities. These materials will originate from either excavation soils or from borrow areas and will be screened and compacted according to specifications. The RCTS on borrow area material was performed on remolded samples.

The RCTS test is performed in a series of steps that incorporate different confining pressures and loading frequencies. The Torsional Shear portion of the test is able to capture physical properties at large strains under lower frequency loading that best resembles the seismic demand. The details of the testing methodology are documented by the procedure, PBRCTS-1, Revision 4, Technical Procedures for RCTS Tests, (UT, 2004a).

© 2007-2012 UniStar Nuclear Services, LLC. All rights reserved.
COPYRIGHT PROTECTED

Resonant Column (RC) and/or Resonant Column Torsional Shear (RCTS) testing are performed to measure two critical parameters in laboratory soil (and sometimes rock) specimens:

1. Shear modulus, which is directly related to shear wave velocity of the soil (Equation 2.5.4-1)

$$G = pV^2_s \qquad \text{Eq. 2.5.4-1}$$

2. Damping, which allows for the dissipation of the energy released during an earthquake or any given vibratory process.

Both the shear modulus and damping depend on:

- The amount of strain (or unit deformation),
- The confining pressure,
- The frequency of the motion, in this context, the frequency of the cyclic load applied during testing.

Table 2.5-41 presents the results for shear modulus and damping at low strains. The table highlights the medium range confining pressure applied during testing. The values of the shear stress in the samples range between the 590 to 5800 ksf and damping ranged between 0.4 and 2.80 percent. The remolded and compacted samples had higher values of shear modulus. A discussion of the recommended values for engineering purposes is included in Section 2.5.4.2.4. The recommended properties take into account the effect that confining pressure has on the low strain shear modulus. The strain dependency variation of the shear modulus and damping is shown in the form of normalized plots by Figure 2.5-154, Figure 2.5-155, Figure 2.5-156, respectively for each of the samples tested. A discussion for recommended values is presented in Section 2.5.4.2.4 and Section 2.5.4.7.

2.5.4.2.3.2.5 Unconfined Resonant Column ”Free-Free” Testing

The Free-Free Resonant Column Tests (FF) was conducted according to the procedure, also developed by UTA, entitled, URC-1, Revision 4, Technical Procedures for URC Tests (UTA, 2004b). The Free-Free resonant column device allows for a simpler approach compared to the RCTS that can measure small-strain shear modulus (Gmax) and small-strain material damping (Dmin). The term "Free-Free" is used to differentiate from the "Fixed-Free" condition of the typical RC test, meaning that one end of the sample is fixed while the other is free to rotate or displace. No confining pressure is used in this test. A total of eight "Free-Free" tests were performed on special care rock samples retrieved from various boring locations. Table 2.5-42 lists the samples and presents the results. A discussion of how the "Free-Free" testing results are used for the analysis is presented in Section 2.5.4.2.4 and Section 2.5.4.7.

2.5.4.2.4 Engineered Soils

Category 1 Granular Structural Fills and Backfills will be created from screened granular soils from either the excavated in-situ soils or borrow areas in the proximity of the project. Cohesive fill (permeability lowered to less than 1.0E-08 m/s) will be required for the construction of the ESWEMS Retention Pond. A distinction is made between fill and backfill as follows: the term "Category 1 Structural Fill" or "fill" is used for engineered soil that will be placed beneath the foundation of Safety Related Facilities; the term "Category 1 Structural Backfill" or "backfill" is

© 2007-2012 UniStar Nuclear Services, LLC. All rights reserved.
COPYRIGHT PROTECTED

used for material that will be placed around and above the foundation level of Safety Related Facilities.

2.5.4.2.4.1 Category 1 Granular Structural Fill

Bowers Construction (Bowers) of Berwick, PA provided excavation of test pits to collect subsurface soil and perform screening of soil samples for the purpose of composite soil sampling soil collection for geotechnical analysis. The borrow site is approximately 4,200 ft (1,280 meters) southwest of the site at the intersection of Rockaway Street and Salem Boulevard (Route 11), Berwick, PA.

Soil samples were collected from two identified test pits (Test Pit # 5 and Test Pit Face). Upon collection of soil, Bowers utilized a Fine Tec 540 screening machine and CAT 960 front end loader along with a 325 track hoe in order to prepare the composite soil sample. After the stockpile was split over the 2 in (5 cm) sieve, Bowers used a Cat 325 track hoe to turn over the stockpile and create a 15 ft x 8 ft x 3 ft (4.5 m x 2.4 m x 0.9 m) pile for each test pit. Rizzo personnel dug 4 holes at the top of the pile at diagonal corners to a depth of 1.5 ft (0.5 m) in depth. Six representative buckets were filled from the 4 holes and shipped the soil buckets to the representative laboratories. The description of the collected soil consisted of well graded Sand with Gravel (sw) - about 70 percent sand fine to coarse, sub rounded to rounded, 25 percent gravel fine to coarse, hard, sub round to rounded, 5 percent silt, no plasticity, no dilatancy no toughness, low strength with slight odor.

A Laboratory Testing Program has been implemented to fully characterize the properties of the proposed material. The tests included:

- Modified Proctor tests,
- Grain size,
- Resonant Column Torsional Shear,
- Chemical Tests

The Modified Proctor Test results, showing optimum moisture content and maximum unit weight are provided by Table 2.5-44. The optimum water content is about 6 percent and the material proved to be quite dense with maximum moist unit weights above 144 pcf (22.4 kN/ m^3).The grain size analysis results are compared against the required specification. Table 2.5-44 provides the recommended properties for structural fill. Structural fill should be compacted to 95 percent of the optimum dry unit weight Modified Proctor. The fill moist, saturated, and dry unit weights exceed the U.S. EPR specified values of 128 pcf (20.1 kN/m^3), 134 pcf (21.1 kN/m^3), and 110 pcf (17.3 kN/m^3), respectively. The unit weight for the structural fills at the BBNPP site will be exceeded (Rizzo, 2009). This represents a departure from the U.S. EPR FSAR.

2.5.4.2.4.2 Category 1 Granular Structural Backfill

Category 1 Granular Structural Backfill will have the same specifications as the structural fill, but compacted to 90 percent Modified Proctor optimum dry unit weight. Table 2.5-45 provides the specifications for Structural Backfill. The backfill moist, saturated, and dry unit weights exceed the U.S. EPR specified values of 128 pcf (20.1 kN/m^3), 134 pcf (21.1 kN/m^3), and 110 pcf (17.3 kN/m^3) respectively. The unit weight for the structural backfills at the BBNPP site will be exceeded (Rizzo, 2009). This represents a departure from the U.S. EPR FSAR.

© 2007-2012 UniStar Nuclear Services, LLC. All rights reserved.
COPYRIGHT PROTECTED

2.5.4.2.5 Recommended Soil, Fill, and Rock Properties

The following sections provide recommendations of soil properties for engineering analysis and design purposes. The properties are based on a combination of field measurements, laboratory testing, engineering analysis, engineering judgment, and available reference material. For a cohesionless structural fills at the site, the soil below and adjacent to the safety-related foundation basemat will have a friction angle in excess of 30 degrees. This strength meets the requirements of the US EPR. The requirement is also met an exceeded by the high strength parameters of the foundation bedrock. Details are provided in the following subsections.

The properties are given for each of the geologic units found during the investigation as described by Section 2.5.4.2.1 and presented by Figure 2.5-129. Those units are listed below:

- Soils - Glacial overburden
- Bedrock - Mahantango Formation

In addition to the existing soils, it is necessary to provide properties for engineered fills that will likely be placed as foundation media for safety related structures . The Nuclear Reactor Building and its adjacent facilities will be placed directly on top of the Mahantango Formation. This will not be the case for the south ESWS Cooling Towers or the south Emergency Power Generating Buildings. Therefore, soil properties are also given for:

- Category I Granular Structural Fill
- Category I Granular Structural Backfill

This Section is divided in:

- Classification and Index Properties,
- Strength Properties,
- Performance Properties,
- Static Elastic Properties,
- Dynamic Elastic Properties, and
- Chemical Properties.

The overburden soils consist of one soil layer: Glacial Overburden (sand and gravel with cobbles and boulders). The existing soil matter is not suitable for the support of large or safety-related structures due to the potential for liquefaction and will be removed in order for the foundation mats to bear directly on either of the Mahantango Formation, concrete fill, or engineered fill. The existing soil matter is not suitable for the support of large or safety-related structures. Additional discussion related to this matter is presented in Section 2.5.4.8. The thickness of the overburden soils varies from about 12.5 to 62 ft (3.8 to 19 m), with an average thickness of 39 ft (12 m). The depth from surface boring elevation to the Mahantango Formation is shown by Figure 2.5-136. The thickness of the soil layers is based on estimating the termination elevations encountered for the layer at the boring locations from the boring logs included with the COLA.

© 2007-2012 UniStar Nuclear Services, LLC. All rights reserved.
COPYRIGHT PROTECTED

2.5.4.2.5.1 Index Properties

Index properties are:

- USCS Classification (or URCS Classification for Rocks),
- Water Content,
- Unit Weight,
- Specific Gravity,
- Grain Size (or Fines Content),

Index properties determined for rocks are:

- Classification
- Unit Weight,
- Specific Gravity.

Selected samples were submitted for laboratory index tests and testing for determination of engineering properties. Section 2.5.4.3 presents the detail of the laboratory testing program. Table 2.5-45 provides the recommended index properties.

Of the index properties, only the dry, moist, and saturated unit weights are discussed in the U. S. EPR Tier 2 FSAR documentation. The site specific unit weights found at the BBNPP site exceed the U. S. EPR FSAR values of:

- Saturated soil = 134 lb/ft^3.

- Moist soil = 128 lb/ft^3.

- Dry soil = 110 lb/ft^3.

At BBNPP:

- Saturated soil = 144 lb/ft^3.

- Moist soil = 141 lb/ft^3.

- Dry soil = 133 lb/ft^3.

This is not necessarily a geotechnical problem. The U. S. EPR FSAR values were established according to one previous site specific experience.

2.5.4.2.5.2 Strength Properties

Strength properties are obtained directly from laboratory tests or from field measurements and supplemental calculations. Triaxial testing on overburden soils was not considered useful due to the heterogeneity of the formation and the presence of large boulders. Undisturbed samples were collected only near the surface. At boring B-331, it was possible to collect an undisturbed sample at a depth of 17 ft (5 m). This sample was used for RCTS testing. The strength of the overburden soils is estimated with the use of soil classification and standard

© 2007-2012 UniStar Nuclear Services, LLC. All rights reserved.
COPYRIGHT PROTECTED

penetration data. The overburden soils will be removed and replaced by engineered fills due to the potential for liquefaction. Strength properties include the Mohr-Coulomb parameters commonly used for many geotechnical analysis issues such as bearing capacity, slope stability, retaining walls, and foundation design.

An equivalent friction and cohesion was estimated for the rock mass of the Mahantango Formation. The parameters were determined according to the classification system proposed by Bieniawski (Bieniawski, 1989). The Mahantango Formation is classified as a "Very Good" Rock Mass with a rating of 82, an equivalent cohesion of 7.3 ksf (350 MPa), and an equivalent friction angle of 40 degrees. Table 2.5-46 provides the detail of the Bienawski classification.

The following recommended strength properties for soil and rock at the site are provided by Table 2.5-46. For each property, the basis for the recommendation is explicitly mentioned in the observations column of the Table 2.5-46.

- Penetration Resistance (SPT)
- Cohesion
- Friction Angle
- Unconfined Compression.

Strength properties were determined by either correlation with SPT blow counts or by statistical averaging of the laboratory tests. Strength properties of the foundation formation (Mahantango Formation) exceed the requirements established in the U.S. EPR FSAR.

The position of the water table is close to the surface at a depth of about 8 ft (2.4 m) at the center line of the reactor footprint, at Elevation 659 ft (201 m) msl. The foundation grade of the BBNPP Nuclear Island (NI) and its adjacent facilities will be placed at Elevation 674 ft (205.4 m) msl , considerably higher due to the elevation of the Probable Maximum Flood level of 671 ft (204.5 m) msl.

2.5.4.2.5.3 Performance Properties

Two performance properties are discussed: (1) hydraulic conductivity, and (2) consolidation.

Permeability

Section 2.4 presents detailed information related to the hydrogeological field investigation, and additional information regarding permeability and hydraulic conductivity is available. The Laboratory Testing Program of Section 2.5 focused on specific values at the site and tests were performed on samples extracted from the geotechnical boring program. As expected, the Glacial Overburden presents relatively high hydraulic conductivity. Table 2.5-48 provides the recommended values for hydraulic conductivity. The recommendation is based on the results from field tests performed on the wells installed as part of the Hydrogeologic investigation.

Consolidation

The soils encountered at the site are granular in nature and long term settlement due to consolidation would not occur if these were used as foundation support.

© 2007-2012 UniStar Nuclear Services, LLC. All rights reserved.
COPYRIGHT PROTECTED

2.5.4.2.5.4 Static Elastic Properties

The static elastic properties of interest are the elastic modulus, the shear modulus, and the Poisson's ratio. The shear modulus is derived directly from the elastic modulus and the Poisson's ratio.

Elastic Modulus

The static elastic modulus of soils and rocks is determined from data retrieved during the field investigation and laboratory testing. Several criteria are used, depending on the soil or fill analyzed:

1. American Society of Civil Engineering (ASCE) Typical recommended values,

2. ASCE N Correlation,

3. American Association of State Highway and Transportation Officials (AASHTO),

4. Rock Mass Rating.

5. American Concrete Institute (ACI).

Each of the criteria is applied and an average or a conservative approach is used for the recommended parameter. Table 2.5-49 presents the values according to each criterion and the recommended elastic modulus value. It is anticipated that static loading in excess of the current in-situ overburden pressure will not occur below the Mahantango Formation, and, therefore, the static elastic modulus is not a critical parameter.

Poisson's Ratio

The most representative value of the Poisson's ratio is obtained directly from the shear wave and compressional wave velocity measurements. Equation 2.5.4-2 is used to establish the Poisson's ratio.

$$\frac{V_p}{V_s} = \sqrt{\frac{2-2\nu}{1-2\nu}} \qquad \text{Eq. 2.5.4-2}$$

Static Shear Modulus

The static shear modulus is directly determined from the Elastic Modulus and the Poisson's Ratio with the use of Eq. 2.5.4-3.

$$G = \frac{E}{2(1+\nu)} \qquad \text{Eq. 2.5.4-3}$$

where G is the static shear modulus, E is the Elastic Modulus and **v** is Poisson's Ratio.

Table 2.5-50 provides the recommendation for the static elastic properties.

© 2007-2012 UniStar Nuclear Services, LLC. All rights reserved.
COPYRIGHT PROTECTED

2.5.4.2.5.5 Dynamic Elastic Properties

A comprehensive field geophysical investigation program and laboratory testing program were undertaken to establish the dynamic properties for the BBNPP. The properties are required for site amplification analysis, Soil Structure Interaction (SSI) analysis, and foundation design. The dynamic properties established are:

- Shear Wave Velocity (V_s),
- Compressional Wave Velocity (V_p),
- Density (ρ),
- Poisson's Ratio (ν),
- Maximum Dynamic Shear Modulus (G_{max}),
- Maximum Dynamic Elastic Modulus (E_{max}),
- Damping at small strain or initial damping (DS_o),
- Strain dependant shear modulus and damping (for Overburden and borrow area soils).

The shear wave velocity profile was determined by means of a data interpretation analysis that incorporated the results from downhole, and P-S Suspension Logging tests. The details of the analysis are described in Section 2.5.4.4. The recommended values for dynamic properties are presented in Table 2.5-51. More descriptions of the procedures followed to provide the recommendation are included in Section 2.5.4.7. The recommended shear wave velocity profile under the Nuclear Island is plotted by Figure 2.5-155.

For the case of the overburden soils, dynamic properties will vary depending on the level of strain present in the soil. The two strain dependant properties of interest are Shear Modulus and Damping. Figure 2.5-158 presents the recommended curves for the engineered fill and/or backfill. The recommended curve for the overburden soils is the generic curve that best adapts to the Torsional Shear experimental data. For Shear Modulus, this curve is generic curve (Vucetic, 1991) that corresponds to a Plastic Index of 30 or 40. For Damping, the curve with a Plastic Index of 50 is recommended (Vucetic, 1991).

2.5.4.2.5.6 Chemical Properties of Soils

The chemical properties of the soils are given by Table 2.5-37.

2.5.4.3 Foundation Interfaces

This section discusses the interfaces between the planned structures and other components and the subsurface characteristics. A plot plan showing the location of the borings, seismic lines, and downhole surveys is provided by Figure 2.5-129. Based on the information obtained during the subsurface investigation and laboratory testing program for the BBNPP, it was determined that exploratory trenches were not necessary in order to characterize the soils at the BBNPP. Cross sections showing the main geologic units are presented by Figure 2.5-131 through Figure 2.5-134. Contour plans of geologic unit elevations are given byFigure 2.5-136 through Figure 2.5-139.

© 2007-2012 UniStar Nuclear Services, LLC. All rights reserved.
COPYRIGHT PROTECTED

2.5.4.3.1 U.S. EPR FSAR

The U.S. EPR FSAR provides criteria related to various sitting issues, which must be satisfied by the particular features of the BBNPP site. The U.S. EPR FSAR identifies the type of information that should be developed to demonstrate that the site is in compliance with the design. Generic soil profiles are listed by the U.S. EPR FSAR and these represent a broad range of foundation media characterized by shear wave velocities ranging from 700 ft/sec (213 m/sec) to those typical of hard rock conditions. It is expected that this range captures the static and dynamic response of plant SSCs which will, in general, envelop the actual response at sites exhibiting foundation soils with shear wave velocity at foundation level greater than 1,000 ft/sec (305 m/sec). At BBNPP, the shear wave velocity of foundation media (Mahantango Formation) for the Nuclear Island (NI), Emergency Power Generation Buildings , and Essential Service Water Cooling Towers facilities is approximately 7000 fps (2135 m/s). The NI basemat is a monolith that includes the Reactor Building (UJA), Safeguards Buildings (UJH- mechanical and UJK-electrical) and Fuel Building. Table 2.5-53 provides the soil conditions that were evaluated by the U.S. EPR FSAR. No departures or deviations were identified.

The seismic ground motion utilized in the design of NI structures is defined as a hypothetical free-field outcrop motion at approximately 36 ft (11 m) below grade, representing the bottom elevation of the containment base mat. On the other hand, the design of adjacent safety related structures founded near the ground surface (Plant Grade) use the free-field soil surface ground motion for design. Section 2.5.2 presents foundation input response spectra (FIRS) for the NI at the base mat elevation. The FIRS are compared with the respective Certified Design Response Spectra (CDRS) presented by the U.S. EPR FSAR. Both the Foundation Input Response Spectra as well as the seismic response of the soil structure system depends on the subsurface soil stratigraphy including the soil layering, layer thickness, layer shear wave velocities and damping and impedance mismatch.

The foundation interface analysis relates to how the foundation medium and its variability affect the bearing pressure distribution and the settlement of the NI Basemat, and other safety related structures (Emergency Power Generation Buildings and Essential Service Water Cooling Towers) in the vicinity, particularly for soil sites. The foundation interface analysis also determines how these same items affect the seismic response of the structures and the foundation medium. The structural design of the NI Basemat is governed by the bearing pressure and its distribution due to dead and live load and seismic forces, as well as the foundation settlements. On the other hand, the seismic loads on the plant structures and foundations are determined by the vertical and the coupled horizontal and rocking response analysis as estimated with Soil-Structure Interaction (SSI) analysis or Rock-Structure Interaction (RSI) analysis, as the case may be.

Dynamic aspects of the foundation interface are discussed in BBNPP FSAR Sections 3.7 and 3.8. Static aspects such as bearing capacities, settlement and horizontal variability of stiffness and subgrade reaction under the base mats are discussed in Section 2.5.4.10. The subsurface soils beneath the NI base mat should have the capacity to support the bearing pressures with a factor of safety of 3.0 under static conditions and 2.0 under Safe Shutdown Earthquake conditions.

2.5.4.3.2 Site Characteristics

Based on the review of the subsurface conditions at existing nuclear power plant sites, the potential sites for the U.S. EPR can be broadly categorized into four primary groups:

- Rock sites,

© 2007-2012 UniStar Nuclear Services, LLC. All rights reserved.
COPYRIGHT PROTECTED

- Thin soil sites,
- Shallow soil sites, and
- Deep soil sites.

This categorization provides a framework for reporting site-specific conditions in a COLA referencing the U.S. EPR FSAR relative to the Plant Parameter Envelope (PPE) considered in the U.S. EPR design. Based on several combinations of site groups and their respective parameters, as specified by Table 2.5-55, the BBNPP site is classified as a Thin Soil Site over Hard or Firm Rock. As such, the Ground Motion Response Spectra (GMRS) is provided at the top of bedrock or top of Mahantango Formation. For the NI, this level corresponds to the top of rock or top of Mahantango Formation. The static and dynamic bearing capacity is verified without the need of time dependant settlement computations. Details related to shear wave velocity are included in Sections 2.5.4.2.5.5 and 2.5.4.2.2.1.3.

2.5.4.3.3 Horizontal Layering

Most geotechnical analyses, including SSI analysis, settlement analysis and bearing capacity analysis, assume that the soil layers are horizontal and effects of non-horizontal layering are practically ignored. This assumption will hold if there is no significant inclination in the soil profiles such as the top of rock horizon.

Figure 2.5-138 shows the inclination of the top surface of the Mahantango Formation. In the direction of maximum gradient (approximately 30 degrees with respect to the North), the top of rock surface drops about 40 ft (12 m) in a distance of 300 ft (91 m), which corresponds to a 7.6 degree sloping angle. It is still applicable to assume a horizontal layered model for both Site Amplification and Soil Structure Interaction Analyses. The following justifications for this assumption apply:

- "The Foundation Interface Document Report on U.S. EPR Design reads: "Depending on the extent of the dip, the physical properties of the foundation medium may or may not vary systematically across a horizontal plane. If the dip is less than approximately 20 degrees, the site layering is defined as horizontal and no further substantiating analysis is required."
- The concrete between the Mahantango formation and the basemat will have a matching shear wave velocity and therefore the sloping effects will be mitigated.

2.5.4.3.4 Uniform Site Conditions

The variation of the dynamic properties between distant points of the NI facilities may be represented by a Lower Bound, Best Estimate and Upper Bound for the Vs value at the center point of the facility. The geotechnical and geophysical exploration programs show conclusive evidence that the subsurface conditions are uniform across the site.

The thickness of the Mahantango Formation was not determined since the BBNPP geotechnical investigation did not be reach the bottom of the formation. The maximum exploration depth was 400 ft (122 m), and the average depth to reach the top of this formation is 39 ft (12 m) with respect the ground level. Based on contour maps, the Mahantango Formation is present across the entire footprint of the power block . As such, the site may be considered as uniform.

© 2007-2012 UniStar Nuclear Services, LLC. All rights reserved.
COPYRIGHT PROTECTED

2.5.4.3.5 Interface Figures

The Interface Figures present cross sections of the site subsurface conditions with the location of the main components of the Project. Safety-related structures are shown at their planned foundation elevation and on top of the corresponding foundation material. Table 2.5-55 provides the depth, elevation, and foundation footprint of the BBNPP safety-related structures. Figure 2.5-159 provides a plan view of an excavation and fill plan with the location of a cross section. Two excavation profiles are shown in Figure 2.5-160 and Figure 2.5-161. A North-South direction cross section is shown in Figure 2.5-162. The Nuclear Island (NI) will sit on top of a concrete fill between its mat and the top of bedrock. The Emergency Power Generation Building and ESWS Cooling Towers will have an engineered soil fill in the south side of the power block. At the north side, these structures will bear directly on top of the Mahantango formation or on top of a concrete fill.

Section 2.5.4.5 provides the excavation details and Section 2.5.4.10 presents bearing capacities and estimated settlements.

2.5.4.4 Geophysical Surveys

Section 2.5.4.2.2.2.3 presents the results of the geophysical investigation surveys .
Section 2.5.4.2.5.5 provides the recommended dynamic soil properties, based on the results from the field investigation and on the post-processing analysis of the retrieved data.

2.5.4.5 Excavation and Backfill

Sections 2.5.4.5.1 through Section 2.5.4.5.5 are added as a supplement to the U.S. EPR FSAR.

BBNPP will utilize a combination of excavation slopes and temporary retaining structures to facilitate construction of below grade portions of the nuclear facility. The planned finish grade is at an elevation of approximately 674 ft (205.4 m).

The materials excavated as part of the site grading are primarily the overburden soils belonging to the sand and gravel units. Due to the presence of loose sand pockets that are prone to liquefaction, these soils are inadequate for foundation purposes and will be removed from the footprint of all the facilities. However, in-situ soils from the excavation may be used for fills and backfills if adequate screening and compaction techniques are implemented. These soils are predominantly of low plasticity or non plastic and their composition consists of sand and gravels with cobbler and boulders. No rebound (heave) in the ground due to the removal of the soils is expected at the Mahantango Formation.

The U.S. EPR minimum shear wave velocity is 1000 fps.

- The Nuclear Island, ESWEMS Pumphouse, North Emergency Power Generation Buildings (1UBP, 2UBP), and North ESWS Cooling Towers (3URB, 4URB) will bear on top of concrete or the Mahantango formation, which have shear wave velocities higher than 1000 fps.

- The South Emergency Power Generation Buildings (1UBP, 2UBP), and South ESWS Cooling Towers (3URB, 4URB) will bear on top of engineered fill, which will be constructed to achieve a shear wave velocity of 1000 fps.

- Category II SSE structures, such as the Fire Protection Building will bear on top of either bedrock, concrete or engineered fill, which will be constructed to achieve a shear wave velocity of 1000 fps.

© 2007-2012 UniStar Nuclear Services, LLC. All rights reserved.
COPYRIGHT PROTECTED

2.5.4.5.1 Source and Quantity of Backfill and Borrow

As previously mentioned in Section 2.5.4.2.4.1, Bowers Construction (Bowers) of Berwick, PA provided excavation of test pits to collect subsurface soil and perform screening of soil samples for the purpose of composite soil sampling soil collection for geotechnical analysis. The borrow site is approximately 4,200 ft (1,280 m) southwest of the site at the intersection of Rockaway Street and Salem Boulevard (Route 11), Berwick, PA and has sufficient material to support site construction needs. Earthwork operations will be performed to achieve the planned site grades. Excavations for foundations of the proposed Category I structures within the Power Block area, including the ESWEMS Pumphouse, will result in removing the overburden soils in their entirety, and will extend to top of the Mahantango Formation. The maximum depth of cut in the overburden soils is estimated to be about 62 ft (19 m). The estimated upper bound of the excavation and backfill volume is 600 thousand cubic yards (460 thousand cubic meters).

2.5.4.5.2 Extent of Excavations

Permanent excavation and fill slopes, created due to site grading, are addressed in Section 2.5.5. Temporary excavation slopes, such as those for foundation excavation, would be graded on an inclination of at least 1.5:1 horizontal to vertical (H:V) or flatter. The ESWEMS Retention Pond will be constructed as a dug reservoir in the natural soils. The bottom of the pond is planned at an elevation of 652 ft (199 m), and side slopes of 3:1 H: V. For the power block area, an excavation plan is provided by Figure 2.5-159. The approach for excavation, confirmed by the slope stability analysis (Section 2.5.5), will implement 1.5:1 H:V slopes, offset by 6 ft (1.8 m) at the base of excavation. A bench (8 ft (2.4 m) wide) should be located at the midpoint of the slope. At BBNPP, engineered fill or concrete will be required beneath the near-ground founded safety related structures. Figure 2.5-159 through Figure 2.5-161 show a excavation scheme for the NI structures (e.g., UJA, UJH, UJK, UKA, UKE and UKS), the Emergency Power Generating Buildings (UBP), the Essential Service Water (UQB and URB) structures, and the Turbine Building (UMA). A cut shown under the Reactor Building is to accommodate the tendon gallery.

2.5.4.5.3 Compaction Specifications

Structural fill sources were identified, as discussed in Section 2.5.4.5.1. Several samples of the materials were obtained and tested for indices and engineering properties, including moisture-density relationships. For foundation support, fill beneath mats is compacted to 95 percent Modified Proctor optimum dry density, and backfill against walls is compacted to 90 percent , as determined based on the Modified Proctor compaction test procedure . The fill is compacted to within 3 percent of its optimum moisture content, which is about 6 percent. Fill placement and compaction control procedures are addressed in a technical specification prepared during the detailed design stage of the project. It includes requirements for suitable fill, sufficient testing to address potential material variations, and in-place density and moisture content testing frequency, e.g., a minimum of one test per 10,000 ft^2 (900 m^2) of fill placed. The technical specification also includes requirements for an on-site testing laboratory for quality control, especially material gradation and plasticity characteristics, the achievement of specified moisture-density criteria, fill placement/compaction, and other requirements to ensure that the fill operations conform to the earthwork specification for BBNPP. The soil testing company is required to be independent of the earthwork contractor and to have an approved quality program. A sufficient number of laboratory tests are required to be performed to ensure that variations in the fill material are accounted for. A trial fill program is normally conducted for the purposes of determining an optimum number of compactor

© 2007-2012 UniStar Nuclear Services, LLC. All rights reserved.
COPYRIGHT PROTECTED

coverages (passes), the maximum loose lift thickness, and other relevant data for optimum achievement of the specified moisture-density (compaction) criteria.

2.5.4.5.4 Dewatering and Excavation Methods

Temporary groundwater control will be required during construction. Measurement of the groundwater conditions at the site indicate that the lower portions of the site excavations will be below the groundwater level. Thus site grading and excavation plans will implement measures to divert these groundwater flows away from excavations, such as, runoff prevention measures or trenches. Seismic Category I foundations are planned within the upper water-bearing Mahantango Formation. Groundwater conditions and dewatering are discussed in detail in Section 2.4.12.5 and 2.5.4.16.

Once the Glacial Overburden materials are dewatered, excavations are expected to be performed using conventional earth-moving equipment. Excavations will not present any major difficulties. Excavations in the top of the Mahantango Formation will not require greater excavating effort, such as ripping tools and explosives. However, excavation into the Mahantango Formation will extend up to about 10 ft (3 m) under the Nuclear Island Facilities. Such excavation will require ripping or minor amounts of explosives. Upon reaching the final excavation levels, all excavations will be cleaned of any loose materials, by either removal or compaction in place. All final subgrades will be inspected and approved prior to being covered by backfill or concrete. The inspection and approval procedure(s) will be addressed in the foundation and earthwork specifications that will be developed during the detailed design stage of the project. These specifications will include measures, such as proof-rolling, excavation and replacement of unsuitable soils, and protection of surfaces from deterioration.

2.5.4.5.5 Monitoring and Quality Control

Monitoring program specifications will be developed during the detailed design stage of the project. The specification document will address issues, such as the installation of a sufficient quantity of instruments in the excavation zone, monitoring and recording frequency, and evaluation of the magnitude of settlement during excavations and foundation construction.

2.5.4.6 Groundwater Conditions

Details of available ground water conditions at the site are given in Section 2.4.12. At the site, the Glacial Overburden is the aquifer that has a direct influence on the foundation of the proposed facilities. The Glacial Overburden aquifer unit includes all of the glacial outwash, kame, kame terrace, till, colluvium, alluvium, and other unconsolidated surficial deposits that overlie the bedrock, are saturated, and transmit groundwater.

Based on groundwater elevation data measured between October 2007 and September 2008, the shallow (surficial) groundwater level in the powerblock area ranges from approximately elevation 655 ft (199.7 m) to elevation 661 ft (202 m), with an average elevation of approximately 658 ft (200.6 m). The adopted design ground water elevation in the geotechnical calculations is 659.0 ft (200.9 m). This value is bounded by the U.S. EPR FSAR value, since plant grade is placed at elevation 674.0 ft (205.5 m). The shallow groundwater levels have been accounted for in the analyses of the stability of foundations. During construction, dewatering along with site grading and excavation plans will divert flows away from excavations.

Sections 2.5.4.6.1 through 2.5.4.6.4 are added as a supplement to U.S. EPR FSAR.

© 2007-2012 UniStar Nuclear Services, LLC. All rights reserved.
COPYRIGHT PROTECTED

2.5.4.6.1 Dewatering During Construction

An active construction dewatering system will be implemented prior to construction to maintain the site conditions dry. The system will continue to operate until the subgrade portions for the structures are completed and the excavation is backfilled. The dewatering system will be decommissioned as the structures are completed and the backfill is placed to establish the final grade. Detailed descriptions of the hydrogeologic conditions are presented in Section 2.4.12.

Prior to initiating dewatering activities, preparations must be made to receive the water discharged from the excavation. Effluent from the dewatering system will be routed through a storm water pond which will be used during plant operation as the detention pond for the plant storm runoff. Thus, it would be beneficial to construct this pond prior to excavation activities in order to use it as a collection area for the dewatering system.

The power block excavation is expected to fully penetrate the glacial soils and the upper weathered bedrock to expose the bearing surface. The depth of excavation in the vicinity of the NI will exceed depths of 60 ft (18.3 m) (from existing grades) through saturated granular deposits. Figure 2.5-160 and Figure 2.5-161 depict cross sections of the excavations in the NI area.

For the ESWEMS pump house and the ESWEMS Retention Pond, the excavation will extend from the current ground surface (about 680 ft (207 m) to at least elevation 640 ft (195 m)) and will terminate at the top of bedrock or well graded gravels, cobbles or shale depending upon the location. This excavation will extend through soils that are generally water bearing granular glacial deposits.

To facilitate quality construction methods in the NI and ESWEMS areas, the excavations should be performed in a dry condition with conventional construction equipment. Given the layout of these areas, a common dewatering system consisting of deep wells surrounding the excavations is designed to facilitate both excavation areas. These excavations can proceed as the dewatering takes place provided the dewatering system maintains the groundwater level below that of the excavations. As the excavation advances, a series of groundwater monitoring wells will be observed to verify the effectiveness of the dewatering system in reducing the groundwater level.

The dewatering system will consist of deep wells penetrating the glacial overburden soils down to the top of the bedrock. The radius of influence of dewatering wells for the NI and the ESWEMS could extend out more than 3,000 ft (915 m) with anticipated drawdown of 20 ft (6.1 m) to 30 ft (9.1 m) being experienced some distance away from the wells if no flow barrier is utilized. This would incur a large impact on the nearby wetlands, flow in Walker Run, and potentially affect (and possibly dry up) any nearby domestic or commercial water wells within the radius of influence of the dewatering activity. Some of the nearby wetlands would most likely dry up as well. To avoid these negative impacts, a flow barrier, such as a soil-bentonite slurry wall, will be implemented around the NI and ESWEMS excavation. This will reduce the drawdown effect of the dewatering wells, since the wells would be located within the limits of the flow barrier. The flow barrier would be installed by keying it into the underlying bedrock. The minimum design permeability of the flow barrier is 1×10^{-7} cm/s (3×10^{-10} ft/s) with an approximate thickness of 3 ft (0.9 m).

Approximately 30 deep wells will be required to maintain a dry condition at the bottom of the excavation. If a build-up of groundwater occurs on the north side of the NI excavation or

© 2007-2012 UniStar Nuclear Services, LLC. All rights reserved.
COPYRIGHT PROTECTED

extreme levels of seepage are encountered, additional pumping wells can be integrated into the system.

There is potential for some water seepage through the bedrock in the bottom of the excavation. Trenches and ditches will be required in the bottom of the excavation to direct any up flow through the rock away from the center of the excavation to the perimeter ditches. Sumps and pumps will be utilized to remove this water from the excavation.

The water removed from the excavation is likely suitable for reuse as dust control, soil compaction, and concrete mixing based on the available water quality information. Chemical testing of the water will be required if it is to be used for concrete mixing. The existing monitoring wells within the NI and ESWEMS excavation limits should be utilized to monitor the effectiveness of the flow barrier. Additional monitoring wells will be installed to provide adequate monitoring on all four sides of the excavation. The monitoring program should include recording water levels on both the inside and outside of the flow barrier.

2.5.4.6.2 Analysis and Interpretation of Seepage

Analysis of the groundwater conditions at the site is described in Section 2.4.12. A groundwater model, based on information currently available, has been prepared for the overall groundwater conditions at the site and is addressed in detail in Section 2.4.12.

2.5.4.6.3 Permeability Testing

Evaluation of permeability of the site soils was performed with lab testing of Shelby-tube samples obtained in shallow soils above the Glacial Overburden aquifer. Slug and pumping tests were performed on screened monitoring wells. A detailed description of the tests and results are provided in Section 2.4.12.

2.5.4.6.4 History of Groundwater Fluctuations

A detailed discussion of the groundwater conditions is provided in Section 2.4.12.

2.5.4.7 Response of Soil and Rock to Dynamic Loading

The Safe Shutdown Earthquake (SSE) spectra and its specific location at a free ground surface reflect the seismic hazard in terms of Probabilistic Seismic Hazard Analysis (PSHA) and geologic characteristics of the site and represent the site-specific ground motion response spectrum. These spectra would be expected to be modified as appropriate to develop ground motion for design considerations. Detailed descriptions on response of site soils and rocks to dynamic loading are addressed in Section 2.5.2.

Sections 2.5.4.7.1 through 2.5.4.7.6 are added as a supplement to the U.S. EPR FSAR.

2.5.4.7.1 Seismic History

The seismic history of the area and the site, including any prior history of seismicity, evidence of liquefaction or boils, is addressed in Section 2.5.1.1 and Section 2.5.1.2.

2.5.4.7.2 Field Dynamic Measurements

The following techniques were used to measure field dynamic properties:

- P-S suspension logging surveys in 4 borings ranging in depth from about 200 to 400 ft (60 to 120 m) below ground surface, including overburden soil and rock.

© 2007-2012 UniStar Nuclear Services, LLC. All rights reserved.
COPYRIGHT PROTECTED

- Downhole seismic velocity surveys in 4 borings ranging in depth from about 200 to 400 ft (60 to 120 m) below ground surface, including overburden soil and rock.
- Seismic refraction surveys were performed along 6 profile lines.
- Geophysical testing borehole locations are shown on Figure 2.5-129. The results for each of the tests are shown in Figure 2.5-144 through Figure 2.5-147.

Data obtained from borehole survey techniques were integrated for development of the site velocity profiles. Each borehole velocity profile was evaluated and compared against the stratigraphic logging and laboratory test data of borehole samples to correlate velocities with soil and rock types by elevation and corresponding depth below ground surface. After each individual borehole velocity data set was evaluated, borehole profiles were grouped based on site-specific location and were compiled using a common reference point (elevation or depth below ground surface).

2.5.4.7.3 Dynamic Laboratory Testing

Dynamic testing, consisting of RCTS and FF tests, to obtain data on shear modulus and damping characteristics of rocks, is described by Section 2.5.4.2.3.2.9.

2.5.4.7.4 Recommended Soil Profile

The Uniform Hazard Spectra (UHS) described in Section 2.5.2 are defined on hard rock, which is located 300 to 350 ft (91 to 107 m) below the ground surface at the BBNPP site. This location was confirmed with shear wave velocity measurements above the 9200 ft/sec (2800 m/sec) threshold. To determine the dynamic motion at the ground surface, it was necessary to adjust the UHS for amplification or de-amplification as the vibratory ground motion propagated through the rock and soil media. The adjustment was made by conducting Site Response Analyses following Approach 2B described in NUREG-6728 (NRC, 2001). These analyses consist of defining the shear wave velocity and material damping characteristics in the soil and rock profile between the ground surface and the depth of hard rock, and then conducting site response studies using a one-dimensional, equivalent linear computer code: SHAKE (Schnabel, 1972).

The NI foundation material is the Mahantango Formation which has a shear-wave velocity of approximately 6,800 ft/sec (2070 m/sec). Consequently, the site amplification to define the GMRS for the BBNPP Site is computed at the top of the Mahantango Formation layer. For the NI, the GMRS corresponds to its FIRS.

The Subsurface Investigation at the BBNPP site included extensive Boring and Geophysical Exploration Programs. The field data available are divided into three sets:

1. Shear-wave velocities,

2. Compressional wave velocities, and

3. Layer thickness.

Six seismic refraction lines were concentrated near the center of the NI Reactor Building. The spatial variability of geotechnical properties along the site was investigated through the boring program, the point geophysical measurements (P-S Suspension and Downhole), and the surface measurements (Refraction). The stratigraphy, layer notation and layer thickness are

© 2007-2012 UniStar Nuclear Services, LLC. All rights reserved.
COPYRIGHT PROTECTED

taken from the geotechnical boring logs. The results from the geophysical investigations are provided in Section 2.5.4.2.2.2.3.

The following steps have been used to develop the best estimate of the compression and shear-wave velocity profiles for the BBNPP site:

- The P-S Suspension Logging Data from B-301 is more reliable since the borehole remained uncased which is the preferred configuration for the methodology, thus suspension logging data from G-301 is discarded at any depth where data from B-301 is available;
- Downhole data is more representative of the elastic properties under the frequency range imposed by seismic ground motion. A higher weight (at least 60 to 65 percent) is given to the downhole than to the measurements closer to the surface;
- As readings get deeper, the P-S Suspension data becomes more reliable since it does not depend on interpretation as much as the downhole data does. Since P-S Suspension data is consistently higher, the shear wave velocity is taken as the average of both methods;
- Closer to the surface, the only P-S Suspension Data available is from borehole G-301. At B-301, there was metal casing left at the hole to support the overburden soils and downhole readings with metal casing are not reliable. The most reliable data within the overburden soils is the one from the downhole and P-S Suspension Tests at G-301;
- Lower bound and upper bound estimates are determined by analyzing the spread in the data through a standard deviation. The standard deviation is obtained by grouping readings from similar formations;
- The best estimate is built using the results from the field tests along with engineering judgment and general knowledge gathered from the field conditions and the borehole conditions.
- Damping is established based on lower bound of rock dynamic testing results.
- Due to liquefaction concerns, overburden soils will be replaced by either engineered soil fills or concrete fills.
- A 7 percent to 17 percent Coefficient of Variation is used to provide an estimate of the upper and lower bound. The actual lower and upper bound used for the Soil Structure Interaction Analysis will be a product of the randomization process of the Site Amplification Analysis. The COV is determined by analyzing the spread in data from the mean and the standard deviation.

Dynamic Parameters of Concrete Fill

A concrete fill is placed between the foundation mat of the NI and the top of rock. The dynamic properties of the fill are determined as follows:

- Match the shear modulus of the concrete to the best estimate of the underlying rock;
- Back calculate the shear modulus and elastic modulus with the use of equations from elasticity;

© 2007-2012 UniStar Nuclear Services, LLC. All rights reserved.
COPYRIGHT PROTECTED

- Back calculate the compressive strength of concrete (f'c, ACI-318 (ACI, 2005))

The shear wave velocity assigned to the concrete fill is 7240 fps (2200 m/s), the unit weight is 150 pcf (23.6 kN/m^3), and the Poisso'n Ratio is 0.2. These parameters are indicated by Table 2.5-51.

Fill and Backfill Dynamic Parameters

Table 2.5-51 provides the dynamic properties assigned to the fill and backfill materials. These properties are not used for the calculation of the GMRS for the NI. When the GMRS are determined as free-field outcrop motions on the uppermost in-situ competent material, only the effects of the materials below this elevation are included in the site response analysis. Therefore, the engineered fill around the structure is not accounted for.

Compliant base

Regulatory Guide 1.208 (NRC, 2007b) defines "Hard Rock" as materials with a shear-wave velocity of 9,200 ft/sec (2,800 m/sec) or higher. Site amplification models need to include the soil and soft rock materials down to a rock formation with a minimum shear-wave velocity of 9,200 ft/sec (2,800 m/sec). The BBNPP Subsurface Exploration Program (Figure 2.5-129) included deep borings with depths of 400 ft (122 m). At depths of about 300 ft (91 m), the geophysical measurements consistently provided measurements in the excess of 9200 ft/sec (2800 m/sec). For the NI amplification model, the base of the foundation is placed 36 ft (11 ft) below grade. The grade elevation is raised 8 ft (2.4 m) due to flooding levels and the compliant base is placed at a distance of 240 ft (73 m) below the position of the foundation mat.

Strain Dependant and Linear Properties

Resonant Column, Torsional Shear, Combined Resonant Column Torsional Shear, and Unconfined Resonant Column ("Free-Free") Laboratory Tests were performed on soil and rock samples. The complete set of results from these tests is reported in Section 2.5.4.2. To account for variations in shear-wave velocity across the site, 60 artificial profiles were generated. The procedures and methodologies to incorporate uncertainties of strain dependant properties are described in Section 2.5.2.5.1.3.

2.5.4.7.5 Amplification Functions

A site amplification analysis was performed to obtain the ground motion response parameters. Section 2.5.2.5.1 provides the amplification functions. Different amplification values are obtained at different elevations and at different locations throughout the power block footprint. The variation in elevation (depth) is due to the soil amplification phenomena related to the travel of vertically propagated seismic shear waves. The variation of the amplification values in location across the site is due to the variation of the depth to bedrock. This variation implies the existence of a different soil column that depends on the specific location of a given facility. Several cases were analyzed as part of a Foundation Input Response Spectra (FIRS) study. The resulting Peak Ground Acceleration (PGA) for these cases is provided by Table 2.5-52. The selection of earthquake coefficients for the analysis of lateral earth pressures, slope stability, and other small building facilities may be obtained from the FIRS analysis (Table 2.5-52).

© 2007-2012 UniStar Nuclear Services, LLC. All rights reserved.
COPYRIGHT PROTECTED

2.5.4.7.6 Acceleration Time History for Soil-Structure Interaction

A spectrum-compatible acceleration-time history was developed for use with the velocity profile described in Section 2.5.4.7.4. This acceleration-time history was chosen based on the probabilistic seismic hazard de-aggregation information described in Section 2.5.2.

The development of the single horizontal component spectrum-compatible time history is based on the mean 10^{-4} uniform hazard target spectrum described in Section 2.5.2. The spectrum compatible time history was developed for the frequency range of 100 Hz to 0.5 Hz.

Using the site-specific soil column extended to the ground surface including the amplification factor, and the performance-based hazard methodology utilized to develop the SSE (refer to Sections 2.5.2.5 and 2.5.2.6), a Ground Motion Response Spectra (GMRS) peak ground acceleration of 0.21g at the top of the Mahantango Formation was computed. These parameters apply to analysis of interaction of soils with structures. For reconciliation of site specific design parameters affecting the SSE analysis results, refer to Sections 3.7.1 and 3.7.2.

2.5.4.8 Liquefaction Potential

The potential for soil liquefaction at the Bell Bend Nuclear Power Plant site was evaluated following NRC Regulatory Guide 1.198 (NRC, 2003c). The soil properties and profiles utilized are those described in Section 2.5.4.2.

Section 2.5.4.8.1 and Section 2.5.4.8.2 are added as a supplement to the U.S. EPR FSAR.

2.5.4.8.1 Regulatory Guide 1.198

Regulatory Guide 1.198, Procedures and Criteria for Assessing Seismic Soil Liquefaction at Nuclear Power Plant Sites, (NRC, 2003c) was used for the evaluation of the potential for soil liquefaction at the BBNPP site.

Under "Screening Techniques for Evaluation of Liquefaction Potential," NRC Regulatory Guide 1.198 (NRC, 2003c) lists the most commonly observed liquefiable soils as fluvial-alluvial deposits, eolian sands and silts, beach sands, reclaimed land, and uncompacted hydraulic fills. The liquefaction evaluation included all soils at the BBNPP site. NRC Regulatory Guide 1.198 (NRC, 2003c) indicates that clay to silt, silty clay to clayey sand, or silty gravel to clayey gravel soils can be considered potentially liquefiable. The geology at the BBNPP site includes glacial overburden soils that consist of wind deposited and glacial transported sands and boulders. These soils will not be used for foundation purposes and are classified as liquefiable due to the presence of loose sand pockets that returned extremely low blow counts. NRC Regulatory Guide 1.198 (NRC, 2003c) indicates that if the geologic site evaluation indicates the presence of potentially liquefiable soils, the resistance of these soils to liquefaction or significant strength loss to cyclic pore pressure generation should be evaluated. The liquefaction evaluation (Section 2.5.4.8.2) indicates that some zones at the BBNPP site are susceptible to liquefaction. Residual shear strength is not evaluated since these soils will be removed from the site and will not be used for the foundation of the facilities.

2.5.4.8.2 Liquefaction Analysis

The in-situ, overburden soils will not be directly used for the foundation of Safety Related Facilities. Even though recorded shear wave velocities were in the excess of 1000 fps (305 m/s), the liquefaction potential evaluation identified "pockets" or zones of loose sand with extremely low blow counts. These zones appear in the south side of the power block area, where the depth to rock is the largest.

© 2007-2012 UniStar Nuclear Services, LLC. All rights reserved.
COPYRIGHT PROTECTED

Assessments of liquefaction for the BBNPP site were based on observations and conclusions from the filed investigation. The NI structures will be built on top of the Mahantango formation. Shallow foundations for other Category I and non-Category I Power Block structures are to be founded on concrete or structural fill.

Based on the information obtained during the investigations of the underlying soil encountered at the BBNPP site, an evaluation of the soil liquefaction potential was performed using the screening techniques proposed in the Regulatory Guide 1.198 (NRC, 2003c).

More than 500 samples of the 48 borings at different depths, from 7 ft to 405 ft (2 m to 123 m), were used in the evaluation.

The guidelines proposed by Youd (Youd, 2001) were followed in the evaluation. The factor of safety against liquefaction is determined by Equation 2.5.4-9

$$FS = \left(\frac{CRR_{7.5}}{CSR} \right) MSF \cdot K_{\sigma} \cdot K_{\alpha} \qquad \text{Eq. 2.5.4-9}$$

$CRR_{7.5}$ → Cyclic Resistance Ratio for a 7.5 Magnitude Earthquake,

CSR → Cyclic Stress Ratio,

MSF → Magnitude Scaling Factor for a different magnitude earthquake,

K_{σ} → Confining Stress Correction Factor,

K_{α} → Sloping Ground Correction Factor,

The CSR is provided by Equation 2.5.4-10

$$CSR = 0.65(a_{max}) \left(\frac{\sigma_{vo}}{\sigma'_{vo}} \right) r_d \qquad \text{Eq. 2.5.4-10}$$

a_{max} → Peak horizontal ground acceleration (0.25 g at BBNPP)

σ_{vo} → Total vertical stress

σ'_{vo} → Effective vertical stress

r_d → Stress reduction coefficient (flexibility of soil profile)

The estimation of the Peak Ground Acceleration (PGA) should correspond to the maximum amplified acceleration at the point of the liquefaction assessment. For the purpose of the liquefaction evaluation, a PGA equal to 0.25 g is used. This value is obtained from the maximum amplified Ground Motion Response Spectra (GMRS). The GMRS PGA of 0.21 g (top of rock condition) and the maximum amplified value, obtained during the Foundation Input Response analysis of the south facilities (i.e., ESWS Cooling Towers (3URB and 4URB) and Emergency Power Generating Building (34UBP) located south of the reactor building) is 0.24g. Refer to Section 2.5.2 for GMRS parameters.

Two criteria are applicable to evaluate the Cyclic Resistance Ratio (CRR):

1. Shear Wave Velocity Criterion

© 2007-2012 UniStar Nuclear Services, LLC. All rights reserved.
COPYRIGHT PROTECTED

2. Standard Penetration Resistance

2.5.4.8.2.1 Shear Wave Velocity Criterion for Liquefaction Analysis

The Shear Wave Velocity criterion uses the shear wave velocity of the soils to provide a reasonable estimate of the CRR. Disadvantages of the shear wave velocity method are that no samples are extracted and that thin liquefiable layers may be undetected. Another disadvantage is that there is usually limited number of measurements at a site and a specific location with liquefaction potential might be left undetected.

The CRR is determined from Equation 2.5.4-11

$$CRR = a\left(\frac{V_{s1}}{100}\right)^2 + b\left(\frac{1}{V_{s1}^* - V_{s1}} - \frac{1}{V_{s1}^*}\right);\ V_{s1} = V_s\left(\frac{P_a}{\sigma'_{vo}}\right)^{0.25} \quad ; \quad V_{s1} \le V_{s1}^* \qquad \text{Eq. 2.5.4-11}$$

CRR → Cyclic Resistance Ratio,

a → Curve fitting parameter (0.022),

b → Curve fitting parameter (2.8),

V_{s1} → Shear wave velocity with correction for overburden stress,

V_{s1}^* → Limiting shear wave velocity,

P_a → Atmospheric Pressure,

σ'_{vo} → Effective vertical stress.

The limiting shear wave velocity varies between 656 fps (200 m/s) for soils with 35 percent fine content and 705 fps (215 m/s) for soils with fines content of 5 percent or less. A value of 690 fps (210 m/s) was used for the evaluation. The potential for liquefaction is analyzed by plotting the CRR against the corrected shear wave velocity and comparing against a curve that represents the onset of liquefaction (Youd, 2001). The plot is provided by Figure 2.5-163. The BBNPP data points are clearly away from the liquefaction zone. The minimum Factor of Safety against liquefaction is 1.7 and it is possible to conclude that, according to the shear wave velocity method, there is no potential for liquefaction at the site. However, as previously stated, one of the disadvantages of this methodology is the limited number of measurements and this is the case at the BBNPP site. Therefore, an SPT analysis approach is required.

2.5.4.8.2.2 SPT Criteria for Liquefaction Analysis

The SPT data was used to estimate liquefaction potential. The abundant amount of gravels and boulders encountered during the investigation may reduce the effectiveness of the SPT method. However, it is the best means to detect liquefiable sand pockets. With this method, the CRR is calculated as follows:

$$CRR_{7.5} = \frac{1}{32 - (N_1)_{60}} + \frac{(N_1)_{60}}{135} + \frac{50}{\left(10 \cdot (N_1)_{60} + 45\right)^2} - \frac{1}{200} \quad ; \quad (N_1)_{60} < 30 \qquad \text{Eq. 2.5.4-12}$$

where $(N1)_{60}$ is the drill rod energy ratio divided by 60.

© 2007-2012 UniStar Nuclear Services, LLC. All rights reserved.
COPYRIGHT PROTECTED

If $(N1)_{60}$ is greater than 30, the soil is considered to be non-liquefiable. $(N1)_{60}$ is calculated by dividing the drill rod energy ratio by 60. The lowest energy ratio recorded at the field from hammer calibration was 78 percent. This value is used to determine $(N1)_{60}$ from the raw blow counts.

Figure 2.5-164 provides the results of the SPT liquefaction analysis. Each sample data point is categorized as liquefied, non-liquefied, or in the fringe of liquefaction. It is worth noting that some instances registered zero blow counts, meaning that the weight of the hammer and the drilling rod was enough to penetrate the soil. These zones correspond to areas of wind deposited sands placed during the coldest period of the glacial event. Figure 2.5-164 provides a diagram of the location of the liquefiable zones. The depth of these zones is variable, ranging in depth from 10 ft (3 m) to 45 ft (14 m). The location of the loose sand pockets is shown in section view by Figure 2.5-131 through Figure 2.5-134.

Based on the SPT analysis, it is concluded that the "In-Situ" overburden soils at the BBNPP site are prone to liquefaction. Since the overburden soil was determined to be liquefiable using SPT data, the lack of CPT data is not an issue.

2.5.4.8.2.3 Liquefaction Analysis - Conclusion

Regardless of the high shear wave velocity of the Glacial Overburden, these soils will be removed from the site and will not be used in their natural condition for foundation or lateral support. The soils from this formation are candidates for engineered fill or backfill through enforcement of appropriate screening and compaction techniques.

Section 2.5.4.5 describes material specifications and compaction for structural fill and backfill. For foundation backfill, compaction will be done to 90 percent of Modified Proctor optimum dry density. For structural fill, a 95 percent Modified Proctor level will be set. The fill will be compacted to within 3 percent of its optimum moisture content.

Liquefaction in engineered fill is not an issue if the recommended compaction practices are followed. Liquefaction occurs in loose sands and/or silts with poor gradation. An engineered fill is a compacted and well graded soil structure. Compaction practices need to be monitored during construction.

Liquefaction of granular engineered fills will be prevented by assuring that the fill and backfill specifications are met during the implementation stages. Particular attention will be placed on the grain size and compaction requirements to ensure the specifications are fully met. Section 2.5.4.2.3 provides information related to the specifications for engineered soils. It is emphasized that the specification will include requirements for an on-site testing laboratory for quality control, especially material gradation and plasticity characteristics, the achievement of specified moisture-density criteria, fill placement/compaction, and other requirements to ensure that the fill operations conform to the earthwork specification for BBNPP.

2.5.4.9 Earthquake Site Characteristics

Section 2.5.2.6 describes the development of the Safe Shutdown Earthquake ground motion for the BBNPP site. The selected ground motion is based on the risk-consistent/ performance-based approach of NRC Regulatory Guide 1.208, "A Performance-Based Approach to Define the Site-Specific Earthquake Ground Motion" (NRC, 2007b) with reference to NUREG/CR-6728 (NRC, 2001) and ASCE/SEI 43-05 (ASCE, 2005). Any deviation from the guidance provided in Regulatory Guide 1.208 is discussed in Section 2.5.2. Horizontal ground motion amplification factors are developed in Section 2.5.2.5 using site-specific data and

© 2007-2012 UniStar Nuclear Services, LLC. All rights reserved.
COPYRIGHT PROTECTED

estimates of near-surface soil and rock properties presented in Sections 2.5.4.2, 2.5.4.4 and 2.5.4.7. These amplification factors are then used to scale the hard rock spectra, presented in Section 2.5.4.2, to develop Uniform Hazard Spectra (UHS), accounting for site-specific conditions using Approach 2B of NUREG/CR-6769 (NRC, 2002). Horizontal SSE spectra are developed from these soil UHS, using the performance-based approach of ASCE/SEI 43-05, accepted by Regulatory Guide 1.208. The Ground Motion Response Spectra (GMRS) is defined at the free ground surface of a hypothetical outcrop at the base of the foundation. Section 2.5.2.6 also describes vertical ground motion, which was developed by scaling the horizontal spectrum by a frequency-dependent vertical-to-horizontal (V:H) factor.

2.5.4.10 Static Stability

The area of planned BBNPP is graded to establish the final site elevation, which is to be at elevation 674 ft msl (205 m msl) at the center of the reactor building. The Reactor, Safeguard, and Fuel Buildings are seismic Category I structures and are supported on a common basemat. The common basemat has an irregular shape, estimated to be approximately 80,170 ft^2, (7450 m^2) in plan. All Category I structures' size and depth ranges are summarized in Table 2.5-55.

Structure locations and designations are shown in Figure 2.5-129. Other major structures in the power block area are the Nuclear Auxiliary Building, RadWaste Building, and the Turbine Building, which are non-Category I structures.

Construction of the Nuclear Island basemat requires an excavation of about 39 ft (12 m) from the existing elevation of approximate elevation 667 ft (203 m) msl. No rebound (heave) in the ground due to the removal of the soils is expected at the Mahantango Formation. The Manhantango rock is extremely dense and was heavily consolidated by marine deposition. The removal of overburden soils will have no effect since the elastic modulus of the rock is very high.}

2.5.4.10.1 Bearing Capacity

The U.S. EPR FSAR includes the following COL Item in Section 2.5.4.10.1:

> A COL applicant that references the U.S. EPR design certification will verify that site-specific foundation soils beneath the foundation basemats of Seismic Category I structures have the capacity to support the bearing pressure with a factor of safety of 3.0 under static conditions, or 2.0 under dynamic conditions, whichever is greater.

This COL Item is addressed as follows:

{The bearing capacity of the subsurface materials depends (1) on the properties of the foundation soils or rocks, including dimensions of bearing strata and geotechnical strength parameters, (2) on the geometry of the building foundations, (3) on the foundation depth, and (4) on the position of the water table, in case drained conditions are assumed for the calculations. Geotechnical properties and soil profiles are detailed in Section 2.5.4.2. The foundation depth and building geometry are provided in Section 2.5.4.3, and particularly in Table 2.5-55 The bearing capacity estimates for the Mahantango Formation are determined with the use of a rock mass equivalent cohesion and friction. The upper bound of the ultimate bearing capacity of structures placed on top of concrete is set at the compressive strength of concrete. If the bearing capacity of rock is higher than this threshold, then the concrete compressive strength is used as the recommended value. The bearing capacities from either concrete or bedrock are very high and they conservatively exceed the minimum requirements

© 2007-2012 UniStar Nuclear Services, LLC. All rights reserved.
COPYRIGHT PROTECTED

established by the U.S. EPR FSAR. Section 2.5.4.10 details the methodologies used to obtain bearing capacity and settlement according to the reference documents. Table 5.0-1 of the U.S. EPR FSAR identifies the soil bearing capacity as a required parameter to be enveloped. It is defined as "Minimum bearing capacity (static) 22 ksf in localized areas at the bottom of the Nuclear Island basemat and 15 ksf on average across the total area of the bottom of the Nuclear Island basemat." Accordingly, the Seismic Category I NI foundation is sized and reinforced to accommodate these bearing pressure values. Other facilities are placed directly on top of engineered backfill. In this case, the bearing capacity estimate is determined using drained conditions with a high water level at the elevation of the Probable Maximum Flood of 671 ft (205 m) msl.

The bearing capacity for the NI is estimated assuming that the foundation stratum is a homogenous layer with the properties of the Mahantango Formation. The backfill unit weight of 140 pcf (22.0 kN/m^3) is used to calculate the embedment contribution to a depth of 36.0 ft (12 m). Other facilities have their foundation base resting on engineered backfill. A friction angle of 35^o is assumed with no cohesion.

The ultimate (gross) bearing capacity is estimated by the Terzaghi theory (ASCE, 1994a) using the Vesic capacity factors (Vesic, 1975).

$$q_{ult} = CN_cS_c + \gamma' D_f N_q S_q + \frac{1}{2}\gamma' B N_\gamma S_\gamma \qquad \text{Eq. 2.5.4-13}$$

C	→	Cohesion,
γ'	→	Effective unit weight of soil,
D_f	→	Depth to calculate effective overburden pressure at base of foundation,
B	→	Width of foundation,
N_c, N_q, N_γ	→	Bearing capacity factors (defined in Vesic, 1975),
S_c, S_q, S_γ	→	Shape factors (defined in Vesic, 1975).

The subsurface conditions and material properties were described in Section 2.5.4.2. Material properties, conservatively designated for the various strata, were used for foundation evaluation, as shown by the recommended strength parameters shown on Table 2.5-47. A summary of the estimated allowable bearing pressures are presented in Table 2.5-57. A factor of safety of 3.0 was applied to obtain the allowable values.

Design values of foundation pressures for the other Category I structures were estimated based on project knowledge. For the BBNPP site-specific conditions, the calculated allowable bearing pressures for the NI meet the minimum 22 ksf and the average 15 ksf identifed in the U.S. EPR FSAR. The site-specific foundation soils beneath the NI basemat and other safety class facilities have been verified to have the capacity to support the required bearing pressures with a Factor of Safety of 3.0 under static conditions and a Factor of Safety of 2.0 under dynamic conditions.}

2.5.4.10.2 Settlement

The U.S. EPR FSAR includes the following COL Items in Section 2.5.4.10.2:

> A COL applicant that references the U.S. EPR design certification will provide an assessment of predicted settlement values across the basemat of Seismic Category I structures during and post construction. The assessment will address both short term (elastic) and long term (heave and consolidation) settlement effects with the

© 2007-2012 UniStar Nuclear Services, LLC. All rights reserved.
COPYRIGHT PROTECTED

site specific soil parameters, including the soil loading effects from adjacent structures.

A COL applicant that references the U.S. EPR design certification will verify that the predicted tilt settlement value of ½ inch per 50 ft in any direction across the foundation basemat of a Seismic Category I structure is not exceeded. Settlement values larger than this may be demonstrated acceptable by performing additional site specific evaluations.

These COL Items are addressed as follows:

{This COL Item is addressed in the following section and in Section 3.8.5.

The safety-related Category I facilities at the BBNPP site will bear either on top of the Mahantango Formation or on top of concrete or engineered soil fill, which in turn bears directly on top of the bedrock. The overburden deposits will not be used for foundation purposes as these have an inherent risk for liquefaction. Elastic short term settlements will occur in either the Mahantango formation or the concrete or engineered fill.

SETTLEMENT ESTIMATION BY SIMPLIFIED METHODS

Three of the ASCE (ASCE, 1994b) recommended methods of analysis were used to estimate settlements:

1. Improved Janbu Approximation - Provides an average estimate of the settlement beneath the foundation. Settlement is estimated using Eq. 2.5.4-14.

$$\rho_i = \mu_o \cdot \mu_1 \cdot \frac{q \cdot B}{E_s^*} \qquad \text{Eq. 2.5.4-14}$$

ρ_i → Settlement,

μ_o → Embedment adjustment coefficient,

μ_o → Shape Adjustment Coefficient,

q → Service pressure load,

B → Foundation width,

E_s^* → Equivalent Young's Modulus.

2. Perloff Approximation - Provides settlement at both center and edge of the foundation. This methodology is useful to analyze differential displacements. Settlement is estimated using Eq. 2.5.4-15.

© 2007-2012 UniStar Nuclear Services, LLC. All rights reserved.
COPYRIGHT PROTECTED

$$\rho_i = I \cdot q \cdot B\left(\frac{1-\nu^2}{E_s}\right) \qquad \text{Eq. 2.5.4-15}$$

ρ_i → Settlement,

I → Stress influence factor at either depth or edge of foundation

q → Service pressure load,

B → Foundation width,

ν → Poisson Ratio,

E_s → Young's Modulus.

3. Kay and Cavagnaro Approach - This approach can adapt to layers of variable elastic properties, and provides settlements at both center and edge of the foundation. It is based on these same principles, as reflected in Eq. 2.5.4-15.

Settlement estimates utilizing the three simplified methods above have been calculated for each of the facilities listed in Table 2.5-58. The adopted elastic modulus is the lesser of that recommended for the Mahantango Formation or the one recommended for the engineered fill. This recommendation is provided by Table 2.5-49. Table 2.5-58 provides the settlement estimates at the site, obtained from the three noted methodologies. Overall, the results indicate very limited to no settlement for the NI and the safety related structures. The load used for the calculation is a U.S. EPR FSAR recommended service pressure of 14 ksf (670 kPa). A more detailed analysis methodology was performed to estimate settlements. The procedure and results are provided by the following section.

SETTLEMENT ESTIMATES FOR THE NI FROM DETAILED ANALYSIS

A detailed analysis was used to evaluate the foundation mat displacements and rotations for the NI Buildings due to potential elastic settlements of the subgrade soils. The loads assigned are different for each area of the NI, according to the [specifications described in the U.S. EPR FSAR. Section 2.5.4.10 details the methodologies used to obtain bearing capacity and settlement according to the reference documents. The calculations are performed assuming a 10 ft (3 m) concrete layer over a 200 ft (61 m) compressible layer with the properties of the Mahantango Formation. The methodology utilized here quantifies the settlements, foundation mat displacements and rotation associated with the proposed site specific subsurface profile.

The first part of the evaluation estimates elastic settlements due to the total construction loads of the Nuclear Island Buildings: Reactor (UJA), Fuel Building (UFA) and four Safeguard Buildings (UJH).

The settlement analysis performs the calculations for two cases: (1) assuming a rigid foundation and (2) a flexible foundation (i.e., the foundation mat which imposes the loads to the foundation medium has no stiffness). The first assumption is more representative of the real conditions. Settlements that are reported correspond to the top of the firm incompressible layer beneath the rock formation (interface between the foundation mat and the sub-laying soft rock) for the rigid foundation case. In the second part of the evaluation, the

© 2007-2012 UniStar Nuclear Services, LLC. All rights reserved.
COPYRIGHT PROTECTED

surface settlements are used to compute equivalent Winkler springs representing the deformation characteristics of the subsurface.

The Winkler springs are incorporated into a three-dimensional structural finite element analysis which assumes a rigid foundation mat for each of the buildings included in the analysis. This analysis uses applied loads on the foundation and calculates the foundation mat deformations. Because the settlements estimated in the first step and, consequently, the equivalent springs vary over the foundation area (soft springs at locations of large settlements and stiff springs at locations of small settlements), the structural analysis redistributes the applied loads on the foundation mat consistent with the stiffness of the mat relative to the subsurface. For example, the elastic settlements are larger near the centers of the loaded disks. Consequently, the soil springs near the center are softer than those at locations closer to the outer edge of the mat, assuming that the mat carries uniformly distributed load. Consistent with this distribution, the structural analysis redistributes the applied loads away from the center of the disks.

In an iterative procedure, the bearing pressures resulting from the structural analysis are used to recalculate the elastic settlements and the corresponding soil springs, and the structural analysis is repeated until a satisfactory agreement is obtained for average settlements.

Surface loads are applied as uniformly loaded flexible disks and the resulting stresses in the soil medium are calculated using an axisymmetric analysis. At-depth stresses are calculated for each of the profile points where settlement is desired due to each of the loaded disks, consistent with the locations of the profile points relative to the center of the disks. The stresses from each of the disks are then superimposed to compute the stresses due to the entire loaded foundation. The at-depth stresses are updated each time the cumulative load is specified.

The analysis uses a three dimensional finite element model representing the soil-structure system. The model considers a rigid plate element for the Nuclear Island base mat. The foundation medium is represented by supports with stiffness of the Winkler Soil Springs. Calculations are performed using computer codes specifically designed to calculate soil settlements (Dapset), and structural response (SAP). Dapset and SAP have been subjected to the verification and validation procedures stipulated in Rizzo's Quality Assurance Manual. Computer software control for Dapset and SAP has been done according to Rizzo’s Quality Assurance Manual. The loads used in the analysis are shown in Figure 2.5-165.

Immediate elastic settlements resulting from the applied loads at different locations across the Nuclear Island are presented in Figure 2.5-166. The differential settlement value of 0.5 in (1.3 cm) in 50 ft (15.2 m) in any direction across the basemat of a Seismic Category I structure is not exceeded.

As a result of a different load distribution among the buildings of the Nuclear Island (the Fuel Building has a bigger load than the Safeguard Buildings 2 and 3) the north-south direction of the [foundation mat presents a slight differential settlement that can be considered as negligible for practical purposes. No considerable differential settlement was observed on the east-west direction since the applied loads are practically symmetrical. As shown in Table 2.5-59, the maximum differential settlement in 50 ft (15.2 m) in any direction across the basemat is less than 0.1 in (0.3 cm).

SETTLEMENT ANALYSIS CONCLUSIONS

© 2007-2012 UniStar Nuclear Services, LLC. All rights reserved.
COPYRIGHT PROTECTED

Displacements will be immediate during and after construction of civil works. Differential settlements estimated using simplified methodologies, as opposed to the detailed analyses described in the previous section, are less than 0.1 in (0.3 cm) in 50 ft (15.2 m) in any direction across the basemat.

Settlements will take place concurrent with construction and these will have taken place prior to placing the equipment, piping, and the final finishes. Hence, post-construction total and differential settlements are expected to be lower than the values noted herein, particularly after accounting for foundation mat rigidity.

The detailed analysis yields lower settlement values since it considers a more realistic distribution load and accounts for the true stress distribution through the subsurface. The results from the detailed analysis are reported in Table 2.5-59. This table provides the best estimate for settlement at the NI.

Settlements are within tolerable thresholds and all foundations will be able to safely tolerate the anticipated total and differential settlements. Additionally, engineering measures are incorporated into design for control of differential movements between adjacent structures, piping, and appurtenances sensitive to movement, consistent with settlement estimates. This includes the development and implementation of a monitoring plan that supplies and requires evaluation of information throughout construction and post-construction on ground heave, settlement, pore water pressure, foundation pressure, building tilt, and other necessary data. This information provides a basis for comparison with design conditions and for projections of future performance.

Analysis indicates favorable conditions for total and differential settling. In order to monitor and verify settling, the BBNPP major structure foundations will be monitored for any settling movement during and after construction.}

2.5.4.10.3 Uniformity and Variability of Foundation Support Media

The U.S. EPR FSAR includes the following COL Item in Section 2.5.4.10.3:

> A COL applicant that references the U.S. EPR design certification will investigate and determine the uniformity of the soil layer(s) underlying the foundation basemats of Seismic Category I structures.

This COL Item is addressed as follows:

{Three criteria are identified in the U.S. EPR FSAR for establishing uniformity in foundation support media, namely, 1) presence of soil and rock, 2) dip angle of soil layers, and 3) shear wave velocity. Each is addressed below:

1. Foundations of all Seismic Category I structures at the BBNPP site are supported on either compacted structural fill or concrete fill which is in turn supported on bedrock. Bedrock at the site is at a depth of 12.5 ft (3.8 m) to 62.0 ft (18.9 m) below ground surface. Regardless of the variable depth to bedrock, as depicted by Figure 2.5-138, non-uniform foundation conditions resulting from combined soil-rock support are not applicable to foundations at the BBNPP site. Each of the Seismic Category 1 structures will be founded either on top of rock, on top of concrete fill, or on top of engineered fill.

© 2007-2012 UniStar Nuclear Services, LLC. All rights reserved.
COPYRIGHT PROTECTED

2. Detailed subsurface information is presented in Section 2.5.4.2. Stratigraphic profiles (presented in Figure 2.5-131 through Figure 2.5-134 of the referenced section) indicate that there is only one stratigraphic line and it corresponds to the boundary between the overburden and the Mahantango formation. In the direction of maximum gradient (approximately 30 degrees with respect to the North), this boundary presents a dipping angle of approximately seven to eight degrees. Figure 2.5-138 shows the inclination of the top surface of the Mahantango Formation. It is still applicable to assume a horizontal layered model for both Site Amplification and Soil Structure Interaction Analyses, and therefore uniform conditions are considered. Section 2.5.4.10.3, of the U.S. EPR Final Safety Analysis Report reads: "If the dip is less than or equal to 20 degrees, the layer is defined as horizontal and analyses using horizontal layers are applicable.". In addition, the concrete above the Mahantango formation will have a matching shear wave velocity and therefore the sloping effects will be mitigated. On this basis, the soil layers at the BBNPP site are considered horizontal.

3. Classification of uniformity (or non-uniformity) in foundation support media resides with the geotechnical engineer, per the U.S. EPR FSAR. Shear wave velocity (V_s) measurements are used for this determination because they are a) in-situ measurements reflecting the natural ground conditions and b) important input to the safety evaluation of structures such as in soil-structure interaction and seismic analyses.

The V_s values were evaluated to a depth of approximately 350 ft (107 m) below the Nuclear Island (NI) foundation basemat, corresponding to El. 280 ft msl (85 m msl). The 350 ft (107 m) value was selected based on the three U.S. EPR FSAR criteria of: 1) 1.5 times an equivalent radius of foundation basemat, 2) 1.0 times the maximum foundation basemat dimension, or 3) no less than 200 ft below the bottom of the foundation basemat; with criterion (2) selected as the governing condition for the BBNPP NI basemat for its greater dimension. It is noted that minor appendages and protrusions in the irregularly-shaped U.S. EPR NI foundation were ignored in selecting this depth.

Detailed V_s data are presented in Section 2.5.4.2.2, along an evaluation of the shear wave velocity conditions. Figure 2.5-144 through Figure 2.5-147 present the plots for compressional and shear wave velocities. The plots provide the results from the two different surveys performed: downhole test, and PS-Suspension Logging. Overburden soils will not be used for foundation purposes and therefore an analysis of the variation of the shear wave velocity is only applicable for the Mahantango formation.

The recommended shear wave velocity profile under the Nuclear Island is plotted by Figure 2.5-157. The shear wave velocity shows an increasing trend, directly related to depth or confining pressure. Therefore, as shown by the figure, the Mahantango formation was subdivided in sub-layers to depict the vertical variation of the shear wave velocity. The minimum value of 6800 fps (2075 m/s) was presented at the uppermost zone in the boundary with the overburden. In a distance of about 350 ft (107 m) the shear wave velocity increases up to 9600 fps (2930 m/s). At each sub-layer the Coefficient of Variation (COV) originated from different readings at different locations and with different methodologies is close to 10% and not exceeding 15%. This relatively low COV is mainly due to the homogeneity of the Mahantango formation. Variation only exists in the vertical direction and this was accounted for in the site amplification analysis by the layer subdivision of this formation. Therefore, they have been accounted for in developing the site-specific horizontal and vertical ground motion response spectra (GMRS) shown in Figure 2.5-57. The GMRS are defined at the foundation level

© 2007-2012 UniStar Nuclear Services, LLC. All rights reserved.
COPYRIGHT PROTECTED

for the U.S. EPR Nuclear Island (NI). Therefore, the GMRS coincide with the FIRS for the NI. There are no significant variations of the shear wave velocity in the horizontal directions.}

2.5.4.10.4 Site Investigation for Uniform Sites

No departures or supplements.

2.5.4.10.5 Site Investigations for Non-uniform Sites

No departures or supplements.

{Section 2.5.4.10.6 is added as a supplement to the U.S. EPR FSAR.

2.5.4.10.6 Earth Pressure

Static and seismic lateral earth pressures are addressed for plant below-ground walls. Seismic earth pressure diagrams are structure-specific and are, therefore, only addressed generically herein. Specific earth pressure diagrams are developed for specific structures based upon each structure's final configuration. Passive earth pressures are not addressed; they are ignored for conservatism for general purpose applications. Fill and backfill will be granular, compacted soils formed by sand/gravel mixtures. Typical values of the friction angle for these types of fills are in excess of 38 degrees (Carter, 1991). A friction angle is conservatively selected. Structural backfill material is verified to meet the design requirements prior to use during construction.

2.5.4.10.6.1 Static Lateral Earth Pressures

$$p_{AS} = K_{AS}\gamma z$$

The static active earth pressure, p_{AS}, is estimated using the following expression:

$$p = K \cdot \gamma \cdot z \qquad \text{Eq. 2.5.4-16}$$

- p → Active (p_a), Passive(p_p), or At Rest (p_o) Pressure,
- K → Active (K_a), Passive (K_p), or At Rest (K_o) Pressure Coefficient as defined by Section 2.5.4.5.6.
- γ → Unit weight of backfill (140 pcf),
- z → Depth below ground surface.

2.5.4.10.6.2 Dynamic Earth Pressures

The following symbols apply:

- P_{ae} -> Dynamic active earth force,
- P_{pe} -> Dynamic passive earth force,
- K_{ae} -> Dynamic active earth pressure coefficient,
- K_{pe} -> Dynamic passive earth pressure coefficient,

© 2007-2012 UniStar Nuclear Services, LLC. All rights reserved.
COPYRIGHT PROTECTED

k_h		Horizontal earthquake acceleration (0.25 g based on FIRS analysis, Section 2.5.4.7.5; the 0.25 g is selected as the best estimate of the range between the 0.21 g value at the top of rock and the 0.30 g value at the ground surface)
k_v		Vertical earthquake acceleration (0.18 g based on FIRS analysis, Section 2.5.4.7.5; the 0.25 g is selected as the best estimate of the range between the 0.18 g value at the top of rock and the 0.33 g value at the ground surface)
γ_{sat}	->	Saturated Unit Weight,
γ'	->	Effective Unit Weight,
F_r	->	Resultant force associated with dynamic soil pressure distribution,
M_r	->	Resultant overturning moment about base of retaining structure,
H	->	Embedment Height,
α_h	->	Horizontal earthquake acceleration (g),
v	->	Poisson's ratio,
C_vD_v	->	Empirical Coefficients as a function of Poisson's ratio.

The active/passive earth force on a wall (cohesionless and dry backfill) is estimated as follows:

$$P_{ae} = \frac{1}{2}\gamma K_{ae} H^2 (1 - k_v) \quad ; \quad P_{pe} = \frac{1}{2}\gamma K_{pe} H^2 (1 - k_v) \qquad \text{Eq. 2.5.4-17}$$

The total active/passive thrust, P_{ae}, can be divided into a static component, P_a, and a dynamic component, ΔP_{ae}:

$$P_{ae} = P_a + \Delta P_{ae} \quad ; \quad P_{pe} = P_a + \Delta P_{pe} \qquad \text{Eq. 2.5.4-18}$$

The static component is known to act at H/3 above the base of the wall. Seed and Whitman (Seed, 1970) recommended that the dynamic component be taken to act at approximately 0.6H. On this basis, the total active thrust will act at a height given by:

$$h = \frac{P_a H/3 + \Delta P_{ae}(0.6H)}{P_{ae}} \qquad \text{Eq. 2.5.4-19}$$

When there is no significant structure-structure interaction, a conservative estimate of dynamic soil pressures may be obtained from a parabolic distribution with a maximum value at a height of 60 to 70 percent of the total fill height (ASCE, 1998). The corresponding resultant force and overturning moment may be obtained by Eq. 2.5.4-20.

$$F_r = \alpha_h C_v \gamma H^2$$
$$Mr = \alpha_h D_v \gamma H^3 \qquad \text{Eq. 2.5.4-20}$$

© 2007-2012 UniStar Nuclear Services, LLC. All rights reserved.
COPYRIGHT PROTECTED

2.5.4.10.6.3 Sample Earth Pressure Diagrams

Using the relationship outlined above and assumed backfill properties, sample earth pressures were estimated. Sample earth pressure diagrams are provided in Figure 2.5-168 for a wall height of 40 ft (12.2 m), level ground surface, and, for conservative purposes, with groundwater level at 3.3 ft (1 m) below the surface. The backfill is a granular soil, with an angle of friction of 35 degrees and a unit weight of 140 pcf (22.4 kN/m^3). The horizontal ground acceleration is taken as 0.25g, which is the PGA at elevation 666 ft (203 m). The validity of assumptions regarding surcharge loads, backfill properties, and structural configurations is confirmed during the detailed design stage. Actual earth pressure evaluations are performed at that time for the design of below-grade walls, based on actual project conditions. The results of these earth pressure evaluations shall be included in an update to this FSAR at that time.

2.5.4.10.6.4 Selected Design Parameters

The field and laboratory test results are discussed in Section 2.5.4.2. The parameters employed for the bearing capacity, settlement, and earth pressure evaluations are based on the material characterization addressed in Section 2.5.4.2. Normal Groundwater Elevation is approximately 15 ft (4.6 m) below grade. A value of 3.0 is commonly used as the factor of safety when determining the bearing capacity of soils. An angle of shearing resistance of 35 degrees was used for characterization of a structural backfill for earth pressure evaluations, which is considered conservative for granular fill compacted to 90 percent Modified Proctor compaction.

2.5.4.10.6.5 Earth Pressure Coefficients

Active, passive, and at-rest lateral earth pressure coefficients, KA, KP, and KO, respectively, were estimated assuming frictionless vertical walls and horizontal backfill by the following relationships:

Active Earth Pressure Coefficient:

$$K_a = \tan^2\left(45 - \frac{\phi'}{2}\right) \qquad \text{Eq. 2.5.4-4}$$

Passive Earth Pressure Coefficient:

$$K_p = \tan^2\left(45 + \frac{\phi'}{2}\right) \qquad \text{Eq. 2.5.4-5}$$

At-Rest Earth Pressure Coefficient:

The At-Rest Earth pressure coefficient depends mainly on the deposition process of the formation, and its subsequent stress history. Its value is between the active and passive earth pressure coefficients and there are documented relationships to estimate its value, for example:

General Application (Bowles, 1996), $K_o = 1 - \sin\varphi$ Eq. 2.5.4-6

In order to account for compaction effects on engineered fills, the Passive Earth Pressure Coefficient is modified with Equation 2.5.4-10 (Bowles, 1996).

© 2007-2012 UniStar Nuclear Services, LLC. All rights reserved.
COPYRIGHT PROTECTED

$$K_{oc} = K_o (5.8\sin(\varphi') - 2.1)$$

Eq. 2.5.4-7

Dynamic Active and Passive Earth Pressure Coefficient:

The Dynamic Active and Passive Earth Pressure Coefficients are determined with the use of the Mononobe-Okabe theory. For a vertical wall and a horizontal grade the theory provides Equations 2.5.4-8(a) through 2.5.4-8(c). .

$$K_{ae} = \frac{\cos^2(\phi-\theta)}{\cos\theta\cos(\delta+\theta)\left(1+\sqrt{\frac{\sin(\phi+\delta)\sin(\phi-\theta)}{\cos(\delta+\theta)}}\right)^2}$$

Eq. 2.5.4-8 (a)

$$K_{pe} = \frac{\cos^2(\phi-\theta)}{\cos\theta\cos(\delta+\theta)\left(1-\sqrt{\frac{\sin(\phi+\delta)\sin(\phi-\theta)}{\cos(\delta+\theta)}}\right)^2}$$

Eq. 2.5.4-8 (b)

$$\theta = a\tan\left(\frac{F_h}{F_v}\right) = \frac{k_h}{1\pm k_v}$$

Eq. 2.5.4-8 (c)

Where:

Where:

K_{ae} → Dynamic active earth pressure coefficient,
K_{pe} → Dynamic passive earth pressure coefficient,
θ → Angle of resultant of seismic load,
ϕ → Friction angle (Drained conditions),
δ → Friction between wall and soil ($\delta = 2\phi/3$ (Das, 1993)),
F_h → Horizontal earthquake force,
F_v → Vertical earthquake force,
k_h → Horizontal earthquake acceleration (0.25 g)
k_v → Vertical earthquake acceleration (0.25 g),

Based on the previous equations, Table 2.5-56 provides the recommended earth pressure coefficients .}

2.5.4.11 Design Criteria

No departures or supplements.

2.5.4.12 Techniques to Improve Subsurface Conditions

{Major structures will derive support from the Mahantango Formation or concrete or engineered structural fills. Ground improvement will be limited to excavation of unsuitable soils, such as liquefiable sands. No in-situ soils in their natural state will be used for foundation or lateral support purposes. Foundation soils will include proof-rolling of foundation subgrade

© 2007-2012 UniStar Nuclear Services, LLC. All rights reserved.
COPYRIGHT PROTECTED

for the purpose of identifying any unsuitable soils for further excavation and replacement, which further densifies the upper portions of the subgrade. In absence of subsurface conditions at the site that require ground improvement, ground control, that is, maintaining the integrity of existing dense or stiff foundation soils, will be the primary focus of earthworks during foundation preparation. These measures will include such steps as groundwater control, use of appropriate measures and equipment for excavation and compaction, subgrade protection, and other similar measures.

2.5.4.13 References

This section is added as a supplement to the U.S. EPR FSAR.

AASHTO, 1998. Load and Resistance Factor Design (LRFD) Bridge Design Specifications, Second Edition, American Association of State Highway and Transportation Officials, 1998.

ACI, 2005. Manual of Concrete Practices, ACI-318, American Concrete Institute, 2005.

ASCE, 2000. Seismic Analysis of Safety-Related Nuclear Structures, ASCE 4-98, American Society of Civil Engineers, 2000.

ASCE, 1994a. Bearing Capacity of Soils, Technical Engineering and Design Guide, American Society of Civil Engineers, 1994.

ASCE, 1994b. Settlement Analysis, Technical Engineering and Design Guide, American Society of Civil Engineers, 1994.

ASCE, 2005. Seismic Design Criteria for Structures, Systems, and Components in Nuclear Facilities, ASCE/SEI 43-05, American Society for Civil Engineers/Structural Engineering Institute, 2005.

ASTM, 1999. Standard Test Method for Penetration Test and Split-Barrel Sampling of Soils, ASTM D1586-99, American Society for Testing and Materials, 1999.

ASTM, 2000a. Standard Practices for Preserving and Transporting Soil Samples, ASTM D4220-95(2000), American Society for Testing and Materials, 2000.

ASTM, 2000b. Standard Practice for Thin-Walled Tube Sampling of Soils for Geotechnical Purposes, ASTM D1587-00, American Society for Testing and Materials,2000.

ASTM, 2000c. Standard Test Method Prebored Pressuremeter Testing in Soils, ASTM D4719-00, American Society for Testing and Materials, 2000.

ASTM, 2002a. Standard Test Method for Particle Size Analysis of Soils, ASTM D422-63 (reapproved 2002), American Society for Testing and Materials, 2002.

ASTM, 2003. Standard Test Methods for Measurement of Hydraulic Conductivity of Saturated Porous Materials Using a Flexible Wall Permeameter, ASTM D5084-03, American Society for Testing and Materials, 2003.

ASTM, 2004a. Standard Test Method for Compressive Strength and Elastic Moduli of Intact Rock Core Specimens under Varying States of Stress and Temperatures, ASTM D7012-04, American Society for Testing and Materials, 2004.

© 2007-2012 UniStar Nuclear Services, LLC. All rights reserved.
COPYRIGHT PROTECTED

ASTM, 2004b. Standard Practice for Determining the Normalized Penetration Resistance of Sands for Evaluation of Liquefaction Potential, ASTM D6066-96(2004), American Society for Testing and Materials, 2004.

ASTM, 2005a. Standard Test Method for Energy Measurement for Dynamic Penetrometers, ASTM D4633-05, American Society for Testing and Materials, 2005.

ASTM, 2005b.. Standard Test Method for Specific Gravity and Absorption of Rock for Erosion Control, ASTM D6473-99(2005), American Society for Testing and Materials, 2005.

ASTM, 2005c. Standard Test Method for Laboratory Determination of Water (Moisture) Content of Soil and Rock by Mass, ASTM D2216-05, American Society for Testing and Materials, 2005.

ASTM, 2005d. Standard Test Method for Standard Guide for Using Rock Mass Classification Systems for Engineering Purposes, ASTM D5878-05, American Society for Testing and Materials, 2005.

ASTM, 2006a. Standard Test Method for Classification of Soils for Engineering Purposes (Unified Soil Classification System), ASTM D2487-06, American Society for Testing and Materials, 2006.

ASTM, 2006b. Test Method for Specific Gravity of Soil Solids by Water Pycnometer, ASTM D854-06, American Society for Testing and Materials, 2006.

ASTM, 2006c. Standard Practice for Description and Identification of Soils (Visual-Manual Procedure), ASTM D2488-06, American Society for Testing and Materials, 2006.

ASTM, 2006e. Standard Practice for Rock Core Drilling and Sampling of Rock for Site Investigation, ASTM D2113-06, American Society for Testing and Materials, 2006.

ASTM, 2006f. Standard Practices for Preserving and Transporting Rock Core Samples, ASTM D5079-02(2006), American Society for Testing and Materials, 2006.

Bieniawski, 1989. Engineering Rock Mass Classifications, Wiley Interscience, Z.T. Bieniawski, 1989.

Carter, 1991. Correlations of Soil Properties, Pentech Press Limited, M. Carter and S.P Bentley, 1991.

Bowles, 1996. Foundation Analysis and Design, 5th Edition, McGraw-Hill Book Company, J. Bowles, 1966.

Dobrin, 1976, Introduction to Geophysical Prospecting, McGraw Hill, Inc., M.B. Dobrin, 1976.

Harper, 1999. Part II. Stratigraphy and Sedimentary Tectonics, Chapter 7: Devonian, in C.H. Shultz ed., The Geology of Pennsylvania: Pennsylvania Bureau of Topographic and Geologic Survey Special Publication 1, J.A. Harper, 1999 .

Inners, 1978. Geology and Mineral Resources of the Berwick Quadrangle, Luzerne and Columbia Counties, Pennsylvania, Pennsylvania Geological Survey, Fourth Series, J.D. Inners, 1978.

© 2007-2012 UniStar Nuclear Services, LLC. All rights reserved.
COPYRIGHT PROTECTED

NRC, 2001. Technical Basis for Revision of Regulatory Guidance on Design Ground Motion: Hazard- and Risk- Consistent Ground Motion Spectra Guidelines, NUREG/CR 6728, Nuclear Regulatory Commission, 2001.

NRC, 2002. Technical Basis for Revision of Regulatory Guidance on Design Ground Motion: Development of Hazard- and Risk- Consistent Seismic Spectra for Two Sites, NUREG/CR 6769, Nuclear Regulatory Commission, 2002.

NRC, 2003a. Site Investigations for Foundations of Nuclear Power Plants, Regulatory Guide 1.132, Revision 2, Nuclear Regulatory Commission, 2003

NRC, 2003b. Laboratory Investigations of Soils for Engineering Analysis and Design of Nuclear Power Plants, Regulatory Guide 1.138, Revision 2, Nuclear Regulatory Commission, 2003.

NRC, 2003c. Procedures and Criteria for Assessing Seismic Soil Liquefaction at Nuclear Power Plant Sites, Regulatory Guide 1.198, Nuclear Regulatory Commission, 2003.

NRC, 2007a. Combined License Applications for Nuclear Power Plants (LWR Edition), Regulatory Guide 1.206, Nuclear Regulatory Commission, 2006.

NRC, 2007b. A performance-Based Approach to Define the Site-Specific Earthquake Ground Motion, Regulatory Guide 1.208, Nuclear Regulatory Commission, 2007.

Peck, 1967. Soil Mechanics in Engineering Practice, 2nd edition, Wiley & Sons, R.B. Peck & K. Terzaghi, 1967.

Peck, 1974. Foundation Engineering, 2nd edition, Wiley & Sons, R. B. Peck,1974.

PPL, 2004. Susquehanna Steam Electric Station, Units 1 and 2, Final Safety Analysis Report, Pennsylvania Power & Light Company, 2004.

Rizzo, 2009. Unit Weight Deviation, Project No. 07-389914.14 Rizzo Engineering and Consultants, 2009.

Schnabel, 1972. SHAKE, A Computer Program for Earthquake Response Analysis Of Horizontally Layered Site, B. Schnabel, J. Lysmer and H.B. Seed, 1972.

Seed, 1970. Design of Earth Retaining Structures for Dynamic Loads, ASCE Specialty Conference on Lateral Stresses and Earth Retaining Structures, H.B. Seed and R.V. Whitman, June 1970.

Terzaghi, 1996. Soil Mechanics in Engineering Practice, 3rd Edition, John Wiley and Sons Inc., Terzaghi, 1996

UTA, 2004a. PBRCTS-1, Revision 4, Technical Procedures for Resonant Column and Torsional Shear (RCTS) Testing of Soil and Rock Samples, Department of Civil Engineering, University of Texas, Austin, Texas, August 2004.

UTA, 2004b. URC-1, Revision 4, Technical Procedures for URC Tests, Department of Civil Engineering, University of Texas, Austin, Texas, August 2004.

Vesic, 1975. Foundation Engineering Handbook, Winterkorn and Fang, A.S. Vesic, 1975.

© 2007-2012 UniStar Nuclear Services, LLC. All rights reserved.
COPYRIGHT PROTECTED

Vucetic, 1991. Effect of Soils Plasticity on Cyclic Response, Journal of Geotechnical Engineering, ASCE 117 (1), M. Vucetic and R. Dobry, 1991.

Weston, 2008. Final Report on Seismic Refraction Survey, Seismic Refraction Surveys For the Bell Bend Site Characterization, Weston Geophysical Corporation, 2008.

Youd, 2001. Liquefaction Resistance of Soils: Summary Report from the 1996 NCEER and 1998 NCEER/NSF Workshops on Evaluation of Liquefaction Resistance of Soils, Journal of Geotechnical and Geoenvironmental Engineering, T.L. Youd, M. Idriss, R.D. Andrus, I. Arango, G. Castro, J.T. Christian, R. Dobry, W.D. Finn, L.F. Harder Jr., M.E. Hynes, K. Ishihara, J.P. Koester, S.S. Liao, W.F. Marcuson III, G.R. Martin, J.K. Mitchell, Y. Moriwaki, M.S. Power, P.K. Robertson, R.B. See, and K.H. Stokoe II, October 2001.}

2.5.5 Stability of Slopes

The U.S. EPR FSAR includes the following COL Item for Section 2.5.5:

> A COL applicant that references the U.S. EPR design certification will evaluate site-specific information concerning the stability of earth and rock slopes, both natural and manmade (e.g., cuts, fill, embankments, dams, etc.), of which failure could adversely affect the safety of the plant.

This COL Item is addressed as follows:

{This section addresses the stability of constructed and natural slopes. It was prepared based on the guidance in relevant Section of NRC Regulatory Guide 1.206, "Combined License Applications for Nuclear Power Plants (LWR Edition)," (NRC, 2007). Constructed slopes evolve as part of the overall site development.

The site of the Bell Bend Nuclear Power Plant (BBNPP) is comprised of generally flat topography in the vicinity of the primary structures and components. The site is planned to be graded in order to establish the final grade for the project, resulting in minor cuts and fills, as well as slopes. The stability of these slopes and their potential impact on safety-related structures are evaluated in this section. In the vicinity of the primary structures and components there are no significant natural slopes at the site or any steep slopes, undergoing continuous erosion. There is a nine degree slope on the North side of the power block, which was analyzed for stability and the results are reported in this section.

2.5.5.1 Slope Characteristics

The characteristics of constructed and natural slopes are described below.

2.5.5.1.1 Characteristics of Constructed Slopes

Site grading areas for the BBNPP include the structures in the power block, switchyard, cooling towers, and Essential Service Water Emergency Makeup System (ESWEMS) Pumphouse Building and Retention Pond. The power block includes the Reactor Building, Fuel Building, Safeguards Building, Emergency Power Generation Building, Nuclear Auxiliary Building, Access Building, Radioactive Waste Building, and Turbine Building. The centerline of the BBNPP power block is planned to be graded to approximately elevation 674 ft (205.4 m) msl. The finished grade in the area of each major structure will be approximately:

- Power block: Elevation 674 ft (205.4 m) msl
- Switchyard: Elevation 680 ft (207.3 m) msl

© 2007-2012 UniStar Nuclear Services, LLC. All rights reserved.
COPYRIGHT PROTECTED

- Cooling Tower: Elevation 753 ft (229.5 m) msl
- ESWEMS: Elevation 674 ft (205.4 m) msl

The site grading will require the excavation of the natural overburden soils, to a current estimated maximum depth of 61 ft (18.6 m) and an average depth of 40 ft (12.2 m). The natural overburden soils are inadequate for the foundation of large safety related facilities. These will be replaced by either granular backfill formed with screen glacial and alluvial soils from either on-site or off-site sources, or concrete. The cut/fill operations will not result in permanent slopes in and around the power block area.

2.5.5.1.1.1 Temporary Slopes

Temporary construction slopes will be constructed in cuts with a minimum 1.5:1 (horizontal to vertical) slope. The maximum possible height will be limited to approximately 40 ft (12.2 m), from the surface to the position of horizontal benches or to the top of the Manhantago Formation. The overburden soil classifications are discussed in Section 2.5.4. Temporary slope cross-sections are shown in Figure 2.5-171.

2.5.5.1.1.2 Permanent Slopes

The only permanent slopes will be the slopes of the ESWEMS Retention Pond. The design of the retention pond is addressed in Section 2.4 and Section 9.2.5 of the BBNPP FSAR. The permanent slope cross sections are found in Figure 2.5-170. Based on the findings of the drilling program, the ground surface elevations near the retention pond center are 691.6 ft (210.8 m) near the north slope and 671.2 ft (204.6 m) near the south slope. The proposed finished grade is 674.0 ft (205.4 m). The excavation line and resulting pond side surface will have a 3:1 (horizontal to vertical) slope. The depth of the excavation is 22.0 ft (6.7 m) down to elevation 652.0 ft (198.7 m). The ESWEMS Pumphouse will be supported on concrete fill on top of the Mahantango bedrock. The stability of the ESWEMS Pumphouse Building is not affected by the adjacent slopes and its presence does not affect the stability of adjacent slopes.

2.5.5.1.2 Characteristics of Natural Slopes

The finish grade elevation along the center line of the Power Block is 674 ft (205.4m) msl. Within the area of the Power Block area the natural grade changes elevation by less than 3 ft (1 m) over distances of approximately 1000 ft (305 m). The same variation extends to the ESWEMS Retention Pond. Overall, the natural grade has variation of one percent. There are no natural slope instability concerns in the plant vicinity. A very mild elevation increase exists on the North side of the Power Block area. This increase forms a slope with an angle of approximately nine degrees. Figure 2.5-169 presents the shape and extent of this slope and the subsurface materials beneath it. Section 2.5.5.2 provides the slope stability analysis results.

2.5.5.1.3 Exploration Program and Geotechnical Conditions

The geotechnical exploration program, groundwater conditions, sampling, materials and properties, liquefaction potential, and other geotechnical parameters are addressed in Section 2.5.4. A summary relevant to the slope stability evaluation is presented below.

A geotechnical subsurface investigation was performed to characterize the upper 400 ft (122 m) of soil and rock materials. The site geology is comprised of glacial soil deposits underlain by the Mahantango formation (bedrock), which is, on average 38.9 ft (11.9 m) below the ground surface and is present down to the bottom of the deepest boring.

© 2007-2012 UniStar Nuclear Services, LLC. All rights reserved.
COPYRIGHT PROTECTED

As explained in Section 2.5.4, the subsurface is divided into the following stratigraphic units:

Overburden Soil: - Glacial Till

Bedrock: - Mahantango Formation

Overall, the subsurface conditions encountered throughout the site are uniform, in both depth and area extension. The thickness of the glacial till varies from 12.5 to 63.5 ft (3.8 to 19.4 m). In general, the till consists of consolidated brown silty sand or sand containing gravel and large rounded cobbles and boulders. The presence of the boulders increases with depth.

The overburden soil is not an adequate foundation strata for safety related structures or facilities that will impose high contact pressures. In the South side of the Power Block area, beneath borings B-313, B-314, B-315, B-316, B-317, B-320, B-321, B-322, and B-323, the glacial till has pockets of loose saturated sands that are susceptible to liquefaction. Figure 2.5-129 provides the locations of these borings.

The overburden soils will be removed in the power block area. No permanent slopes will be implemented except for the slopes of the ESWEMS Retention Pond. At the ESWEMS Pond, the lack of cohesion of the in-situ soils would result in sloughing failures of the ESWEMS Pond slopes with a high probability of erosion. These soils will be replaced with a cohesive fill. The slopes of the ESWEMS will be protected from erosion through the use of cohesive fill to avoid soil debris falling into the pond and diminishing the design retention capacity.

The depth of the groundwater table at the site varies from 0 ft (0 m) to 10 ft (3 m) depending on location. On average, the groundwater depth is 4 ft (1.2 m) to 6 ft (1.8 m) below the ground surface. Since the plant grade is placed at elevation 674.0 ft (205.4 m) msl, the slope stability analysis of the ESWEMS Retention Pond slopes is governed by the forces imposed by the pond water level.

Temporary slopes will be developed under dry conditions within a dewatered zone.

2.5.5.2 Design Criteria and Analysis

The stability of constructed slopes was assessed using limit equilibrium methods, which generally consider moment or force equilibrium of a potential sliding mass by discretizing the mass into vertical slices. This approach results in a Factor of Safety (FOS) that can be defined as (Duncan, 2005) :

$$FOS = \frac{\text{Shear Strength of Soil}}{\text{Shear Stress Required for Equilibrium}} \qquad \text{(Eq. 2.5.5-1)}$$

Factor of Safety is defined as the ratio of the available strength of the cross section versus the forces placed upon it, such as water or seismic force. A Factor of Safety greater than one indicates that the available strength is greater than the stresses being placed upon the cross section and implies that under these particular circumstances there should be no measureable damage or permanent displacements of the cross section.

Various limit equilibrium methods are available for slope stability evaluation, including the Ordinary method (Fellenius, 1936), Bishop's simplified method (Bishop, 1955), Janbu's simplified method (Janbu, 1968), and the Morgenstern-Price method (Morgenstern, 1965),

© 2007-2012 UniStar Nuclear Services, LLC. All rights reserved.
COPYRIGHT PROTECTED

among others. These methods were selected for evaluation of slopes because they are routinely used, and their limitations, and advantages, are well documented. The main differences are:

1. Equations of statics that are included and satisfied.
2. Interslice forces that are included in the analysis.
3. Assumed relationship between the interslice shear and normal forces.

The Ordinary (Fellenius, 1936) method is one of the earliest methods developed. It ignores all interslice forces and satisfies only moment equilibrium. Both Bishop's (Bishop, 1955) simplified method and Janbu's (Janbu, 1968) simplified method include the interslice normal force, E, but ignore the interslice shear force. Bishop's (Bishop, 1955) and Janbu's (Janbu, 1968) simplified methods satisfy only moment equilibrium and horizontal force equilibrium, respectively.

The slope stability analysis is performed using the latest version of Computer Program GSTABL7 with STEDwin (Gregory 2003). This program was originally developed by Purdue University for the Indiana State Highway Commission in 1986 and later revised and marketed by Geotechnical Engineering Software Company. The program calculates the factor of safety against slope failure utilizing a two-dimensional limit equilibrium method. The calculation of the factor of safety against slope instability is performed using the Simplified Bishop method of slices, which is applicable to circular shaped failure surfaces, or the Simplified Janbu method of slices, which is applicable to failure surfaces of a general shape. GSTABL7 may incorporate up to 20 soil options with nonlinear undrained shear strength parameters, isotropic or anisotropic soils, and fiber reinforcement. Stabilizing structures such as piles, tiebacks, or nails may also be considered. None of these stabilizing options are required at the BBNPP site and isotropic soils are used in the analysis.

Dynamic analysis of the slopes can be performed using a pseudo-static approach, which represents the effects of seismic shaking by accelerations that create inertial forces. These forces act in the horizontal and vertical directions at the centroid of each slice, and are defined as:

$$F_h = (a_h / g)W = k_h W \qquad \text{(Eq. 2.5.5-2)}$$

$$F_v = (a_v / g)W = k_v W \qquad \text{(Eq. 2.5.5-3)}$$

Where a_h and a_v are horizontal and vertical ground accelerations, respectively, W is the slice weight, and g is the gravitational acceleration constant. The inertial effect is specified by k_h and k_v coefficients, based on site seismic considerations.

Typical minimum acceptable values of FOS are 1.5 for normal long-term loading conditions and 1.0 to 1.2 for infrequent loading conditions (Duncan, 2005), e.g., during earthquakes.

2.5.5.2.1 Stability of Constructed Slopes

The ESWEMS Retention Pond at the BBNPP will be constructed primarily via excavation of overburden soils and replacement of soils with cohesive fill material. The cohesive fill material will compose the entirety of the earthen embankment sides of the ESWEMS Retention Pond.

The excavation will cut in part through the overburden soil layer. The soil profile was verified with seven borings placed directly within the area near and surrounding the ESWEMS

© 2007-2012 UniStar Nuclear Services, LLC. All rights reserved.
COPYRIGHT PROTECTED

Retention Pond. The location of the borings (B-331, B-332, B-333, B-334, B-341, B-342, and B-343) is shown in Figure 2.5-129. Four separate sections are analyzed to represent the various design differences of slopes for the ESWEMS Retention Pond. These sections are shown in Figure 2.5-170. These sections represent the elevations on each side of the rectangular ESWEMS Pond. The overall design and elevations are similar. They will be composed primarily of cohesive fill which will replace the overburden present on-site. The embankment sides will be built up to the ESWEMS Pumphouse Building grade at elevation 674.5 ft (205.6 m).

The ESWEMS Retention Pond is constructed by excavation from grade, therefore there is no downstream slope of significance to require a stability analysis. The upstream sections govern the analysis.

The analyses are performed for steady state loading conditions as well as earthquake loading conditions. The total stress strength parameters of the soils provided in Section 2.5.4 are utilized in the analyses.

Both circular and wedge analyses are performed on the cross sections. The circular failure analysis uses the Simplified Bishop Method. Wedge analysis utilizes the Simplified Janbu method.

For the ESWEMS Retention Pond, the phreatic surface is defined as the boundary between the saturated and unsaturated zones in the cross sectional profile. Normally, Casagrande's solution for seepage through an earthen dam can be used to calculate the expected phreatic surface (Das, 2002). Under the conditions presented for the ESWEMS Retention Pond there is no significant downstream slope, thereby making Casagrande's equation and approach to determining the phreatic surface non-applicable to this situation. Instead, engineering judgment was substituted to visually approximate a conservative phreatic surface for the cross section. The phreatic surface is conservative for a gradual drop in water surface from elevation 670 ft (204.2 m) (the normal water level) as it passes through the slope. The phreatic surface is shown in Figure 2.5-170, noted as the normal pool water level on the cross sections.

The Safe Shutdown Earthquake (SSE) load consists of horizontal and vertical seismic loads applied pseudo-statically to the model. Using data derived from a Foundation Input Response Spectra (FIRS), a peak horizontal seismic acceleration was found to be $a_h = 0.28g$ and a peak vertical ground acceleration $a_v = 0.30g$. The higher of the two, $a_v = 0.30g$, is used in the analysis. Total stress parameters for the soil properties are used for the earthquake loading analysis. The seismic coefficients are considered to be half of the peak ground acceleration according to the Hynes-Griffin and Franklin model (Abramson, 2001) resulting in $k_h = 0.14g$ and $k_v = 0.15g$. The method of analysis and data are presented in Section 2.5.2.

In order to find the worst case slope failure, the program GSTABL7 allows the calculation of numerous iterations and provides the corresponding location and Factor of Safety of the worst case scenario. The worst case is the location exhibiting the lowest Factor of Safety.

The slope stability analyses results are summarized in Table 2.5-60 and the critical failure surfaces are shown in Figure 2.5-170. The static case analysis indicate that the BBNPP ESWEMS Retention Pond side slopes have Factor of Safety values ranging from 4.4 to 9.2 depending upon the slope configuration and analysis method. The Factor of Safety under dynamic conditions is between 2.0 and 4.1. Therefore, it can be stated that the current design is safe.

© 2007-2012 UniStar Nuclear Services, LLC. All rights reserved.
COPYRIGHT PROTECTED

The North Side Slope critical failure surfaces are shown by Figure 2.5-169. The Factors of Safety provided by Table 2.5-60 (1.6 dynamic and 5.7 static) indicate that this slope does not represent a threat to the integrity of the facilities in the power block area.

At the BBNPP site, there are no dams or embankments, for which adverse conditions such as high water levels attributable to the Probable Maximum Flood (PMF), sudden drawdown, or steady seepage at various levels may occur.

The slope stability analysis at the ESWEMS site was performed with the phreatic surface at elevation 670 ft (204.2 m), compared to the PMF level of 671 ft (204.5 m). Earthquake loading was incorporated without modifying the water level of 670 ft (204.2 m). As such, the unlikely event of simultaneous flooding and an earthquake is considered to be adequately addressed in the analysis.

2.5.5.2.2 Stability of Temporary Fill Slopes

Temporary cut and fill slopes will exist in dry conditions during construction. The slope stability analyses are performed for the sections shown by Figure 2.5-171. Results are summarized in Table 2.5-60 and the critical failure surfaces are shown in the sections of Figure 2.5-171. Analysis for temporary construction slopes was performed for the static condition. The Factor of Safety is 1.3 for minor, close to the surface planes.

2.5.5.2.3 Concluding Remarks

Based on analyses provided in this Section, it is concluded that the constructed and natural slopes at the site are sufficiently stable and present no failure potential under any conditions to which they could be exposed during the life of the plant that would adversely affect the safety of the proposed BBNPP.

2.5.5.3 Logs of Borings

Logs of borings, and associated references, are provided in Part 11 of the COLA.

2.5.5.4 Compacted Fill

Compacted fill, and associated references, are addressed in Section 2.5.4.5.

2.5.5.5 References

Abramson, 2001. Slope Stability and Stabilization Methods, Second Edition, Wiley and Sons, L.W. Abramson, et al., 2001.

Bishop, 1955, The Use of Slip Surface Circle in Stability Analysis of Slopes, Geotechnique Volume 5, Number 1, pp. 7-17, A.W. Bishop, 1955.

Das, 2002. Principles of Geotechnical Engineering, Fifth Edition, Brooks/Cole, B. Das, 2002.

Duncan, 2005. Soil Strength and Slope Stability, Wiley and Sons, J.M. Duncan and S.G. Wright, 2005.

Fellenius, 1936, Calculation of the Stability of Earth Dams, Proceedings of the Second Congress of Large Dams, Volume 4, pp. 445-463, 1936.

Gregory, 2003. GSTABL7 with STEDwin: Slope Stability Analysis System Program Manual, G.H. Gregory, 2003.

© 2007-2012 UniStar Nuclear Services, LLC. All rights reserved.
COPYRIGHT PROTECTED

Janbu, 1968. Slope Stability Computations, Soil Mechanics and Foundation Engineering, The Technical University of Norway, N. Janbu, 1968.

Morgenstern, 1965. The Analysis of the Stability of General Slip Surfaces, Geotechnique, Volume 15, pp. 79-93, N.R. Morgenstern and V.E. Price, 1965.

NRC, 2007. Combined License Applications For Nuclear Power Plants (LWR Edition), Regulatory Guide 1.206, U.S. Nuclear Regulatory Commission, 2007.}

2.5.6 References

No departures or supplements.

© 2007-2012 UniStar Nuclear Services, LLC. All rights reserved.
COPYRIGHT PROTECTED

Table 2.5-1— {Updated Earthquake catalog (1534-April 2010) Including events with $m_b \geq 3.0$}

(Page 1 of 75)

Year	Month	Day	Hour	Min	Sec	Lat (deg)	Lon (deg)	Depth (km)	mb	Source
1534	1	1	0	0	0.0	47.70	-70.10	0.0	6.3	DNAG
1627	1	1	0	0	0.0	42.60	-70.80	0.0	3.8	NCEER
1638	6	11	19	0	0.0	44.40	-71.80	0.0	6.5	Ebel
1643	3	15	12	0	0.0	42.80	-70.80	0.0	3.3	NCEER
1643	6	11	18	0	0.0	42.80	-70.80	0.0	3.3	NCEER
1658	4	14	0	0	0.0	42.50	-70.90	0.0	3.5	NCEER
1661	2	10	12	0	0.0	45.50	-73.00	0.0	5.2	NCEER
1663	2	5	22	30	0.0	47.60	-70.10	0.0	7.0	Ebel
1665	10	15	21	30	0.0	46.82	-71.22	0.0	3.3	NCEER
1668	4	3	9	0	0.0	42.35	-71.10	0.0	3.3	NCEER
1668	4	13	13	0	0.0	47.10	-70.50	0.0	3.8	NCEER
1668	12	19	0	0	0.0	42.50	-71.50	0.0	3.5	Ebel
1672	2	1	0	0	0.0	48.15	-69.70	0.0	3.3	NCEER
1677	12	13	0	0	0.0	41.10	-73.50	0.0	3.3	NCEER
1685	2	18	21	0	0.0	42.80	-70.80	0.0	3.5	Ebel
1697	2	20	11	15	0.0	42.00	-70.80	0.0	3.0	Ebel
1698	1	1	0	0	0.0	41.38	-73.47	0.0	3.3	NCEER
1702	1	1	0	0	0.0	41.40	-73.50	0.0	3.3	NCEER
1705	6	27	0	0	0.0	42.40	-71.10	0.0	3.3	NCEER
1727	11	10	3	40	0.0	42.80	-70.60	0.0	5.1	NCEER
1728	5	16	0	0	0.0	42.80	-70.60	0.0	3.3	NCEER
1728	7	30	15	0	0.0	42.80	-70.60	0.0	3.3	NCEER
1729	2	10	14	0	0.0	42.80	-70.60	0.0	3.5	NCEER
1729	3	30	19	0	0.0	42.80	-70.60	0.0	3.3	NCEER
1729	8	6	0	0	0.0	41.40	-73.50	0.0	3.3	NCEER
1729	9	19	20	30	0.0	42.80	-70.60	0.0	3.3	NCEER
1729	10	10	21	30	0.0	42.80	-70.60	0.0	3.3	NCEER
1729	11	25	13	0	0.0	42.80	-70.60	0.0	3.3	NCEER
1730	2	20	1	0	0.0	42.80	-70.60	0.0	3.3	NCEER
1730	4	24	1	0	0.0	42.80	-70.60	0.0	3.3	NCEER
1730	12	7	1	20	0.0	42.80	-70.60	0.0	3.3	NCEER
1731	1	13	0	0	0.0	42.80	-70.60	0.0	3.3	NCEER
1731	7	16	10	0	0.0	42.80	-70.60	0.0	3.3	NCEER
1731	10	13	4	0	0.0	42.80	-70.60	0.0	3.3	NCEER
1732	2	19	0	0	0.0	42.80	-70.60	0.0	3.3	NCEER
1732	9	16	16	0	0.0	45.50	-73.60	0.0	5.8	NCEER
1734	11	23	5	0	0.0	42.80	-70.60	0.0	3.3	NCEER
1736	2	13	22	45	0.0	42.80	-70.60	0.0	3.3	NCEER
1736	10	12	6	30	0.0	42.80	-70.60	0.0	3.3	NCEER
1736	11	23	7	0	0.0	42.80	-70.60	0.0	3.3	NCEER
1737	2	17	21	30	0.0	42.40	-71.00	0.0	3.3	NCEER
1737	9	20	15	20	0.0	42.80	-70.60	0.0	3.3	NCEER
1737	12	19	3	45	0.0	40.80	-74.00	0.0	5.2	NCEER
1739	8	13	7	30	0.0	42.80	-70.60	0.0	3.3	NCEER
1741	2	5	20	50	0.0	42.80	-70.60	0.0	3.3	NCEER
1744	5	27	0	0	0.0	46.80	-71.20	0.0	3.3	NCEER

© 2007-2012 UniStar Nuclear Services, LLC. All rights reserved.
COPYRIGHT PROTECTED

Table 2.5-1— {Updated Earthquake catalog (1534-April 2010) Including events with $m_b \geq 3.0$}

(Page 2 of 75)

Year	Month	Day	Hour	Min	Sec	Lat (deg)	Lon (deg)	Depth (km)	mb	Source
1744	6	14	15	15	0.0	42.50	-70.90	0.0	4.6	NCEER
1752	12	17	23	30	0.0	40.00	-76.30	0.0	3.6	SRA
1755	11	18	9	12	0.0	42.70	-70.30	0.0	5.8	NCEER
1757	7	8	19	15	0.0	42.30	-71.10	0.0	3.3	NCEER
1758	4	25	2	30	0.0	38.90	-76.50	0.0	3.5	NCEER
1759	2	2	7	0	0.0	42.35	-71.00	0.0	3.3	NCEER
1761	3	12	7	15	0.0	42.50	-71.00	0.0	4.3	NCEER
1761	11	2	1	0	0.0	43.10	-71.50	0.0	3.3	NCEER
1764	9	30	0	0	0.0	45.30	-66.00	0.0	3.5	NCEER
1766	1	23	10	0	0.0	43.70	-70.30	0.0	3.3	NCEER
1766	3	2	8	0	0.0	43.07	-70.77	0.0	3.3	NCEER
1766	12	17	11	48	0.0	43.10	-70.80	0.0	3.3	NCEER
1769	10	19	0	0	0.0	43.70	-70.30	0.0	3.3	NCEER
1774	2	21	19	0	0.0	37.20	-77.40	0.0	4.6	NCEER
1775	3	16	19	15	0.0	37.70	-78.80	0.0	3.3	NCEER
1776	1	1	0	0	0.0	39.90	-82.00	0.0	4.0	NCEER
1776	11	5	0	0	0.0	35.20	-83.00	0.0	3.3	NCEER
1777	11	16	7	0	0.0	36.00	-84.00	0.0	3.3	NCEER
1780	2	6	0	0	0.0	30.40	-87.20	0.0	3.8	NCEER
1780	11	29	0	0	0.0	42.50	-70.90	0.0	3.3	NCEER
1783	11	30	3	50	0.0	41.00	-74.50	0.0	4.9	NCEER
1784	1	2	10	0	0.0	46.80	-71.20	0.0	3.3	NCEER
1785	1	2	12	15	0.0	40.00	-67.00	0.0	5.2	NCEER
1791	1	13	9	0	0.0	37.70	-78.80	0.0	3.3	NCEER
1791	1	15	10	0	0.0	37.50	-77.50	0.0	3.3	NCEER
1791	5	16	13	22	0.0	41.50	-72.40	0.0	4.5	NCEER
1791	12	6	20	0	0.0	47.40	-70.50	0.0	6.0	NCEER
1792	8	29	3	0	0.0	41.50	-72.50	0.0	3.3	NCEER
1794	3	6	19	0	0.0	41.50	-72.50	0.0	3.3	NCEER
1795	1	8	9	0	0.0	39.00	-89.90	0.0	3.4	NCEER
1796	12	26	11	0	0.0	42.90	-79.00	0.0	4.0	NCEER
1799	4	11	8	20	0.0	32.90	-80.00	0.0	4.4	NCEER
1800	11	20	5	0	0.0	40.12	-76.39	0.0	3.9	NCEER
1800	12	20	0	0	0.0	43.70	-72.30	0.0	3.3	NCEER
1800	12	25	0	0	0.0	41.90	-71.10	0.0	3.3	NCEER
1801	3	1	20	30	0.0	43.10	-70.80	0.0	3.3	NCEER
1802	8	23	10	0	0.0	37.40	-79.10	0.0	3.5	NCEER
1803	1	18	14	50	0.0	42.50	-70.90	0.0	3.3	NCEER
1804	8	20	20	10	0.0	42.00	-87.80	0.0	4.4	USH
1804	8	24	20	10	0.0	42.00	-89.00	0.0	4.2	NCEER
1805	4	25	0	0	0.0	42.50	-70.90	0.0	3.3	NCEER
1805	6	12	12	30	0.0	44.50	-69.00	0.0	3.3	NCEER
1805	12	30	11	0	0.0	41.50	-72.50	0.0	3.3	NCEER
1807	1	14	4	0	0.0	43.00	-71.10	0.0	3.3	NCEER
1807	5	1	9	0	0.0	37.40	-79.10	0.0	3.5	NCEER
1807	5	6	18	0	0.0	43.50	-70.50	0.0	3.3	NCEER

© 2007-2012 UniStar Nuclear Services, LLC. All rights reserved.
COPYRIGHT PROTECTED

Table 2.5-1— {Updated Earthquake catalog (1534-April 2010) Including events with $m_b \geq 3.0$}

(Page 3 of 75)

Year	Month	Day	Hour	Min	Sec	Lat (deg)	Lon (deg)	Depth (km)	mb	Source
1808	6	26	2	50	0.0	44.40	-69.00	0.0	3.5	NCEER
1810	11	10	2	15	0.0	43.00	-70.90	0.0	3.9	NCEER
1811	11	27	8	0	0.0	36.10	-80.20	0.0	3.3	NCEER
1812	2	2	9	30	0.0	37.60	-77.40	0.0	3.3	NCEER
1812	2	7	9	45	0.0	36.50	-89.60	0.0	7.4	NCEER
1812	4	22	4	0	0.0	37.50	-77.50	0.0	3.3	NCEER
1814	11	29	0	14	0.0	43.70	-70.30	0.0	4.0	NCEER
1816	7	25	15	0	0.0	36.60	-89.50	0.0	3.0	NCEER
1816	9	9	0	0	0.0	45.50	-73.60	0.0	5.2	NCEER
1817	1	8	4	0	0.0	33.00	-70.00	0.0	4.8	NCEER
1817	1	8	9	0	0.0	32.90	-80.00	0.0	5.0	USH
1817	5	22	20	0	0.0	45.00	-67.20	0.0	4.7	NCEER
1817	10	5	16	45	0.0	42.50	-71.20	0.0	4.2	NCEER
1817	12	11	0	0	0.0	38.50	-84.50	0.0	3.1	NCEER
1818	4	11	20	0	0.0	38.60	-90.20	0.0	3.0	NCEER
1818	10	11	0	0	0.0	46.90	-71.20	0.0	3.3	NCEER
1818	12	7	0	0	0.0	44.00	-76.50	0.0	3.3	NCEER
1819	9	2	8	0	0.0	37.70	-89.70	0.0	3.4	NCEER
1819	9	17	4	0	0.0	38.10	-89.80	0.0	3.1	NCEER
1820	1	1	0	0	0.0	36.60	-89.50	0.0	3.0	NCEER
1820	9	3	8	30	0.0	33.40	-79.30	0.0	3.3	NCEER
1820	11	9	22	0	0.0	37.30	-89.50	0.0	3.4	NCEER
1821	5	5	12	30	0.0	44.80	-68.80	0.0	3.8	NCEER
1823	3	7	15	0	0.0	43.90	-70.00	0.0	3.3	NCEER
1823	6	10	17	0	0.0	44.80	-68.80	0.0	3.5	NCEER
1823	7	23	11	55	0.0	42.90	-70.60	0.0	3.8	NCEER
1824	7	9	0	0	0.0	46.50	-66.50	0.0	3.5	NCEER
1824	7	15	16	20	0.0	39.70	-80.50	0.0	4.1	NCEER
1826	2	26	14	0	0.0	30.08	-81.56	0.0	3.3	NCEER
1827	5	11	0	0	0.0	36.10	-81.20	0.0	3.3	NCEER
1827	7	5	11	30	0.0	38.00	-87.50	0.0	4.8	NCEER
1827	8	7	4	30	0.0	38.00	-88.00	0.0	4.8	NCEER
1827	8	7	7	0	0.0	38.30	-85.80	0.0	4.0	NCEER
1827	8	23	0	0	0.0	41.40	-72.10	0.0	3.3	NCEER
1828	3	9	0	0	0.0	37.00	-80.00	0.0	4.8	NCEER
1828	7	25	11	0	0.0	43.90	-70.00	0.0	3.3	NCEER
1829	8	27	21	45	0.0	44.20	-69.80	0.0	3.3	NCEER
1830	3	29	7	0	0.0	39.65	-77.72	0.0	3.7	NCEER
1831	1	23	6	0	0.0	45.51	-73.54	0.0	3.3	NCEER
1831	4	2	14	0	0.0	37.73	-88.34	0.0	3.8	NCEER
1831	5	8	0	0	0.0	47.30	-70.50	0.0	5.2	NCEER
1831	7	8	0	0	0.0	46.87	-71.18	0.0	3.8	NCEER
1831	7	14	0	0	0.0	47.60	-70.10	0.0	5.0	NCEER
1832	1	1	0	0	0.0	45.00	-64.00	0.0	3.3	NCEER
1832	1	22	23	30	0.0	44.69	-75.50	0.0	3.9	NCEER
1832	3	24	22	0	0.0	44.85	-74.29	0.0	3.3	NCEER

© 2007-2012 UniStar Nuclear Services, LLC. All rights reserved.
COPYRIGHT PROTECTED

Table 2.5-1— {Updated Earthquake catalog (1534-April 2010) Including events with $m_b \geq 3.0$}

(Page 4 of 75)

Year	Month	Day	Hour	Min	Sec	Lat (deg)	Lon (deg)	Depth (km)	mb	Source
1832	8	12	7	0	0.0	44.50	-64.50	0.0	4.3	NCEER
1833	2	4	0	0	0.0	42.30	-85.60	0.0	4.0	NCEER
1833	3	1	0	0	0.0	47.65	-70.17	0.0	3.3	NCEER
1833	4	1	0	0	0.0	47.70	-70.20	0.0	3.3	NCEER
1833	6	20	2	0	0.0	42.70	-78.38	0.0	3.0	NCEER
1833	8	27	11	0	0.0	37.70	-78.00	0.0	4.6	NCEER
1834	2	5	22	30	0.0	39.85	-76.14	0.0	3.8	NCEER
1834	5	24	12	0	0.0	44.26	-72.58	0.0	3.3	NCEER
1834	11	20	19	40	0.0	38.00	-86.00	0.0	3.4	NCEER
1835	1	4	18	0	0.0	41.80	-72.72	0.0	3.3	NCEER
1835	1	11	18	0	0.0	41.77	-71.13	0.0	3.3	NCEER
1836	7	9	2	15	0.0	41.50	-81.70	0.0	3.1	NCEER
1836	7	15	20	30	0.0	41.49	-71.31	0.0	3.8	NCEER
1836	8	30	14	0	0.0	41.33	-72.15	0.0	3.2	NCEER
1837	1	15	7	0	0.0	42.50	-70.90	0.0	3.3	NCEER
1837	2	9	3	0	0.0	46.82	-71.22	0.0	4.2	NCEER
1837	4	12	0	0	0.0	41.70	-72.70	0.0	3.5	NCEER
1837	6	22	20	30	0.0	41.94	-71.62	0.0	3.1	NCEER
1838	6	9	14	45	0.0	38.50	-88.00	0.0	5.0	NCEER
1839	9	5	0	0	0.0	38.60	-83.80	0.0	3.1	NCEER
1840	1	16	20	0	0.0	43.00	-75.00	0.0	3.7	NCEER
1840	4	1	0	0	0.0	41.99	-70.74	0.0	3.8	NCEER
1840	8	9	20	30	0.0	41.50	-72.90	0.0	3.7	NCEER
1840	9	10	0	0	0.0	43.20	-79.85	0.0	4.0	NCEER
1841	1	25	5	30	0.0	40.79	-74.25	0.0	3.3	NCEER
1841	12	28	5	50	0.0	36.60	-89.20	0.0	4.2	NCEER
1842	5	7	15	0	0.0	30.77	-91.92	0.0	3.9	NCEER
1842	5	28	5	0	0.0	36.60	-89.20	0.0	3.1	NCEER
1842	11	4	6	30	0.0	36.60	-89.20	0.0	3.4	NCEER
1842	11	9	0	0	0.0	46.00	-73.20	0.0	3.8	NCEER
1843	1	5	2	45	0.0	35.50	-89.60	0.0	5.4	NCEER
1843	2	16	0	0	0.0	38.80	-90.30	0.0	3.1	NCEER
1843	2	17	5	0	0.0	35.50	-90.50	0.0	4.4	NCEER
1843	3	14	0	0	0.0	44.40	-72.50	0.0	3.3	NCEER
1843	8	1	0	0	0.0	34.77	-89.45	0.0	3.3	NCEER
1843	8	9	0	0	0.0	35.60	-87.10	0.0	4.1	NCEER
1843	8	12	12	0	0.0	39.83	-74.78	0.0	3.3	NCEER
1843	10	17	7	50	0.0	42.16	-71.14	0.0	3.0	NCEER
1844	8	18	21	0	0.0	41.10	-73.25	0.0	3.8	NCEER
1844	9	19	22	0	0.0	42.94	-77.80	0.0	3.0	NCEER
1844	10	22	7	0	0.0	43.05	-78.33	0.0	3.5	NCEER
1844	11	1	0	0	0.0	45.50	-73.60	0.0	3.3	NCEER
1844	11	28	8	0	0.0	35.79	-83.27	0.0	3.6	NCEER
1845	2	3	4	0	0.0	41.93	-73.92	0.0	3.8	NCEER
1845	4	29	16	30	0.0	45.51	-73.54	0.0	3.3	NCEER
1845	10	26	23	15	0.0	41.22	-73.67	0.0	3.8	NCEER

© 2007-2012 UniStar Nuclear Services, LLC. All rights reserved.
COPYRIGHT PROTECTED

Table 2.5-1— {Updated Earthquake catalog (1534-April 2010) Including events with $m_b \geq 3.0$}

(Page 5 of 75)

Year	Month	Day	Hour	Min	Sec	Lat (deg)	Lon (deg)	Depth (km)	mb	Source
1846	5	30	18	30	0.0	42.70	-70.30	0.0	3.3	NCEER
1846	8	25	9	45	0.0	42.50	-70.80	0.0	4.1	NCEER
1847	1	1	0	0	0.0	43.80	-66.10	0.0	3.3	NCEER
1847	2	2	0	0	0.0	44.20	-69.10	0.0	3.3	NCEER
1847	8	8	15	0	0.0	41.70	-70.10	0.0	4.2	NCEER
1847	9	2	0	0	0.0	40.20	-72.00	0.0	3.5	NCEER
1848	1	1	0	0	0.0	45.00	-63.50	0.0	3.3	NCEER
1848	4	6	0	0	0.0	39.65	-82.53	0.0	3.7	NCEER
1848	9	9	0	0	0.0	41.11	-73.85	0.0	4.4	NCEER
1849	1	24	0	0	0.0	36.60	-89.20	0.0	3.4	NCEER
1850	4	5	2	5	0.0	37.00	-88.00	0.0	4.3	NCEER
1850	10	1	10	25	0.0	41.50	-81.70	0.0	3.1	NCEER
1850	10	17	0	0	0.0	37.30	-78.40	0.0	3.3	NCEER
1851	1	4	4	30	0.0	44.60	-69.60	0.0	3.3	NCEER
1852	1	10	11	40	0.0	41.20	-71.40	0.0	3.3	NCEER
1852	2	16	6	0	0.0	39.33	-76.30	0.0	3.8	NCEER
1852	4	29	18	0	0.0	36.60	-81.60	0.0	4.9	NCEER
1852	5	10	8	0	0.0	29.73	-84.99	0.0	4.2	NCEER
1852	6	30	12	0	0.0	43.48	-72.47	0.0	3.3	NCEER
1852	8	25	2	40	0.0	33.48	-82.00	0.0	3.3	NCEER
1852	11	2	23	35	0.0	37.60	-78.60	0.0	4.4	NCEER
1852	11	28	4	45	0.0	43.00	-70.90	0.0	3.7	NCEER
1853	3	12	7	0	0.0	43.70	-75.50	0.0	4.5	NCEER
1853	3	13	10	0	0.0	43.10	-79.40	0.0	3.3	NCEER
1853	5	2	14	20	0.0	38.50	-79.50	0.0	4.4	NCEER
1853	5	20	5	10	0.0	33.49	-81.96	0.0	4.0	NCEER
1853	7	17	10	30	0.0	43.50	-70.20	0.0	3.3	NCEER
1853	11	27	0	0	0.0	43.00	-69.00	0.0	3.3	NCEER
1853	11	28	0	0	0.0	43.00	-71.90	0.0	3.3	NCEER
1853	12	12	0	0	0.0	36.60	-89.20	0.0	4.1	NCEER
1854	2	12	0	0	0.0	37.20	-83.80	0.0	3.0	NCEER
1854	2	28	0	0	0.0	37.60	-84.00	0.0	3.6	NCEER
1854	3	8	0	0	0.0	38.20	-85.20	0.0	3.1	NCEER
1854	3	20	6	15	0.0	32.82	-83.62	0.0	3.3	NCEER
1854	10	24	0	0	0.0	42.90	-72.30	0.0	3.3	NCEER
1854	12	11	5	30	0.0	43.00	-70.80	0.0	3.4	NCEER
1855	1	16	23	0	0.0	44.00	-71.00	0.0	4.0	NCEER
1855	2	2	8	0	0.0	37.00	-78.60	0.0	3.9	NCEER
1855	2	8	11	30	0.0	46.00	-64.50	0.0	5.2	NCEER
1855	2	19	0	0	0.0	44.60	-69.60	0.0	3.3	NCEER
1855	4	19	13	0	0.0	40.22	-74.76	0.0	3.3	NCEER
1855	5	3	3	33	0.0	37.00	-89.20	0.0	3.1	NCEER
1855	5	29	10	0	0.0	44.70	-71.60	0.0	3.3	NCEER
1855	6	1	0	0	0.0	44.70	-65.50	0.0	3.3	NCEER
1855	6	28	0	18	0.0	39.07	-76.58	0.0	3.9	NCEER
1855	9	24	6	0	0.0	42.08	-78.43	0.0	3.1	NCEER

© 2007-2012 UniStar Nuclear Services, LLC. All rights reserved.
COPYRIGHT PROTECTED

Table 2.5-1— {Updated Earthquake catalog (1534-April 2010) Including events with $m_b \geq 3.0$}

Year	Month	Day	Hour	Min	Sec	Lat (deg)	Lon (deg)	Depth (km)	mb	Source
1855	12	17	19	0	0.0	43.30	-73.70	0.0	3.3	NCEER
1856	1	4	6	0	0.0	39.94	-77.66	0.0	3.3	NCEER
1856	1	5	12	0	0.0	44.69	-75.50	0.0	3.8	NCEER
1856	1	16	8	0	0.0	39.20	-78.20	0.0	3.3	NCEER
1856	1	26	4	0	0.0	39.47	-77.39	0.0	3.3	NCEER
1856	3	13	3	0	0.0	41.40	-72.60	0.0	3.3	NCEER
1856	7	16	13	40	0.0	37.57	-77.45	0.0	3.3	NCEER
1856	11	9	10	0	0.0	36.60	-89.50	0.0	4.1	NCEER
1856	12	6	12	0	0.0	37.22	-77.40	0.0	3.3	NCEER
1857	2	10	23	30	0.0	40.08	-74.75	0.0	3.1	NCEER
1857	2	11	0	0	0.0	40.27	-74.52	0.0	3.2	NCEER
1857	2	27	20	30	0.0	42.22	-81.05	0.0	3.9	NCEER
1857	3	1	1	40	0.0	41.80	-80.60	0.0	3.3	NCEER
1857	3	1	22	45	0.0	33.00	-83.18	0.0	3.4	NCEER
1857	10	8	10	0	0.0	38.70	-89.20	0.0	5.1	NCEER
1857	10	23	20	15	0.0	42.74	-78.97	0.0	4.0	NCEER
1857	12	8	20	0	0.0	46.70	-68.00	0.0	3.3	NCEER
1857	12	19	8	50	0.0	32.78	-80.73	0.0	4.1	NCEER
1857	12	23	18	30	0.0	44.10	-70.20	0.0	3.9	NCEER
1858	1	1	7	0	0.0	42.90	-78.50	0.0	3.3	NCEER
1858	3	3	14	0	0.0	43.65	-70.28	0.0	3.8	NCEER
1858	4	10	11	30	0.0	41.70	-81.30	0.0	3.1	NCEER
1858	5	17	20	0	0.0	45.50	-72.10	0.0	3.3	NCEER
1858	7	1	3	45	0.0	41.30	-73.00	0.0	3.3	NCEER
1858	8	24	12	0	0.0	43.74	-71.60	0.0	3.3	NCEER
1858	9	21	0	0	0.0	36.50	-89.20	0.0	4.0	NCEER
1859	1	10	4	0	0.0	41.49	-71.31	0.0	3.8	NCEER
1859	3	22	0	0	0.0	37.10	-81.50	0.0	3.1	NCEER
1859	10	26	15	0	0.0	44.99	-66.79	0.0	3.9	NCEER
1860	1	1	0	0	0.0	46.00	-94.80	0.0	4.5	NCEER
1860	1	19	18	0	0.0	33.68	-80.57	0.0	4.3	NCEER
1860	3	17	2	30	0.0	42.20	-70.50	0.0	3.3	NCEER
1860	4	24	20	0	0.0	34.92	-83.52	0.0	4.0	NCEER
1860	8	7	15	30	0.0	37.50	-87.50	0.0	4.3	NCEER
1860	10	17	11	15	0.0	47.50	-70.10	0.0	6.0	NCEER
1860	10	22	5	0	0.0	34.13	-82.64	0.0	3.2	NCEER
1861	1	3	16	30	0.0	35.09	-83.36	0.0	4.3	NCEER
1861	7	12	0	0	0.0	45.40	-75.40	0.0	5.0	NCEER
1861	8	31	5	0	0.0	36.18	-82.30	0.0	5.2	NCEER
1861	10	1	0	0	0.0	45.60	-73.70	0.0	3.5	NCEER
1862	2	2	19	0	0.0	41.43	-72.47	0.0	3.4	NCEER
1862	12	10	20	52	0.0	37.57	-77.45	0.0	3.8	NCEER
1863	6	9	21	30	0.0	44.50	-73.00	0.0	3.3	NCEER
1864	4	20	18	15	0.0	46.90	-71.20	0.0	3.8	NCEER
1864	10	21	9	10	0.0	45.50	-73.60	0.0	3.3	NCEER
1865	1	29	4	0	0.0	42.89	-78.88	0.0	3.8	NCEER

© 2007-2012 UniStar Nuclear Services, LLC. All rights reserved.
COPYRIGHT PROTECTED

Table 2.5-1— {Updated Earthquake catalog (1534-April 2010) Including events with $m_b \geq 3.0$}
(Page 7 of 75)

Year	Month	Day	Hour	Min	Sec	Lat (deg)	Lon (deg)	Depth (km)	mb	Source
1865	8	17	15	0	0.0	36.50	-89.50	0.0	4.6	NCEER
1865	9	17	12	0	0.0	40.05	-76.30	0.0	3.3	NCEER
1866	9	3	5	0	0.0	39.00	-76.89	0.0	3.4	NCEER
1866	11	9	16	10	0.0	46.80	-71.20	0.0	3.3	NCEER
1867	1	7	18	0	0.0	42.97	-77.75	0.0	3.1	NCEER
1867	2	25	3	0	0.0	33.85	-89.90	0.0	3.9	NCEER
1867	4	24	20	22	0.0	39.20	-96.30	0.0	5.2	NCEER
1867	4	28	0	0	0.0	40.70	-95.80	0.0	3.1	NCEER
1867	9	25	6	0	0.0	35.98	-83.92	0.0	3.3	NCEER
1867	10	14	12	0	0.0	42.88	-76.16	0.0	3.2	NCEER
1867	12	18	8	0	0.0	44.65	-75.15	0.0	4.7	NCEER
1868	1	15	0	0	0.0	45.15	-67.20	0.0	4.5	NCEER
1868	2	22	11	0	0.0	36.78	-81.75	0.0	3.4	NCEER
1868	2	26	0	0	0.0	45.51	-73.54	0.0	3.8	NCEER
1868	7	11	21	0	0.0	33.43	-86.10	0.0	3.3	NCEER
1868	8	7	2	0	0.0	41.09	-73.59	0.0	3.5	NCEER
1868	11	15	22	0	0.0	40.62	-74.19	0.0	3.0	NCEER
1868	11	28	19	0	0.0	31.31	-92.46	0.0	3.8	NCEER
1869	1	1	0	0	0.0	32.90	-80.00	0.0	3.3	NCEER
1869	2	15	1	0	0.0	38.81	-77.04	0.0	3.3	NCEER
1869	2	20	0	0	0.0	38.10	-84.50	0.0	3.4	NCEER
1869	4	9	8	0	0.0	42.68	-80.80	0.0	3.3	NCEER
1869	9	5	21	0	0.0	36.02	-83.42	0.0	3.8	NCEER
1869	10	22	11	0	0.0	45.00	-67.20	0.0	5.1	NCEER
1869	11	6	0	40	0.0	35.22	-93.15	0.0	3.3	NCEER
1869	12	1	0	0	0.0	47.50	-70.50	0.0	4.0	NCEER
1870	1	9	5	0	0.0	31.14	-92.29	0.0	4.2	NCEER
1870	2	8	0	0	0.0	44.10	-69.80	0.0	3.3	NCEER
1870	3	17	11	0	0.0	45.50	-66.50	0.0	3.3	NCEER
1870	10	20	16	30	0.0	47.40	-70.50	0.0	6.5	NCEER
1870	12	14	0	0	0.0	36.60	-89.20	0.0	3.0	NCEER
1871	1	3	0	0	0.0	45.60	-74.60	0.0	3.5	NCEER
1871	1	29	12	0	0.0	34.12	-93.05	0.0	3.3	NCEER
1871	5	20	7	0	0.0	46.80	-71.20	0.0	3.3	NCEER
1871	5	21	1	30	0.0	45.00	-78.00	0.0	4.6	NCEER
1871	6	18	22	0	0.0	40.61	-73.44	0.0	3.8	NCEER
1871	7	20	1	0	0.0	43.38	-70.82	0.0	3.9	NCEER
1871	7	25	6	40	0.0	38.50	-90.00	0.0	3.4	NCEER
1871	10	9	14	40	0.0	39.70	-75.50	0.0	3.8	NCEER
1871	10	16	0	0	0.0	43.21	-71.54	0.0	3.3	NCEER
1871	10	19	16	40	0.0	44.31	-69.78	0.0	3.3	NCEER
1872	2	6	14	0	0.0	43.50	-83.80	0.0	3.4	NCEER
1872	2	8	11	0	0.0	37.00	-89.20	0.0	3.0	NCEER
1872	2	26	0	0	0.0	35.98	-83.92	0.0	3.3	NCEER
1872	4	16	2	30	0.0	32.36	-88.70	0.0	4.1	NCEER
1872	6	5	3	0	0.0	37.70	-78.00	0.0	3.7	NCEER

© 2007-2012 UniStar Nuclear Services, LLC. All rights reserved.
COPYRIGHT PROTECTED

Table 2.5-1— {Updated Earthquake catalog (1534-April 2010) Including events with $m_b \geq 3.0$}

Year	Month	Day	Hour	Min	Sec	Lat (deg)	Lon (deg)	Depth (km)	mb	Source
1872	6	17	14	30	0.0	33.06	-83.22	0.0	3.0	NCEER
1872	7	9	2	30	0.0	39.80	-93.50	0.0	3.1	NCEER
1872	7	11	10	25	0.0	40.90	-73.80	0.0	3.0	NCEER
1872	10	9	16	0	0.0	42.70	-97.00	0.0	3.6	NCEER
1872	11	18	19	0	0.0	43.20	-71.60	0.0	3.4	NCEER
1873	1	4	23	40	0.0	39.96	-83.00	0.0	3.8	NCEER
1873	4	23	4	14	0.0	39.70	-84.20	0.0	3.0	NCEER
1873	4	25	19	0	0.0	44.80	-74.20	0.0	3.5	NCEER
1873	4	30	0	0	0.0	43.30	-79.90	0.0	3.1	NCEER
1873	4	30	0	0	0.0	45.00	-74.70	0.0	3.3	NCEER
1873	5	1	4	30	0.0	30.20	-97.70	0.0	3.0	NCEER
1873	5	3	21	0	0.0	36.00	-89.60	0.0	3.7	NCEER
1873	7	6	0	0	0.0	42.69	-78.94	0.0	4.0	NCEER
1873	9	30	11	50	0.0	45.50	-73.20	0.0	3.3	NCEER
1873	9	30	11	50	0.0	46.50	-76.00	0.0	3.3	NCEER
1873	10	3	12	45	0.0	37.20	-78.20	0.0	3.6	NCEER
1873	10	4	0	0	0.0	33.00	-83.90	0.0	3.2	NCEER
1874	1	6	0	0	0.0	43.60	-71.20	0.0	3.3	NCEER
1874	1	25	17	0	0.0	42.60	-71.40	0.0	3.3	NCEER
1874	1	26	7	0	0.0	43.00	-71.50	0.0	3.3	NCEER
1874	2	22	0	0	0.0	35.70	-82.10	0.0	3.3	NCEER
1874	2	28	3	40	0.0	45.18	-67.28	0.0	3.7	NCEER
1874	3	17	0	0	0.0	35.70	-82.10	0.0	3.3	NCEER
1874	4	14	0	0	0.0	35.70	-82.10	0.0	3.3	NCEER
1874	7	9	22	0	0.0	37.00	-89.20	0.0	3.0	NCEER
1874	7	31	9	0	0.0	48.60	-69.10	0.0	3.3	NCEER
1874	11	24	0	0	0.0	42.70	-70.90	0.0	3.0	NCEER
1874	12	11	3	25	0.0	40.90	-73.80	0.0	3.4	NCEER
1875	4	10	0	0	0.0	35.29	-82.51	0.0	3.4	NCEER
1875	6	18	13	43	0.0	40.20	-84.00	0.0	4.7	NCEER
1875	7	28	9	10	0.0	41.90	-73.00	0.0	3.4	NCEER
1875	10	7	0	0	0.0	36.10	-89.60	0.0	4.1	NCEER
1875	10	28	3	0	0.0	35.10	-90.00	0.0	3.1	NCEER
1875	11	1	22	30	0.0	33.49	-82.90	0.0	4.8	NCEER
1875	11	8	10	40	0.0	39.00	-95.70	0.0	3.8	NCEER
1875	11	12	7	0	0.0	36.00	-84.00	0.0	3.6	NCEER
1875	12	1	9	0	0.0	42.90	-72.30	0.0	3.3	NCEER
1875	12	23	4	45	0.0	37.60	-78.50	0.0	4.8	NCEER
1876	2	20	8	0	0.0	41.91	-83.48	0.0	3.3	NCEER
1876	6	1	0	0	0.0	40.40	-84.20	0.0	3.4	NCEER
1876	8	17	5	25	0.0	44.10	-99.60	0.0	3.1	NCEER
1876	9	22	4	30	0.0	41.50	-71.30	0.0	3.6	NCEER
1876	9	25	6	15	0.0	38.50	-87.00	0.0	4.7	NCEER
1876	12	12	0	0	0.0	32.90	-80.00	0.0	3.3	NCEER
1876	12	23	4	45	0.0	37.40	-77.50	0.0	3.3	NCEER
1877	1	23	21	0	0.0	38.80	-83.50	0.0	3.4	NCEER

© 2007-2012 UniStar Nuclear Services, LLC. All rights reserved.
COPYRIGHT PROTECTED

Table 2.5-1— {Updated Earthquake catalog (1534-April 2010) Including events with $m_b \geq 3.0$}

(Page 9 of 75)

Year	Month	Day	Hour	Min	Sec	Lat (deg)	Lon (deg)	Depth (km)	mb	Source
1877	3	20	6	0	0.0	44.90	-72.41	0.0	3.8	NCEER
1877	5	25	0	0	0.0	36.00	-84.00	0.0	3.6	NCEER
1877	5	26	21	0	0.0	38.20	-87.90	0.0	3.0	NCEER
1877	7	15	0	40	0.0	36.80	-89.70	0.0	4.2	NCEER
1877	8	17	16	50	0.0	42.30	-83.30	0.0	3.1	NCEER
1877	9	10	14	59	0.0	40.30	-74.90	0.0	3.3	NCEER
1877	10	14	18	0	0.0	46.75	-72.00	0.0	3.3	NCEER
1877	11	4	0	0	0.0	45.20	-73.90	0.0	4.7	NCEER
1877	11	15	17	45	0.0	41.00	-97.00	0.0	5.0	NCEER
1877	11	16	7	38	0.0	35.50	-84.00	0.0	3.7	NCEER
1877	11	19	11	10	0.0	37.00	-89.20	0.0	3.0	NCEER
1877	12	18	10	0	0.0	45.70	-76.85	0.0	3.5	NCEER
1878	1	9	4	30	0.0	37.00	-89.20	0.0	3.0	NCEER
1878	3	12	10	0	0.0	36.80	-89.10	0.0	3.9	NCEER
1878	10	4	7	30	0.0	41.50	-74.00	0.0	3.4	NCEER
1878	11	19	5	52	0.0	35.50	-90.70	0.0	5.2	NCEER
1879	3	1	0	0	0.0	39.60	-99.10	0.0	3.3	NCEER
1879	3	26	0	30	0.0	39.20	-75.50	0.0	3.3	NCEER
1879	6	11	0	0	0.0	45.60	-73.60	0.0	3.3	NCEER
1879	8	21	8	0	0.0	43.20	-79.20	0.0	3.3	NCEER
1879	9	26	3	10	0.0	35.30	-90.30	0.0	3.7	NCEER
1879	10	26	2	30	0.0	43.00	-71.50	0.0	3.3	NCEER
1879	10	26	20	0	0.0	34.37	-81.08	0.0	3.1	NCEER
1879	12	29	6	30	0.0	42.90	-97.30	0.0	3.6	NCEER
1880	5	12	12	45	0.0	42.70	-71.00	0.0	3.4	NCEER
1880	5	31	0	0	0.0	45.20	-75.30	0.0	3.3	NCEER
1880	7	14	2	30	0.0	35.30	-90.30	0.0	3.7	NCEER
1880	7	20	0	0	0.0	43.00	-71.50	0.0	3.3	NCEER
1880	9	6	5	30	0.0	45.20	-73.80	0.0	3.3	NCEER
1880	10	31	20	0	0.0	43.92	-78.58	0.0	3.3	NCEER
1880	11	28	13	30	0.0	47.45	-70.50	0.0	3.3	NCEER
1880	12	28	7	15	0.0	49.00	-97.20	0.0	3.0	NCEER
1881	1	21	2	40	0.0	44.00	-70.00	0.0	3.3	NCEER
1881	2	3	2	0	0.0	41.62	-74.15	0.0	3.6	NCEER
1881	4	20	0	0	0.0	41.60	-85.80	0.0	3.1	NCEER
1881	5	27	0	0	0.0	41.30	-89.10	0.0	4.0	NCEER
1881	10	1	6	40	0.0	47.60	-70.20	0.0	3.3	NCEER
1881	10	6	5	3	0.0	43.20	-71.60	0.0	3.3	NCEER
1881	10	7	16	52	0.0	35.10	-90.00	0.0	3.1	NCEER
1882	2	9	20	0	0.0	40.40	-84.20	0.0	3.1	NCEER
1882	4	17	0	0	0.0	43.20	-71.70	0.0	3.3	NCEER
1882	7	20	10	0	0.0	36.90	-89.20	0.0	3.4	NCEER
1882	7	28	0	0	0.0	37.60	-90.60	0.0	3.9	NCEER
1882	8	15	15	30	0.0	49.30	-67.40	0.0	3.3	NCEER
1882	9	27	10	20	0.0	38.70	-89.50	0.0	4.4	NCEER
1882	10	22	22	15	0.0	33.60	-95.60	0.0	4.8	NCEER

© 2007-2012 UniStar Nuclear Services, LLC. All rights reserved.
COPYRIGHT PROTECTED

Table 2.5-1— {Updated Earthquake catalog (1534-April 2010) Including events with $m_b \geq 3.0$}
(Page 10 of 75)

Year	Month	Day	Hour	Min	Sec	Lat (deg)	Lon (deg)	Depth (km)	mb	Source
1882	11	8	1	30	0.0	40.50	-105.50	0.0	6.6	USH
1882	11	27	23	30	0.0	43.00	-79.25	0.0	3.1	NCEER
1882	12	19	22	24	0.0	43.20	-71.40	0.0	3.6	NCEER
1883	1	1	2	55	0.0	45.00	-67.00	0.0	3.5	NCEER
1883	1	1	7	58	0.0	44.60	-67.70	0.0	3.3	NCEER
1883	1	11	7	12	0.0	37.00	-88.50	0.0	4.7	NCEER
1883	2	4	11	0	0.0	42.30	-85.60	0.0	4.7	NCEER
1883	2	4	20	5	0.0	43.60	-71.20	0.0	3.3	NCEER
1883	2	28	3	30	0.0	41.50	-71.30	0.0	3.6	NCEER
1883	3	11	23	57	0.0	39.50	-76.40	0.0	3.1	NCEER
1883	3	12	0	0	0.0	45.10	-74.50	0.0	3.3	NCEER
1883	4	12	8	30	0.0	37.00	-89.20	0.0	4.5	NCEER
1883	5	23	4	30	0.0	38.40	-82.60	0.0	3.1	NCEER
1883	6	11	18	16	0.0	35.10	-90.00	0.0	4.0	NCEER
1883	7	14	7	30	0.0	37.00	-89.10	0.0	3.7	NCEER
1883	11	15	3	14	0.0	38.70	-90.20	0.0	3.1	NCEER
1883	12	5	15	20	0.0	35.70	-91.20	0.0	4.0	NCEER
1884	1	18	7	0	0.0	43.20	-71.70	0.0	3.3	NCEER
1884	1	18	8	0	0.0	34.59	-77.59	0.0	3.7	NCEER
1884	3	17	20	0	0.0	41.10	-100.70	0.0	3.1	NCEER
1884	3	21	4	30	0.0	32.80	-83.05	0.0	3.6	NCEER
1884	8	10	19	7	0.0	40.60	-74.00	0.0	5.2	NCEER
1884	8	11	6	0	0.0	42.78	-71.07	0.0	3.3	NCEER
1884	8	24	19	45	0.0	36.07	-83.83	0.0	3.3	NCEER
1884	9	18	20	0	0.0	32.30	-85.17	0.0	3.3	NCEER
1884	9	19	20	14	0.0	40.70	-84.10	0.0	4.8	NCEER
1884	11	23	5	30	0.0	43.20	-71.70	0.0	3.7	NCEER
1884	11	30	5	0	0.0	35.50	-89.70	0.0	3.5	NCEER
1884	12	17	7	0	0.0	43.70	-71.50	0.0	3.3	NCEER
1885	1	3	2	12	0.0	39.20	-77.50	0.0	3.9	NCEER
1885	1	4	11	6	0.0	41.30	-73.90	0.0	3.4	NCEER
1885	1	18	10	30	0.0	41.16	-81.60	0.0	3.5	NCEER
1885	2	2	12	10	0.0	36.90	-81.10	0.0	3.3	NCEER
1885	6	1	0	0	0.0	45.10	-66.10	0.0	3.3	NCEER
1885	8	6	9	0	0.0	36.12	-81.83	0.0	3.4	NCEER
1885	10	10	4	35	0.0	37.70	-78.80	0.0	4.4	NCEER
1885	10	17	18	20	0.0	33.17	-82.71	0.0	3.6	NCEER
1886	1	6	0	10	0.0	42.90	-71.50	0.0	3.3	NCEER
1886	1	25	0	4	0.0	41.60	-73.80	0.0	3.3	NCEER
1886	2	5	1	0	0.0	32.80	-88.00	0.0	3.5	NCEER
1886	2	5	2	0	0.0	35.93	-81.52	0.0	3.3	NCEER
1886	2	13	6	0	0.0	32.34	-88.05	0.0	3.5	NCEER
1886	2	27	12	0	0.0	43.08	-73.87	0.0	3.3	NCEER
1886	3	1	16	0	0.0	39.00	-85.50	0.0	3.0	NCEER
1886	3	18	5	59	0.0	37.00	-89.20	0.0	4.2	NCEER
1886	4	23	6	0	0.0	43.09	-76.32	0.0	3.1	NCEER

© 2007-2012 UniStar Nuclear Services, LLC. All rights reserved.
COPYRIGHT PROTECTED

Table 2.5-1— {Updated Earthquake catalog (1534-April 2010) Including events with $m_b \geq 3.0$}

Year	Month	Day	Hour	Min	Sec	Lat (deg)	Lon (deg)	Depth (km)	mb	Source
1886	5	3	3	0	0.0	39.36	-82.24	0.0	3.8	NCEER
1886	5	18	19	30	0.0	49.30	-67.40	0.0	3.3	NCEER
1886	8	12	0	0	0.0	46.00	-74.00	0.0	3.3	NCEER
1886	8	14	0	0	0.0	39.70	-86.10	0.0	3.0	NCEER
1886	8	27	8	30	0.0	33.38	-80.14	0.0	3.8	NCEER
1886	9	1	0	0	0.0	44.27	-76.63	0.0	3.8	NCEER
1886	9	1	0	0	0.0	30.40	-81.70	0.0	3.3	NCEER
1886	9	1	2	51	0.0	32.90	-80.00	0.0	6.8	NCEER
1886	9	1	8	55	0.0	33.93	-81.94	0.0	4.4	NCEER
1886	9	1	9	45	0.0	34.30	-82.86	0.0	4.2	NCEER
1886	9	1	23	50	0.0	33.41	-81.56	0.0	4.3	NCEER
1886	9	2	23	0	0.0	34.72	-81.23	0.0	3.6	NCEER
1886	9	5	0	0	0.0	41.50	-72.50	0.0	3.3	NCEER
1886	9	7	11	42	0.0	33.05	-80.97	0.0	4.1	NCEER
1886	9	7	17	0	0.0	32.70	-80.68	0.0	4.3	NCEER
1886	9	19	0	0	0.0	32.23	-80.96	0.0	3.7	NCEER
1886	9	21	6	20	0.0	41.18	-73.19	0.0	3.0	NCEER
1886	9	23	23	0	0.0	41.13	-91.44	0.0	3.3	NCEER
1886	9	25	2	0	0.0	36.70	-80.05	0.0	3.2	NCEER
1886	9	27	22	0	0.0	34.70	-81.62	0.0	3.4	NCEER
1886	10	22	0	0	0.0	34.71	-81.66	0.0	4.1	NCEER
1886	10	22	14	45	0.0	33.87	-81.01	0.0	5.2	NCEER
1886	10	31	14	20	0.0	33.90	-80.39	0.0	3.9	NCEER
1886	11	5	12	25	0.0	33.40	-80.42	0.0	5.3	NCEER
1886	12	2	2	20	0.0	33.04	-81.06	0.0	3.8	NCEER
1886	12	11	16	0	0.0	34.18	-82.06	0.0	3.6	NCEER
1887	1	2	22	30	0.0	39.57	-77.00	0.0	3.3	NCEER
1887	1	5	11	35	0.0	30.17	-97.22	0.0	3.4	NCEER
1887	1	7	14	22	0.0	30.33	-81.66	0.0	3.8	NCEER
1887	1	12	6	0	0.0	34.35	-82.42	0.0	3.1	NCEER
1887	1	27	20	0	0.0	41.45	-96.64	0.0	3.2	NCEER
1887	1	31	20	14	0.0	30.53	-96.30	0.0	3.8	NCEER
1887	2	6	22	15	0.0	39.00	-88.50	0.0	4.5	NCEER
1887	2	10	21	30	0.0	42.37	-93.82	0.0	3.3	NCEER
1887	2	19	0	0	0.0	45.35	-80.00	0.0	3.1	NCEER
1887	2	22	22	59	0.0	49.30	-67.40	0.0	3.3	NCEER
1887	3	2	16	30	0.0	40.72	-73.45	0.0	3.5	NCEER
1887	3	11	0	0	0.0	47.50	-70.50	0.0	3.3	NCEER
1887	4	5	3	0	0.0	43.29	-71.89	0.0	3.3	NCEER
1887	5	22	20	45	0.0	33.90	-80.37	0.0	3.7	NCEER
1887	5	27	6	15	0.0	47.45	-70.50	0.0	4.0	NCEER
1887	6	3	8	45	0.0	34.00	-81.00	0.0	3.6	NCEER
1887	6	30	17	0	0.0	43.06	-72.01	0.0	3.7	NCEER
1887	7	10	13	5	0.0	33.74	-80.77	0.0	3.7	NCEER
1887	8	2	1	0	0.0	34.41	-78.83	0.0	3.8	NCEER
1887	8	2	18	36	0.0	37.20	-88.50	0.0	4.6	NCEER

© 2007-2012 UniStar Nuclear Services, LLC. All rights reserved.
COPYRIGHT PROTECTED

Table 2.5-1— {Updated Earthquake catalog (1534-April 2010) Including events with $m_b \geq 3.0$}
(Page 12 of 75)

Year	Month	Day	Hour	Min	Sec	Lat (deg)	Lon (deg)	Depth (km)	mb	Source
1887	8	10	7	1	0.0	33.83	-79.95	0.0	3.9	NCEER
1887	8	26	23	45	0.0	32.49	-80.62	0.0	4.2	NCEER
1887	8	27	4	56	0.0	33.52	-81.22	0.0	4.0	NCEER
1887	8	28	22	57	0.0	33.66	-80.86	0.0	3.9	NCEER
1887	12	23	0	0	0.0	41.64	-70.93	0.0	3.4	NCEER
1888	1	11	5	0	0.0	45.42	-75.70	0.0	4.2	NCEER
1888	1	12	9	55	0.0	34.18	-80.17	0.0	4.4	NCEER
1888	1	23	0	0	0.0	42.81	-70.88	0.0	3.3	NCEER
1888	2	1	11	0	0.0	44.35	-71.65	0.0	4.1	NCEER
1888	2	9	20	0	0.0	41.49	-81.69	0.0	3.3	NCEER
1888	3	17	0	0	0.0	36.40	-82.50	0.0	3.0	NCEER
1888	3	27	2	0	0.0	42.76	-71.45	0.0	3.8	NCEER
1888	4	19	1	0	0.0	47.45	-70.50	0.0	3.6	NCEER
1888	7	8	23	0	0.0	44.39	-77.06	0.0	3.7	NCEER
1888	8	15	1	15	0.0	44.30	-70.00	0.0	3.3	NCEER
1888	8	15	18	30	0.0	34.37	-81.08	0.0	3.1	NCEER
1888	8	23	5	40	0.0	34.87	-85.84	0.0	3.8	NCEER
1888	9	17	21	30	0.0	33.42	-83.35	0.0	3.5	NCEER
1888	11	3	0	0	0.0	35.40	-90.40	0.0	3.1	NCEER
1888	11	17	4	0	0.0	42.18	-71.55	0.0	3.0	NCEER
1888	12	7	6	0	0.0	47.64	-69.70	0.0	4.2	NCEER
1888	12	19	6	0	0.0	43.36	-73.74	0.0	3.6	NCEER
1889	1	7	22	15	0.0	39.48	-88.38	0.0	3.3	NCEER
1889	2	5	19	40	0.0	33.16	-79.20	0.0	3.9	NCEER
1889	3	8	0	0	0.0	43.50	-71.60	0.0	3.3	NCEER
1889	3	8	23	40	0.0	40.00	-76.00	0.0	4.1	NCEER
1889	5	11	3	45	0.0	38.98	-76.49	0.0	3.3	NCEER
1889	6	6	16	25	0.0	35.90	-88.10	0.0	3.7	NCEER
1889	6	7	10	35	0.0	41.67	-71.05	0.0	3.2	NCEER
1889	7	8	0	0	0.0	44.67	-70.15	0.0	3.8	NCEER
1889	7	11	21	47	0.0	32.40	-80.33	0.0	4.4	NCEER
1889	7	20	1	32	0.0	35.20	-90.00	0.0	4.0	NCEER
1889	8	10	9	0	0.0	43.78	-73.75	0.0	3.9	NCEER
1889	9	29	0	0	0.0	35.03	-84.87	0.0	3.5	NCEER
1889	10	24	10	0	0.0	34.72	-82.60	0.0	3.1	NCEER
1889	12	2	1	0	0.0	43.47	-71.24	0.0	3.2	NCEER
1890	2	7	16	20	0.0	40.33	-74.20	0.0	3.6	NCEER
1890	3	28	22	0	0.0	43.20	-71.75	0.0	3.2	NCEER
1890	4	11	3	0	0.0	45.19	-69.23	0.0	3.3	NCEER
1890	5	25	7	0	0.0	43.11	-74.24	0.0	3.8	NCEER
1890	12	23	6	0	0.0	35.98	-83.92	0.0	3.8	NCEER
1891	1	8	6	0	0.0	31.70	-95.20	0.0	3.8	NCEER
1891	1	14	0	0	0.0	35.10	-90.00	0.0	3.0	NCEER
1891	1	14	3	0	0.0	43.35	-75.40	0.0	3.3	NCEER
1891	1	15	5	0	0.0	42.67	-71.58	0.0	3.2	NCEER
1891	4	3	0	0	0.0	47.26	-70.67	0.0	4.2	NCEER

© 2007-2012 UniStar Nuclear Services, LLC. All rights reserved.
COPYRIGHT PROTECTED

Table 2.5-1— {Updated Earthquake catalog (1534-April 2010) Including events with $m_b \geq 3.0$}
(Page 13 of 75)

Year	Month	Day	Hour	Min	Sec	Lat (deg)	Lon (deg)	Depth (km)	mb	Source
1891	5	2	0	10	0.0	43.20	-71.60	0.0	3.7	NCEER
1891	5	8	15	30	0.0	28.62	-96.63	0.0	3.3	NCEER
1891	6	7	11	0	0.0	40.49	-74.45	0.0	3.3	NCEER
1891	7	27	2	28	0.0	37.90	-87.50	0.0	4.2	NCEER
1891	8	9	18	0	0.0	40.93	-71.94	0.0	3.8	NCEER
1891	8	18	3	0	0.0	41.34	-73.41	0.0	3.5	NCEER
1891	8	28	20	0	0.0	41.96	-73.10	0.0	3.2	NCEER
1891	9	27	4	55	0.0	38.30	-88.50	0.0	5.5	NCEER
1891	10	13	5	55	0.0	32.90	-80.00	0.0	3.3	NCEER
1892	2	11	0	0	0.0	39.86	-74.74	0.0	3.8	NCEER
1892	2	17	12	0	0.0	44.84	-68.36	0.0	3.3	NCEER
1892	3	10	21	0	0.0	42.58	-70.90	0.0	3.3	NCEER
1892	4	12	11	45	0.0	43.34	-74.46	0.0	3.8	NCEER
1892	4	15	5	25	0.0	40.55	-84.57	0.0	3.8	NCEER
1892	5	1	9	0	0.0	43.21	-71.54	0.0	3.2	NCEER
1892	5	6	3	0	0.0	40.18	-76.17	0.0	3.8	NCEER
1892	8	4	18	0	0.0	42.68	-88.28	0.0	3.2	NCEER
1892	12	11	16	30	0.0	44.30	-71.70	0.0	3.3	NCEER
1892	12	25	6	32	0.0	45.08	-74.58	0.0	3.3	NCEER
1893	1	11	20	0	0.0	38.28	-85.75	0.0	3.8	NCEER
1893	1	15	20	30	0.0	40.62	-74.42	0.0	3.8	NCEER
1893	3	9	5	30	0.0	40.60	-74.00	0.0	3.3	NCEER
1893	3	14	0	0	0.0	42.30	-72.70	0.0	3.3	NCEER
1893	4	26	4	0	0.0	40.05	-76.30	0.0	3.3	NCEER
1893	6	21	7	7	0.0	30.40	-81.70	0.0	3.3	NCEER
1893	7	5	8	10	0.0	32.90	-80.00	0.0	3.3	NCEER
1893	9	19	7	5	0.0	32.90	-80.00	0.0	3.3	NCEER
1893	11	8	4	40	0.0	32.90	-80.00	0.0	3.3	NCEER
1893	11	27	16	50	0.0	45.50	-73.30	0.0	5.2	NCEER
1893	12	1	5	0	0.0	50.20	-66.38	0.0	3.3	NCEER
1893	12	25	3	0	0.0	40.41	-77.97	0.0	3.8	NCEER
1893	12	27	6	51	0.0	32.90	-80.00	0.0	3.3	NCEER
1894	1	11	9	0	0.0	49.70	-66.80	0.0	3.3	NCEER
1894	1	11	14	25	0.0	40.59	-98.39	0.0	3.8	NCEER
1894	1	25	20	40	0.0	38.98	-76.49	0.0	3.8	NCEER
1894	1	30	4	5	0.0	32.90	-80.00	0.0	3.3	NCEER
1894	2	25	5	30	0.0	41.42	-99.12	0.0	3.8	NCEER
1894	2	27	22	0	0.0	42.12	-86.46	0.0	3.8	NCEER
1894	3	27	20	0	0.0	30.12	-97.32	0.0	3.3	NCEER
1894	4	10	0	0	0.0	41.60	-72.50	0.0	3.3	NCEER
1894	6	16	2	16	0.0	32.90	-80.00	0.0	3.3	NCEER
1894	6	25	0	0	0.0	42.90	-106.30	0.0	4.3	NCEER
1894	7	27	0	0	0.0	44.33	-78.75	0.0	3.8	NCEER
1894	9	27	8	0	0.0	47.97	-70.78	0.0	3.7	NCEER
1894	11	9	3	0	0.0	42.12	-86.46	0.0	3.8	NCEER
1894	11	11	23	40	0.0	46.00	-72.75	0.0	3.8	NCEER

© 2007-2012 UniStar Nuclear Services, LLC. All rights reserved.
COPYRIGHT PROTECTED

Table 2.5-1— {Updated Earthquake catalog (1534-April 2010) Including events with $m_b \geq 3.0$}
(Page 14 of 75)

Year	Month	Day	Hour	Min	Sec	Lat (deg)	Lon (deg)	Depth (km)	mb	Source
1894	11	12	22	35	0.0	41.91	-72.38	0.0	3.1	NCEER
1894	11	23	8	0	0.0	41.32	-72.17	0.0	3.3	NCEER
1894	11	24	4	0	0.0	39.27	-81.56	0.0	3.8	NCEER
1894	12	2	10	50	0.0	39.61	-90.81	0.0	3.3	NCEER
1894	12	11	5	27	0.0	32.90	-80.00	0.0	3.3	NCEER
1894	12	17	3	0	0.0	42.47	-73.80	0.0	3.4	NCEER
1895	1	8	5	40	0.0	32.90	-80.00	0.0	3.3	NCEER
1895	1	9	23	30	0.0	45.72	-77.00	0.0	3.3	NCEER
1895	3	4	22	0	0.0	36.10	-80.25	0.0	3.3	NCEER
1895	4	27	7	40	0.0	32.90	-80.00	0.0	3.3	NCEER
1895	5	28	11	51	0.0	42.85	-72.56	0.0	3.8	NCEER
1895	7	25	4	1	0.0	32.90	-80.00	0.0	3.3	NCEER
1895	7	27	0	0	0.0	35.20	-88.20	0.0	3.0	NCEER
1895	8	19	15	0	0.0	38.53	-83.75	0.0	3.2	NCEER
1895	9	1	11	9	0.0	40.46	-74.30	0.0	4.3	NCEER
1895	9	12	5	0	0.0	36.00	-83.00	0.0	3.3	NCEER
1895	10	6	6	25	0.0	32.90	-80.00	0.0	3.3	NCEER
1895	10	7	4	30	0.0	35.90	-77.50	0.0	3.5	NCEER
1895	10	11	23	55	0.0	43.90	-103.30	0.0	3.5	NCEER
1895	10	31	11	8	0.0	37.00	-89.40	0.0	5.4	NCEER
1895	11	12	23	33	0.0	32.90	-80.00	0.0	3.3	NCEER
1895	11	15	22	30	0.0	41.08	-74.07	0.0	3.3	NCEER
1895	11	20	3	0	0.0	39.98	-75.75	0.0	3.3	NCEER
1896	1	6	4	0	0.0	43.70	-72.29	0.0	3.8	NCEER
1896	1	11	7	30	0.0	44.31	-69.97	0.0	3.3	NCEER
1896	2	11	1	45	0.0	36.30	-78.60	0.0	3.3	NCEER
1896	3	1	19	17	0.0	37.03	-97.62	0.0	3.3	NCEER
1896	3	4	0	0	0.0	40.33	-75.83	0.0	3.8	NCEER
1896	3	15	7	0	0.0	40.30	-84.20	0.0	3.1	NCEER
1896	3	19	8	22	0.0	32.90	-80.00	0.0	3.3	NCEER
1896	3	23	0	56	0.0	45.20	-67.20	0.0	3.8	NCEER
1896	5	16	4	0	0.0	45.90	-66.60	0.0	3.3	NCEER
1896	7	13	1	0	0.0	43.87	-78.93	0.0	3.8	NCEER
1896	8	11	5	58	0.0	32.90	-80.00	0.0	3.3	NCEER
1896	9	17	6	0	0.0	47.50	-70.50	0.0	3.3	NCEER
1896	10	22	10	30	0.0	44.30	-71.80	0.0	3.3	NCEER
1896	11	14	8	15	0.0	32.90	-80.00	0.0	3.3	NCEER
1896	11	20	15	0	0.0	39.73	-75.39	0.0	3.3	NCEER
1896	12	6	17	0	0.0	45.07	-94.07	0.0	3.3	NCEER
1897	1	2	0	0	0.0	45.42	-75.70	0.0	3.8	NCEER
1897	1	19	21	0	0.0	44.42	-72.03	0.0	3.3	NCEER
1897	1	26	11	30	0.0	44.71	-67.46	0.0	3.8	NCEER
1897	1	28	0	0	0.0	44.50	-66.80	0.0	3.3	NCEER
1897	3	3	6	15	0.0	42.39	-76.87	0.0	3.3	NCEER
1897	3	5	22	40	0.0	43.12	-79.05	0.0	3.2	NCEER
1897	3	21	6	0	0.0	42.83	-71.25	0.0	3.6	NCEER

© 2007-2012 UniStar Nuclear Services, LLC. All rights reserved.
COPYRIGHT PROTECTED

Table 2.5-1— {Updated Earthquake catalog (1534-April 2010) Including events with $m_b \geq 3.0$}
(Page 15 of 75)

Year	Month	Day	Hour	Min	Sec	Lat (deg)	Lon (deg)	Depth (km)	mb	Source
1897	3	23	23	7	0.0	45.50	-73.60	0.0	5.0	NCEER
1897	3	24	6	0	0.0	40.57	-74.61	0.0	3.8	NCEER
1897	4	20	3	0	0.0	41.26	-95.94	0.0	3.3	NCEER
1897	4	26	4	0	0.0	35.80	-89.60	0.0	3.7	NCEER
1897	5	1	4	0	0.0	37.00	-89.00	0.0	3.3	NCEER
1897	5	2	20	0	0.0	42.79	-86.11	0.0	3.3	NCEER
1897	5	6	20	45	0.0	33.48	-81.31	0.0	3.5	NCEER
1897	5	28	3	16	0.0	44.50	-73.50	0.0	4.5	NCEER
1897	5	31	18	58	0.0	37.30	-80.70	0.0	5.0	NCEER
1897	6	3	0	30	0.0	42.74	-73.68	0.0	3.3	NCEER
1897	6	4	23	48	0.0	36.95	-81.09	0.0	3.3	NCEER
1897	6	6	4	0	0.0	43.33	-91.51	0.0	3.4	NCEER
1897	7	1	9	20	0.0	43.70	-71.60	0.0	3.3	NCEER
1897	7	22	3	0	0.0	43.08	-73.87	0.0	3.4	NCEER
1897	9	5	0	0	0.0	41.50	-72.50	0.0	3.3	NCEER
1897	9	25	18	5	0.0	44.70	-68.70	0.0	4.1	NCEER
1897	10	22	3	20	0.0	36.90	-81.10	0.0	4.1	NCEER
1897	11	9	22	0	0.0	41.40	-73.45	0.0	3.8	NCEER
1897	11	14	0	0	0.0	42.90	-106.30	0.0	4.5	NCEER
1897	11	27	20	56	0.0	37.70	-77.50	0.0	3.3	NCEER
1897	12	2	7	10	0.0	37.70	-97.70	0.0	4.0	NCEER
1897	12	3	0	0	0.0	43.14	-89.75	0.0	3.8	NCEER
1897	12	18	23	45	0.0	37.70	-77.50	0.0	4.6	NCEER
1898	1	2	5	0	0.0	42.98	-70.95	0.0	3.8	NCEER
1898	1	7	13	20	0.0	44.85	-74.29	0.0	4.0	NCEER
1898	1	11	9	0	0.0	44.70	-66.80	0.0	3.3	NCEER
1898	1	27	1	35	0.0	34.60	-90.60	0.0	3.1	NCEER
1898	2	5	20	0	0.0	37.00	-81.00	0.0	4.3	NCEER
1898	2	22	0	0	0.0	43.25	-73.50	0.0	3.3	NCEER
1898	6	1	22	15	0.0	44.85	-74.29	0.0	3.3	NCEER
1898	6	11	6	45	0.0	42.80	-72.60	0.0	3.3	NCEER
1898	6	14	15	6	0.0	36.50	-88.70	0.0	4.0	NCEER
1898	6	19	15	0	0.0	36.07	-83.67	0.0	4.0	NCEER
1898	7	23	21	30	0.0	36.75	-82.83	0.0	3.9	NCEER
1898	9	16	9	59	0.0	42.60	-97.30	0.0	3.1	NCEER
1898	11	25	20	0	0.0	37.00	-81.00	0.0	4.3	NCEER
1899	1	1	20	30	0.0	40.31	-74.27	0.0	3.4	NCEER
1899	1	30	2	30	0.0	43.08	-73.87	0.0	3.3	NCEER
1899	2	11	0	0	0.0	43.35	-85.40	0.0	3.1	NCEER
1899	2	13	9	30	0.0	37.00	-81.00	0.0	4.4	NCEER
1899	3	3	0	0	0.0	36.90	-76.30	0.0	3.3	NCEER
1899	3	10	5	45	0.0	32.90	-80.00	0.0	3.3	NCEER
1899	4	30	2	5	0.0	38.50	-87.40	0.0	4.6	NCEER
1899	4	30	12	24	0.0	43.53	-71.47	0.0	3.8	NCEER
1899	5	17	1	15	0.0	41.60	-72.60	0.0	3.6	NCEER
1899	6	26	19	10	0.0	41.47	-72.60	0.0	3.7	NCEER

© 2007-2012 UniStar Nuclear Services, LLC. All rights reserved.
COPYRIGHT PROTECTED

Table 2.5-1— {Updated Earthquake catalog (1534-April 2010) Including events with $m_b \geq 3.0$}
(Page 16 of 75)

Year	Month	Day	Hour	Min	Sec	Lat (deg)	Lon (deg)	Depth (km)	mb	Source
1899	8	25	5	0	0.0	43.21	-71.54	0.0	3.8	NCEER
1899	9	14	3	0	0.0	41.17	-82.12	0.0	3.3	NCEER
1899	10	5	11	30	0.0	44.00	-69.50	0.0	3.3	NCEER
1899	10	11	4	0	0.0	42.10	-86.50	0.0	3.2	NCEER
1899	11	12	14	0	0.0	39.30	-83.00	0.0	3.1	NCEER
1899	12	1	18	50	0.0	36.80	-94.40	0.0	3.1	NCEER
1899	12	4	12	48	0.0	32.90	-80.00	0.0	3.3	NCEER
1899	12	6	12	0	0.0	44.50	-99.00	0.0	3.5	NCEER
1900	3	14	3	0	0.0	45.50	-89.50	0.0	3.0	NCEER
1900	4	9	13	0	0.0	41.40	-81.80	0.0	4.0	NCEER
1900	4	28	19	7	0.0	39.84	-75.15	0.0	3.4	NCEER
1900	6	26	14	0	0.0	41.05	-73.53	0.0	3.2	NCEER
1900	10	31	16	15	0.0	30.40	-81.70	0.0	3.5	NCEER
1900	12	1	0	0	0.0	36.00	-96.80	0.0	3.1	NCEER
1901	1	4	3	12	0.0	37.80	-94.00	0.0	3.5	NCEER
1901	1	30	14	0	0.0	39.89	-75.13	0.0	3.0	NCEER
1901	2	15	0	15	0.0	36.00	-90.00	0.0	3.8	NCEER
1901	3	5	18	0	0.0	42.99	-71.46	0.0	3.3	NCEER
1901	5	17	7	0	0.0	38.95	-82.66	0.0	4.3	NCEER
1901	10	31	22	0	0.0	42.71	-71.60	0.0	3.6	NCEER
1901	12	2	0	26	0.0	32.90	-80.00	0.0	3.3	NCEER
1901	12	10	18	0	0.0	41.65	-70.48	0.0	3.2	NCEER
1902	1	12	21	0	0.0	43.08	-73.87	0.0	3.3	NCEER
1902	1	24	10	18	0.0	42.30	-89.00	0.0	4.3	NCEER
1902	3	5	8	0	0.0	38.14	-83.76	0.0	3.8	NCEER
1902	3	10	6	0	0.0	39.90	-85.20	0.0	3.0	NCEER
1902	5	18	4	0	0.0	37.30	-80.60	0.0	3.4	NCEER
1902	5	29	7	30	0.0	35.10	-85.30	0.0	4.2	NCEER
1902	5	30	6	0	0.0	34.85	-82.40	0.0	3.3	NCEER
1902	6	14	7	0	0.0	40.30	-81.40	0.0	3.3	NCEER
1902	7	18	5	25	0.0	44.85	-74.29	0.0	4.2	NCEER
1902	7	19	17	50	0.0	43.44	-71.82	0.0	3.1	NCEER
1902	7	28	18	0	0.0	42.50	-97.50	0.0	4.2	NCEER
1902	8	25	12	48	0.0	40.57	-75.09	0.0	3.3	NCEER
1902	10	9	12	0	0.0	30.34	-97.73	0.0	3.3	NCEER
1902	10	9	19	0	0.0	30.10	-97.60	0.0	3.6	SRA
1902	10	18	22	0	0.0	35.00	-85.30	0.0	3.2	NCEER
1903	1	24	1	0	0.0	32.90	-80.00	0.0	4.1	NCEER
1903	2	9	0	21	0.0	37.80	-89.30	0.0	4.8	NCEER
1903	3	10	6	0	0.0	34.80	-84.97	0.0	3.8	NCEER
1903	3	17	11	50	0.0	39.10	-89.50	0.0	3.0	NCEER
1903	4	24	7	0	0.0	42.78	-71.07	0.0	3.2	NCEER
1903	9	20	0	0	0.0	39.40	-86.30	0.0	3.1	NCEER
1903	9	21	0	0	0.0	38.70	-88.10	0.0	3.1	NCEER
1903	10	5	2	56	0.0	38.30	-90.20	0.0	3.7	NCEER
1903	11	3	18	0	0.0	37.80	-89.30	0.0	3.0	NCEER

© 2007-2012 UniStar Nuclear Services, LLC. All rights reserved.
COPYRIGHT PROTECTED

Table 2.5-1— {Updated Earthquake catalog (1534-April 2010) Including events with $m_b \geq 3.0$}
(Page 17 of 75)

Year	Month	Day	Hour	Min	Sec	Lat (deg)	Lon (deg)	Depth (km)	mb	Source
1903	11	4	19	14	0.0	36.50	-89.80	0.0	4.9	NCEER
1903	11	27	7	0	0.0	37.00	-89.50	0.0	3.9	NCEER
1903	12	2	15	0	0.0	39.12	-88.54	0.0	3.3	NCEER
1903	12	25	12	30	0.0	44.70	-75.50	0.0	3.5	NCEER
1904	3	5	0	30	0.0	35.70	-83.50	0.0	3.4	NCEER
1904	3	21	6	4	0.0	45.00	-67.20	0.0	5.0	NCEER
1904	9	14	8	52	0.0	45.42	-75.70	0.0	3.9	NCEER
1904	10	21	12	0	0.0	38.65	-90.25	0.0	3.3	NCEER
1904	10	28	4	30	0.0	37.50	-100.20	0.0	3.5	NCEER
1905	2	3	0	0	0.0	30.50	-91.10	0.0	3.4	NCEER
1905	2	7	12	0	0.0	29.88	-97.68	0.0	3.8	NCEER
1905	3	13	16	30	0.0	45.10	-87.70	0.0	3.4	NCEER
1905	4	13	16	30	0.0	40.40	-91.60	0.0	3.6	NCEER
1905	7	15	10	10	0.0	44.20	-70.00	0.0	4.4	NCEER
1905	7	27	0	20	0.0	47.30	-88.40	0.0	4.5	NCEER
1905	8	22	5	8	0.0	37.20	-89.30	0.0	5.2	NCEER
1905	8	30	22	40	0.0	43.10	-70.70	0.0	3.4	NCEER
1905	10	22	6	0	0.0	44.94	-72.21	0.0	4.2	NCEER
1905	11	26	0	30	0.0	41.50	-71.30	0.0	3.3	NCEER
1905	12	23	0	0	0.0	39.70	-78.18	0.0	3.1	NCEER
1906	1	8	0	15	0.0	39.20	-96.50	0.0	4.9	NCEER
1906	3	6	0	0	0.0	39.70	-91.40	0.0	3.1	NCEER
1906	4	23	7	12	0.0	40.70	-83.60	0.0	3.4	NCEER
1906	5	8	6	58	0.0	39.50	-85.80	0.0	3.6	NCEER
1906	5	8	13	30	0.0	41.50	-72.50	0.0	3.3	NCEER
1906	5	8	17	41	0.0	38.70	-75.70	0.0	3.0	NCEER
1906	5	9	6	38	0.0	39.20	-85.90	0.0	3.1	NCEER
1906	5	10	0	27	0.0	43.00	-101.30	0.0	4.2	NCEER
1906	5	11	6	15	0.0	38.50	-87.20	0.0	3.3	NCEER
1906	5	20	15	0	0.0	40.25	-75.83	0.0	3.8	NCEER
1906	5	21	19	0	0.0	38.70	-88.40	0.0	3.4	NCEER
1906	5	26	14	42	0.0	47.30	-88.40	0.0	3.3	NCEER
1906	6	27	21	10	0.0	40.40	-81.60	0.0	3.2	NCEER
1906	8	8	0	0	0.0	47.30	-88.40	0.0	3.7	NCEER
1906	8	13	13	19	0.0	39.70	-86.80	0.0	3.1	NCEER
1906	9	7	16	33	0.0	38.20	-87.70	0.0	3.8	NCEER
1906	10	19	19	30	0.0	43.00	-70.00	0.0	4.2	NCEER
1906	11	17	14	0	0.0	45.61	-75.41	0.0	3.3	NCEER
1906	12	5	6	0	0.0	38.67	-76.08	0.0	3.3	NCEER
1907	1	10	9	45	0.0	41.20	-77.10	0.0	3.3	NCEER
1907	1	11	7	45	0.0	37.10	-97.00	0.0	3.1	NCEER
1907	1	30	5	30	0.0	39.50	-86.60	0.0	3.4	NCEER
1907	1	31	5	30	0.0	38.90	-89.50	0.0	3.6	SRA
1907	2	11	13	22	0.0	37.70	-78.30	0.0	4.0	NCEER
1907	4	19	8	30	0.0	32.90	-80.00	0.0	3.9	NCEER
1907	6	29	0	0	0.0	43.50	-70.50	0.0	3.3	NCEER

© 2007-2012 UniStar Nuclear Services, LLC. All rights reserved.
COPYRIGHT PROTECTED

Table 2.5-1— {Updated Earthquake catalog (1534-April 2010) Including events with $m_b \geq 3.0$}
(Page 18 of 75)

Year	Month	Day	Hour	Min	Sec	Lat (deg)	Lon (deg)	Depth (km)	mb	Source
1907	7	4	9	0	0.0	37.80	-90.40	0.0	3.2	NCEER
1907	8	5	12	43	0.0	47.65	-70.16	0.0	3.3	NCEER
1907	10	16	0	10	0.0	42.80	-71.00	0.0	3.5	NCEER
1907	11	14	5	0	0.0	45.47	-76.68	0.0	3.3	NCEER
1907	11	28	16	30	0.0	42.30	-89.80	0.0	3.1	NCEER
1907	12	11	4	32	0.0	38.60	-90.20	0.0	3.1	NCEER
1908	3	10	0	0	0.0	47.45	-70.50	0.0	3.3	NCEER
1908	5	14	4	45	0.0	44.00	-65.80	0.0	4.0	NCEER
1908	5	31	17	42	0.0	40.60	-75.50	0.0	3.1	NCEER
1908	6	16	20	41	0.0	45.10	-74.80	0.0	3.5	NCEER
1908	7	17	7	10	0.0	45.43	-76.35	0.0	3.3	NCEER
1908	8	8	12	0	0.0	46.30	-67.60	0.0	3.5	NCEER
1908	8	23	9	30	0.0	37.50	-77.90	0.0	3.5	NCEER
1908	9	28	19	34	0.0	36.60	-89.60	0.0	3.5	NCEER
1908	10	28	0	27	0.0	37.00	-89.20	0.0	3.6	NCEER
1908	11	12	12	0	0.0	38.70	-93.20	0.0	3.8	SRA
1908	11	23	13	0	0.0	43.50	-71.70	0.0	3.3	NCEER
1908	12	27	21	15	0.0	37.50	-88.00	0.0	3.7	NCEER
1909	1	23	3	15	0.0	47.20	-88.60	0.0	3.4	NCEER
1909	1	26	20	15	0.0	42.30	-97.80	0.0	3.3	NCEER
1909	2	1	8	20	0.0	45.51	-73.57	0.0	3.3	NCEER
1909	4	2	7	25	0.0	39.40	-78.00	0.0	3.5	NCEER
1909	5	10	1	20	0.0	46.10	-74.30	0.0	3.3	NCEER
1909	5	16	4	15	0.0	49.00	-104.00	0.0	5.5	NCEER
1909	5	26	14	42	0.0	41.60	-88.10	0.0	5.0	USH
1909	6	8	8	25	0.0	46.05	-74.28	0.0	3.3	NCEER
1909	7	19	4	34	0.0	40.30	-90.70	0.0	4.3	NCEER
1909	8	16	22	45	0.0	38.30	-90.10	0.0	3.8	NCEER
1909	9	22	0	0	0.0	38.70	-86.50	0.0	3.7	NCEER
1909	9	27	9	45	0.0	39.50	-87.40	0.0	4.8	NCEER
1909	10	8	10	0	0.0	34.90	-85.00	0.0	3.3	NCEER
1909	10	22	22	0	0.0	37.60	-90.60	0.0	3.1	NCEER
1909	10	22	22	30	0.0	41.80	-89.70	0.0	3.3	NCEER
1909	10	23	7	10	0.0	37.00	-89.50	0.0	4.3	NCEER
1909	10	23	9	47	0.0	39.00	-87.80	0.0	3.9	NCEER
1909	12	10	6	24	10.0	45.40	-75.60	0.0	3.3	NCEER
1910	2	1	0	0	0.0	48.00	-70.00	0.0	3.8	NCEER
1910	2	8	14	0	0.0	38.80	-78.70	0.0	3.2	NCEER
1910	2	25	0	0	0.0	43.20	-79.80	0.0	3.1	NCEER
1910	2	26	8	0	0.0	41.40	-97.40	0.0	3.8	NCEER
1910	5	8	21	10	0.0	37.70	-78.40	0.0	3.5	NCEER
1910	5	12	0	0	0.0	30.10	-96.00	0.0	3.2	NCEER
1910	7	26	1	30	0.0	41.50	-109.30	0.0	4.3	DNA
1910	8	21	18	45	0.0	42.70	-71.10	0.0	3.3	NCEER
1910	8	30	14	30	0.0	43.40	-72.10	0.0	3.3	NCEER
1910	10	20	21	50	0.0	44.30	-68.80	0.0	3.3	NCEER

© 2007-2012 UniStar Nuclear Services, LLC. All rights reserved.
COPYRIGHT PROTECTED

Table 2.5-1— {Updated Earthquake catalog (1534-April 2010) Including events with $m_b \geq 3.0$}
(Page 19 of 75)

Year	Month	Day	Hour	Min	Sec	Lat (deg)	Lon (deg)	Depth (km)	mb	Source
1910	10	25	9	30	0.0	47.60	-69.80	0.0	4.0	NCEER
1911	2	10	10	22	0.0	36.60	-79.40	0.0	3.3	NCEER
1911	2	28	9	0	0.0	38.70	-90.30	0.0	3.1	NCEER
1911	3	2	21	30	0.0	43.20	-71.50	0.0	3.3	NCEER
1911	3	31	16	57	0.0	34.00	-91.80	0.0	4.6	NCEER
1911	3	31	18	10	0.0	33.80	-92.20	0.0	3.5	NCEER
1911	4	8	1	0	0.0	38.30	-75.50	0.0	3.3	NCEER
1911	4	20	22	0	0.0	35.10	-82.70	0.0	3.5	NCEER
1911	6	2	22	34	0.0	44.20	-98.20	0.0	4.2	NCEER
1911	7	29	0	0	0.0	41.80	-87.60	0.0	3.3	NCEER
1912	1	2	16	21	0.0	42.30	-89.00	0.0	4.7	NCEER
1912	5	27	12	52	0.0	43.20	-79.70	0.0	3.4	NCEER
1912	6	12	10	30	0.0	32.90	-80.00	0.0	4.9	NCEER
1912	6	20	0	0	0.0	32.00	-81.00	0.0	3.5	NCEER
1912	8	8	1	0	0.0	37.70	-78.40	0.0	3.3	NCEER
1912	9	25	0	0	0.0	42.30	-89.10	0.0	3.0	NCEER
1912	10	23	0	0	0.0	49.50	-68.00	0.0	3.3	NCEER
1912	10	23	1	15	0.0	32.70	-83.50	0.0	3.3	NCEER
1912	11	17	12	30	0.0	32.90	-80.00	0.0	3.3	NCEER
1912	12	7	19	10	0.0	34.70	-81.70	0.0	3.3	NCEER
1913	1	1	18	28	0.0	34.70	-81.70	0.0	5.0	NCEER
1913	3	13	5	0	0.0	34.50	-85.00	0.0	3.3	NCEER
1913	3	28	21	50	0.0	36.20	-83.70	0.0	4.0	NCEER
1913	4	17	16	30	0.0	35.30	-84.20	0.0	3.7	NCEER
1913	4	29	0	28	57.0	44.87	-75.33	0.0	4.4	NCEER
1913	6	8	6	30	0.0	45.68	-74.40	0.0	3.3	NCEER
1913	6	9	15	30	0.0	35.80	-88.90	0.0	3.7	NCEER
1913	8	3	16	45	0.0	36.00	-84.00	0.0	3.8	NCEER
1913	8	10	5	15	0.0	44.00	-74.00	0.0	3.4	NCEER
1913	10	17	2	15	0.0	41.80	-89.70	0.0	3.7	NCEER
1913	11	3	14	30	0.0	41.50	-71.50	0.0	3.3	NCEER
1913	11	11	14	0	0.0	38.20	-85.80	0.0	3.1	NCEER
1914	1	13	8	0	0.0	45.10	-67.20	0.0	3.3	NCEER
1914	1	24	3	24	0.0	35.60	-84.50	0.0	3.5	NCEER
1914	2	10	18	31	0.0	46.00	-75.00	0.0	5.5	NCEER
1914	2	14	9	34	0.0	46.40	-73.60	0.0	3.5	NCEER
1914	2	22	19	15	0.0	45.00	-70.50	0.0	3.8	NCEER
1914	3	5	20	5	0.0	33.50	-83.50	0.0	4.6	NCEER
1914	3	7	1	20	0.0	34.20	-79.80	0.0	3.3	NCEER
1914	4	12	0	0	0.0	49.31	-67.61	0.0	3.3	NCEER
1914	7	14	1	53	0.0	32.90	-80.00	0.0	3.3	NCEER
1914	9	22	7	4	0.0	32.90	-80.00	0.0	4.3	NCEER
1914	10	7	21	0	0.0	43.10	-89.40	0.0	3.1	NCEER
1914	12	30	1	0	0.0	30.50	-95.90	0.0	3.5	NCEER
1915	1	14	9	20	0.0	36.60	-82.20	0.0	3.6	NCEER
1915	2	5	6	55	0.0	37.70	-88.60	0.0	3.1	NCEER

© 2007-2012 UniStar Nuclear Services, LLC. All rights reserved.
COPYRIGHT PROTECTED

Table 2.5-1— {Updated Earthquake catalog (1534-April 2010) Including events with $m_b \geq 3.0$}
(Page 20 of 75)

Year	Month	Day	Hour	Min	Sec	Lat (deg)	Lon (deg)	Depth (km)	mb	Source
1915	2	19	4	35	0.0	37.10	-89.20	0.0	3.1	NCEER
1915	2	21	1	20	0.0	42.70	-71.40	0.0	3.5	NCEER
1915	2	21	23	41	0.0	44.70	-73.40	0.0	3.3	NCEER
1915	3	3	7	45	0.0	47.30	-88.40	0.0	3.0	NCEER
1915	4	15	13	20	0.0	38.70	-88.10	0.0	3.7	NCEER
1915	4	28	23	40	0.0	36.50	-89.50	0.0	3.1	NCEER
1915	7	27	16	30	0.0	44.00	-65.00	0.0	4.0	NCEER
1915	8	8	15	15	0.0	48.10	-103.60	0.0	3.1	NCEER
1915	9	16	19	0	0.0	42.80	-99.30	0.0	3.0	NCEER
1915	10	4	14	2	0.0	47.30	-88.40	0.0	3.3	NCEER
1915	10	8	16	50	0.0	35.70	-95.30	0.0	3.7	NCEER
1915	10	23	6	5	0.0	43.80	-101.50	0.0	3.8	NCEER
1915	10	26	7	40	0.0	36.70	-88.60	0.0	3.4	NCEER
1915	12	7	18	40	0.0	36.00	-90.00	0.0	4.4	NCEER
1916	1	5	13	56	0.0	43.70	-73.70	0.0	4.0	NCEER
1916	1	7	19	45	0.0	39.10	-87.00	0.0	3.7	NCEER
1916	2	3	4	26	0.0	43.00	-74.00	0.0	3.8	NCEER
1916	2	21	22	39	0.0	35.62	-83.55	0.0	5.2	Chapman
1916	2	29	5	15	0.0	46.80	-70.90	0.0	3.3	NCEER
1916	3	2	5	2	0.0	34.50	-82.70	0.0	3.3	NCEER
1916	4	24	16	7	45.0	47.00	-77.00	0.0	4.0	NCEER
1916	5	21	18	24	0.0	36.60	-89.50	0.0	3.6	NCEER
1916	6	8	21	15	0.0	41.00	-73.80	0.0	3.3	NCEER
1916	8	24	9	0	0.0	37.00	-89.20	0.0	3.5	NCEER
1916	8	26	19	36	0.0	36.00	-81.00	0.0	3.6	NCEER
1916	10	18	22	3	40.0	33.50	-86.20	0.0	5.2	NCEER
1916	11	2	2	32	0.0	43.30	-73.70	0.0	3.5	NCEER
1916	12	19	5	42	0.0	36.60	-89.20	0.0	3.7	NCEER
1917	1	25	21	15	0.0	36.10	-83.50	0.0	3.4	NCEER
1917	1	26	19	35	0.0	46.80	-74.50	0.0	3.5	NCEER
1917	2	6	17	26	0.0	47.90	-95.00	0.0	3.1	NCEER
1917	2	16	9	0	0.0	41.50	-72.50	0.0	3.3	NCEER
1917	3	5	2	7	0.0	36.00	-84.00	0.0	3.4	NCEER
1917	3	25	19	15	0.0	36.10	-83.50	0.0	3.6	NCEER
1917	3	27	19	56	0.0	35.30	-101.30	0.0	3.8	NCEER
1917	4	9	20	52	0.0	37.00	-90.00	0.0	4.9	NCEER
1917	4	9	23	38	0.0	38.10	-90.20	0.0	3.1	NCEER
1917	5	9	9	0	0.0	36.80	-90.40	0.0	3.9	SRA
1917	5	22	9	0	26.0	45.10	-75.60	0.0	3.9	NCEER
1917	6	9	13	14	0.0	36.80	-89.40	0.0	3.8	NCEER
1917	6	12	2	0	0.0	49.00	-68.00	0.0	4.0	NCEER
1917	6	21	0	0	0.0	36.00	-83.00	0.0	3.8	NCEER
1917	6	30	1	23	0.0	32.70	-87.50	0.0	3.4	NCEER
1917	9	3	21	30	0.0	46.30	-94.80	0.0	4.2	NCEER
1918	1	1	0	0	0.0	35.50	-97.70	0.0	3.0	NCEER
1918	1	16	15	45	0.0	35.90	-83.90	0.0	3.3	NCEER

© 2007-2012 UniStar Nuclear Services, LLC. All rights reserved.
COPYRIGHT PROTECTED

Table 2.5-1— {Updated Earthquake catalog (1534-April 2010) Including events with $m_b \geq 3.0$}

Year	Month	Day	Hour	Min	Sec	Lat (deg)	Lon (deg)	Depth (km)	mb	Source
1918	2	17	8	10	0.0	37.00	-89.20	0.0	3.7	NCEER
1918	2	22	0	0	0.0	42.80	-84.20	0.0	3.1	NCEER
1918	4	10	2	9	0.0	38.70	-78.40	0.0	4.7	NCEER
1918	6	22	1	0	0.0	36.10	-84.10	0.0	3.5	NCEER
1918	7	1	19	2	0.0	39.70	-91.40	0.0	3.1	NCEER
1918	7	23	12	0	0.0	46.85	-71.35	0.0	3.3	NCEER
1918	8	21	4	11	54.0	44.20	-70.50	0.0	4.2	USH
1918	9	10	16	30	0.0	35.50	-98.00	0.0	3.6	NCEER
1918	10	4	9	21	0.0	35.00	-91.10	0.0	4.0	NCEER
1918	10	13	9	30	0.0	36.10	-91.00	0.0	3.5	NCEER
1918	10	16	2	15	0.0	36.00	-90.00	0.0	4.2	NCEER
1919	2	11	3	37	0.0	37.80	-87.50	0.0	3.5	NCEER
1919	4	8	12	30	0.0	36.20	-91.30	0.0	3.0	NCEER
1919	5	23	12	30	0.0	36.60	-89.20	0.0	3.7	NCEER
1919	5	25	9	45	0.0	38.30	-87.50	0.0	3.8	NCEER
1919	5	27	4	0	0.0	37.70	-97.30	0.0	3.7	NCEER
1919	5	28	13	45	0.0	36.40	-89.50	0.0	3.7	NCEER
1919	7	11	1	40	0.0	43.90	-70.00	0.0	3.3	NCEER
1919	7	23	11	50	0.0	43.70	-70.30	0.0	3.3	NCEER
1919	7	26	13	55	0.0	37.70	-97.30	0.0	3.6	NCEER
1919	9	6	2	46	0.0	38.80	-78.20	0.0	3.8	NCEER
1919	10	26	10	28	0.0	47.60	-70.00	0.0	3.3	NCEER
1919	11	3	20	40	0.0	36.30	-91.00	0.0	3.6	NCEER
1920	2	6	0	0	0.0	48.15	-69.71	0.0	3.3	NCEER
1920	2	29	3	5	0.0	37.20	-93.30	0.0	3.9	NCEER
1920	4	7	20	45	0.0	36.30	-88.20	0.0	3.7	NCEER
1920	4	30	15	12	0.0	38.60	-89.10	0.0	3.5	NCEER
1920	5	1	15	15	0.0	38.00	-89.60	0.0	3.9	NCEER
1920	5	23	8	0	0.0	43.10	-71.50	0.0	3.3	NCEER
1920	6	7	8	0	0.0	43.50	-70.50	0.0	3.3	NCEER
1920	7	14	23	0	0.0	43.20	-103.20	0.0	3.5	NCEER
1920	7	24	0	0	0.0	38.70	-78.40	0.0	3.3	NCEER
1920	10	3	14	15	0.0	38.60	-94.30	0.0	3.7	NCEER
1920	11	8	0	0	0.0	46.01	-73.43	0.0	3.4	NCEER
1920	11	9	0	40	0.0	45.00	-67.10	0.0	3.3	NCEER
1920	12	24	7	30	0.0	36.00	-85.00	0.0	3.4	NCEER
1921	1	9	21	54	0.0	36.40	-89.50	0.0	3.3	NCEER
1921	1	26	23	40	0.0	40.01	-74.91	0.0	3.2	NCEER
1921	2	27	22	16	0.0	37.00	-89.20	0.0	3.7	NCEER
1921	3	14	12	15	0.0	40.00	-88.00	0.0	4.0	NCEER
1921	3	16	23	45	0.0	43.50	-96.70	0.0	3.0	NCEER
1921	3	31	20	3	0.0	37.90	-87.80	0.0	3.1	NCEER
1921	7	29	21	14	0.0	42.50	-70.40	0.0	3.3	NCEER
1921	8	7	6	30	0.0	37.80	-78.40	0.0	3.8	NCEER
1921	8	27	8	12	16.0	47.00	-76.00	0.0	3.4	NCEER
1921	9	9	3	0	0.0	38.30	-90.10	0.0	3.5	NCEER

© 2007-2012 UniStar Nuclear Services, LLC. All rights reserved.
COPYRIGHT PROTECTED

Table 2.5-1— {Updated Earthquake catalog (1534-April 2010) Including events with $m_b \geq 3.0$}
(Page 22 of 75)

Year	Month	Day	Hour	Min	Sec	Lat (deg)	Lon (deg)	Depth (km)	mb	Source
1921	9	24	0	30	0.0	43.70	-98.70	0.0	3.1	NCEER
1921	10	1	9	0	0.0	37.70	-88.60	0.0	3.5	NCEER
1921	10	9	7	50	0.0	38.30	-90.10	0.0	3.7	NCEER
1921	10	10	13	0	0.0	44.80	-67.00	0.0	3.3	NCEER
1921	12	15	13	20	0.0	35.80	-84.60	0.0	3.4	NCEER
1922	1	2	14	50	0.0	43.80	-99.30	0.0	4.0	NCEER
1922	1	11	3	42	0.0	37.90	-87.80	0.0	3.7	NCEER
1922	3	22	22	30	0.0	37.90	-88.40	0.0	4.6	NCEER
1922	3	23	2	22	0.0	37.40	-89.40	0.0	4.6	USH
1922	3	23	21	45	0.0	37.00	-88.90	0.0	3.8	NCEER
1922	3	28	16	42	0.0	36.70	-90.40	0.0	3.8	NCEER
1922	3	30	1	20	0.0	35.50	-86.70	0.0	3.1	NCEER
1922	3	30	3	21	0.0	36.80	-82.30	0.0	3.3	NCEER
1922	3	30	16	53	0.0	36.10	-89.60	0.0	3.9	NCEER
1922	3	30	22	20	0.0	36.50	-82.20	0.0	3.3	NCEER
1922	5	7	22	40	0.0	43.40	-71.40	0.0	3.3	NCEER
1922	7	2	22	25	35.0	46.50	-66.60	0.0	3.5	NCEER
1922	7	7	0	0	0.0	43.80	-88.50	0.0	3.4	NCEER
1922	11	27	3	31	0.0	37.40	-88.20	0.0	4.6	NCEER
1922	12	8	21	24	0.0	44.40	-75.10	0.0	3.5	NCEER
1923	3	9	2	45	0.0	38.90	-89.40	0.0	3.9	SRA
1923	3	27	8	0	0.0	34.60	-89.70	0.0	3.7	NCEER
1923	5	6	7	50	0.0	37.00	-89.20	0.0	3.7	NCEER
1923	9	10	6	30	0.0	41.70	-96.20	0.0	3.0	NCEER
1923	10	28	17	10	0.0	35.30	-90.00	0.0	4.1	NCEER
1923	11	10	4	0	0.0	40.00	-89.90	0.0	3.3	NCEER
1923	11	26	23	25	0.0	35.50	-90.40	0.0	3.6	NCEER
1923	11	29	23	20	0.0	37.00	-89.20	0.0	3.1	NCEER
1923	12	31	20	6	0.0	34.80	-82.50	0.0	3.3	NCEER
1924	1	1	3	5	0.0	36.00	-90.00	0.0	4.3	NCEER
1924	1	5	0	0	0.0	39.10	-78.10	0.0	3.3	NCEER
1924	3	4	19	15	0.0	47.80	-70.20	0.0	3.5	NCEER
1924	4	2	11	15	0.0	37.00	-88.80	0.0	4.0	NCEER
1924	6	7	5	42	0.0	36.50	-89.80	0.0	3.7	NCEER
1924	7	15	0	10	0.0	45.70	-76.50	0.0	3.7	NCEER
1924	8	13	4	23	0.0	36.00	-104.50	0.0	3.4	NCEER
1924	9	24	11	0	0.0	40.90	-100.10	0.0	3.1	NCEER
1924	10	20	8	30	0.0	35.00	-82.60	0.0	4.4	NCEER
1924	11	13	10	30	0.0	36.60	-82.20	0.0	4.0	NCEER
1924	11	14	1	32	0.0	45.50	-76.30	0.0	3.3	NCEER
1924	12	26	4	30	0.0	37.30	-79.90	0.0	3.5	NCEER
1924	12	30	22	10	0.0	43.50	-103.50	0.0	3.6	NCEER
1925	1	7	13	7	0.0	42.60	-70.60	0.0	3.9	NCEER
1925	1	27	22	42	0.0	36.20	-91.70	0.0	3.6	NCEER
1925	3	1	2	19	14.7	47.76	-69.84	9.0	6.6	NCEER
1925	3	9	0	0	0.0	42.90	-71.50	0.0	3.3	NCEER

© 2007-2012 UniStar Nuclear Services, LLC. All rights reserved.
COPYRIGHT PROTECTED

Table 2.5-1— {Updated Earthquake catalog (1534-April 2010) Including events with $m_b \geq 3.0$}
(Page 23 of 75)

Year	Month	Day	Hour	Min	Sec	Lat (deg)	Lon (deg)	Depth (km)	mb	Source
1925	3	27	4	6	0.0	39.50	-83.90	0.0	3.4	NCEER
1925	4	24	7	56	0.0	41.70	-70.80	0.0	3.6	NCEER
1925	4	27	4	5	0.0	38.00	-88.20	0.0	4.9	NCEER
1925	5	4	17	51	0.0	42.50	-70.90	0.0	3.3	NCEER
1925	5	13	12	0	0.0	36.70	-88.60	0.0	3.6	NCEER
1925	5	16	1	30	0.0	37.30	-77.50	0.0	3.5	NCEER
1925	7	8	16	0	0.0	36.20	-93.20	0.0	3.5	NCEER
1925	7	13	0	0	0.0	38.80	-90.00	0.0	3.8	NCEER
1925	7	14	21	20	0.0	37.60	-77.50	0.0	3.3	NCEER
1925	7	29	11	30	0.0	34.50	-101.20	0.0	3.1	NCEER
1925	7	30	8	0	0.0	34.50	-100.30	0.0	3.4	NCEER
1925	7	30	12	17	0.0	35.40	-101.30	0.0	4.8	NCEER
1925	8	25	6	27	0.0	42.80	-97.40	0.0	3.1	NCEER
1925	9	2	11	55	0.0	37.90	-87.20	0.0	4.5	NCEER
1925	10	9	5	0	0.0	46.82	-71.22	0.0	3.3	NCEER
1925	10	9	13	55	0.0	43.70	-71.10	0.0	4.0	NCEER
1925	10	18	21	30	0.0	44.10	-70.20	0.0	3.3	NCEER
1925	10	19	12	5	17.0	47.00	-73.00	0.0	3.5	NCEER
1925	11	14	13	4	0.0	41.70	-72.40	0.0	3.4	NCEER
1925	11	16	6	20	0.0	41.80	-72.70	0.0	3.3	NCEER
1925	11	18	1	50	0.0	44.60	-107.00	0.0	4.3	NCEER
1926	1	4	0	0	0.0	41.60	-71.80	0.0	3.3	NCEER
1926	1	20	0	0	0.0	35.60	-94.90	0.0	4.0	NCEER
1926	1	26	23	40	0.0	40.00	-75.00	0.0	3.5	NCEER
1926	1	27	0	0	0.0	44.30	-74.10	0.0	3.3	NCEER
1926	2	19	20	20	0.0	47.70	-71.00	0.0	3.3	NCEER
1926	3	18	21	9	0.0	42.80	-71.80	0.0	3.5	NCEER
1926	3	22	14	30	0.0	37.80	-88.60	0.0	3.5	NCEER
1926	4	28	2	16	0.0	36.20	-89.00	0.0	3.9	SRA
1926	5	12	3	30	0.0	40.90	-73.90	0.0	3.0	NCEER
1926	6	20	14	20	0.0	35.60	-94.90	0.0	4.0	NCEER
1926	7	8	9	50	0.0	35.90	-82.10	0.0	3.5	NCEER
1926	7	18	6	0	0.0	47.00	-71.50	0.0	3.3	NCEER
1926	8	23	16	40	0.0	45.80	-77.10	0.0	3.3	NCEER
1926	8	28	21	0	0.0	44.70	-70.00	0.0	3.4	NCEER
1926	10	27	16	22	0.0	36.70	-90.40	0.0	3.5	NCEER
1926	10	28	8	42	0.0	41.70	-83.60	0.0	3.4	NCEER
1926	11	5	16	53	0.0	39.10	-82.10	0.0	3.8	USH
1926	11	24	19	30	0.0	45.00	-67.50	0.0	3.3	NCEER
1926	12	13	23	3	0.0	36.70	-89.40	0.0	3.7	NCEER
1926	12	17	0	0	0.0	36.40	-89.50	0.0	3.5	NCEER
1927	1	7	9	30	0.0	38.30	-97.70	0.0	3.6	NCEER
1927	2	2	1	30	0.0	37.40	-89.70	0.0	3.9	SRA
1927	2	3	8	0	0.0	36.70	-90.40	0.0	3.8	SRA
1927	2	17	5	30	0.0	40.70	-82.50	0.0	3.1	NCEER
1927	3	9	4	8	0.0	43.30	-71.40	0.0	3.4	NCEER

© 2007-2012 UniStar Nuclear Services, LLC. All rights reserved.
COPYRIGHT PROTECTED

Table 2.5-1— {Updated Earthquake catalog (1534-April 2010) Including events with $m_b \geq 3.0$}
(Page 24 of 75)

Year	Month	Day	Hour	Min	Sec	Lat (deg)	Lon (deg)	Depth (km)	mb	Source
1927	3	12	22	12	0.0	44.60	-75.20	0.0	3.3	NCEER
1927	3	18	17	25	0.0	39.90	-95.30	0.0	3.9	NCEER
1927	3	30	0	0	0.0	41.70	-72.80	0.0	3.3	NCEER
1927	4	18	10	30	0.0	36.30	-89.50	0.0	3.5	NCEER
1927	5	7	8	28	0.0	36.00	-90.20	0.0	4.7	NCEER
1927	6	1	12	23	0.0	40.30	-74.00	0.0	3.9	NCEER
1927	6	10	7	16	0.0	38.00	-79.00	0.0	3.6	NCEER
1927	6	16	12	0	0.0	34.70	-86.00	0.0	3.6	NCEER
1927	7	25	0	56	0.0	47.30	-71.00	0.0	4.0	NCEER
1927	8	13	16	10	0.0	36.40	-89.50	0.0	4.1	NCEER
1927	10	8	4	30	0.0	35.10	-85.30	0.0	3.3	NCEER
1927	10	14	16	10	0.0	41.60	-98.90	0.0	3.1	NCEER
1927	10	24	11	0	0.0	44.70	-73.80	0.0	3.3	NCEER
1927	10	27	0	0	0.0	36.30	-76.20	0.0	3.3	NCEER
1927	10	29	0	0	0.0	40.90	-81.20	0.0	3.4	NCEER
1927	11	13	0	50	0.0	43.10	-79.06	0.0	3.1	NCEER
1927	11	13	16	21	0.0	32.30	-90.20	0.0	3.4	NCEER
1927	11	23	0	50	0.0	33.90	-78.00	0.0	3.3	NCEER
1927	12	15	4	30	0.0	28.90	-89.40	0.0	3.5	NCEER
1928	1	13	19	50	0.0	41.20	-71.60	0.0	3.3	NCEER
1928	1	23	9	19	0.0	42.00	-90.00	0.0	3.1	NCEER
1928	1	27	0	0	0.0	48.00	-70.20	0.0	3.3	NCEER
1928	2	8	0	0	0.0	45.30	-69.00	0.0	3.5	NCEER
1928	3	7	2	45	0.0	35.60	-87.00	0.0	3.5	NCEER
1928	3	17	21	15	0.0	38.60	-90.20	0.0	3.3	NCEER
1928	3	18	15	25	0.0	44.50	-74.30	0.0	4.0	NCEER
1928	3	22	13	30	0.0	45.30	-69.00	0.0	3.3	NCEER
1928	4	15	11	0	0.0	36.60	-89.50	0.0	3.1	NCEER
1928	4	15	15	5	0.0	37.30	-89.50	0.0	3.1	NCEER
1928	4	23	11	0	0.0	36.50	-89.20	0.0	3.1	NCEER
1928	4	25	23	38	0.0	44.50	-71.20	0.0	3.8	NCEER
1928	5	31	22	40	0.0	36.60	-89.50	0.0	3.1	NCEER
1928	10	27	0	0	0.0	40.40	-84.10	0.0	3.0	NCEER
1928	10	30	11	45	0.0	37.50	-77.50	0.0	3.4	NCEER
1928	11	3	4	2	49.8	36.11	-82.83	0.0	4.6	NCEER
1928	11	8	14	15	0.0	39.50	-89.10	0.0	3.1	NCEER
1928	11	10	6	20	0.0	36.10	-91.10	0.0	3.1	NCEER
1928	11	16	13	45	0.0	44.10	-103.70	0.0	3.5	NCEER
1928	11	20	2	30	0.0	45.00	-67.20	0.0	3.2	NCEER
1928	11	20	3	45	0.0	35.80	-82.30	0.0	3.7	NCEER
1928	12	1	0	0	0.0	50.00	-81.50	0.0	4.0	NCEER
1928	12	23	2	30	0.0	35.30	-80.30	0.0	3.3	NCEER
1928	12	23	6	10	0.0	47.60	-93.90	0.0	3.1	NCEER
1928	12	26	3	25	0.0	36.10	-91.10	0.0	3.1	NCEER
1929	1	3	12	5	0.0	33.90	-80.30	0.0	3.3	NCEER
1929	2	5	19	9	0.0	44.00	-70.30	0.0	3.3	NCEER

© 2007-2012 UniStar Nuclear Services, LLC. All rights reserved.
COPYRIGHT PROTECTED

Table 2.5-1— {Updated Earthquake catalog (1534-April 2010) Including events with $m_b \geq 3.0$}
(Page 25 of 75)

Year	Month	Day	Hour	Min	Sec	Lat (deg)	Lon (deg)	Depth (km)	mb	Source
1929	2	14	20	12	0.0	38.30	-87.60	0.0	3.2	NCEER
1929	2	26	8	15	0.0	37.60	-90.60	0.0	3.1	NCEER
1929	3	8	9	6	0.0	40.40	-84.20	0.0	3.7	NCEER
1929	5	11	9	30	0.0	45.40	-71.90	0.0	3.3	NCEER
1929	5	13	3	50	0.0	36.40	-89.50	0.0	3.5	NCEER
1929	7	28	17	0	0.0	28.90	-89.40	0.0	3.4	NCEER
1929	8	12	11	24	48.7	42.91	-78.40	9.0	5.2	NCEER
1929	9	23	11	0	0.0	39.00	-96.60	0.0	3.9	NCEER
1929	10	6	12	30	0.0	42.80	-97.40	0.0	3.4	NCEER
1929	10	28	2	15	0.0	34.30	-82.40	0.0	3.3	NCEER
1929	11	26	16	20	0.0	37.20	-99.80	0.0	3.1	NCEER
1929	12	7	8	2	0.0	39.20	-96.60	0.0	3.4	NCEER
1929	12	26	2	56	0.0	38.10	-78.50	0.0	3.6	NCEER
1929	12	28	0	30	0.0	35.50	-97.90	0.0	4.0	NCEER
1930	1	4	14	30	38.0	46.73	-65.83	0.0	4.6	NCEER
1930	1	26	21	0	0.0	36.10	-91.10	0.0	3.1	NCEER
1930	2	25	12	45	0.0	37.00	-90.20	0.0	3.0	NCEER
1930	3	19	0	15	0.0	43.30	-71.60	0.0	3.3	NCEER
1930	3	26	8	56	0.0	35.10	-90.00	0.0	3.5	SRA
1930	4	2	9	39	0.0	36.10	-89.70	0.0	3.1	NCEER
1930	6	19	12	6	56.0	45.73	-71.22	0.0	3.6	NCEER
1930	6	26	21	45	0.0	40.50	-84.00	0.0	3.2	NCEER
1930	7	11	0	15	0.0	40.60	-83.20	0.0	3.1	NCEER
1930	7	13	4	52	39.3	47.50	-69.83	0.0	3.1	NCEER
1930	8	1	2	0	0.0	41.50	-70.80	0.0	3.1	NCEER
1930	8	8	18	31	0.0	39.70	-91.40	0.0	3.1	NCEER
1930	8	29	6	26	54.0	37.00	-89.10	0.0	3.5	NCEER
1930	8	30	9	28	0.0	35.90	-84.40	0.0	3.5	NCEER
1930	9	1	20	27	24.0	36.60	-89.40	0.0	3.7	NCEER
1930	9	30	20	40	0.0	40.30	-84.30	0.0	3.5	NCEER
1930	10	8	1	8	41.0	48.93	-68.70	0.0	3.9	NCEER
1930	10	16	21	50	0.0	36.00	-83.90	0.0	3.6	NCEER
1930	10	19	12	12	0.0	30.10	-91.00	0.0	4.2	NCEER
1930	11	1	1	34	0.0	39.10	-76.50	0.0	3.3	NCEER
1930	11	16	12	30	0.0	34.30	-92.80	0.0	3.3	NCEER
1930	12	13	23	18	23.7	47.65	-70.17	0.0	3.5	NCEER
1930	12	23	14	44	0.0	38.50	-90.70	0.0	3.2	NCEER
1930	12	26	3	0	0.0	34.50	-80.30	0.0	3.1	NCEER
1931	1	6	2	51	0.0	39.00	-87.00	0.0	3.5	SRA
1931	1	8	0	13	0.3	47.30	-70.40	0.0	5.4	NCEER
1931	1	17	18	45	0.0	43.70	-98.70	0.0	3.1	NCEER
1931	3	21	15	48	0.0	40.40	-84.20	0.0	3.0	NCEER
1931	4	1	23	20	9.0	36.90	-88.30	0.0	3.5	NCEER
1931	4	6	15	37	3.0	36.80	-89.00	0.0	3.1	NCEER
1931	4	20	19	54	30.6	43.47	-73.78	5.0	4.8	NCEER
1931	4	22	0	0	0.0	42.90	-78.90	0.0	3.1	NCEER

© 2007-2012 UniStar Nuclear Services, LLC. All rights reserved.
COPYRIGHT PROTECTED

Table 2.5-1— {Updated Earthquake catalog (1534-April 2010) Including events with $m_b \geq 3.0$}
(Page 26 of 75)

Year	Month	Day	Hour	Min	Sec	Lat (deg)	Lon (deg)	Depth (km)	mb	Source
1931	5	5	12	18	0.0	33.70	-86.60	0.0	4.2	NCEER
1931	7	1	2	45	0.0	41.60	-73.40	0.0	3.0	NCEER
1931	7	18	14	52	0.0	36.60	-89.50	0.0	3.3	NCEER
1931	8	7	0	0	0.0	44.62	-65.77	0.0	3.3	NCEER
1931	8	9	6	18	37.0	39.10	-94.70	0.0	3.8	NCEER
1931	9	20	23	4	54.0	40.43	-84.27	5.0	4.7	NCEER
1931	9	23	22	47	37.0	47.00	-76.07	0.0	4.5	NCEER
1931	11	14	14	2	29.5	47.33	-70.17	0.0	3.4	NCEER
1931	12	10	8	11	36.0	35.90	-89.90	0.0	3.3	NCEER
1931	12	17	3	36	0.0	34.10	-89.80	0.0	4.7	NCEER
1932	1	5	4	5	0.0	37.60	-78.40	0.0	3.1	NCEER
1932	1	21	0	0	0.0	41.10	-81.60	0.0	3.1	NCEER
1932	1	29	0	15	0.0	39.00	-99.60	0.0	3.8	NCEER
1932	3	9	5	23	38.8	46.47	-74.67	0.0	3.8	NCEER
1932	4	9	10	15	0.0	31.70	-96.40	0.0	3.6	NCEER
1932	11	22	7	56	42.0	36.00	-90.20	0.0	3.4	NCEER
1932	12	7	3	15	0.0	44.40	-74.10	0.0	3.2	NCEER
1933	1	11	23	32	0.0	47.45	-70.50	0.0	3.2	NCEER
1933	1	21	16	4	39.5	45.30	-74.65	0.0	3.8	NCEER
1933	1	25	2	0	0.0	40.20	-74.70	0.0	3.3	NCEER
1933	2	20	17	0	0.0	39.80	-99.90	0.0	3.8	NCEER
1933	2	23	3	20	0.0	40.30	-84.20	0.0	3.3	NCEER
1933	2	25	9	43	2.7	47.43	-69.93	0.0	3.4	NCEER
1933	3	11	12	48	0.0	36.70	-90.40	0.0	3.1	NCEER
1933	5	28	15	10	0.0	38.60	-83.70	0.0	3.4	NCEER
1933	6	9	11	30	0.0	33.30	-83.50	0.0	3.3	NCEER
1933	6	26	14	10	0.0	41.00	-73.80	0.0	3.0	NCEER
1933	7	13	14	42	39.0	37.90	-89.90	0.0	3.3	NCEER
1933	7	14	4	48	40.0	45.42	-75.70	0.0	3.9	NCEER
1933	8	4	4	34	15.0	37.90	-89.90	0.0	3.1	NCEER
1933	8	8	0	0	0.0	41.90	-103.70	0.0	3.3	NCEER
1933	8	19	19	30	0.0	35.50	-98.00	0.0	3.4	NCEER
1933	10	29	0	0	0.0	43.00	-73.70	0.0	3.1	NCEER
1933	11	16	9	29	1.0	38.60	-90.60	0.0	3.3	NCEER
1933	12	7	5	55	0.0	42.90	-89.20	0.0	3.1	NCEER
1933	12	9	8	50	0.0	35.80	-90.20	0.0	4.0	NCEER
1933	12	23	9	40	0.0	32.90	-80.00	0.0	3.5	NCEER
1934	1	29	12	30	0.0	45.90	-97.70	0.0	3.1	NCEER
1934	1	30	10	30	0.0	41.80	-72.60	0.0	3.3	NCEER
1934	3	17	0	0	0.0	43.50	-65.50	0.0	3.0	NCEER
1934	4	11	3	0	0.0	44.00	-72.70	0.0	3.6	NCEER
1934	4	12	1	40	0.0	33.90	-95.50	0.0	3.9	SRA
1934	4	15	2	58	0.0	44.70	-73.80	0.0	3.9	NCEER
1934	4	15	18	5	0.0	44.80	-74.30	0.0	3.3	NCEER
1934	5	11	10	40	0.0	41.50	-98.70	0.0	3.2	NCEER
1934	5	15	14	28	0.0	37.90	-89.90	0.0	3.0	NCEER

© 2007-2012 UniStar Nuclear Services, LLC. All rights reserved.
COPYRIGHT PROTECTED

Table 2.5-1— {Updated Earthquake catalog (1534-April 2010) Including events with $m_b \geq 3.0$}
(Page 27 of 75)

Year	Month	Day	Hour	Min	Sec	Lat (deg)	Lon (deg)	Depth (km)	mb	Source
1934	7	3	3	10	41.0	35.20	-90.00	0.0	3.1	NCEER
1934	7	30	7	20	0.0	42.70	-103.00	0.0	4.3	NCEER
1934	8	2	14	59	0.0	43.70	-70.30	0.0	3.2	NCEER
1934	8	20	0	47	0.0	36.90	-89.20	0.0	4.3	NCEER
1934	8	26	11	36	0.0	44.90	-67.00	0.0	3.0	NCEER
1934	8	30	3	50	0.0	43.40	-99.10	0.0	3.1	NCEER
1934	10	29	20	7	0.0	42.00	-80.20	0.0	3.2	NCEER
1934	10	30	2	25	47.0	37.50	-88.50	0.0	3.3	NCEER
1934	11	8	4	45	0.0	42.60	-100.20	0.0	3.4	NCEER
1934	11	12	14	45	0.0	41.50	-90.50	0.0	3.9	NCEER
1934	12	9	9	0	0.0	32.90	-80.00	0.0	3.3	NCEER
1935	1	1	8	15	0.0	35.10	-83.60	0.0	3.4	NCEER
1935	1	5	18	40	0.0	41.50	-90.60	0.0	3.0	NCEER
1935	2	10	23	45	0.0	37.20	-77.40	0.0	3.3	NCEER
1935	3	1	10	59	44.0	40.30	-96.20	0.0	4.8	NCEER
1935	4	24	1	24	0.0	42.20	-70.20	0.0	3.3	NCEER
1935	7	24	1	38	0.0	36.40	-89.50	0.0	3.1	NCEER
1935	11	1	6	3	40.0	46.78	-79.07	0.0	6.2	NCEER
1935	11	1	8	30	0.0	38.90	-78.90	0.0	3.3	NCEER
1935	11	2	14	31	58.0	47.23	-78.17	0.0	4.9	NCEER
1935	11	14	3	30	0.0	29.60	-81.70	0.0	3.3	NCEER
1936	1	31	19	30	0.0	41.20	-83.20	0.0	3.1	NCEER
1936	2	17	5	5	8.0	36.20	-89.70	0.0	3.1	NCEER
1936	3	14	17	20	0.0	34.00	-95.20	0.0	3.4	NCEER
1936	3	29	0	49	23.4	47.33	-70.25	0.0	4.0	NCEER
1936	6	14	5	40	0.0	43.50	-71.50	0.0	3.4	NCEER
1936	6	20	3	24	3.5	35.31	-100.77	5.0	4.4	NCEER
1936	6	21	4	20	0.0	44.70	-74.20	0.0	3.3	NCEER
1936	7	12	0	23	0.0	36.90	-102.90	0.0	3.0	NCEER
1936	8	2	22	16	25.0	36.70	-89.00	0.0	3.9	NCEER
1936	10	8	16	30	0.0	39.30	-84.40	0.0	3.3	NCEER
1936	10	30	10	30	0.0	43.50	-103.50	0.0	3.1	NCEER
1936	11	10	2	46	0.0	43.60	-71.40	0.0	3.3	NCEER
1936	11	10	4	2	0.0	44.70	-71.70	0.0	3.2	NCEER
1937	1	30	8	57	9.0	36.20	-89.70	2.0	3.3	NCEER
1937	2	3	1	26	0.0	37.70	-78.70	0.0	3.6	NCEER
1937	3	2	14	47	33.3	40.49	-84.27	2.0	4.9	NCEER
1937	3	10	5	29	0.0	44.60	-75.20	0.0	3.3	NCEER
1937	5	17	0	49	46.0	36.10	-90.60	0.0	4.0	NCEER
1937	6	8	14	26	0.0	35.30	-96.90	0.0	3.2	NCEER
1937	7	19	3	51	0.0	40.72	-73.71	0.0	3.5	NCEER
1937	9	30	7	58	3.4	47.80	-65.43	5.0	4.5	NCEER
1937	11	6	14	31	20.6	46.78	-75.82	24.0	4.0	NCEER
1937	11	12	16	57	31.3	46.10	-74.47	1.0	3.7	NCEER
1937	11	17	17	4	0.0	38.60	-89.10	0.0	4.0	NCEER
1938	1	2	17	5	0.0	44.50	-98.20	0.0	3.5	NCEER

© 2007-2012 UniStar Nuclear Services, LLC. All rights reserved.
COPYRIGHT PROTECTED

Table 2.5-1— {Updated Earthquake catalog (1534-April 2010) Including events with $m_b \geq 3.0$}
(Page 28 of 75)

Year	Month	Day	Hour	Min	Sec	Lat (deg)	Lon (deg)	Depth (km)	mb	Source
1938	1	6	13	28	42.2	44.90	-75.18	0.0	3.2	NCEER
1938	1	24	5	29	2.0	45.57	-76.27	0.0	3.0	NCEER
1938	2	12	6	27	0.0	41.60	-87.00	0.0	3.8	NCEER
1938	2	23	17	56	35.7	46.38	-75.40	0.0	3.2	NCEER
1938	3	13	16	10	0.0	42.40	-83.20	0.0	3.1	NCEER
1938	3	24	13	11	0.0	42.70	-103.40	0.0	3.3	NCEER
1938	3	31	10	10	0.0	35.60	-83.50	0.0	3.6	NCEER
1938	4	12	18	55	47.0	46.72	-79.08	0.0	3.2	NCEER
1938	4	26	5	42	0.0	34.20	-93.50	0.0	3.1	NCEER
1938	5	5	0	33	0.3	45.37	-74.50	0.0	3.0	NCEER
1938	5	17	18	32	0.0	49.00	-68.00	0.0	3.9	NCEER
1938	6	15	5	7	43.0	46.50	-66.80	0.0	3.0	NCEER
1938	7	15	22	46	12.0	40.68	-78.43	1.0	3.2	NCEER
1938	8	2	9	2	30.0	41.08	-73.70	0.0	3.1	NCEER
1938	8	22	12	48	9.4	44.89	-68.79	5.0	3.8	NCEER
1938	8	23	5	4	53.4	40.05	-74.36	21.0	3.8	NCEER
1938	9	7	23	18	18.9	45.87	-74.90	0.0	3.0	NCEER
1938	9	17	3	34	28.3	35.41	-90.25	1.0	4.8	USH
1938	9	20	0	0	0.0	41.50	-72.20	0.0	3.2	NCEER
1938	9	28	4	33	16.0	48.78	-69.58	0.0	4.1	NCEER
1938	10	1	22	15	0.0	43.80	-99.30	0.0	3.8	NCEER
1938	10	11	9	37	0.0	43.50	-96.70	0.0	3.8	NCEER
1938	11	4	22	10	0.0	43.20	-98.90	0.0	3.3	NCEER
1938	11	18	22	19	6.0	44.75	-75.25	0.0	3.5	NCEER
1938	11	26	7	47	57.5	47.03	-76.20	0.0	4.2	NCEER
1938	12	25	7	46	0.0	47.60	-75.40	0.0	3.9	NCEER
1939	1	14	8	10	16.0	43.25	-79.85	0.0	3.3	NCEER
1939	1	28	17	55	0.0	46.80	-95.80	0.0	3.6	NCEER
1939	2	24	0	20	0.0	42.90	-78.30	0.0	3.0	NCEER
1939	3	16	20	21	0.0	46.40	-77.50	0.0	3.6	NCEER
1939	3	18	14	3	0.0	40.40	-84.00	0.0	3.3	NCEER
1939	4	15	17	25	0.0	36.80	-89.40	0.0	3.2	NCEER
1939	5	5	2	45	0.0	33.70	-85.80	0.0	3.3	NCEER
1939	6	1	7	30	0.0	35.00	-96.40	0.0	3.9	NCEER
1939	6	10	18	30	0.0	43.00	-98.90	0.0	3.1	NCEER
1939	6	18	3	20	0.0	40.30	-84.00	0.0	3.1	NCEER
1939	6	19	21	43	12.0	34.10	-92.60	0.0	4.1	NCEER
1939	6	24	10	27	0.0	34.70	-86.60	0.0	3.4	NCEER
1939	6	24	17	20	18.3	47.59	-69.98	14.0	4.5	NCEER
1939	10	19	11	53	58.0	47.80	-69.80	15.0	5.6	NCEER
1939	11	7	2	40	32.0	47.80	-70.50	0.0	4.1	NCEER
1939	11	15	2	53	48.7	39.58	-75.05	3.0	3.8	NCEER
1939	11	23	15	14	52.0	38.18	-90.14	0.0	4.9	NCEER
1939	11	26	5	20	0.0	39.50	-76.60	0.0	3.5	NCEER
1939	12	8	1	17	47.0	47.97	-71.40	0.0	3.6	NCEER
1940	1	5	0	34	14.0	46.72	-79.08	0.0	3.0	NCEER

© 2007-2012 UniStar Nuclear Services, LLC. All rights reserved.
COPYRIGHT PROTECTED

Table 2.5-1— {Updated Earthquake catalog (1534-April 2010) Including events with $m_b \geq 3.0$}
(Page 29 of 75)

Year	Month	Day	Hour	Min	Sec	Lat (deg)	Lon (deg)	Depth (km)	mb	Source
1940	1	28	23	12	0.0	41.60	-70.80	0.0	3.4	NCEER
1940	2	10	20	57	17.3	46.50	-76.83	0.0	4.0	NCEER
1940	3	26	0	1	0.0	38.80	-78.50	0.0	3.5	NCEER
1940	4	13	8	13	34.0	47.73	-70.73	0.0	3.8	NCEER
1940	5	16	14	0	17.1	45.80	-73.20	0.0	3.6	NCEER
1940	5	31	19	3	0.0	37.10	-88.60	0.0	3.4	NCEER
1940	6	16	4	30	0.0	40.90	-82.30	0.0	3.1	NCEER
1940	8	4	16	20	52.0	46.25	-74.78	0.0	3.1	NCEER
1940	8	7	23	57	35.3	45.77	-74.83	0.0	3.0	NCEER
1940	9	11	1	6	55.4	47.00	-71.13	0.0	3.5	NCEER
1940	10	13	19	50	51.0	47.80	-69.80	0.0	4.7	NCEER
1940	10	19	5	54	0.0	34.70	-85.10	0.0	3.3	NCEER
1940	12	2	16	16	0.0	33.00	-94.00	0.0	3.1	NCEER
1940	12	20	7	27	26.2	43.87	-71.37	10.0	5.5	NCEER
1940	12	25	6	5	0.0	35.90	-82.90	0.0	3.2	NCEER
1940	12	29	2	30	0.0	37.90	-87.30	0.0	3.6	SRA
1941	3	4	6	15	0.0	36.00	-83.90	0.0	3.4	NCEER
1941	3	5	7	29	23.2	46.27	-75.50	0.0	3.0	NCEER
1941	4	4	8	10	43.7	44.73	-73.92	0.0	3.3	NCEER
1941	5	10	11	12	0.0	35.60	-82.60	0.0	3.3	NCEER
1941	5	25	6	25	0.0	43.50	-103.50	0.0	3.7	NCEER
1941	6	22	9	59	31.0	47.39	-70.34	0.0	3.0	NCEER
1941	6	26	4	5	44.9	47.40	-76.83	0.0	4.1	NCEER
1941	6	28	18	30	0.0	32.30	-90.80	0.0	3.0	NCEER
1941	8	30	10	21	0.0	46.10	-67.90	0.0	3.7	NCEER
1941	9	8	9	45	0.0	35.00	-85.30	0.0	3.0	NCEER
1941	10	6	16	34	27.6	47.63	-70.73	0.0	4.0	NCEER
1941	10	8	7	51	0.0	36.20	-89.70	0.0	3.3	NCEER
1941	10	11	8	15	0.0	42.30	-72.30	0.0	3.0	NCEER
1941	10	18	7	48	0.0	35.40	-99.00	0.0	3.2	NCEER
1941	10	21	6	10	41.0	44.77	-74.80	0.0	3.3	NCEER
1941	10	21	16	53	0.0	37.00	-89.10	0.0	3.3	NCEER
1941	10	24	14	13	59.3	45.70	-74.30	0.0	3.6	NCEER
1941	11	15	3	7	0.0	35.10	-90.00	0.0	3.1	NCEER
1941	11	17	3	8	0.0	35.50	-89.70	0.0	4.2	NCEER
1942	1	14	18	5	0.0	38.40	-90.30	0.0	3.3	NCEER
1942	1	19	0	0	0.0	26.50	-81.00	0.0	3.3	NCEER
1942	2	18	7	55	12.0	46.83	-74.77	0.0	3.1	NCEER
1942	3	1	14	43	10.0	41.20	-89.70	0.0	3.6	NCEER
1942	3	8	23	37	0.0	44.20	-70.40	0.0	3.2	NCEER
1942	3	11	16	55	0.0	44.40	-103.50	0.0	3.0	NCEER
1942	3	29	12	43	0.0	37.70	-88.60	0.0	3.0	NCEER
1942	5	20	12	19	22.8	45.77	-74.67	0.0	4.4	NCEER
1942	5	24	11	33	0.0	44.70	-73.80	0.0	3.9	NCEER
1942	6	12	4	50	0.0	36.40	-97.90	0.0	3.5	NCEER
1942	8	26	17	54	0.0	46.80	-77.50	0.0	3.7	NCEER

© 2007-2012 UniStar Nuclear Services, LLC. All rights reserved.
COPYRIGHT PROTECTED

Table 2.5-1— {Updated Earthquake catalog (1534-April 2010) Including events with $m_b \geq 3.0$}
(Page 30 of 75)

Year	Month	Day	Hour	Min	Sec	Lat (deg)	Lon (deg)	Depth (km)	mb	Source
1942	8	31	9	28	0.0	37.00	-89.20	0.0	3.1	NCEER
1942	9	5	14	30	24.1	46.97	-71.50	0.0	3.1	NCEER
1942	9	10	9	0	0.0	38.80	-99.30	0.0	3.4	NCEER
1942	9	11	11	5	13.0	49.22	-67.40	0.0	3.7	NCEER
1942	9	15	22	32	46.0	46.78	-76.00	0.0	3.3	NCEER
1942	10	2	22	29	50.5	42.57	-73.80	0.0	3.0	NCEER
1942	10	7	2	15	0.0	37.60	-78.40	0.0	3.3	NCEER
1942	10	24	17	27	3.6	40.97	-75.25	0.0	3.4	NCEER
1942	11	16	0	13	29.4	46.42	-75.05	0.0	3.6	NCEER
1942	11	17	18	18	0.0	38.60	-90.20	0.0	3.0	NCEER
1942	12	5	21	10	51.2	46.97	-76.07	0.0	4.2	NCEER
1943	1	14	21	32	38.0	45.16	-69.33	0.0	4.4	NCEER
1943	2	28	16	40	1.2	46.50	-75.77	0.0	3.7	NCEER
1943	3	9	3	25	24.9	41.63	-81.31	7.0	4.4	NCEER
1943	3	14	14	2	0.0	43.70	-71.60	0.0	3.9	NCEER
1943	4	13	17	0	0.0	38.30	-85.80	0.0	3.1	NCEER
1943	5	9	11	3	12.5	44.77	-73.83	0.0	3.2	NCEER
1943	5	16	19	40	0.0	43.50	-103.50	0.0	3.1	NCEER
1943	6	8	19	50	0.0	38.60	-90.40	0.0	3.0	NCEER
1943	6	25	4	25	0.0	48.50	-105.00	0.0	4.0	NCEER
1943	7	6	22	10	16.0	44.84	-73.03	22.0	3.8	NCEER
1943	9	25	5	52	36.1	47.55	-70.65	0.0	3.3	NCEER
1943	9	28	16	30	25.2	47.27	-70.40	0.0	3.8	NCEER
1943	11	6	0	6	40.5	47.38	-70.08	0.0	3.9	NCEER
1943	12	6	7	19	40.0	47.68	-74.87	0.0	3.2	NCEER
1943	12	19	9	0	44.0	44.60	-69.60	0.0	3.0	NCEER
1943	12	28	10	25	0.0	33.00	-80.20	0.0	3.3	NCEER
1944	1	7	5	18	0.0	37.50	-89.70	0.0	3.2	NCEER
1944	1	8	0	0	0.0	39.80	-75.50	0.0	4.3	DNA
1944	1	22	21	55	9.1	45.83	-76.78	0.0	4.3	NCEER
1944	1	28	17	30	0.0	32.90	-80.00	0.0	3.3	NCEER
1944	2	5	12	37	52.5	47.40	-70.50	0.0	4.0	NCEER
1944	2	5	16	22	0.0	40.80	-76.20	0.0	3.7	NCEER
1944	3	8	12	49	0.0	46.70	-78.90	0.0	4.1	NCEER
1944	4	9	12	44	0.0	49.90	-67.40	0.0	4.9	NCEER
1944	6	9	15	19	8.7	47.30	-70.28	0.0	3.7	NCEER
1944	6	23	6	37	53.0	49.42	-67.75	0.0	5.1	NCEER
1944	6	24	23	48	38.5	46.00	-74.25	0.0	3.7	NCEER
1944	9	5	4	38	45.7	44.96	-74.72	12.0	5.8	NCEER
1944	9	9	4	12	20.0	39.00	-107.50	0.0	5.0	DNA
1944	9	25	11	37	23.0	37.90	-90.00	0.0	3.9	NCEER
1944	10	14	13	26	17.0	48.50	-67.00	0.0	4.2	NCEER
1944	11	5	19	7	0.0	48.70	-80.80	0.0	4.4	NCEER
1944	11	13	11	52	0.0	40.40	-84.40	0.0	4.1	NCEER
1944	12	10	11	0	0.0	45.70	-87.10	0.0	3.1	NCEER
1944	12	14	3	15	0.0	41.60	-72.80	0.0	3.6	NCEER

© 2007-2012 UniStar Nuclear Services, LLC. All rights reserved.
COPYRIGHT PROTECTED

Table 2.5-1— {Updated Earthquake catalog (1534-April 2010) Including events with $m_b \geq 3.0$}
(Page 31 of 75)

Year	Month	Day	Hour	Min	Sec	Lat (deg)	Lon (deg)	Depth (km)	mb	Source
1944	12	23	7	23	0.0	36.20	-89.70	0.0	3.1	NCEER
1945	1	16	2	0	0.0	37.80	-90.20	0.0	3.2	NCEER
1945	1	30	20	20	0.0	32.90	-80.00	0.0	3.3	NCEER
1945	3	28	1	45	58.0	38.60	-90.20	0.0	3.7	NCEER
1945	4	15	13	15	0.0	43.00	-76.40	0.0	3.1	NCEER
1945	5	2	11	22	0.0	36.50	-89.70	0.0	3.3	NCEER
1945	5	21	7	51	0.0	38.60	-90.20	0.0	3.1	NCEER
1945	6	12	7	58	15.1	47.08	-75.40	0.0	4.3	NCEER
1945	6	14	3	25	0.0	35.00	-84.50	0.0	3.6	NCEER
1945	6	18	15	20	4.7	47.34	-71.09	5.0	4.7	NCEER
1945	7	2	13	29	52.1	48.47	-76.80	0.0	3.9	NCEER
1945	7	15	10	44	0.0	44.90	-67.00	0.0	3.3	NCEER
1945	7	26	10	32	16.4	33.75	-81.38	5.0	4.0	NCEER
1945	9	23	6	22	0.0	37.00	-89.80	0.0	3.1	NCEER
1945	10	9	13	18	42.0	47.99	-69.81	5.0	4.7	NCEER
1945	10	12	19	0	0.0	37.50	-78.50	0.0	3.3	NCEER
1945	11	10	8	0	0.0	43.00	-97.90	0.0	3.1	NCEER
1945	11	13	8	21	0.0	37.00	-89.20	0.0	3.7	NCEER
1945	12	2	15	22	32.0	45.00	-74.90	0.0	3.0	SRA
1946	1	17	8	4	52.0	49.40	-68.70	0.0	4.3	NCEER
1946	2	25	0	52	0.0	38.60	-89.10	0.0	3.3	NCEER
1946	4	7	5	0	0.0	35.20	-84.90	0.0	3.8	NCEER
1946	4	21	5	5	55.5	45.73	-73.43	0.0	3.6	NCEER
1946	5	15	6	10	0.0	36.60	-90.80	0.0	4.0	NCEER
1946	6	27	21	6	22.0	44.65	-74.53	0.0	3.0	NCEER
1946	7	23	6	45	0.0	44.10	-98.60	0.0	4.0	NCEER
1946	9	1	4	39	41.0	47.33	-71.47	0.0	3.3	NCEER
1946	9	4	19	30	0.0	44.90	-74.88	0.0	3.0	NCEER
1946	9	19	0	53	28.8	47.72	-75.00	0.0	3.2	NCEER
1946	9	26	21	19	8.2	46.43	-72.15	0.0	3.4	NCEER
1946	10	8	1	12	2.0	37.50	-90.60	0.0	4.0	NCEER
1946	10	26	20	37	0.0	48.10	-103.60	0.0	3.1	NCEER
1946	10	28	20	36	0.0	41.50	-76.60	0.0	3.6	NCEER
1946	11	10	11	41	23.1	42.87	-77.45	0.0	3.1	NCEER
1946	11	11	10	20	47.0	45.00	-74.90	0.0	3.0	SRA
1946	11	24	10	20	47.2	45.17	-74.68	0.0	3.1	NCEER
1946	12	25	4	48	3.0	44.90	-74.90	0.0	3.0	NCEER
1947	1	4	18	51	0.0	41.00	-73.60	0.0	3.3	NCEER
1947	1	19	0	45	1.7	46.80	-76.70	0.0	3.9	NCEER
1947	2	2	16	50	32.3	47.67	-70.53	0.0	4.2	NCEER
1947	3	16	15	30	0.0	42.10	-88.30	0.0	3.1	NCEER
1947	3	26	0	0	0.0	37.00	-88.40	0.0	4.0	NCEER
1947	3	29	12	28	52.4	47.37	-70.23	0.0	4.0	NCEER
1947	5	6	21	27	0.0	43.00	-87.90	0.0	3.5	NCEER
1947	5	14	5	2	0.0	46.00	-100.90	0.0	3.1	NCEER
1947	5	16	5	45	0.0	44.40	-100.30	0.0	3.0	NCEER

© 2007-2012 UniStar Nuclear Services, LLC. All rights reserved.
COPYRIGHT PROTECTED

Table 2.5-1— {Updated Earthquake catalog (1534-April 2010) Including events with $m_b \geq 3.0$}
(Page 32 of 75)

Year	Month	Day	Hour	Min	Sec	Lat (deg)	Lon (deg)	Depth (km)	mb	Source
1947	6	6	12	55	0.0	36.00	-84.00	0.0	3.4	NCEER
1947	6	30	4	23	53.0	38.40	-90.20	0.0	4.2	NCEER
1947	8	8	5	39	0.0	46.50	-81.10	0.0	4.4	NCEER
1947	8	10	2	46	41.3	41.93	-85.00	2.0	4.5	NCEER
1947	8	25	14	0	0.0	43.10	-98.90	0.0	3.1	NCEER
1947	9	14	19	29	0.0	47.00	-81.30	0.0	4.3	NCEER
1947	9	20	21	30	0.0	31.90	-92.60	0.0	3.3	NCEER
1947	10	22	9	36	38.3	47.55	-70.72	0.0	3.8	NCEER
1947	11	2	4	30	0.0	32.90	-80.00	0.0	3.3	NCEER
1947	11	3	19	51	0.0	45.70	-81.20	0.0	4.5	NCEER
1947	12	1	7	47	33.0	36.70	-90.60	0.0	3.7	NCEER
1947	12	16	3	27	0.0	35.60	-90.10	0.0	4.0	SRA
1947	12	27	19	0	0.0	35.00	-85.30	0.0	3.2	NCEER
1947	12	28	19	58	0.0	45.20	-69.20	0.0	3.8	NCEER
1948	1	1	18	33	45.3	47.30	-70.40	0.0	4.5	NCEER
1948	1	5	2	45	0.0	37.70	-78.30	0.0	3.3	NCEER
1948	1	5	3	20	0.0	37.50	-78.50	0.0	3.5	NCEER
1948	1	6	1	34	0.0	38.60	-89.10	0.0	3.1	NCEER
1948	1	15	17	40	0.0	43.10	-89.70	0.0	3.1	NCEER
1948	1	16	6	2	56.0	50.00	-69.00	0.0	3.7	NCEER
1948	2	10	0	4	0.0	36.40	-84.10	0.0	3.4	NCEER
1948	3	12	4	29	6.3	36.22	-102.48	5.0	4.6	NCEER
1948	4	3	3	0	0.0	37.70	-97.30	0.0	3.1	NCEER
1948	4	20	14	17	0.0	41.70	-91.80	0.0	3.1	NCEER
1948	5	4	2	23	0.0	41.40	-71.80	0.0	3.2	NCEER
1948	5	7	12	2	27.3	45.86	-73.69	3.0	4.0	NCEER
1948	6	9	3	4	12.2	45.23	-73.87	0.0	3.7	NCEER
1948	11	8	17	44	0.0	26.50	-82.20	0.0	3.3	NCEER
1948	11	13	16	49	56.6	46.70	-70.30	0.0	3.5	NCEER
1948	11	29	4	56	0.0	45.20	-69.20	0.0	3.0	NCEER
1949	1	14	3	49	0.0	36.40	-89.70	0.0	3.5	NCEER
1949	2	2	10	52	0.0	32.90	-80.00	0.0	3.3	NCEER
1949	5	8	11	1	0.0	37.60	-77.60	0.0	3.6	NCEER
1949	5	13	4	15	0.0	42.50	-99.00	0.0	3.3	NCEER
1949	6	3	0	0	0.0	45.00	-100.00	0.0	3.1	NCEER
1949	6	27	6	53	0.0	32.90	-80.00	0.0	3.3	NCEER
1949	7	9	18	44	43.0	32.25	-70.75	0.0	5.7	NCEER
1949	9	17	9	30	0.0	36.70	-83.00	0.0	3.2	NCEER
1949	10	5	2	33	47.8	44.84	-70.58	20.0	4.7	NCEER
1949	10	16	23	33	45.4	45.49	-74.90	14.0	4.2	NCEER
1949	10	30	20	51	13.7	46.47	-72.12	0.0	3.4	NCEER
1950	1	17	0	51	0.0	35.70	-109.50	0.0	5.0	DNA
1950	1	18	1	55	51.0	40.50	-110.50	0.0	5.3	USH
1950	2	8	10	37	0.0	37.70	-92.70	0.0	3.7	NCEER
1950	2	15	10	5	0.0	46.10	-95.20	0.0	3.3	NCEER
1950	3	6	16	14	11.8	46.00	-74.50	0.0	4.0	NCEER

© 2007-2012 UniStar Nuclear Services, LLC. All rights reserved.
COPYRIGHT PROTECTED

Table 2.5-1— {Updated Earthquake catalog (1534-April 2010) Including events with $m_b \geq 3.0$}
(Page 33 of 75)

Year	Month	Day	Hour	Min	Sec	Lat (deg)	Lon (deg)	Depth (km)	mb	Source
1950	3	20	13	24	0.0	33.50	-97.10	0.0	3.1	NCEER
1950	3	20	22	55	11.5	41.50	-75.80	0.0	3.3	NCEER
1950	4	14	18	20	48.5	47.83	-75.50	0.0	4.9	NCEER
1950	4	20	0	0	0.0	39.80	-84.20	0.0	3.1	NCEER
1950	6	19	4	19	0.0	35.80	-84.00	0.0	3.5	NCEER
1950	6	29	9	13	33.0	49.90	-68.10	0.0	4.3	NCEER
1950	8	4	6	45	21.0	47.33	-70.25	0.0	3.2	NCEER
1950	8	4	14	29	28.7	45.20	-74.72	0.0	4.0	NCEER
1950	9	17	5	48	0.0	35.70	-89.90	0.0	3.0	NCEER
1950	10	29	5	59	26.0	45.82	-77.12	0.0	3.0	NCEER
1950	11	26	7	45	0.0	37.70	-78.30	0.0	3.3	NCEER
1951	1	26	3	27	0.0	41.50	-72.50	0.0	3.2	NCEER
1951	3	4	2	55	0.0	32.90	-80.00	0.0	3.3	NCEER
1951	3	9	7	0	0.0	37.60	-77.60	0.0	3.5	NCEER
1951	6	10	17	20	37.7	41.52	-71.53	5.0	3.7	NCEER
1951	6	20	18	37	11.1	35.22	-103.04	1.0	4.3	NCEER
1951	6	28	1	3	57.0	50.00	-67.50	0.0	4.2	NCEER
1951	7	25	0	22	51.5	47.20	-71.37	0.0	3.3	NCEER
1951	8	8	9	36	24.1	45.93	-74.67	0.0	3.3	NCEER
1951	9	3	21	26	24.8	41.35	-73.86	18.0	3.6	NCEER
1951	9	19	8	19	38.0	49.30	-66.25	0.0	4.3	NCEER
1951	9	20	2	38	0.0	38.70	-89.90	0.0	3.3	NCEER
1951	9	25	15	45	0.0	46.22	-75.37	0.0	3.7	NCEER
1951	10	25	7	7	52.8	45.27	-74.73	0.0	3.8	NCEER
1951	11	6	17	54	45.9	44.92	-73.55	31.0	3.9	NCEER
1951	11	23	6	45	0.0	40.60	-75.50	0.0	3.3	NCEER
1951	12	30	7	55	0.0	32.90	-80.00	0.0	3.3	NCEER
1952	1	30	4	0	0.0	44.50	-73.20	0.0	3.1	NCEER
1952	2	18	20	56	7.0	46.33	-69.38	0.0	3.3	NCEER
1952	2	20	22	34	39.0	36.40	-89.50	0.0	3.9	NCEER
1952	2	26	0	56	0.0	46.80	-70.20	0.0	3.7	NCEER
1952	3	17	4	14	41.0	47.10	-76.17	0.0	3.8	NCEER
1952	3	30	13	11	7.0	47.83	-69.88	0.0	4.1	NCEER
1952	4	9	16	29	28.4	35.52	-97.85	10.0	5.1	NCEER
1952	4	19	2	50	52.8	47.47	-70.58	0.0	3.8	NCEER
1952	4	26	4	59	0.0	47.00	-78.50	0.0	3.7	NCEER
1952	5	28	9	54	14.0	36.60	-89.70	0.0	3.3	NCEER
1952	6	11	20	20	0.0	36.30	-82.30	0.0	3.3	NCEER
1952	6	20	9	38	8.6	39.64	-82.02	9.0	3.9	NCEER
1952	7	16	23	48	10.0	36.20	-89.60	0.0	4.0	NCEER
1952	7	19	1	16	17.2	46.87	-75.84	1.0	4.3	NCEER
1952	8	25	0	7	0.0	43.00	-74.50	0.0	3.2	NCEER
1952	10	8	4	15	0.0	35.10	-96.50	0.0	3.1	NCEER
1952	10	8	21	40	0.0	41.70	-74.00	0.0	4.3	DNA
1952	10	14	22	3	44.8	47.80	-69.80	0.0	4.9	NCEER
1952	10	17	4	16	18.0	36.20	-89.60	0.0	3.1	NCEER

© 2007-2012 UniStar Nuclear Services, LLC. All rights reserved.
COPYRIGHT PROTECTED

Table 2.5-1— {Updated Earthquake catalog (1534-April 2010) Including events with $m_b \geq 3.0$}
(Page 34 of 75)

Year	Month	Day	Hour	Min	Sec	Lat (deg)	Lon (deg)	Depth (km)	mb	Source
1952	10	17	15	48	0.0	30.10	-93.70	0.0	3.1	NCEER
1952	11	15	0	0	0.0	44.10	-103.50	0.0	3.1	NCEER
1952	11	18	20	12	0.0	30.60	-84.60	0.0	3.3	NCEER
1952	11	19	0	0	0.0	32.90	-80.00	0.0	3.1	NCEER
1952	12	25	0	0	0.0	43.80	-81.00	0.0	3.1	NCEER
1952	12	25	4	23	24.0	35.90	-89.80	0.0	3.6	NCEER
1953	1	24	9	58	37.0	49.07	-66.00	0.0	4.6	NCEER
1953	1	26	23	18	0.0	36.00	-89.50	0.0	3.1	NCEER
1953	2	7	7	5	0.0	37.70	-78.10	0.0	3.3	NCEER
1953	2	11	10	50	54.0	36.50	-89.50	0.0	3.3	NCEER
1953	2	17	11	45	0.0	36.10	-89.80	0.0	3.1	NCEER
1953	2	28	6	24	2.5	48.07	-74.43	0.0	3.5	NCEER
1953	3	17	14	25	0.0	35.60	-98.00	0.0	4.2	NCEER
1953	3	26	0	0	0.0	28.60	-81.40	0.0	3.3	NCEER
1953	3	27	8	50	0.0	41.10	-73.50	0.0	3.0	NCEER
1953	3	31	2	50	0.0	43.70	-73.00	0.0	3.6	NCEER
1953	4	26	1	17	0.0	44.70	-73.50	0.0	3.0	NCEER
1953	5	12	18	50	0.0	35.60	-90.30	0.0	3.1	NCEER
1953	6	6	17	40	0.0	34.70	-96.70	0.0	3.1	NCEER
1953	6	12	0	0	0.0	41.70	-83.60	0.0	3.5	NCEER
1953	7	30	5	45	0.0	39.00	-110.16	0.0	4.3	DNA
1953	8	17	4	22	50.0	41.00	-74.00	0.0	3.1	NCEER
1953	9	11	18	26	28.0	38.80	-90.10	0.0	3.9	NCEER
1953	9	14	22	52	57.0	49.10	-65.20	0.0	4.4	NCEER
1953	10	11	4	0	0.0	36.00	-83.90	0.0	3.3	NCEER
1953	12	21	22	43	0.0	45.20	-102.90	0.0	3.0	NCEER
1953	12	30	22	0	0.0	38.60	-89.10	0.0	3.3	NCEER
1953	12	31	20	30	0.0	43.10	-99.30	0.0	3.1	NCEER
1954	1	1	2	30	0.0	37.30	-83.20	0.0	3.8	NCEER
1954	1	2	3	25	0.0	36.60	-83.70	0.0	4.4	NCEER
1954	1	7	7	25	0.0	40.30	-76.00	0.0	3.2	NCEER
1954	1	10	21	4	30.0	49.17	-68.23	0.0	3.1	NCEER
1954	1	17	7	15	0.0	36.00	-89.40	0.0	3.1	NCEER
1954	1	20	20	50	1.0	41.50	-105.50	0.0	3.4	NCEER
1954	1	23	1	0	0.0	35.30	-84.40	0.0	3.1	NCEER
1954	1	31	12	30	0.0	42.90	-77.30	0.0	3.1	NCEER
1954	2	1	0	37	50.0	43.03	-76.65	0.0	3.3	NCEER
1954	2	2	16	53	0.0	36.70	-90.30	0.0	4.3	NCEER
1954	2	7	20	24	16.0	47.60	-70.25	0.0	3.8	NCEER
1954	2	21	9	0	37.0	47.67	-70.62	0.0	3.5	NCEER
1954	4	11	0	0	0.0	35.00	-96.40	0.0	3.1	NCEER
1954	4	12	21	22	0.1	47.00	-76.12	6.0	4.3	NCEER
1954	4	21	15	45	0.0	44.70	-73.50	0.0	3.1	NCEER
1954	4	27	2	14	8.0	43.10	-79.20	0.0	4.1	NCEER
1954	4	27	4	9	0.0	35.10	-90.00	0.0	3.9	NCEER
1954	5	20	22	0	0.0	45.00	-74.20	0.0	3.0	NCEER

© 2007-2012 UniStar Nuclear Services, LLC. All rights reserved.
COPYRIGHT PROTECTED

Table 2.5-1— {Updated Earthquake catalog (1534-April 2010) Including events with $m_b \geq 3.0$}
(Page 35 of 75)

Year	Month	Day	Hour	Min	Sec	Lat (deg)	Lon (deg)	Depth (km)	mb	Source
1954	6	30	7	41	7.0	47.00	-70.12	0.0	3.7	NCEER
1954	7	29	19	56	56.0	42.81	-70.70	1.0	3.5	NCEER
1954	8	9	0	0	0.0	38.50	-87.30	0.0	3.1	NCEER
1954	8	11	3	40	0.0	40.30	-76.00	0.0	3.3	NCEER
1954	9	8	1	29	53.0	49.03	-68.37	0.0	3.6	NCEER
1954	9	11	18	55	55.6	47.18	-75.66	28.0	4.6	NCEER
1954	12	13	3	53	0.0	44.60	-74.60	0.0	3.0	NCEER
1955	1	5	20	0	0.0	47.30	-88.40	0.0	3.1	NCEER
1955	1	6	20	30	0.0	36.60	-82.20	0.0	3.1	NCEER
1955	1	7	5	0	0.0	47.10	-88.60	0.0	3.4	NCEER
1955	1	17	12	37	0.0	37.30	-78.40	0.0	3.3	NCEER
1955	1	21	8	40	0.0	43.00	-73.80	0.0	4.0	DNA
1955	1	25	7	24	39.1	36.07	-89.83	8.0	4.3	NCEER
1955	1	25	19	34	0.0	36.00	-83.90	0.0	3.1	NCEER
1955	2	1	12	40	27.0	47.67	-70.50	0.0	4.0	NCEER
1955	2	1	14	45	0.0	30.40	-89.10	0.0	4.1	NCEER
1955	2	10	17	30	0.0	40.50	-107.00	0.0	4.3	NCEER
1955	2	25	1	45	0.0	41.30	-98.60	0.0	3.3	NCEER
1955	4	4	3	17	7.0	51.58	-79.30	0.0	3.6	NCEER
1955	4	9	13	1	23.3	38.23	-89.78	11.0	4.3	NCEER
1955	5	26	18	9	0.0	41.30	-81.40	0.0	3.2	NCEER
1955	6	29	1	16	33.0	41.30	-81.40	0.0	3.1	NCEER
1955	6	29	1	17	40.0	43.77	-79.63	0.0	3.0	NCEER
1955	8	16	7	35	0.0	42.90	-78.30	0.0	3.5	NCEER
1955	9	6	1	45	0.0	36.00	-89.50	0.0	3.4	NCEER
1955	9	24	18	45	0.0	36.40	-89.50	0.0	3.1	NCEER
1955	9	28	7	1	41.5	36.60	-81.30	0.0	3.5	NCEER
1955	10	7	18	9	52.0	45.22	-73.90	0.0	3.5	NCEER
1955	10	20	21	31	6.0	48.93	-70.20	0.0	3.4	NCEER
1955	11	1	7	45	52.0	46.50	-75.87	0.0	3.5	NCEER
1955	11	21	16	10	41.0	50.58	-63.50	0.0	4.0	NCEER
1955	12	13	7	43	0.0	36.00	-89.50	0.0	3.4	NCEER
1956	1	5	8	0	0.0	34.30	-82.40	0.0	3.3	NCEER
1956	1	6	11	58	7.4	37.58	-98.35	29.0	4.0	NCEER
1956	1	7	23	30	0.0	29.30	-94.80	0.0	3.8	SRA
1956	1	10	12	8	18.0	45.67	-75.47	0.0	3.3	NCEER
1956	1	27	11	3	27.0	40.50	-84.00	0.0	3.7	NCEER
1956	1	29	4	44	15.5	35.76	-89.80	16.0	3.9	NCEER
1956	1	30	9	43	13.0	47.05	-71.17	0.0	3.7	NCEER
1956	2	2	19	24	16.0	45.45	-74.82	0.0	3.1	NCEER
1956	2	16	23	30	0.0	35.40	-97.30	0.0	3.9	NCEER
1956	3	6	23	38	10.0	44.85	-75.38	0.0	3.1	NCEER
1956	3	13	15	5	0.0	40.50	-90.40	0.0	3.7	SRA
1956	4	2	16	3	18.0	34.20	-95.60	0.0	3.5	NCEER
1956	5	19	19	0	0.0	34.30	-82.40	0.0	3.3	NCEER
1956	6	15	0	53	37.0	47.10	-76.43	0.0	3.9	NCEER

© 2007-2012 UniStar Nuclear Services, LLC. All rights reserved.
COPYRIGHT PROTECTED

Table 2.5-1— {Updated Earthquake catalog (1534-April 2010) Including events with $m_b \geq 3.0$}
(Page 36 of 75)

Year	Month	Day	Hour	Min	Sec	Lat (deg)	Lon (deg)	Depth (km)	mb	Source
1956	7	18	21	30	0.0	43.60	-87.70	0.0	3.1	NCEER
1956	7	27	1	34	44.0	44.70	-73.78	0.0	3.4	NCEER
1956	8	3	12	52	9.0	49.42	-66.17	0.0	3.6	NCEER
1956	9	7	13	35	50.8	36.44	-83.79	5.0	4.0	NCEER
1956	9	7	13	49	29.0	35.50	-84.00	0.0	4.2	NCEER
1956	9	9	22	45	0.0	35.80	-86.70	0.0	3.2	SRA
1956	9	27	14	15	0.0	31.90	-88.40	0.0	3.8	NCEER
1956	10	13	0	0	0.0	42.90	-87.90	0.0	3.1	NCEER
1956	10	27	14	40	6.0	48.25	-69.00	0.0	3.4	NCEER
1956	10	29	9	23	44.0	36.10	-89.70	0.0	3.4	NCEER
1956	10	30	10	36	21.0	36.20	-95.80	0.0	4.0	USH
1956	11	4	11	53	29.2	45.96	-75.42	1.0	4.0	NCEER
1956	11	26	4	12	43.3	36.91	-90.39	1.0	4.3	NCEER
1957	1	8	16	0	0.0	43.50	-88.80	0.0	3.0	NCEER
1957	1	25	18	15	0.0	36.60	-83.70	0.0	4.0	NCEER
1957	2	19	5	18	33.0	48.40	-69.93	0.0	3.5	NCEER
1957	2	20	15	45	0.0	44.90	-74.90	0.0	3.3	NCEER
1957	3	19	16	37	38.0	32.60	-94.70	0.0	4.0	NCEER
1957	3	23	19	2	0.0	40.60	-74.80	0.0	3.5	NCEER
1957	3	26	8	27	6.0	37.00	-88.40	0.0	3.1	NCEER
1957	4	23	9	23	39.0	33.77	-86.72	5.0	4.3	NCEER
1957	4	24	0	41	59.0	44.42	-72.00	0.0	3.3	NCEER
1957	4	26	11	40	8.6	43.53	-70.25	5.0	4.4	NCEER
1957	5	13	14	24	51.1	35.80	-82.14	5.0	4.1	NCEER
1957	6	23	6	34	16.0	35.95	-84.10	5.0	3.3	NCEER
1957	6	29	11	25	9.0	42.90	-81.30	0.0	3.1	NCEER
1957	7	2	9	33	1.0	35.60	-82.70	0.0	3.9	NCEER
1957	8	4	12	40	58.0	46.58	-67.08	0.0	3.7	NCEER
1957	8	6	23	50	38.0	47.48	-70.42	0.0	4.0	NCEER
1957	8	17	1	30	7.0	46.73	-70.12	0.0	3.3	NCEER
1957	8	17	23	0	0.0	36.20	-89.50	0.0	3.1	NCEER
1957	8	21	2	40	33.0	44.80	-76.17	0.0	3.0	NCEER
1957	10	9	14	16	58.0	48.42	-69.90	0.0	3.1	NCEER
1957	10	16	19	13	27.0	50.50	-64.87	0.0	4.1	NCEER
1957	10	27	8	48	27.0	46.38	-78.75	0.0	3.2	NCEER
1957	11	7	17	15	0.0	36.00	-84.00	0.0	3.3	NCEER
1957	11	13	20	49	19.0	48.67	-69.55	0.0	3.5	NCEER
1957	11	24	20	6	17.0	35.00	-83.50	0.0	3.9	NCEER
1957	12	3	7	30	0.0	43.80	-98.20	0.0	3.1	NCEER
1958	1	8	2	41	43.0	38.40	-87.90	0.0	4.5	DNA
1958	1	11	16	36	0.0	44.90	-74.90	0.0	3.3	NCEER
1958	1	24	17	10	0.0	45.00	-81.30	0.0	3.5	NCEER
1958	1	26	16	55	37.0	36.10	-89.70	0.0	3.8	NCEER
1958	1	28	5	56	40.0	37.10	-89.20	0.0	3.9	NCEER
1958	3	1	17	41	49.0	46.90	-76.03	0.0	3.9	NCEER
1958	3	5	11	53	43.0	34.20	-77.80	0.0	3.4	NCEER

© 2007-2012 UniStar Nuclear Services, LLC. All rights reserved.
COPYRIGHT PROTECTED

Table 2.5-1— {Updated Earthquake catalog (1534-April 2010) Including events with $m_b \geq 3.0$}
(Page 37 of 75)

Year	Month	Day	Hour	Min	Sec	Lat (deg)	Lon (deg)	Depth (km)	mb	Source
1958	3	19	6	39	25.0	46.00	-77.13	0.0	3.1	NCEER
1958	3	23	22	4	17.0	45.55	-67.12	0.0	3.4	NCEER
1958	4	8	22	25	33.0	36.30	-89.20	0.0	3.4	NCEER
1958	4	26	7	30	0.0	36.40	-89.50	0.0	3.2	NCEER
1958	5	1	22	46	31.0	41.50	-81.80	0.0	3.1	NCEER
1958	5	6	16	2	49.0	48.57	-70.32	0.0	3.7	NCEER
1958	5	14	17	41	16.7	47.09	-76.82	1.0	5.0	NCEER
1958	5	16	22	30	0.0	35.60	-82.60	0.0	3.3	NCEER
1958	5	20	1	25	0.0	35.50	-90.40	0.0	3.1	NCEER
1958	7	18	23	56	27.0	46.70	-71.40	0.0	3.2	NCEER
1958	7	22	1	46	40.0	43.00	-79.50	0.0	4.4	NCEER
1958	7	25	3	45	11.0	46.57	-75.80	0.0	3.8	NCEER
1958	7	27	8	58	0.0	47.32	-70.30	0.0	3.0	NCEER
1958	8	4	20	25	58.0	43.13	-80.00	0.0	3.8	NCEER
1958	8	7	0	46	43.0	41.10	-106.00	0.0	3.1	NCEER
1958	8	8	22	15	3.0	47.93	-70.38	0.0	3.6	NCEER
1958	8	12	3	22	12.0	48.60	-69.38	0.0	3.9	NCEER
1958	8	22	14	25	5.0	43.00	-79.00	0.0	3.6	NCEER
1958	9	19	17	45	0.0	43.60	-70.20	0.0	3.0	NCEER
1958	9	29	10	45	29.0	48.38	-69.27	0.0	3.3	NCEER
1958	9	30	0	13	58.0	45.18	-73.73	0.0	3.7	NCEER
1958	10	20	6	16	0.0	34.50	-82.70	0.0	3.5	NCEER
1958	10	21	9	32	51.0	49.60	-68.00	0.0	4.1	NCEER
1958	10	23	2	29	44.3	37.20	-81.90	5.0	3.0	NCEER
1958	11	6	23	8	0.0	29.90	-90.10	0.0	3.1	NCEER
1958	11	8	2	41	12.6	38.44	-88.01	5.0	4.4	NCEER
1958	11	19	18	15	0.0	30.50	-91.20	0.0	3.3	NCEER
1958	11	21	23	30	0.0	44.00	-71.70	0.0	3.3	NCEER
1958	12	23	23	14	16.0	46.98	-69.82	0.0	3.7	NCEER
1959	1	12	13	0	0.0	44.90	-98.10	0.0	3.1	NCEER
1959	1	21	15	35	0.0	36.30	-89.50	0.0	3.1	NCEER
1959	2	9	0	0	0.0	43.00	-81.00	0.0	3.1	NCEER
1959	2	10	20	5	0.0	35.50	-100.90	0.0	4.2	NCEER
1959	2	13	8	37	0.0	36.10	-89.50	0.0	3.2	NCEER
1959	4	13	21	20	19.0	41.92	-73.27	0.0	3.4	NCEER
1959	4	16	16	36	25.0	47.12	-70.33	0.0	3.5	NCEER
1959	4	23	20	58	39.5	37.39	-80.68	1.0	3.7	NCEER
1959	5	21	9	38	51.0	46.55	-76.45	0.0	3.9	NCEER
1959	5	24	10	52	0.0	48.80	-79.20	0.0	3.5	NCEER
1959	6	13	1	0	0.0	35.40	-84.30	0.0	3.6	SRA
1959	6	15	12	45	0.0	34.70	-96.70	0.0	3.7	NCEER
1959	6	17	10	27	10.6	34.64	-98.06	5.0	4.1	NCEER
1959	7	7	23	17	0.0	37.30	-80.70	0.0	3.1	NCEER
1959	8	1	13	52	49.0	48.42	-68.32	0.0	4.1	NCEER
1959	8	3	6	8	36.8	33.05	-80.13	1.0	4.6	NCEER
1959	8	12	18	6	1.4	34.79	-86.56	5.0	3.9	NCEER

© 2007-2012 UniStar Nuclear Services, LLC. All rights reserved.
COPYRIGHT PROTECTED

Table 2.5-1— {Updated Earthquake catalog (1534-April 2010) Including events with $m_b \geq 3.0$}
(Page 38 of 75)

Year	Month	Day	Hour	Min	Sec	Lat (deg)	Lon (deg)	Depth (km)	mb	Source
1959	8	21	17	20	0.0	37.30	-80.70	0.0	3.2	NCEER
1959	8	22	3	52	30.0	46.95	-70.78	0.0	3.2	NCEER
1959	9	25	1	36	30.0	50.18	-68.20	0.0	3.9	NCEER
1959	10	15	15	45	0.0	29.80	-93.10	0.0	3.4	NCEER
1959	10	27	2	7	28.0	34.50	-80.20	0.0	4.0	NCEER
1959	12	21	16	23	39.6	36.03	-89.34	5.0	3.4	NCEER
1959	12	25	9	50	0.0	41.10	-106.20	0.0	4.3	NCEER
1960	1	20	20	7	40.0	46.97	-75.67	0.0	3.7	NCEER
1960	1	22	20	53	22.0	41.50	-75.50	0.0	3.4	SRA
1960	1	28	21	38	0.0	36.00	-89.50	0.0	3.2	NCEER
1960	2	6	0	44	2.0	47.80	-70.38	0.0	3.3	NCEER
1960	3	12	12	47	44.0	33.07	-80.12	9.0	4.2	NCEER
1960	4	15	10	10	10.0	35.80	-84.00	0.0	3.5	NCEER
1960	4	21	10	45	0.0	36.00	-89.50	0.0	3.4	NCEER
1960	4	23	11	47	47.1	47.88	-70.34	5.0	4.0	NCEER
1960	5	4	16	31	32.0	34.20	-92.00	0.0	3.1	NCEER
1960	7	24	3	37	30.0	32.90	-80.00	0.0	3.7	NCEER
1960	9	4	18	40	0.0	37.40	-79.30	0.0	3.3	NCEER
1960	10	11	8	5	30.5	38.30	-107.60	49.0	5.5	USH
1961	1	11	1	40	0.0	34.90	-95.50	0.0	3.6	NCEER
1961	1	29	0	49	39.0	46.38	-66.93	0.0	3.8	NCEER
1961	2	22	9	45	3.0	41.20	-83.30	0.0	3.7	NCEER
1961	3	13	10	55	45.0	45.17	-75.28	0.0	3.2	NCEER
1961	4	13	21	14	55.2	39.98	-99.77	1.0	3.6	NCEER
1961	4	20	13	13	0.0	45.00	-74.80	0.0	3.2	NCEER
1961	4	26	7	5	0.0	34.60	-95.00	0.0	3.6	NCEER
1961	4	27	7	30	0.0	34.90	-95.30	0.0	3.8	NCEER
1961	7	5	22	43	44.0	50.25	-66.68	0.0	4.3	NCEER
1961	8	22	18	55	51.0	47.33	-70.50	0.0	3.4	NCEER
1961	9	9	22	42	55.0	35.96	-90.19	5.0	3.8	NCEER
1961	9	15	2	16	56.0	40.80	-75.50	0.0	4.3	DNA
1961	9	29	6	30	0.0	44.90	-74.90	0.0	3.1	NCEER
1961	10	7	22	36	51.0	48.67	-76.58	0.0	3.8	NCEER
1961	12	14	1	49	0.0	43.80	-67.80	0.0	3.9	NCEER
1961	12	25	12	58	16.8	39.32	-94.24	9.0	3.9	NCEER
1961	12	27	17	6	0.0	40.50	-74.80	0.0	3.3	NCEER
1961	12	31	16	36	5.8	44.25	-100.72	23.0	4.0	NCEER
1962	1	27	12	11	17.0	45.92	-74.85	0.0	3.8	NCEER
1962	1	31	14	32	38.0	47.50	-67.13	0.0	3.5	NCEER
1962	2	2	6	43	30.0	36.37	-89.51	4.0	4.3	NCEER
1962	2	16	0	0	0.0	37.00	-88.70	0.0	3.0	NCEER
1962	3	23	2	2	21.0	47.18	-69.47	0.0	3.3	NCEER
1962	3	25	5	15	5.0	47.57	-66.02	0.0	4.0	NCEER
1962	3	27	6	35	0.0	43.00	-79.30	0.0	3.0	NCEER
1962	4	10	14	30	45.2	44.11	-72.97	5.0	4.3	NCEER
1962	4	28	6	9	11.0	35.30	-98.60	0.0	3.3	NCEER

© 2007-2012 UniStar Nuclear Services, LLC. All rights reserved.
COPYRIGHT PROTECTED

Table 2.5-1— {Updated Earthquake catalog (1534-April 2010) Including events with $m_b \geq 3.0$}
(Page 39 of 75)

Year	Month	Day	Hour	Min	Sec	Lat (deg)	Lon (deg)	Depth (km)	mb	Source
1962	5	24	0	0	0.0	36.50	-89.50	0.0	3.0	NCEER
1962	6	1	11	23	38.6	35.38	-90.39	1.0	3.2	NCEER
1962	6	21	2	6	47.0	45.44	-72.64	1.0	3.2	NCEER
1962	6	27	1	28	59.3	37.90	-88.64	0.0	5.4	NCEER
1962	7	14	2	23	44.0	36.56	-89.82	1.0	3.2	NCEER
1962	7	23	6	5	15.7	36.04	-89.40	8.0	3.6	NCEER
1962	7	27	17	56	57.0	47.25	-70.67	0.0	3.9	NCEER
1962	8	10	20	47	19.0	34.80	-97.40	0.0	3.2	SRA
1962	8	11	3	5	16.0	47.53	-70.05	0.0	3.6	NCEER
1962	9	4	23	40	0.0	39.50	-77.70	0.0	3.3	NCEER
1962	9	7	14	0	0.0	39.70	-78.20	0.0	3.3	NCEER
1962	9	7	16	50	23.8	39.20	-110.89	7.0	3.1	SRA
1962	9	7	22	53	44.0	34.70	-98.40	0.0	3.2	SRA
1962	10	2	23	45	0.0	44.80	-74.30	0.0	3.3	NCEER
1962	12	1	21	29	23.0	45.57	-69.13	0.0	3.0	NCEER
1962	12	11	10	28	13.5	39.36	-110.42	7.0	3.4	SRA
1962	12	15	0	58	32.0	50.20	-66.38	0.0	4.0	NCEER
1962	12	29	6	19	0.0	42.80	-71.70	0.0	3.0	NCEER
1963	1	17	14	26	50.8	37.30	-80.10	0.0	3.3	NCEER
1963	1	30	14	50	0.0	44.00	-75.90	0.0	3.0	NCEER
1963	2	7	21	18	36.0	34.40	-92.10	0.0	3.4	NCEER
1963	2	25	18	45	16.5	42.60	-109.20	33.0	4.3	SRA
1963	2	27	6	0	0.0	43.20	-79.57	0.0	3.0	NCEER
1963	3	2	20	24	32.0	41.51	-75.73	0.0	3.4	NCEER
1963	3	3	17	30	10.6	36.64	-90.05	15.0	4.8	NCEER
1963	3	13	9	33	34.0	34.60	-95.90	0.0	3.1	NCEER
1963	4	3	9	55	12.6	45.10	-109.80	33.0	3.9	SRA
1963	4	6	8	12	22.7	36.46	-89.58	6.0	3.1	NCEER
1963	4	24	13	33	3.3	39.44	-110.33	7.0	4.6	SRA
1963	5	2	1	9	21.4	36.67	-89.54	10.0	3.1	NCEER
1963	5	4	21	1	50.3	32.97	-80.19	5.0	3.3	NCEER
1963	5	7	20	3	29.0	34.30	-96.40	0.0	3.0	SRA
1963	5	19	19	14	0.0	43.50	-75.20	0.0	3.5	NCEER
1963	6	5	0	13	50.6	39.30	-104.00	0.0	4.4	NCEER
1963	6	6	8	5	33.0	36.60	-104.40	0.0	4.0	SNM
1963	7	1	19	59	12.0	42.37	-73.75	0.0	3.3	NCEER
1963	7	8	23	51	42.1	36.97	-90.47	0.0	3.1	NCEER
1963	8	1	6	34	16.0	46.80	-66.50	0.0	3.0	NCEER
1963	8	3	0	37	49.1	36.98	-88.77	7.0	4.4	NCEER
1963	8	26	16	29	35.0	45.18	-73.95	0.0	3.5	NCEER
1963	9	30	9	17	39.3	38.10	-111.22	7.0	4.5	SRA
1963	10	8	6	1	43.4	33.90	-82.50	0.0	3.2	SRA
1963	10	10	14	59	52.3	39.66	-78.20	0.0	3.6	SRA
1963	10	14	8	31	23.0	42.20	-108.30	30.0	4.5	SRA
1963	10	15	13	59	50.8	46.37	-77.47	8.0	4.2	NCEER
1963	10	16	15	30	59.7	42.40	-70.42	14.0	3.8	NCEER

© 2007-2012 UniStar Nuclear Services, LLC. All rights reserved.
COPYRIGHT PROTECTED

Table 2.5-1— {Updated Earthquake catalog (1534-April 2010) Including events with $m_b \geq 3.0$}
(Page 40 of 75)

Year	Month	Day	Hour	Min	Sec	Lat (deg)	Lon (deg)	Depth (km)	mb	Source
1963	10	25	8	49	39.0	51.40	-61.90	0.0	3.3	NCEER
1963	10	28	22	38	0.3	36.70	-81.00	0.0	3.7	NCEER
1963	10	30	22	36	57.9	42.70	-70.80	0.0	3.4	NCEER
1963	11	5	22	45	3.4	27.49	-92.58	15.0	4.8	NCEER
1963	12	4	21	32	34.8	43.60	-71.60	9.0	3.2	NCEER
1963	12	5	6	51	0.5	37.15	-86.97	1.0	3.2	NCEER
1963	12	19	16	47	28.0	35.13	-104.13	0.0	3.4	SNM
1964	1	5	13	57	16.7	41.26	-109.14	7.0	3.9	SRA
1964	1	8	10	3	26.0	46.23	-77.53	0.0	3.9	NCEER
1964	1	16	5	9	58.0	36.84	-89.46	0.0	3.3	NCEER
1964	1	20	18	57	45.3	46.92	-70.70	27.0	3.1	NCEER
1964	1	25	19	54	10.0	36.50	-89.50	0.0	3.0	NCEER
1964	2	2	8	23	0.0	35.10	-99.70	0.0	3.4	NCEER
1964	2	13	19	46	40.8	40.38	-77.96	1.0	3.3	NCEER
1964	2	18	9	31	10.4	34.67	-85.39	15.0	4.4	SRA
1964	3	7	18	2	58.6	33.72	-82.39	5.0	3.3	NCEER
1964	3	13	1	20	17.5	33.19	-83.31	1.0	3.9	NCEER
1964	3	17	2	16	6.0	36.20	-89.60	0.0	3.5	NCEER
1964	3	24	6	12	0.0	43.50	-103.50	0.0	3.5	NCEER
1964	3	28	3	0	0.0	42.70	-104.10	0.0	3.4	NCEER
1964	3	28	10	8	46.5	43.00	-101.80	30.0	4.5	NCEER
1964	3	29	9	16	0.0	44.90	-74.90	0.0	4.3	NCEER
1964	4	1	11	21	34.0	43.60	-71.50	0.0	3.1	NCEER
1964	4	5	13	21	0.0	46.40	-81.10	0.0	3.8	NCEER
1964	4	20	19	4	44.1	33.84	-81.10	3.0	3.7	NCEER
1964	4	24	7	33	51.9	31.42	-93.81	5.0	3.6	NCEER
1964	5	12	6	45	10.7	40.30	-76.41	1.0	3.2	NCEER
1964	5	23	11	25	34.5	36.58	-90.02	3.0	3.9	NCEER
1964	6	2	23	0	0.0	31.30	-94.00	0.0	4.2	SRA
1964	6	3	9	37	0.0	31.00	-94.00	0.0	3.0	NCEER
1964	6	16	0	0	0.0	40.90	-74.30	0.0	3.3	NCEER
1964	6	26	11	4	49.0	43.40	-71.68	1.0	3.8	NCEER
1964	6	27	19	17	0.0	47.80	-79.20	0.0	3.7	NCEER
1964	7	1	21	41	30.0	49.43	-67.42	0.0	3.8	NCEER
1964	7	12	0	0	41.0	46.72	-71.41	0.0	3.4	NCEER
1964	7	24	10	34	11.0	46.65	-76.25	0.0	3.3	NCEER
1964	7	28	0	0	0.0	36.00	-83.90	0.0	3.0	NCEER
1964	8	4	11	13	25.2	39.70	-106.00	0.0	4.0	NCEER
1964	8	5	15	17	56.2	38.95	-110.92	7.0	3.0	SRA
1964	8	12	9	35	27.0	50.47	-64.87	0.0	3.7	NCEER
1964	8	16	11	35	31.0	31.40	-93.80	0.0	3.0	NCEER
1964	8	22	3	28	11.0	42.90	-104.70	0.0	4.5	NCEER
1964	8	26	16	58	55.1	43.77	-102.25	20.0	3.0	NCEER
1964	9	9	6	16	26.0	48.40	-73.87	0.0	3.1	NCEER
1964	9	10	6	19	50.7	41.90	-107.80	33.0	4.1	SRA
1964	9	19	20	51	5.0	50.00	-109.70	33.0	4.0	DNA

© 2007-2012 UniStar Nuclear Services, LLC. All rights reserved.
COPYRIGHT PROTECTED

Table 2.5-1— {Updated Earthquake catalog (1534-April 2010) Including events with $m_b \geq 3.0$}
(Page 41 of 75)

Year	Month	Day	Hour	Min	Sec	Lat (deg)	Lon (deg)	Depth (km)	mb	Source
1964	9	24	8	9	34.0	37.10	-91.10	0.0	3.0	NCEER
1964	9	28	15	41	0.0	44.00	-96.40	0.0	3.4	NCEER
1964	10	10	8	30	0.0	47.40	-89.80	0.0	3.0	NCEER
1964	10	10	11	30	0.0	47.30	-90.30	0.0	3.0	NCEER
1964	10	13	16	30	0.0	36.00	-83.90	0.0	3.2	NCEER
1964	10	17	14	13	7.0	47.67	-67.25	0.0	3.9	NCEER
1964	11	4	8	42	51.8	39.36	-110.29	7.0	4.0	SRA
1964	11	17	17	8	0.0	41.20	-73.70	0.0	3.1	NCEER
1964	11	25	2	50	6.4	37.39	-81.70	6.0	3.6	SRA
1964	12	16	21	39	25.2	38.92	-110.92	7.0	3.1	DNA
1965	1	3	17	5	1.0	43.50	-72.00	0.0	3.0	NCEER
1965	1	8	12	29	45.0	48.00	-78.50	0.0	3.5	NCEER
1965	1	14	12	30	10.8	39.44	-110.35	7.0	4.5	SRA
1965	2	3	11	32	34.0	35.10	-103.80	0.0	3.4	SNM
1965	2	3	19	59	32.0	31.90	-103.00	0.0	3.0	SRA
1965	2	11	3	40	24.8	36.52	-89.59	3.0	3.3	NCEER
1965	2	14	20	3	20.0	36.90	-93.30	0.0	3.0	NCEER
1965	3	1	2	22	8.0	47.50	-71.25	0.0	3.1	NCEER
1965	3	5	12	11	1.0	47.72	-78.83	0.0	3.2	NCEER
1965	3	6	21	8	50.3	37.40	-91.03	7.0	4.0	NCEER
1965	3	6	21	13	0.0	45.00	-83.00	0.0	3.1	NCEER
1965	3	18	12	9	5.0	49.77	-67.53	0.0	3.1	NCEER
1965	3	25	12	59	27.7	36.46	-89.52	3.0	3.7	NCEER
1965	4	1	6	30	20.0	46.00	-80.50	0.0	3.4	NCEER
1965	4	26	15	26	19.7	37.32	-81.60	5.0	3.5	NCEER
1965	5	25	7	15	43.0	36.10	-89.90	0.0	3.3	NCEER
1965	5	30	17	31	4.1	39.40	-106.30	33.0	4.3	SRA
1965	6	1	7	24	57.0	36.50	-89.50	0.0	3.0	NCEER
1965	6	3	19	30	25.8	43.60	-106.50	33.0	4.7	SRA
1965	7	8	7	3	50.0	36.50	-89.50	0.0	3.3	NCEER
1965	7	16	11	6	57.0	43.04	-78.08	18.0	3.0	NCEER
1965	7	18	3	55	51.4	39.50	-109.90	33.0	3.1	SRA
1965	8	6	15	39	49.2	44.70	-109.80	33.0	3.9	SRA
1965	8	14	13	13	56.9	37.23	-89.31	1.0	3.8	NCEER
1965	8	22	17	54	33.3	42.30	-110.60	33.0	3.3	SRA
1965	8	28	1	55	0.0	43.00	-78.10	0.0	3.1	SRA
1965	8	30	5	17	38.0	32.10	-102.30	0.0	3.5	NCEER
1965	8	31	8	38	44.0	46.00	-65.28	0.0	3.2	NCEER
1965	9	9	14	42	20.0	34.70	-81.20	0.0	3.2	NCEER
1965	9	15	17	56	28.0	46.72	-79.05	0.0	3.8	NCEER
1965	9	29	20	57	0.0	41.40	-74.40	0.0	3.3	NCEER
1965	10	5	14	36	55.0	49.78	-67.66	0.0	3.9	NCEER
1965	10	8	2	17	27.0	40.08	-79.75	0.0	3.3	NCEER
1965	10	10	23	51	33.0	36.10	-97.70	0.0	3.1	NCEER
1965	10	21	2	4	39.1	37.48	-90.94	5.0	4.9	NCEER
1965	10	24	17	45	0.0	41.30	-70.10	0.0	3.0	NCEER

© 2007-2012 UniStar Nuclear Services, LLC. All rights reserved.
COPYRIGHT PROTECTED

Table 2.5-1— {Updated Earthquake catalog (1534-April 2010) Including events with $m_b \geq 3.0$}
(Page 42 of 75)

Year	Month	Day	Hour	Min	Sec	Lat (deg)	Lon (deg)	Depth (km)	mb	Source
1965	11	4	7	43	37.9	37.03	-90.92	4.0	3.4	NCEER
1965	11	7	20	57	41.8	47.25	-76.36	10.0	4.2	NCEER
1965	11	8	12	58	1.0	33.20	-83.20	0.0	3.3	SRA
1965	11	24	21	28	1.0	46.93	-76.28	0.0	3.7	NCEER
1965	12	8	3	2	0.0	41.70	-71.40	0.0	3.2	NCEER
1965	12	16	13	53	19.0	47.83	-70.60	0.0	4.1	NCEER
1965	12	19	0	49	0.0	51.20	-80.80	0.0	4.9	NCEER
1965	12	19	22	19	12.0	36.03	-89.76	1.0	3.8	NCEER
1966	1	1	13	23	39.0	42.84	-78.25	2.0	3.9	NCEER
1966	1	14	15	29	25.0	48.90	-67.47	0.0	3.9	NCEER
1966	2	12	4	32	12.8	35.95	-89.87	1.0	3.6	NCEER
1966	2	13	6	29	43.0	33.60	-87.00	0.0	3.5	SRA
1966	2	13	23	19	37.8	37.04	-90.90	6.0	3.6	NCEER
1966	3	13	14	24	42.0	36.20	-90.00	0.0	3.0	NCEER
1966	3	20	23	45	33.0	46.50	-76.16	0.0	3.2	NCEER
1966	4	21	14	14	19.0	35.28	-103.33	0.0	3.4	SNM
1966	4	28	12	2	0.0	44.10	-71.90	0.0	3.3	NCEER
1966	5	20	0	5	42.0	44.25	-66.50	0.0	3.8	NCEER
1966	5	31	6	18	59.5	37.66	-78.13	2.0	4.3	NCEER
1966	6	22	11	27	53.0	38.60	-88.20	0.0	3.1	NCEER
1966	6	25	0	5	51.0	45.16	-73.83	0.0	3.4	NCEER
1966	6	26	11	59	43.1	44.30	-103.43	2.0	3.1	NCEER
1966	7	12	1	6	38.0	49.50	-66.00	0.0	3.3	NCEER
1966	7	20	9	4	58.8	35.64	-101.33	3.0	3.7	NCEER
1966	7	20	20	8	29.0	47.75	-70.00	0.0	3.2	NCEER
1966	7	24	1	59	0.0	44.50	-67.60	0.0	3.0	NCEER
1966	7	24	22	19	46.0	49.63	-68.55	0.0	3.7	NCEER
1966	7	30	3	25	31.0	39.44	-110.36	7.0	4.1	SRA
1966	8	14	15	25	53.7	32.12	-102.34	3.0	4.3	USH
1966	8	24	6	0	0.0	35.80	-84.00	0.0	3.0	NCEER
1966	9	4	9	52	34.5	38.30	-107.60	33.0	4.2	SRA
1966	9	9	9	50	34.2	41.30	-98.81	27.0	3.1	NCEER
1966	9	28	0	0	0.0	39.30	-80.30	0.0	3.1	NCEER
1966	9	28	20	11	35.0	46.92	-65.25	0.0	3.2	NCEER
1966	10	1	17	23	55.0	47.66	-70.33	0.0	3.0	NCEER
1966	10	3	2	26	2.3	37.40	-104.10	0.0	4.5	NCEER
1966	10	13	0	33	0.0	39.30	-104.60	0.0	3.0	SRA
1966	10	23	23	5	0.0	43.00	-71.80	0.0	3.2	NCEER
1966	11	1	7	40	28.0	40.20	-106.90	33.0	4.0	SRA
1966	11	13	15	43	0.0	47.00	-76.30	0.0	3.6	NCEER
1966	12	6	8	0	47.0	38.90	-92.80	0.0	3.0	NCEER
1966	12	12	21	4	12.0	49.00	-68.17	0.0	3.4	NCEER
1966	12	16	2	0	40.0	36.98	-107.02	0.0	3.7	SNM
1966	12	19	20	52	33.3	39.00	-106.50	5.0	4.6	SRA
1967	1	12	3	52	6.2	38.98	-107.51	33.0	4.4	SRA
1967	1	16	9	22	45.9	37.67	-107.86	33.0	4.1	SRA

© 2007-2012 UniStar Nuclear Services, LLC. All rights reserved.
COPYRIGHT PROTECTED

Table 2.5-1— {Updated Earthquake catalog (1534-April 2010) Including events with $m_b \geq 3.0$}
(Page 43 of 75)

Year	Month	Day	Hour	Min	Sec	Lat (deg)	Lon (deg)	Depth (km)	mb	Source
1967	1	18	6	12	0.6	40.05	-107.05	33.0	3.8	SRA
1967	1	21	0	18	16.0	44.74	-109.77	33.0	3.6	SRA
1967	2	1	20	15	10.1	37.83	-110.17	7.0	3.8	SRA
1967	2	2	6	30	0.0	42.70	-84.60	0.0	3.1	NCEER
1967	2	2	13	40	9.0	41.40	-71.40	0.0	3.3	NCEER
1967	2	5	10	7	16.6	39.55	-110.10	33.0	3.0	SRA
1967	2	12	0	0	0.0	36.00	-90.00	0.0	3.1	SRA
1967	2	15	15	2	16.5	39.27	-110.37	5.0	3.4	SRA
1967	2	21	0	53	0.0	52.00	-81.30	0.0	3.9	NCEER
1967	2	22	14	21	55.0	50.50	-63.33	0.0	3.5	NCEER
1967	3	10	2	20	33.2	42.05	-110.28	7.0	3.7	SRA
1967	3	28	20	31	35.4	45.16	-109.90	33.0	3.6	SRA
1967	4	4	22	53	39.5	38.32	-107.75	33.0	4.5	SRA
1967	4	8	5	40	30.5	39.65	-82.53	1.0	3.7	NCEER
1967	4	11	23	44	45.0	36.10	-89.70	0.0	3.0	NCEER
1967	4	26	10	17	59.4	43.41	-108.77	5.0	4.7	SRA
1967	5	11	21	15	6.6	43.66	-105.90	0.0	4.8	NCEER
1967	5	15	22	47	12.0	42.30	-69.90	0.0	3.2	NCEER
1967	6	4	16	14	12.6	33.55	-90.84	6.0	4.3	NCEER
1967	6	11	1	49	39.0	46.58	-75.03	0.0	3.7	NCEER
1967	6	13	19	8	55.5	42.84	-78.23	1.0	3.9	NCEER
1967	7	1	16	11	18.9	44.40	-69.90	0.0	3.8	SRA
1967	7	6	16	43	51.0	35.80	-90.40	0.0	3.4	NCEER
1967	7	21	9	14	48.8	37.44	-90.44	15.0	4.6	NCEER
1967	8	5	8	8	32.0	48.57	-64.97	0.0	4.0	NCEER
1967	8	25	19	15	18.0	37.10	-91.10	0.0	3.1	NCEER
1967	9	17	1	19	38.0	50.67	-75.25	0.0	4.0	NCEER
1967	9	23	16	27	55.0	46.93	-70.70	0.0	3.4	NCEER
1967	9	30	22	39	48.0	49.44	-65.63	15.0	4.7	NCEER
1967	10	18	5	8	36.0	36.50	-89.50	0.0	3.0	NCEER
1967	10	23	9	4	2.5	32.80	-80.22	19.0	3.4	NCEER
1967	10	25	7	5	31.0	50.15	-63.52	0.0	3.4	NCEER
1967	11	22	22	10	0.0	41.20	-73.80	0.0	3.2	NCEER
1967	11	23	6	23	42.1	43.56	-99.60	1.0	3.5	NCEER
1967	12	16	12	23	33.4	37.36	-81.60	2.0	3.5	NCEER
1968	1	4	22	30	0.0	34.85	-95.55	0.0	3.1	NCEER
1968	1	9	2	16	39.3	42.70	-106.80	33.0	3.8	SRA
1968	1	23	16	16	0.0	36.20	-89.80	0.0	3.3	NCEER
1968	2	10	1	34	30.6	36.52	-89.86	7.0	3.8	NCEER
1968	2	20	6	34	26.4	41.72	-110.61	7.0	3.7	SRA
1968	3	8	5	38	15.7	37.28	-80.77	8.0	3.4	NCEER
1968	3	30	15	28	59.0	47.94	-70.49	18.0	3.1	NCEER
1968	3	31	17	58	9.6	38.02	-89.85	1.0	4.5	NCEER
1968	4	11	9	18	0.0	47.60	-70.40	0.0	3.5	NCEER
1968	4	21	7	8	7.0	37.80	-102.10	0.0	3.8	NCEER
1968	5	27	19	21	56.0	46.90	-66.66	18.0	3.3	NCEER

© 2007-2012 UniStar Nuclear Services, LLC. All rights reserved.
COPYRIGHT PROTECTED

Table 2.5-1— {Updated Earthquake catalog (1534-April 2010) Including events with $m_b \geq 3.0$}
(Page 44 of 75)

Year	Month	Day	Hour	Min	Sec	Lat (deg)	Lon (deg)	Depth (km)	mb	Source
1968	5	30	1	59	33.0	36.50	-89.50	0.0	3.5	NCEER
1968	6	2	18	59	23.2	39.21	-110.45	7.0	3.8	SRA
1968	6	14	21	11	15.3	41.93	-110.47	7.0	3.0	SRA
1968	6	23	20	16	13.0	39.31	-107.41	33.0	3.8	SRA
1968	7	8	16	50	14.7	46.59	-100.74	27.0	3.7	NCEER
1968	7	12	1	12	0.0	32.80	-79.70	0.0	3.8	DNA
1968	7	14	4	21	25.0	36.50	-89.50	0.0	3.1	SRA
1968	7	15	4	21	25.0	35.70	-90.80	0.0	3.0	NCEER
1968	7	24	23	16	37.0	47.01	-71.30	18.0	3.1	NCEER
1968	7	26	15	2	53.7	40.40	-84.20	0.0	3.0	SRA
1968	9	22	21	41	18.2	34.11	-81.48	1.0	3.1	NCEER
1968	9	23	15	38	50.0	45.17	-69.45	18.0	3.3	NCEER
1968	9	29	10	4	48.0	50.14	-67.22	18.0	3.6	NCEER
1968	10	10	20	10	41.0	45.80	-81.66	18.0	3.4	NCEER
1968	10	11	5	0	11.0	39.03	-110.17	7.0	3.2	SRA
1968	10	14	14	42	54.0	34.00	-96.80	0.0	3.5	NCEER
1968	10	19	10	37	0.0	45.30	-74.10	0.0	3.2	NCEER
1968	10	20	2	36	0.0	47.50	-70.60	0.0	3.6	NCEER
1968	10	31	0	0	0.0	43.00	-83.00	0.0	3.7	NCEER
1968	11	3	8	33	0.0	41.40	-72.50	0.0	3.3	NCEER
1968	11	3	20	50	49.0	46.17	-76.30	18.0	3.1	NCEER
1968	11	9	17	1	40.5	37.91	-88.37	21.0	5.5	NCEER
1968	11	25	20	0	0.0	34.10	-77.90	0.0	3.3	NCEER
1968	12	10	9	12	0.0	39.70	-74.60	0.0	3.2	NCEER
1968	12	11	15	0	0.0	37.80	-87.60	0.0	3.4	NCEER
1968	12	11	16	0	0.0	38.30	-85.80	0.0	3.0	NCEER
1969	1	1	23	35	38.7	34.99	-92.69	7.0	4.4	NCEER
1969	1	20	19	25	0.0	37.80	-90.40	0.0	3.4	NCEER
1969	4	13	6	27	51.0	34.20	-96.30	0.0	3.5	NCEER
1969	5	2	11	33	21.7	35.29	-96.31	8.0	3.3	NCEER
1969	5	10	18	43	29.0	47.47	-70.65	18.0	3.6	NCEER
1969	5	18	0	0	0.0	33.95	-82.58	0.0	3.5	NCEER
1969	5	22	14	59	51.6	39.61	-78.25	0.0	3.1	SRA
1969	5	26	1	30	8.6	40.40	-104.40	0.0	3.5	NCEER
1969	5	30	14	8	5.0	34.80	-97.80	0.0	3.0	NCEER
1969	6	4	9	36	2.0	49.67	-81.45	18.0	3.1	NCEER
1969	7	1	3	36	58.0	37.40	-97.00	0.0	3.0	NCEER
1969	7	13	21	51	9.8	36.12	-83.69	1.0	4.1	NCEER
1969	7	14	3	6	59.0	47.83	-70.09	18.0	3.8	NCEER
1969	7	27	0	0	0.0	36.50	-89.50	0.0	3.1	SRA
1969	8	6	16	2	0.5	43.80	-71.40	0.0	3.5	NCEER
1969	8	31	7	20	27.0	47.49	-70.07	18.0	3.2	NCEER
1969	10	6	0	0	0.0	41.10	-74.60	0.0	3.3	NCEER
1969	10	6	20	24	53.0	48.29	-106.58	18.0	3.1	NCEER
1969	10	10	0	7	4.9	46.31	-75.06	2.0	4.5	NCEER
1969	11	20	1	0	9.3	37.45	-80.93	5.0	4.6	NCEER

© 2007-2012 UniStar Nuclear Services, LLC. All rights reserved.
COPYRIGHT PROTECTED

Table 2.5-1— {Updated Earthquake catalog (1534-April 2010) Including events with $m_b \geq 3.0$}
(Page 45 of 75)

Year	Month	Day	Hour	Min	Sec	Lat (deg)	Lon (deg)	Depth (km)	mb	Source
1969	12	11	23	44	37.4	37.84	-77.67	1.0	3.6	NCEER
1969	12	13	10	19	29.7	35.04	-82.85	6.0	3.7	NCEER
1970	1	7	17	45	0.0	35.20	-89.90	0.0	3.1	NCEER
1970	1	12	11	21	15.0	35.90	-103.42	0.0	3.8	SNM
1970	2	3	0	0	0.0	31.00	-97.00	0.0	3.1	NCEER
1970	2	3	5	59	35.6	37.92	-108.31	33.0	4.0	SRA
1970	2	6	4	53	2.0	37.90	-90.60	0.0	3.4	NCEER
1970	2	27	8	8	36.0	48.24	-77.78	18.0	3.1	NCEER
1970	3	27	3	44	29.2	36.60	-89.54	5.0	3.3	NCEER
1970	4	25	0	46	27.0	49.70	-81.22	18.0	3.1	NCEER
1970	5	27	17	59	41.4	39.62	-78.28	0.0	3.2	SRA
1970	7	30	15	15	16.9	36.99	-82.21	12.0	3.7	SRA
1970	7	31	0	31	0.0	37.70	-83.40	0.0	3.5	SRA
1970	8	8	0	10	30.0	45.80	-66.12	18.0	3.3	NCEER
1970	8	11	6	14	25.5	38.23	-82.05	10.0	3.2	NCEER
1970	9	7	21	39	27.0	47.92	-70.30	18.0	3.2	NCEER
1970	9	10	1	41	5.2	36.02	-81.42	1.0	3.1	NCEER
1970	10	9	16	35	1.0	48.72	-71.03	18.0	3.0	NCEER
1970	10	15	18	56	11.0	47.07	-76.25	18.0	3.3	NCEER
1970	11	5	10	25	35.0	36.00	-90.00	0.0	3.0	NCEER
1970	11	17	2	13	54.1	35.86	-89.95	16.0	4.4	NCEER
1970	11	30	4	46	53.0	36.30	-89.50	0.0	3.0	NCEER
1970	12	8	23	16	0.0	36.00	-89.00	0.0	3.0	NCEER
1970	12	8	23	16	0.0	38.00	-89.00	0.0	3.0	SRA
1970	12	12	15	57	19.1	43.96	-107.55	15.0	4.9	SRA
1970	12	24	10	17	56.8	36.71	-89.55	15.0	3.4	NCEER
1971	1	6	6	22	8.0	47.17	-75.96	18.0	3.0	NCEER
1971	1	7	20	39	52.1	39.49	-107.31	33.0	4.3	SRA
1971	1	19	13	44	25.0	46.92	-75.18	18.0	3.1	NCEER
1971	2	12	12	44	27.5	38.50	-87.85	15.0	3.1	NCEER
1971	2	19	23	11	42.0	37.10	-83.20	0.0	3.0	NCEER
1971	3	14	17	27	54.6	33.18	-87.84	12.0	3.6	NCEER
1971	3	16	2	37	28.0	32.80	-88.30	0.0	3.7	NCEER
1971	3	18	9	8	59.9	40.70	-106.97	10.0	4.4	SRA
1971	4	1	5	5	11.0	37.40	-81.60	0.0	3.0	NCEER
1971	4	13	14	0	51.0	35.80	-90.10	0.0	3.0	NCEER
1971	5	14	6	20	9.0	45.10	-73.37	18.0	3.2	NCEER
1971	5	19	12	54	3.6	33.36	-80.66	1.0	3.7	NCEER
1971	5	21	4	48	24.0	40.72	-63.98	18.0	3.5	NCEER
1971	5	23	6	24	27.9	43.90	-74.48	2.0	4.1	NCEER
1971	7	6	17	47	49.0	46.55	-76.28	18.0	3.0	NCEER
1971	7	9	5	5	26.0	46.74	-81.20	18.0	3.1	NCEER
1971	7	10	17	22	36.8	40.24	-109.60	7.0	3.8	SRA
1971	7	13	2	3	0.0	36.00	-84.00	0.0	3.4	SRA
1971	7	13	3	3	0.0	36.00	-84.30	0.0	3.4	NCEER
1971	7	13	11	42	26.0	34.80	-83.00	0.0	3.6	NCEER

© 2007-2012 UniStar Nuclear Services, LLC. All rights reserved.
COPYRIGHT PROTECTED

Table 2.5-1— {Updated Earthquake catalog (1534-April 2010) Including events with $m_b \geq 3.0$}
(Page 46 of 75)

Year	Month	Day	Hour	Min	Sec	Lat (deg)	Lon (deg)	Depth (km)	mb	Source
1971	7	14	0	0	0.0	39.70	-75.60	0.0	3.3	NCEER
1971	7	30	1	45	51.4	31.64	-103.17	5.0	3.6	NCEER
1971	7	31	20	16	55.0	33.34	-80.63	4.0	3.8	NCEER
1971	9	12	0	6	27.6	38.15	-77.59	5.0	3.6	NCEER
1971	9	12	8	31	43.0	47.56	-70.24	18.0	3.2	NCEER
1971	9	24	1	1	54.0	31.60	-103.20	0.0	3.0	SRA
1971	9	27	8	47	23.0	45.71	-75.17	18.0	3.2	NCEER
1971	10	1	18	49	38.5	35.77	-90.49	9.0	4.1	NCEER
1971	10	9	16	43	32.7	35.80	-83.37	8.0	3.7	NCEER
1971	10	13	2	38	59.0	51.65	-80.90	18.0	3.4	NCEER
1971	10	18	6	39	31.0	36.70	-89.60	0.0	3.0	NCEER
1971	10	19	21	7	37.4	43.69	-101.26	17.0	3.7	NCEER
1971	10	21	0	54	0.0	42.70	-71.20	0.0	3.4	NCEER
1971	10	22	21	55	0.0	36.00	-83.00	0.0	3.3	SRA
1971	10	27	7	13	24.0	49.23	-67.13	18.0	3.0	NCEER
1971	11	3	5	53	49.0	50.17	-66.42	18.0	3.2	NCEER
1971	11	12	9	30	44.6	38.91	-108.68	5.0	4.0	SRA
1971	11	15	10	38	55.0	45.06	-73.87	18.0	3.0	NCEER
1971	11	22	5	29	7.0	47.24	-76.28	18.0	3.0	NCEER
1971	11	23	16	32	30.0	45.83	-76.62	18.0	3.0	NCEER
1971	12	3	7	44	59.2	42.49	-110.34	7.0	4.2	SRA
1971	12	18	15	36	24.5	46.01	-74.67	13.0	4.0	NCEER
1971	12	29	0	0	0.0	39.70	-75.60	0.0	3.3	NCEER
1972	1	9	23	24	29.0	37.40	-81.60	0.0	3.7	NCEER
1972	2	1	5	42	9.5	36.37	-90.85	3.0	3.7	NCEER
1972	2	3	23	11	9.7	33.31	-80.58	2.0	4.5	NCEER
1972	2	11	0	16	0.3	39.70	-75.60	0.0	3.3	NCEER
1972	2	18	11	43	38.1	44.29	-105.12	0.0	4.3	NCEER
1972	3	29	20	38	31.7	36.12	-89.74	7.0	3.7	NCEER
1972	4	25	3	24	25.0	46.67	-75.99	18.0	3.3	NCEER
1972	5	7	2	12	8.7	35.93	-89.97	1.0	3.4	NCEER
1972	5	20	19	39	6.0	37.00	-82.20	0.0	3.9	NCEER
1972	6	9	19	15	18.9	37.62	-90.37	12.0	3.1	NCEER
1972	6	19	16	15	18.8	37.00	-89.08	13.0	4.5	NCEER
1972	7	17	1	58	46.0	47.90	-77.86	18.0	3.0	NCEER
1972	7	26	3	58	19.0	49.35	-104.93	5.0	4.3	NCEER
1972	7	26	4	35	40.0	32.65	-104.03	0.0	3.1	SNM
1972	8	14	1	9	0.0	39.70	-75.60	0.0	3.3	NCEER
1972	8	14	15	5	19.0	33.20	-81.40	0.0	3.0	NCEER
1972	8	22	19	17	48.0	49.54	-66.47	18.0	3.9	NCEER
1972	9	5	16	0	0.0	37.60	-77.70	0.0	3.4	NCEER
1972	9	12	9	15	38.0	46.18	-77.56	18.0	3.2	NCEER
1972	9	15	5	22	15.9	41.64	-89.37	10.0	4.4	NCEER
1972	10	16	5	47	33.0	42.30	-99.60	0.0	3.7	NCEER
1972	10	19	2	22	0.1	45.80	-64.70	0.0	3.0	NCEER
1972	11	2	5	15	8.8	44.76	-74.56	0.0	3.0	SRA

© 2007-2012 UniStar Nuclear Services, LLC. All rights reserved.
COPYRIGHT PROTECTED

Table 2.5-1— {Updated Earthquake catalog (1534-April 2010) Including events with $m_b \geq 3.0$}
(Page 47 of 75)

Year	Month	Day	Hour	Min	Sec	Lat (deg)	Lon (deg)	Depth (km)	mb	Source
1972	11	21	6	8	46.0	49.12	-112.74	18.0	3.3	DNA
1972	12	8	3	0	33.3	40.14	-76.24	2.0	3.5	NCEER
1972	12	8	18	47	39.4	43.65	-108.39	20.0	4.1	SRA
1972	12	16	19	1	37.2	45.64	-75.10	10.0	3.9	NCEER
1973	1	7	22	56	6.2	37.40	-87.22	14.0	3.2	NCEER
1973	1	8	9	11	37.0	33.80	-90.60	0.0	3.5	NCEER
1973	1	12	11	56	56.2	37.89	-90.48	17.0	3.2	NCEER
1973	1	28	13	7	50.0	47.98	-70.00	10.0	3.1	NCEER
1973	2	9	17	38	37.0	36.43	-110.43	5.0	3.2	SRA
1973	2	26	13	42	0.0	44.50	-70.00	0.0	3.0	SRA
1973	2	28	8	21	33.2	39.69	-75.43	12.0	3.8	NCEER
1973	4	9	23	11	0.0	37.30	-77.70	0.0	3.4	NCEER
1973	4	22	6	7	12.4	42.64	-107.85	33.0	4.8	SRA
1973	5	25	14	40	14.0	33.90	-90.80	0.0	3.4	NCEER
1973	6	14	15	9	55.0	49.48	-66.50	18.0	3.1	NCEER
1973	6	15	1	9	5.1	45.31	-71.12	12.0	4.8	NCEER
1973	7	10	4	38	0.2	39.70	-75.70	0.0	3.3	NCEER
1973	7	15	8	20	30.7	43.87	-74.47	2.0	3.5	NCEER
1973	7	20	17	6	39.0	49.56	-66.96	18.0	3.1	NCEER
1973	9	23	3	58	54.9	37.15	-104.57	5.0	4.2	NCEER
1973	10	3	3	50	19.8	35.87	-90.05	6.0	3.4	NCEER
1973	10	9	20	15	26.5	36.49	-89.62	3.0	3.8	NCEER
1973	10	13	1	39	14.0	49.57	-61.36	18.0	3.1	NCEER
1973	10	23	12	37	10.0	51.26	-62.39	18.0	3.2	NCEER
1973	10	27	6	21	2.0	28.48	-80.65	5.0	3.5	NCEER
1973	10	30	22	58	39.0	35.76	-84.12	1.0	3.5	NCEER
1973	11	15	17	31	35.0	49.60	-69.01	18.0	3.1	NCEER
1973	11	16	1	36	34.0	47.55	-70.29	10.0	3.1	NCEER
1973	11	18	10	3	53.0	35.00	-94.70	0.0	3.1	NCEER
1973	11	30	7	48	40.5	35.89	-83.99	12.0	4.6	NCEER
1973	12	19	10	16	8.7	32.97	-80.27	6.0	3.0	NCEER
1973	12	20	10	45	0.9	36.14	-89.69	10.0	3.1	NCEER
1973	12	25	2	46	0.0	29.00	-98.30	0.0	3.1	NCEER
1974	1	8	1	12	38.1	36.18	-89.47	7.0	3.9	NCEER
1974	2	15	13	33	49.2	36.40	-100.69	0.0	4.5	NCEER
1974	2	15	22	49	4.4	34.03	-93.04	10.0	3.8	NCEER
1974	2	17	12	57	28.0	49.54	-67.09	18.0	3.0	NCEER
1974	3	4	14	24	28.1	35.69	-90.41	5.0	3.0	NCEER
1974	3	12	12	30	29.2	35.64	-89.80	5.0	3.2	SRA
1974	3	31	11	58	47.1	40.70	-107.05	5.0	3.5	SRA
1974	4	3	23	5	2.8	38.55	-88.07	15.0	4.7	NCEER
1974	4	20	23	46	10.0	29.00	-98.00	0.0	3.0	SRA
1974	4	27	14	45	39.9	40.97	-75.91	0.0	3.2	SRA
1974	4	28	14	19	0.0	39.80	-75.60	0.0	3.3	NCEER
1974	5	13	6	52	18.7	36.74	-89.36	4.0	3.8	NCEER
1974	5	30	21	28	35.3	37.46	-80.54	5.0	3.6	NCEER

© 2007-2012 UniStar Nuclear Services, LLC. All rights reserved.
COPYRIGHT PROTECTED

Table 2.5-1— {Updated Earthquake catalog (1534-April 2010) Including events with $m_b \geq 3.0$}
(Page 48 of 75)

Year	Month	Day	Hour	Min	Sec	Lat (deg)	Lon (deg)	Depth (km)	mb	Source
1974	6	5	0	16	40.2	38.48	-84.75	10.0	3.2	NCEER
1974	6	5	8	6	10.7	38.65	-89.91	12.0	3.2	NCEER
1974	6	5	8	7	11.0	36.80	-89.90	0.0	3.6	SRA
1974	6	24	18	3	10.0	29.00	-98.00	0.0	3.4	SRA
1974	7	2	4	46	51.0	49.58	-67.22	10.0	3.4	NCEER
1974	8	1	13	33	10.0	29.00	-98.00	0.0	3.0	SRA
1974	8	2	8	52	11.1	33.91	-82.53	4.0	4.1	NCEER
1974	8	8	11	55	33.0	45.93	-76.08	18.0	3.2	NCEER
1974	8	11	14	29	45.4	36.93	-91.16	6.0	3.2	NCEER
1974	9	19	15	36	11.4	44.11	-107.38	10.0	4.4	SRA
1974	9	29	2	26	19.1	41.21	-83.49	1.0	3.0	NCEER
1974	10	8	23	22	28.0	33.90	-82.40	0.0	3.1	NCEER
1974	10	20	15	13	55.6	39.06	-81.61	4.0	3.8	NCEER
1974	10	23	22	52	57.0	46.08	-75.48	10.0	3.2	NCEER
1974	10	28	11	33	0.0	33.79	-81.92	0.0	3.0	NCEER
1974	11	2	13	47	56.0	46.07	-75.03	10.0	3.2	NCEER
1974	11	5	3	0	0.0	33.73	-82.22	0.0	3.7	NCEER
1974	11	22	5	25	56.7	32.92	-80.16	6.0	4.3	NCEER
1974	11	27	10	28	51.7	43.33	-79.11	0.0	3.3	SRA
1974	11	28	3	35	20.0	32.63	-104.02	0.0	4.0	SNM
1974	12	2	10	58	5.0	46.25	-75.50	10.0	3.5	NCEER
1974	12	3	8	25	0.0	33.95	-82.50	0.0	3.6	NCEER
1974	12	10	6	1	35.0	31.23	-87.46	18.0	3.2	NCEER
1974	12	13	5	3	55.5	34.49	-91.86	3.0	3.1	NCEER
1974	12	22	20	46	48.7	42.37	-69.80	0.0	3.0	SRA
1974	12	25	13	21	35.0	35.78	-90.01	10.0	3.0	PDE
1974	12	27	0	50	12.0	49.14	-67.44	18.0	3.5	NCEER
1974	12	30	8	5	27.1	30.92	-103.11	5.0	3.7	NCEER
1975	1	2	9	19	0.0	34.90	-90.90	0.0	3.0	NCEER
1975	1	15	19	16	0.0	44.90	-74.60	0.0	3.1	NCEER
1975	1	30	14	48	40.3	39.27	-108.65	5.0	4.4	SRA
1975	2	2	20	39	23.0	35.07	-103.10	0.0	3.0	SNM
1975	2	3	10	31	0.0	41.30	-83.20	0.0	3.3	NCEER
1975	2	13	19	43	58.0	36.55	-89.59	3.0	3.4	NCEER
1975	2	16	23	21	34.4	38.88	-82.35	4.0	3.0	NCEER
1975	3	1	11	50	0.2	33.55	-87.98	18.0	3.5	NCEER
1975	3	7	12	45	13.5	37.32	-80.48	5.0	3.0	NCEER
1975	3	25	14	59	58.0	42.67	-108.10	10.0	4.8	SRA
1975	4	3	19	3	17.0	45.73	-74.24	5.0	3.1	NCEER
1975	4	28	5	46	52.6	33.00	-80.22	10.0	3.0	NCEER
1975	5	13	7	53	40.0	42.07	-98.50	1.0	3.3	NCEER
1975	5	16	5	57	1.0	43.20	-103.70	0.0	3.1	NCEER
1975	5	29	21	19	16.0	47.23	-75.19	18.0	3.2	NCEER
1975	6	7	4	36	21.7	41.91	-108.80	5.0	3.7	SRA
1975	6	9	18	39	22.7	44.87	-73.65	11.0	3.5	NCEER
1975	6	13	22	40	27.5	36.54	-89.68	9.0	3.9	NCEER

© 2007-2012 UniStar Nuclear Services, LLC. All rights reserved.
COPYRIGHT PROTECTED

Table 2.5-1— {Updated Earthquake catalog (1534-April 2010) Including events with $m_b \geq 3.0$}
(Page 49 of 75)

Year	Month	Day	Hour	Min	Sec	Lat (deg)	Lon (deg)	Depth (km)	mb	Source
1975	6	20	7	29	6.6	36.21	-89.44	7.0	3.5	DNA
1975	6	24	11	11	36.6	33.70	-87.84	4.0	3.7	NCEER
1975	6	30	20	15	23.0	43.40	-79.77	10.0	3.0	NCEER
1975	7	9	14	54	21.3	45.50	-96.10	8.0	4.6	NCEER
1975	7	12	12	37	13.8	46.54	-76.31	17.0	4.2	NCEER
1975	7	18	4	21	6.0	49.16	-66.81	18.0	3.1	NCEER
1975	8	21	4	29	37.0	47.44	-70.18	5.0	3.1	NCEER
1975	8	21	21	42	51.1	48.12	-78.12	1.0	3.6	PDE
1975	8	25	7	11	8.0	36.05	-89.84	11.0	3.0	NCEER
1975	8	27	22	28	22.0	46.80	-65.34	18.0	3.0	NCEER
1975	8	29	4	22	52.1	33.66	-86.59	4.0	4.4	NCEER
1975	9	2	6	21	17.0	48.29	-69.74	2.0	3.3	NCEER
1975	9	5	20	47	40.7	48.37	-104.38	0.0	3.8	NCEER
1975	9	9	11	52	44.0	30.70	-89.30	0.0	3.0	NCEER
1975	9	13	1	25	5.6	34.13	-97.22	5.0	3.2	NCEER
1975	10	12	2	58	11.5	35.50	-97.70	5.0	3.2	NCEER
1975	10	15	3	26	17.0	45.11	-65.89	18.0	3.1	NCEER
1975	10	18	4	31	0.0	34.90	-83.00	0.0	3.3	NCEER
1975	10	21	20	50	2.0	49.13	-68.13	18.0	3.1	NCEER
1975	10	23	21	17	48.7	49.83	-68.62	2.0	4.1	NCEER
1975	11	3	20	54	55.3	43.91	-74.65	5.0	4.0	NCEER
1975	11	7	23	39	31.7	33.31	-87.33	4.0	3.5	NCEER
1975	11	11	8	10	37.6	37.22	-80.89	1.0	3.2	NCEER
1975	11	25	15	17	34.8	34.93	-82.90	10.0	3.2	NCEER
1975	11	29	14	29	44.9	34.68	-97.42	14.0	3.5	NCEER
1975	12	4	18	59	59.9	38.24	-94.62	0.0	3.3	SRA
1975	12	19	15	25	0.1	47.01	-78.89	0.0	3.6	NCEER
1975	12	19	23	26	19.5	42.85	-107.65	0.0	3.5	SRA
1976	1	5	6	23	33.9	35.82	-108.21	0.0	4.6	SNM
1976	1	16	19	42	56.9	35.90	-92.16	7.0	3.4	NCEER
1976	1	19	4	3	30.0	31.90	-103.10	0.0	3.3	NCEER
1976	1	19	6	20	39.6	36.87	-83.86	1.0	3.8	NCEER
1976	1	25	4	48	28.5	31.90	-100.09	4.0	3.3	SRA
1976	2	2	21	14	2.3	41.88	-83.73	5.0	3.4	NCEER
1976	2	4	19	53	53.0	34.97	-84.70	14.0	3.6	NCEER
1976	3	11	8	29	32.2	41.56	-71.21	0.0	3.5	NCEER
1976	3	14	23	12	24.6	41.66	-69.97	0.0	3.1	NCEER
1976	3	16	7	39	45.3	35.43	-95.60	5.0	3.1	NCEER
1976	3	25	0	12	16.0	49.39	-104.27	5.0	3.5	NCEER
1976	3	25	0	41	20.8	35.58	-90.48	17.0	4.9	NCEER
1976	3	29	21	23	27.0	49.34	-67.86	18.0	3.3	NCEER
1976	4	8	7	38	53.0	39.30	-86.70	0.0	3.0	NCEER
1976	4	13	15	39	12.9	40.80	-74.03	0.0	3.2	NCEER
1976	4	15	7	3	34.4	37.38	-87.31	4.0	3.3	NCEER
1976	4	19	4	42	46.9	36.04	-99.79	8.0	3.5	NCEER
1976	4	19	23	35	45.5	35.39	-109.10	5.0	3.5	SRA

© 2007-2012 UniStar Nuclear Services, LLC. All rights reserved.
COPYRIGHT PROTECTED

Table 2.5-1— {Updated Earthquake catalog (1534-April 2010) Including events with $m_b \geq 3.0$}
(Page 50 of 75)

Year	Month	Day	Hour	Min	Sec	Lat (deg)	Lon (deg)	Depth (km)	mb	Source
1976	5	1	11	13	40.8	32.27	-103.14	0.0	3.0	SRA
1976	5	5	3	1	4.0	49.56	-73.90	18.0	3.1	NCEER
1976	5	6	18	46	8.1	39.60	-79.90	0.0	3.1	NCEER
1976	5	15	21	6	52.0	49.84	-68.62	3.0	3.3	NCEER
1976	5	22	7	40	46.1	36.03	-89.83	9.0	3.2	NCEER
1976	5	30	1	43	37.3	37.41	-104.02	5.0	3.0	SRA
1976	6	19	5	54	13.4	37.34	-81.60	1.0	3.3	NCEER
1976	6	24	15	27	32.0	35.62	-103.28	0.0	3.0	SNM
1976	7	13	3	51	14.0	45.18	-74.10	9.0	3.1	NCEER
1976	7	30	22	19	0.2	40.75	-110.30	7.0	3.1	SRA
1976	8	5	18	53	9.0	31.57	-103.02	0.0	3.0	SRA
1976	8	7	7	50	11.0	49.77	-74.98	18.0	3.1	NCEER
1976	8	10	13	54	57.5	45.03	-106.57	5.0	3.4	SRA
1976	9	3	4	18	16.2	44.04	-106.15	10.0	4.8	SRA
1976	9	13	18	54	38.0	36.62	-80.77	9.0	4.3	NCEER
1976	9	17	2	47	45.4	32.21	-103.10	0.0	3.0	SRA
1976	9	17	3	56	29.0	31.40	-102.50	0.0	3.1	DNA
1976	9	18	0	40	32.0	49.36	-67.10	18.0	3.4	NCEER
1976	9	25	14	6	55.8	35.58	-90.47	8.0	3.5	NCEER
1976	10	8	13	54	0.0	45.03	-106.57	0.0	3.5	SRA
1976	10	22	17	15	50.5	35.38	-97.06	5.0	3.0	NCEER
1976	10	22	18	50	56.0	48.16	-78.05	18.0	3.0	NCEER
1976	10	23	0	40	59.2	32.00	-88.98	10.0	3.1	NCEER
1976	10	23	20	58	18.0	47.82	-69.78	18.0	4.2	NCEER
1976	11	6	6	9	29.0	47.11	-75.96	18.0	3.0	NCEER
1976	11	7	12	27	15.0	50.82	-101.99	5.0	3.0	NCEER
1976	12	11	7	5	1.1	38.10	-91.04	0.0	4.2	NCEER
1976	12	13	8	35	55.1	37.81	-90.26	9.0	3.5	NCEER
1976	12	27	6	57	15.2	32.06	-82.50	14.0	3.7	NCEER
1977	1	3	22	56	48.5	37.58	-89.71	5.0	3.6	NCEER
1977	1	18	18	29	14.1	33.06	-80.17	1.0	3.0	NCEER
1977	2	6	9	1	19.0	46.88	-66.73	18.0	4.5	DNA
1977	2	14	0	35	4.1	47.54	-70.42	8.0	3.1	NCEER
1977	2	27	20	5	34.6	37.90	-78.63	0.0	3.4	NCEER
1977	3	2	18	7	24.2	44.61	-109.90	1.0	3.1	DNA
1977	3	3	17	50	28.0	41.24	-107.15	5.0	4.2	SRA
1977	3	5	3	0	55.8	35.75	-108.22	0.0	4.2	SNM
1977	3	24	8	55	0.0	44.60	-107.00	0.0	3.7	DNA
1977	4	26	9	3	7.0	31.90	-103.10	0.0	3.3	NCEER
1977	5	4	2	0	24.3	31.96	-88.44	0.0	3.3	NCEER
1977	6	2	23	29	10.6	34.56	-94.17	10.0	3.6	NCEER
1977	6	17	15	39	46.9	40.71	-84.71	1.0	3.2	NCEER
1977	6	20	5	5	54.7	47.77	-70.16	8.0	3.1	NCEER
1977	7	14	7	39	29.8	46.04	-74.38	4.0	3.4	NCEER
1977	7	22	4	1	10.0	31.80	-102.70	0.0	3.0	DNA
1977	7	27	22	3	20.8	35.42	-84.41	5.0	3.5	NCEER

© 2007-2012 UniStar Nuclear Services, LLC. All rights reserved.
COPYRIGHT PROTECTED

Table 2.5-1— {Updated Earthquake catalog (1534-April 2010) Including events with $m_b \geq 3.0$}

Year	Month	Day	Hour	Min	Sec	Lat (deg)	Lon (deg)	Depth (km)	mb	Source
1977	8	4	4	20	7.7	33.37	-80.70	9.0	3.1	NCEER
1977	8	8	23	8	40.0	49.77	-67.05	18.0	3.9	NCEER
1977	8	25	4	20	7.0	33.39	-80.69	0.0	3.1	NCEER
1977	9	24	11	16	48.4	39.31	-107.31	5.0	4.0	SRA
1977	9	28	17	21	44.7	44.39	-73.89	3.0	3.1	SRA
1977	9	30	10	19	20.4	40.47	-110.47	6.0	5.0	USH
1977	10	16	21	29	19.1	46.52	-73.82	1.0	3.0	NCEER
1977	10	24	18	9	12.0	47.00	-67.05	18.0	3.0	NCEER
1977	11	4	11	21	10.2	33.93	-89.17	16.0	3.4	SRA
1977	11	7	20	48	52.7	46.27	-75.15	5.0	3.0	NCEER
1977	11	13	8	39	6.0	50.62	-64.82	18.0	3.1	NCEER
1977	11	25	18	47	24.4	46.69	-75.86	1.0	3.0	NCEER
1977	11	26	4	18	18.1	34.39	-92.91	10.0	3.1	NCEER
1977	12	15	19	16	43.1	32.88	-80.18	9.0	3.0	NCEER
1977	12	20	17	44	23.8	41.79	-70.68	0.0	3.1	NCEER
1977	12	22	14	57	1.3	46.84	-76.91	11.0	3.5	NCEER
1977	12	25	15	35	53.5	43.20	-71.64	0.0	3.2	NCEER
1978	1	4	19	28	10.8	44.07	-70.55	9.0	3.2	NCEER
1978	1	8	11	34	23.4	32.70	-88.21	1.0	3.1	NCEER
1978	1	12	21	10	0.0	28.10	-81.60	0.0	3.8	DNA
1978	1	16	3	50	3.1	42.43	-105.31	5.0	3.0	SRA
1978	1	28	16	40	58.8	38.24	-88.01	5.0	3.0	DNA
1978	2	7	5	3	10.4	42.50	-109.70	30.0	3.3	SRA
1978	2	18	14	48	25.0	46.35	-74.11	7.0	4.1	NCEER
1978	3	2	10	4	53.0	31.55	-102.50	1.0	3.5	NCEER
1978	4	3	12	24	21.5	36.63	-90.00	9.0	3.1	NCEER
1978	4	8	8	21	45.0	47.75	-69.89	22.0	3.0	PDE
1978	4	26	19	30	23.3	39.70	-78.24	15.0	3.1	SRA
1978	5	7	16	6	23.0	42.26	-101.95	38.0	3.6	NCEER
1978	5	26	2	31	0.4	47.72	-69.99	3.0	3.2	NCEER
1978	5	29	16	45	18.0	39.28	-107.32	5.0	3.0	SRA
1978	6	1	7	22	25.0	49.95	-63.68	18.0	3.0	NCEER
1978	6	2	2	7	28.9	38.41	-88.46	20.0	3.2	NCEER
1978	6	6	21	23	34.7	43.63	-107.83	5.0	4.0	SRA
1978	6	9	23	15	19.6	32.04	-88.60	2.0	3.3	SRA
1978	6	29	20	58	45.1	31.05	-101.94	0.0	3.4	DNA
1978	6	30	0	17	0.0	48.75	-68.39	18.0	3.2	NCEER
1978	7	8	17	14	0.0	38.50	-70.40	0.0	3.1	NCEER
1978	7	16	6	39	29.7	39.90	-76.22	0.0	3.1	NCEER
1978	7	21	5	2	36.2	34.68	-105.04	0.0	3.1	SNM
1978	7	24	8	6	16.9	26.38	-88.72	15.0	4.9	NCEER
1978	7	29	13	56	43.0	49.30	-65.61	18.0	3.4	NCEER
1978	7	30	10	54	44.0	45.68	-74.44	7.0	3.6	NCEER
1978	8	10	21	12	5.1	40.27	-70.99	5.0	3.5	NCEER
1978	8	21	8	47	0.0	44.52	-74.51	0.0	3.1	NCEER
1978	8	26	3	54	34.1	47.17	-76.43	5.0	3.0	NCEER

© 2007-2012 UniStar Nuclear Services, LLC. All rights reserved.
COPYRIGHT PROTECTED

Table 2.5-1— {Updated Earthquake catalog (1534-April 2010) Including events with $m_b \geq 3.0$}
(Page 52 of 75)

Year	Month	Day	Hour	Min	Sec	Lat (deg)	Lon (deg)	Depth (km)	mb	Source
1978	8	30	16	33	21.2	48.49	-111.48	5.0	3.5	SRA
1978	8	31	0	31	0.6	36.09	-89.44	1.0	3.5	NCEER
1978	9	20	12	24	8.9	38.58	-90.28	1.0	3.0	NCEER
1978	9	23	7	34	3.7	33.96	-91.92	33.0	3.1	NCEER
1978	10	6	19	25	47.4	40.08	-76.15	0.0	3.0	NCEER
1978	11	4	1	23	52.0	50.72	-101.80	10.0	3.1	NCEER
1978	11	6	23	0	0.0	30.20	-82.65	0.0	3.8	DNA
1978	12	2	8	36	44.0	48.96	-67.62	18.0	3.3	NCEER
1978	12	5	1	48	2.0	38.56	-88.37	23.0	3.5	NCEER
1978	12	11	2	6	50.1	31.91	-88.47	3.0	3.5	NCEER
1979	1	20	6	59	8.4	40.82	-107.86	5.0	3.3	SRA
1979	1	30	16	30	52.0	40.32	-74.26	0.0	3.0	NCEER
1979	2	5	5	31	9.4	35.84	-90.10	10.0	3.2	NCEER
1979	2	24	15	49	15.5	49.23	-113.30	5.0	3.3	PDE
1979	2	27	22	54	54.8	35.96	-91.20	10.0	3.4	NCEER
1979	3	10	4	49	39.6	40.72	-74.50	0.0	3.2	NCEER
1979	3	18	8	28	23.0	49.99	-63.98	18.0	3.2	NCEER
1979	3	18	16	31	12.0	45.84	-76.46	18.0	3.0	NCEER
1979	3	19	14	59	29.7	40.18	-108.90	2.0	3.1	SRA
1979	3	23	22	53	5.0	47.69	-70.10	10.0	3.2	NCEER
1979	4	14	9	39	6.4	48.59	-112.41	5.0	3.2	SRA
1979	4	16	6	40	16.7	46.70	-95.54	20.0	3.1	SRA
1979	4	18	2	34	15.3	43.97	-69.79	17.0	4.0	NCEER
1979	4	20	10	32	49.2	45.24	-66.03	18.0	3.2	NCEER
1979	4	23	0	5	45.7	43.04	-71.24	0.0	3.1	NCEER
1979	4	30	2	7	10.3	37.88	-111.02	7.0	3.8	SRA
1979	5	26	21	58	32.8	46.18	-75.68	1.0	3.3	NCEER
1979	5	29	20	48	49.1	45.00	-74.99	2.0	3.0	NCEER
1979	6	5	8	58	20.0	49.37	-67.54	18.0	3.3	NCEER
1979	6	7	7	39	36.3	35.22	-99.76	2.0	3.0	NCEER
1979	6	7	13	45	53.3	44.43	-73.86	0.0	3.1	NCEER
1979	6	11	4	12	17.1	36.15	-89.64	15.0	3.8	NCEER
1979	6	16	1	8	44.7	37.86	-110.90	7.0	3.0	DNA
1979	6	20	19	20	17.8	41.35	-74.38	0.0	3.0	SRA
1979	6	25	17	11	13.8	35.56	-90.45	7.0	3.0	NCEER
1979	6	30	20	46	42.3	39.92	-97.29	7.0	3.0	NCEER
1979	7	8	1	29	18.0	46.87	-76.60	18.0	3.8	NCEER
1979	7	8	12	35	15.5	36.91	-89.31	2.0	3.1	NCEER
1979	7	9	8	16	26.0	46.54	-74.65	18.0	3.7	NCEER
1979	7	16	0	3	48.4	40.18	-100.32	4.0	3.2	NCEER
1979	7	25	23	56	11.7	37.59	-110.59	7.0	3.1	DNA
1979	7	28	23	29	12.0	43.29	-70.44	11.0	3.5	NCEER
1979	8	7	19	32	17.2	34.33	-81.36	3.0	3.0	SRA
1979	8	9	17	12	55.4	48.49	-111.47	5.0	3.8	SRA
1979	8	13	5	18	56.8	35.21	-84.36	10.0	3.7	NCEER
1979	8	13	5	19	25.2	33.90	-82.54	23.0	4.1	SRA

© 2007-2012 UniStar Nuclear Services, LLC. All rights reserved.
COPYRIGHT PROTECTED

Table 2.5-1— {Updated Earthquake catalog (1534-April 2010) Including events with $m_b \geq 3.0$}

(Page 53 of 75)

Year	Month	Day	Hour	Min	Sec	Lat (deg)	Lon (deg)	Depth (km)	mb	Source
1979	8	19	22	49	30.4	47.67	-69.90	10.0	4.6	NCEER
1979	8	26	1	31	45.0	34.92	-82.96	1.0	3.7	USH
1979	8	26	11	28	0.0	36.30	-91.50	0.0	3.8	DNA
1979	9	6	20	38	16.3	35.30	-83.24	10.0	3.2	NCEER
1979	9	12	6	24	4.0	35.58	-83.91	12.0	3.2	NCEER
1979	9	13	0	49	21.5	35.19	-99.47	1.0	3.4	NCEER
1979	10	8	8	53	52.8	36.44	-82.08	5.0	3.6	SRA
1979	10	23	4	17	19.9	37.89	-110.93	7.0	3.5	SRA
1979	11	5	16	35	25.9	36.46	-91.04	6.0	3.2	NCEER
1979	11	9	21	29	59.8	38.49	-82.81	1.0	3.6	NCEER
1979	11	27	9	10	36.7	35.63	-98.41	5.0	3.3	NCEER
1979	12	19	18	58	10.0	49.43	-66.72	18.0	3.8	NCEER
1980	1	10	19	16	23.5	24.13	-85.71	15.0	3.9	NCEER
1980	2	1	5	22	23.0	40.40	-66.10	0.0	3.4	NCEER
1980	2	27	6	13	41.0	49.62	-91.22	18.0	3.5	NCEER
1980	2	29	5	53	56.1	42.58	-74.20	12.0	3.1	SRA
1980	3	11	4	15	55.0	46.79	-71.87	18.0	3.7	NCEER
1980	3	11	6	0	26.9	40.15	-75.09	0.0	3.3	NCEER
1980	3	11	10	7	0.0	38.60	-64.30	0.0	3.4	NCEER
1980	3	13	2	23	13.0	37.89	-88.44	20.0	3.0	NCEER
1980	3	23	21	38	16.2	37.60	-86.76	9.0	3.3	NCEER
1980	4	3	16	57	24.0	48.77	-67.95	18.0	4.0	NCEER
1980	4	10	15	36	43.8	44.71	-68.36	0.0	3.2	NCEER
1980	4	13	22	40	23.0	49.64	-81.64	18.0	4.1	NCEER
1980	4	14	3	27	33.8	48.79	-112.34	5.0	3.6	SRA
1980	4	24	6	16	57.2	34.33	-81.32	3.0	3.0	SRA
1980	5	2	19	2	0.0	40.30	-75.00	0.0	3.0	NCEER
1980	5	19	23	40	50.0	45.26	-75.25	19.0	3.0	DNA
1980	5	23	8	39	44.0	44.89	-74.55	0.0	3.4	NCEER
1980	6	6	13	15	51.9	43.56	-75.23	1.0	3.5	NCEER
1980	6	9	22	37	12.3	35.48	-101.01	1.0	3.4	NCEER
1980	6	10	23	47	32.2	35.46	-82.81	1.0	3.0	NCEER
1980	6	25	18	2	1.6	35.73	-84.03	1.0	3.3	NCEER
1980	7	1	3	6	38.0	47.56	-70.75	10.0	3.4	NCEER
1980	7	2	7	50	33.0	47.30	-70.33	10.0	3.1	NCEER
1980	7	5	8	54	40.1	36.56	-89.60	4.0	3.5	NCEER
1980	7	18	14	29	46.8	35.18	-99.70	5.0	3.2	NCEER
1980	7	25	6	22	34.0	45.14	-74.17	5.0	3.1	NCEER
1980	7	25	15	30	12.5	33.94	-87.44	0.0	3.1	SRA
1980	7	27	18	52	21.4	38.19	-83.89	16.0	5.2	NCEER
1980	7	29	1	10	22.7	34.35	-81.36	1.0	3.2	SRA
1980	7	31	10	10	4.0	49.90	-82.04	18.0	3.0	NCEER
1980	8	2	17	20	59.7	40.43	-74.15	8.0	3.1	SRA
1980	8	11	14	54	46.1	43.54	-75.16	0.0	3.3	NCEER
1980	8	20	9	34	53.4	41.99	-82.99	1.0	3.2	NCEER
1980	8	23	3	49	3.7	37.98	-84.87	1.0	3.1	NCEER

© 2007-2012 UniStar Nuclear Services, LLC. All rights reserved.
COPYRIGHT PROTECTED

Table 2.5-1— {Updated Earthquake catalog (1534-April 2010) Including events with $m_b \geq 3.0$}
(Page 54 of 75)

Year	Month	Day	Hour	Min	Sec	Lat (deg)	Lon (deg)	Depth (km)	mb	Source
1980	8	25	13	14	23.4	41.40	-67.78	0.0	3.0	DNA
1980	8	30	9	19	0.0	39.80	-74.90	0.0	3.0	NCEER
1980	9	4	4	30	55.8	41.11	-73.78	13.0	3.2	SRA
1980	9	8	5	59	55.2	44.67	-69.00	8.0	3.2	NCEER
1980	9	12	22	33	55.4	41.18	-105.12	0.0	3.2	SRA
1980	9	21	4	7	31.0	45.69	-74.34	4.0	3.2	DNA
1980	9	21	20	52	45.1	43.63	-74.02	0.0	3.2	DNA
1980	9	30	18	26	1.0	47.67	-69.90	6.0	3.0	NCEER
1980	10	14	0	58	56.4	43.15	-80.57	5.0	3.4	NCEER
1980	10	24	17	27	38.2	41.30	-72.90	0.0	3.1	NCEER
1980	11	2	10	0	48.9	35.46	-97.76	1.0	3.0	NCEER
1980	11	5	21	48	14.7	38.18	-79.90	4.0	3.0	NCEER
1980	12	2	8	59	29.7	36.17	-89.43	5.0	3.8	NCEER
1981	1	10	8	34	31.0	51.89	-103.45	5.0	3.1	NCEER
1981	1	23	2	57	50.0	50.07	-69.46	5.0	3.0	NCEER
1981	2	11	13	44	16.4	37.72	-78.44	6.0	3.4	NCEER
1981	2	13	2	15	0.0	30.00	-91.80	0.0	3.8	DNA
1981	2	18	6	33	32.0	28.23	-91.36	10.0	3.0	NCEER
1981	2	19	7	7	10.0	45.96	-74.93	18.0	3.3	NCEER
1981	4	2	16	10	6.4	39.91	-104.96	8.0	4.3	NCEER
1981	4	8	1	53	13.0	38.87	-89.38	1.0	3.5	SRA
1981	4	9	7	10	31.2	35.51	-82.05	0.0	3.3	NCEER
1981	4	13	3	28	21.0	50.66	-101.85	5.0	3.2	NCEER
1981	4	13	17	31	38.0	45.93	-65.70	18.0	3.7	NCEER
1981	5	5	21	21	56.7	35.33	-82.42	10.0	3.5	NCEER
1981	5	25	22	50	18.2	36.76	-91.63	1.0	3.0	SRA
1981	5	29	3	9	2.2	36.83	-110.37	1.0	3.0	SRA
1981	6	3	20	54	22.4	36.18	-81.67	1.0	3.0	SRA
1981	6	9	1	46	32.7	31.99	-94.32	5.0	3.2	NCEER
1981	6	9	14	15	47.8	37.82	-89.03	19.0	3.4	NCEER
1981	6	12	15	30	0.0	43.90	-89.90	0.0	3.8	DNA
1981	6	16	17	55	4.0	47.47	-70.00	8.0	3.7	NCEER
1981	6	26	8	33	27.0	35.85	-90.07	9.0	3.5	NCEER
1981	6	28	22	42	35.0	43.57	-71.55	0.0	3.1	NCEER
1981	7	4	23	16	32.0	45.14	-74.62	13.0	3.7	NCEER
1981	7	11	21	9	21.8	34.85	-97.73	5.0	3.5	NCEER
1981	7	13	4	48	4.0	49.82	-66.80	18.0	3.7	NCEER
1981	7	14	19	29	51.0	36.82	-110.31	0.0	3.0	SRA
1981	8	7	11	53	44.0	36.03	-89.18	11.0	4.0	NCEER
1981	8	10	23	6	59.3	44.07	-73.54	1.0	3.0	DNA
1981	8	23	23	17	20.0	48.66	-72.24	5.0	3.3	NCEER
1981	8	28	10	51	33.0	43.15	-80.59	1.0	3.3	NCEER
1981	9	4	17	21	44.5	34.63	-85.17	3.0	3.0	NCEER
1981	9	5	5	49	21.0	42.80	-81.41	9.0	3.1	NCEER
1981	9	7	0	38	9.1	42.89	-100.52	5.0	3.1	SRA
1981	9	10	7	55	9.0	37.50	-110.56	2.0	3.1	SRA

© 2007-2012 UniStar Nuclear Services, LLC. All rights reserved.
COPYRIGHT PROTECTED

Table 2.5-1— {Updated Earthquake catalog (1534-April 2010) Including events with $m_b \geq 3.0$}
(Page 55 of 75)

Year	Month	Day	Hour	Min	Sec	Lat (deg)	Lon (deg)	Depth (km)	mb	Source
1981	9	13	22	16	29.7	43.04	-101.85	5.0	3.4	NCEER
1981	9	18	2	24	11.0	49.53	-66.11	18.0	3.1	NCEER
1981	9	18	7	16	7.0	46.11	-75.02	0.0	3.5	NCEER
1981	9	30	23	41	39.0	46.37	-75.56	0.0	3.5	NCEER
1981	10	9	21	54	27.8	41.17	-98.54	5.0	3.3	NCEER
1981	10	20	3	47	36.0	49.29	-112.92	18.0	3.0	DNA
1981	10	21	16	49	6.9	41.14	-72.57	5.0	3.7	NCEER
1981	10	28	19	56	14.0	49.83	-65.25	18.0	3.9	NCEER
1981	11	6	12	36	40.5	32.02	-95.26	5.0	3.2	NCEER
1981	11	8	17	11	19.0	36.09	-89.39	12.0	3.0	NCEER
1981	11	12	18	40	14.0	46.98	-77.04	18.0	3.4	NCEER
1981	11	28	5	12	3.0	47.03	-66.61	5.0	3.7	NCEER
1981	12	6	16	11	27.0	45.38	-72.64	3.0	3.3	NCEER
1982	1	2	2	0	26.2	35.18	-86.43	13.0	3.1	NCEER
1982	1	4	16	56	8.1	31.18	-102.49	5.0	3.9	NCEER
1982	1	9	12	53	52.0	47.00	-66.60	5.0	5.7	NCEER
1982	1	19	0	14	42.6	43.51	-71.62	7.0	4.7	NCEER
1982	1	24	3	22	44.4	35.22	-92.22	0.0	4.3	NCEER
1982	1	27	1	35	56.0	47.45	-70.38	6.0	3.3	NCEER
1982	1	27	18	50	4.6	41.87	-70.94	0.0	3.0	NCEER
1982	1	28	4	52	51.9	32.98	-81.39	7.0	3.4	SRA
1982	1	30	15	44	35.0	49.18	-67.48	18.0	3.0	DNA
1982	2	2	9	26	46.3	35.92	-90.06	10.0	3.1	NCEER
1982	3	9	13	10	50.1	48.51	-104.03	18.0	3.3	NCEER
1982	3	13	4	34	32.0	46.65	-82.48	1.0	3.0	NCEER
1982	3	16	11	3	2.7	35.36	-103.27	5.0	3.1	NCEER
1982	3	19	16	48	13.0	46.30	-79.88	18.0	3.0	NCEER
1982	3	21	21	43	21.0	49.07	-113.25	18.0	3.4	DNA
1982	3	28	23	24	32.9	29.85	-98.46	5.0	3.0	NCEER
1982	4	13	13	4	13.3	36.51	-82.04	3.0	3.0	NCEER
1982	4	17	6	0	12.5	38.22	-111.30	9.0	3.0	SRA
1982	4	21	21	17	55.0	35.18	-92.24	0.0	3.5	NCEER
1982	5	3	7	54	48.6	33.99	-96.47	5.0	3.1	NCEER
1982	5	9	21	7	36.5	44.64	-109.70	11.0	3.4	SRA
1982	5	12	18	29	33.0	40.41	-77.96	0.0	3.0	SRA
1982	5	31	18	21	19.7	35.20	-92.23	2.0	3.5	NCEER
1982	6	23	0	22	0.0	47.38	-76.95	18.0	3.5	NCEER
1982	7	5	4	13	52.0	35.22	-92.21	6.0	3.5	NCEER
1982	7	11	19	42	28.4	44.01	-96.72	5.0	3.6	NCEER
1982	7	13	2	18	49.0	46.09	-74.55	17.0	3.8	NCEER
1982	7	15	7	27	55.4	46.08	-69.02	6.0	3.0	SRA
1982	7	16	14	16	2.9	34.32	-81.55	2.0	3.1	SRA
1982	8	6	6	29	10.0	45.89	-75.46	19.0	3.7	NCEER
1982	8	9	11	12	31.6	35.19	-92.24	4.0	3.2	SRA
1982	8	11	10	32	38.8	37.25	-88.73	5.0	3.1	NCEER
1982	8	13	1	6	42.0	46.67	-78.61	18.0	3.7	NCEER

© 2007-2012 UniStar Nuclear Services, LLC. All rights reserved.
COPYRIGHT PROTECTED

Table 2.5-1— {Updated Earthquake catalog (1534-April 2010) Including events with $m_b \geq 3.0$}
(Page 56 of 75)

Year	Month	Day	Hour	Min	Sec	Lat (deg)	Lon (deg)	Depth (km)	mb	Source
1982	8	17	4	49	25.0	49.06	-105.38	18.0	4.3	NCEER
1982	8	29	2	7	11.0	47.37	-70.38	20.0	3.4	NCEER
1982	8	31	10	16	28.4	43.20	-74.19	5.0	3.0	NCEER
1982	8	31	22	2	18.5	42.72	-108.85	5.0	3.2	SRA
1982	9	2	21	52	45.5	34.96	-82.90	3.0	3.0	SRA
1982	9	3	23	14	3.0	45.67	-76.61	12.0	3.7	NCEER
1982	9	5	10	11	9.4	35.19	-84.51	13.0	3.2	NCEER
1982	9	24	22	19	16.9	35.68	-84.25	8.0	3.4	NCEER
1982	9	25	23	17	5.5	35.21	-92.23	5.0	3.5	SRA
1982	9	28	7	17	49.0	50.73	-101.85	5.0	3.5	NCEER
1982	9	28	22	24	12.5	43.13	-73.06	8.0	3.0	DNA
1982	10	3	4	31	5.0	51.25	-62.81	18.0	3.3	NCEER
1982	10	14	12	52	46.3	36.10	-102.57	5.0	3.9	NCEER
1982	10	29	21	50	57.0	49.82	-65.30	18.0	3.3	NCEER
1982	10	31	3	12	12.2	32.64	-84.89	0.0	3.1	NCEER
1982	11	3	17	54	1.9	35.31	-108.70	0.0	3.3	SNM
1982	11	7	0	4	19.0	35.20	-100.20	0.0	3.1	SRA
1982	11	15	2	58	22.9	43.01	-97.85	5.0	4.3	NCEER
1982	11	21	16	35	31.0	35.25	-92.08	0.0	3.5	NCEER
1982	11	24	7	34	39.0	45.34	-73.43	5.0	3.0	PDE
1982	12	1	22	52	22.9	43.62	-71.52	6.0	3.0	SRA
1982	12	4	16	8	32.0	47.54	-70.22	16.0	3.9	NCEER
1982	12	11	0	25	0.0	32.85	-83.53	0.0	3.0	NCEER
1983	1	10	21	31	27.0	46.82	-78.83	18.0	3.3	NCEER
1983	1	17	19	35	52.0	49.11	-67.06	18.0	4.1	NCEER
1983	1	19	2	30	42.0	35.28	-92.16	0.0	3.9	NCEER
1983	1	20	9	16	45.0	48.72	-83.45	18.0	3.1	NCEER
1983	1	20	14	17	21.0	47.46	-67.86	15.0	3.1	NCEER
1983	1	22	7	46	58.0	41.75	-81.02	10.0	3.3	NCEER
1983	1	26	14	7	44.7	32.85	-83.56	0.0	3.5	NCEER
1983	1	27	22	9	35.1	36.06	-83.63	13.0	3.1	NCEER
1983	1	27	23	37	11.8	37.78	-110.67	7.0	3.3	SRA
1983	2	5	13	8	19.0	34.73	-88.31	0.0	3.2	NCEER
1983	2	11	15	46	56.0	48.98	-68.33	18.0	3.5	NCEER
1983	2	13	13	44	44.0	42.23	-105.73	5.0	4.0	SRA
1983	2	16	6	22	9.3	48.54	-112.37	14.0	3.5	SRA
1983	2	23	8	51	27.0	36.19	-89.60	1.0	3.6	NCEER
1983	2	26	19	59	35.4	41.55	-73.66	7.0	3.0	NCEER
1983	3	4	6	32	18.6	44.21	-99.41	5.0	4.4	NCEER
1983	3	6	23	19	30.0	51.34	-66.83	18.0	3.2	NCEER
1983	3	14	9	11	21.0	50.70	-74.89	18.0	3.7	NCEER
1983	3	24	14	27	20.4	42.96	-71.72	1.0	3.4	NCEER
1983	3	25	2	47	11.1	35.33	-82.46	12.0	3.3	NCEER
1983	3	30	4	15	26.0	35.20	-92.15	0.0	3.2	NCEER
1983	4	3	4	55	24.2	35.32	-102.38	5.0	3.4	NCEER
1983	4	13	16	6	53.0	49.34	-66.98	18.0	3.0	DNA

© 2007-2012 UniStar Nuclear Services, LLC. All rights reserved.
COPYRIGHT PROTECTED

Table 2.5-1— {Updated Earthquake catalog (1534-April 2010) Including events with $m_b \geq 3.0$}
(Page 57 of 75)

Year	Month	Day	Hour	Min	Sec	Lat (deg)	Lon (deg)	Depth (km)	mb	Source
1983	5	3	12	43	37.7	38.31	-110.63	2.0	3.0	SRA
1983	5	6	6	14	46.9	42.96	-102.20	5.0	3.3	SRA
1983	5	13	23	40	57.0	47.00	-66.60	5.0	3.9	NCEER
1983	5	15	5	16	22.0	38.77	-89.57	0.0	4.3	NCEER
1983	5	16	2	1	57.0	47.70	-69.89	11.0	3.8	NCEER
1983	5	16	14	3	4.0	38.48	-92.36	0.0	3.0	NCEER
1983	5	27	23	4	35.2	45.54	-69.46	10.0	3.7	NCEER
1983	5	29	5	45	49.9	44.49	-70.40	3.0	4.4	NCEER
1983	6	2	6	30	23.0	47.45	-70.22	10.0	3.4	NCEER
1983	6	4	5	0	23.0	47.46	-69.65	10.0	3.0	NCEER
1983	6	28	8	5	49.0	47.04	-66.68	5.0	3.5	NCEER
1983	7	8	9	41	40.0	37.10	-90.94	0.0	3.0	NCEER
1983	7	8	19	29	5.9	35.55	-84.15	10.0	3.4	NCEER
1983	7	17	22	47	45.0	46.06	-74.91	18.0	3.0	NCEER
1983	7	23	3	25	38.0	46.53	-70.95	10.0	3.0	NCEER
1983	7	23	15	24	38.2	28.74	-98.13	5.0	3.4	SRA
1983	8	12	14	8	47.6	44.97	-67.68	12.0	3.7	NCEER
1983	8	17	14	3	15.0	38.47	-82.77	10.0	3.5	NCEER
1983	8	17	15	3	27.6	37.47	-104.31	5.0	3.4	SRA
1983	8	28	22	45	7.4	36.68	-83.82	18.0	3.1	NCEER
1983	9	8	19	35	6.0	40.25	-72.06	8.0	3.2	NCEER
1983	9	14	17	37	5.0	50.31	-65.03	18.0	3.4	NCEER
1983	9	15	23	25	37.5	34.92	-104.43	0.0	3.1	SNM
1983	9	24	16	57	45.7	40.79	-108.84	5.0	4.1	SRA
1983	10	4	17	18	40.0	43.44	-79.79	2.0	3.1	NCEER
1983	10	7	10	18	47.0	44.03	-74.31	7.0	5.2	NCEER
1983	10	11	4	10	55.0	45.21	-75.77	15.0	4.2	NCEER
1983	10	16	3	0	47.0	45.62	-75.05	11.0	3.1	NCEER
1983	10	16	19	40	50.8	30.24	-93.39	5.0	3.8	NCEER
1983	10	17	22	58	56.0	47.21	-66.31	5.0	3.2	NCEER
1983	10	24	1	0	6.0	48.14	-77.97	1.0	3.1	NCEER
1983	11	1	10	16	52.0	45.68	-73.90	18.0	3.5	NCEER
1983	11	6	9	2	19.8	32.94	-80.16	10.0	3.3	NCEER
1983	11	15	12	33	12.1	43.02	-105.96	5.0	3.0	SRA
1983	11	17	15	32	18.0	47.00	-66.60	5.0	3.8	NCEER
1983	12	4	10	48	33.6	45.19	-69.16	2.0	3.3	NCEER
1983	12	8	12	23	5.0	45.11	-67.17	7.0	3.0	NCEER
1983	12	9	20	52	10.5	33.18	-92.70	5.0	3.0	SRA
1983	12	14	1	52	3.0	46.69	-76.29	18.0	3.2	NCEER
1983	12	21	15	4	44.0	45.24	-73.97	18.0	3.1	NCEER
1983	12	28	12	24	21.0	47.01	-76.33	18.0	3.4	NCEER
1984	1	12	2	48	15.7	37.59	-89.75	2.0	3.0	SRA
1984	1	14	9	9	32.0	44.88	-67.16	18.0	3.5	NCEER
1984	1	14	20	14	31.0	41.65	-83.43	0.0	3.0	NCEER
1984	1	16	19	50	25.2	47.15	-110.85	5.0	3.3	SRA
1984	1	17	19	4	46.0	45.56	-75.12	19.0	3.1	NCEER

© 2007-2012 UniStar Nuclear Services, LLC. All rights reserved.
COPYRIGHT PROTECTED

Table 2.5-1— {Updated Earthquake catalog (1534-April 2010) Including events with $m_b \geq 3.0$}
(Page 58 of 75)

Year	Month	Day	Hour	Min	Sec	Lat (deg)	Lon (deg)	Depth (km)	mb	Source
1984	1	28	21	29	22.1	36.61	-89.92	1.0	3.2	SRA
1984	2	3	4	38	28.0	34.67	-97.36	5.0	3.2	NCEER
1984	2	11	11	26	41.0	50.23	-92.24	18.0	3.9	PDE
1984	2	14	20	54	30.9	36.13	-83.74	10.0	3.6	NCEER
1984	2	14	22	56	10.0	37.21	-89.00	0.0	3.6	NCEER
1984	2	24	3	17	14.0	47.00	-66.60	5.0	3.7	PDE
1984	3	1	18	13	0.9	41.54	-108.64	2.0	3.2	SRA
1984	3	3	1	3	26.5	28.85	-98.46	5.0	3.8	SRA
1984	3	17	23	26	11.4	35.83	-84.05	7.0	3.0	NCEER
1984	3	27	22	56	24.0	46.91	-66.49	5.0	3.0	DNA
1984	3	29	22	52	50.0	49.61	-66.46	18.0	3.2	DNA
1984	4	3	4	55	24.0	35.32	-102.40	0.0	3.4	SRA
1984	4	11	19	7	42.0	49.30	-67.52	18.0	3.8	DNA
1984	4	13	15	35	51.0	47.00	-66.60	5.0	3.1	DNA
1984	4	17	4	44	44.0	38.38	-88.44	0.0	3.4	NCEER
1984	4	22	17	30	56.7	39.28	-107.19	5.0	3.1	SRA
1984	4	23	1	36	0.0	39.95	-76.37	4.0	4.1	NCEER
1984	5	14	10	14	17.2	39.32	-107.23	5.0	3.2	SRA
1984	5	21	13	30	14.0	35.40	-102.40	0.0	3.4	SRA
1984	5	21	13	31	13.5	35.07	-102.23	5.0	3.1	SRA
1984	5	27	23	30	19.3	39.22	-102.16	5.0	3.6	SRA
1984	5	28	21	4	52.0	49.60	-66.33	18.0	3.2	DNA
1984	6	20	16	10	22.0	46.63	-80.78	1.0	3.5	PDE
1984	6	26	15	15	19.9	36.10	-89.39	12.0	3.2	NCEER
1984	6	28	3	8	49.0	46.23	-75.68	0.0	3.1	DNA
1984	6	29	7	58	29.3	37.70	-88.47	2.0	3.8	NCEER
1984	7	2	5	24	54.0	47.00	-66.60	5.0	3.0	DNA
1984	7	6	17	24	52.0	46.53	-81.17	1.0	4.0	PDE
1984	7	16	3	50	53.5	36.50	-89.53	7.0	3.0	NCEER
1984	7	28	23	39	27.4	39.22	-87.07	10.0	4.0	NCEER
1984	7	30	7	33	46.5	37.82	-90.92	7.0	3.0	NCEER
1984	8	3	13	41	11.0	45.32	-67.05	18.0	3.0	DNA
1984	8	8	1	31	27.3	29.13	-98.36	5.0	3.0	SRA
1984	8	9	2	42	35.8	34.62	-86.30	8.0	3.2	NCEER
1984	8	17	18	5	46.9	37.87	-78.32	8.0	4.2	SRA
1984	8	20	10	58	17.0	44.88	-73.48	11.0	3.2	SRA
1984	8	29	6	50	59.5	39.11	-87.45	10.0	3.1	NCEER
1984	8	30	16	26	28.4	35.57	-84.34	13.0	3.1	NCEER
1984	9	8	0	59	31.1	44.14	-106.11	15.0	5.0	USH
1984	9	11	14	47	33.5	31.99	-100.70	5.0	3.2	SRA
1984	9	14	19	4	26.3	41.61	-108.58	2.0	3.2	SRA
1984	9	23	8	56	31.0	46.00	-64.80	18.0	3.9	PDE
1984	9	27	8	48	10.0	50.61	-101.88	1.0	3.5	DNA
1984	9	27	13	3	6.0	35.25	-92.21	5.0	3.4	NCEER
1984	9	27	13	16	22.9	35.72	-91.70	5.0	3.0	NCEER
1984	10	9	11	54	26.9	34.75	-85.20	12.0	4.2	NCEER

© 2007-2012 UniStar Nuclear Services, LLC. All rights reserved.
COPYRIGHT PROTECTED

Table 2.5-1— {Updated Earthquake catalog (1534-April 2010) Including events with $m_b \geq 3.0$}
(Page 59 of 75)

Year	Month	Day	Hour	Min	Sec	Lat (deg)	Lon (deg)	Depth (km)	mb	Source
1984	10	13	1	45	15.0	47.08	-66.59	5.0	3.0	DNA
1984	10	13	12	53	45.0	44.72	-65.66	18.0	3.3	DNA
1984	10	18	15	30	22.0	42.32	-105.74	22.0	5.5	USH
1984	10	22	18	58	41.7	36.36	-81.68	11.0	3.2	NCEER
1984	10	23	6	26	21.9	43.59	-73.93	0.0	3.5	NCEER
1984	11	2	10	24	21.0	50.68	-101.90	5.0	3.0	DNA
1984	11	3	9	30	8.4	42.53	-108.92	5.0	4.5	USH
1984	11	20	10	57	31.9	34.71	-97.41	5.0	3.1	NCEER
1984	11	26	9	3	49.0	45.19	-75.05	14.0	3.2	PDE
1984	11	30	5	54	22.0	46.98	-66.58	14.0	3.7	PDE
1984	12	3	11	55	44.6	36.16	-89.70	11.0	3.0	NCEER
1984	12	9	18	12	21.0	47.52	-66.04	1.0	3.6	DNA
1984	12	17	9	38	36.0	46.50	-82.60	0.0	3.5	PDE
1984	12	22	12	46	30.0	47.40	-70.25	19.0	3.0	DNA
1985	1	30	9	35	12.4	35.93	-89.91	9.0	3.0	SRA
1985	2	7	23	44	35.3	36.29	-89.51	7.0	3.1	NCEER
1985	2	13	10	22	24.0	38.42	-87.50	3.0	3.0	SRA
1985	2	15	15	56	9.9	37.23	-89.34	6.0	3.3	NCEER
1985	3	3	12	15	17.0	47.39	-70.48	14.0	3.2	PDE
1985	3	16	21	55	2.4	38.56	-105.85	5.0	3.2	SRA
1985	4	10	5	52	57.0	47.52	-69.96	12.0	3.1	DNA
1985	4	12	5	27	30.5	45.36	-70.70	2.0	3.1	SRA
1985	4	14	11	39	54.0	41.59	-80.40	18.0	3.2	DNA
1985	4	14	21	48	2.9	35.26	-108.92	0.0	3.4	SNM
1985	5	4	7	7	12.5	36.27	-90.77	9.0	3.1	SRA
1985	5	15	10	39	3.0	50.70	-101.81	1.0	3.0	DNA
1985	5	16	13	39	7.0	46.83	-75.90	18.0	3.2	DNA
1985	6	10	12	22	38.3	37.25	-80.49	11.0	3.2	SRA
1985	6	19	22	28	8.9	37.22	-82.04	1.0	3.6	SRA
1985	7	12	18	20	28.4	35.20	-85.16	3.0	3.0	SRA
1985	8	13	20	57	0.8	41.82	-108.65	5.0	3.5	SRA
1985	8	16	6	5	22.6	42.81	-108.06	10.0	4.3	SRA
1985	8	16	22	48	37.0	49.30	-67.67	0.0	3.1	DNA
1985	8	22	2	12	5.0	46.11	-110.23	5.0	3.0	SRA
1985	8	24	6	4	2.0	45.67	-76.64	18.0	3.1	PDE
1985	9	6	22	17	2.8	35.81	-93.12	10.0	3.6	SRA
1985	9	9	22	6	31.0	41.85	-88.01	5.0	3.0	SRA
1985	9	18	15	54	4.6	33.55	-97.05	5.0	3.3	SRA
1985	10	5	5	34	14.0	47.00	-66.60	5.0	4.0	PDE
1985	10	7	20	33	40.1	40.41	-109.50	21.0	3.0	SRA
1985	10	15	20	0	38.4	42.53	-71.47	13.0	3.1	SRA
1985	10	19	10	7	40.3	40.98	-73.83	6.0	3.6	USH
1985	11	1	23	33	39.0	45.29	-73.45	5.0	3.3	PDE
1985	11	8	19	56	48.5	35.22	-92.19	4.0	3.3	SRA
1985	12	4	8	38	14.0	49.18	-113.36	18.0	3.2	DNA
1985	12	5	22	59	41.2	35.88	-89.99	5.0	3.9	SRA

© 2007-2012 UniStar Nuclear Services, LLC. All rights reserved.
COPYRIGHT PROTECTED

Table 2.5-1— {Updated Earthquake catalog (1534-April 2010) Including events with $m_b \geq 3.0$}
(Page 60 of 75)

Year	Month	Day	Hour	Min	Sec	Lat (deg)	Lon (deg)	Depth (km)	mb	Source
1985	12	15	7	14	52.6	35.44	-104.67	0.0	3.0	SNM
1985	12	21	6	3	11.0	47.00	-66.60	5.0	3.1	DNA
1985	12	22	0	56	5.0	35.70	-83.72	13.0	3.3	SRA
1985	12	29	8	56	56.3	38.55	-88.97	5.0	3.5	SRA
1986	1	7	1	26	43.3	35.61	-84.76	22.0	3.2	SRA
1986	1	10	9	59	48.0	45.80	-77.32	18.0	3.3	PDE
1986	1	11	13	30	28.0	47.70	-70.18	18.0	4.0	PDE
1986	1	30	22	26	37.0	32.07	-100.69	5.0	3.3	SRA
1986	1	31	16	46	42.3	41.65	-81.16	2.0	4.9	USH
1986	2	13	11	35	45.3	34.79	-82.91	5.0	3.5	SRA
1986	3	3	11	45	17.4	35.31	-102.51	5.0	3.1	SRA
1986	3	6	8	34	51.0	47.00	-66.60	5.0	3.5	PDE
1986	4	19	7	40	53.0	35.19	-85.51	27.0	3.0	SRA
1986	5	7	2	27	0.4	33.34	-87.35	1.0	4.5	SRA
1986	5	9	9	4	33.0	46.54	-66.14	18.0	3.3	PDE
1986	5	12	4	18	2.4	27.70	-88.73	10.0	3.6	PDE
1986	5	14	15	2	55.7	37.29	-110.32	8.0	3.2	SRA
1986	5	24	8	16	1.5	35.18	-92.22	5.0	3.0	SRA
1986	5	24	12	48	13.5	36.58	-89.88	10.0	3.4	SRA
1986	5	25	7	13	22.1	43.94	-98.29	5.0	3.4	SRA
1986	6	1	14	53	14.0	47.00	-66.60	5.0	3.4	PDE
1986	6	2	4	4	5.2	39.34	-99.78	5.0	3.0	SRA
1986	6	5	12	13	22.0	46.34	-75.09	8.0	3.3	PDE
1986	6	12	15	14	34.0	42.40	-105.69	20.0	3.0	SRA
1986	7	11	14	26	14.8	34.94	-84.99	13.0	3.8	USH
1986	7	12	8	19	37.9	40.54	-84.37	10.0	4.6	USH
1986	7	12	20	32	48.4	46.17	-68.20	9.0	3.4	SRA
1986	8	6	11	19	36.0	46.37	-75.22	18.0	3.5	PDE
1986	8	13	4	55	18.4	45.13	-74.25	24.0	3.3	PDE
1986	8	22	13	26	33.3	37.42	-110.57	5.0	4.0	SRA
1986	8	26	16	41	24.8	38.32	-89.79	5.0	3.7	SRA
1986	8	27	18	6	58.0	35.12	-105.17	0.0	3.1	SNM
1986	9	3	6	20	50.9	38.91	-107.09	5.0	3.5	SRA
1986	9	19	15	53	1.0	47.30	-70.32	22.0	4.2	PDE
1986	10	17	14	47	59.0	47.00	-66.60	5.0	4.1	PDE
1986	10	20	4	32	49.0	37.92	-101.37	5.0	3.0	SRA
1986	10	25	17	16	38.4	43.40	-71.59	5.0	3.9	SRA
1986	11	3	0	23	45.0	41.92	-108.90	5.0	3.3	SRA
1986	11	7	1	31	53.7	37.43	-110.30	1.0	3.0	SRA
1986	11	7	13	53	18.5	34.67	-70.90	10.0	4.0	PDE
1986	12	11	14	7	11.5	34.90	-82.88	9.0	3.0	SRA
1986	12	30	7	15	19.1	36.42	-89.58	14.0	3.5	SRA
1987	1	1	8	2	24.0	42.79	-103.48	5.0	3.5	PDE
1987	1	16	3	25	35.7	35.89	-89.98	5.0	3.0	PDE
1987	1	24	16	8	17.0	35.83	-98.10	5.0	3.1	PDE
1987	3	5	3	2	50.4	40.44	-110.62	1.0	4.0	PDE

© 2007-2012 UniStar Nuclear Services, LLC. All rights reserved.
COPYRIGHT PROTECTED

Table 2.5-1— {Updated Earthquake catalog (1534-April 2010) Including events with $m_b \geq 3.0$}
(Page 61 of 75)

Year	Month	Day	Hour	Min	Sec	Lat (deg)	Lon (deg)	Depth (km)	mb	Source
1987	3	27	7	29	30.4	35.57	-84.23	19.0	4.2	USH
1987	6	10	23	48	54.8	38.71	-87.95	10.0	5.2	USH
1987	6	13	21	17	12.8	36.61	-89.69	5.0	4.1	PDE
1987	7	7	19	19	5.7	36.84	-89.17	5.0	3.6	PDE
1987	7	9	22	6	45.4	44.33	-98.29	10.0	3.0	PDE
1987	7	11	0	4	29.4	36.10	-83.82	25.0	3.3	PDE
1987	7	13	5	49	17.4	41.90	-80.77	5.0	3.8	PDE
1987	7	23	9	32	28.5	43.49	-79.47	6.0	3.4	PDE
1987	8	31	17	12	35.5	38.31	-89.69	5.0	3.1	PDE
1987	9	22	17	23	50.1	35.62	-84.31	19.0	3.3	PDE
1987	9	26	17	44	6.9	44.38	-74.52	10.0	3.8	PDE
1987	9	29	0	4	57.2	36.84	-89.21	5.0	4.5	USH
1987	10	5	18	54	49.3	45.77	-107.38	5.0	3.7	PDE
1987	10	14	15	49	39.5	37.05	-88.79	5.0	3.8	PDE
1987	10	15	10	54	33.8	44.47	-98.60	5.0	3.0	PDE
1987	11	27	18	58	29.5	36.85	-83.10	14.0	3.5	PDE
1987	12	8	1	42	40.3	36.06	-98.02	5.0	3.7	PDE
1987	12	12	3	53	28.7	34.24	-82.63	5.0	3.0	PDE
1988	1	9	1	7	40.7	35.28	-84.20	12.0	3.3	PDE
1988	1	14	17	23	36.5	46.56	-89.62	5.0	3.6	PDE
1988	1	23	1	57	16.3	32.94	-80.16	7.0	3.3	PDE
1988	1	28	8	38	28.0	48.00	-65.58	18.0	4.9	PDE
1988	1	31	0	12	43.4	35.68	-90.47	10.0	3.5	PDE
1988	2	14	18	32	40.5	40.63	-108.53	5.0	3.3	PDE
1988	2	16	15	26	54.5	36.56	-82.30	5.0	3.3	PDE
1988	2	18	0	37	45.9	35.37	-83.85	5.0	3.5	PDE
1988	2	18	5	27	5.5	50.77	-101.89	0.0	3.1	PDE
1988	3	6	18	13	18.1	47.00	-66.60	5.0	3.3	PDE
1988	3	10	14	42	55.2	46.34	-75.72	18.0	3.9	PDE
1988	3	25	22	14	0.6	50.60	-102.14	1.0	3.7	PDE
1988	4	14	9	39	31.4	39.09	-99.16	5.0	3.2	PDE
1988	4	14	23	37	31.1	37.24	-81.99	0.0	4.1	PDE
1988	4	24	1	14	52.1	45.96	-64.88	18.0	3.7	PDE
1988	5	9	1	23	3.6	47.00	-66.60	5.0	3.4	PDE
1988	5	15	6	10	5.6	45.17	-75.58	7.0	3.5	PDE
1988	5	20	23	6	22.6	37.29	-92.77	5.0	3.3	PDE
1988	7	15	0	38	9.5	36.37	-110.45	5.0	3.3	PDE
1988	8	9	13	57	26.9	45.00	-74.96	10.0	3.4	PDE
1988	8	14	20	3	3.9	39.13	-110.87	10.0	5.5	USH
1988	8	26	5	59	10.2	46.99	-66.59	5.0	3.8	PDE
1988	9	7	2	28	9.5	38.14	-83.88	10.0	4.6	USH
1988	10	5	0	38	52.2	38.69	-87.93	5.0	3.6	PDE
1988	10	20	13	9	50.1	44.54	-71.16	5.0	3.9	USH
1988	11	14	6	15	43.1	44.42	-70.39	5.0	3.8	PDE
1988	11	25	23	46	4.5	48.12	-71.18	28.0	5.9	PDE
1988	12	25	15	57	57.7	34.19	-92.70	13.0	3.3	PDE

© 2007-2012 UniStar Nuclear Services, LLC. All rights reserved.
COPYRIGHT PROTECTED

Table 2.5-1— {Updated Earthquake catalog (1534-April 2010) Including events with $m_b \geq 3.0$}
(Page 62 of 75)

Year	Month	Day	Hour	Min	Sec	Lat (deg)	Lon (deg)	Depth (km)	mb	Source
1988	12	28	6	28	44.4	44.51	-69.34	10.0	3.5	PDE
1988	12	31	14	24	20.5	36.19	-89.43	5.0	3.5	PDE
1989	1	1	17	55	53.6	49.26	-67.36	18.0	3.6	PDE
1989	1	4	18	50	9.7	49.06	-112.86	5.0	3.1	PDE
1989	1	29	5	7	15.6	35.18	-104.10	0.0	3.4	SNM
1989	2	9	5	15	45.8	42.69	-101.90	5.0	3.8	PDE
1989	2	10	1	4	24.0	50.07	-64.66	18.0	4.4	PDE
1989	2	28	17	31	50.8	33.64	-87.09	0.0	3.5	PDE
1989	3	11	8	31	52.1	47.70	-69.90	18.0	4.4	PDE
1989	4	6	2	35	51.3	44.51	-71.14	5.0	3.5	PDE
1989	4	7	8	26	48.9	47.72	-105.60	5.0	3.9	PDE
1989	4	15	16	39	51.1	36.56	-89.71	5.0	3.0	PDE
1989	4	27	16	47	49.8	36.01	-89.77	10.0	4.3	USH
1989	5	14	0	16	9.5	36.74	-89.71	2.0	3.7	PDE
1989	6	8	18	18	43.3	39.17	-99.48	5.0	3.8	PDE
1989	7	13	18	35	22.9	39.17	-99.47	5.0	3.4	PDE
1989	7	15	0	8	2.6	38.61	-83.57	10.0	3.1	PDE
1989	7	20	6	7	50.4	36.43	-98.88	5.0	3.1	PDE
1989	8	5	21	7	59.1	43.21	-79.53	18.0	3.3	PDE
1989	8	10	21	17	43.5	46.65	-65.82	18.0	3.5	PDE
1989	8	13	20	16	2.9	33.63	-87.09	0.0	3.4	PDE
1989	8	20	0	3	17.8	34.74	-87.65	10.0	3.9	USH
1989	8	24	15	56	59.3	41.61	-70.90	5.0	3.0	PDE
1989	8	31	4	2	38.3	47.55	-108.95	5.0	3.0	PDE
1989	9	14	17	31	28.0	36.55	-89.62	11.0	3.5	PDE
1989	11	2	6	23	56.2	41.21	-107.03	5.0	3.0	PDE
1989	11	16	9	24	52.0	46.57	-76.59	18.0	4.0	PDE
1989	11	19	3	21	13.6	38.06	-107.77	5.0	3.0	PDE
1989	11	26	1	6	14.6	45.32	-99.91	5.0	3.3	PDE
1989	12	25	8	29	26.9	35.25	-90.74	5.0	3.2	PDE
1990	1	24	18	20	24.4	38.13	-86.43	5.0	4.0	PDE
1990	1	28	4	59	59.1	43.31	-102.50	5.0	4.0	PDE
1990	3	2	7	1	47.7	38.87	-89.22	10.0	3.6	PDE
1990	3	18	16	22	33.0	36.72	-91.49	5.0	3.0	PDE
1990	3	30	1	54	9.0	47.28	-68.23	18.0	3.5	PDE
1990	4	4	21	42	33.6	48.72	-112.37	6.0	3.1	PDE
1990	4	7	15	37	54.8	40.08	-109.52	3.0	3.5	PDE
1990	4	17	10	27	34.7	40.46	-84.85	5.0	3.0	PDE
1990	4	24	9	41	24.3	39.56	-88.23	10.0	3.0	PDE
1990	5	5	20	48	56.1	36.04	-71.67	10.0	3.7	PDE
1990	6	25	17	15	33.5	38.95	-110.83	11.0	3.0	PDE
1990	7	18	2	47	3.9	41.51	-98.95	5.0	3.0	PDE
1990	8	7	5	5	56.4	36.85	-89.24	6.0	3.0	PDE
1990	8	17	21	1	17.9	36.79	-83.34	10.0	3.5	PDE
1990	8	29	19	34	59.9	35.83	-89.66	13.0	3.5	PDE
1990	9	8	0	3	57.4	38.06	-83.73	5.0	3.3	PDE

© 2007-2012 UniStar Nuclear Services, LLC. All rights reserved.
COPYRIGHT PROTECTED

Table 2.5-1— {Updated Earthquake catalog (1534-April 2010) Including events with $m_b \geq 3.0$}
(Page 63 of 75)

Year	Month	Day	Hour	Min	Sec	Lat (deg)	Lon (deg)	Depth (km)	mb	Source
1990	9	12	21	38	57.6	39.70	-106.21	5.0	3.0	PDE
1990	9	26	13	18	51.3	37.17	-89.58	12.0	4.8	PDE
1990	9	30	0	6	24.0	41.82	-101.51	5.0	3.0	PDE
1990	10	7	8	47	30.5	46.32	-75.19	17.0	3.9	PDE
1990	10	19	7	1	57.4	46.47	-75.59	13.0	5.1	PDE
1990	10	24	8	20	4.3	38.31	-88.99	5.0	3.2	PDE
1990	10	25	6	25	25.5	43.79	-98.47	5.0	3.9	PDE
1990	11	9	3	39	15.9	36.54	-89.62	8.0	3.6	PDE
1990	11	13	15	22	13.0	32.95	-80.14	3.0	3.2	PDE
1990	11	15	11	44	41.4	34.76	-97.59	5.0	3.6	PDE
1990	11	15	13	47	15.7	47.13	-76.22	18.0	4.1	PDE
1990	11	20	8	19	11.2	39.13	-110.89	2.0	3.2	PDE
1990	12	12	5	15	7.1	47.00	-66.60	5.0	3.5	PDE
1990	12	17	5	24	59.1	40.07	-87.04	10.0	3.2	PDE
1990	12	20	14	4	17.1	39.57	-86.67	10.0	3.6	PDE
1990	12	31	3	53	58.3	47.58	-72.56	18.0	4.4	PDE
1991	1	23	9	25	23.5	37.95	-88.86	5.0	3.0	PDE
1991	1	24	5	0	26.9	36.38	-97.30	5.0	3.0	PDE
1991	1	26	3	21	22.6	41.54	-81.45	5.0	3.4	PDE
1991	1	26	21	49	38.0	37.68	-111.43	9.0	3.5	PDE
1991	2	11	0	0	6.1	35.98	-89.95	14.0	3.0	PDE
1991	3	2	8	41	37.4	40.09	-109.48	1.0	3.0	PDE
1991	3	6	5	26	53.6	46.28	-76.87	18.0	3.9	PDE
1991	3	15	6	54	8.2	37.75	-77.92	17.0	3.8	PDE
1991	3	21	4	10	59.3	49.70	-66.59	18.0	3.9	PDE
1991	4	13	19	8	5.1	42.03	-106.86	5.0	3.2	PDE
1991	4	16	4	6	39.3	38.56	-87.99	15.0	3.0	PDE
1991	4	22	1	1	20.2	37.94	-80.21	14.0	3.5	PDE
1991	4	23	3	19	19.0	47.00	-66.60	5.0	3.6	PDE
1991	5	4	1	18	54.9	36.56	-89.82	5.0	4.6	PDE
1991	5	17	18	8	47.0	45.50	-74.40	18.0	3.2	PDE
1991	5	30	22	7	44.0	39.20	-99.40	5.0	3.5	PDE
1991	6	5	9	24	7.6	48.37	-112.01	5.0	3.6	PDE
1991	6	16	16	46	53.0	47.00	-76.70	18.0	4.2	PDE
1991	6	17	8	53	16.7	42.63	-74.68	5.0	4.1	PDE
1991	6	25	21	2	13.6	37.21	-110.36	1.0	3.0	PDE
1991	6	28	18	34	51.9	38.28	-81.67	5.0	3.2	PDE
1991	7	2	3	49	1.7	37.49	-91.71	5.0	3.3	PDE
1991	7	5	1	47	36.7	45.23	-73.90	18.0	3.8	PDE
1991	7	7	21	24	2.6	36.66	-91.64	5.0	3.8	PDE
1991	7	8	23	49	7.4	36.14	-89.44	12.0	3.0	PDE
1991	7	20	23	38	19.2	28.91	-98.04	10.0	3.4	PDE
1991	8	7	12	49	16.6	43.50	-108.86	5.0	3.5	PDE
1991	8	15	7	16	7.1	40.79	-77.66	1.0	3.0	PDE
1991	8	26	11	49	15.4	42.16	-100.53	5.0	3.4	PDE
1991	9	24	7	21	6.4	35.71	-84.10	5.0	3.0	PDE

© 2007-2012 UniStar Nuclear Services, LLC. All rights reserved.
COPYRIGHT PROTECTED

Table 2.5-1— {Updated Earthquake catalog (1534-April 2010) Including events with $m_b \geq 3.0$}
(Page 64 of 75)

Year	Month	Day	Hour	Min	Sec	Lat (deg)	Lon (deg)	Depth (km)	mb	Source
1991	10	3	11	46	4.8	36.84	-89.43	5.0	3.1	PDE
1991	10	28	20	58	26.1	41.07	-73.58	10.0	3.0	PDE
1991	11	11	9	20	47.4	38.71	-87.89	10.0	3.8	PDE
1991	11	13	9	43	15.9	35.72	-90.27	9.0	3.0	PDE
1991	12	5	10	10	0.7	47.95	-108.90	10.0	3.0	PDE
1991	12	8	3	0	30.0	47.70	-69.80	18.0	4.1	PDE
1991	12	18	21	36	47.9	41.94	-106.92	5.0	3.1	PDE
1991	12	23	20	32	27.2	45.82	-106.72	5.0	3.6	PDE
1992	1	2	11	45	35.3	32.30	-103.19	0.0	5.0	SNM
1992	1	3	4	21	22.2	33.95	-82.47	5.0	3.2	PDE
1992	1	9	8	50	45.2	40.36	-74.34	7.0	3.0	PDE
1992	1	21	11	36	21.0	38.00	-92.67	5.0	3.1	PDE
1992	2	22	4	21	34.6	26.36	-78.89	10.0	3.2	PDE
1992	3	15	6	13	55.2	41.91	-81.25	5.0	3.5	PDE
1992	3	31	14	59	39.6	26.02	-85.73	5.0	3.8	PDE
1992	4	3	3	6	3.9	35.83	-89.48	12.0	3.2	PDE
1992	4	15	22	46	5.0	37.34	-104.77	5.0	3.3	PDE
1992	5	1	0	37	51.4	47.45	-70.41	2.0	3.2	PDE
1992	5	19	5	59	41.0	46.44	-74.96	18.0	3.7	PDE
1992	7	10	14	44	43.0	50.64	-101.84	1.0	3.4	PDE
1992	7	15	2	56	40.7	38.76	-99.55	5.0	3.3	PDE
1992	8	21	16	31	55.1	33.05	-80.12	10.0	4.4	PDE
1992	8	22	12	20	32.6	39.11	-70.32	10.0	4.7	PDE
1992	8	26	3	24	52.6	32.17	-102.71	5.0	3.0	PDE
1992	8	26	5	41	38.4	37.63	-89.68	5.0	3.2	PDE
1992	8	31	1	40	14.2	43.83	-107.04	5.0	3.6	PDE
1992	9	27	17	2	34.3	28.17	-88.44	10.0	3.8	PDE
1992	10	6	15	38	4.0	43.32	-71.58	5.0	3.4	PDE
1992	10	10	15	40	56.2	42.82	-108.24	5.0	4.0	PDE
1992	11	2	6	54	10.3	42.74	-104.39	5.0	3.0	PDE
1992	11	17	3	37	22.9	49.00	-112.61	5.0	3.4	PDE
1992	11	17	3	58	0.9	45.76	-74.86	18.0	4.2	PDE
1992	12	17	7	18	4.2	34.74	-97.58	5.0	3.5	PDE
1992	12	27	10	12	58.9	37.50	-89.63	5.0	3.2	PDE
1993	1	1	5	8	5.3	35.88	-82.09	3.0	3.0	PDE
1993	1	1	15	57	41.9	48.90	-112.19	5.0	3.3	PDE
1993	1	8	13	1	18.8	35.83	-90.03	21.0	3.5	PDE
1993	1	14	17	6	10.4	36.60	-98.28	5.0	3.1	PDE
1993	1	15	2	2	51.8	35.08	-84.97	1.0	3.1	PDE
1993	1	21	19	46	19.3	36.22	-89.62	13.0	3.0	PDE
1993	1	22	6	2	32.7	49.21	-112.40	5.0	3.4	PDE
1993	1	29	13	56	23.2	39.04	-89.04	5.0	3.2	PDE
1993	2	6	2	9	45.5	36.66	-89.73	7.0	3.5	PDE
1993	2	20	13	8	10.1	42.83	-101.46	5.0	3.5	PDE
1993	2	25	3	44	15.5	44.93	-106.06	5.0	3.5	PDE
1993	3	2	0	29	11.8	36.67	-89.49	8.0	3.1	PDE

© 2007-2012 UniStar Nuclear Services, LLC. All rights reserved.
COPYRIGHT PROTECTED

Table 2.5-1— {Updated Earthquake catalog (1534-April 2010) Including events with $m_b \geq 3.0$}
(Page 65 of 75)

Year	Month	Day	Hour	Min	Sec	Lat (deg)	Lon (deg)	Depth (km)	mb	Source
1993	3	10	3	54	31.1	43.40	-106.62	5.0	3.2	PDE
1993	3	16	7	38	10.2	35.67	-90.55	10.0	3.3	PDE
1993	3	24	2	32	5.9	35.15	-104.44	0.0	3.0	SNM
1993	3	31	20	23	21.2	36.79	-89.42	5.0	3.3	PDE
1993	4	9	12	29	19.1	28.81	-98.12	5.0	4.3	PDE
1993	4	28	22	40	1.9	36.19	-89.44	7.0	3.6	PDE
1993	5	6	1	23	25.9	46.30	-75.50	18.0	3.5	PDE
1993	6	1	21	33	22.9	42.30	-107.58	5.0	3.7	PDE
1993	6	5	1	24	53.0	45.67	-96.29	10.0	4.1	PDE
1993	6	30	6	50	57.8	42.99	-105.37	5.0	3.0	PDE
1993	7	8	4	3	52.2	39.23	-106.72	5.0	3.1	PDE
1993	7	16	10	54	32.8	31.75	-88.34	5.0	3.7	PDE
1993	7	23	6	30	23.8	42.48	-105.70	5.0	3.7	PDE
1993	7	30	22	30	54.0	45.26	-74.12	8.0	3.9	PDE
1993	8	5	7	21	37.4	36.00	-89.88	11.0	3.0	PDE
1993	8	8	9	24	31.1	33.63	-81.60	5.0	3.2	PDE
1993	8	23	5	29	47.6	43.58	-109.92	5.0	3.0	PDE
1993	8	23	13	12	13.8	42.03	-106.84	5.0	3.0	PDE
1993	8	27	0	8	34.0	38.09	-90.36	16.0	3.3	PDE
1993	8	30	5	15	28.5	46.46	-75.05	15.0	3.3	PDE
1993	9	23	6	45	28.4	46.07	-74.61	18.0	3.5	PDE
1993	9	24	18	27	15.0	36.56	-89.58	6.0	3.0	PDE
1993	9	29	2	1	28.5	35.57	-103.56	0.0	3.0	SNM
1993	10	10	4	17	46.7	42.42	-105.87	5.0	3.7	PDE
1993	10	16	6	30	5.3	41.70	-81.01	5.0	3.4	PDE
1993	11	16	7	26	4.0	43.88	-107.38	5.0	3.5	PDE
1993	11	16	9	31	44.2	45.18	-73.50	17.0	4.1	PDE
1993	11	30	3	7	36.3	35.81	-103.16	0.0	3.3	SNM
1993	12	1	12	47	15.0	47.53	-70.06	8.0	3.5	PDE
1993	12	13	14	51	3.0	42.33	-105.50	5.0	3.2	PDE
1993	12	25	16	44	22.3	46.51	-75.61	18.0	4.3	PDE
1993	12	28	21	2	28.7	43.48	-110.13	8.0	4.7	PDE
1993	12	30	23	1	47.5	47.45	-70.37	7.0	3.8	PDE
1994	1	16	1	49	16.2	40.33	-76.04	5.0	4.6	PDE
1994	1	25	2	44	39.8	42.63	-100.14	5.0	3.3	PDE
1994	2	5	14	55	37.7	37.37	-89.18	16.0	4.2	PDE
1994	2	9	8	45	35.5	45.00	-95.00	5.0	3.1	PDE
1994	3	12	10	43	15.7	42.78	-77.88	1.0	3.5	PDE
1994	3	28	16	28	23.0	48.99	-65.74	18.0	3.6	PDE
1994	4	5	22	21	59.0	34.96	-85.49	5.0	3.2	PDE
1994	4	6	17	38	55.8	38.12	-89.27	10.0	3.1	PDE
1994	5	4	9	12	2.7	34.20	-87.17	5.0	3.0	PDE
1994	6	10	23	34	2.9	33.01	-92.67	5.0	3.2	PDE
1994	6	30	1	8	24.2	27.91	-90.18	10.0	4.2	PDE
1994	7	14	12	41	52.0	47.00	-66.60	5.0	4.0	PDE
1994	8	6	19	54	9.9	35.07	-76.75	5.0	3.6	PDE

© 2007-2012 UniStar Nuclear Services, LLC. All rights reserved.
COPYRIGHT PROTECTED

Table 2.5-1— {Updated Earthquake catalog (1534-April 2010) Including events with $m_b \geq 3.0$}
(Page 66 of 75)

Year	Month	Day	Hour	Min	Sec	Lat (deg)	Lon (deg)	Depth (km)	mb	Source
1994	8	16	11	3	41.7	48.49	-111.33	5.0	3.9	PDE
1994	8	20	10	45	44.6	36.14	-91.06	5.0	3.5	PDE
1994	9	2	21	23	6.5	42.80	-84.60	5.0	3.4	PDE
1994	9	5	14	13	52.2	43.86	-69.23	5.0	3.0	PDE
1994	9	13	6	1	23.0	38.15	-107.98	10.0	4.4	PDE
1994	9	16	4	22	42.5	45.31	-68.22	5.0	3.6	PDE
1994	9	25	0	53	28.0	47.77	-69.96	17.0	4.3	PDE
1994	9	26	14	23	22.0	36.93	-88.94	5.0	3.6	PDE
1994	10	2	11	27	22.5	42.35	-72.28	10.0	3.5	PDE
1994	11	3	11	40	10.1	40.04	-108.27	5.0	3.4	PDE
1994	12	25	19	6	7.5	39.29	-104.81	10.0	4.0	PDE
1995	1	18	15	51	39.4	34.77	-97.60	5.0	4.0	PDE
1995	2	3	15	26	10.6	41.53	-109.64	1.0	5.3	PDE
1995	2	11	5	54	10.1	40.51	-94.95	5.0	3.1	PDE
1995	2	15	15	53	57.0	45.90	-75.04	18.0	3.4	PDE
1995	2	19	12	57	6.0	39.12	-83.47	10.0	3.6	PDE
1995	3	2	5	33	51.4	44.23	-74.43	4.0	3.0	PDE
1995	3	5	12	17	11.5	48.65	-112.35	10.0	3.3	PDE
1995	3	18	22	6	21.0	35.43	-84.92	17.0	3.3	PDE
1995	3	19	18	36	43.9	35.00	-104.21	5.0	3.3	PDE
1995	3	20	12	46	16.3	40.18	-108.93	5.0	4.2	PDE
1995	4	17	13	45	57.8	32.95	-80.07	10.0	3.9	PDE
1995	4	20	4	37	5.0	49.15	-67.73	15.0	3.3	PDE
1995	5	6	7	51	35.0	47.00	-66.60	5.0	3.9	PDE
1995	5	27	19	51	10.4	36.17	-89.43	6.0	3.8	PDE
1995	5	28	15	28	36.9	33.19	-87.83	1.0	3.4	PDE
1995	6	1	4	49	29.3	34.29	-96.73	5.0	3.0	PDE
1995	6	3	22	44	32.0	47.02	-76.29	18.0	3.4	PDE
1995	6	16	12	13	11.4	44.29	-71.92	5.0	3.8	PDE
1995	6	26	0	36	17.0	36.75	-81.45	5.0	3.5	PDE
1995	6	29	9	27	20.1	36.59	-89.79	5.0	3.0	PDE
1995	7	4	3	59	4.5	36.25	-104.81	5.0	3.8	PDE
1995	7	5	14	16	44.4	35.37	-84.21	10.0	3.7	PDE
1995	7	7	21	1	2.8	36.52	-81.87	11.0	3.0	PDE
1995	7	15	1	3	28.3	33.48	-87.67	1.0	3.3	PDE
1995	7	20	2	10	34.4	36.53	-89.63	5.0	3.2	PDE
1995	8	17	23	18	50.8	36.10	-89.41	5.0	3.1	PDE
1995	9	12	3	59	5.0	45.61	-74.43	18.0	3.7	PDE
1995	9	15	0	31	33.2	36.87	-98.69	5.0	3.8	PDE
1995	9	21	23	3	27.0	45.08	-74.21	18.0	3.1	PDE
1995	10	10	7	19	20.0	46.42	-78.77	18.0	3.2	PDE
1995	10	20	15	57	18.7	45.79	-96.86	5.0	3.7	PDE
1995	12	23	6	51	48.8	38.73	-104.92	5.0	3.6	PDE
1996	1	6	12	55	58.6	39.12	-110.88	0.0	4.3	PDE
1996	2	6	15	10	28.2	42.51	-97.54	5.0	3.6	PDE
1996	2	6	16	8	36.7	43.98	-103.73	5.0	3.7	PDE

© 2007-2012 UniStar Nuclear Services, LLC. All rights reserved.
COPYRIGHT PROTECTED

Table 2.5-1— {Updated Earthquake catalog (1534-April 2010) Including events with $m_b \geq 3.0$}
(Page 67 of 75)

Year	Month	Day	Hour	Min	Sec	Lat (deg)	Lon (deg)	Depth (km)	mb	Source
1996	3	14	10	42	26.0	45.99	-74.43	18.0	4.5	PDE
1996	3	22	20	22	12.5	41.69	-71.24	11.0	3.1	PDE
1996	3	25	6	43	46.8	35.61	-102.60	5.0	3.5	PDE
1996	3	25	14	15	50.5	32.13	-88.67	5.0	3.5	PDE
1996	4	9	2	48	8.1	43.07	-104.10	5.0	3.7	PDE
1996	4	11	21	54	57.6	34.97	-91.16	5.0	3.3	PDE
1996	6	29	19	30	42.6	37.19	-81.95	1.0	3.9	PDE
1996	8	1	5	44	22.7	37.40	-104.25	5.0	3.8	PDE
1996	8	11	18	17	49.8	33.58	-90.87	10.0	3.5	PDE
1996	8	15	20	7	29.9	49.08	-112.41	5.0	3.6	PDE
1996	8	16	4	56	46.0	49.21	-82.92	18.0	3.6	PDE
1996	8	21	7	54	14.0	44.18	-71.35	10.0	3.8	PDE
1996	10	19	13	27	57.9	43.09	-106.06	5.0	4.2	PDE
1996	10	21	13	51	39.5	42.55	-109.27	5.0	3.7	PDE
1996	11	1	3	9	28.3	37.35	-104.23	5.0	3.2	PDE
1996	11	23	10	54	18.5	35.04	-100.50	5.0	3.0	PDE
1996	11	29	5	41	33.6	35.92	-89.93	20.0	4.3	PDE
1996	11	29	10	47	9.0	36.29	-89.37	5.0	3.6	PDE
1996	12	16	1	58	31.3	39.50	-87.40	5.0	3.1	PDE
1997	1	18	22	4	39.0	39.10	-105.10	5.0	3.3	PDE
1997	2	12	23	53	10.7	34.95	-100.89	5.0	3.0	PDE
1997	2	15	9	8	55.4	34.97	-100.57	5.0	3.2	PDE
1997	3	16	19	7	27.9	34.21	-93.44	5.0	3.4	PDE
1997	3	24	22	31	34.5	27.72	-98.05	5.0	3.8	PDE
1997	4	3	4	44	12.0	45.98	-72.33	5.0	3.5	PDE
1997	4	18	14	57	35.3	25.78	-86.55	33.0	3.9	PDE
1997	4	25	10	39	6.7	42.68	-108.73	5.0	3.1	PDE
1997	5	1	21	38	36.0	49.13	-112.65	5.0	3.8	PDE
1997	5	4	3	39	12.9	31.00	-87.40	5.0	3.1	PDE
1997	5	24	18	52	6.3	45.98	-74.42	10.0	4.2	PDE
1997	5	31	3	26	41.3	33.18	-95.97	5.0	3.4	PDE
1997	7	19	17	6	34.3	35.06	-84.81	10.0	3.5	PDE
1997	7	30	12	29	23.3	36.44	-83.51	5.0	3.8	PDE
1997	7	31	7	15	29.7	43.62	-75.37	5.0	3.2	PDE
1997	8	9	17	46	3.9	41.80	-97.19	5.0	3.4	PDE
1997	8	20	9	12	4.0	47.53	-70.29	18.0	3.7	PDE
1997	9	6	23	38	0.9	34.66	-96.44	5.0	4.5	PDE
1997	9	17	18	16	31.6	35.62	-90.46	5.0	3.8	PDE
1997	9	20	5	55	50.4	37.18	-90.92	5.0	3.1	PDE
1997	9	24	4	20	24.8	36.55	-89.82	5.0	3.2	PDE
1997	9	27	12	14	9.3	36.20	-89.48	5.0	3.0	PDE
1997	10	13	23	6	40.2	44.36	-74.97	4.0	3.0	PDE
1997	10	24	8	35	17.8	31.12	-87.34	10.0	4.9	PDE
1997	10	28	11	44	18.0	47.67	-69.91	11.0	4.7	PDE
1997	11	6	2	34	33.0	46.80	-71.41	22.0	5.1	PDE
1997	11	14	3	44	11.0	40.15	-76.25	5.0	3.0	PDE

© 2007-2012 UniStar Nuclear Services, LLC. All rights reserved.
COPYRIGHT PROTECTED

Table 2.5-1— {Updated Earthquake catalog (1534-April 2010) Including events with $m_b \geq 3.0$}
(Page 68 of 75)

Year	Month	Day	Hour	Min	Sec	Lat (deg)	Lon (deg)	Depth (km)	mb	Source
1997	12	12	8	42	20.2	33.47	-87.31	1.0	4.0	PDE
1998	1	2	15	47	16.4	37.83	-103.41	5.0	3.4	PDE
1998	2	12	9	37	49.5	36.12	-89.71	10.0	3.0	PDE
1998	2	13	2	28	4.0	44.33	-107.51	5.0	3.0	PDE
1998	2	26	14	20	31.0	46.07	-76.36	18.0	3.7	PDE
1998	3	9	5	5	58.0	46.49	-81.07	1.0	3.9	PDE
1998	3	29	12	12	42.0	38.25	-111.35	3.0	3.0	PDE
1998	4	8	18	16	49.0	36.94	-89.02	13.0	3.2	PDE
1998	4	13	9	56	11.3	34.61	-80.47	5.0	3.9	PDE
1998	4	18	16	22	52.0	45.57	-74.99	18.0	4.1	PDE
1998	4	27	15	22	46.2	35.45	-102.38	5.0	3.2	PDE
1998	4	28	14	13	1.6	34.78	-98.42	5.0	4.2	PDE
1998	5	25	15	47	2.0	46.46	-81.17	1.0	3.9	PDE
1998	6	5	2	31	1.9	35.48	-80.82	5.0	3.2	PDE
1998	6	9	8	53	51.0	44.75	-73.72	4.0	3.4	PDE
1998	6	17	8	0	23.4	35.93	-84.41	10.0	3.6	PDE
1998	6	18	16	26	38.3	42.62	-103.00	5.0	3.4	PDE
1998	6	24	15	20	1.3	32.50	-87.95	5.0	3.4	PDE
1998	7	6	6	54	3.7	25.02	-93.63	10.0	3.4	PDE
1998	7	7	18	44	44.4	34.72	-97.59	5.0	3.2	PDE
1998	7	12	16	28	49.6	43.55	-101.11	5.0	3.1	PDE
1998	7	15	4	24	51.0	36.69	-89.52	13.0	3.1	PDE
1998	7	15	7	8	4.0	47.02	-66.61	5.0	4.0	PDE
1998	7	29	3	31	58.9	48.37	-104.71	5.0	3.7	PDE
1998	7	30	8	57	22.0	46.16	-74.73	10.0	4.4	PDE
1998	8	6	18	22	7.1	41.95	-107.19	10.0	3.6	PDE
1998	9	25	19	52	52.0	41.50	-80.39	5.0	5.2	PDE
1998	10	18	7	13	10.6	36.03	-111.09	5.0	3.4	PDE
1998	10	21	5	56	47.2	37.38	-78.37	13.0	3.8	PDE
1998	10	22	9	43	35.0	49.34	-66.88	18.0	4.1	PDE
1998	10	30	17	41	22.2	36.80	-97.60	5.0	3.5	PDE
1998	11	11	11	59	37.6	48.55	-104.03	5.0	3.5	PDE
1998	12	25	13	30	26.0	43.83	-77.93	18.0	3.6	PDE
1999	1	7	5	16	26.9	38.67	-99.38	5.0	3.0	PDE
1999	1	10	10	52	16.1	42.84	-70.98	2.0	3.1	PDE
1999	1	17	18	38	4.7	36.85	-83.69	5.0	3.0	PDE
1999	1	18	7	0	53.4	33.41	-87.26	1.0	4.0	PDE
1999	2	1	22	22	5.6	49.27	-80.94	18.0	3.4	PDE
1999	2	26	3	38	43.0	44.48	-69.52	3.0	3.8	PDE
1999	3	16	12	50	48.0	49.61	-66.32	18.0	5.1	PDE
1999	4	6	0	41	9.5	41.45	-107.74	10.0	4.3	PDE
1999	5	13	14	18	22.7	39.10	-94.70	5.0	3.0	PDE
1999	7	21	2	36	6.9	42.56	-108.46	5.0	3.1	PDE
1999	8	23	12	12	41.1	36.26	-89.50	9.0	3.1	PDE
1999	9	2	16	17	29.7	41.72	-89.43	5.0	3.5	PDE
1999	10	21	8	18	0.0	36.49	-91.02	19.0	3.9	PDE

© 2007-2012 UniStar Nuclear Services, LLC. All rights reserved.
COPYRIGHT PROTECTED

Table 2.5-1— {Updated Earthquake catalog (1534-April 2010) Including events with $m_b \geq 3.0$}
(Page 69 of 75)

Year	Month	Day	Hour	Min	Sec	Lat (deg)	Lon (deg)	Depth (km)	mb	Source
1999	10	25	23	19	58.3	36.85	-99.66	26.0	3.0	PDE
1999	10	31	20	14	10.0	45.85	-74.32	18.0	4.2	PDE
1999	11	3	13	28	52.0	45.51	-105.47	10.0	3.5	PDE
1999	11	9	8	17	41.1	43.48	-107.48	5.0	3.1	PDE
1999	11	26	22	33	1.4	43.71	-79.00	12.0	3.8	PDE
1999	11	28	11	0	9.3	33.42	-87.25	1.0	3.8	PDE
1999	12	17	21	0	0.0	51.60	-89.84	18.0	3.9	PDE
1999	12	25	0	21	41.0	44.94	-69.37	5.0	3.0	PDE
2000	1	1	11	22	57.0	46.89	-78.93	18.0	5.2	PDE
2000	1	3	21	5	50.0	44.31	-70.17	9.0	3.5	PDE
2000	1	8	22	43	37.0	42.10	-110.34	12.0	3.2	PDE
2000	1	17	8	16	20.0	44.57	-70.44	16.0	3.6	PDE
2000	1	18	22	19	31.9	32.99	-83.21	5.0	3.5	PDE
2000	1	27	14	49	40.0	43.00	-71.18	1.0	3.0	PDE
2000	1	30	14	46	51.3	41.46	-109.68	1.0	4.4	PDE
2000	2	1	22	15	45.3	42.24	-106.73	5.0	3.0	PDE
2000	2	7	17	24	54.3	40.60	-106.67	5.0	3.0	PDE
2000	4	14	3	54	20.0	39.76	-86.75	5.0	3.6	PDE
2000	4	20	8	46	55.4	43.95	-74.26	5.0	4.0	PDE
2000	5	24	10	22	46.2	43.81	-79.10	18.0	3.1	PDE
2000	5	26	21	58	46.6	42.20	-107.57	5.0	4.0	PDE
2000	5	28	11	32	7.0	33.81	-87.82	5.0	3.0	PDE
2000	6	15	9	25	54.0	47.67	-69.81	10.0	3.7	PDE
2000	6	16	4	2	53.0	42.10	-72.82	9.0	3.3	PDE
2000	6	20	17	55	46.0	40.69	-109.31	1.0	3.0	PDE
2000	6	27	1	28	45.0	35.80	-92.75	0.0	3.9	PDE
2000	6	27	6	2	57.0	37.13	-88.87	4.0	3.0	PDE
2000	7	12	15	1	49.0	47.52	-71.10	10.0	4.2	PDE
2000	8	6	8	52	24.0	46.19	-74.97	18.0	4.2	PDE
2000	8	17	1	8	5.4	35.39	-101.81	5.0	3.9	PDE
2000	8	19	2	55	43.7	42.55	-108.26	5.0	3.2	PDE
2000	8	22	20	12	14.0	36.49	-91.11	8.0	3.9	PDE
2000	9	7	10	7	40.7	44.36	-69.38	5.0	3.2	PDE
2000	10	6	13	59	4.0	45.13	-74.02	18.0	3.8	PDE
2000	11	8	2	16	49.9	43.44	-107.69	5.0	3.0	PDE
2000	11	11	21	17	53.0	40.28	-109.23	5.0	3.7	PDE
2000	12	7	14	8	49.4	37.97	-87.66	5.0	4.0	PDE
2000	12	9	6	46	9.1	28.03	-90.17	10.0	4.2	PDE
2000	12	16	22	8	54.0	35.40	-101.80	5.0	3.9	PDE
2001	1	26	3	3	20.0	41.94	-80.80	5.0	4.4	PDE
2001	2	3	20	15	15.0	42.35	-77.39	0.0	3.2	PDE
2001	3	3	10	46	13.0	33.19	-92.66	5.0	3.0	PDE
2001	3	7	17	12	25.0	35.51	-84.81	6.0	3.2	PDE
2001	3	16	4	39	7.6	28.36	-89.03	10.0	3.6	PDE
2001	3	19	10	40	17.0	47.05	-76.28	18.0	3.9	PDE
2001	3	21	23	35	35.0	34.86	-85.44	3.0	3.2	PDE

© 2007-2012 UniStar Nuclear Services, LLC. All rights reserved.
COPYRIGHT PROTECTED

Table 2.5-1— {Updated Earthquake catalog (1534-April 2010) Including events with $m_b \geq 3.0$}
(Page 70 of 75)

Year	Month	Day	Hour	Min	Sec	Lat (deg)	Lon (deg)	Depth (km)	mb	Source
2001	3	24	11	57	18.3	50.03	-63.35	18.0	4.2	PDE
2001	3	30	17	13	55.6	37.93	-93.33	5.0	3.1	PDE
2001	4	13	16	36	20.7	36.53	-83.34	0.0	3.0	PDE
2001	5	4	6	42	12.6	35.21	-92.19	10.0	4.7	PDE
2001	6	2	1	55	53.7	32.33	-103.14	5.0	3.3	PDE
2001	6	3	22	36	46.4	41.91	-80.77	5.0	3.4	PDE
2001	6	11	18	27	54.2	30.23	-79.89	10.0	3.3	PDE
2001	7	7	20	45	42.7	36.28	-89.40	14.0	3.0	PDE
2001	7	22	19	22	45.5	39.02	-105.13	5.0	3.1	PDE
2001	7	24	14	2	35.0	37.70	-97.00	5.0	3.0	PDE
2001	7	26	5	26	44.7	35.93	-83.58	5.0	3.2	PDE
2001	8	4	1	13	25.3	34.29	-93.21	5.0	3.1	PDE
2001	8	9	22	38	54.5	39.66	-107.38	5.0	4.0	PDE
2001	9	5	10	52	7.8	37.14	-104.62	5.0	4.5	PDE
2001	9	16	6	20	26.0	50.64	-63.33	5.0	3.7	PDE
2001	9	22	16	1	20.5	38.03	-78.40	2.0	3.2	PDE
2001	9	27	22	5	21.7	43.46	-110.05	5.0	4.3	PDE
2001	10	25	0	24	29.8	45.20	-68.67	9.0	3.3	PDE
2001	11	13	1	56	13.1	40.00	-100.21	5.0	3.3	PDE
2001	11	22	0	7	8.0	31.79	-102.63	5.0	3.1	PDE
2001	12	8	1	8	21.5	34.74	-86.25	5.0	3.9	PDE
2001	12	15	7	58	31.3	36.86	-104.80	5.0	3.3	PDE
2001	12	24	16	58	21.0	46.87	-76.49	18.0	3.8	PDE
2002	1	20	14	11	55.0	49.49	-66.95	30.0	4.1	PDE
2002	1	26	1	6	3.8	36.86	-104.78	5.0	3.4	PDE
2002	1	31	18	17	45.4	40.29	-107.69	5.0	4.3	PDE
2002	2	8	16	7	13.6	34.73	-98.36	5.0	3.8	PDE
2002	2	11	11	41	37.0	46.06	-73.46	10.0	3.8	PDE
2002	2	24	21	38	33.0	45.29	-75.17	18.0	3.1	PDE
2002	3	12	7	13	25.7	41.62	-69.33	1.0	3.0	PDE
2002	3	12	8	30	48.2	37.17	-89.97	5.0	3.6	PDE
2002	3	23	6	34	32.5	40.47	-106.91	1.0	3.1	PDE
2002	4	5	1	18	48.2	43.94	-108.10	5.0	3.3	PDE
2002	4	14	18	16	33.7	40.49	-106.89	1.0	3.3	PDE
2002	4	20	10	50	47.5	44.51	-73.70	11.0	5.2	PDE
2002	5	21	20	35	34.4	32.80	-88.10	5.0	3.1	PDE
2002	5	27	0	28	16.9	27.12	-94.44	10.0	3.8	PDE
2002	5	28	9	15	38.0	45.63	-76.62	18.0	3.4	PDE
2002	5	31	9	57	10.0	34.03	-97.62	5.0	3.3	PDE
2002	6	1	11	35	29.0	45.59	-73.86	18.0	3.2	PDE
2002	6	18	9	12	36.6	36.88	-104.78	5.0	3.5	PDE
2002	6	18	17	37	15.1	37.99	-87.78	5.0	5.0	PDE
2002	6	19	12	14	20.3	36.57	-103.03	5.0	3.7	PDE
2002	6	20	4	29	40.3	41.51	-98.62	5.0	3.5	PDE
2002	7	23	2	8	59.0	49.59	-66.95	18.0	4.0	PDE
2002	7	26	8	32	17.2	44.36	-98.22	5.0	3.1	PDE

© 2007-2012 UniStar Nuclear Services, LLC. All rights reserved.
COPYRIGHT PROTECTED

Table 2.5-1— {Updated Earthquake catalog (1534-April 2010) Including events with $m_b \geq 3.0$}
(Page 71 of 75)

Year	Month	Day	Hour	Min	Sec	Lat (deg)	Lon (deg)	Depth (km)	mb	Source
2002	8	17	5	53	54.0	47.33	-70.51	13.0	3.8	PDE
2002	9	7	21	27	45.0	46.96	-76.29	18.0	3.7	PDE
2002	9	19	14	44	36.1	27.82	-89.14	10.0	3.7	PDE
2002	9	26	10	32	10.0	37.41	-110.53	3.0	3.0	PDE
2002	10	20	2	18	13.0	34.27	-96.08	5.0	3.4	PDE
2002	10	26	20	5	55.9	34.03	-90.68	5.0	3.1	PDE
2002	11	1	11	8	56.2	39.12	-99.09	5.0	3.0	PDE
2002	11	3	20	41	56.9	42.77	-98.90	5.0	4.3	PDE
2002	11	6	12	45	36.0	48.60	-112.33	1.0	3.1	PDE
2002	11	7	16	55	6.0	44.05	-77.43	18.0	3.0	PDE
2002	11	11	23	39	29.7	32.40	-79.94	2.0	4.4	PDE
2002	11	14	4	56	52.2	36.92	-104.77	5.0	3.2	PDE
2002	12	25	18	25	19.0	44.56	-73.79	14.0	3.3	PDE
2003	1	3	16	17	9.0	37.83	-88.07	18.0	3.1	PDE
2003	1	9	0	2	17.0	46.02	-110.36	10.0	3.7	PDE
2003	1	20	2	38	5.0	48.53	-112.34	1.0	3.5	PDE
2003	2	1	18	44	11.5	43.08	-106.18	5.0	3.7	PDE
2003	2	9	16	18	3.0	46.51	-75.20	18.0	3.3	PDE
2003	3	18	6	4	24.2	33.69	-82.89	5.0	3.5	PDE
2003	4	8	15	6	14.4	44.62	-74.34	10.0	3.7	PDE
2003	4	13	4	52	53.9	26.09	-86.09	10.0	3.2	PDE
2003	4	17	17	31	59.0	39.26	-99.48	5.0	3.0	PDE
2003	4	29	8	59	39.0	34.49	-85.63	19.0	4.9	PDE
2003	4	30	4	56	22.0	35.94	-89.92	23.0	4.0	PDE
2003	5	2	3	25	3.0	36.73	-89.68	1.0	3.0	PDE
2003	5	2	8	10	13.0	37.96	-88.65	0.0	3.1	PDE
2003	5	5	16	32	32.7	37.76	-78.07	5.0	3.9	PDE
2003	5	25	7	32	33.3	43.09	-101.79	5.0	4.0	PDE
2003	5	30	2	18	24.0	36.13	-89.39	6.0	3.0	PDE
2003	6	6	12	29	34.0	36.87	-88.98	2.0	4.0	PDE
2003	6	13	11	34	40.0	47.70	-70.09	11.0	4.1	PDE
2003	6	15	0	22	17.9	36.91	-104.76	5.0	3.6	PDE
2003	6	30	19	21	17.2	41.80	-81.20	4.0	3.6	PDE
2003	7	13	20	15	16.9	32.34	-82.14	5.0	3.6	PDE
2003	7	22	11	41	15.6	42.77	-70.02	11.0	3.6	PDE
2003	8	16	5	9	22.5	36.81	-91.61	5.0	3.9	PDE
2003	8	20	1	58	17.0	46.01	-74.95	18.0	3.5	PDE
2003	8	26	2	26	56.7	37.10	-88.72	5.0	3.2	PDE
2003	8	26	18	24	18.4	40.61	-75.11	3.0	3.8	PDE
2003	9	8	11	2	49.3	37.37	-104.69	5.0	3.0	PDE
2003	9	24	15	2	9.0	35.28	-101.74	5.0	3.3	PDE
2003	9	30	2	28	3.3	31.12	-87.52	5.0	3.3	PDE
2003	10	10	14	48	14.5	23.15	-84.97	10.0	4.4	PDE
2003	10	12	8	26	7.0	47.01	-76.37	18.0	4.5	PDE
2003	10	15	4	13	14.0	45.08	-66.91	18.0	3.1	PDE
2003	10	18	16	25	7.0	46.94	-67.19	18.0	3.5	PDE

© 2007-2012 UniStar Nuclear Services, LLC. All rights reserved.
COPYRIGHT PROTECTED

Table 2.5-1— {Updated Earthquake catalog (1534-April 2010) Including events with $m_b \geq 3.0$}
(Page 72 of 75)

Year	Month	Day	Hour	Min	Sec	Lat (deg)	Lon (deg)	Depth (km)	mb	Source
2003	11	21	1	9	11.6	44.26	-98.78	5.0	3.5	PDE
2003	11	24	7	5	57.7	36.96	-104.83	5.0	3.1	PDE
2003	12	9	20	59	14.1	37.59	-77.90	5.0	4.5	PDE
2003	12	29	9	2	8.6	38.14	-90.17	5.0	3.0	PDE
2004	2	15	3	18	18.0	42.94	-105.40	10.0	3.5	PDE
2004	3	1	9	50	5.8	43.61	-109.80	2.0	3.0	PDE
2004	3	22	12	9	56.4	36.86	-104.85	5.0	4.4	PDE
2004	5	9	8	56	10.4	33.23	-86.96	5.0	3.3	PDE
2004	6	8	0	15	9.9	34.23	-97.25	5.0	3.5	PDE
2004	6	15	8	34	21.0	36.73	-89.68	4.0	3.8	PDE
2004	6	28	6	10	52.1	41.46	-88.90	10.0	4.2	PDE
2004	6	30	4	3	14.5	41.78	-81.08	5.0	3.3	PDE
2004	7	16	3	25	17.0	36.86	-89.18	4.0	3.5	PDE
2004	7	16	12	17	30.6	40.63	-95.55	5.0	3.3	PDE
2004	7	20	9	13	14.4	32.97	-80.25	10.0	3.1	PDE
2004	8	4	23	55	26.6	43.69	-78.25	5.0	3.2	PDE
2004	8	13	1	19	24.3	42.29	-106.96	5.0	3.5	PDE
2004	8	19	23	51	49.4	33.20	-86.97	5.0	3.5	PDE
2004	8	29	18	49	44.2	42.89	-105.49	5.0	3.8	PDE
2004	9	12	13	5	19.1	39.59	-85.80	6.0	3.6	PDE
2004	9	17	15	21	43.6	36.93	-84.01	1.0	3.7	PDE
2004	11	7	11	20	21.4	32.65	-87.93	5.0	4.0	PDE
2004	11	22	23	42	13.4	34.86	-97.67	5.0	3.0	PDE
2004	12	23	6	54	21.0	35.43	-84.20	7.0	3.0	PDE
2005	1	5	15	32	42.0	47.01	-66.57	5.0	3.7	PDE
2005	1	9	13	10	51.9	41.39	-107.35	5.0	3.0	PDE
2005	1	10	10	14	59.1	37.01	-104.68	5.0	3.4	PDE
2005	2	10	14	4	54.0	35.76	-90.25	15.0	4.1	PDE
2005	3	3	2	22	1.0	45.06	-74.20	18.0	3.5	PDE
2005	3	6	6	17	49.0	47.75	-69.73	13.0	5.3	PDE
2005	3	13	17	8	14.0	46.54	-80.98	18.0	3.6	PDE
2005	3	22	8	11	50.5	31.84	-88.06	5.0	3.3	PDE
2005	3	31	15	13	8.0	46.28	-75.64	18.0	3.4	PDE
2005	4	3	14	39	16.9	28.39	-100.31	5.0	3.5	PDE
2005	4	8	4	32	38.0	46.26	-73.45	18.0	3.4	PDE
2005	4	22	5	17	4.0	34.18	-95.19	5.0	3.0	PDE
2005	5	1	12	37	32.0	35.83	-90.15	9.0	4.2	PDE
2005	5	18	19	59	42.9	38.46	-93.97	5.0	3.3	PDE
2005	6	2	11	35	11.0	36.15	-89.47	14.0	3.9	PDE
2005	6	20	12	21	42.0	36.92	-89.00	21.0	3.6	PDE
2005	6	27	15	46	52.0	37.63	-89.42	5.0	3.0	PDE
2005	7	31	7	7	7.9	38.72	-92.73	5.0	3.3	PDE
2005	8	10	22	8	22.6	36.95	-104.83	5.0	5.0	PDE
2005	8	25	3	9	42.0	35.88	-82.80	8.0	3.6	PDE
2005	9	6	14	10	51.0	46.27	-75.29	18.0	3.6	PDE
2005	9	25	3	8	57.9	45.02	-67.20	6.0	3.5	PDE

© 2007-2012 UniStar Nuclear Services, LLC. All rights reserved.
COPYRIGHT PROTECTED

Table 2.5-1— {Updated Earthquake catalog (1534-April 2010) Including events with $m_b \geq 3.0$}
(Page 73 of 75)

Year	Month	Day	Hour	Min	Sec	Lat (deg)	Lon (deg)	Depth (km)	mb	Source
2005	10	1	5	57	3.0	40.58	-106.61	5.0	3.9	PDE
2005	10	12	6	27	30.0	35.51	-84.54	8.0	3.6	PDE
2005	10	19	2	43	46.1	44.08	-97.54	5.0	3.1	PDE
2005	10	20	21	16	28.7	44.68	-80.48	11.0	4.2	PDE
2005	10	27	10	49	19.6	40.03	-107.72	5.0	3.1	PDE
2005	12	11	13	30	38.0	49.27	-112.83	30.0	3.2	PDE-W
2005	12	20	0	52	20.5	30.26	-90.71	5.0	3.0	PDE-W
2005	12	28	17	13	35.0	47.22	-111.74	27.0	3.6	PDE-W
2006	1	2	21	48	57.1	37.80	-88.35	10.0	3.6	PDE-W
2006	1	3	11	5	10.0	49.32	-81.12	19.0	3.7	PDE-W
2006	1	5	14	44	45.0	40.97	-109.98	4.0	3.2	PDE-W
2006	1	9	15	35	39.9	45.03	-73.90	15.0	3.5	PDE-W
2006	1	27	6	47	12.0	39.17	-110.88	0.0	3.8	PDE-W
2006	2	10	4	14	17.8	27.60	-90.16	5.0	4.1	PDE-W
2006	2	10	21	48	13.7	39.59	-107.44	5.0	3.8	PDE-W
2006	2	18	5	49	41.4	35.67	-101.79	5.0	3.5	PDE-W
2006	2	25	1	39	22.0	45.66	-75.23	18.0	4.5	PDE-W
2006	2	26	4	9	22.4	45.55	-74.71	18.0	3.2	PDE-W
2006	3	1	17	42	42.0	37.50	-88.98	6.0	3.0	PDE-W
2006	3	4	2	13	10.7	49.52	-81.58	18.0	3.4	PDE-W
2006	3	11	12	27	15.6	41.78	-81.39	5.0	3.1	PDE-W
2006	3	15	8	30	25.8	35.09	-96.30	5.0	3.0	PDE-W
2006	3	28	23	55	11.4	35.36	-101.87	5.0	3.0	PDE-W
2006	4	5	18	46	23.1	34.07	-97.31	5.0	3.0	PDE-W
2006	4	7	8	31	40.0	47.29	-70.47	0.0	4.1	PDE-W
2006	4	7	12	44	26.7	46.83	-76.62	18.0	3.1	PDE-W
2006	4	11	3	29	21.0	35.36	-84.48	19.0	3.3	PDE-W
2006	4	13	5	50	12.8	40.48	-106.96	1.0	3.3	PDE-W
2006	5	6	17	7	1.3	37.01	-104.77	5.0	3.1	PDE-W
2006	5	9	3	15	3.5	49.99	-66.29	18.0	3.0	PDE-W
2006	5	10	12	17	29.0	35.53	-84.40	24.0	3.2	PDE-W
2006	5	11	6	35	38.5	46.27	-72.68	18.0	3.1	PDE-W
2006	5	26	6	14	25.1	36.80	-104.83	5.0	3.1	PDE-W
2006	5	28	11	20	47.8	49.56	-66.28	18.0	3.6	PDE-W
2006	6	1	9	34	25.7	46.58	-67.45	5.0	3.6	PDE-W
2006	6	16	0	57	27.7	35.52	-83.23	4.0	3.1	PDE-W
2006	6	20	20	11	18.5	41.84	-81.23	5.0	3.8	PDE-W
2006	6	27	20	21	14.1	41.84	-108.73	1.0	3.0	PDE-W
2006	7	14	9	34	49.3	46.93	-68.68	23.0	4.0	PDE-W
2006	8	11	9	2	2.5	44.80	-65.36	5.0	3.2	PDE-W
2006	8	29	11	46	53.6	44.22	-106.29	5.0	3.2	PDE-W
2006	9	7	13	51	13.0	36.27	-89.50	7.0	3.3	PDE-W
2006	9	9	23	14	35.5	37.30	-104.79	5.0	3.6	PDE-W
2006	9	10	14	56	8.1	26.32	-86.61	14.0	5.8	PDE-W
2006	9	22	11	22	0.2	34.55	-79.58	5.0	3.4	PDE-W
2006	9	25	5	44	25.0	34.75	-79.88	5.0	3.7	PDE-W

© 2007-2012 UniStar Nuclear Services, LLC. All rights reserved.
COPYRIGHT PROTECTED

Table 2.5-1— {Updated Earthquake catalog (1534-April 2010) Including events with $m_b \geq 3.0$}
(Page 74 of 75)

Year	Month	Day	Hour	Min	Sec	Lat (deg)	Lon (deg)	Depth (km)	mb	Source
2006	10	3	0	7	38.2	44.35	-68.15	6.0	4.3	PDE-W
2006	10	6	22	13	16.7	34.12	-97.63	5.0	3.5	PDE-W
2006	10	18	20	59	21.0	36.54	-89.64	8.0	3.4	PDE-W
2006	11	2	17	53	2.1	37.20	-81.92	1.0	4.3	PDE-W
2006	11	21	19	37	58.3	38.17	-108.00	5.0	3.3	PDE-W
2006	11	29	7	22	55.1	46.48	-81.17	1.0	4.1	PDE-W
2006	12	7	4	44	59.2	49.52	-81.54	16.0	4.2	PDE-W
2006	12	18	8	34	27.0	35.36	-84.35	17.0	3.3	PDE-W
2006	12	24	11	50	21.4	36.94	-104.75	5.0	3.6	PDE-W
2006	12	29	21	21	10.7	44.35	-68.17	8.0	3.2	PDE-W
2006	12	30	13	53	49.6	49.26	-112.79	20.0	3.5	PDE-W
2007	1	6	4	8	45.0	47.03	-76.23	18.0	3.5	ANSS
2007	2	24	6	50	38.0	47.22	-76.51	18.0	3.0	EC
2007	3	12	23	18	16.0	41.28	-81.38	5.0	3.8	ANSS
2007	5	11	5	55	23.0	46.71	-76.09	18.0	3.3	ANSS
2007	6	2	2	19	55.0	46.09	-74.96	14.6	3.1	ANSS
2007	7	19	17	7	58.0	43.71	-78.19	5.1	3.1	ANSS
2007	7	24	1	56	49.0	42.6	-74.12	15.1	3.2	ANSS
2007	8	30	3	47	46.0	44.32	-74.36	2.2	3.3	ANSS
2007	9	30	17	35	35.0	46.88	-76.52	13.0	4.0	ANSS
2007	10	1	16	42	8.0	47.08	-76.88	18.0	4.2	ANSS
2007	10	13	5	53	32.0	46.53	-75.13	11.0	3.4	ANSS
2007	10	17	20	4	10.0	41.75	-81.42	5.0	3.6	ANSS
2007	10	28	9	47	19.0	46.52	-77.14	3.4	3.5	ANSS
2007	12	12	15	51	21.0	46.3	-75.15	15.0	3.1	ANSS
2007	12	20	12	16	41.0	45.79	-76.96	18.0	3.3	ANSS
2007	12	23	23	48	35.0	46.26	-77.32	18.0	3.8	ANSS
2008	1	9	1	34	47.0	41.72	-81.43	5.0	3.4	ANSS
2008	1	10	6	12	43.0	46.11	-74.82	16.7	3.2	ANSS
2008	3	31	20	3	40.0	46.87	-76.04	18.0	3.1	EC
2008	6	11	4	36	35.0	45.64	-75.39	18.4	3.3	ANSS
2008	8	30	21	52	14.0	46.75	-75.47	10.7	3.2	ANSS
2008	9	11	11	21	49.0	46.48	-81.04	1.0	3.9	ANSS
2008	10	11	2	47	14.0	46.33				ANSS
2008	10	20	8	26	18.0	46.44				ANSS
2008	11	2	7	26	27.0	47.43	-71.44	18.0	3.8	ANSS
2008	12	27	5	4	35.0	40.11	-76.4	3.6	3.4	ANSS
2008	12	31	6	54	49.0	46.15	-75.45	-72.55	5.0	3.1
2009	2	3	3	34	19.0	40.87	-74.53	-75.76	10.5	3.1
2009	4	24	13	42	46.0	38.81	-82.27	5.0	3.5	ANSS
2009	4	29	19	37	8.0	46.85	-71.06	18.0	3.4	PDE
2009	5	8	19	47	2.0	45.49	-75.96	21.2	3.2	ANSS
2009	5	16	8	8	18.0	37.25	-80	12.9	3.1	ANSS
2009	5	18	0	53	30.0	42.57	-74.11	8.6	3.1	ANSS
2009	5	28	9	19	25.0	45.83	-75.83	3.9	3.1	ANSS
2009	6	5	15	7	52.0	42.86	-78.25	18.0	3.4	EC

© 2007-2012 UniStar Nuclear Services, LLC. All rights reserved.
COPYRIGHT PROTECTED

Table 2.5-1— {Updated Earthquake catalog (1534-April 2010) Including events with $m_b \geq 3.0$}

Year	Month	Day	Hour	Min	Sec	Lat (deg)	Lon (deg)	Depth (km)	mb	Source
2009	6	17	8	20	22.0	47.26	-77.14	18.0	3.1	EC
2009	8	19	21	18	39.0	45.4	-73.54	17.1	3.4	ANSS
2009	10	3	6	4	33.0	45.97	-77.02	18.0	3.4	ANSS
2009	11	2	3	16	45.0	46.11	-74.75	3.9	3.6	ANSS
2009	12	13	22	0	51.0	42.57	-74.11	10.2	3.2	ANSS
2010	2	25	22	13	16.0	41.35	-83.41	5.0	3.0	EC
2010	2	28	3	51	25.0	45.73	-74.46	7.4	3.8	ANSS
2010	3	6	13	18	2.0	47.05	-70.92	18.0	3.2	EC
2010	3	6	15	9	24.0	45.97	-75.38	18.0	3.2	EC
2010	3	10	13	9	4.0	45.73	-74.45	18.0	3.3	EC
2010	3	30	20	42	19.0	44.67	-68.75	4.3	4.0	ANSS
2010	4	4	9	19	14.0	38.6	-80.92	0.0	3.4	ANSS
2010	4	5	5	54	12.0	46.17	-72.76	2.5	3.6	ANSS
2010	4	15	7	57	20.0	45.51	-72.49	0.2	5.5	ANSS

© 2007-2012 UniStar Nuclear Services, LLC. All rights reserved.
COPYRIGHT PROTECTED

Table 2.5-2— {Conversion Between Body-Wave (m_b) and Moment (M) Magnitude}

Conversion Model	m_b to M	M to m_b	Weight
Atkinson and Boore 1987	$M = 2.715 - 0.277m_b + 0.127 m_b^2$	$m_b = -4.249 + 3.3935M^2 + 0.0168M^3$	0.333
EPRI 1993	$M=0.3281 + 1.9437m_b-0.43m_b^2+0.0419m_b^3$	$m_b=-10.23+6.105M-0.7632M^2+0.03436M^3$	0.334
Johnston 1996	$M=1.14+0.24m_b+0.0933m_b^2$	$m_b=-0.919+1.7864M-0.1351M^2+0.0052M^3$	0.333
Notes: m_b indicates body wave magnitude M indicates moment magnitude			

© 2007-2012 UniStar Nuclear Services, LLC. All rights reserved.
COPYRIGHT PROTECTED

Table 2.5-3— {Summary of Bechtel Group Seismic Sources}
(Page 1 of 2)

Source	Name	Probability of Activity (Pa)	b-value and Weight	Mmax (mb) and Weight
3	La Malbaie (Charlevoix)	0.8	0.704 [0.33] 0.704 [0.34] 0.713 [0.33]	6.4 [0.10] 6.6 [0.10] 6.7 [0.40] 7.0 [0.40]
8	Clinton-Newberry	0.2	1.199 [0.33] 1.203 [0.34] 1.122 [0.33]	5.7 [0.10] 6.0 [0.40] 6.3 [0.40] 6.6 [0.10]
11	Clarendon-Linden	0.4	0.497 [0.33] 0.498 [0.34] 0.808 [0.33]	5.4 [0.10] 5.7 [0.40] 6.0 [0.40] 6.6 [0.10]
D	Niagara Area	0.35	0.952 [0.33] 0.953 [0.34] 0.998 [0.33]	5.4 [0.10] 5.7 [0.40] 6.0 [0.40] 6.6 [0.10]
13	Mesozoic Basins	0.1	0.991 [0.33] 0.985 [0.34] 1.037 [0.33]	5.4 [0.10] 5.7 [0.40] 6.0 [0.40] 6.6 [0.10]
17	Stafford Fault Zone	0.1	1.862 [0.33] 1.862 [0.34] 1.222 [0.33]	5.4 [0.10] 5.7 [0.40] 6.0 [0.40] 6.6 [0.10]
23	Lebanon Trend	0.05	1.040 [0.33] 1.040 [0.34] 1.040 [0.33]	5.4 [0.10] 5.7 [0.40] 6.0 [0.40] 6.6 [0.10]
24	Bristol Block	0.25	0.844 [0.33] 0.836 [0.34] 0.979 [0.33]	5.7 [0.10] 6.0 [0.40] 6.3 [0.40] 6.6 [0.10]
25	NY-AL Lineament	0.3	1.057 [0.33] 1.055 [0.34] 1.043 [0.33]	5.4 [0.10] 5.7 [0.40] 6.0 [0.40] 6.6 [0.10]
BZ4 (Background)	Atlantic Coastal region	1	1.064 [0.33] 1.090 [0.34] 1.105 [0.33]	6.6 [0.10] 6.8 [0.10] 7.1 [0.40] 7.4 [0.40]
BZ5 (Background)	Southern Appalachian	1	0.912 [0.33] 0.920 [0.34] 0.937 [0.33]	5.7 [0.10] 6.0 [0.40] 6.3 [0.40] 6.6 [0.10]
BZ6 (Background)	Southern Eastern Craton	1	1.074 [0.33] 1.073 [0.34] 1.084 [0.33]	5.4 [0.10] 5.7 [0.40] 6.0 [0.40] 6.6 [0.10]

© 2007-2012 UniStar Nuclear Services, LLC. All rights reserved.
COPYRIGHT PROTECTED

Table 2.5-3— {Summary of Bechtel Group Seismic Sources}
(Page 2 of 2)

Source	Name	Probability of Activity (Pa)	b-value and Weight	Mmax (mb) and Weight
BZ7 (Background)	Northern Eastern Craton	1	1.066 [0.33] 1.075 [0.34] 1.087 [0.33]	6.0 [0.10] 6.3 [0.40] 6.6 [0.50]
BZ8 (Background)	Northern Appalachian	1	1.173 [0.33] 1.128 [0.34] 1.140 [0.33]	5.7 [0.10] 6.0 [0.40] 6.3 [0.40] 6.6 [0.10]

© 2007-2012 UniStar Nuclear Services, LLC. All rights reserved.
COPYRIGHT PROTECTED

Table 2.5-4— {Summary of Dames & Moore Seismic Sources}

Source	Name	Probability of Activity (P_a)	b-value and Weight	M_{max} (m_b) and Weight
3	Adirondacks Zone	0.05	1.043 [0.75] 1.047 [0.25]	6.3 [0.80] 7.2 [0.20]
4 (Default Zone)	Appalachian Fold Belts	0.35	1.042 [0.75] 1.046 [0.25]	6.0 [0.80] 7.2 [0.20]
4A	Kink in Fold Belt	0.65	1.049 [0.75] 1.075 [0.25]	6.8 [0.75] 7.2 [0.25]
4C	Kink in Fold Belt	0.65	1.041 [0.75] 1.045 [0.25]	5.0 [0.75] 7.2 [0.25]
4D	Kink in Fold Belt	0.65	1.048 [0.75] 1.080 [0.25]	5.6 [0.75] 7.2 [0.25]
8	Eastern Marginal Basin	0.08	1.042 [0.75] 1.052 [0.25]	5.6 [0.80] 7.2 [0.20]
9	Clarendon-Linden Zone	0.51	1.035 [0.37] 1.011 [0.12] 1.031 [0.38] 1.004 [0.13]	6.5 [0.75] 7.2 [0.25]
40	Central Virginia Seismic Zone	0.05	1.056 [0.75] 1.090 [0.25]	6.6[0.80] 7.2[0.20]
41 (Default Zone)	Southern Cratonic Margin	0.12	1.035 [0.75] 1.028 [0.25]	6.1 [0.80] 7.2 [0.20]
42	Newark-Gettysburg Basin	0.4	1.015 [0.75] 0.947 [0.25]	6.3 [0.75] 7.2 [0.25]
43	Ramapo Fault Zone	0.2	1.066 [0.75] 1.152 [0.25]	6.1 [0.75] 7.2 [0.25]
47	Connecticut Basin	0.28	1.045 [0.75] 1.063 [0.25]	6.0 [0.75] 7.2 [0.25]
53 (Default Zone)	Southern Appalachian Mobile Belt	0.26	1.043 [0.75] 1.053 [0.25]	5.6 [0.80] 7.2 [0.20]
59	La Malbaie/Charlevoix	0.65	0.63* [1.00]	7.2 [1.00]

* Re-estimated using the updated (1534-April 2010) catalog and Dames and Moore geometry for the source zone.

© 2007-2012 UniStar Nuclear Services, LLC. All rights reserved.
COPYRIGHT PROTECTED

Table 2.5-5— {Summary of Law Engineering Seismic Sources}

Source	Name	Probability of Activity (Pa)	b-value and Weight	Mmax (mb) and Weight
17-Aug	Mesozoic Basins - 17	0.27	1.050 [1.00]	6.8 [1.00]
12	La Malbaie/Chalevoix	1	0.756 [1.00]	6.4 [0.20] 7.4 [0.80]
17	Eastern Basement	0.62	0.992 [1.00]	5.7 [0.20] 6.8 [0.80]
20	Clarendon-Linden	0.7	0.828 [1.00]	5.0 [0.50] 5.5 [0.50]
22	Reactivated E. Seaboard Normal	0.27	1.054 [1.00]	6.8 [1.00]
M15	Mafic Pluton	0.43	0.992 [1.00]*	6.8 [1.00]
M16	Mafic Pluton	0.43	1.040 [1.00]*	6.8 [1.00]
M17	Mafic Pluton	0.43	1.040 [1.00]*	6.8 [1.00]
M18	Mafic Pluton	0.43	1.040 [1.00]*	6.8 [1.00]
M19	Mafic Pluton	0.43	0.992 [1.00]*	6.8 [1.00]
101 (Background)	Western New England	1	0.955 [1.00]	4.5 [0.15] 5.5 [0.85]
107 (Background)	Eastern Piedmont	1	1.042 [1.00]	4.9 [0.30] 5.5 [0.40] 5.7 [0.30]
110 (Background)	Adirondacks	0.9	0.972 [1.00]	5.5 [0.50] 5.7 [0.50]
111 (Background)	Laurentian Block	0.9	0.955 [1.00]	5.5 [0.50] 6.0 [0.50]
112 (Background)	Ohio-Pennsylvania Block	0.85	1.060 [1.00]	4.6 [0.20] 5.1 [0.50] 5.5 [0.30]
217	Eastern Basement Background	0.38	0.992 [1.00]	4.9 [0.50] 5.7 [0.50]
C09	Combination Zone (8-bridged)	NA	1.052 [1.00]	6.8 [1.00]
C11	Combination Zone (22-35)	NA	1.054 [1.00]	6.8 [1.00]

*b-values of “Mafic Plutons” are not provided by LAW EST. The b-value of the backgrounds hosting these zones are presented in the table and used in the hazard analysis.

© 2007-2012 UniStar Nuclear Services, LLC. All rights reserved.
COPYRIGHT PROTECTED

Table 2.5-6— {Summary of Rondout Associates Seismic Sources}

Source	Name	Probability of Activity (P_a)	b-value and Weight	M_{max} (m_b) and Weight
30	Shenandoah	0.96	1.010 [1.00]	5.2 [0.30] 6.3 [0.55] 6.5 [0.15]
31	Quakers	1.00	0.960 [1.00]	5.8 [0.15] 6.5 [0.60] 6.8 [0.25]
33	Niagara	1.00	1.000 [1.00]	5.2 [0.30] 6.3 [0.55] 6.5 [0.15]
34	Nessmuk	1.00	0.920 [1.00]	5.2 [0.30] 6.3 [0.55] 6.5 [0.15]
37	La Malbaie/Charlevoix	1.00	0.700 [1.00]	7.1 [0.10] 7.3 [0.80] 7.4 [0.10]
41	Vermont	1.00	1.100 [1.00]	5.2 [0.30] 6.3 [0.55] 6.5 [0.15]
49-3 (Background)	Appalachian Basement-3	1.00	1.000 [1.00]	4.8 [0.20] 5.5 [0.60] 5.8 [0.20]
50-2 (Background)	Grenville Province-2	1.00	1.010 [1.00]	4.8 [0.20] 5.5 [0.60] 5.8 [0.20]

© 2007-2012 UniStar Nuclear Services, LLC. All rights reserved.
COPYRIGHT PROTECTED

Table 2.5-7— {Summary of Weston Geophysical Seismic Sources}

Source	Name	Probability of Activity (P_a)	b-value and Weight	M_{max} (m_b) and Weight
1	La Malbaie/Charlevoix	1.00	0.790 [1.00]	7.2 [1.00]
6	Adirondack Mountains	1.00	0.933 [0.50] 0.936 [0.50]	5.4 [0.38] 6.0 [0.46] 6.6 [0.16]
7	Niagara Peninsula	0.36	0.911 [1.00]	5.4 [0.62] 6.0 [0.29] 6.6 [0.09]
8	Clarendon-Linden Faults	0.83	0.846 [1.00]	5.4 [0.26] 6.0 [0.50] 6.6 [0.24]
10	Hudson Valley	1.00	0.847 [1.00]	5.4 [0.51] 6.0 [0.33] 6.6 [0.16]
10-A	Hudson Valley	0.54	1.083 [1.00]	5.4 [0.65] 6.0 [0.25] 6.6 [0.10]
19	Moodus	1.00	1.608 [1.00]	5.4 [0.56] 6.0 [0.32] 6.6 [0.12]
20	Western New England Fold Belt	1.00	0.929 [1.00]	5.4 [0.62] 6.0 [0.29] 6.6 [0.09]
21	New York Nexus	1.00	0.934 [1.00]	5.4 [0.62] 6.0 [0.29] 6.6 [0.09]
28-A	Zone of Mesozoic Basin	0.26	0.899 [1.00]	5.4 [0.65] 6.0 [0.25] 6.6 [0.10]
28-B	Zone of Mesozoic Basin	0.26	0.854 [1.00]	5.4 [0.65] 6.0 [0.25] 6.6 [0.10]
28-E	Zone of Mesozoic Basin	0.26	0.918 [1.00]	5.4 [0.65] 6.0 [0.25] 6.6 [0.10]
101 (Background)	S. Ontario-Ohio-Indiana	1.00	1.005 [0.20] 1.007 [0.80]	5.4 [0.19] 6.0 [0.68] 6.6 [0.13]
102 (Background)	Appalachian Plateau	1.00	1.007 [0.20] 1.007 [0.80]	5.4 [0.62] 6.0 [0.29] 6.6 [0.09]
103 (Background)	Southern Appalachian	1.00	0.993 [0.20] 0.996 [0.80]	5.4 [0.26] 6.0 [0.58] 6.6 [0.16]
104 (Background)	Southern Coastal Plain	1.00	0.997 [0.20] 0.997 [0.80]	5.4 [0.24] 6.0 [0.61] 6.6 [0.15]

© 2007-2012 UniStar Nuclear Services, LLC. All rights reserved.
COPYRIGHT PROTECTED

Table 2.5-8— {Summary of Woodward-Clyde Consultants Seismic Sources}

(Page 1 of 2)

Source	Name	Probability of Activity (Pa)	b-value and Weight	Mmax (mb) and Weight
10	Moodus Seismic Zone	0.900	1.229 [0.10]	5.7 [0.33]
			1.174 [0.33]	6.3 [0.34]
			1.121 [0.57]	6.9 [0.33]
12	La Malbaie/Charlevoix	0.894	0.65*[1.00]	6.5 [0.33]
				7.0 [0.34]
				7.5 [0.33]
18	Adirondack Dome/Uplift	0.288	1.006 [0.25]	5.4 [0.33]
			1.001[0.25]	6.3 [0.34]
			0.930 [0.25]	6.9 [0.33]
			0.861 [0.25]	
20-A	Mohawk River Trend	0.090	1.010 [0.33]	5.5 [0.33]
			0.922 [0.34]	6.0 [0.34]
			0.836 [0.33]	7.0 [0.33]
21	New Jersey Isostatic Gravity Saddle	0.135	0.781 [0.25]	5.3 [0.33]
			0.950 [0.25]	6.5 [0.34]
			0.873 [0.25]	6.9 [0.33]
			0.798 [0.25]	
21A	New Jersey Isostatic Gravity Saddle	0.045	0.638 [0.25]	5.5 [0.33]
			0.914 [0.25]	6.3 [0.34]
			0.835 [0.25]	6.9 [0.33]
			0.758 [0.25]	
22	Newark Basin	0.075	0.518 [0.25]	5.5 [0.33]
			0.852 [0.25]	6.5 [0.34]
			0.780 [0.25]	7.1 [0.33]
			0.708 [0.25]	
23	Newark Basin Perimeter	0.359	0.766 [0.25]	5.5 [0.33]
			0.920 [0.25]	6.3 [0.34]
			0.852 [0.25]	6.8 [0.33]
			0.786 [0.25]	
24	Ramapo Fault Zone	0.123	0.828 [0.33]	5.8 [0.33]
			0.760 [0.34]	6.8 [0.34]
			0.693 [0.33]	7.1 [0.33]
25	Hudson River Trend	0.137	1.201 [0.25]	5.5 [0.33]
			1.056 [0.25]	6.3 [0.34]
			0.989 [0.25]	6.8 [0.33]
			0.926 [0.25]	
33	Western New York-S. Ontario Seismic Zone	0.418	0.951 [0.25]	5.5 [0.33]
			0.977 [0.25]	6.5 [0.34]
			0.924 [0.25]	7.0 [0.33]
			0.873 [0.25]	
34	Attica, New York Intersection	0.471	0.780 [0.33]	5.6 [0.33]
			0.725 [0.34]	6.3 [0.34]
			0.672 [0.33]	7.4 [0.33]
53	New York-New Jersey-E. Pennsylvania Default	0.120	0.782 [0.25]	5.5 [0.33]
			0.935 [0.25]	6.3 [0.34]
			0.863 [0.25]	6.8 [0.33]
			0.795 [0.25]	

© 2007-2012 UniStar Nuclear Services, LLC. All rights reserved.
COPYRIGHT PROTECTED

Table 2.5-8— {Summary of Woodward-Clyde Consultants Seismic Sources}
(Page 2 of 2)

Source	Name	Probability of Activity (Pa)	b-value and Weight	Mmax (mb) and Weight
61	Pittsburg-Washington Lineament	0.037	1.030 [0.33]	5.4 [0.33]
			0.939 [0.34]	6.5 [0.34]
			0.850 [0.33]	7.1 [0.33]
63	Tyrone-Mt. Union Lineament	0.042	0.997 [0.33]	5.4 [0.33]
			0.904 [0.34]	6.3 [0.34]
			0.811 [0.33]	7.1 [0.33]
BZ16	Susquehanna Background	1.00	0.924 [0.25]	4.9 [0.17]
			0.993 [0.25]	5.4 [0.28]
			0.903 [0.25]	5.8 [0.27]
			0.814 [0.25]	6.5 [0.28]

* Re-estimated using the updated (1534-April 2010) catalog and Woodward-Clyde geometry for the source zone.

© 2007-2012 UniStar Nuclear Services, LLC. All rights reserved.
COPYRIGHT PROTECTED

Table 2.5-9— {Alternative New Madrid Fault Locations}
(Metric Units)

Fault arm	New Madrid South		Reelfoot		New Madrid North		Combined Weight
Faults set	Distance to Site (km)	Weight	Distance to Site (km)	Weight	Distance to Site (km)	Weight	
1	1268	0.6	1259	0.7	1213	0.7	0.294
2					1185	0.3	0.126
3			1259	0.3	1213	0.7	0.126
4					1185	0.3	0.054
5	1280	0.4	1259	0.7	1213	0.7	0.196
6					1185	0.3	0.084
7			1259	0.3	1213	0.7	0.084
8					1185	0.3	0.036

© 2007-2012 UniStar Nuclear Services, LLC. All rights reserved.
COPYRIGHT PROTECTED

Table 2.5-9— {Alternative New Madrid Fault Locations}
(SI Units)

Fault arm	New Madrid South		Reelfoot		New Madrid North		Combined Weight
Faults set	Distance to Site (mile)	Weight	Distance to Site (mile)	Weight	Distance to Site (mile)	Weight	
1	788	0.6	782	0.7	754	0.7	0.294
2					736	0.3	0.126
3			782	0.3	754	0.7	0.126
4					736	0.3	0.054
5	796	0.4	782	0.7	754	0.7	0.196
6					736	0.3	0.084
7			782	0.3	754	0.7	0.084
8					736	0.3	0.036

© 2007-2012 UniStar Nuclear Services, LLC. All rights reserved.
COPYRIGHT PROTECTED

Table 2.5-10— {Earthquake Frequencies for Repeating New Madrid Earthquake Sequences}

Rupture Set	Weight	Magnitude, M			Weight	Rupture Model	Weight	Combined Weight
		NMS	RF	NMN				
1	0.1667	7.8	7.7	7.5	1	A	0.667	0.1112
		7.8	7.7	7.5	0.333	B	0.333	0.0185
		7.3	7.7	7.5	0.333			0.0185
		7.8	7.7	7.0	0.333			0.0185
2	0.1667	7.9	7.8	7.6	1	A	0.667	0.1112
		7.9	7.8	7.6	0.333	B	0.333	0.0185
		7.4	7.8	7.6	0.333			0.0185
		7.9	7.8	7.1	0.333			0.0185
3	0.2500	7.6	7.8	7.5	1	A	0.667	0.1668
		7.6	7.8	7.5	0.333	B	0.333	0.0277
		7.1	7.8	7.5	0.333			0.0277
		7.6	7.8	7.0	0.333			0.0277
4	0.0833	7.2	7.4	7.2	1	A	0.667	0.0556
		7.2	7.4	7.2	0.333	B	0.333	0.0092
		7.0	7.4	7.2	0.333			0.0092
		7.2	7.4	7.2	0.333			0.0092
5	0.1667	7.2	7.4	7.0	1	A	0.667	0.1112
		7.2	7.4	7.0	0.333	B	0.333	0.0185
		7.0	7.4	7.0	0.333			0.0185
		7.2	7.4	7.0	0.333			0.0185
6	0.1667	7.3	7. 5	7.0	1	A	0.667	0.1112
		7.3	7.5	7.0	0.333	B	0.333	0.0185
		7.0	7.5	7.0	0.333			0.0185
		7.3	7.5	7.0	0.333			0.0185

Notes:
1) Adapted from the Seismic Hazards Report for the EGC ESP Site
See Table 4.1-2 of Appendix B (EGC, 2006)
2) NMS indicates New Madrid South Arm
3) RF indicates New Madrid Reelfoot Arm
4) NMN indicates New Madrid North Arm

© 2007-2012 UniStar Nuclear Services, LLC. All rights reserved.
COPYRIGHT PROTECTED

Table 2.5-11— {Controlling Earthquakes for BBNPP}

Mean Annual Frequency of Exceedance and Spectral Frequency Range	Reference Earthquake		Deaggregation Earthquake			
	Magnitude (M)	Distance (km [mi])	ID	Magnitude (M)	Distance (km [mi])	Weight
1E-4 Average of 1 and 2.5 Hz	7.3	686 [426]	DEL	6.0	53 [33]	0.466
			DEM	7.5	864 [537]	0.247
			DEH	7.5	1236 [768]	0.287
1E-4 Average of 5 and 10 Hz	5.8	46 [29]	DEL	5.3	12 [7]	0.377
			DEM	5.9	79 [49]	0.561
			DEH	7.5	1007 [626]	0.062
1E-5 Average of 1 and 2.5 Hz	7.4	709 [441]	DEL	6.1	28 [17]	0.606
			DEM	7.7	858 [533]	0.149
			DEH	7.5	1236 [768]	0.245
1E-5 Average of 5 and 10 Hz	5.6	15 [9]	DEL	5.4	10 [6]	0.776
			DEM	6.3	62 [39]	0.217
			DEH	7.7	973 [605]	0.007

Note:

Distance ranges for low spectral frequency range (1 to 2.5 Hz) controlling earthquakes are:

DEL – 0 to 500 km

DEM – 500 to 1000 km

DEH – 1000 to 3000 km

REF – >100 km

Distance ranges for high spectral frequency range (5 to 10 Hz) controlling earthquakes are:

DEL – 0 to 25 km

DEM – 25 to 500 km

DEH – >500 km

REF – > 0 km

© 2007-2012 UniStar Nuclear Services, LLC. All rights reserved.
COPYRIGHT PROTECTED

Table 2.5-12— {Recommended Horizontal and Vertical SSE Amplitudes and common V/H Ratio}

Freq (Hz)	Horizontal SSE (g)	Vertical SSE (g)	V/H
0.1000	0.0015	0.0010	0.6667
0.1269	0.0027	0.0018	0.6667
0.1610	0.0052	0.0034	0.6667
0.2043	0.0099	0.0066	0.6667
0.2593	0.0170	0.0117	0.6896
0.3290	0.0282	0.0201	0.7133
0.4175	0.0434	0.0320	0.7378
0.5298	0.0604	0.0461	0.7631
0.6723	0.0650	0.0513	0.7894
0.8532	0.0688	0.0562	0.8165
1.0826	0.0799	0.0675	0.8446
1.3738	0.1118	0.0977	0.8736
1.7433	0.1593	0.1439	0.9036
2.2122	0.2321	0.2169	0.9347
2.8072	0.3481	0.3366	0.9668
3.5622	0.5010	0.5010	1.0000
4.5204	0.5260	0.5260	1.0000
5.7362	0.4183	0.4183	1.0000
7.2790	0.3986	0.3986	1.0000
9.2367	0.4495	0.4495	1.0000
11.7210	0.4965	0.4965	1.0000
14.8741	0.5077	0.5077	1.0000
18.8740	0.5131	0.5131	1.0000
23.9498	0.4599	0.4599	1.0000
30.3924	0.3962	0.3962	1.0000
38.5654	0.3425	0.3425	1.0000
48.9380	0.2789	0.2789	1.0000
62.1002	0.2337	0.2337	1.0000
78.8022	0.2005	0.2005	1.0000
100.0000	0.1809	0.1809	1.0000

© 2007-2012 UniStar Nuclear Services, LLC. All rights reserved.
COPYRIGHT PROTECTED

Table 2.5-13— {Amplification Factors for 10^{-4} and 10^{-5} Input Motions and HF and LF Rock Spectra}

Mean Frequency of Exceedence: 10^{-4}								
	LF				HF			
	DEL	DEM	DEH		DEL	DEM	DEH	
Frequency,	weights				weights			
Hz	0.4660	0.2470	0.2870	Average	0.3770	0.5610	0.0623	Average
0.1000	1.0766	1.0780	2.0705	1.3622	1.2508	1.0566	1.3642	1.1493
0.1269	1.0551	1.0599	2.0604	1.3448	1.1672	1.0461	1.2714	1.1061
0.1610	1.0385	1.0856	2.0610	1.3436	1.1099	1.0511	1.1393	1.0791
0.2043	1.0622	1.0580	1.8439	1.2855	1.1130	1.0622	1.1331	1.0861
0.2593	1.0582	1.0749	1.6877	1.2430	1.0800	1.0698	1.0922	1.0753
0.3290	1.0713	1.0922	1.6677	1.2476	1.1342	1.0608	1.1090	1.0918
0.4175	1.0873	1.1275	1.5046	1.2170	1.1377	1.0619	1.1021	1.0933
0.5298	1.1359	1.1367	1.4440	1.2245	1.1506	1.1363	1.1293	1.1416
0.6723	1.1545	1.1327	1.4280	1.2276	1.2568	1.1683	1.1407	1.2003
0.8532	1.1420	1.1535	1.4815	1.2423	1.1452	1.1511	1.1822	1.1512
1.0826	1.2667	1.1936	1.4513	1.3017	1.2355	1.2599	1.1731	1.2457
1.3738	1.3618	1.3064	1.5312	1.3967	1.3815	1.3266	1.3202	1.3473
1.7433	1.5707	1.4991	1.7348	1.6001	1.5536	1.4690	1.4661	1.5011
2.2122	1.8547	1.7631	2.0919	1.9002	1.8893	1.8260	1.8445	1.8516
2.8072	2.6530	2.4939	2.8145	2.6601	2.4562	2.3714	2.6038	2.4186
3.5622	3.9809	3.6799	4.1698	3.9608	3.5990	3.7395	3.7372	3.6875
4.5204	4.1311	4.6647	4.1310	4.2629	4.1979	4.7518	4.6059	4.5353
5.7362	3.1429	3.6794	2.8491	3.1911	3.6327	3.6548	3.4906	3.6373
7.2790	2.0598	2.5036	1.9168	2.1284	2.2839	2.3242	2.2797	2.3069
9.2367	1.7893	1.7179	1.7155	1.7505	1.7602	1.7248	1.8325	1.7454
11.7210	1.9796	2.2008	2.0316	2.0492	2.1917	2.1826	2.1724	2.1861
14.8741	1.9563	2.2201	1.8180	1.9818	2.3829	2.2118	2.1742	2.2746
18.8740	1.6743	1.9705	1.7538	1.7703	1.9313	1.9115	1.9321	1.9208
23.9498	1.4834	1.7732	1.4728	1.5519	1.6810	1.7651	1.7595	1.7335
30.3924	1.3172	1.6411	1.3763	1.4142	1.5496	1.5450	1.6510	1.5538
38.5654	1.2428	1.5141	1.2878	1.3227	1.4228	1.4212	1.5122	1.4279
48.9380	1.1388	1.5363	1.2615	1.2722	1.3339	1.2797	1.5353	1.3164
62.1002	1.1931	1.6425	1.4445	1.3762	1.3153	1.3532	1.7017	1.3610
78.8022	1.4251	1.9851	1.7799	1.6653	1.4199	1.5532	2.0671	1.5355
100.0000	1.6683	2.3156	2.0050	1.9248	1.6347	1.8182	2.3123	1.7803

Note: Distance range of each event
DEL: Low distance range
DEM: Medium distance range
DEH: High distance range

© 2007-2012 UniStar Nuclear Services, LLC. All rights reserved.
COPYRIGHT PROTECTED

Table 2.5-13— {Amplification Factors for 10^{-4} and 10^{-5} Input Motions and HF and LF Rock Spectra}

Mean Frequency of Exceedence: 10^{-5}								
	LF				**HF**			
	DEL	**DEM**	**DEH**		**DEL**	**DEM**	**DEH**	
Frequency	**weights**				**weights**			
(Hz)	**0.6060**	**0.1490**	**0.2450**	**Average**	**0.7760**	**0.2160**	**0.0074**	**Average**
0.1000	1.0478	1.0892	2.0773	1.3062	1.1493	1.0560	1.2036	1.1289
0.1269	1.0310	1.0987	1.9199	1.2589	1.0836	1.0413	1.1782	1.0746
0.1610	1.0338	1.0792	2.0335	1.2855	1.0428	1.0707	1.1574	1.0491
0.2043	1.0305	1.0801	1.9205	1.2560	1.0614	1.0438	1.0964	1.0572
0.2593	1.0230	1.0876	1.6921	1.1965	1.1038	1.0735	1.1210	1.0968
0.3290	1.0355	1.0870	1.6636	1.1971	1.1298	1.0901	1.1527	1.1208
0.4175	1.0638	1.1327	1.5168	1.1851	1.1510	1.0906	1.1755	1.1375
0.5298	1.0927	1.1221	1.5607	1.2118	1.0986	1.0862	1.1919	1.0960
0.6723	1.1839	1.1558	1.5362	1.2660	1.2358	1.1348	1.2342	1.2133
0.8532	1.2379	1.2103	1.4861	1.2946	1.2255	1.2081	1.2580	1.2213
1.0826	1.2661	1.2996	1.6278	1.3597	1.4103	1.2543	1.3279	1.3752
1.3738	1.4887	1.4324	1.6887	1.5293	1.5227	1.4728	1.5751	1.5115
1.7433	1.7729	1.7611	2.1466	1.8627	1.8528	1.8383	1.9546	1.8494
2.2122	2.5042	2.1961	2.7762	2.5249	2.3551	2.3916	2.6280	2.3637
2.8072	3.0869	3.2831	3.5243	3.2233	3.2967	3.2247	3.3913	3.2800
3.5622	3.5975	3.7466	3.1587	3.5122	3.7405	3.3158	3.0017	3.6412
4.5204	2.5446	3.1539	2.2952	2.5743	2.9329	2.7451	2.4052	2.8868
5.7362	1.8705	2.2431	1.5781	1.8544	1.8798	1.8622	1.6619	1.8733
7.2790	1.5059	1.7028	1.4153	1.5130	1.5802	1.5001	1.4023	1.5607
9.2367	1.4470	1.5106	1.3124	1.4235	1.6649	1.4501	1.3523	1.6152
11.7210	1.3609	1.6084	1.2194	1.3631	1.4625	1.2979	1.2753	1.4247
14.8741	1.1690	1.4857	1.0732	1.1927	1.2252	1.2010	1.1374	1.2186
18.8740	1.0002	1.3071	0.9813	1.0413	1.1450	1.0777	1.0191	1.1289
23.9498	0.8362	1.1315	0.8311	0.8790	0.9249	0.9264	0.8817	0.9244
30.3924	0.7127	1.0552	0.7658	0.7768	0.7636	0.7209	0.8146	0.7544
38.5654	0.6905	0.9735	0.7290	0.7421	0.7097	0.7303	0.7890	0.7143
48.9380	0.6453	0.9944	0.7407	0.7207	0.6316	0.7114	0.8039	0.6498
62.1002	0.7082	1.1172	0.9168	0.8202	0.6852	0.7680	0.9520	0.7047
78.8022	0.8834	1.4294	1.1234	1.0236	0.8038	0.9650	1.2118	0.8412
100.0000	1.0523	1.5833	1.2920	1.1901	0.9566	1.1561	1.3783	1.0023
Note: Distance range of each event DEL: Low distance range DEM: Medium distance range DEH: High distance range								

© 2007-2012 UniStar Nuclear Services, LLC. All rights reserved.
COPYRIGHT PROTECTED

Table 2.5-14— {Uniform Hazard Response Spectra (Hard Rock Conditions)}

Frequency (Hz)	10^{-4} SA, g		10^{-5} SA, g		10^{-6} SA, g	
	Mean	Median	Mean	Median	Mean	Median
0.5	0.0337	0.018	0.1027	0.041	0.2225	0.084
1	0.0425	0.029	0.1097	0.069	0.2381	0.147
2.5	0.0743	0.061	0.2033	0.171	0.5192	0.412
5	0.12	0.109	0.3822	0.347	1.064	0.894
10	0.1739	0.164	0.6154	0.574	1.787	1.51
25	0.2606	0.223	0.9573	0.827	3.138	2.177
100	0.0899	0.082	0.3456	0.314	1.111	0.0808

© 2007-2012 UniStar Nuclear Services, LLC. All rights reserved.
COPYRIGHT PROTECTED

Table 2.5-15— {Earthquake Frequencies for Repeating New Madrid Earthquake Sequences}

Model	Weight of model	Mean repeat time (years)	Equivalent annual frequency, $?_{rate\ of\ cluster}$	Weight of $?_{rate\ of\ cluster}$	Combined weight, w_c	$?_{rate\ of\ cluster}$ times w_c
Poisson	0.5	161	6.20E-03	0.10108	0.05054	0.00031
		262	3.82E-03	0.24429	0.12215	0.00047
		410	2.44E-03	0.30926	0.15463	0.00038
		694	1.44E-03	0.24429	0.12215	0.00018
		1563	6.40E-04	0.10108	0.05054	0.00003
Renewal a = 0.3	0.5x0.2 = 0.1	333	3.39E-03	0.10108	0.01011	0.00003
		410	1.07E-03	0.24429	0.02443	0.00003
		485	3.02E-04	0.30926	0.03093	0.00001
		574	5.95E-05	0.24429	0.02443	0.00000
		709	4.30E-06	0.10108	0.01011	0.00000
Renewal a = 0.5	0.5x0.5 = 0.25	316	4.85E-03	0.10108	0.02527	0.00012
		440	2.18E-03	0.24429	0.06107	0.00013
		573	8.89E-04	0.30926	0.07732	0.00007
		746	2.58E-04	0.24429	0.06107	0.00002
		1032	2.97E-05	0.10108	0.02527	0.00000
Renewal a = 0.7	0.5x0.3 0.15	325	4.45E-03	0.10108	0.01516	0.00007
		506	2.25E-03	0.24429	0.03664	0.00008
		719	1.02E-03	0.30926	0.04639	0.00005
		1011	3.37E-04	0.24429	0.03664	0.00001
		1521	4.49E-05	0.10108	0.01516	0.00000
sums	1.00				1.00	0.00199
				Average return period =	503	years

Note:
Adapted from the Seismic Hazards Report for the Clinton ESP Site
See Figure 4.1-1 and Table 4.1-3 (EGC 2006)

© 2007-2012 UniStar Nuclear Services, LLC. All rights reserved.
COPYRIGHT PROTECTED

Table 2.5-16— {USGS 2008 Seismicity Smoothing Models}

Model	Incompleteness Year	Minimum Magnitude, m_b	Correlation Distance		Weight	
			km	mile	Main Source	Background
1	1924	3.0	50	31	0.50	0.40
2	1860	4.0	75	47	0.25	0.20
3	1700	5.0	75	47	0.25	0.20
4	Uniformly distributed		-	-	-	0.20

© 2007-2012 UniStar Nuclear Services, LLC. All rights reserved.
COPYRIGHT PROTECTED

Table 2.5-17— {Seed Time Histories Selected for Controlling Deaggregation Earthquakes}

1E-4 Annual Frequency of Exceedance, Response Spectral Frequency Range: 5 to 10 Hz								
Controlling Deaggregation Earthquake				Seed Time History				
Identification	Magnitude (M)	Distance (km)	Distance (mi)	Earthquake	Station	Magnitude (M)	Distance (km)	Distance (mi)
DEL	5.3	12	7	Coalinga	Anticline Ridge Free-Field	5.2	11	6.8
				North Palm Springs	Hurkey Creek Park	6.0	34.9	21.7
DEM	5.9	78	49	North Palm Springs	Puerta La Cruz	6.0	71.9	44.7
				San Fernando	Cedar Springs, Allen Ranch	6.6	86.6	53.8
DEH	7.5	1007	626	Landers	Sun Valley – Sunland	7.3	162.6	101.0
				Borrego Mountain	San Onofre – So Cal Edison	6.8	124.7	77.5

© 2007-2012 UniStar Nuclear Services, LLC. All rights reserved.
COPYRIGHT PROTECTED

Table 2.5-17— {Seed Time Histories Selected for Controlling Deaggregation Earthquakes}

1E-4 Annual Frequency of Exceedance, Response Spectral Frequency Range: 1 to 2.5 Hz								
Controlling Deaggregation Earthquake				Seed Time History				
Identification	Magnitude (M)	Distance (km)	Distance (mi)	Earthquake	Station	Magnitude (M)	Distance (km)	Distance (mi)
DEL	6.0	53	33	Whittier Narrows	Riverside Airport	6.0	56.8	35.3
				Northridge	Duarte Mel Canyon Rd.	6.7	51.6	32.1
DEM	7.5	864	537	Landers	Calabasas – N Las Virg	7.3	194.1	120.6
				Borrego Mountain	San Onofre – So Cal Edison	6.8	124.7	77.5
DEH	7.5	1236	768	Landers	Sun Valley – Sunland	7.3	162.6	101.0
				Landers	Calabasas – N Las Virg	7.3	194.1	120.6

© 2007-2012 UniStar Nuclear Services, LLC. All rights reserved.
COPYRIGHT PROTECTED

Table 2.5-17— {Seed Time Histories Selected for Controlling Deaggregation Earthquakes}

1E-5 Annual Frequency of Exceedance, Response Spectral Frequency Range: 5 to 10 Hz								
Controlling Deaggregation Earthquake				Seed Time History				
Identification	Magnitude (M)	Distance (km)	Distance (mi)	Earthquake	Station	Magnitude (M)	Distance (km)	Distance (mi)
DEL	5.4	10	6	Coalinga	Palmer Ave	5.2	12.2	7.6
				Lytle Creek	Wrightwood – 6074 Park Dr	5.4	15.4	9.6
DEM	6.3	62	39	North Palm Springs	Santa Rosa Mountain	6.0	43.8	27.2
				Northridge	Rancho Palos Verdes Hawth	6.7	55.2	34.3
DEH	7.7	973	605	Landers	Sun Valley – Sunland	7.3	162.6	101.0
				Borrego Mountain	San Onofre – So Cal Edison	6.8	124.7	77.5

© 2007-2012 UniStar Nuclear Services, LLC. All rights reserved.
COPYRIGHT PROTECTED

Table 2.5-17— {Seed Time Histories Selected for Controlling Deaggregation Earthquakes}

1E-5 Annual Frequency of Exceedance, Response Spectral Frequency Range: 1 to 2.5 Hz								
Controlling Deaggregation Earthquake				Seed Time History				
Identification	Magnitude (M)	Distance (km)	Distance (mi)	Earthquake	Station	Magnitude (M)	Distance (km)	Distance (mi)
DEL	6.1	28	17	North Palm Springs	Hurkey Creek Park	6.0	34.9	21.7
				San Fernando	Lake Hughes #4	6.6	24.2	15.0
DEM	7.7	858	533	Landers	Calabasas – N Las Virg	7.3	194.1	120.6
				Borrego Mountain	San Onofre – So Cal Edison	6.8	124.7	77.5
DEH	7.5	1236	768	Landers	Sun Valley – Sunland	7.3	162.6	101.0
				Landers	Calabasas – N Las Virg	7.3	194.1	120.6

© 2007-2012 UniStar Nuclear Services, LLC. All rights reserved.
COPYRIGHT PROTECTED

Table 2.5-18— Comparison of Post-EPRI NP-6395-D 1989 Magnitude Estimates for the 1886 Charleston Earthquake

Study	Magnitude Estimation Method	Reported Magnitude Estimate	Assigned Weights	Mean Magnitude (M)
EPRI (1994)	worldwide survey of passive-margin, extended-crust earthquakes	**M**7.56 ± 0.35	--	7.56
Martin (1994)	geotechnical assessment of 1886 liquefaction data	**M**7 - 7.5	--	7.25
Johnston (1996)	isoseismal area regression, accounting for eastern North America anelastic attenuation	**M**7.3 ± 0.26	--	7.3
Chapman (2002) (South Carolina Department of Transportation)	consideration of available magnitude estimates	**M**7.1 **M**7.3 **M**7.5	0.2 0.6 0.2	7.3
Frankel et al., (2002) (USGS National seismic hazard mapping project)	consideration of available magnitude estimates	**M**6.8 **M**7.1 **M**7.3 **M**7.5	0.20 0.20 0.45 0.15	7.2
Bakun (2004)	isoseismal area regression, including empirical site corrections	$\mathbf{M}_I$ 6.4 - 7.2	--	6.9
95% confidence interval estimate; MI (intensity magnitude) is considered equivalent to **M** (Bakun and Hopper 2004) Adopted from the Seismic Hazard Report for CCNPP Unit 3 FSAR 2007				

© 2007-2012 UniStar Nuclear Services, LLC. All rights reserved.
COPYRIGHT PROTECTED

Table 2.5-19— {Mean and Fractile Rock Hazard Curves for PGA}

Ground Motion Level (g)	Annual probability of Exceedance					
	Mean	5 % Fractile	16 % Fractile	50 % Fractile	84 % Fractile	95 % Fractile
0.01	3.53E-03	1.05E-03	1.68E-03	2.94E-03	5.17E-03	7.42E-03
0.03	9.16E-04	1.84E-04	3.57E-04	7.14E-04	1.42E-03	2.30E-03
0.05	2.81E-04	4.65E-05	1.05E-04	2.31E-04	4.43E-04	7.19E-04
0.08	1.37E-04	2.10E-05	4.92E-05	1.17E-04	2.25E-04	3.48E-04
0.10	8.32E-05	1.22E-05	2.85E-05	7.23E-05	1.42E-04	2.12E-04
0.20	2.55E-05	2.94E-06	7.13E-06	2.23E-05	4.80E-05	7.12E-05
0.30	1.28E-05	1.08E-06	2.76E-06	1.10E-05	2.58E-05	3.93E-05
0.40	7.75E-06	4.19E-07	1.23E-06	6.05E-06	1.63E-05	2.55E-05
0.50	5.18E-06	1.95E-07	5.94E-07	3.62E-06	1.12E-05	1.81E-05
0.60	3.68E-06	1.07E-07	3.22E-07	2.25E-06	7.98E-06	1.35E-05
0.70	2.72E-06	5.64E-08	1.96E-07	1.50E-06	5.82E-06	1.04E-05
0.80	2.07E-06	3.12E-08	1.28E-07	1.03E-06	4.38E-06	8.25E-06
0.90	1.61E-06	1.84E-08	8.40E-08	7.24E-07	3.34E-06	6.63E-06
1.00	1.28E-06	1.09E-08	5.40E-08	5.26E-07	2.62E-06	5.45E-06
1.25	7.58E-07	3.21E-09	1.98E-08	2.58E-07	1.49E-06	3.36E-06
1.50	4.80E-07	1.07E-09	8.25E-09	1.34E-07	9.08E-07	2.16E-06
2.00	2.16E-07	1.83E-10	1.89E-09	4.13E-08	3.67E-07	9.67E-07
2.75	7.94E-08	1.93E-11	2.78E-10	1.00E-08	1.15E-07	3.56E-07
3.50	3.39E-08	3.01E-12	5.52E-11	3.02E-09	4.45E-08	1.59E-07
5.00	8.26E-09	1.57E-13	4.12E-12	4.21E-10	9.34E-09	4.02E-08

© 2007-2012 UniStar Nuclear Services, LLC. All rights reserved.
COPYRIGHT PROTECTED

Table 2.5-20— {Mean and Fractile Rock Hazard Curves for 25 Hz}

Ground motion level (g)	Annual Probability of Exceedance					
	Mean	5% Fractile	16% Fractile	50% Fractile	84% Fractile	95% Fractile
0.01	1.37E-03	2.74E-04	4.79E-04	1.05E-03	2.23E-03	3.26E-03
0.03	2.93E-04	2.32E-05	4.69E-05	1.45E-04	5.18E-04	1.11E-03
0.05	7.17E-05	2.52E-06	5.71E-06	2.40E-05	9.66E-05	2.88E-04
0.08	2.76E-05	5.54E-07	1.50E-06	7.95E-06	3.26E-05	1.04E-04
0.10	1.31E-05	1.69E-07	5.63E-07	3.58E-06	1.53E-05	4.66E-05
0.20	1.72E-06	6.44E-09	3.17E-08	3.61E-07	2.63E-06	7.54E-06
0.30	4.87E-07	6.87E-10	4.38E-09	7.71E-08	9.37E-07	2.61E-06
0.40	2.02E-07	1.18E-10	9.21E-10	2.62E-08	4.48E-07	1.18E-06
0.50	1.04E-07	2.59E-11	2.47E-10	1.01E-08	2.37E-07	6.59E-07
0.60	6.09E-08	7.16E-12	8.34E-11	4.45E-09	1.33E-07	4.15E-07
0.70	3.89E-08	2.04E-12	2.90E-11	2.11E-09	7.83E-08	2.81E-07
0.80	2.64E-08	6.16E-13	1.11E-11	1.07E-09	5.14E-08	1.99E-07
0.90	1.87E-08	2.09E-13	4.78E-12	5.91E-10	3.48E-08	1.44E-07
1.00	1.37E-08	7.89E-14	2.26E-12	3.37E-10	2.44E-08	1.06E-07
1.25	6.96E-09	5.99E-16	4.04E-13	9.51E-11	1.05E-08	5.69E-08
1.50	3.93E-09	0.00E+00	8.05E-14	3.24E-11	5.11E-09	3.46E-08
2.00	1.52E-09	0.00E+00	0.00E+00	5.57E-12	1.53E-09	1.36E-08
2.75	4.92E-10	0.00E+00	0.00E+00	5.63E-13	3.93E-10	4.28E-09
3.50	1.98E-10	0.00E+00	0.00E+00	8.38E-14	1.23E-10	1.65E-09
5.00	4.63E-11	0.00E+00	0.00E+00	3.60E-17	1.82E-11	3.42E-10

© 2007-2012 UniStar Nuclear Services, LLC. All rights reserved.
COPYRIGHT PROTECTED

Table 2.5-21— {Mean and Fractile Rock Hazard Curves for 10 Hz}

Ground motion level (g)	Annual Probability of Exceedance					
	Mean	5% Fractile	16% Fractile	50% Fractile	84% Fractile	95% Fractile
0.01	7.89E-03	3.40E-03	4.74E-03	7.10E-03	1.03E-02	1.35E-02
0.03	2.57E-03	7.72E-04	1.25E-03	2.19E-03	3.74E-03	5.28E-03
0.05	8.97E-04	2.04E-04	3.92E-04	7.47E-04	1.37E-03	2.04E-03
0.08	4.52E-04	8.80E-05	1.95E-04	3.84E-04	7.03E-04	1.04E-03
0.10	2.71E-04	4.94E-05	1.14E-04	2.36E-04	4.27E-04	6.30E-04
0.20	7.77E-05	1.28E-05	2.95E-05	7.12E-05	1.32E-04	1.87E-04
0.30	3.75E-05	5.82E-06	1.27E-05	3.39E-05	6.68E-05	9.42E-05
0.40	2.23E-05	3.07E-06	6.94E-06	2.03E-05	4.11E-05	5.91E-05
0.50	1.48E-05	1.76E-06	4.11E-06	1.32E-05	2.81E-05	4.11E-05
0.60	1.05E-05	1.10E-06	2.55E-06	9.13E-06	2.04E-05	3.03E-05
0.70	7.80E-06	7.46E-07	1.68E-06	6.60E-06	1.53E-05	2.34E-05
0.80	6.00E-06	5.18E-07	1.17E-06	4.86E-06	1.19E-05	1.86E-05
0.90	4.73E-06	3.55E-07	8.54E-07	3.77E-06	9.56E-06	1.51E-05
1.00	3.80E-06	2.55E-07	6.35E-07	2.93E-06	7.75E-06	1.25E-05
1.25	2.34E-06	1.22E-07	3.17E-07	1.67E-06	4.90E-06	8.19E-06
1.50	1.54E-06	6.00E-08	1.66E-07	1.02E-06	3.28E-06	5.68E-06
2.00	7.57E-07	1.81E-08	6.09E-08	4.36E-07	1.66E-06	3.04E-06
2.75	3.19E-07	4.09E-09	1.72E-08	1.50E-07	7.11E-07	1.41E-06
3.50	1.56E-07	1.18E-09	6.25E-09	6.20E-08	3.45E-07	7.36E-07
5.00	4.90E-08	1.52E-10	1.02E-09	1.43E-08	1.07E-07	2.50E-07

© 2007-2012 UniStar Nuclear Services, LLC. All rights reserved.
COPYRIGHT PROTECTED

Table 2.5-22— {Mean and Fractile Rock Hazard Curves for 5 Hz}

Ground motion level (g)	Annual Probability of Exceedance					
	Mean	5% Fractile	16% Fractile	50% Fractile	84% Fractile	95% Fractile
0.01	6.28E-03	2.62E-03	3.66E-03	5.65E-03	8.40E-03	1.08E-02
0.03	1.68E-03	4.84E-04	7.81E-04	1.41E-03	2.50E-03	3.59E-03
0.05	5.19E-04	1.08E-04	2.05E-04	4.20E-04	8.11E-04	1.32E-03
0.08	2.47E-04	4.35E-05	9.24E-05	2.03E-04	3.92E-04	6.52E-04
0.10	1.43E-04	2.34E-05	5.18E-05	1.18E-04	2.33E-04	3.73E-04
0.20	3.68E-05	5.31E-06	1.14E-05	3.19E-05	6.54E-05	9.60E-05
0.30	1.64E-05	2.07E-06	4.33E-06	1.36E-05	3.04E-05	4.52E-05
0.40	9.11E-06	9.74E-07	2.06E-06	7.43E-06	1.77E-05	2.64E-05
0.50	5.69E-06	5.10E-07	1.10E-06	4.48E-06	1.14E-05	1.75E-05
0.60	3.84E-06	3.05E-07	6.43E-07	2.88E-06	7.86E-06	1.23E-05
0.70	2.72E-06	1.77E-07	3.92E-07	1.95E-06	5.69E-06	9.20E-06
0.80	2.00E-06	1.07E-07	2.51E-07	1.38E-06	4.26E-06	7.02E-06
0.90	1.51E-06	7.03E-08	1.66E-07	9.82E-07	3.27E-06	5.49E-06
1.00	1.17E-06	4.56E-08	1.13E-07	7.23E-07	2.58E-06	4.41E-06
1.25	6.66E-07	1.71E-08	5.02E-08	3.62E-07	1.50E-06	2.69E-06
1.50	4.10E-07	7.17E-09	2.38E-08	1.96E-07	9.39E-07	1.74E-06
2.00	1.83E-07	1.64E-09	6.46E-09	6.97E-08	4.30E-07	8.50E-07
2.75	6.96E-08	2.81E-10	1.27E-09	2.02E-08	1.64E-07	3.64E-07
3.50	3.18E-08	6.28E-11	3.46E-10	7.14E-09	7.31E-08	1.77E-07
5.00	9.16E-09	6.09E-12	4.11E-11	1.29E-09	2.05E-08	5.36E-08

© 2007-2012 UniStar Nuclear Services, LLC. All rights reserved.
COPYRIGHT PROTECTED

Table 2.5-23— {Mean and Fractile Rock Hazard Curves for 2.5 Hz}

Ground motion level (g)	Annual Probability of Exceedance					
	Mean	5% Fractile	16% Fractile	50% Fractile	84% Fractile	95% Fractile
0.01	3.60E-03	1.31E-03	1.90E-03	3.19E-03	5.04E-03	6.87E-03
0.03	8.22E-04	1.78E-04	3.03E-04	6.33E-04	1.30E-03	2.09E-03
0.05	2.25E-04	3.24E-05	6.27E-05	1.53E-04	3.46E-04	6.82E-04
0.08	9.81E-05	1.21E-05	2.48E-05	6.36E-05	1.50E-04	3.00E-04
0.10	5.23E-05	5.67E-06	1.19E-05	3.41E-05	8.30E-05	1.60E-04
0.20	1.04E-05	7.72E-07	1.76E-06	7.02E-06	1.93E-05	3.40E-05
0.30	3.88E-06	1.94E-07	4.79E-07	2.42E-06	7.87E-06	1.38E-05
0.40	1.91E-06	6.20E-08	1.79E-07	1.10E-06	4.04E-06	7.35E-06
0.50	1.10E-06	2.35E-08	8.06E-08	5.48E-07	2.40E-06	4.57E-06
0.60	6.94E-07	9.96E-09	3.77E-08	2.93E-07	1.56E-06	3.06E-06
0.70	4.68E-07	4.58E-09	1.91E-08	1.75E-07	1.06E-06	2.18E-06
0.80	3.30E-07	2.27E-09	1.02E-08	1.07E-07	7.68E-07	1.61E-06
0.90	2.41E-07	1.20E-09	5.67E-09	6.99E-08	5.57E-07	1.20E-06
1.00	1.81E-07	6.70E-10	3.40E-09	4.74E-08	4.29E-07	9.52E-07
1.25	9.73E-08	1.79E-10	1.02E-09	1.95E-08	2.36E-07	5.42E-07
1.50	5.72E-08	5.69E-11	3.67E-10	9.03E-09	1.38E-07	3.41E-07
2.00	2.38E-08	8.27E-12	6.31E-11	2.54E-09	5.81E-08	1.61E-07
2.75	8.35E-09	8.25E-13	7.66E-12	5.35E-10	1.99E-08	6.41E-08
3.50	3.57E-09	1.07E-13	1.39E-12	1.45E-10	7.95E-09	2.83E-08
5.00	9.24E-10	0.00E+00	7.41E-14	1.83E-11	1.66E-09	7.25E-09

© 2007-2012 UniStar Nuclear Services, LLC. All rights reserved.
COPYRIGHT PROTECTED

Table 2.5-24— {Mean and Fractile Rock Hazard Curves for 1 Hz}

Ground motion level (g)	Annual Probability of Exceedance					
	Mean	5% Fractile	16% Fractile	50% Fractile	84% Fractile	95% Fractile
0.01	1.37E-03	2.74E-04	4.79E-04	1.05E-03	2.23E-03	3.26E-03
0.03	2.93E-04	2.32E-05	4.69E-05	1.45E-04	5.18E-04	1.11E-03
0.05	7.17E-05	2.52E-06	5.71E-06	2.40E-05	9.66E-05	2.88E-04
0.08	2.76E-05	5.54E-07	1.50E-06	7.95E-06	3.26E-05	1.04E-04
0.10	1.31E-05	1.69E-07	5.63E-07	3.58E-06	1.53E-05	4.66E-05
0.20	1.72E-06	6.44E-09	3.17E-08	3.61E-07	2.63E-06	7.54E-06
0.30	4.87E-07	6.87E-10	4.38E-09	7.71E-08	9.37E-07	2.61E-06
0.40	2.02E-07	1.18E-10	9.21E-10	2.62E-08	4.48E-07	1.18E-06
0.50	1.04E-07	2.59E-11	2.47E-10	1.01E-08	2.37E-07	6.59E-07
0.60	6.09E-08	7.16E-12	8.34E-11	4.45E-09	1.33E-07	4.15E-07
0.70	3.89E-08	2.04E-12	2.90E-11	2.11E-09	7.83E-08	2.81E-07
0.80	2.64E-08	6.16E-13	1.11E-11	1.07E-09	5.14E-08	1.99E-07
0.90	1.87E-08	2.09E-13	4.78E-12	5.91E-10	3.48E-08	1.44E-07
1.00	1.37E-08	7.89E-14	2.26E-12	3.37E-10	2.44E-08	1.06E-07
1.25	6.96E-09	5.99E-16	4.04E-13	9.51E-11	1.05E-08	5.69E-08
1.50	3.93E-09	0.00E+00	8.05E-14	3.24E-11	5.11E-09	3.46E-08
2.00	1.52E-09	0.00E+00	0.00E+00	5.57E-12	1.53E-09	1.36E-08
2.75	4.92E-10	0.00E+00	0.00E+00	5.63E-13	3.93E-10	4.28E-09
3.50	1.98E-10	0.00E+00	0.00E+00	8.38E-14	1.23E-10	1.65E-09
5.00	4.63E-11	0.00E+00	0.00E+00	3.60E-17	1.82E-11	3.42E-10

© 2007-2012 UniStar Nuclear Services, LLC. All rights reserved.
COPYRIGHT PROTECTED

Table 2.5-25— {Mean and Fractile Rock Hazard Curves for 0.5 Hz}

Ground motion level (g)	Annual Probability of Exceedance					
	Mean	5% Fractile	16% Fractile	50% Fractile	84% Fractile	95% Fractile
0.01	7.33E-04	5.17E-05	1.14E-04	4.32E-04	1.44E-03	2.22E-03
0.03	1.71E-04	2.61E-06	7.45E-06	4.41E-05	2.61E-04	9.27E-04
0.05	4.93E-05	1.66E-07	6.75E-07	5.65E-06	3.81E-05	2.72E-04
0.08	2.14E-05	2.51E-08	1.30E-07	1.47E-06	1.09E-05	9.44E-05
0.10	1.08E-05	5.33E-09	3.57E-08	5.58E-07	4.73E-06	3.82E-05
0.20	1.45E-06	9.58E-11	1.07E-09	3.77E-08	7.17E-07	3.90E-06
0.30	3.52E-07	3.81E-12	9.69E-11	5.61E-09	2.23E-07	1.05E-06
0.40	1.18E-07	2.51E-13	1.27E-11	1.14E-09	8.58E-08	4.92E-07
0.50	4.91E-08	1.59E-14	2.04E-12	3.20E-10	3.57E-08	2.85E-07
0.60	2.39E-08	0.00E+00	3.71E-13	1.05E-10	1.80E-08	1.68E-07
0.70	1.31E-08	0.00E+00	6.11E-14	4.15E-11	9.55E-09	1.01E-07
0.80	7.82E-09	0.00E+00	1.50E-14	1.84E-11	5.71E-09	6.37E-08
0.90	5.03E-09	0.00E+00	7.29E-17	8.07E-12	3.51E-09	4.42E-08
1.00	3.40E-09	0.00E+00	0.00E+00	4.00E-12	2.22E-09	2.71E-08
1.25	1.53E-09	0.00E+00	0.00E+00	8.46E-13	8.18E-10	1.17E-08
1.50	8.03E-10	0.00E+00	0.00E+00	1.93E-13	3.31E-10	5.75E-09
2.00	2.89E-10	0.00E+00	0.00E+00	1.50E-14	7.56E-11	1.78E-09
2.75	8.99E-11	0.00E+00	0.00E+00	0.00E+00	1.11E-11	4.90E-10
3.50	3.53E-11	0.00E+00	0.00E+00	0.00E+00	1.85E-12	1.77E-10
5.00	8.03E-12	0.00E+00	0.00E+00	0.00E+00	1.74E-13	2.96E-11

© 2007-2012 UniStar Nuclear Services, LLC. All rights reserved.
COPYRIGHT PROTECTED

Table 2.5-26— {Summary Of Thicknesses And Termination Elevations For Various Strata}
English Units

	Thickness (feet)			Top (feet msl)		
	Minimum	**Maximum**	**Average**	**Minimum**	**Maximum**	**Average**
Glacial Overburden	12.5	62.0	38.7	656.6	801.3	678.7
Mahantango Formation	*	*	*	594.3	774.2	639.3
Note: * This layer was not fully penetrated						

© 2007-2012 UniStar Nuclear Services, LLC. All rights reserved.
COPYRIGHT PROTECTED

Table 2.5-26— {Summary Of Thicknesses And Termination Elevations For Various Strata}
SI Units

	Thickness (m)			Top (m msl)		
	Minimum	**Maximum**	**Average**	**Minimum**	**Maximum**	**Average**
Glacial Overburden	3.8	18.9	11.8	200.2	244.3	206.9
Mahantango Formation	*	*	*	181.2	236.0	194.9
Note: * This layer was not fully penetrated						

© 2007-2012 UniStar Nuclear Services, LLC. All rights reserved.
COPYRIGHT PROTECTED

Table 2.5-27— {Summary Of Geotechnical Field Tests}

Test	Specification	Quantity
Soil and Rock Borings	ASTM D1586/1587	48
Seismic Refraction Survey	NA	6
P-S Suspension Logging Surveys (boreholes)	NA	4
Downhole Velocity Measurements	NA	4
Pressuremeter Test (PMT)	ASTM D4719-00	8
SPT Hammer Energy Measurements	ASTM D4633	2

© 2007-2012 UniStar Nuclear Services, LLC. All rights reserved.
COPYRIGHT PROTECTED

Table 2.5-28— {Summary of Site Borings}

(Page 1 of 2)

STRUCTURE		BORING	Horizontal Coordinates		EL. [ft]	Boring Depth to [ft]		
			Northing (ft)	Easting (ft)		Weathered Rock	Transition Zone	Sound Rock
Reactor Building	RB	B-401	340123.51	2405131.34	747.68	19.5	35.0	90.0
		B-402	340214.84	2405121.84	761.79	15.0	60.0	95.0
		B-403	340114.59	2405041.43	737.56	19.9	26.0	75.6
		B-404	340031.69	2405136.97	744.44	17.8	64.0	95.2
		B-405	340131.91	2405221.36	757.56	11.0	39.0	99.0
Nuclear Island Facilities: Safeguard Building Mechanical Safeguard Building Electrical Fuel Building Nuclear Auxiliary Building Access Building	NI	B-406	340286.99	2405115.50	771.88	11.0	***	74.0
		B-407	340169.21	2404971.67	734.19	25.5	60.0	71.0
		B-408	340045.08	2404983.01	728.44	25.0	33.0	76.0
		B-409	339978.74	2405035.71	735.15	17.5	***	71.0
		B-410	339957.85	2405145.85	744.85	17.5	61.0	80.0
		B-411	339979.47	2405273.90	758.15	23.5	40.0	80.0
		B-412	340068.40	2405294.49	763.35	22.0	41.0	100.0
		B-413	340208.12	2405283.00	772.20	9.0	***	110.5
Radioactive Waste Processing Building	RWPB	B-414	339887.65	2404983.51	730.32	16.5	34.3	39.3
		B-415	339896.90	2405085.97	739.64	15.5	31.5	115.5
		B-416	339788.65	2404992.39	728.86	25.0	30.0	45.0
		B-417	339799.26	2405095.47	734.74	20.0	30.4	35.5
Emergency Power Generation Building	EPBG	B-418	339853.39	2405203.43	744.02	20.0	***	41.5
		B-419	339860.44	2405278.15	748.14	23.8	***	54.0
		B-420	340403.18	2405150.67	778.81	15.6	46.5	70.0
		B-421	340410.50	2405228.92	783.85	15.4	57.0	70.0
Essential Service Water Building	ESWB	B-422	339721.35	2405472.52	724.95	16.0	16.0	16.0
		B-423	339727.11	2405533.75	724.06	13.2	13.2	39.0
		B-424	339868.96	2405458.50	745.40	23.4	31.2	89.6
		B-425	339874.33	2405519.37	744.91	23.9	37.0	86.8
		B-426	340296.20	2404892.65	745.20	20.0	***	58.0
		B-427	340301.39	2404954.97	753.97	12.7	54.2	59.3
		B-428	340444.20	2404878.07	750.57	17.0	25.0	47.0
		B-429	340449.24	2404939.62	757.19	21.0	28.0	52.0

© 2007-2012 UniStar Nuclear Services, LLC. All rights reserved.
COPYRIGHT PROTECTED

Table 2.5-28— {Summary of Site Borings}

(Page 2 of 2)

STRUCTURE		BORING	Horizontal Coordinates		EL. [ft]	Boring Depth to [ft]		
			Northing (ft)	Easting (ft)		Weathered Rock	Transition Zone	Sound Rock
Turbine Building	TB	B-430	340146.97	2405389.90	775.32	21.8	***	83.0
		B-431	340160.61	2405519.42	783.22	20.3	44.0	99.0
		B-432	340173.52	2405665.64	789.49	28.0	47.0	97.0
Demineralized Water Tanks	DWT	B-433	340485.71	2405380.47	792.77	25.0	70.0	77.0
Fire Protection Storage	FPSB	B-434	339641.97	2404822.94	709.00	15.7	15.7	29.8
Essential Service Water Emergency Makeup System	ESWEMS	B-435	339687.56	2406056.31	687.27	12.2	12.2	35.4
		B-436	339698.74	2406180.69	682.97	33.0	33.0	33.0
		B-437	339709.67	2406305.29	679.59	40.9	40.9	40.9
		B-438	339721.41	2406429.61	679.00	39.0	39.0	39.0
		B-439	339757.11	2406541.81	677.06	44.8	44.8	44.8
		B-440	339706.74	2406546.24	675.97	34.3	34.3	34.3
		B-441	339619.81	2407095.21	666.90	54.5	54.5	54.5
		B-442	339570.73	2406579.03	673.20	40.1	40.1	40.1
Cooling Tower	CT	B-443	341137.47	2405090.24	728.19	35.0	***	40.0
		B-444	341108.61	2405751.32	782.61	24.5	30.0	30.0
Auxiliary Geophysics	AG	G-401	340119.93	2405141.09	748.81	***	***	***
		G-423	339738.64	2405527.45	725.5	***	***	***
		G-426	340306.23	2404892.64	764.31	***	***	***

© 2007-2012 UniStar Nuclear Services, LLC. All rights reserved.
COPYRIGHT PROTECTED

Table 2.5-29— {Summary of Hammer-Rod Energy Measurements}

Drill Rig	Measurement in Boring No.	ETR Range (%)	Average ETR (%)	EnergyAdjustment (ETR%/60%)
CME - 55 340665	B-336	75-87	84	1.40
CME 55 300 Carrier	B-327	60-80	78	1.30
Note: ETR = Percentage of theoretical hammer energy measured in the field				

© 2007-2012 UniStar Nuclear Services, LLC. All rights reserved.
COPYRIGHT PROTECTED

Table 2.5-30— {Summary Of Field-Measured Standard Penetration Test (Spt) N-Values}

Stratum	SPT N-values (blows / feet)		
	Minimum	Maximum	Average
Glacial Overburden	0	131	35

© 2007-2012 UniStar Nuclear Services, LLC. All rights reserved.
COPYRIGHT PROTECTED

Table 2.5-31— {Summary Of Adjusted Spt N-Values Based On Energy Measurements}

Stratum	Adjusted Minimum N-Value (blows/feet)	Adjusted Maximum N-Value (blows/feet)	Adjusted Average N-Value (blows/feet)	Recommended N-Value for Engineering Purposes (blows/ft)
Glacial Overburden	0	97	27	20

© 2007-2012 UniStar Nuclear Services, LLC. All rights reserved.
COPYRIGHT PROTECTED

Table 2.5-32— {Summary Of Borehole Pressuremeter Test Results}
English Units

Boring	Depth (ft)	E_p (ksf)	p_{creep} (ksf)	p_{limit} (ksf)
B-301	45	12932	*	*
B-301	55	29098	*	*
B-322	64	104006	*	*
B-322	74	9124	*	*
B-325	22	22908	*	*
B-325	31.5	25932	*	*
B-327	25	9986	*	*
B-327	35	11122	*	*

© 2007-2012 UniStar Nuclear Services, LLC. All rights reserved.
COPYRIGHT PROTECTED

Table 2.5-32— {Summary Of Borehole Pressuremeter Test Results}
SI Units

Boring	Depth (m)	E_p (kPa)	p_l (kPa)	E_s (kPa)
B-301	13.9	619200	*	*
B-301	17.0	1393200	*	*
B-322	19.8	4979800	*	*
B-322	22.9	436900	*	*
B-325	6.8	1096800	*	*
B-325	9.8	1241600	*	*
B-327	7.7	478100	*	*
B-327	10.8	532500	*	*

Note:
* Tests terminated before creep and limit pressures could be established
p_l - Pressuremeter limit pressure
E_p - Pressuremeter Modulus

© 2007-2012 UniStar Nuclear Services, LLC. All rights reserved.
COPYRIGHT PROTECTED

Table 2.5-33— {Summary Of Laboratory Tests}

Test	Specification	Quantity
Engineering Classification	ASTM D2487-06 / ASTM D5878-05	114
Moisture Content	ASTM D2216-05	35
Unit Weight	From weight-volume relationship	19
Specific Gravity	ASTM D854-06 / ASTM D6473-99(2005)	13
Grain Size Analysis	ASTM D422-63 (2002)	114
Hydraulic Conductivity	ASTM D5084-03	3
Compaction Tests	ASTM D1557-07 Method C	2
Unconfined Compression	ASTM D7012-04	19
Resonant Column Torsional Shear	Technical Procedures for RCTS Tests (1)	5
Free-Free Test	Technical Procedures for URC Tests (2)	8
Sonic Pulse Test	ASTM D 2845-05	3
Organic Content	ASTM D2974-07	2
pH	ASTM D4792	38
Resistivity	ASTM G187-05	38
Chloride ion content	AASHTO T291	38
Sulphate ion content	AASHTO T290	38

(1) PBRCTS-1 Rev. 4, October 2004, University of Texas at Austin, Performed at FUGRO
(2) URC-1 Rev. 1, August 2004, University of Texas at Austin, Performed at FUGRO

© 2007-2012 UniStar Nuclear Services, LLC. All rights reserved.
COPYRIGHT PROTECTED

Table 2.5-34— {Summary Of Moisture Content}

(Page 1 of 2)

Formation	Boring	Depth		Moisture Content (%)	
		(ft)	(m)		
Glacial Overburden	B-301	5.8	1.8	3.8	10.8
	B-301	8.8	2.7	2.6	
	B-302	0.8	0.2	16.7	
	B-302	2.0	0.6	13.2	
	B-302	8.8	2.7	3.3	
	B-303	6.3	1.9	7.0	
	B-303	9.3	2.8	13.6	
	B-303	12.3	3.7	5.2	
	B-303	2.5	0.8	9.9	
	B-305	2.3	0.7	4.6	
	B-305	3.8	1.1	8.6	
	B-305	6.8	2.1	14.1	
	B-308	5.8	1.8	10.2	
	B-308	13.3	4.0	11.2	
	B-309	5.3	1.6	20.9	
	B-309	8.3	2.5	20.6	
	B-309	11.3	3.4	18.9	
	B-311	0.8	0.2	9.0	
	B-311	5.3	1.6	4.7	
	B-311	6.8	2.1	4.7	
	B-317	0.8	0.2	21.2	
	B-317	3.8	1.1	19.9	
	B-317	14.3	4.3	25.6	
	B-318	0.8	0.2	13.5	
	B-318	3.8	1.1	13.2	
	B-319	4.0	1.2	12.8	
	B-324	2.3	0.7	6.3	
	B-324	5.3	1.6	3.4	
	B-324	8.3	2.5	3.2	
	B-326	2.3	0.7	4.4	
	B-326	6.8	2.1	10.8	
	B-327	3.0	0.9	10.4	
	B-333	5.8	1.8	12.2	
	B-333	13.3	4.0	5.7	
	B-303 U2	2.5	0.8	9.9	
	B-319 U2	4.0	1.2	12.8	
	B-327 ST2	3.0	0.9	10.4	

© 2007-2012 UniStar Nuclear Services, LLC. All rights reserved.
COPYRIGHT PROTECTED

Table 2.5-34— {Summary Of Moisture Content}

(Page 2 of 2)

Formation	Boring	Depth		Moisture Content (%)	
		(ft)	(m)		
Mahantango Formation	B-301	197.8	60.3	NR	0.5
	B-301	152.4	46.4	NR	
	B-302	318.1	97.0	0.3	
	B-302	52.3	15.9	0.4	
	B-302	214.1	65.3	0.4	
	B-302	110.6	33.7	0.5	
	B-303	142.7	43.5	0.0	
	B-304	109.8	33.5	0.3	
	B-304	170.8	52.1	0.3	
	B-304	273.5	83.4	0.3	
	B-309	54.7	16.7	0.6	
	B-310	57.2	17.4	0.6	
	B-318	93.5	28.5	0.0	
	B-319	41.1	12.5	NR	
	B-324	27.6	8.4	0.6	
	B-326	41.1	12.5	1.2	
	B-327	34.0	10.4	1.1	
	B-331	67.5	20.6	0.9	
	B-334	64.6	19.7	NR	

© 2007-2012 UniStar Nuclear Services, LLC. All rights reserved.
COPYRIGHT PROTECTED

Table 2.5-35— {Summary Of Unit Weight Tests Special Care Rock Samples And Undisturbed Samples}

English Units

Formation	Boring	Depth (ft)	Dry Unit Weight (pcf)		Moist Unit Weight (pcf)	
Glacial Overburden	B-303 U2	2.5	99	102	109	121
	B-319 U2	4.0	118		133	
	B-327 ST2	3.0	86		95	
	B-331 ST2	17.0	105		126	
	B-310 U3	6.0	100		124	
Mahantango Formation	B-301, R20	197.8	NR	171	170	171
	B-301, R15	152.4	NR		171	
	B-302, R32	318.1	172		173	
	B-302, R3	52.3	171		172	
	B-302, R21	214.1	172		173	
	B-302, R11	110.6	172		173	
	B-303, R24	142.7	172		172	
	B-304, R8	109.8	172		173	
	B-304, R-14	170.8	172		173	
	B-304, R26	273.5	171		172	
	B-309, R7	54.7	NR		ND	
	B-310, R2	57.2	170		171	
	B-318, R14	93.5	172		172	
	B-319, R4	41.1	NR		172	
	B-324, R2	27.6	171		172	
	B-326, R1	41.1	166		168	
	B-327, R3	34.0	164		166	
	B-331, R7	67.5	170		172	
	B-334, R9	64.6	NR		172	

NR - Not Recorded
ND - Not Detected

© 2007-2012 UniStar Nuclear Services, LLC. All rights reserved.
COPYRIGHT PROTECTED

Table 2.5-35— {Summary Of Unit Weight Tests Special Care Rock Samples And Undisturbed Samples}
(SI Units)

Formation	Boring	Depth (m)	Dry Unit Weight (N/m^3)		Moist Unit Weight (N/m^3)	
Glacial Overburden	B-303 U2	0.8	15550		17090	
	B-303 U2	1.2	18470		20840	
	B-319 U2	0.9	13510	17010	14910	18965
	B-331 ST2	5.2	16500		19810	
	B-310 U3	1.8	15730		19540	
Mahantango Formation	B-301, R20	60.3	NR		26770	
	B-301, R15	46.4	NR		26890	
	B-302, R32	97.0	27030		27110	
	B-302, R3	15.9	26930		27030	
	B-302, R21	65.3	27010		27110	
	B-302, R11	33.7	27090		27220	
	B-303, R24	43.5	27080		27080	
	B-304, R8	33.5	27030		27110	
	B-304, R-14	52.1	27020		27100	
	B-304, R26	83.4	26920	27027	27000	27047
	B-309, R7	16.7	NR		ND	
	B-310, R2	17.4	26700		26860	
	B-318, R14	28.5	27030		27030	
	B-319, R4	12.5	NR		26990	
	B-324, R2	8.4	26900		27070	
	B-326, R1	12.5	26080		26390	
	B-327, R3	10.4	25730		26010	
	B-331, R7	20.6	26730		26970	
	B-334, R9	19.7	NR		26990	

NR - Not Recorded
ND - Not Detected

© 2007-2012 UniStar Nuclear Services, LLC. All rights reserved.
COPYRIGHT PROTECTED

Table 2.5-36— {Summary Of Specific Gravity Tests Special Care Rock Samples And Undisturbed Samples}

English Units

Formation	Boring	Depth (ft)	Depth (m)	SG
Glacial Overburden	B-303 U2	2.5	0.8	2.69
	B-319 U2	4.0	1.2	2.72
	B-327 ST2	3.0	0.9	2.69
Mahantango Formation	B-301 R20	197.8	60.3	2.77
	B-302 R3	152.4	46.4	2.76
	B-302 R11	318.1	97.0	2.76
	B-304 R8	52.3	15.9	2.76
	B-310 R2	214.1	65.3	2.77
	B-318 R14	110.6	33.7	2.76
	B-319 R4	142.7	43.5	2.83
	B-324 R2	109.8	33.5	2.76
	B-326 R1	170.8	52.1	2.67
	B-334 R9	273.5	83.4	2.77

© 2007-2012 UniStar Nuclear Services, LLC. All rights reserved.
COPYRIGHT PROTECTED

Table 2.5-37— {Chemical Test Results Of Soil And Rock Samples}

(Page 1 of 2)

Location		Depth		Formation	pH	Resistivity (O-cm)		Sulfates* (ppm)	Chlorides* (ppm)
Boring	ID	(ft)	(m)			As Received	100% Saturated		
B-301	S-12	18.5	5.6	Glacial Overburden	7.7	18130	12432	94	20
B-301	R-1	41.0	12.5	Mahantango Formation	8.6	>3.11e6	566000	62	<10
B-302	S-10	17.0	5.2	Glacial Overburden	7.1	59570	41440	70	<10
B-302	R-1	28.5	8.7	Mahantango Formation	8.8	>2.13e6	776000	29	<10
B-303	S-3	7.0	2.1	Glacial Overburden	7.0	62160	41440	73	<10
B-303	S-5	10.0	3.0	Glacial Overburden	7.1	18907	17353	43	<10
B-303	R-1	30.0	9.1	Mahantango Formation	8.0	>5.90e6	4.34E+06	20	<10
B-308	S-2	3.5	1.1	Glacial Overburden	6.4	59570	38850	24	<10
B-310	S-5	12.0	3.7	Glacial Overburden	7.0	20202	18389	81	<10
B-310	S-27	45.0	13.7	Glacial Overburden	4.3	11396	7511	1443	13
B-311	R-2	50.8	15.5	Mahantango Formation	8.7	>3.2e6	1.89E+06	21	<10
B-312	S-5	6.0	1.8	Glacial Overburden	8.5	699300	108780	20	13
B-312	S-6	7.5	2.3	Glacial Overburden	7.3	284900	62160	26	<10
B-312	S-7	9.0	2.7	Glacial Overburden	7.1	602100	73590	23	13
B-312	S-8	10.5	3.2	Glacial Overburden	7.8	21238	20720	33	13
B-314	S-11	15.0	4.6	Glacial Overburden	8.0	22523	16725	21	13
B-314	S-12	16.5	5.0	Glacial Overburden	7.8	16056	9812	45	<10
B-314	S-13	18.0	5.5	Glacial Overburden	6.0	14272	12934	77	<10
B-314	S-14	19.5	5.9	Glacial Overburden	8.3	7136	5798	127	13
B-314	S-15	21.0	6.4	Glacial Overburden	7.7	21631	12934	111	13
B-315	S-10	22.5	6.9	Glacial Overburden	6.9	33670	28490	64	<10
B-315	S-11	25.0	7.6	Glacial Overburden	6.8	12950	10878	150	<10
B-315	S-12	27.5	8.4	Glacial Overburden	7.7	8697	8028	91	<10
B-317	S-2	1.5	0.5	Glacial Overburden	6.3	31080	25123	42	13
B-317	S-9	12.0	3.7	Glacial Overburden	7.5	13468	10360	74	13
B-317	S-36	52.5	16.0	Glacial Overburden	8.5	7770	5957	366	13
B-318	R-1	28.0	8.5	Mahantango Formation	8.1	>6.29e6	1.54E+06	133	<10
B-320	S-1	0.0	0.0	Glacial Overburden	6.7	2676	2453	19	20
B-320	S-2	1.5	0.5	Glacial Overburden	6.2	38850	20979	46	<10
B-322	S-16	22.5	6.9	Glacial Overburden	7.7	31080	25900	90	<10
B-322	S-17	24.0	7.3	Glacial Overburden	6.5	13209	12691	148	<10

© 2007-2012 UniStar Nuclear Services, LLC. All rights reserved.
COPYRIGHT PROTECTED

Table 2.5-37— {Chemical Test Results Of Soil And Rock Samples}

(Page 2 of 2)

Location		Depth		Formation	pH	Resistivity (O-cm)		Sulfates* (ppm)	Chlorides* (ppm)
Boring	ID	(ft)	(m)			As Received	100% Saturated		
B-322	S-18	25.5	7.8	Glacial Overburden	7.2	33670	28490	89	<10
B-324	S-6	9.0	2.7	Glacial Overburden	6.9	468300	26760	71	40
B-324	R-2	22.0	6.7	Glacial Overburden	8.8	>3.73e6	780000	36	<10
B-327	S-5	15.0	4.6	Glacial Overburden	7.8	37910	33450	32	20
B-327	R-1	20.5	6.3	Mahantango Formation	6.5	>6.04e6	2.25E+06	530	<10
Test Pit Face(1)		NA	NA	Borrow area material	6.2	96690	82040	16	<10
Test Pit #5(1)		NA	NA	Borrow area material	5.8	73250	52740	13	10

(*) Water Soluble Ion Content
1 Borrow area fill Material

© 2007-2012 UniStar Nuclear Services, LLC. All rights reserved.
COPYRIGHT PROTECTED

Table 2.5-38— {Summary Of Unconfined Compressive Strength Tests Special Care Rock Samples}

English Units
Page 1 of 2

Formation	Boring	Depth (ft)	UCS (psi		UCS (psf)	
Mahantango Formation	B-301, R20	197.8	3687	9250	530900	1331350
	B-301, R15	152.4	9929		1429800	
	B-302, R32	318.1	13833		1992000	
	B-302, R3	52.3	8495		1223300	
	B-302, R21	214.1	9042		1302000	
	B-302, R11	110.6	8666		1247900	
	B-303, R24	142.7	9207		1325800	
	B-304, R8	109.8	12070		1738100	
	B-304, R-14	170.8	8381		1206900	
	B-304, R26	273.5	9924		1429100	
	B-309, R7	54.7	(*)		(*)	
	B-310, R2	57.2	12580		1811500	
	B-318, R14	93.5	7556		1088100	
	B-319, R4	41.1	6770		974900	
	B-324, R2	27.6	(*)		(*)	
	B-326, R1	41.1	(*)		(*)	
	B-327, R3	34.0	9006		1296900	
	B-331, R7	67.5	9535		1373000	
	B-334, R9	64.6	(*)		(*)	

(*) Specimen broke during preparation

© 2007-2012 UniStar Nuclear Services, LLC. All rights reserved.
COPYRIGHT PROTECTED

Table 2.5-38— {Summary Of Unconfined Compressive Strength Tests Special Care Rock Samples}

SI Units
Page 2 of 2

Formation	Boring	Depth (m)	UCS (MPa)	
Mahantango Formation	B-301	60.3	25	64
	B-301	46.4	68	
	B-302	97.0	95	
	B-302	15.9	59	
	B-302	65.3	62	
	B-302	33.7	60	
	B-303	43.5	63	
	B-304	33.5	83	
	B-304	52.1	58	
	B-304	83.4	68	
	B-309	16.7	(*)	
	B-310	17.4	87	
	B-318	28.5	52	
	B-319	12.5	47	
	B-324	8.4	(*)	
	B-326	12.5	(*)	
	B-327	10.4	62	
	B-331	20.6	66	
	B-334	19.7	(*)	
(*) Specimen broke during preparation				

© 2007-2012 UniStar Nuclear Services, LLC. All rights reserved.
COPYRIGHT PROTECTED

Table 2.5-39— {Hydraulic Conductivity Test Results}

English Units
Page 1 of 2

Soil Type	Boring	Depth (ft)	Eff. Confining Pressure (psf)	Hydraulic Conductivity (fps)
Glacial Overburden	B-303	2.5	500	6.89E-06
Glacial Overburden	B-319	4.0	500	9.84E-07
Glacial Overburden	B-327	3.0	500	2.89E-06

© 2007-2012 UniStar Nuclear Services, LLC. All rights reserved.
COPYRIGHT PROTECTED

Table 2.5-39— {Hydraulic Conductivity Test Results}

SI Units
Page 2 of 2

Soil Type	Boring	Depth (m)	Eff. Confining Pressure (kPA)	Hydraulic Conductivity (cm/s)
Glacial Overburden	B-303	0.8	24	2.10E-04
Glacial Overburden	B-319	1.2	24	3.00E-05
Glacial Overburden	B-327	0.9	24	8.80E-05

© 2007-2012 UniStar Nuclear Services, LLC. All rights reserved.
COPYRIGHT PROTECTED

Table 2.5-40— {Dynamic Testing Program Samples}

Location		Depth		Formation	Test
Boring	ID	(ft)	(m)		
B-331	ST2	17.0	5.2	Glacial Overburden	RCTS
B-310	U3	6.0	1.8	Glacial Overburden	RCTS
B-304	R2	41.0	12.5	Mahantango Formation	RCTS
Test Pit Face				Fill and Backfill Borrow Material	RCTS
Test Pit #5				Fill and Backfill Borrow Material	RCTS
B-301	R-1	48.3	14.7	Mahantango Formation	URC
B-301	R-10	108.4	33.0	Mahantango Formation	URC
B-309	R-34	189.6	57.8	Mahantango Formation	URC
B-301	R-25	242.2	73.8	Mahantango Formation	URC
B-302	R-27	272.1	82.9	Mahantango Formation	URC
B-304	R-30	305.8	93.2	Mahantango Formation	URC
B-302	R-35	344.1	104.9	Mahantango Formation	URC
B-301	R-42	395.0	120.4	Mahantango Formation	URC
B-303	R-4	44.3	13.5	Mahantango Formation	SP
B-309	R-25	147.0	44.8	Mahantango Formation	SP
B-313	R-11	95.9	29.2	Mahantango Formation	SP

RCTS: Resonant Column Torsional Shear
URC: Unconfined Resonant Column, Free-Free Test
SP: Sonic Pulse Test

© 2007-2012 UniStar Nuclear Services, LLC. All rights reserved.
COPYRIGHT PROTECTED

Table 2.5-41— {Resonant Column Low Strain Properties}

English Units
Page 1 of 2

Sample	Location		Depth (ft)	Formation	Confining Pressures (psf)		? (psf)	G_{max} (ksf)	V_s (fps)	D (%)
	Boring	ID								
B-331-ST2	B-331	B-331	17	Glacial Overburden	$s_{o(min)}$	288	126	472	347	1.32
					$s_{o(site)}$	1008	126	980	500	1.12
					$s_{o(max)}$	3888	126	2191	748	0.96
B-310-U3	U3	U3	6	Glacial Overburden	$s_{o(min)}$	288	124	575	386	1.06
					$s_{o(site)}$	1152	124	1091	531	0.84
					$s_{o(max)}$	4752	124	2268	766	0.55
Test Pit Face				Borrow Area Fill	$s_{o(min)}$	576	133	1093	515	2.07
					$s_{o(site)}$	2448	133	2564	788	1.75
					$s_{o(max)}$	9936	133	5735	1179	1.68
Test Pit #5				Borrow Area Fill	$s_{o(min)}$	576	136	1307	556	1.64
					$s_{o(site)}$	2448	136	2839	820	1.47
					$s_{o(max)}$	9936	136	5877	1180	1.34

© 2007-2012 UniStar Nuclear Services, LLC. All rights reserved.
COPYRIGHT PROTECTED

Table 2.5-41— {Resonant Column Low Strain Properties}

SI Units
Page 2 of 2

Sample	Location		Depth (m)	Formation	Confining Pressures (kPA)		? (kN/m^3)	G_{max} (MPa)	V_s (m/s)	D (%)
	Boring	ID								
B-331-ST2	B-331	B-331	5.18	Glacial Overburden	$s_{o(min)}$	14	20	23	106	1.32
					$s_{o(site)}$	48	20	47	153	1.12
					$s_{o(max)}$	186	20	105	228	0.96
B-310-U3	U3	U3	1.83	Glacial Overburden	$s_{o(min)}$	14	20	28	118	1.06
					$s_{o(site)}$	55	20	52	162	0.84
					$s_{o(max)}$	228	20	109	234	0.55
Test Pit Face				Borrow Area Fill	$s_{o(min)}$	28	21	52	157	2.07
					$s_{o(site)}$	117	21	123	240	1.75
					$s_{o(max)}$	476	21	275	359	1.68
Test Pit #5				Borrow Area Fill	$s_{o(min)}$	28	21	63	170	1.64
					$s_{o(site)}$	117	21	136	250	1.47
					$s_{o(max)}$	476	21	281	360	1.34

© 2007-2012 UniStar Nuclear Services, LLC. All rights reserved.
COPYRIGHT PROTECTED

Table 2.5-42— {"Free-Free" Test Results}
English Units

Location		Depth (ft)	? (pcf)	V_s (fps)	D_s (%)	V_c (fps)	D_c (%)	V_p (fps)
Boring	**ID**							
B-301	R-1	48.3	169.9	7680	2.51	12020	1.58	12940
B-301	R-10	108.4	171.0	9030	0.98	13590	1.26	13810
B-309	R-34	189.6	171.5	9360	0.75	14260	1.26	14690
B-301	R-25	242.2	170.9	9670	1.14	15030	1.37	15980
B-302	R-27	272.1	171.6	9290	0.86	14100	1.68	14490
B-304	R-30	305.8	170.8	9460	0.79	14390	1.46	14850
B-302	R-35	344.1	169.5	9600	0.7	14690	1.38	15120
B-301	R-42	395.0	171.1	9670	0.79	14870	1.16	15320

? - Unit Weight
V_s - Shear Wave Velocity
D_s - Shear Wave Damping
V_c - Compression Wave Velocity (Unconstrained Test)
D_c - Compression Wave Damping
V_p - Compression Wave Velocity (Constrained Test)

© 2007-2012 UniStar Nuclear Services, LLC. All rights reserved.
COPYRIGHT PROTECTED

Table 2.5-42— {"Free-Free" Test Results}

SI Units

Location		Depth (m)	? (kN/m^3)	V_s (m/s)	D_s (%)	V_c (m/s)	D_c (%)	V_p (m/s)
Boring	**ID**							
B-301	R-1	14.7	26.7	2341	2.51	3665	1.58	3945
B-301	R-10	33.0	26.9	2753	0.98	4143	1.26	4210
B-309	R-34	57.8	26.9	2854	0.75	4348	1.26	4479
B-301	R-25	73.8	26.8	2948	1.14	4582	1.37	4872
B-302	R-27	82.9	27.0	2832	0.86	4299	1.68	4418
B-304	R-30	93.2	26.8	2884	0.79	4387	1.46	4527
B-302	R-35	104.9	26.6	2927	0.7	4479	1.38	4610
B-301	R-42	120.4	26.9	2948	0.79	4534	1.16	4671

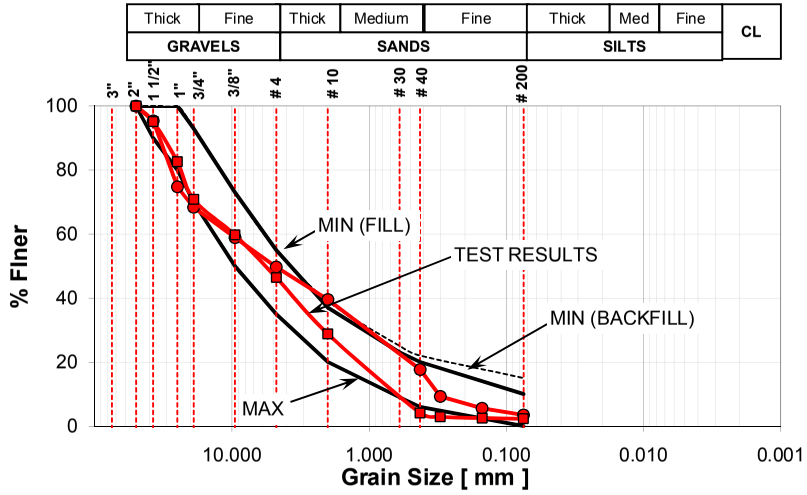
? - Unit Weight
V_s - Shear Wave Velocity
D_s - Shear Wave Damping
V_c - Compression Wave Velocity (Unconstrained Test)
D_c - Compression Wave Damping
V_p - Compression Wave Velocity (Constrained Test)

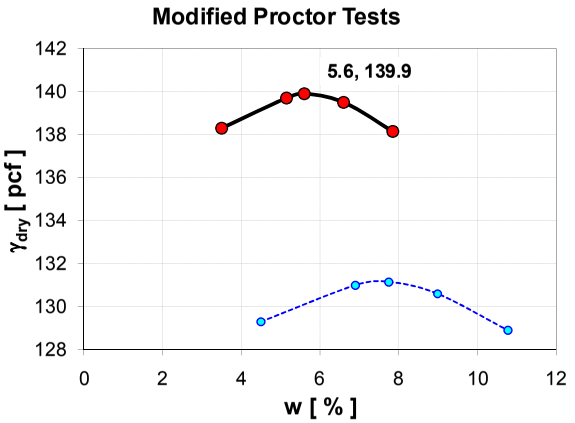
© 2007-2012 UniStar Nuclear Services, LLC. All rights reserved.
COPYRIGHT PROTECTED

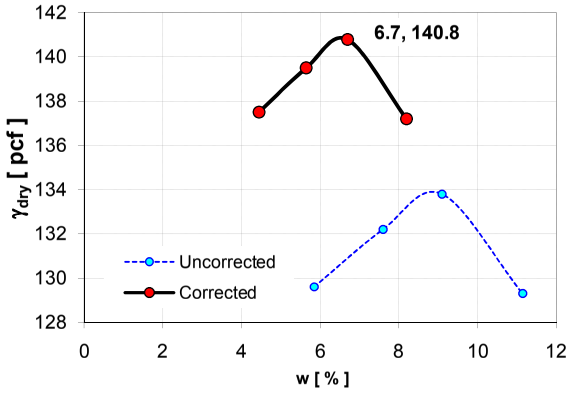
Table 2.5-43— {Category 1 Structural Fill and Backfill Properties}

English Units

Parameter				Category 1 Structural Fill[1]	Category 1 Backfill[2]
Grain Size Analysis	% Gravel		[%]	57.0	57.0
	% Sands		[%]	37.7	37.7
	% Fines		[%]	7.6	7.6
Mass (in 1 ft^3)	Solids	m_s	[lbm]	133	126
	Water	m_w	[lbm]	8	8
	Total	m_t	[lbm]	141	134
Comb	Moisture Content	w	[%]	6.1	6.1
	Saturation	S	[%]	88.3	73.2
	Specific Gravity	SG	[ ]	2.6	2.6
Unit Weight	Dry	γ_{dry}	[pcf]	133	126
	Moist	γ_{moist}	[pcf]	141	134
	Saturated	γ_{sat}	[pcf]	144	140







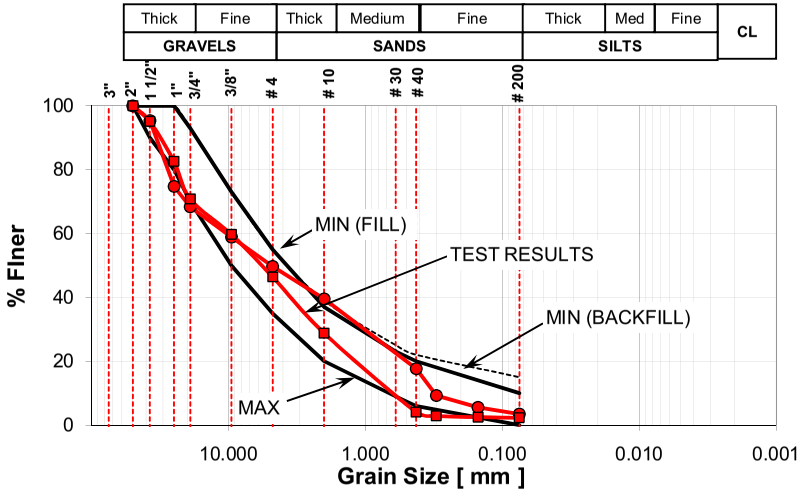
[1] 95% Modified Proctor [2] 90% Modified Proctor

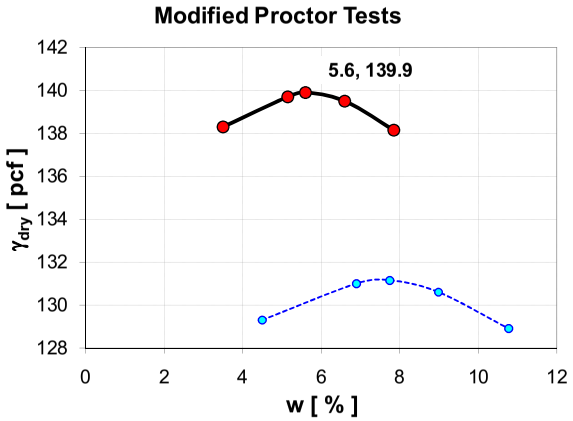
© 2007-2012 UniStar Nuclear Services, LLC. All rights reserved.
COPYRIGHT PROTECTED

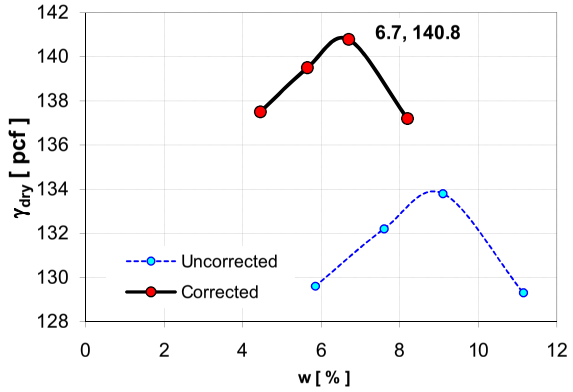
Table 2.5-44— {Category 1 Structural Fill and Backfill Properties}

SI Units

Parameter				Category 1 Structural Fill[1]	Category 1 Backfill[2]
Grain Size Analysis	% Gravel		[%]	57.0	57.0
	% Sands		[%]	37.7	37.7
	% Fines		[%]	7.6	7.6
Mass (in 1 ft^3)	Solids	m_s	[lbm]	133	126
	Water	m_w	[lbm]	8	8
	Total	m_t	[lbm]	141	134
Comb	Moisture Content	w	[%]	6.1	6.1
	Saturation	S	[%]	88.3	73.2
	Specific Gravity	SG	[ ]	2.6	2.6
Unit Weight	Dry	γ_{dry}	[pcf]	133	126
	Moist	γ_{moist}	[pcf]	141	134
	Saturated	γ_{sat}	[pcf]	144	140







[1] 95% Modified Proctor [2] 90% Modified Proctor

© 2007-2012 UniStar Nuclear Services, LLC. All rights reserved.
COPYRIGHT PROTECTED

Table 2.5-45— {Recommended Values Of Index Properties}

English Units

Unit	USCS or URCS	Water Content (%)	Unit Weight (pcf)			Observations
			Dry	Moist	Sat	
Glacial Overburden	SW	11.0	109	121	144	-URCS Classification: (Weathering, Strength, Discontinuity, Weight) NA: Not Applicable
Mahantango Formation	ABAA	0.5	169	170	170	
Category 1 Granular Fill	SW	6.1	133	141	144	
Category 1 GranularBackfill	SW	6.1	126	134	140	
Concrete Fill	NA	NA	NA	150	NA	

© 2007-2012 UniStar Nuclear Services, LLC. All rights reserved.
COPYRIGHT PROTECTED

Table 2.5-45— {Recommended Values Of Index Properties}

SI Units

Unit	USCS or URCS	Water Content (%)	Unit Weight (kN/m^3)			Observations
			Dry	Moist	Sat	
Glacial Overburden	SW	11.0	17.1	19.0	22.7	-URCS Classification: (Weathering, Strength, Discontinuity, Weight) NA: Not Applicable
Mahantango Formation	ABAA	0.5	26.6	26.7	26.7	
Category 1 Granular Fill	SW	6.1	20.9	22.2	22.7	
Category 1 GranularBackfill	SW	6.1	19.8	21.1	22.2	
Concrete Fill	NA	NA	NA	23.6	NA	

© 2007-2012 UniStar Nuclear Services, LLC. All rights reserved.
COPYRIGHT PROTECTED

Table 2.5-46— {Rock Mass Rating For Mahantango Formation}
English Units

Item	Value	Rating
Unconfined Compressive Strength (ksf)	1040	12
Rock Quality Designation (%)	83	17
Spacing of Discontinuities (m)	>0.61	20
Condition of Discontinuities	Slightly Rough Weathered Walls	25
Groundwater Conditions	Damp, less than 0.35 cf/min	10
Adjustment for Orientation	Favorable	-2
Total Rating		82
Type of Rock	**Very Good Rock**	**I**
Equivalent Cohesion (ksf)	**7.3**	
Equivalent Friction (º)	**40.0**	

© 2007-2012 UniStar Nuclear Services, LLC. All rights reserved.
COPYRIGHT PROTECTED

Table 2.5-46— {Rock Mass Rating For Mahantango Formation}
SI Units

Item	Value	Rating
Unconfined Compressive Strength (ksf)	50	12
Rock Quality Designation (%)	83	17
Spacing of Discontinuities (m)	>2	20
Condition of Discontinuities	Slightly Rough Weathered Walls	25
Groundwater Conditions	Damp, less than 10 l/min	10
Adjustment for Orientation	Favorable	-2
Total Rating		82
Type of Rock	**Very Good Rock**	**I**
Equivalent Cohesion (kPa)	**7.3**	
Equivalent Friction (º)	**40.0**	

© 2007-2012 UniStar Nuclear Services, LLC. All rights reserved.
COPYRIGHT PROTECTED

Table 2.5-47— {Recommended Values For Strength Properties}

English Units

Formation	SPT	c [ksf]	f [º]	q_u [ksf]	Observations
Glacial Overburden	20	0	32.0	NA	♦ Friction obtained from SPT Correlation for Dense Sands and Gravels (Peck, 1974)
Mahantango Formation	NA	7.3	40.0	1050	♦ qu determined from Unconfined Compressive Test
Category 1 Granular Fill	NM	0.0	35.0	NA	♦ For the Mahantango Formation equivalent cohesion and friction based on Rock Mass Rating (Bieniawski, 1989)- Concrete strength consistent with Vs = 6800 fps
Category 1 Granular Backfill	NM	0.0	35.0	NA	♦ Friction for granular fill based on common practice and conservatism
Concrete Fill	f'c = 5000				♦ NM: Not Measured ♦ NA: Not Applicable

© 2007-2012 UniStar Nuclear Services, LLC. All rights reserved.
COPYRIGHT PROTECTED

Table 2.5-47— {Recommended Values For Strength Properties}

SI Units

Formation	SPT	c [kPa]	f [º]	q_u [kPa]	Observations
Glacial Overburden	20	0	32.0	NA	♦ Friction obtained from SPT Correlation for Dense Sands and Gravels (Peck, 1974)
Mahantango Formation	NA	350	40.0	50270	♦ qu determined from Unconfined Compressive Test
Category 1 Granular Fill	NM	0.0	35.0	NA	♦ For the Mahantango Formation equivalent cohesion and friction based on Rock Mass Rating (Bieniawski, 1989)- Concrete strength consistent with Vs = 6800 fps
Category 1 Granular Backfill	NM	0.0	35.0	NA	♦ Friction for granular fill based on common practice and conservatism
Concrete Fill	f'c = 34450				♦ NM: Not Measured ♦ NA: Not Applicable

© 2007-2012 UniStar Nuclear Services, LLC. All rights reserved.
COPYRIGHT PROTECTED

Table 2.5-48— {Recommended Values For Hydraulic Conductivity}

English Units

Formation	K (Laboratory) (fps)	K (Field) (fps)	K (Recommended) (fps)	Observations
Glacial Overburden	3.6E-06	1.2E-03	1.2E-03	NM: Not MeasuredFill and Compacted Fill recommendation based on typical values for clean sands and gravels (Terzaghi, Peck 1967, 1996)
MahantangoFormation	NM	2.0E-05	2.0E-05	
Category 1 Granular Fill	NM	NM	3.3E-03	
Category 1 Granular Backfill	NM	NM	3.3E-03	
Concrete Fill	NM	NM	3.3E-12	

© 2007-2012 UniStar Nuclear Services, LLC. All rights reserved.
COPYRIGHT PROTECTED

Table 2.5-48— {Recommended Values For Hydraulic Conductivity}
SI Units

Formation	K (Laboratory) (cm/s)	K (Field) (cm/s)	K (Recommended) (cm/s)	Observations
Glacial Overburden	3.6E-06	1.2E-03	1.2E-03	NM: Not Measured Fill and Compacted Fill recommendation based on typical values for clean sands and gravels (Terzaghi, Peck 1967, 1996)
MahantangoFormation	NM	2.0E-05	2.0E-05	
Category 1 Granular Fill	NM	NM	3.3E-03	
Category 1 Granular Backfill	NM	NM	3.3E-03	
Concrete Fill	NM	NM	3.3E-12	

© 2007-2012 UniStar Nuclear Services, LLC. All rights reserved.
COPYRIGHT PROTECTED

Table 2.5-49— {Recommended Values For Elastic Modulus}

English Units

Formation	E (ksf)						Observations
	Method 1	Method 2	Method 3	Method 4	Method 5	Recomm	
Glacial Overburden	2000	3600	2000	-	-	2000	Method 1: ASCE Typical Method 2: ASCE N Correlation Method 3: AASHTO Typical Method 4: Rock Mass Rating Method 5: Concrete strength ACI318
MahantangoFormation	-	-	523000	376000	-	376000	
Category 1 Granular Fill	-	-	2000	-	-	2000	
Category 1 Granular Backfill	-	-	2000	-	-	2000	
Concrete Fill	-	-	-	-	500000	500000	

© 2007-2012 UniStar Nuclear Services, LLC. All rights reserved.
COPYRIGHT PROTECTED

Table 2.5-49— {Recommended Values For Elastic Modulus}

SI Units

Formation	E (MPa)						Observations
	Method 1	Method 2	Method 3	Method 4	Method 5	Recomm	
Glacial Overburden	96	172	96	-	-	96	Method 1: ASCE Typical Method 2: ASCE N Correlation Method 3: AASHTO Typical Method 4: Rock Mass Rating Method 5: Concrete strength ACI318
Mahantango Formation	-	-	25000	18000	-	18000	
Category 1 Granular Fill	-	-	96	-	-	96	
Category 1 Granular Backfill	-	-	96	-	-	96	
Concrete Fill	-	-	-	-	23900	23900	

© 2007-2012 UniStar Nuclear Services, LLC. All rights reserved.
COPYRIGHT PROTECTED

Table 2.5-50— {Recommended Values For Static Elastic Properties}

English Units

Formation	E (ksf)	?	G (ksf)	Observations
Glacial Overburden	2000	0.40	710	Elastic Properties obtained from field measurements and published values References:- Peck, 1974 - AASHTO, 1998
Mahantango Formation	3.76E+05	0.30	144620	
Category 1 Granular Fill	2000	0.35	740	
Category 1 Granular Backfill	2000	0.35	740	
Concrete Fill	500000	0.20	208300	

© 2007-2012 UniStar Nuclear Services, LLC. All rights reserved.
COPYRIGHT PROTECTED

Table 2.5-50— {Recommended Values For Static Elastic Properties}

SI Units

Formation	E (MPa)	?	G (MPa)	Observations
Glacial Overburden	100	0.40	36	Elastic Properties obtained from field measurements and published values References:- Peck, 1974- AASHTO, 1998
Mahantango Formation	18000	0.30	6923	
Category 1 Granular Fill	100	0.35	40	
Category 1 Granular Backfill	100	0.35	37	
Concrete Fill	23940	0.20	9975	

© 2007-2012 UniStar Nuclear Services, LLC. All rights reserved.
COPYRIGHT PROTECTED

Table 2.5-51— {Recommended Values For Low Strain Dynamic Elastic Properties At Center Of Nuclear Island Footprint}

English Units

Unit		Depth (ft) (*)		V_s (fps)	V_p (fps)	? ($p_m$cf)	?	G_{max} (ksf)	E_{max} (ksf)	DS_o (%)	Observations
SOILS	Glacial Overburden 1	0.0	20.0	1150	2550	126	0.37	5180	14220	1.00	$G_{max} = ?V_s^2$ $E_{max} = 2(1 + ?)G_s$ - Velocities determined from best estimate soil profile - Poisson's Ration determined from velocity ratio squared -Initial Shear Damping (DSo): determined from "Free-Free" Testing for Rocks, and RCTS Testing for Overburden
	Glacial Overburden 2	20.0	40.0	2300	7000	126	0.44	20700	59590	1.00	
ROCK FORMATIONS	Mahantango Formation Layer 1	40.0	60.0	6800	12900	170	0.31	244120	638430	0.80	
	Mahantango Formation Layer 2	60.0	100.0	7150	15300	170	0.36	269900	734290	0.80	
	Mahantango Formation Layer 3	100.0	155.0	7600	16100	170	0.36	304940	827390	0.70	
	Mahantango Formation Layer 4	155.0	220.0	8500	16100	170	0.31	381440	996910	0.70	
	Mahantango Formation Layer 5	220.0	270.0	8950	16750	170	0.30	422900	1099710	0.70	
	Mahantango Formation Layer 6	270.0	-	9600	16850	170	0.26	486560	1225840	0.70	
FILLS	Category 1 Granular Fill/Backfill	0.0	10.0	600	1250	140	0.35	1570	4240	1.00	NA: Not Applicable
		10.0	20.0	800	1670	140	0.35	2780	7510	1.00	
		> 20.0		1000	2100	140	0.35	4350	11770	1.00	
	Concrete	NA	NA	7240	11820	150	0.20	244180	585920	0.80	

© 2007-2012 UniStar Nuclear Services, LLC. All rights reserved.
COPYRIGHT PROTECTED

Table 2.5-51— {Recommended Values For Low Strain Dynamic Elastic Properties At Center Of Nuclear Island Footprint}

SI Units

Unit		Depth (m) (*)		V_s (m/s)	V_p (m/s)	? (kg/m^3)	?	G_{max} (MPa)	E_{max} (MPa)	DS_o (%)	Observations
SOILS	Glacial Overburden 1	0.0	6.1	351	777	2020	0.37	250	690	1.00	$G_{max} = ?V_s^2$ $E_{max} = 2(1 + ?)G_s$ - Velocities determined from best estimate soil profile - Poisson's Ration determined from velocity ratio squared -Initial Shear Damping (DSo): determined from "Free-Free" Testing for Rocks, and RCTS Testing for Overburden
	Glacial Overburden 2	6.1	12.2	701	2134	2020	0.44	990	2850	1.00	
ROCK FORMATIONS	Mahantango Formation Layer 1	12.2	18.3	2073	3933	2720	0.31	11690	30570	0.80	
	Mahantango Formation Layer 2	18.3	30.5	2180	4665	2720	0.36	12930	35180	0.80	
	Mahantango Formation Layer 3	30.5	47.3	2317	4909	2720	0.36	14600	39610	0.70	
	Mahantango Formation Layer 4	67.1	67.1	2729	5107	2720	0.30	20250	52660	0.70	
	Mahantango Formation Layer 5	82.3	82.3	2927	5137	2720	0.26	23300	58700	0.70	
	Mahantango Formation Layer 6	82.3	-	2927	5137	2720	0.26	23300	58700	0.70	
FILLS	Category 1 Granular Fill/Backfill	0.0	3.0	183	381	2240	0.35	70	190	1.00	NA: Not Applicable
		3.0	6.1	244	509	2240	0.35	130	350	1.00	
		> 6.1		305	640	2240	0.35	210	570	1.00	
	Concrete	NA	NA	2207	3604	2400	0.20	11690	28050	0.80	

© 2007-2012 UniStar Nuclear Services, LLC. All rights reserved.
COPYRIGHT PROTECTED

Table 2.5-52— {Peak Ground Acceleration from FIRS Study}

English Units

Structure		Foundation		Base to Rock (ft)(2)	Base to OGS (ft)(3)	Eng Fill[4] (ft)	Contact Soil[5]	Hor PGA (g)	Ver PGA (g)
		Depth (ft)	El.[1] (ft msl)						
Nuclear Island(6)	NI	36.0	638.0	12.6	-28.0	12.6	C-M	0.21	0.18
ESWEMS Cooling Towers (URB)	URB1	22.0	652.0	3.0	-23.0	3.0	C	0.21	0.18
	URB2	22.0	652.0	4.5	-17.0	4.5	C	0.21	0.18
	URB3	22.0	652.0	58.5	-5.5	58.5	EF	0.21	0.21
	URB4	22.0	652.0	41.0	-5.5	41.0	EF	0.24	0.25
Emergency Power Building (UBP)	UBP12(7)	5.0	669.0	27.0	-3.0	27.0	C	0.21	0.19
	UBP12	5.0	669.0	27.0	-3.0	27.0	EF	0.30	0.33
	UBP34	5.0	669.0	67.0	12.0	67.0	EF	0.21	0.22
ESWEMS Pumphouse		33.0	641.0	7.0	-40.0	7.0	C	0.21	0.18

[1] Plant Grade El. (ft msl) 674
[2] Distance between rock and base of foundation
[3] Distance between foundation base original ground surface
[4] Engineered fill (Concrete for NI and soil for other facilities)
[5] Concrete (C), Mahantango Formation (M), Glacial Overburden (GO), Engineered Fill (EF)
[6] Depth given for containment building, other NI facilities have 41.3 ft
[7] Concrete fill is the preferred configuration for this facility

© 2007-2012 UniStar Nuclear Services, LLC. All rights reserved.
COPYRIGHT PROTECTED

Table 2.5-52— {Peak Ground Acceleration from FIRS Study}

SI Units

Structure		Foundation		Base to Rock (m)[2]	Base to OGS (m)[3]	Eng Fill[4] (m)	Contact Soil[5]	Hor PGA (g)	Ver PGA (g)
		Depth (m)	El.[1] (m msl)						
Nuclear Island[6]	NI	11.0	194.5	3.8	-8.5	3.8	C-M	0.21	0.18
ESWEMS Cooling Towers (URB)	URB1	6.7	198.8	0.9	-7.0	0.9	C	0.21	0.18
	URB2	6.7	198.8	1.4	-5.2	1.4	C	0.21	0.18
	URB3	6.7	198.8	17.8	-1.7	17.8	EF	0.21	0.21
	URB4	6.7	198.8	12.5	-1.7	12.5	EF	0.24	0.25
Emergency Power Building (UBP)	UBP12[7]	1.5	204.0	8.2	-0.9	8.2	C	0.21	0.19
	UBP12	1.5	204.0	8.2	-0.9	8.2	S	0.30	0.33
	UBP34	1.5	204.0	20.4	3.7	20.4	EF	0.21	0.22
ESWEMS Pumphouse		10.1	195.4	2.1	-12.2	2.1	C	0.21	0.18

[1] Plant Grade El. (m msl) 205
[2] Distance between rock and base of foundation
[3] Distance between foundation base original ground surface
[4] Engineered fill (Concrete for NI and soil for other facilities)
[5] Concrete (C), Mahantango Formation (M), Glacial Overburden (GO), Engineered Fill (EF)
[6] Depth given for containment building, other NI facilities have 12.6 m
[7] Concrete fill is the preferred configuration for this facility

© 2007-2012 UniStar Nuclear Services, LLC. All rights reserved.
COPYRIGHT PROTECTED

Table 2.5-53— {Soil Conditions For The U.S. EPR Standard Plant}

English Units

Soil Case No.	Seismic Control Motion Applied	Soil Profile (Half Space or Layered)	Shear-wave Velocity of Soil[1] (fps)
1u	EUR Soft	Half-space	700
2u (A and B)	EUR Soft and Medium	Half-space	1,640
3u	EUR Medium	Half-space	2,625
4u (A and B)	EUR Medium and Hard	Half-space	3,937
5u	EUR Hard	Half-space	5,249
5a	EUR Hard	Half-space	13,123
1n2u	EUR Soft	Linear gradient within a 100 ft layer over a half-space	820 to 1,640
2sn4u	EUR Medium	49 ft uniform layer over a half- space	1,640/3,937
2n3u	EUR Medium	Linear gradient within a 200 ft layer over a half-space	1,640 to 2,625
3r3u	EUR Medium	20 ft uniform layer over 46 ft stiffer layer followed by soil half-space	2,625/5,249/2,625

[1] Shear wave velocities of generic soil profiles are taken as strain-compatible properties

© 2007-2012 UniStar Nuclear Services, LLC. All rights reserved.
COPYRIGHT PROTECTED

Table 2.5-53— {Soil Conditions For The U.S. EPR Standard Plant}

SI Units

Soil Case No.	Seismic Control Motion Applied	Soil Profile (Half Space or Layered)	Shear-wave Velocity of Soil[1] (m/s)
1u	EUR Soft	Half-space	215
2u (A and B)	EUR Soft and Medium	Half-space	500
3u	EUR Medium	Half-space	800
4u (A and B)	EUR Medium and Hard	Half-space	1,200
5u	EUR Hard	Half-space	1,600
5a	EUR Hard	Half-space	4,000
1n2u	EUR Soft	Linear gradient within a 30 m layer over a half-space	250 to 500
2sn4u	EUR Medium	15 m uniform layer over a half- space	500/1,200
2n3u	EUR Medium	Linear gradient within a 60 m layer over a half-space	500 to 800
3r3u	EUR Medium	6 m uniform layer over 14 m stiffer layer followed by soil half-space	800/1,600/800

[1] Shear wave velocities of generic soil profiles are taken as strain-compatible properties

© 2007-2012 UniStar Nuclear Services, LLC. All rights reserved.
COPYRIGHT PROTECTED

Table 2.5-54— {Soil Conditions For The U.S. EPR Standard Plant}
English Units

Site Class		Shear Wave Velocity (mean) (fps)	Location of GMRS	Geotechnical Analysis Requirements
Rock Site (Rock is at the ground surface at the site)	**Hard and Firm Rock Site**	Vs>3,500	At top of Rock	Static and dynamic bearing capacity to be verified; no time-dependent settlement analysis required.
	Soft Rock Site	2,400<Vs<3,500	At top of Rock	Static and dynamic bearing capacity to be verified; no time-dependent settlement analysis required.
Thin Soil Site (Rock is generally within 40 to 60 feet of the ground surface and the EPR Nuclear Island is founded on rock)	**Thin Soil Site over Hard or Firm Rock**	At depth below Nuclear Island Basemat,Vs > 3,500	At Top of Outcropping Rock	Static and dynamic bearing capacity to be verified; no time-dependent settlement analysis required.
	Thin Soil Site over Soft Rock	At depth below Nuclear Island Basemat,Vs < 3,500	At Grade Elevation	Static and dynamic bearing capacity to be verified; no time-dependent settlement analysis required.
Soil Sites (Foundation underlain by < 200′ of soil for Shallow and > 200′ feet for Deep)	**Shallow Soil and Deep Soil Sites**	1,000<Vs<3,500with soil below Nuclear Island Basemat of unlimited thickness	At free-field soil surface	Static and dynamic bearing capacity analysis required; requires verification that time-dependent settlement falls within EPR envelope.

© 2007-2012 UniStar Nuclear Services, LLC. All rights reserved.
COPYRIGHT PROTECTED

Table 2.5-54— {Soil Conditions For The U.S. EPR Standard Plant}
SI Units

Site Class		Shear Wave Velocity (mean) (m/s)	Location of GMRS	Geotechnical Analysis Requirements
Rock Site (Rock is at the ground surface at the site)	**Hard and Firm Rock Site**	Vs>1,070	At top of Rock	Static and dynamic bearing capacity to be verified; no time-dependent settlement analysis required.
	Soft Rock Site	730<Vs<1,070	At top of Rock	Static and dynamic bearing capacity to be verified; no time-dependent settlement analysis required.
Thin Soil Site (Rock is generally within 40 to 60 feet of the ground surface and the EPR Nuclear Island is founded on rock)	**Thin Soil Site over Hard or Firm Rock**	At depth below Nuclear Island Basemat,Vs > 1,070	At Top of Outcropping Rock	Static and dynamic bearing capacity to be verified; no time-dependent settlement analysis required.
	Thin Soil Site over Soft Rock	At depth below Nuclear Island Basemat,Vs < 1,070	At Grade Elevation	Static and dynamic bearing capacity to be verified; no time-dependent settlement analysis required.
Soil Sites (Foundation underlain by < 200′ of soil for Shallow and > 200′ feet for Deep)	**Shallow Soil and Deep Soil Sites**	305<Vs<1,070with soil below Nuclear Island Basemat of unlimited thickness	At free-field soil surface	Static and dynamic bearing capacity analysis required; requires verification that time-dependent settlement falls within EPR envelope.

© 2007-2012 UniStar Nuclear Services, LLC. All rights reserved.
COPYRIGHT PROTECTED

Table 2.5-55— {Foundation Elevations}

English Units

Structure		Foundation		Shape	Base to Rock (ft)[2]	Base to OGS (ft)[3]	Fill Thickness		Contact Soil[5]	Area (ft^2)	Contact Pressure (ksf)[6]		
		Depth (ft)	El.[1] (ft msl)				In-Situ	Eng[4]			Average Static	Maximum Static	Dynamic
Nuclear Island[(7)]	NI	36.0	638.0		12.6	-28.0	0.0	12.6	C-M	80,170	14.7	22.0	25.0
Nuclear Auxiliary Building	UKA	41.5	632.5		19.5	-27.5	0.0	19.5	EF	12,510	9.8	22.0	25.0
Rad Waste Building	UKS	36.0	638.0		41.0	-19.5	0.0	41.0	EF	16,880	4.3	22.0	25.0
EWSW Cooling Towers	URB1	22.0	652.0		3.0	-23.0	0.0	3.0	C	22,120	5.4	22.0	25.0
	URB2	22.0	652.0		4.5	-17.0	0.0	4.5	C	22,120	5.4	22.0	25.0
	URB3	22.0	652.0		58.5	-5.5	0.0	58.5	EF	22,120	5.4	22.0	25.0
	URB4	22.0	652.0		41.0	-5.5	0.0	41.0	EF	22,120	5.4	22.0	25.0
Emergency Power Building (UBP)	UBP12	5.0	669.0		27.0	-3.0	0.0	27.0	C	12,650	3.2	22.0	25.0
	UBP34	5.0	669.0		67.0	12.0	0.0	67.0	EF	12,650	3.2	22.0	25.0
Turbine Building	UMA	33.0	641.0		33.0	-27.0	0.0	33.0	EF	100,000	4.2	10.0	12.0

[1] Plant Grade El. [ft msl] 674
[2] Distance between rock and base of foundation
[3] Distance between foundation base original ground surface
[4] Engineered fill (Concrete for NI and soil for other facilities)
[5] Concrete (C), Mahantango Formation (M), Glacial Overburden (GO), Engineered Fill (EF)
[6] As prescribed by the U.S. EPR FSAR and Foundation Interface Document
[7] Depth given for containment building, other NI facilities have 41.3 ft

© 2007-2012 UniStar Nuclear Services, LLC. All rights reserved.
COPYRIGHT PROTECTED

Table 2.5-55— {Foundation Elevations}

SI Units

Structure		Foundation		Shape	Base to Rock (m)[2]	Base to OGS (m)[3]	Fill Thickness		Contact Soil[5]	Area (m^2)	Contact Pressure (kPa)[6]		
		Depth (m)	El.[1] (m msl)				In-Situ	Eng[4]			Average Static	Maximum Static	Dynamic
Nuclear Island	NI	11.0	194.5		3.8	-8.5	0.0	3.8	C-M	7,452	700	1,050	1,200
Nuclear AuxiliaryBuilding	UKA	12.7	192.8		5.9	-8.4	0.0	5.9	EF	1,163	470	1,050	1,200
Rad WasteBuilding	UKS	11.0	194.5		12.5	-5.9	0.0	12.5	EF	1,569	210	1,050	1,200
ESWS Cooling Towers	URB1	6.7	198.8		0.9	-7.0	0.0	0.9	C	2,056	260	1,050	1,200
	URB2	6.7	198.8		1.4	-5.2	0.0	1.4	C	2,056	260	1,050	1,200
	URB3	6.7	198.8		17.8	-1.7	0.0	17.8	EF	2,056	260	1,050	1,200
	URB4	6.7	198.8		12.5	-1.7	0.0	12.5	EF	2,056	260	1,050	1,200
Emergency PowerBuilding(UBP)	UBP12	1.5	204.0		8.2	-0.9	0.0	8.2	C	1,176	150	1,050	1,200
	UBP34	1.5	204.0		20.4	3.7	0.0	20.4	EF	1,176	150	1,050	1,200
Turbine Building	UMA	10.1	195.4		10.1	-8.2	0.0	10.1	EF	9,295	200	480	570

[1] Plant Grade El. [m msl] 205.5
[2] Distance between rock and base of foundation
[3] Distance between foundation base original ground surface
[4] Engineered fill (Concrete for NI and soil for other facilities)
[5] Concrete (C), Mahantango Formation (M), Glacial Overburden (GO), Engineered Fill (EF)
[6] As prescribed by the U.S. EPR FSAR and Foundation Interface Document

© 2007-2012 UniStar Nuclear Services, LLC. All rights reserved.
COPYRIGHT PROTECTED

Table 2.5-56— {Earth Pressure Coefficients}

Formation	f (º)	k_a	k_p	k_o	k_{AE}	k_{PE}	Observations
Glacial Overburden	35	0.27	3.69	0.43	0.58	8.12	NA - Not Applicable ka - Active Earth Pressure Coefficient kp - Passive Earth Pressure Coefficient ko - At Rest Earth Pressure Coefficient
Mahantango Formation	NA	NA	NA	NA	NA	NA	
Granular Fill/Backfill	35	0.27	3.69	0.43	0.58	8.12	
Concrete Fill	NA	NA	NA	NA	NA	NA	

© 2007-2012 UniStar Nuclear Services, LLC. All rights reserved.
COPYRIGHT PROTECTED

Table 2.5-57— {Bearing Capacity (Failure Controlled)}
English Units

Structure		Foundation		Footprint Shape	Simplified		Contact Surface[2]	Bearing Capacity (ksf)	
		Depth (ft)	El.[1] (ft msl)		B (ft)	L (ft)		Ultimate	Allowable FS=3.0
Nuclear Island	NI	36.0	638.0		284	284	C-M	720.0	240.0
Nuclear Auxiliary Building	UKA	41.5	632.5		105	120	C	239.6	79.9
Radioactive Waste Building	UKS	36.0	638.0		130	130	C	245.3	81.8
ESWS Cooling Towers	URB1	22.0	652.0		124	180	C	720.0	240.0
	URB2	22.0	652.0		124	180	C	720.0	240.0
	URB3	22.0	652.0		124	180	EF	222.8	74.3
	URB4	22.0	652.0		124	180	EF	222.8	74.3
Emergency Power Generation Building	UBP1	5.0	669.0		90	140	C	720.0	240.0
	UBP2	5.0	669.0		90	140	EF	139.1	46.4
Turbine Building	UMA	33.0	641.0		300	330	EF	436.6	145.5
10′ x 10′ Footing on Fill (3′ Deep)		3.0	671.0		10	10	EF	22.9	7.6

[1] Plant Grade El. (ft msl) 674
[2] Concrete (C), Mahantango Formation (M), Glacial Overburden (GO), Engineered Fill (EF)

© 2007-2012 UniStar Nuclear Services, LLC. All rights reserved.
COPYRIGHT PROTECTED

Table 2.5-57— {Bearing Capacity (Failure Controlled)}
SI Units

Structure		Foundation		Footprint Shape	Simplified		Contact Surface[2]	Bearing Capacity (kPa)	
		Depth (m)	El.[1] (m msl)		B (m)	L (m)		Ultimate	Allowable FS=3.0
Nuclear Island	NI	11.0	194.5		87	87	C-M	34,470	11,490
Nuclear Auxiliary Building	UKA	12.7	192.8		32	37	C	11,470	3,820
Radioactive Waste Building	UKS	11.0	194.5		40	40	C	11,750	3,920
ESWS Cooling Towers	URB1	6.7	198.8		38	55	C	34,470	11,490
	URB2	6.7	198.8		38	55	C	34,470	11,490
	URB3	6.7	198.8		38	55	EF	10,670	3,560
	URB4	6.7	198.8		38	55	EF	10,670	3,560
Emergency Power Generation Building	UBP1	1.5	204.0		27	43	C	34,470	11,490
	UBP2	1.5	204.0		27	43	EF	6,660	2,220
Turbine Building	UMA	10.1	195.4		91	101	EF	20,900	6,970
10′ x 10′ Footing on Fill (3′ Deep)		0.9	204.6		3	3	EF	1,100	370

[1] Plant Grade El. [m msl] 205
[2] Concrete (C), Mahantango Formation (M), Glacial Overburden (GO), Engineered Fill (EF)

© 2007-2012 UniStar Nuclear Services, LLC. All rights reserved.
COPYRIGHT PROTECTED

Table 2.5-58— {Elastic Settlement Analysis By Simplified Approximations}
English Units

Structure		Foundation		Contact Surface[2]	Service Load (ksf)	Settlement Approximation (in)					
		Depth (ft)	El.[1] (ft msl)			Janbu		Perloff		Kay & Cav.	
						Center	Edge	Center	Edge	Center	Edge
Nuclear Island	NI	36.0	638.0	C-M	14.7	0.0	-	0.0	0.0	0.0	0.0
Nuclear Auxiliary Building	UKA	41.5	632.5	C	9.8	0.3	-	1.1	0.4	0.4	0.2
Radioactive Waste Building	UKS	36.0	638.0	C	4.3	0.3	-	0.9	0.4	0.4	0.2
ESWS Cooling Towers	URB1	22.0	652.0	C	5.4	0.0	-	0.0	0.0	0.0	0.0
	URB2	22.0	652.0	C	5.4	0.0	-	0.0	0.0	0.0	0.0
	URB3	22.0	652.0	EF	5.4	0.6	-	1.8	0.7	0.9	0.4
	URB4	22.0	652.0	EF	5.4	0.4	-	1.1	0.4	0.6	0.3
Emergency Power Generation	UBP1	5.0	669.0	C	3.2	0.0	-	0.0	0.0	0.0	0.0
	UBP2	5.0	669.0	EF	3.2	0.4	-	0.9	0.4	0.7	0.3
Turbine Building	UMA	33.0	641.0	EF	4.2	0.4	-	0.7	0.3	0.3	0.1
10′ x 10′ Footing on Fill (3′ Deep)		3.0	671.0	EF	2.0	0.0	-	0.1	0.0	0.1	0.0

[1] Plant Grade El. (ft msl) 674.0
[2] Concrete (C), Mahantango Formation (M), Glacial Overburden (GO), Engineered Fill (EF)

© 2007-2012 UniStar Nuclear Services, LLC. All rights reserved.
COPYRIGHT PROTECTED

Table 2.5-58— {Elastic Settlement Analysis By Simplified Approximations}
SI Units

Structure		Foundation		Contact Surface[2]	Service Load (kPa)	Settlement Approximation (in)					
		Depth (m)	El.[1] (m msl)			Janbu		Perloff		Kay & Cav.	
						Center	Edge	Center	Edge	Center	Edge
Nuclear Island	NI	11.0	194.5	C-M	700	0.0	-	0.1	0.0	0.1	0.0
Nuclear Auxiliary Building	UKA	12.7	192.8	C	470	0.7	-	2.9	1.1	1.1	0.5
Radioactive Waste Building	UKS	11.0	194.5	C	210	0.8	-	2.3	0.9	1.1	0.5
ESWS Cooling Towers	URB1	6.7	198.8	C	260	0.0	-	0.0	0.0	0.0	0.0
	URB2	6.7	198.8	C	260	0.0	-	0.0	0.0	0.0	0.0
	URB3	6.7	198.8	EF	260	1.5	-	4.6	1.9	2.4	1.0
	URB4	6.7	198.8	EF	260	1.0	-	2.8	1.1	1.4	0.6
Emergency Power Generation	UBP1	1.5	204.0	C	150	0.0	-	0.0	0.0	0.0	0.0
	UBP2	1.5	204.0	EF	150	1.1	-	2.4	1.1	1.8	0.7
Turbine Building	UMA	10.1	195.4	EF	200	1.0	-	1.7	0.7	0.7	0.4
10′ x 10′ Footing on Fill (3′ Deep)		0.9	204.6	EF	100	0.1	-	0.2	0.1	0.2	0.1

[1] Plant Grade El. (m msl) 205.5
[2] Concrete (C), Mahantango Formation (M), Glacial Overburden (GO), Engineered Fill (EF)

© 2007-2012 UniStar Nuclear Services, LLC. All rights reserved.
COPYRIGHT PROTECTED

Table 2.5-59— {Detailed Elastic Settlement Analysis}
English Units

Structure		Depth (ft)	El.[1] (ft msl)	Contact Surface	Service Load (ksf)	Settlement	
						Total (in)	Differential (in/50ft)
Nuclear Island[3]	NI	36.0	638.0	C-M	14.7	< .5	<.1
1 Plant Grade El. (ft msl) 674.0 2 Concrete (C), Mahantango Formation (M), Glacial Overburden (GO), Engineered Fill (EF) 3 Depth shown for UJA (Containment Building). Depth is 41.5 feet around containment							

© 2007-2012 UniStar Nuclear Services, LLC. All rights reserved.
COPYRIGHT PROTECTED

Table 2.5-59— {Detailed Elastic Settlement Analysis}
SI Units

Structure		Depth (m)	El.[1] (m msl)	Contact Surface	Service Load (kPa)	Settlement	
						Total (cm)	Differential (cm/100 m)
Nuclear Island[3]	NI	11.0	194.5	C-M	700.0	<0.2	<2
1 Plant Grade El. (m msl) 205.5 2 Concrete (C), Mahantango Formation (M), Glacial Overburden (GO), Engineered Fill (EF 3 Depth shown for UJA (Containment Building). Depth is 12.7 m around containment							

© 2007-2012 UniStar Nuclear Services, LLC. All rights reserved.
COPYRIGHT PROTECTED

Table 2.5-60— {Factor Of Safety Against Sliding}

		Circular Failure		Wedge Failure		Observations
		Static	Dynamic	Static	Dynamic	
Permanent Slopes (ESWEMS Retention Pond)	Section 1	5.6	2.9	7.9	3.3	
	Section 2	6.9	2.4	9.2	4.1	
	Section 3	4.4	2.0	5.9	2.2	
	Section 4	5.7	2.1	7.0	2.9	
Temporary Slopes	Section 1	1.3			1.4	Dynamic case not applicable for temporary slopes.
	Section 2	2.5		2.5		
North Slope	Section 1			5.7	1.6	North slope analyzed to examine risk of landslide on-site.Only wedge failure is applicable.

© 2007-2012 UniStar Nuclear Services, LLC. All rights reserved.
COPYRIGHT PROTECTED

Table 2.5-61— {Smooth Uniform Hazard Response Spectra}

Frequency(Hz)	SmoothUHRS1 E-4	SmoothUHRS1 E-5	SmoothUHRS1 E-6
0.100	0.004	0.011	0.025
0.127	0.006	0.017	0.039
0.161	0.008	0.026	0.057
0.204	0.012	0.036	0.080
0.259	0.016	0.050	0.111
0.329	0.022	0.068	0.151
0.418	0.029	0.090	0.200
0.500	0.036	0.110	0.244
0.672	0.042	0.124	0.272
0.853	0.045	0.126	0.276
1.000	0.045	0.118	0.261
1.374	0.058	0.152	0.347
1.750	0.068	0.180	0.425
2.212	0.077	0.207	0.507
2.500	0.081	0.220	0.556
3.562	0.103	0.294	0.767
4.520	0.121	0.358	0.957
5.000	0.131	0.407	1.108
7.500	0.162	0.534	1.484
10.000	0.189	0.647	1.825
11.721	0.210	0.728	2.104
14.874	0.238	0.837	2.477
18.874	0.262	0.931	2.815
25.000	0.280	1.004	3.100
30.392	0.272	0.981	3.019
38.566	0.257	0.930	2.854
48.939	0.229	0.832	2.544
62.102	0.182	0.665	2.026
78.805	0.129	0.475	1.443
100.000	0.097	0.361	1.091

© 2007-2012 UniStar Nuclear Services, LLC. All rights reserved.
COPYRIGHT PROTECTED

Table 2.5-62— {Relation of the Tectonic History of the Site Region to the Associated Tectonic Features}

(Page 1 of 4)

Tectonic Event	Principal Duration of Event	Brief Description of Conditions during Event near Site Region	Named Features and Text Sections for Detailed Descriptions	
Grenville Orogeny	Meso- Proterozoic (Precambrian)	Collision of N. America and S. America created the supercontinent of Rodinia, and created a band of highly metamorphosed rocks along the southern and eastern edge of the N. American craton.		
Late Precambrian Rifting	Late Precambrian to Middle Ordovician	During the breakup of Rodinia, and the opening of the Iapetus Ocean, rift basins developed along the continental margin and the normal faults along the margins of the rifts.	**New Madrid Seismic Zone** (and Reelfoot Rift)	**2.5.1.1.4.4.1.1**
			Charlevoix-La Malbaie Seismic Zone (related to the St. Lawrence Rift Valley)	**2.5.1.1.4.4.1.3**
			St Lawrence Rift Valley	**2.5.1.1.4.4.1.4**
			Bristol Block Geopotential Trends	**2.5.1.4.4.3.4**
			Transylvania Fault Zone	2.5.1.1.4.4.4.9
			Ramapo Fault (active since Proterozoic)	**2.5.1.1.4.4.2.2**
			Pittsburgh-Washington Lineament	2.5.1.1.4.4.3.3
			Tyrone-Mt. Union Lineament	2.5.1.1.4.4.3.3
			Reading Prong	**2.5.1.1.4.4.3.5**
Taconic Orogeny	Middle Ordovician to Middle Silurian	Collision of the N. American continent with island arc terranes, and accretion of volcanics and sea floor crust to the continent. Folding, thrust faulting, and metamorphism were common.	Mountain Run Fault (thrust fault)	2.5.1.4.4.2.16
			Pittsburgh-Washington Lineament	2.5.1.1.4.4.3.3
			Tyrone-Mt. Union Lineament	2.5.1.1.4.4.3.3
			Rome Trough	2.5.1.1.4.4.4.7
			Pleasant Valley-Huntington Valley Fault	2.5.1.1.4.4.4.8
			Transylvania Fault Zone	2.5.1.1.4.4.4.9
			Plummers Island and Pleasant Grove Shear Zones	2.5.1.1.4.4.4.10
			Martic Fault	2.5.1.1.4.4.4.15
			Broadtop Synclinorium	2.5.1.1.4.4.4.17
			Philadelphia Structural Block	2.5.1.1.4.4.4.20
			Rosemont Shear Zone	2.5.1.1.4.4.4.20
			Potomac and Westminster Terranes	2.5.1.1.4.4.4.21
			Baltimore Gneiss Terrane	2.5.1.1.4.4.4.22
			Everona Fault-Mountain Run Fault Zone	**2.5.1.1.4.4.2.16**
			Reading Prong (west of the Ramapo)	**2.5.1.1.4.4.3.5**

© 2007-2012 UniStar Nuclear Services, LLC. All rights reserved.
COPYRIGHT PROTECTED

Table 2.5-62— {Relation of the Tectonic History of the Site Region to the Associated Tectonic Features}

(Page 2 of 4)

Tectonic Event	Principal Duration of Event	Brief Description of Conditions during Event near Site Region	Named Features and Text Sections for Detailed Descriptions	
Acadian Orogeny	Devonian to Middle Mississippian	Collision of Laurentia (N. American continent) with the Avalonia and Baltica terranes (eastern Europe craton). Mainly affected New England area with intrusives and metamorphism, but the site area became a basin with deposition of extensive clastics.	**Charlevoix-La Malbaie Seismic Zone** (meteorite impact)	**2.5.1.1.4.4.1.3**
			Plummers Island and Pleasant Grove Shear Zones	2.5.1.1.4.4.4.10
			Martic Fault	2.5.1.1.4.4.4.15
			Rosemont Shear Zone	2.5.1.1.4.4.4.20
Alleghanian Orogeny	Middle Pennsylvanian to Permian	Convergence of N. America and N. Africa continents (and others) to form the supercontinent of Pangaea. The principal effects were folding, thrusting and metamorphism with the reactivation of some older faults.	Anthracite Region	2.5.1.1.4.4.4.3
			Berwick Anticlinorium,	2.5.1.1.4.4.4.1
			Lackawanna Synclinorium	2.5.1.1.4.4.4.2
			Catawissa-McCauley Mountain Synclinorium	2.5.1.1.4.4.4.4
			Light Street Fault	2.5.1.1.4.4.4.1.1
			Berwick Fault	2.5.1.1.4.4.4.1.2
			Yellow Breeches Fault Zone	2.5.1.1.4.4.4.6
			Transylvania Fault Zone (reactivated)	2.5.1.1.4.4.4.9
			Plummers Island and Pleasant Grove Shear Zones (reactivated)	2.5.1.1.4.4.4.10
			Martic Fault	2.5.1.1.4.4.4.15
			Broadtop Synclinorium (reactivated)	2.5.1.1.4.4.4.17
			Sweet Arrow Fault	2.5.1.1.4.4.4.18
			Chestnut Ridge Anticline	2.5.1.1.4.4.4.19
			Furlong-Flemington Fault System (border fault for rift basin)	2.5.1.1.4.4.2.3
			Reading Prong (west of the Ramapo)	**2.5.1.1.4.4.3.5**

© 2007-2012 UniStar Nuclear Services, LLC. All rights reserved.
COPYRIGHT PROTECTED

Table 2.5-62— {Relation of the Tectonic History of the Site Region to the Associated Tectonic Features}

(Page 3 of 4)

Tectonic Event	Principal Duration of Event	Brief Description of Conditions during Event near Site Region	Named Features and Text Sections for Detailed Descriptions	
Mesozoic Rifting	Triassic to Jurassic	The breakup of Pangaea led to the formation of new rift basins along the crustal margin, when the Atlantic Ocean was opened. Intrusion of diabase dikes, and accumulation of volcanic and sediments. Outboard of the basins, carbonate platform deposition along the continental margin occurred.	**Charlevoix-La Malbaie Seismic Zone** (reactivated by renewed rifting)	**2.5.1.1.4.4.1.3**
			Ramapo Fault (Border fault of the Newark Basin)	**2.5.1.1.4.4.2.2**
			Reading Prong (west of the Ramapo)	**2.5.1.1.4.4.3.5**
			Furlong-Flemington Fault System (border fault for rift basin)	2.5.1.1.4.4.2.3
			Kingston Fault (border fault for the Newark Basin)	2.5.1.1.4.4.2.4.
			Dobbs Ferry Fault (Multi episodes of movement?)	**2.5.1.1.4.4.2.9**
			Lancaster Seismic Zone (Rift basin boundary?)	**2.5.1.1.4.4.2.10**
			East Border Fault	2.5.1.1.4.4.4.16
			Everona Fault-Mountain Run Fault Zone (Culpepper Basin)	**2.5.1.1.4.4.2.16**
			Transylvania Fault Zone (reactivated)	2.5.1.1.4.4.4.9
			Gettysburg, Culpepper, & Newark Basins	2.5.1.1.4.4.4.11
			Hartford Basin	2.5.1.1.4.4.4.12
			Connecticut Basin	2.5.1.1.4.4.4.13

© 2007-2012 UniStar Nuclear Services, LLC. All rights reserved.
COPYRIGHT PROTECTED

Table 2.5-62— {Relation of the Tectonic History of the Site Region to the Associated Tectonic Features}

(Page 4 of 4)

Tectonic Event	Principal Duration of Event	Brief Description of Conditions during Event near Site Region	Named Features and Text Sections for Detailed Descriptions	
Cenozoic Passive Margin	Late Cretaceous to Present	Site area becomes a Passive Continental Margin. Uplift and erosion inland, with inundation of the Atlantic Coastal Plain by a transgressive sea during much of the Cenozoic Era with continental shelf deposition. This was followed by the advance of at least three glaciers to the site vicinity during the Pleistocene.	**New Madrid Seismic Zone** (and Reelfoot Rift) (as a reactivated fault along a Precambrian rift?)	**2.5.1.1.4.4.1.1**
			Charleston Seismic Zone	**2.5.1.1.4.4.1.2**
			Charlevoix-La Malbaie Seismic Zone	**2.5.1.1.4.4.1.3**
			St Lawrence Rift Valley	**2.5.1.1.4.4.1.4**
			Newbury Liquefaction Features (Class A)	**2.5.1.1.4.4.2.1**
			Ramapo Fault (seismic activity indicates reactivation?)	**2.5.1.1.4.4.2.2**
			Furlong-Flemington Fault System (border fault for rift basin)	2.5.1.1.4.4.2.3
			Kingston Fault (border fault for the Newark Basin)	2.5.1.1.4.4.2.4
			New York Bight Fault (offshore)	**2.5.1.1.4.4.2.5**
			Moshulu Fault	**2.5.1.1.4.4.2.6**
			New Castle County Faults (Delaware)	**2.5.1.1.4.4.2.7**
			Upper Marlboro Faults (Landslides?)	2.5.1.1.4.4.2.8
			Dobbs Ferry Fault (Multi episodes of movement?)	**2.5.1.1.4.4.2.9**
			Lancaster Seismic Zone (Pennsylvania)	**2.5.1.1.4.4.2.10**
			Cacoosing Valley EQ Sequence (Quarry unloading)	2.5.1.1.4.4.2.11
			Moodus Seismic Zone	**2.5.1.1.4.4.2.12**
			Clarendon-Linden Fault Zone	**2.5.1.1.4.4.2.13**
			Offset Glaciated Surfaces	2.5.1.1.4.4.2.14
			Fall Lines of Weems	2.5.1.1.4.4.2.15
			Everona Fault-Mountain Run Fault Zone	**2.5.1.1.4.4.2.16**
			Stafford Fault System	**2.5.1.1.4.4.2.17**
			New York-Alabama Lineament	**2.5.1.1.4.4.3.1**
			Hudson River Valley Trend	**2.5.1.1.4.4.3.2**
			Pittsburgh-Washington Lineament	2.5.1.1.4.4.3.3
			Tyrone-Mt. Union Lineament	2.5.1.1.4.4.3.3
			Bristol Block Geopotential Trends	2.5.1.1.4.4.3.4
			Reading Prong (west of the Ramapo)	**2.5.1.1.4.4.3.5**
			Peekskill-Stamford Seismic Boundary	**2.5.1.1.4.4.3.6**
			Dillsburg Microearthquake Swarm	**2.5.1.1.4.4.3.7**
			Scranton Gravity High	2.5.1.1.4.4.4.5
			Brandywine Fault System	2.5.1.1.4.4.4.14

NOTE: Features that are considered to be capable are shown in **BOLD FONT**

© 2007-2012 UniStar Nuclear Services, LLC. All rights reserved.
COPYRIGHT PROTECTED

Table 2.5-63— {2002-2007 Events In 500 Mile (805 km) Radius}

(Page 1 of 2)

mb	Longitude (degree)	Latitude (degree)	Depth (km)	Year	Month	Day	Hour	Minute	Second	Catalog Reference
3.80	-73.46	46.06	10	2002	2	11	11	41	37	**USGS (PDE)**
3.10	-75.17	45.29	18	2002	2	24	21	38	33	**USGS (PDE)**
3.04	-69.33	41.62	1	2002	3	12	7	13	24	**ANSS**
5.30	-73.70	44.51	11	2002	4	20	10	50	47	**ANSS**
3.60	-73.68	44.50	10	2002	5	24	23	46	0	**USGS (PDE)**
3.40	-76.62	45.63	18	2002	5	28	9	15	38	**USGS (PDE)**
3.17	-68.98	44.99	27.93	2002	6	5	20	18	44	**ANSS**
3.20	-73.86	45.59	18	2002	6	1	11	35	29	**USGS (PDE)**
3.40	-73.70	44.50	9	2002	6	25	13	40	28	**USGS (PDE)**
3.70	-76.29	46.96	18	2002	9	7	21	27	45	**USGS (PDE)**
3.00	-77.43	44.05	18	2002	11	7	16	55	6	**USGS (PDE)**
3.30	-73.79	44.56	14	2002	12	25	18	25	19	**USGS (PDE)**
3.30	-75.20	46.51	18	2003	2	9	16	18	3	**ANSS**
3.50	-82.89	44.69	5	2003	3	18	6	4	24	**ANSS**
3.70	-74.34	44.62	10	2003	4	8	15	6	14	**USGS (PDE)**
3.90	-78.07	37.76	5	2003	5	5	16	32	32	**USGS (PDE)**
3.60	-81.20	41.80	4	2003	6	30	19	21	17	**USGS (PDE)**
3.60	-70.02	42.77	11	2003	7	22	11	41	15	**USGS (PDE)**
3.50	-74.95	46.01	18	2003	8	20	1	58	17	**USGS (PDE)**
3.80	-75.11	40.61	3	2003	8	26	18	24	18	**USGS (PDE)**
4.50	-76.37	47.01	18	2003	10	12	8	26	7	**ANSS**
4.50	-77.90	37.59	5	2003	12	9	20	59	14	**USGS (PDE)**
3.30	-81.08	41.78	5	2004	6	30	4	3	14	**USGS (PDE)**
3.20	-78.25	43.69	5	2004	8	4	23	55	26	**USGS (PDE)**
3.30	-77.97	48.05	19.68	2005	1	30	18	6	45	**ANSS**
3.50	-74.20	45.06	18	2005	3	3	2	22	1	**USGS (PDE)**
3.60	-80.98	46.54	18	2005	3	13	17	8	14	**USGS (PDE)**
3.40	-75.64	46.28	18	2005	3	31	15	13	8	**USGS (PDE)**
3.40	-73.45	46.26	18	2005	4	8	4	32	38	**USGS (PDE)**
3.27	-75.61	46.29	5	2005	5	25	19	22	13	**ANSS**
3.30	-76.89	46.24	13.4	2005	7	4	11	47	14	**ANSS**
3.00	-75.13	47.06	10	2005	7	23	2	48	20	**ANSS**
3.60	-75.29	46.27	18	2005	9	6	14	10	51	**USGS (PDE)**
3.10	-76.52	46.63	12.88	2005	10	1	7	1	46	**ANSS**
4.20	-80.48	44.68	11	2005	10	20	21	16	28	**USGS (PDE)**
3.70	-73.90	45.03	12.69	2006	1	9	15	35	40	**ANSS**
4.50	-75.23	45.66	18	2006	2	25	1	39	22	**USGS (PDE)**
3.20	-74.71	45.55	18	2006	2	26	4	9	22	**USGS (PDE)**
3.10	-81.39	41.78	5	2006	3	11	12	27	15	**USGS (PDE)**
3.10	-76.62	46.83	18	2006	4	7	12	44	26	**USGS (PDE)**
3.10	-72.68	46.27	18	2006	5	11	6	35	38	**USGS (PDE)**
3.50	-81.23	41.84	5	2006	6	20	20	11	18	**USGS (PDE)**
3.40	-68.19	44.35	7	2006	9	22	10	39	21	**USGS (PDE)**
3.40	-79.58	34.55	5	2006	9	22	11	22	0	**USGS (PDE)**
3.70	-79.88	34.75	5	2006	9	25	5	44	25	**USGS (PDE)**
4.17	-68.14	44.35	10.83	2006	10	3	0	7	38	**ANSS**

© 2007-2012 UniStar Nuclear Services, LLC. All rights reserved.
COPYRIGHT PROTECTED

Table 2.5-63— {2002-2007 Events In 500 Mile (805 km) Radius}

(Page 2 of 2)

mb	Longitude (degree)	Latitude (degree)	Depth (km)	Year	Month	Day	Hour	Minute	Second	Catalog Reference
4.30	-81.92	37.20	1	2006	11	2	17	53	2	**USGS (PDE)**
4.30	-81.97	37.16	0	2006	11	23	10	42	57	**USGS (PDE)**
4.10	-81.17	46.48	1	2006	11	29	7	22	55	**USGS (PDE)**
3.20	-68.17	44.35	8	2006	12	29	21	21	10	**USGS (PDE)**
3.30	-76.23	47.03	18	2007	1	6	4	8	44	**USGS (PDE)**
3.70	-81.38	41.28	5	2007	3	12	23	18	16	**USGS (PDE)**
3.20	-76.09	46.71	18	2007	5	11	5	55	22	**USGS (PDE)**
3.00	-72.89	46.99	18	2007	5	31	1	57	44	**USGS (PDE)**
3.00	-74.96	46.09	14.64	2007	6	2	2	19	54	**ANSS**
3.10	-78.17	43.71	5	2007	7	19	17	7	58	**USGS (PDE)**
3.10	-74.12	42.60	15	2007	7	24	1	56	48	**USGS (PDE)**
3.20	-74.36	44.32	2	2007	8	30	3	47	45	**USGS (PDE)**
3.90	-76.52	46.88	13	2007	9	30	17	35	35	**USGS (PDE)**
4.10	-76.88	47.08	18	2007	10	1	16	42	8	**USGS (PDE)**
3.50	-75.13	46.53	11	2007	10	13	5	53	31	**USGS (PDE)**
3.40	-81.42	41.75	5	2007	10	17	20	4	9	**USGS (PDE)**
3.53	-77.14	46.52	3.41	2007	10	28	9	47	18	**ANSS**
3.00	-75.12	46.31	18	2007	12	12	15	51	20	**USGS (PDE)**
3.00	-76.96	45.79	18	2007	12	20	12	16	41	**USGS (PDE)**
3.60	-77.32	46.26	18	2007	12	23	23	48	34	**USGS (PDE)**

© 2007-2012 UniStar Nuclear Services, LLC. All rights reserved.
COPYRIGHT PROTECTED

Table 2.5-64— {Uniform Hazard Response Spectra Comparison of 500-mi Sensitivity Analysis}

Spectral Frequency (Hz)	Probability of Exceedance Levels								
	2002 Catalog with 2002-2007 Update (500 miles) Spectral Value (g)			2002 Catalog (Base Case) Spectral Value (g)			Difference (%)		
	10^{-4}	10^{-5}	10^{-6}	10^{-4}	10^{-5}	10^{-6}	10^{-4}	10^{-5}	10^{-6}
0.5	0.0355	0.1100	0.2430	0.0357	0.1103	0.2437	-0.5%	-0.3%	-0.3%
1.0	0.0450	0.1175	0.2582	0.0454	0.1183	0.2606	-0.8%	-0.7%	-0.9%
2.5	0.0795	0.2166	0.5464	0.0807	0.2202	0.5565	-1.5%	-1.7%	-1.8%
5.0	0.1279	0.3978	1.0866	0.1307	0.4068	1.1081	-2.1%	-2.2%	-1.9%
10.0	0.1840	0.6314	1.7888	0.1888	0.6474	1.8252	-2.5%	-2.5%	-2.0%
25.0	0.2729	0.9777	3.0327	0.2802	1.0043	3.1000	-2.6%	-2.6%	-2.2%
100.0	0.0947	0.3512	1.0692	0.0973	0.3611	1.0914	-2.6%	-2.7%	-2.0%

© 2007-2012 UniStar Nuclear Services, LLC. All rights reserved.
COPYRIGHT PROTECTED

Table 2.5-65— {Uniform Hazard Response Spectra Comparison for the 625 mile (1006 km) Charlevoix Sensitivity Analysis Case 1}

Spectral Frequency (Hz)	Probability of Exceedance Levels								
	Modified Charlevoix Approach Case 1 Spectral Value (g)			Base Case Spectral Value (g)			Difference (%)		
	10^{-4}	10^{-5}	10^{-6}	10^{-4}	10^{-5}	10^{-6}	10^{-4}	10^{-5}	10^{-6}
0.5	0.0356	0.1101	0.2432	0.0357	0.1103	0.2437	-0.3%	-0.2%	-0.2%
1.0	0.0451	0.1176	0.2585	0.0454	0.1183	0.2606	-0.7%	-0.6%	-0.8%
2.5	0.0796	0.2169	0.5474	0.0807	0.2202	0.5565	-1.4%	-1.5%	-1.6%
5.0	0.1281	0.3986	1.0888	0.1307	0.4068	1.1081	-2.0%	-2.0%	-1.7%
10.0	0.1844	0.6329	1.7924	0.1888	0.6474	1.8252	-2.3%	-2.2%	-1.8%
25.0	0.2734	0.9801	3.0392	0.2802	1.0043	3.1000	-2.4%	-2.4%	-2.0%
100.0	0.0949	0.3521	1.0714	0.0973	0.3611	1.0914	-2.4%	-2.5%	-1.8%

© 2007-2012 UniStar Nuclear Services, LLC. All rights reserved.
COPYRIGHT PROTECTED

Table 2.5-66— {Maximum Magnitude Distribution used for the for the 625 mile (1006 km) Charlevoix Sensitivity Analyses}

Maximum Magnitude	Weight
5.9	0.33
6.3	0.34
6.7	0.33

© 2007-2012 UniStar Nuclear Services, LLC. All rights reserved.
COPYRIGHT PROTECTED

Table 2.5-67— {Uniform Hazard Response Spectra Comparison for the 625 mile (1006 km) Charlevoix Sensitivity Analysis Case 2}

Spectral Frequency (Hz)	Probability of Exceedance Levels								
	Modified Charlevoix Approach Case 2 Spectral Value (g)			Base Case Spectral Value (g)			Difference (%)		
	10^{-4}	10^{-5}	10^{-6}	10^{-4}	10^{-5}	10^{-6}	10^{-4}	10^{-5}	10^{-6}
0.5	0.0357	0.1102	0.2433	0.0357	0.1103	0.2437	0.0%	-0.1%	-0.1%
1.0	0.0452	0.1177	0.2587	0.0454	0.1183	0.2606	-0.4%	-0.5%	-0.7%
2.5	0.0797	0.2170	0.5475	0.0807	0.2202	0.5565	-1.3%	-1.5%	-1.6%
5.0	0.1282	0.3986	1.0888	0.1307	0.4068	1.1081	-1.9%	-2.0%	-1.7%
10.0	0.1844	0.6329	1.7924	0.1888	0.6474	1.8252	-2.3%	-2.2%	-1.8%
25.0	0.2735	0.9801	3.0392	0.2802	1.0043	3.1000	-2.4%	-2.4%	-2.0%
100.0	0.0949	0.3521	1.0714	0.0973	0.3611	1.0914	-2.4%	-2.5%	-1.8%

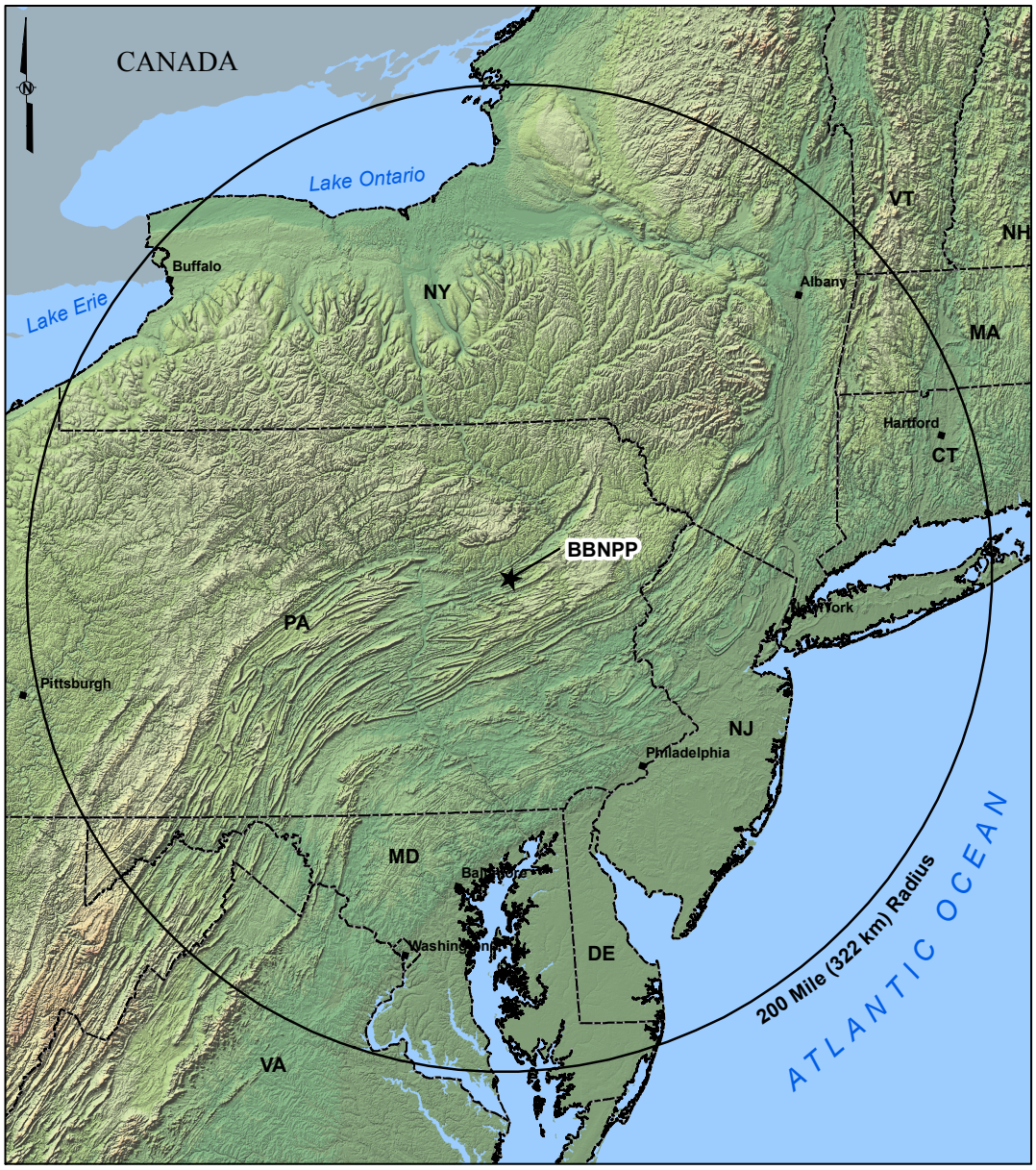
© 2007-2012 UniStar Nuclear Services, LLC. All rights reserved.
COPYRIGHT PROTECTED

Table 2.5-68— {Maximum Magnitude Distribution for the RSZ EST Zones}

EST	Zone(s) Emcompassing RSZ	Mmax Distribution		Mean M_{max}
		M_{max}	Weight	
Bechtel	Zone 13	5.4	0.1	5.82
		5.7	0.4	
		6.0	0.4	
		6.6	0.1	
	BZ5	5.7	0.1	6.15
		6.0	0.4	
		6.3	0.4	
		6.6	0.1	
Dames & Moore	Zone 41	6.1	0.8	6.32
		7.2	0.2	
	Zone 42	6.3	0.75	6.52
		7.2	0.25	
Law	Zone 17	5.7	0.2	6.58
		6.8	0.8	
Rondout	Zone 31	5.8	0.15	6.47
		6.5	0.60	
		6.8	0.25	
WCC	Zone 21	5.3	0.33	6.23
		6.5	0.34	
		6.9	0.33	
Weston	Zone 21	5.4	0.62	5.68
		6.0	0.29	
		6.6	0.09	

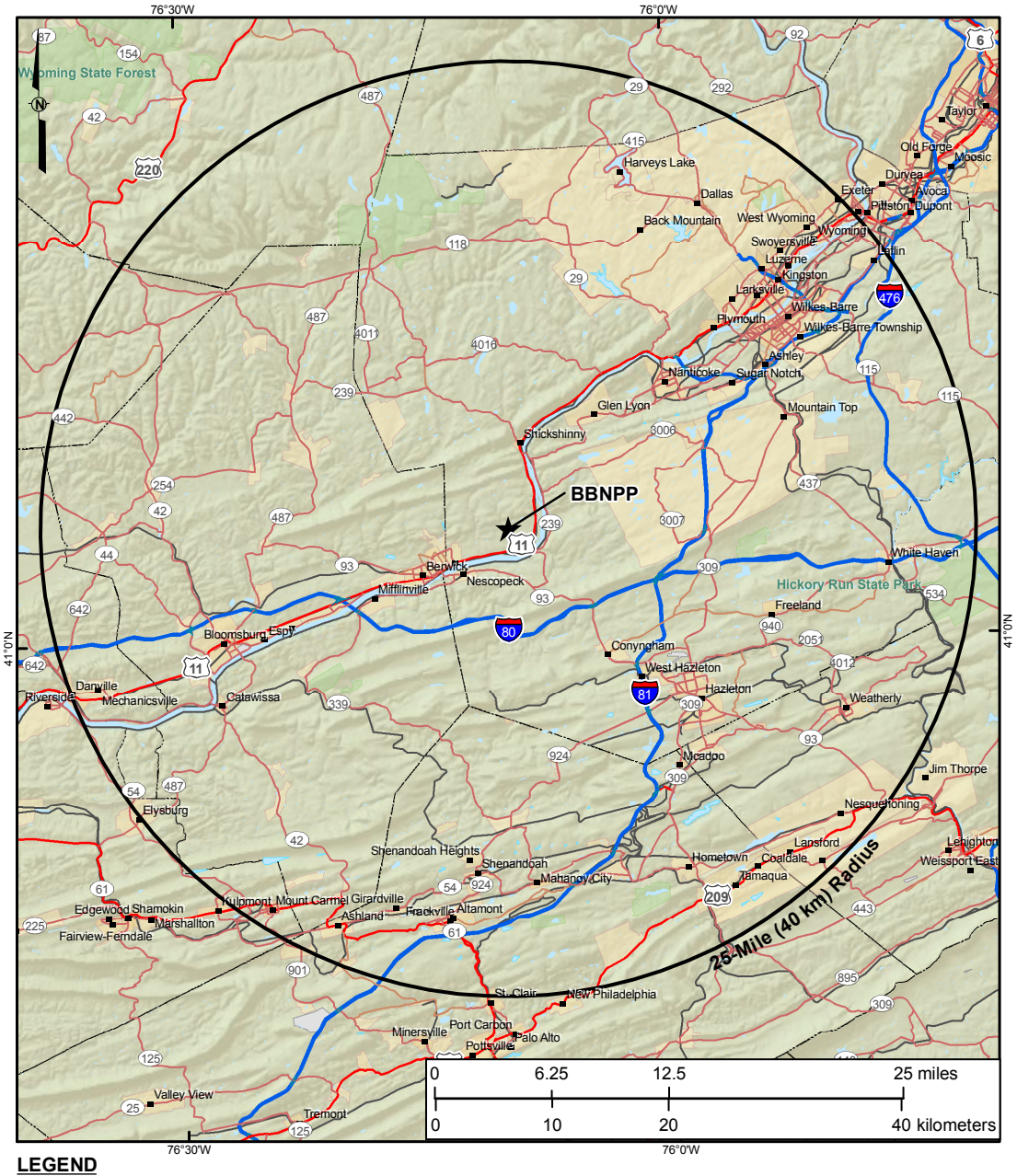
© 2007-2012 UniStar Nuclear Services, LLC. All rights reserved.
COPYRIGHT PROTECTED

Figure 2.5-1— {Site Region Relief Map 200 Mile (322 km) Radius}



© 2007-2012 UniStar Nuclear Services, LLC. All rights reserved.
COPYRIGHT PROTECTED

Figure 2.5-2— {Site Vicinity Shaded Relief Map 25 Mile (40 km) Radius}



LEGEND

★ Center Point of Proposed Bell Bend NPP (BBNPP)

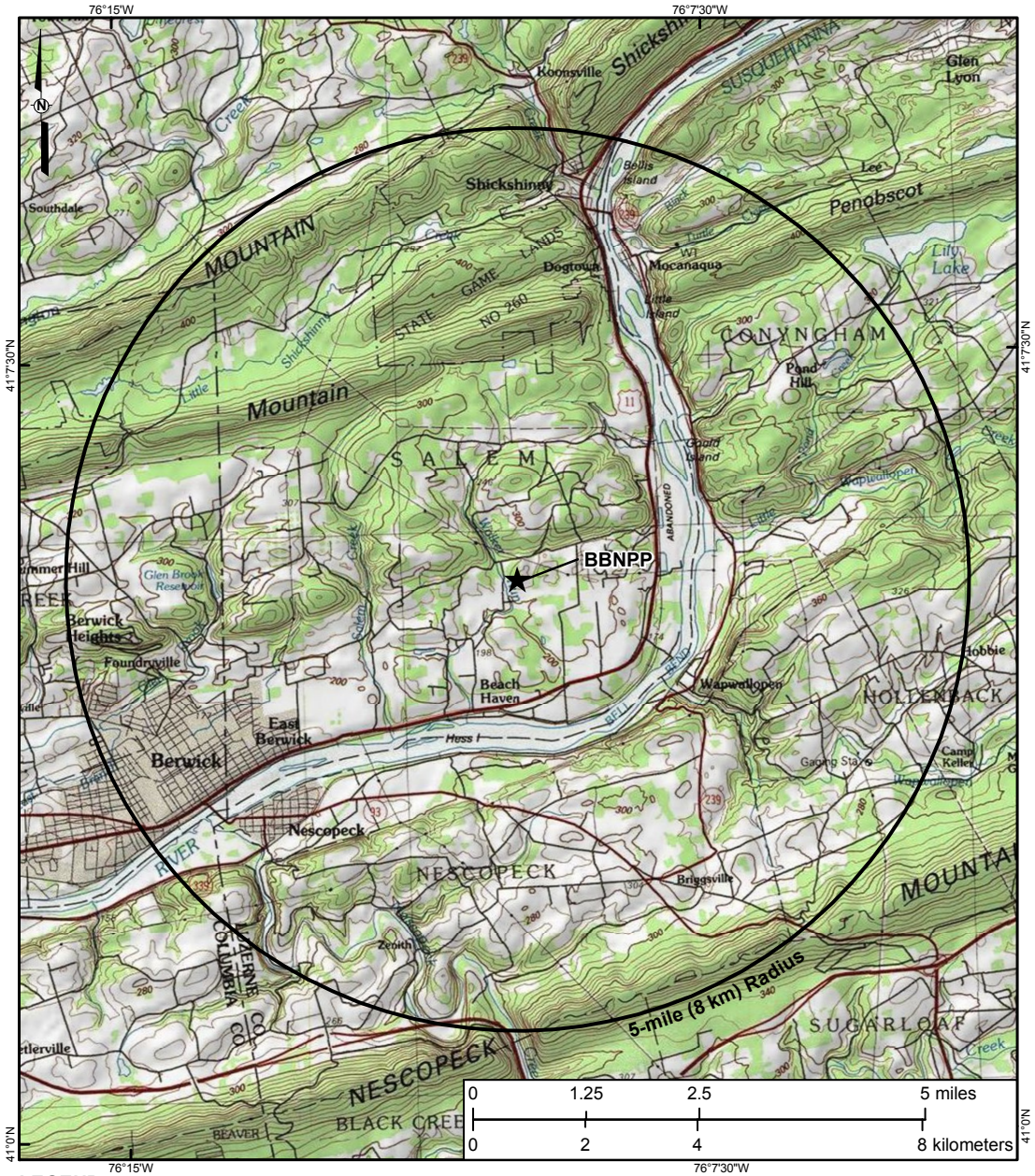
○ NPP Reactor 25-Mile (40 km) Radius

REFERENCE:
• ESRI, 2007.

10-4310-GIS-A028

© 2007-2012 UniStar Nuclear Services, LLC. All rights reserved.
COPYRIGHT PROTECTED

Figure 2.5-3— {Site Area Topographic Map 5 Mile (8 km) Radius}



LEGEND

★ Center Point of Proposed Bell Bend NPP (BBNPP)

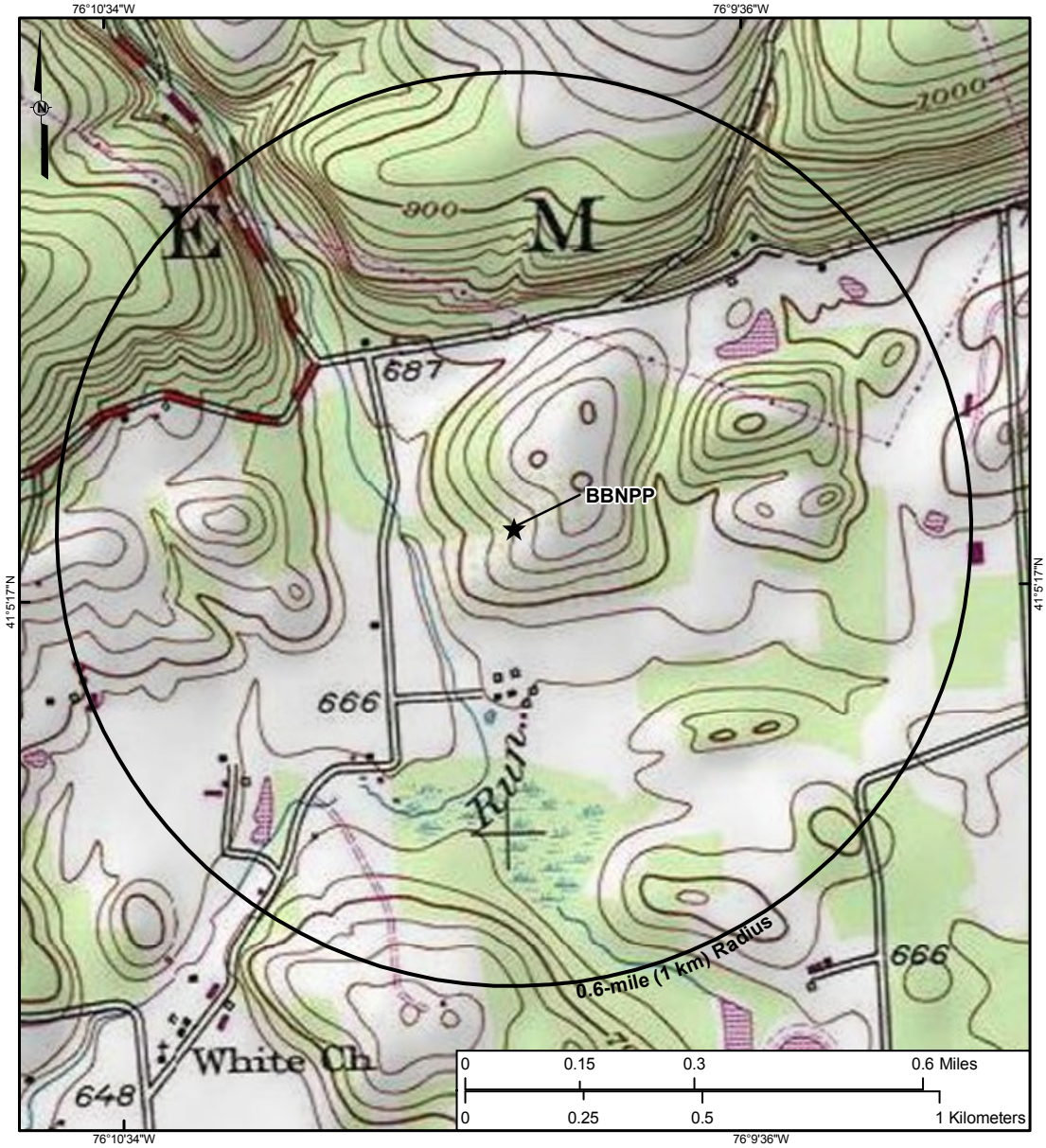
○ NPP Reactor 5-mile (8 km) Radius

REFERENCE:
• NGS, 2009.

10-4310-GIS-A029

© 2007-2012 UniStar Nuclear Services, LLC. All rights reserved.
COPYRIGHT PROTECTED

Figure 2.5-4— {Site Topographic Map 0.6 Mile (1 km) Radius}



LEGEND

★ Center Point of Proposed Bell Bend NPP (BBNPP)

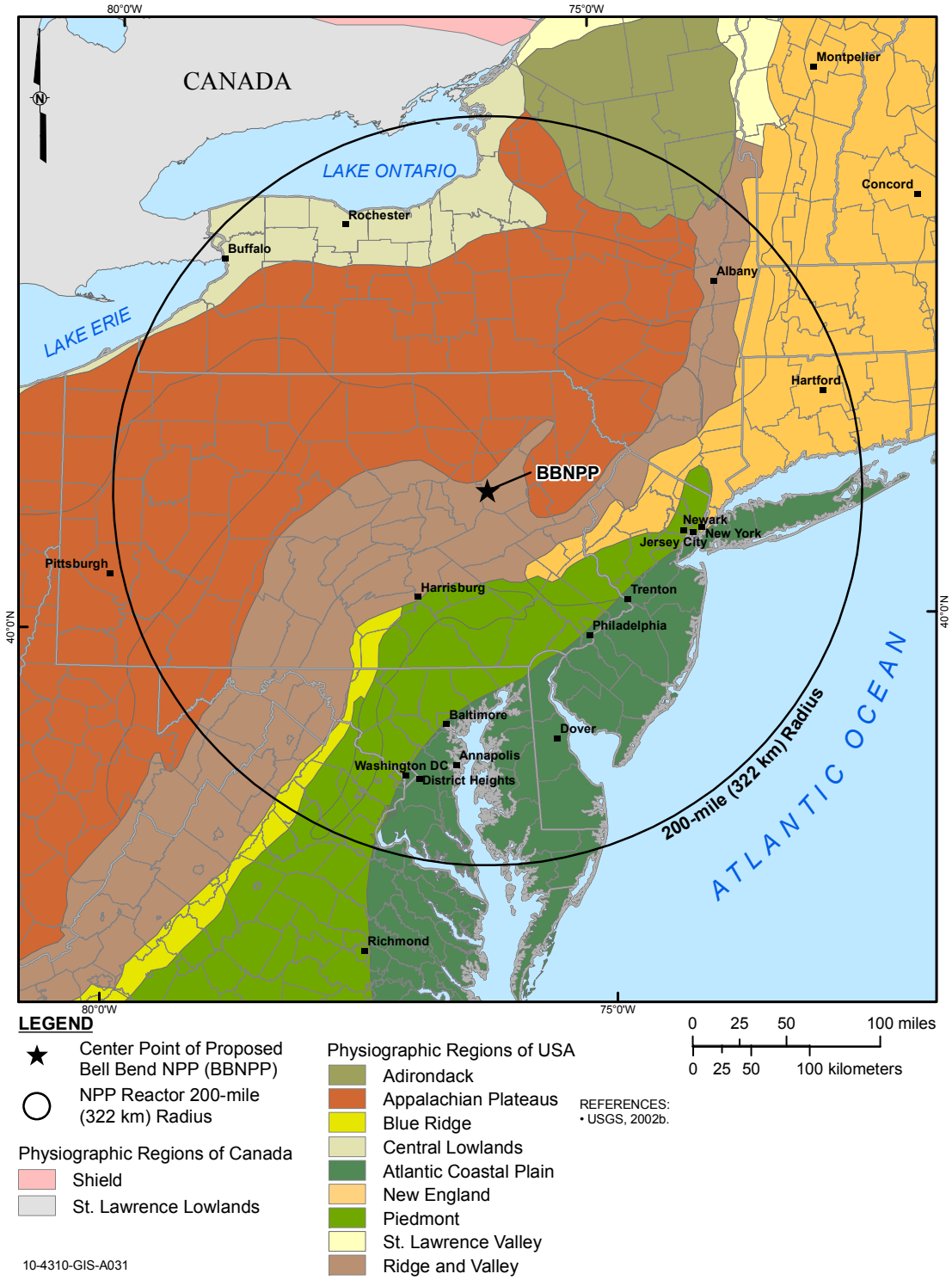
○ NPP Reactor 0.6-mile (1 km) Radius

REFERENCE:
• NGS, 2009.

10-4310-GIS-A030

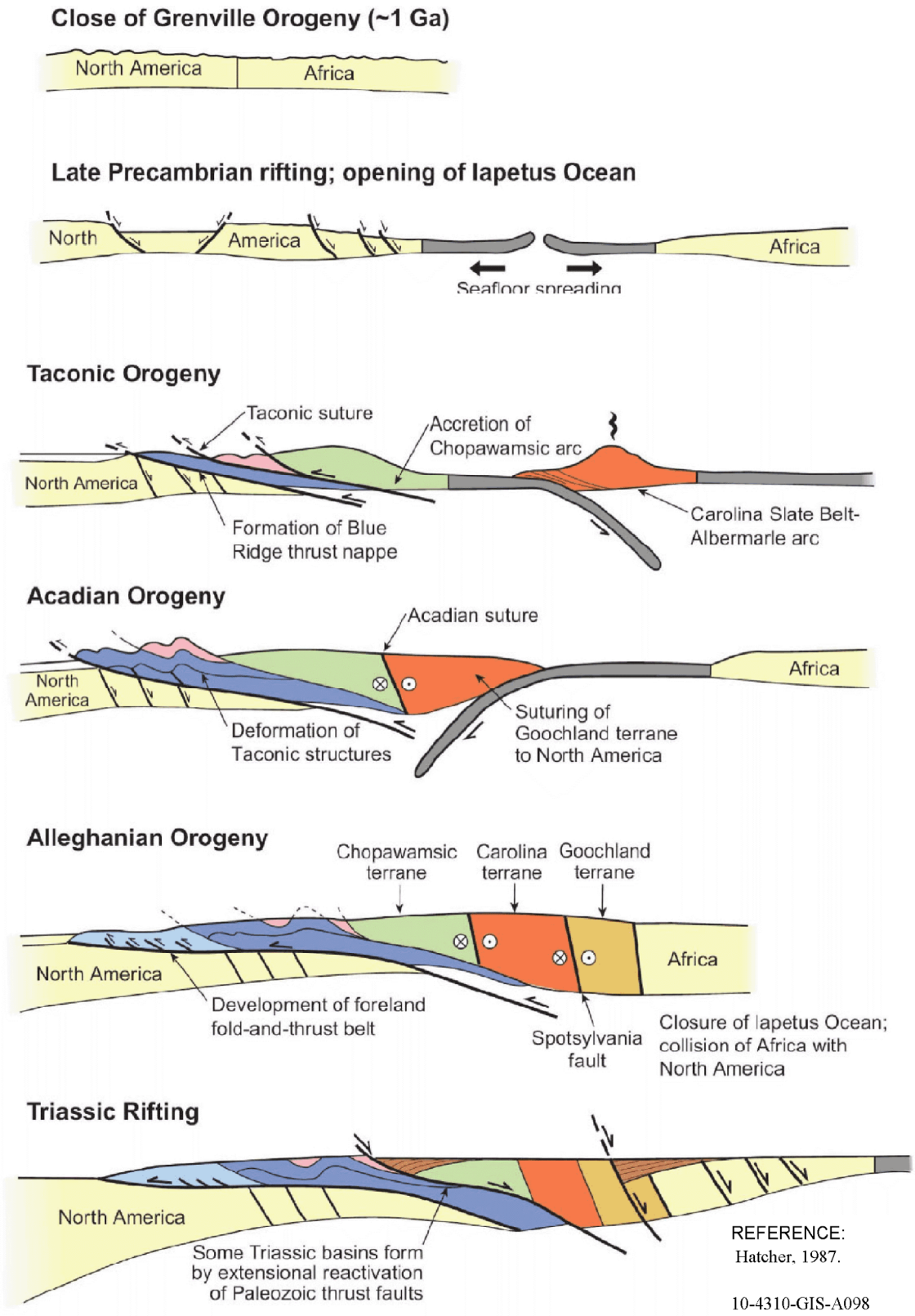
© 2007-2012 UniStar Nuclear Services, LLC. All rights reserved.
COPYRIGHT PROTECTED

Figure 2.5-5— {Physiographic Provinces Within the Site Region 200 Mile (322 km) Radius}



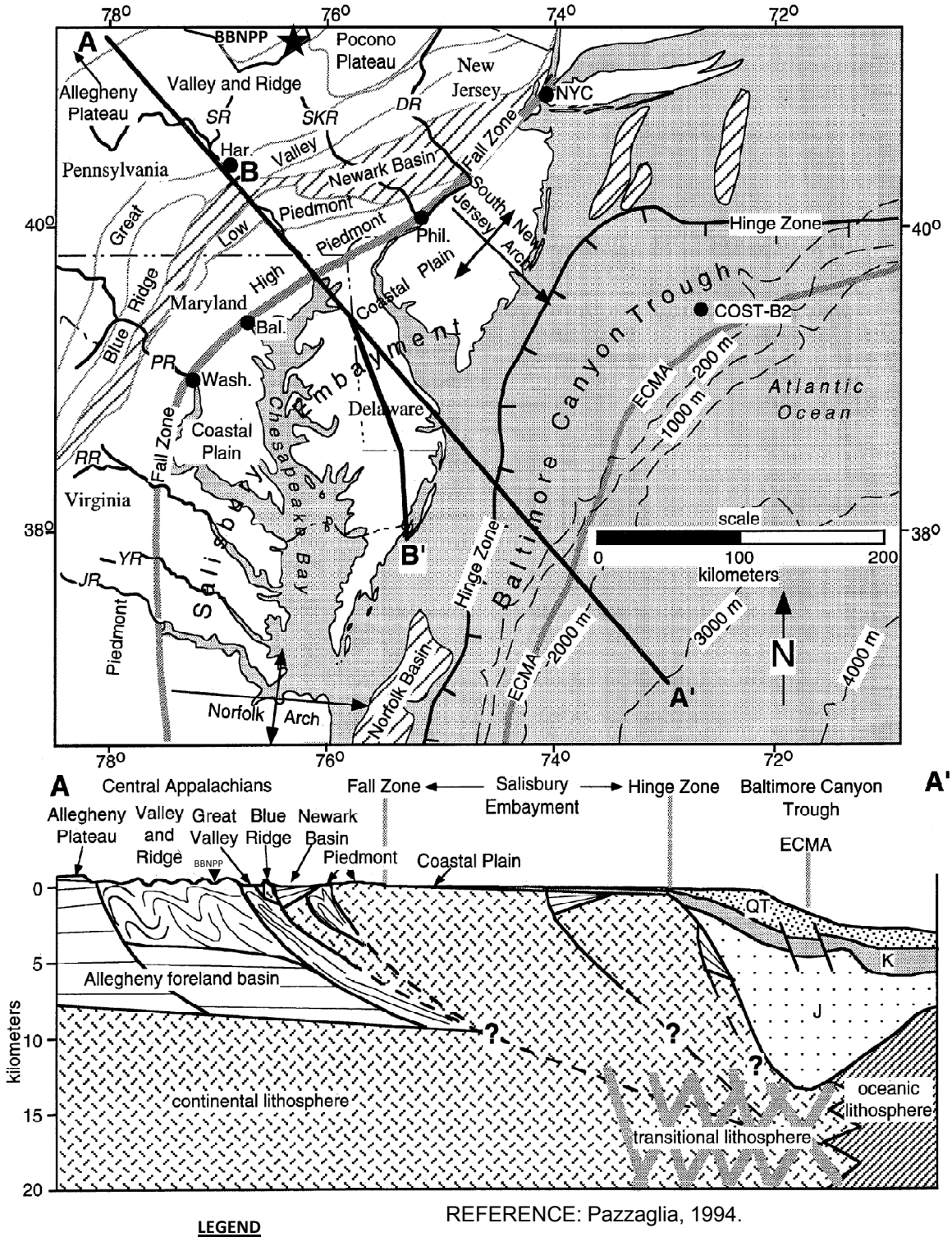
© 2007-2012 UniStar Nuclear Services, LLC. All rights reserved.
COPYRIGHT PROTECTED

Figure 2.5-6— {Evolution of the Appalachian Orogenic Belt}



© 2007-2012 UniStar Nuclear Services, LLC. All rights reserved.
COPYRIGHT PROTECTED

Figure 2.5-7— {Location Map and Cross Section of the Middle U.S. Atlantic Passive Margin}



REFERENCE: Pazzaglia, 1994.

LEGEND

Syn-rift basins shown with the diagonal-line ruled pattern

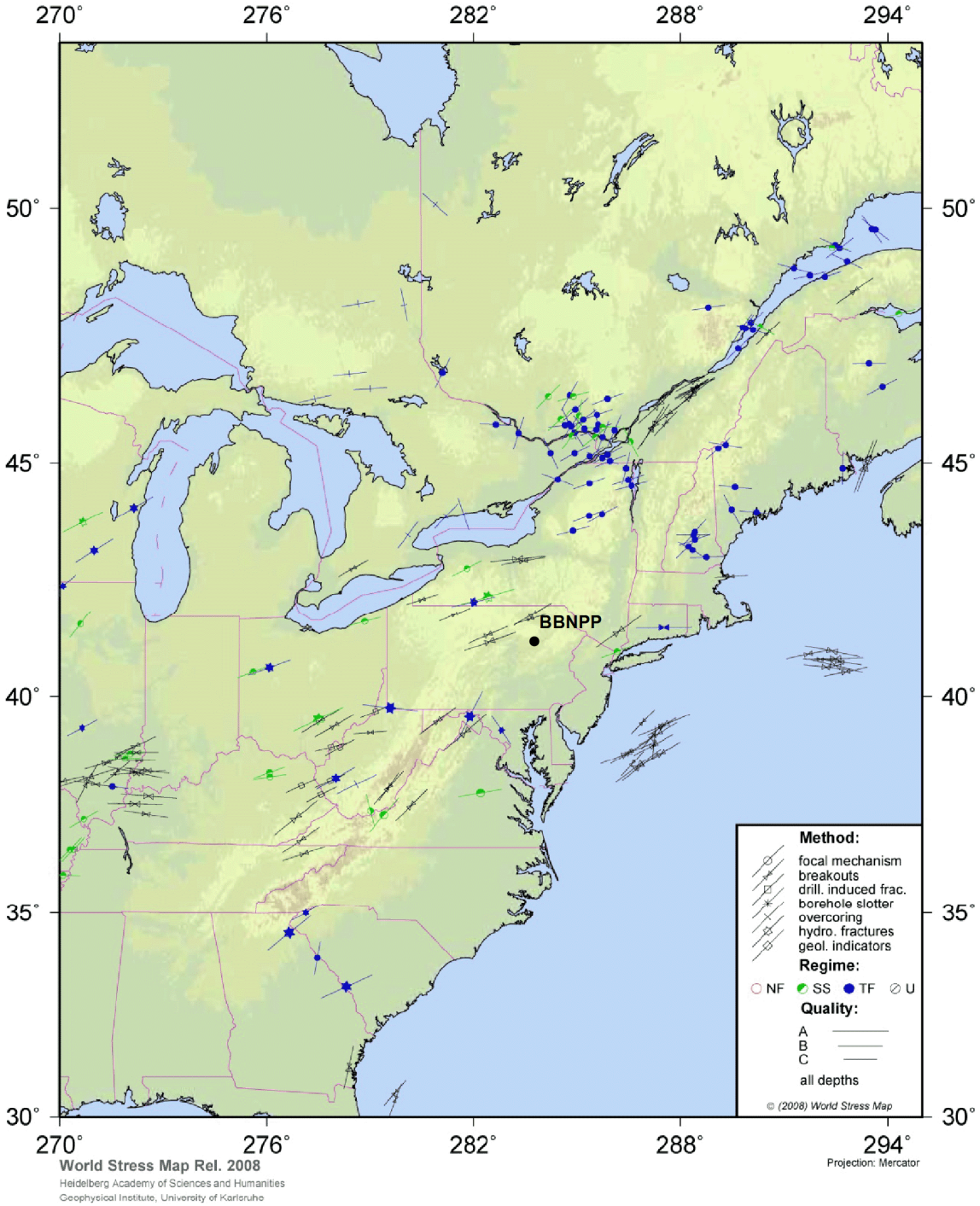
DR, Delaware River; **JR**, James River; **PT**, Potomac River; **RR**, Rappahannock River; **SKR**, Schuylkill River; **SR**, Susquehanna River; **YR**, York River; **Bal**, Baltimore; **Har**, Harrisburg; **NYC**, New York City; **Phil**, Philadelphia; **Wash**, Washington

★ **Bell Bend NPP**

BBNPP ▼ Approximate Location of Bell Bend NPP

© 2007-2012 UniStar Nuclear Services, LLC. All rights reserved.
COPYRIGHT PROTECTED

Figure 2.5-8— {Maximum Horizontal Stress Directions in Eastern North America}



Reference: Heidbach, 2008.

© 2007-2012 UniStar Nuclear Services, LLC. All rights reserved.
COPYRIGHT PROTECTED

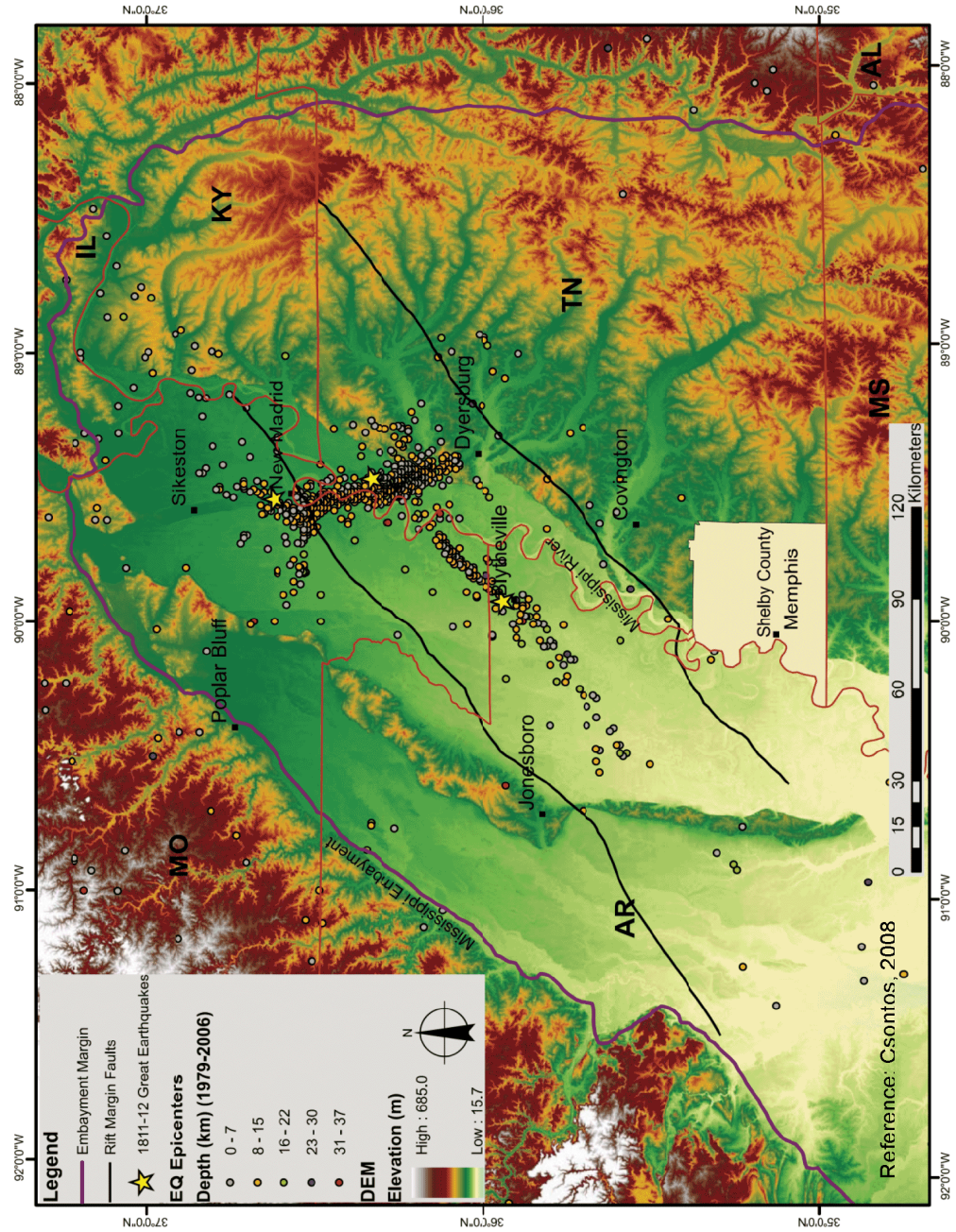
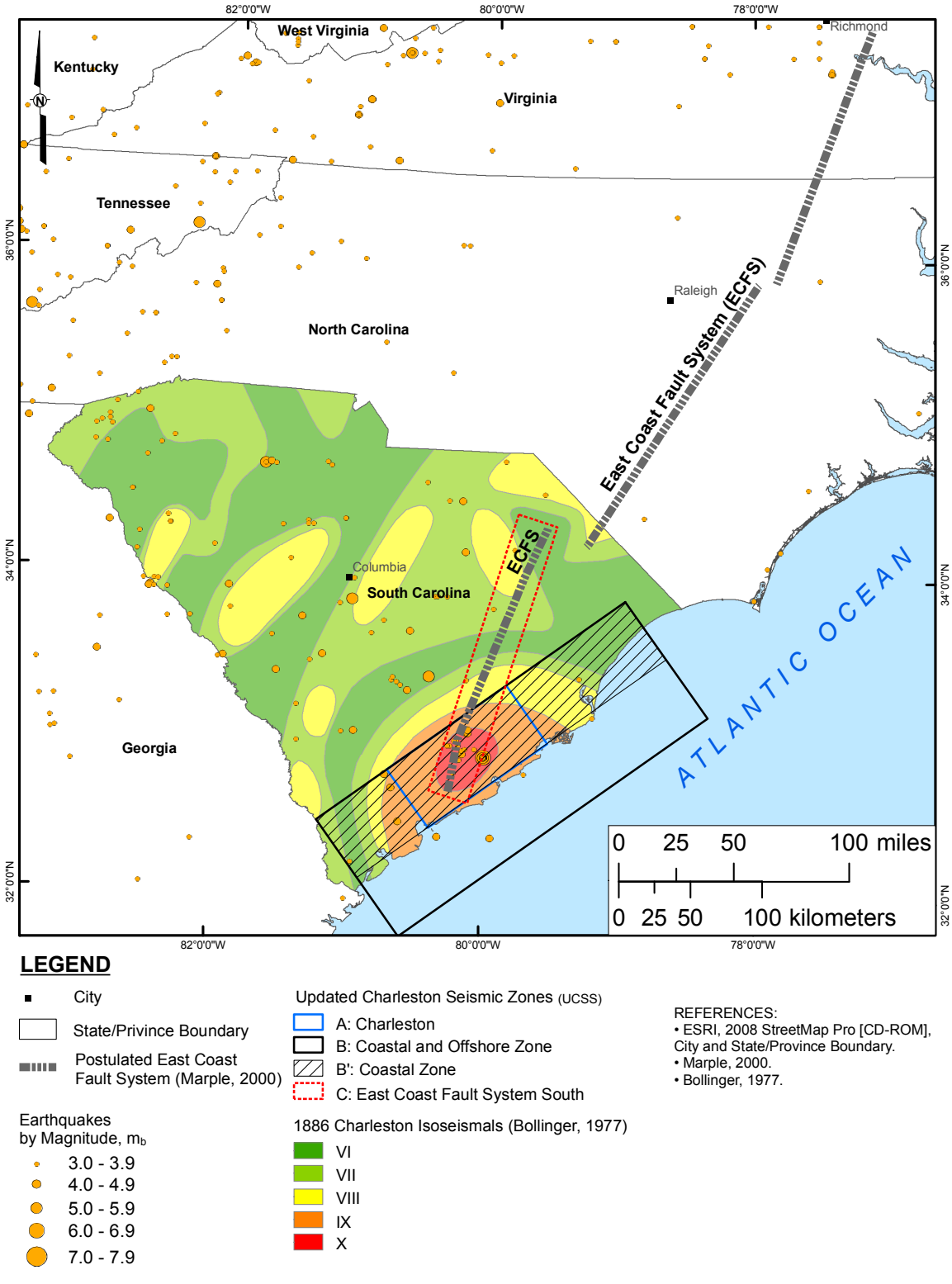


Figure 2.5-9— {New Madrid Seismic Zone with Earthquake Activity (1979-2006)}

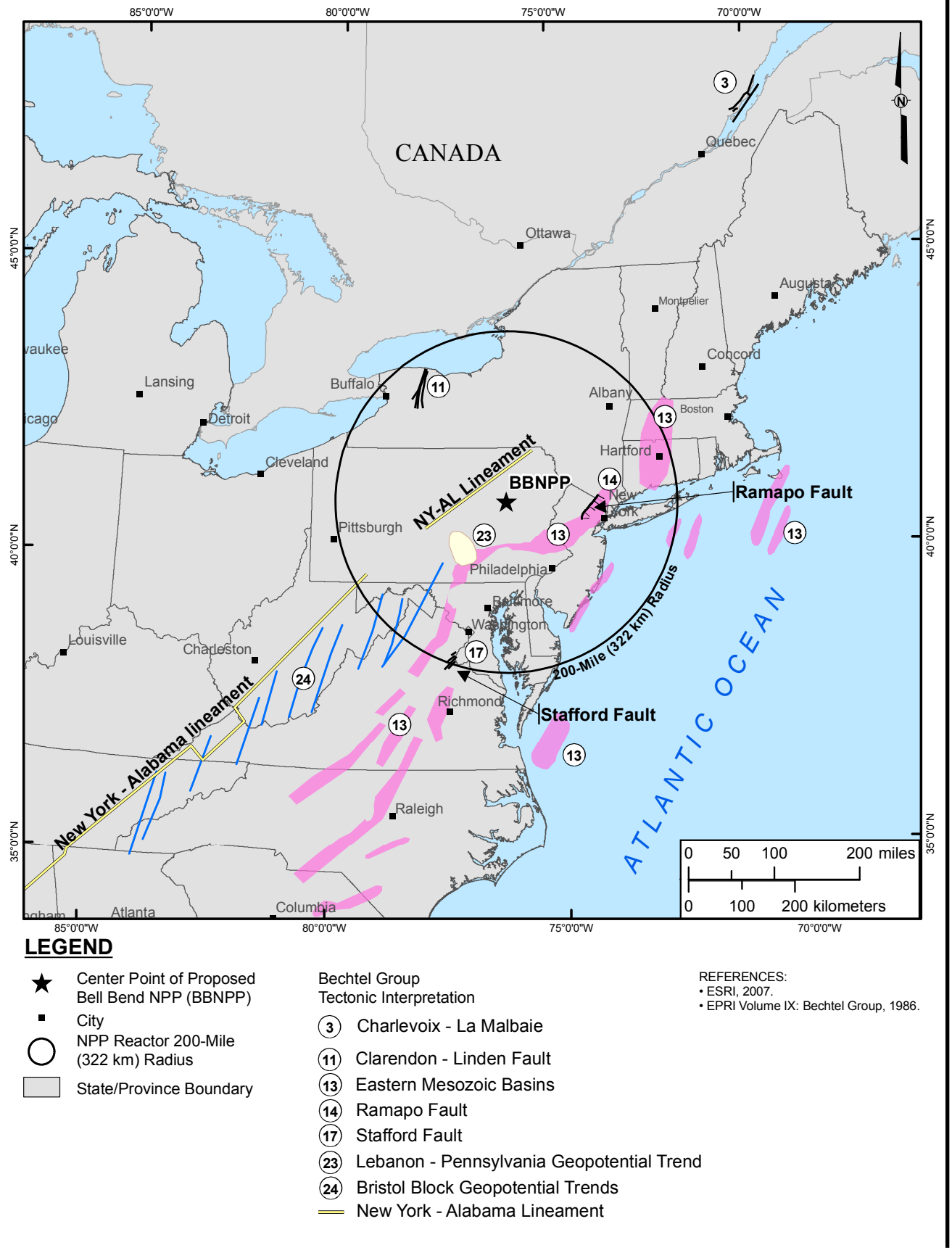
© 2007-2012 UniStar Nuclear Services, LLC. All rights reserved.
COPYRIGHT PROTECTED

Figure 2.5-10— {Charleston Seismic Zone (UCSS) Map with East Coast Fault System}



© 2007-2012 UniStar Nuclear Services, LLC. All rights reserved.
COPYRIGHT PROTECTED

Figure 2.5-11— {Tectonic Interpretations by Bechtel Group}



LEGEND

- ★ Center Point of Proposed Bell Bend NPP (BBNPP)
- ■ City
- ○ NPP Reactor 200-Mile (322 km) Radius
- State/Province Boundary

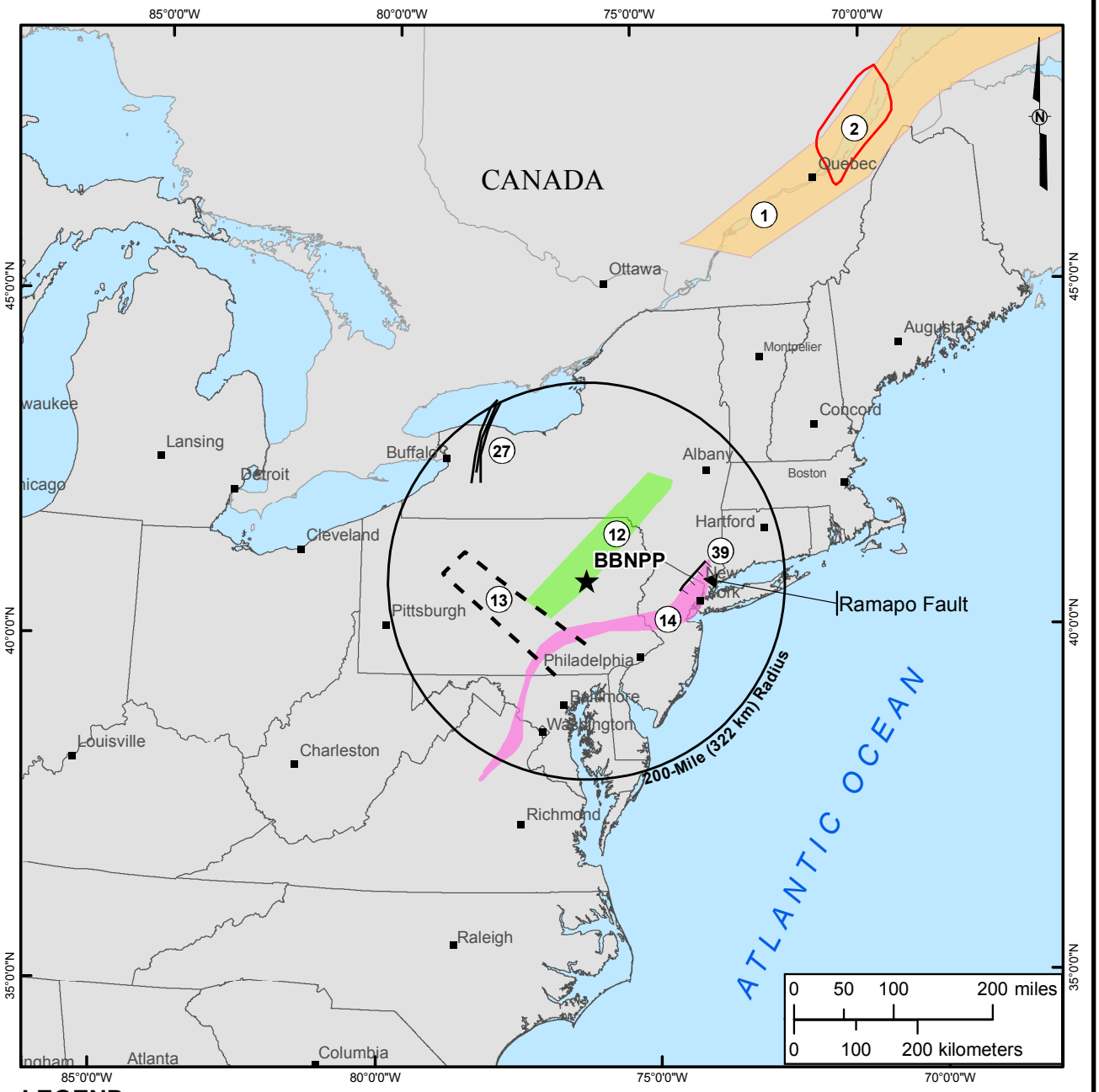
Bechtel Group
Tectonic Interpretation

- (3) Charlevoix - La Malbaie
- (11) Clarendon - Linden Fault
- (13) Eastern Mesozoic Basins
- (14) Ramapo Fault
- (17) Stafford Fault
- (23) Lebanon - Pennsylvania Geopotential Trend
- (24) Bristol Block Geopotential Trends
- New York - Alabama Lineament

REFERENCES:
- ESRI, 2007.
- EPRI Volume IX: Bechtel Group, 1986.

© 2007-2012 UniStar Nuclear Services, LLC. All rights reserved.
COPYRIGHT PROTECTED

Figure 2.5-12— {Tectonic Interpretations by Dames and Moore}



LEGEND

- ★ Center Point of Proposed Bell Bend NPP (BBNPP)
- ■ City
- ○ NPP Reactor 200-Mile (322 km) Radius
- State/Province Boundary

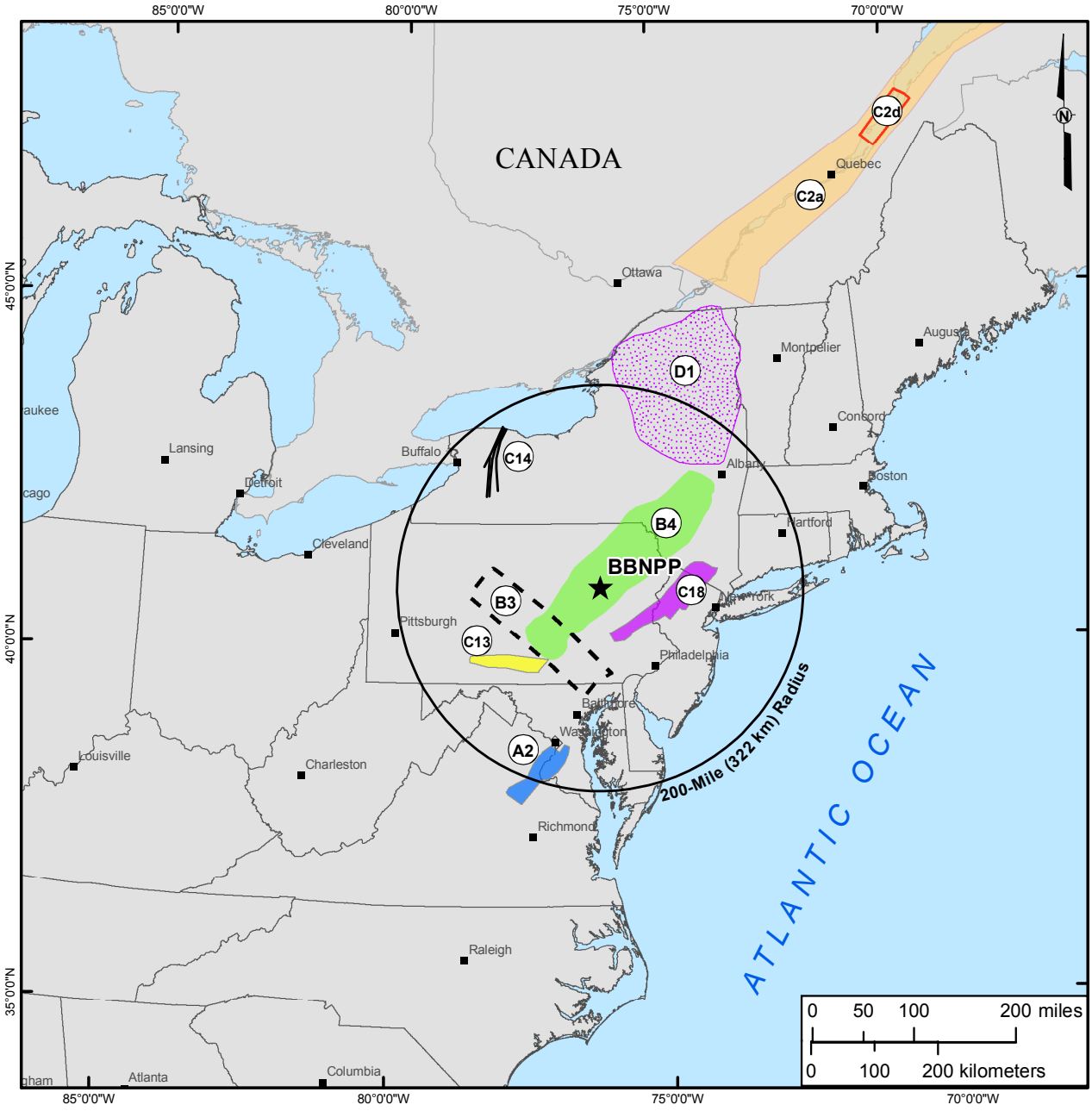
Dames and Moore Tectonic Interpretation

1. St. Lawrence Valley Rift
2. La Malbaie/Charlevoix Zone
12. Scranton Gravity Anomaly
13. Pennsylvania Aulacogen
14. Newark - Gettysburg Basin
27. Clarendon - Linden Fault Zone
39. Ramapo Fault

REFERENCES:
- ESRI, 2007.
- EPRI Volume VI: Dames and Moore, 1986.

© 2007-2012 UniStar Nuclear Services, LLC. All rights reserved.
COPYRIGHT PROTECTED

Figure 2.5-13— {Tectonic Interpretations by Law Engineering}



LEGEND

- ★ Center Point of Proposed Bell Bend NPP (BBNPP)
- ▪ City
- ○ NPP Reactor 200-Mile (322 km) Radius
- State/Province Boundary

Law Engineering Tectonic Interpretation

Regional Features

- (B3) Pennsylvania Aulacogen (EOCAMBRIAN RIFTS)
- (B4) Scranton Gravity High (EOCAMBRIAN RIFTS)
- (C2a) St Lawrence Valley Rift (ST. LAWRENCE RIFT SYSTEM)
- (C2d) Charlevoix - La Malbaie Area (ST. LAWRENCE RIFT SYSTEM)
- (D1) Adirondacks (MESOZOIC RIFTS)

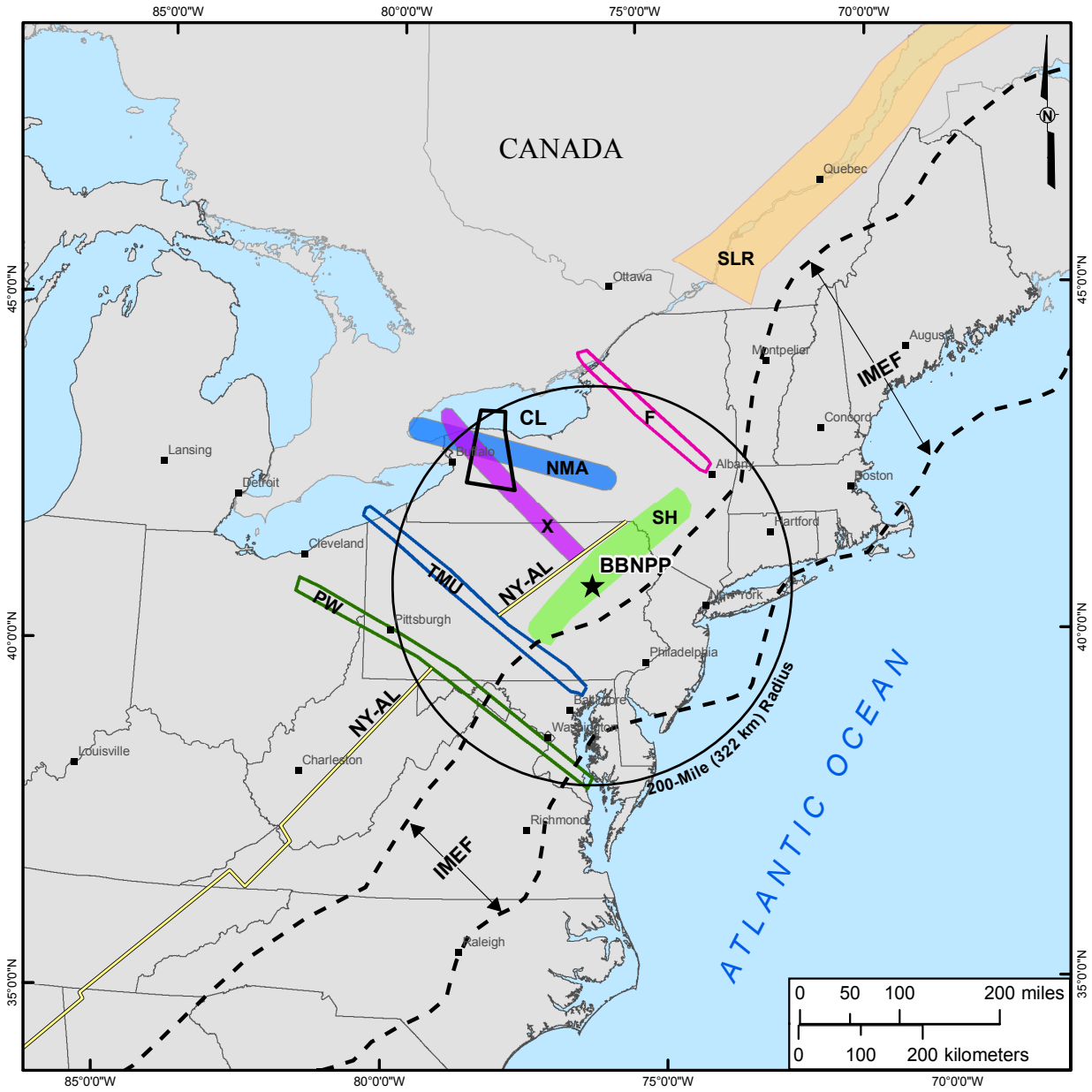
Faults and Shear Zones

- (A2) Stafford - Brandywine Fault Zone
- (C14) Clarendon - Linden Structure
- (C13) Latitude 40° N Fault Zone
- (C18) Ramapo Fault

REFERENCES:
- ESRI, 2007.
- EPRI Volume VII: Law Engineering, 1986.

© 2007-2012 UniStar Nuclear Services, LLC. All rights reserved.
COPYRIGHT PROTECTED

Figure 2.5-14— {Tectonic Interpretations by Rondout Associates}



LEGEND

- ★ Center Point of Proposed Bell Bend NPP (BBNPP)
- ▪ City
- ○ NPP Reactor 200-Mile (322 km) Radius
- State/Province Boundary

Rondout Associates
Tectonic Interpretations

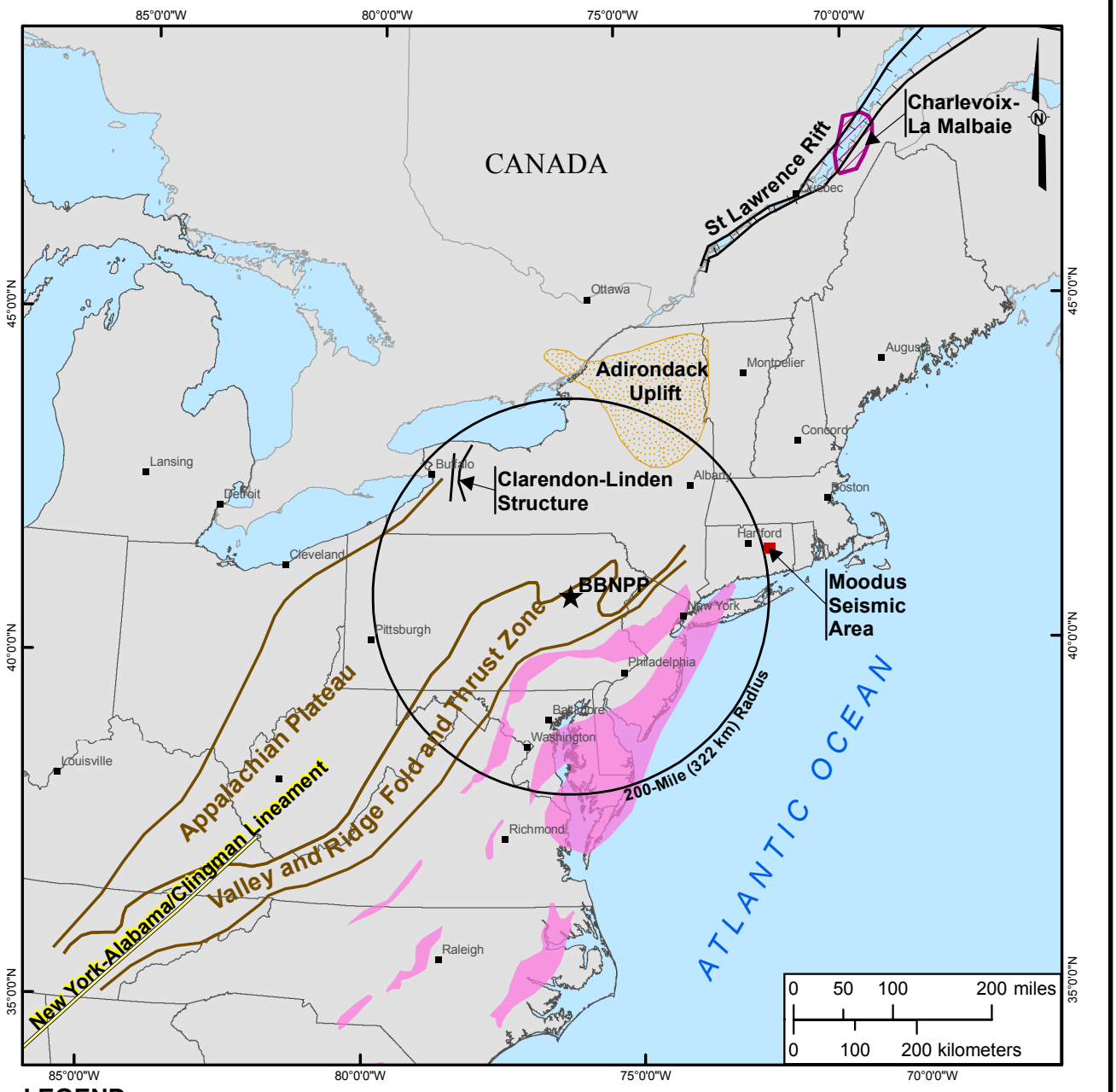
CL	Clarendon-Linden
F	Gravity Lineament
IMEF	Inboard Mesozoic Extentional Fault Realm
NMA	Niagara Magnetic Anomaly
NY-AL	New York - Alabama Lineament
PW	Pittsburgh - Washington Lineament
SH	Scranton Gravity HIgh
SLR	St. Lawrence Rift
TMU	Tyrone - Mt. Union Lineament
X	Gravity Anomaly

REFERENCES:
- ESRI, 2007.
- EPRI Volume X: Rondout Associates, 1986.

10-4310-GIS-A037

© 2007-2012 UniStar Nuclear Services, LLC. All rights reserved.
COPYRIGHT PROTECTED

Figure 2.5-15— {Tectonic Interpretation by Weston Geophycial}



LEGEND

- ★ Center Point of Proposed Bell Bend NPP (BBNPP)
- ▪ City
- ○ NPP Reactor 200-Mile (322 km) Radius

Weston Geophysical Tectonic Features

- Adirondack Uplift
- Charlevoix - La Malbaie
- Clarendon - Linden Structure
- N.Y. - Alabama/Clingman Lineaments
- St. Lawrence Rift
- Appalachian Plateau
- Valley and Ridge Fold and Thrust Zone
- Moodus Seismic Area
- Zone of Mesozoic Basins

REFERENCES:
- ESRI, 2007.
- EPRI Volume V: Weston Geophysical, 1986.

© 2007-2012 UniStar Nuclear Services, LLC. All rights reserved.
COPYRIGHT PROTECTED

Figure 2.5-16— {Tectonic Interpretations by Woodward-Clyde Consultants}



LEGEND

- ★ Center Point of Proposed Bell Bend NPP (BBNPP)
- ▪ City
- ○ NPP Reactor 200-Mile (322 km) Radius

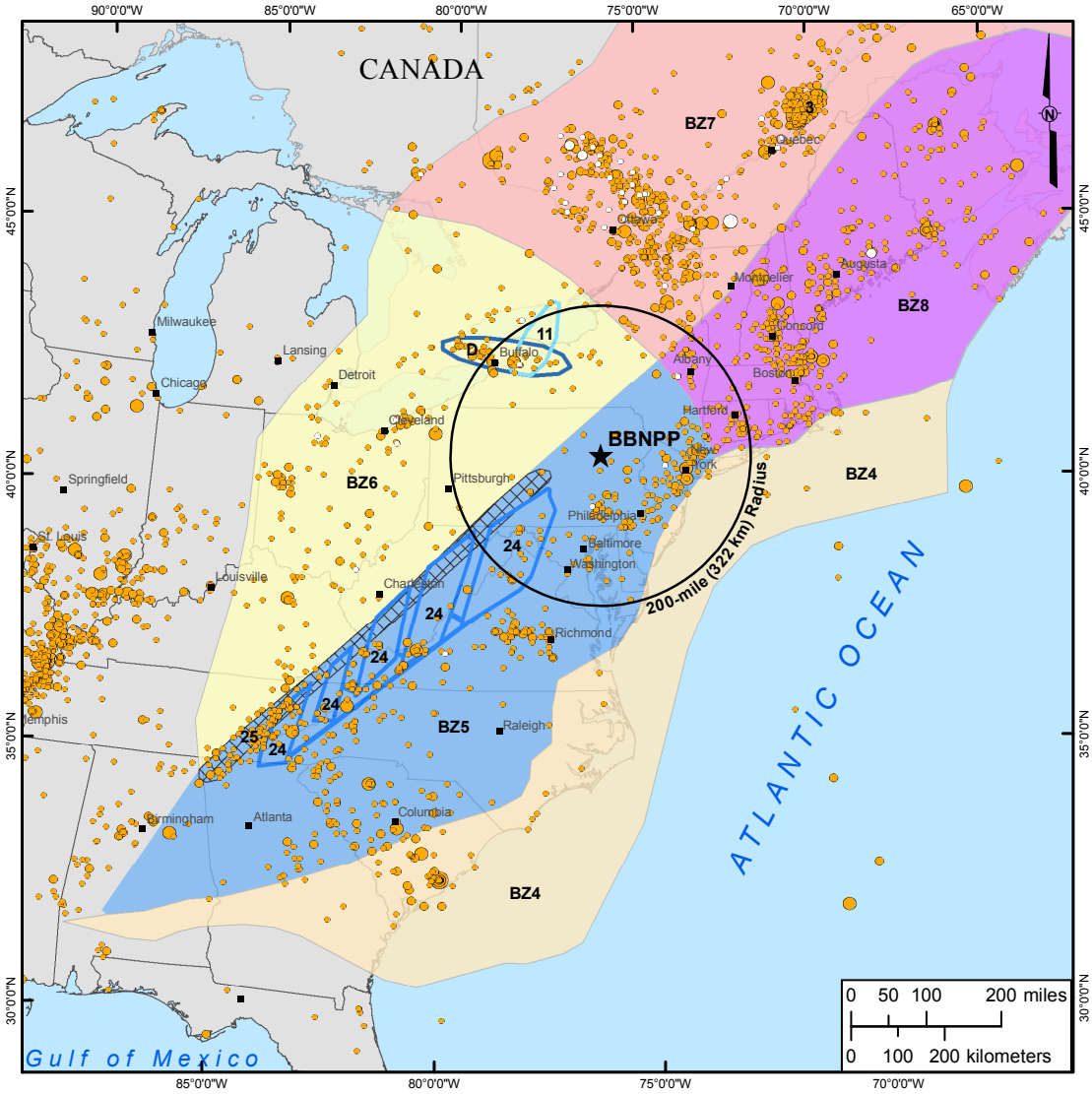
Woodward-Clyde Tectonic Interpretations

- **18** Adirondack Uplift
- **20** Mohawk River Trend
- **21** NJ Isostatic Gravity Saddle
- **25** Hudson River Valley Trend
- **33** Western NY - Southern Ontario Trend
- **34** Attica, NY Intersection Feature
- **63** Pittsburgh-Washington Lineament
- **12** Charlevoix - La Malbaie Structure
- **61** Tyrone - Mt. Union Lineament

REFERENCES:
- ESRI, 2007.
- EPRI Volume VIII: Woodward-Clyde Consultants, 1986.

© 2007-2012 UniStar Nuclear Services, LLC. All rights reserved.
COPYRIGHT PROTECTED

Figure 2.5-17— {Bechtel Group EPRI Source Zones}



LEGEND

- ★ Center Point of Proposed Bell Bend NPP (BBNPP)
- ▪ City
- ◯ NPP Reactor 200-mile (322 km) Radius

Earthquake Epicenters (by Magnitude, mb)

USGS 2008 Catalog (1534-2006)	2007 to April 2010
3.0 - 3.9	3.0 - 3.9
4.0 - 4.9	4.0 - 4.9
5.0 - 5.9	5.0 - 5.9
6.0 - 6.9	
7.0 - 7.9	

NOTE: The 2007 to 2010 seismicity shown in 500-mile (800 km) radius.

Bechtel Group Sources contributing to 99% of BBNPP Site Hazard

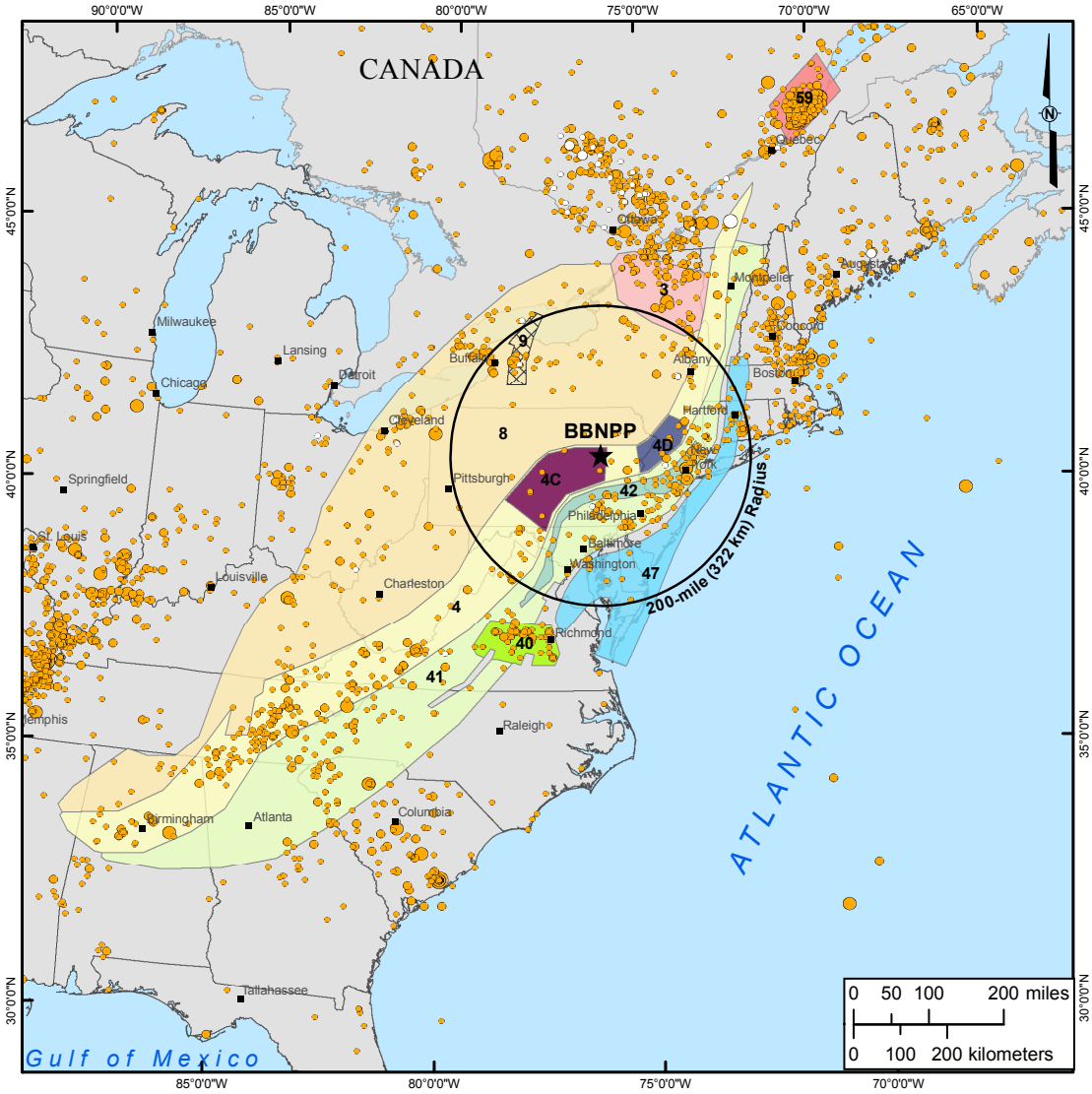
- 3 La Malbaie/Charlevoix
- 11 Clarendon-Linden
- 24 Bristol Block
- 25 NY-AL Lineament
- BZ4 Atlantic Coastal Region Background
- BZ5 Southern Appalachians Background
- BZ6 Southern Eastern Craton Background
- BZ7 Northern Eastern Craton Background
- BZ8 Northern Appalachians Background
- D Niagara Area

REFERENCES:
- ESRI, 2007.
- USGS 2008.
- USGS, PDE, 2010.
- ANSS, 2010.
- EC, 2010.
- EPRI Volume IX: Bechtel Group, 1986.

10-4310-GIS-A071

© 2007-2012 UniStar Nuclear Services, LLC. All rights reserved.
COPYRIGHT PROTECTED

Figure 2.5-18— {Dames & Moore EPRI Source Zones}



LEGEND

- ★ Center Point of Proposed Bell Bend NPP (BBNPP)
- ▪ City
- ◯ NPP Reactor 200-mile (322 km) Radius

Earthquake Epicenters (by Magnitude, mb)

USGS 2008 Catalog (1534-2006)	2007 to April 2010
3.0 - 3.9	3.0 - 3.9
4.0 - 4.9	4.0 - 4.9
5.0 - 5.9	5.0 - 5.9
6.0 - 6.9	
7.0 - 7.9	

NOTE: The 2007 to 2010 seismicity shown in 500-mile (800 km) radius.

Dames and Moore Sources contributing to 99% of BBNPP Site Hazard

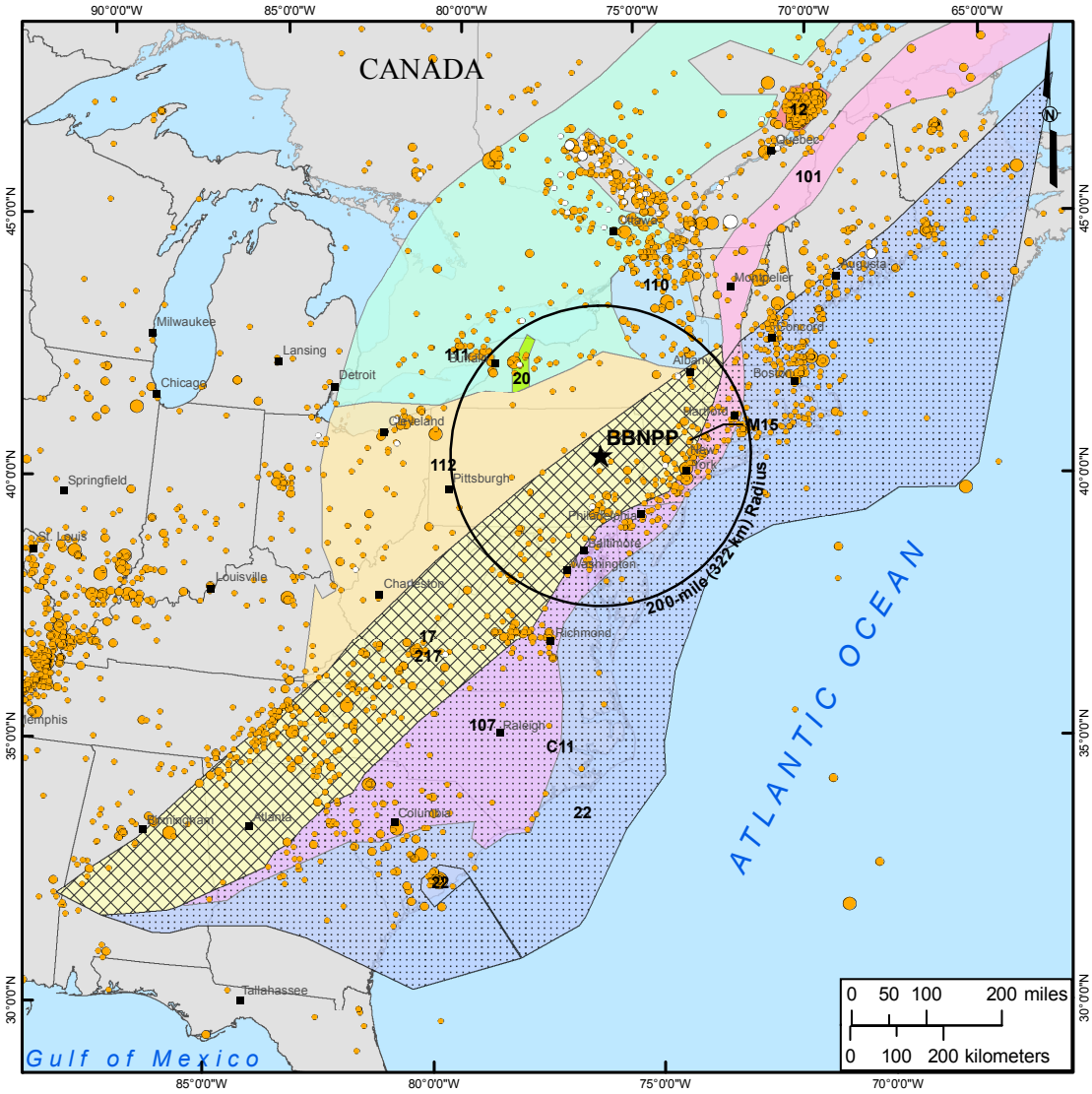
- 3 Adirondacks Zone
- 4 Appalachian Fold Belts
- 4C Kink in Fold Belt
- 4D Kink in Fold Belt
- 8 Eastern Marginal Basin
- 9 Clarendon-Linden Zone
- 40 Central Virginia Seismic Zone
- 41 Southern Cratonic Margin (default)
- 42 Newark-Gettysburg Basin
- 47 Connecticut Basin
- 59 La Malbaie/Charlevoix Zone

REFERENCES:
- ESRI, 2007.
- USGS 2008.
- USGS, PDE, 2010.
- ANSS, 2010.
- EC, 2010.
- EPRI Volume VI: Dames and Moore, 1986.

10-4310-GIS-A078

© 2007-2012 UniStar Nuclear Services, LLC. All rights reserved.
COPYRIGHT PROTECTED

Figure 2.5-19— {Law Engineering EPRI Source Zones}



LEGEND

- ★ Center Point of Proposed Bell Bend NPP (BBNPP)
- ■ City
- ◯ NPP Reactor 200-mile (322 km) Radius

Earthquake Epicenters (by Magnitude, mb)

USGS 2008 Catalog (1534-2006)	2007 to April 2010
3.0 - 3.9	3.0 - 3.9
4.0 - 4.9	4.0 - 4.9
5.0 - 5.9	5.0 - 5.9
6.0 - 6.9	
7.0 - 7.9	

NOTE: The 2007 to 2010 seismicity shown in 500-mile (800 km) radius.

Law Engineering Sources contributing to 99% of BBNPP Site Hazard

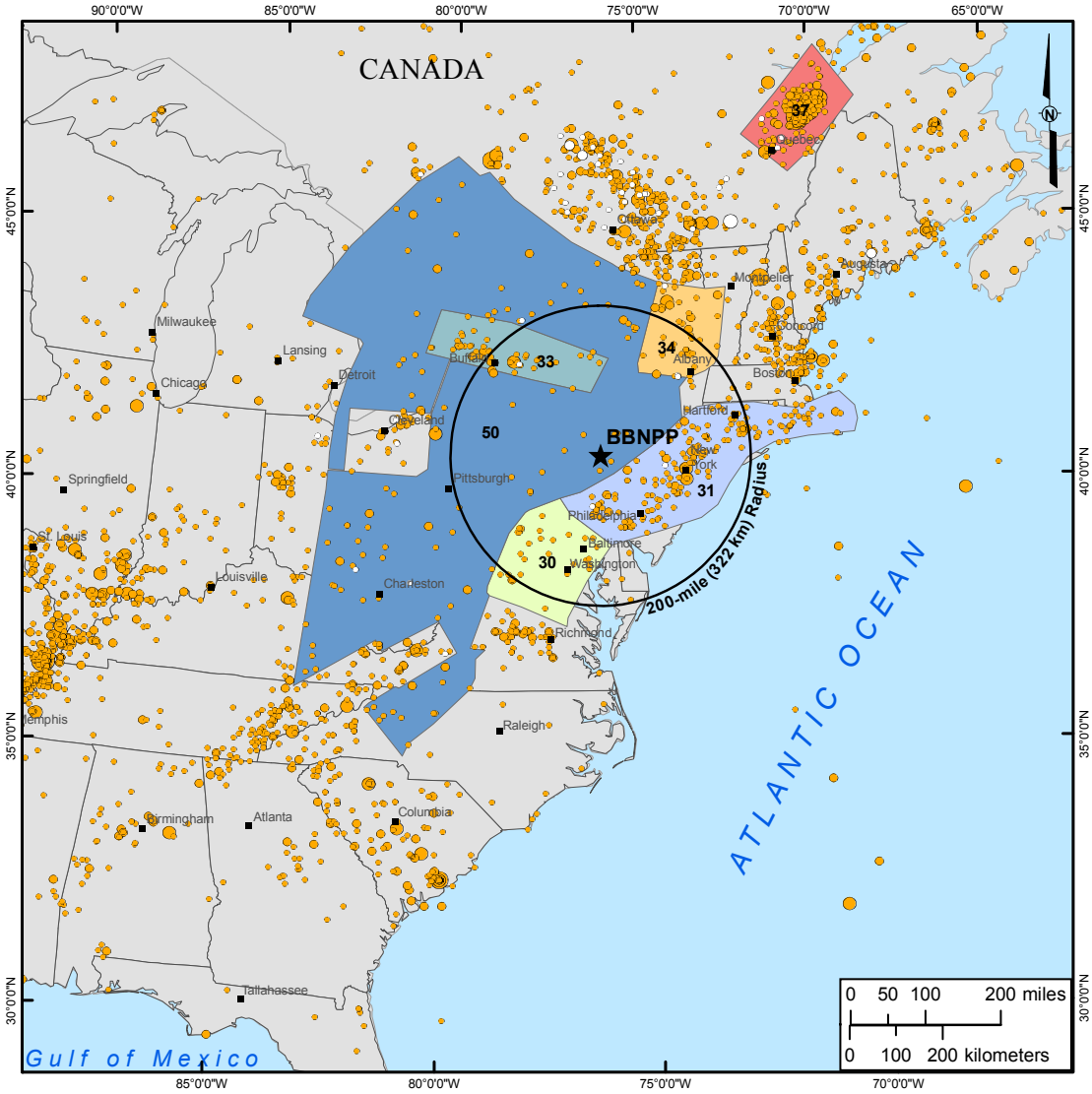
M15	Mafic Pluton
C11	Combination (22-35)
217	Eastern Basement Background
12	La Malbaie/Charlevoix
17	Eastern Basement
20	Clarendon-Linden
22	Reactivated Eastern Seaboard Normal
101	Western New England Background
107	Eastern Piedmont Background
110	Adirondacks Background
111	Laurentian Block
112	Ohio-Pennsylvania Block

REFERENCES:
- ESRI, 2007.
- USGS 2008.
- USGS, PDE, 2010.
- ANSS, 2010.
- EC, 2010.
- EPRI Volume VII: Law Engineering, 1986.

10-4310-GIS-A079

© 2007-2012 UniStar Nuclear Services, LLC. All rights reserved.
COPYRIGHT PROTECTED

Figure 2.5-20— {Roundout Associates EPRI Source Zones}



LEGEND

- ★ Center Point of Proposed Bell Bend NPP (BBNPP)
- ▪ City
- ◯ NPP Reactor 200-mile (322 km) Radius

Earthquake Epicenters (by Magnitude, mb)

USGS 2008 Catalog (1534-2006)	2007 to April 2010
3.0 - 3.9	3.0 - 3.9
4.0 - 4.9	4.0 - 4.9
5.0 - 5.9	5.0 - 5.9
6.0 - 6.9	
7.0 - 7.9	

NOTE: The 2007 to 2010 seismicity shown in 500-mile (800 km) radius.

Rondout Associates Sources contributing to 99% of BBNPP Site Hazard

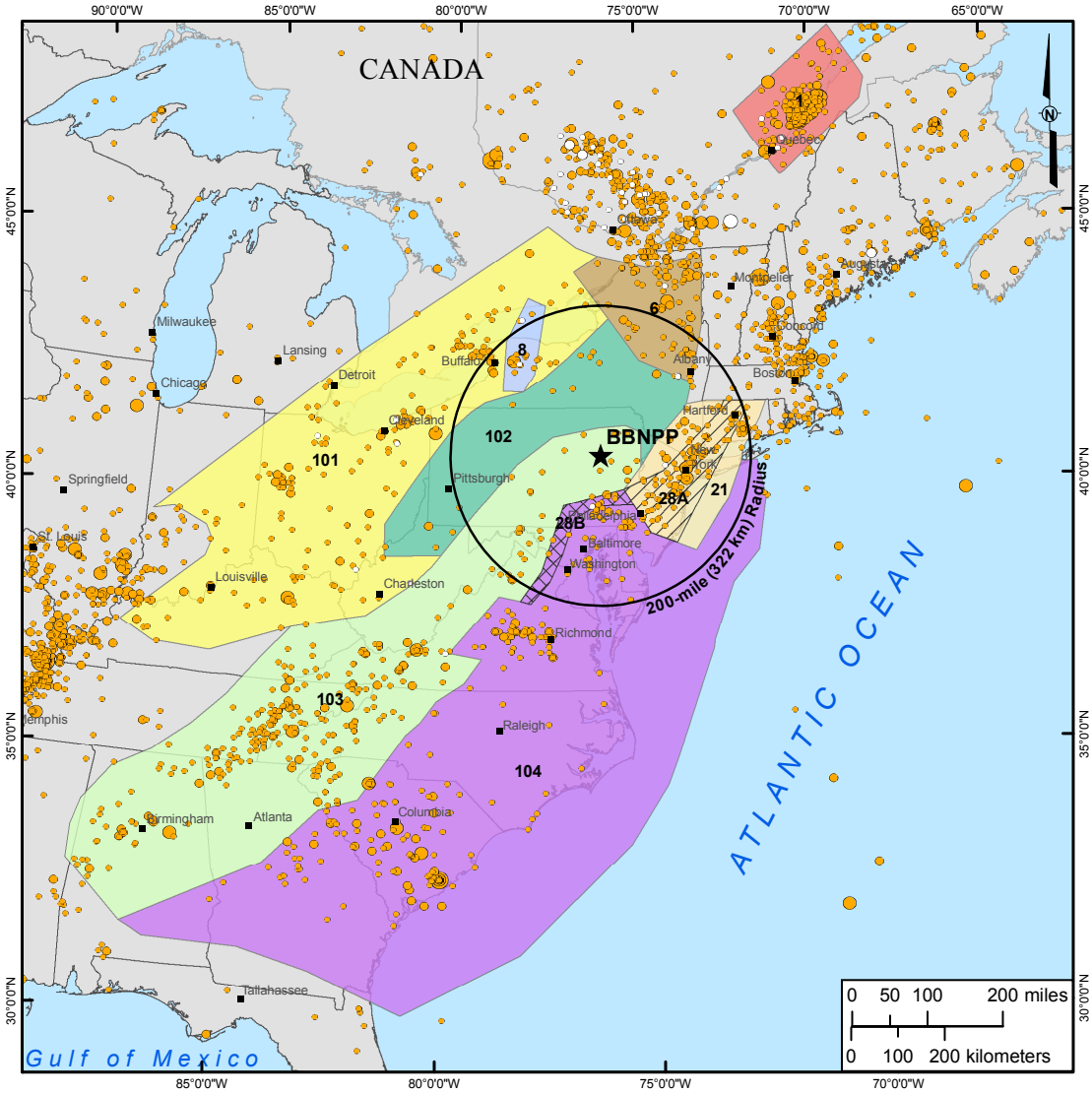
- 30 Shenandoah
- 31 Quakers
- 33 Niagara
- 34 Nessmuk
- 37 La Malbaie (Charlevoix) Seismic Zone
- 50 Grenville Province (Background)

REFERENCES:
- ESRI, 2007.
- USGS 2008.
- USGS, PDE, 2010.
- ANSS, 2010.
- EC, 2010.
- EPRI Volume X: Rondout Associates, 1986.

10-4310-GIS-A056

© 2007-2012 UniStar Nuclear Services, LLC. All rights reserved.
COPYRIGHT PROTECTED

Figure 2.5-21— {Weston Geophysical EPRI Source Zones}



LEGEND

- ★ Center Point of Proposed Bell Bend NPP (BBNPP)
- ■ City
- ◯ NPP Reactor 200-mile (322 km) Radius

Earthquake Epicenters (by Magnitude, mb)

USGS 2008 Catalog (1534-2006)	2007 to April 2010
3.0 - 3.9	3.0 - 3.9
4.0 - 4.9	4.0 - 4.9
5.0 - 5.9	5.0 - 5.9
6.0 - 6.9	
7.0 - 7.9	

NOTE: The 2007 to 2010 seismicity shown in 500-mile (800 km) radius.

Weston Geophysical Sources contributing to 99% of BBNPP Site Hazard

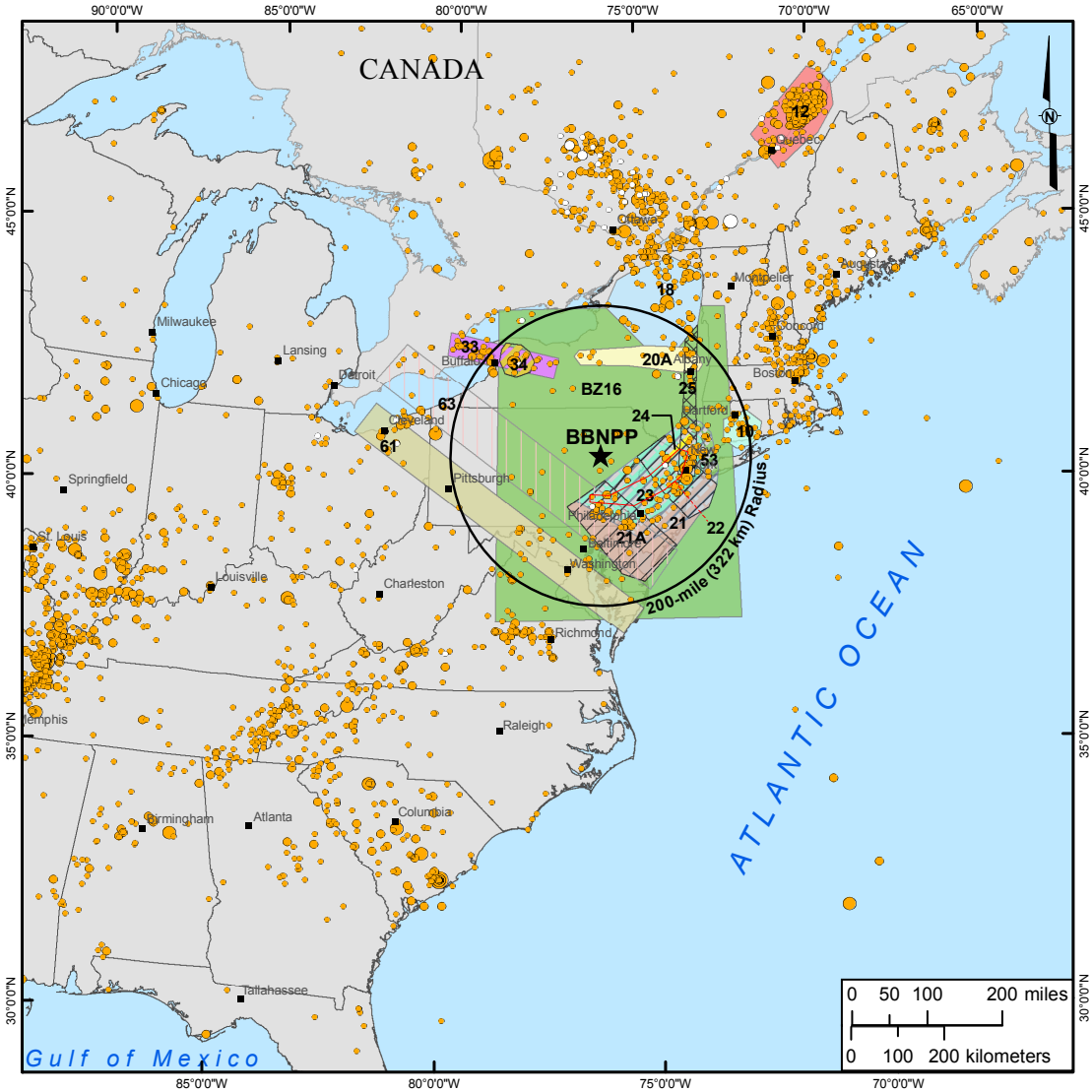
- 1 Charlevoix - La Malbaie Seismic Zone
- 6 Adirondack Mountains
- 8 Clarendon-Linden
- 21 New York Nexus
- 28A Zone of Mesozoic Basin
- 28B Zone of Mesozoic Basin
- 101 South Ontario-Ohio-Indiana Background
- 102 Appalachian Plateau Background
- 103 Southern Appalachian Background
- 104 Southern Coastal Plain Background

REFERENCES:
- ESRI, 2007.
- USGS 2008.
- USGS, PDE, 2010.
- ANSS, 2010.
- EC, 2010.
- EPRI Volume V: Weston Geophysical, 1986.

10-4310-GIS-A075

© 2007-2012 UniStar Nuclear Services, LLC. All rights reserved.
COPYRIGHT PROTECTED

Figure 2.5-22— {Woodward-Clyde Consultants EPRI Source Zones}



LEGEND

- ★ Center Point of Proposed Bell Bend NPP (BBNPP)
- ▪ City
- ◯ NPP Reactor 200-mile (322 km) Radius

Earthquake Epicenters (by Magnitude, mb)

USGS 2008 Catalog (1534-2006)	2007 to April 2010
3.0 - 3.9	3.0 - 3.9
4.0 - 4.9	4.0 - 4.9
5.0 - 5.9	5.0 - 5.9
6.0 - 6.9	
7.0 - 7.9	

NOTE: The 2007 to 2010 seismicity shown in 500-mile (800 km) radius.

Woodward-Clyde Sources contributing to 99% of BBNPP Site Hazard

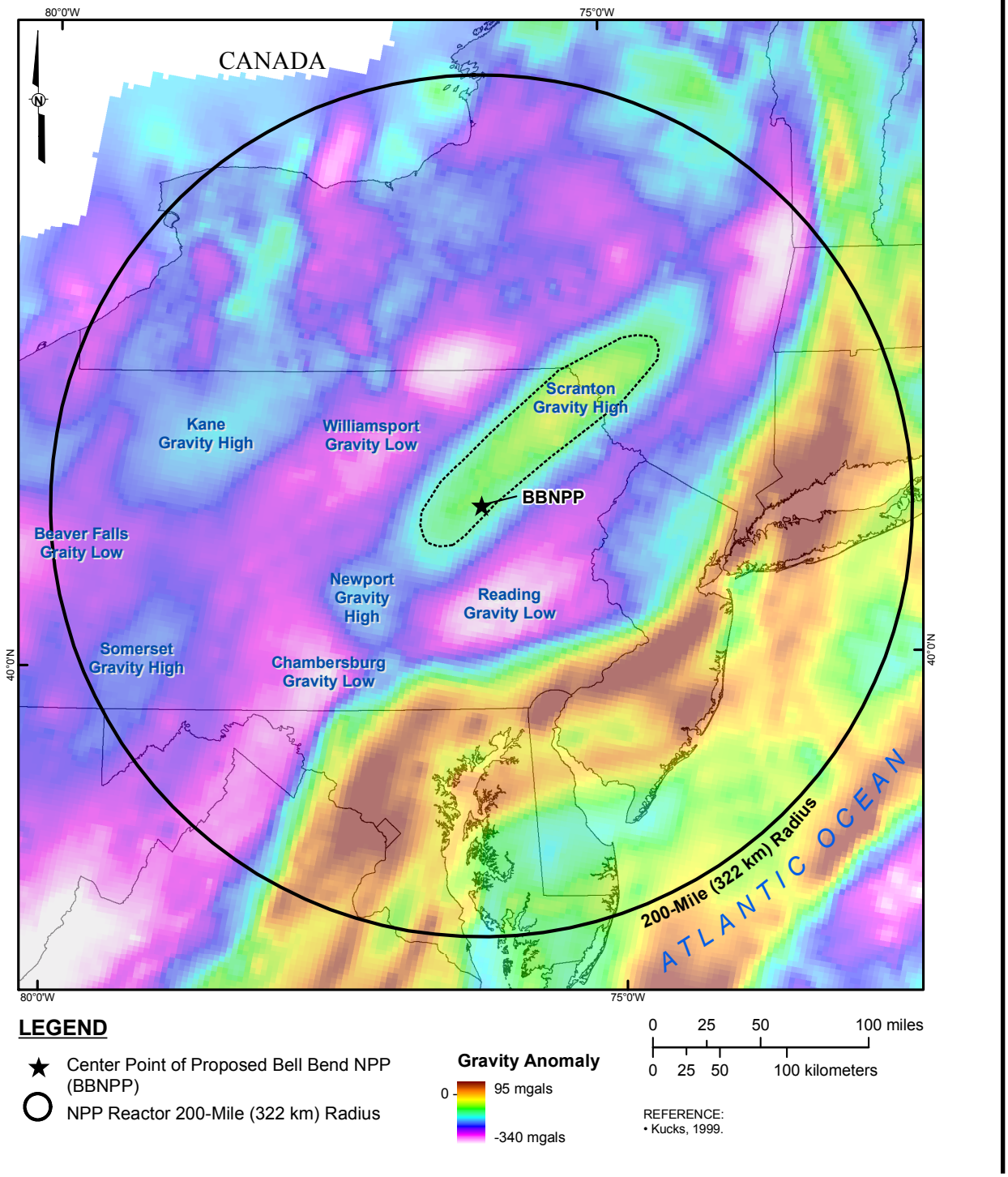
18	Adirondack Uplift
20A	Mohawk River Trend
21	NJ Isostatic Gravity Saddle
21A	NJ Isostatic Gravity Saddle
22	Newark Basin
23	Newark Basin Perimeter
24	Ramapo Fault Zone
25	Hudson River Valley Trend
33	W. NY-S Ontario Trend
34	Attica, NY Intersection
63	Tyron-Mt. Union Lineament
BZ16	Susquehanna Background
12	Charlevoix Seismic Zone
61	Pittsburgh-Washington Lineament
10	Moodus Seismic Zone
53	New York-New Jersey-E. Pennsylvania Default

REFERENCES:
- ESRI, 2007.
- USGS 2008.
- USGS, PDE, 2010.
- ANSS, 2010.
- EC, 2010.
- EPRI Volume VIII: Woodward-Clyde Consultants, 1986.

10-4310-GIS-A076

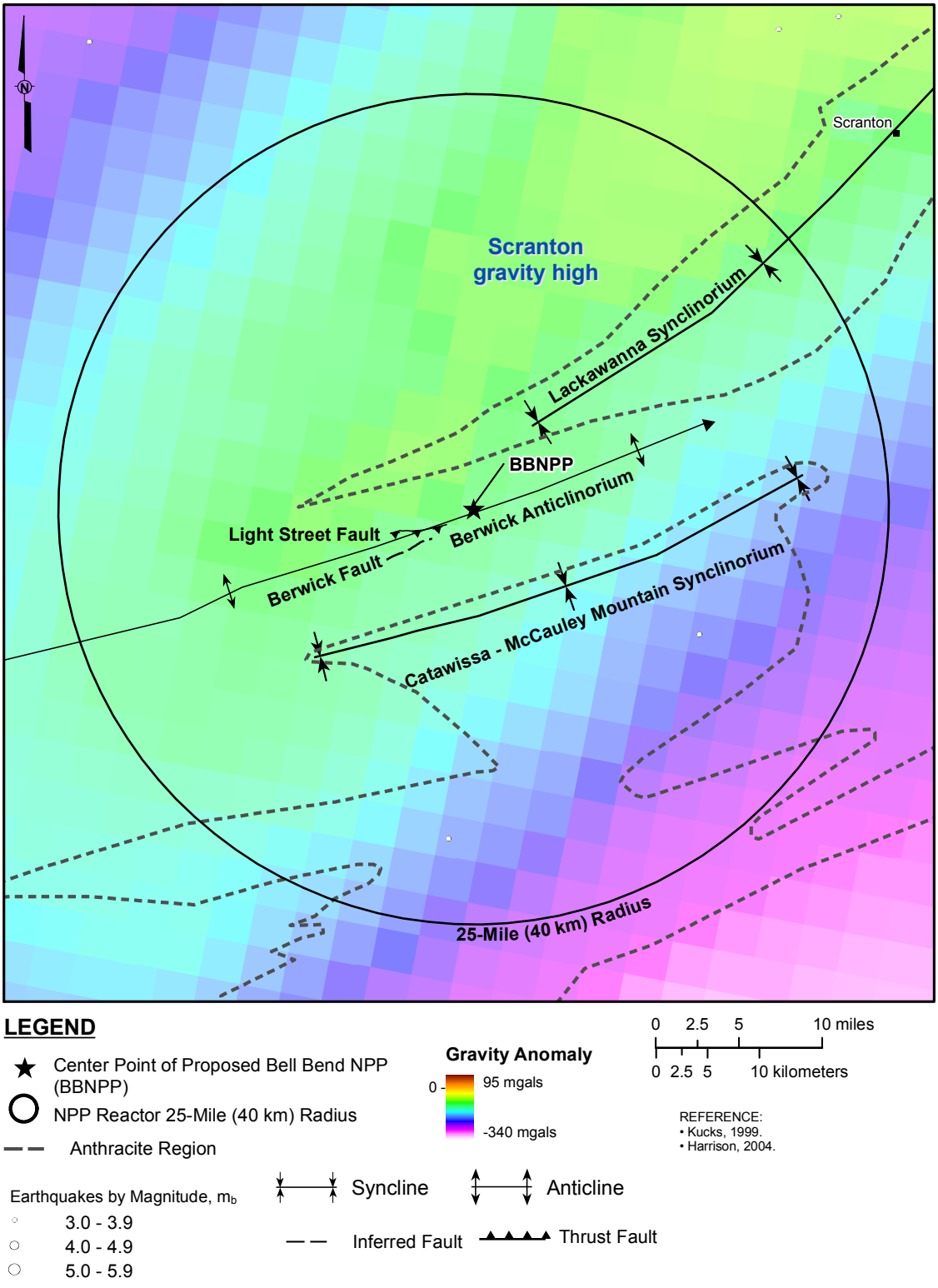
© 2007-2012 UniStar Nuclear Services, LLC. All rights reserved.
COPYRIGHT PROTECTED

Figure 2.5-23— {Regional Bouguer Gravity Anomaly Map}



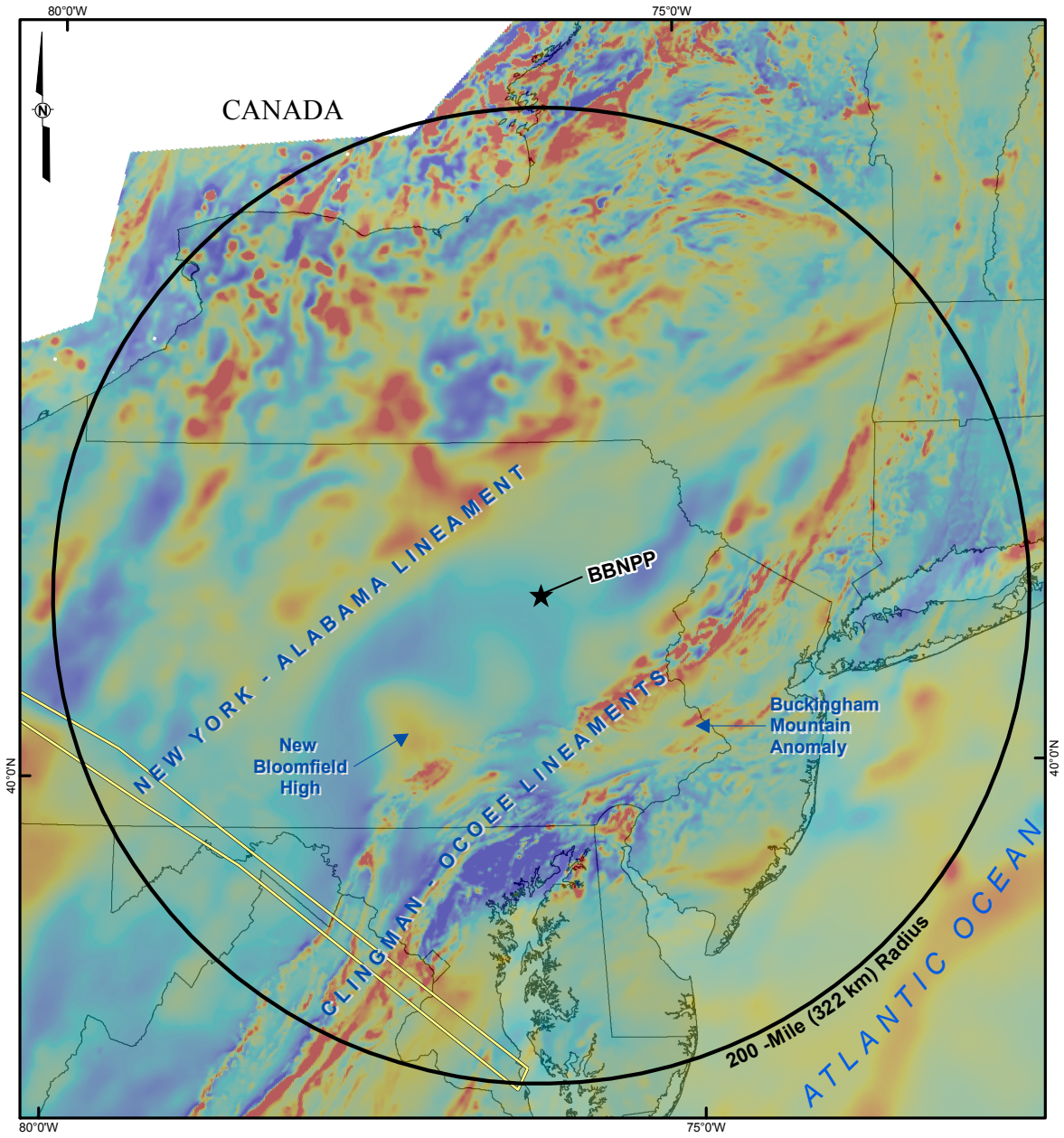
© 2007-2012 UniStar Nuclear Services, LLC. All rights reserved.
COPYRIGHT PROTECTED

Figure 2.5-24— {Site Vicinity Bouguer Gravity Anomaly Map}



© 2007-2012 UniStar Nuclear Services, LLC. All rights reserved.
COPYRIGHT PROTECTED

Figure 2.5-25— {Regional Magnetic Anomaly Map}



© 2007-2012 UniStar Nuclear Services, LLC. All rights reserved.
COPYRIGHT PROTECTED